



日中笹川医学奨学金制度
第44期〈学位取得コース〉研究者

報 告 書

2022年4月～2024年3月

公益財団法人 日中医学協会

日中笹川医学奨学金制度＜学位取得コース＞：第 44 期研究者

研究者 No.	氏 名	所 属 機 関	受 け 入 れ 機 関	指導責任者	掲載頁
		研究テーマ			
G 4401	李 君鵬	吉林省人民医院・主治医師	東北大学大学院医学系研究科 消化器外科学分野	亀井 尚 教授	p. 1
		胃癌、食道胃接合部癌における癌微小免疫環境の解析と至適治療の確立			
G 4402	黄 璐嬌	四川省医学科学院・四川省人民医院・主管技師	筑波大学医学医療系国際発達ケア： エンパワメント科学研究室	安梅 勅江 教授	p. 7
		高齢栄養リスクの指数と高齢入院者の入院時間、入院費用との関係			
G 4403	楊 勇	懷化市第一人民医院・主治医師	千葉大学社会精神保健教育研究センター	橋本 謙二 副センター 長・教授	p. 13
		脳疾患の病因解明と新規治療法の開発			
G 4404	蔣 夢恬	東京医科歯科大学大学院医歯学総合研究科 ・博士課程学生	東京医科歯科大学大学院医歯学総合研究科 生体補綴歯科学分野	若林 則幸 教授	p. 70
		暗条件下での血清及び唾液中の二酸化チタンの殺菌効果に及ぼす 3 種類のイオン性抗菌剤の影響に関する研究			
G 4405	陳 曹傑	慶應義塾大学大学院医学研究科・博士課程学生	慶應義塾大学医学部形成外科学	貴志 和生 教授	p. 88
		創傷治癒とオートファジーの関係			
G 4406	趙 宏波	中国医学科学院腫瘍医院深圳医院・副主任医師	東海大学医学部外科学系消化器外科学	小柳 和夫 教授	p. 119
		食道癌術後縫合不全に対する ICG 蛍光イメージング法の有用性の検討			
G 4407	周 英	金沢大学大学院人間社会環境研究科 ・博士課程学生	金沢大学大学院人間社会環境研究科	堤 敦朗 教授	p. 162
		日本における精神科医療通訳が受ける心理的影響に関する研究：質的研究			
G 4408	劉 天驕	成都市婦女児童センター医院・幹事	京都大学大学院医学研究科 分子遺伝学分野	篠原 隆司 教授	p. 178
		α-Klotho を要因とする老化過程における精子幹細胞の微小環境制御			
G 4409	馬 快	大阪大学大学院医学系研究科・博士課程学生	大阪大学大学院医学系研究科腎臓内科学 国立成育医療研究センター研究所 RI 管理室/移植免疫研究室	猪阪 善隆 教授 李 小康 室長	p. 219
		腎移植における腎臓線維化発生機序の解明と新規治療法の開発に関する研究			
G 4410	徐 勇	長崎大学大学院医歯薬学総合研究科・博士課程学生	長崎大学原爆後障害医療研究所 生物学研究分野	李 桃生 教授	p. 272
		ニカラベンによる間葉系幹細胞の放射線損傷の軽減			
G 4411	李 佩霖	長崎大学大学院医歯薬学総合研究科・博士課程学生	長崎大学大学院医歯薬学総合研究科 移植・消化器外科学	江口 晋 教授	p. 330
		小分子誘導肝前駆細胞 (CLiP) からの 3D 胆管形成			

日中笹川医学奨学金制度<学位取得コース>評価書

課程博士：指導教官用



第 44 期

研究者番号：G4401

作成日：2024年3月10日

氏名	李君鵬	LI JUNPENG	性別	M	生年月日	1983/01/15
所属機関(役職)	吉林省人民医院急診外科(主治医師)					
研究先(指導教官)	東北大学大学院医学系研究科消化器外科学分野(亀井尚教授)					
研究テーマ	SIRP α -CD47 経路が食道癌に与える影響の解明と治療標的としての有用性の検討 The impact of the immune checkpoint SIRP α -CD47 on esophageal cancer and its efficacy as a therapeutic target.					
専攻種別	<input type="checkbox"/> 論文博士			<input checked="" type="checkbox"/> 課程博士		

研究者評価(指導教官記入欄)

成績状況	優 良 可 不可 学業成績係数=	取得単位数
		12/30
学生本人が行った研究の概要	食道癌手術患者における SIRP α ・CD47 の発現を 120 名の手術検体の免疫染色にて評価し、長期予後との関連について検討をおこなった。特に CD47 については臨床で実際に使用されている PD-L1 発現の染色評価基準に準じて CPS・TPS で評価するという新たな試みをおこなった。その結果、食道癌周囲の免疫細胞の SIRP α の高発現や癌微小環境内の腫瘍や免疫細胞の CD47 高発現が食道癌患者の予後不良因子であるという知見を新たに得ることが出来た。また、In vitro 実験のため食道癌細胞株の培養・継代・保存の手技を獲得し、細胞増殖試験や蛋白抽出などの手技も取得したため今後の細胞実験の準備は整っている。	
総合評価	【良かった点】 実験についてはいつも積極的に取り組む姿勢を評価したい。当初に設定した研究テーマで思うような結果が得られず途中でテーマを変更し課題に当たってもらったが、それまでの研究で得た知識も生かし、スピード感を持って結果を得ることが出来た。また、実験だけでなくグループ内のミーティングや抄読会などにも積極的に参加し、自身の専門的知識の獲得と周囲との円滑なコミュニケーションの獲得に努めていたことは素晴らしい姿勢であった。	
	【改善すべき点】 特にないが、独自で研究を進め発表をおこなっていくためには、英語のスキルはもう少し向上することが望まれる。	
	【今後の展望】 今回の結果を基に、In vitro でマクロファージの食道癌細胞に対する貪食機能の評価を、チェックポイント阻害剤を用いて評価・検討していく予定である。	
学位取得見込	奨学金支援の終了後、2年以内に博士学位を取得見込みである。	
評価者(指導教官名) 東北大学大学院消化器外科学教授 亀井 尚		

日中笹川医学奨学金制度<学位取得コース>報告書 研究者用



第44期

研究者番号: G4401

作成日: 2024年3月7日

氏名	李君鹏	LI JUNPENG	性別	M	生年月日	1983/01/15
所属機関(役職)	吉林省人民医院急診外科(主治医師)					
研究先(指導教官)	東北大学大学院医学系研究科消化器外科学分野(亀井尚 教授)					
研究テーマ	SIRP α -CD47経路が食道癌に与える影響の解明と治療標的としての有用性の検討 The impact of the immune checkpoint SIRP α -CD47 on esophageal cancer and its efficacy as a therapeutic target.					
専攻種別	論文博士	<input type="checkbox"/>	課程博士	<input checked="" type="checkbox"/>		
<p>1. 研究概要(1)</p> <p>1) 目的(Goal) This study aimed to conduct a detailed evaluation of the expression of SIRPα and CD47 in cancer cells and immune cells within the cancer microenvironment of ESCC (esophageal squamous cell carcinoma) surgical specimens using immunohistochemistry. Furthermore, it investigated the relationship between the CD47-SIRPα pathway and the long-term prognosis after ESCC surgery. Additionally, the study aimed to stratify the risk for esophageal cancer and to prove the utility of this stratification as a therapeutic target.</p> <p>2) 戦略(Approach) Esophageal cancer is one of the major causes of death worldwide, including in Japan. Particularly in East Asia and Africa, the incidence of esophageal squamous cell carcinoma (ESCC) is high, and its prognosis is known to be poor. In Japan, according to data from 2015, the incidence rate was 31.2 cases per 100,000 men and 5.9 cases per 100,000 women. In 2019, there were 11,619 deaths due to esophageal cancer, accounting for 3.1% of all cancer deaths, highlighting the need for the development of new treatments and improved intervention strategies. Recently, the inhibition of the PD-1/PD-L1 pathway through anti-PD1 antibody drugs has been widely used in cancer immunotherapy, and several immune checkpoints other than the PD-1/PD-L1 pathway have been reported and are attracting attention as therapeutic targets.</p> <p>Signal-regulatory protein alpha (SIRPα) and Cluster of Differentiation 47 (CD47) are known as immune checkpoints that control innate immunity. It has been reported that the binding of these two proteins suppresses the phagocytic activity of myeloid cells such as macrophages. In the field of oncology, high expression of CD47 in various tumors has been reported as a poor prognostic factor, and inhibition of the SIRPα-CD47 pathway is being focused on as a new therapeutic strategy. However, in esophageal cancer, a detailed examination of the SIRPα-CD47 pathway has not yet been conducted.</p> <p>3) 材料と方法(Materials and methods) Our institution targeted 100 patients with ESCC (esophageal squamous cell carcinoma) who underwent esophagectomy. From the resected specimens, slides including the deepest part of the tumor were selected for immunohistochemical staining of SIRPα and CD47. The expression of SIRPα in immune cells was classified into high and low expression groups using a cutoff value of 3% positivity. For CD47, the expression status in both tumor cells and immune cells was evaluated using Combined Positive Score (CPS) and Tumor Proportion Score (TPS), with a cutoff value of 10% used to categorize into high and low expression groups. Long-term survival was compared between the groups using 5-year overall survival (5y-OS) and 5-year recurrence-free survival (5y-RFS) rates.</p> <p>4) 実験結果(Results) In this study, 79 males and 21 females were included, with an average age of 68.7 years. The median follow-up period was 61 months. The high SIRPα expression group (48 patients) showed a statistically significant poorer 5-year overall survival rate (5y-OS) compared to the low expression group (52 patients) (56.4% vs. 82.8%, P=0.0098). For CD47, high expression in both CPS and TPS was significantly associated with poorer 5y-OS (48.8% vs. 89.5%, P<0.0001, and 48.4% vs. 87.5%, P<0.0001). The 5-year recurrence-free survival (5y-RFS) was also significantly worse in the high expression groups for both SIRPα and CD47. Furthermore, multivariate analysis using the Cox proportional hazards model identified high expression of CD47 and high expression of SIRPα as poor prognostic factors for overall survival (OS), and high expression of CD47 as a poor prognostic factor for recurrence-free survival (RFS).</p>						

5) 考察 (Discussion)

This study investigated the importance of SIRP α and CD47 expression in esophageal squamous cell carcinoma (ESCC) and its implications for prognosis. Our main findings are:

Impact of High SIRP α and CD47 Expression: We found that high levels of SIRP α and CD47 in ESCC are associated with worse survival rates. This suggests that these proteins play a significant role in the progression of this cancer.

Potential Therapeutic Targets: The link between high expression of SIRP α and CD47 and poor outcomes highlights the potential of these molecules as targets for new treatments in ESCC.

Use in Clinical Practice: Identifying patients with high SIRP α and CD47 expression could help in choosing more effective treatments, as these patients might have more aggressive cancer.

Limitations and Future Research: Our study, while informative, has limitations due to its retrospective design and small sample size. Further research with larger groups of patients is needed to confirm our findings and understand the mechanisms behind them. We plan to investigate the expression levels of SIRP α and CD47 in esophageal squamous cell carcinoma (ESCC) and conduct cellular experiments to verify the reduction in macrophage phagocytic ability using anti-CD47 and anti-SIRP α antibodies. In conclusion, SIRP α and CD47 are important in understanding ESCC and could be key targets for improving treatment strategies for this cancer.

6) 参考文献 (References)

1. Huang, C.-Y., Ye, Z.-H., Huang, M.-Y., & Lu, J.-J. (2020). Regulation of CD47 expression in cancer cells. *Translational Oncology*, 13, Article 100862.
2. Koga, N., Hu, Q., Sakai, A., Takada, K., Nakanishi, R., Hisamatsu, Y., Ando, K., Kimura, Y., Oki, E., Oda, Y., & Mori, M. (2021). Clinical significance of signal regulatory protein alpha (SIRP α) expression in esophageal squamous cell carcinoma. *Cancer Science*. <https://doi.org/10.1111/cas.14971>.
3. Son, J., Hsieh, R. C.-E., Lin, H. Y., Krause, K. J., Yuan, Y., Biter, A. B., Welsh, J., Curran, M. A., & Hong, D. S. (2022). Inhibition of the CD47-SIRP α axis for cancer therapy: A systematic review and meta-analysis of emerging clinical data. *Frontiers in Immunology*. <https://doi.org/10.3389/fimmu.2022.1027235>.
4. Zhao, C.-L., Yu, S., Wang, S.-H., Li, S.-G., Wang, Z.-J., & Han, S.-N. (2018). Characterization of cluster of differentiation 47 expression and its potential as a therapeutic target in esophageal squamous cell cancer. *Oncology Letters*, 15, 2017-2023. <https://doi.org/10.3892/ol.2017.7447>.
5. Logtenberg, M. E. W., Scheeren, F. A., & Schumacher, T. N. (2020). The CD47-SIRP α Immune Checkpoint. *Immunity*, 52(5), 742-752. <https://doi.org/10.1016/j.immuni.2020.04.011>.

2. 執筆論文 Publication of thesis ※記載した論文を添付してください。Attach all of the papers listed below.

論文名 1 Title					
掲載誌名 Published journal					
	年	月	巻(号)	頁 ~	頁 言語 Language
第1著者名 First author	第2著者名 Second author		第3著者名 Third author		
その他著者名 Other authors					
論文名 2 Title					
掲載誌名 Published journal					
	年	月	巻(号)	頁 ~	頁 言語 Language
第1著者名 First author	第2著者名 Second author		第3著者名 Third author		
その他著者名 Other authors					
論文名 3 Title					
掲載誌名 Published journal					
	年	月	巻(号)	頁 ~	頁 言語 Language
第1著者名 First author	第2著者名 Second author		第3著者名 Third author		
その他著者名 Other authors					
論文名 4 Title					
掲載誌名 Published journal					
	年	月	巻(号)	頁 ~	頁 言語 Language
第1著者名 First author	第2著者名 Second author		第3著者名 Third author		
その他著者名 Other authors					
論文名 5 Title					
掲載誌名 Published journal					
	年	月	巻(号)	頁 ~	頁 言語 Language
第1著者名 First author	第2著者名 Second author		第3著者名 Third author		
その他著者名 Other authors					

3. 学会発表 Conference presentation ※筆頭演者として総会・国際学会を含む主な学会で発表したものを記載してください

※Describe your presentation as the principal presenter in major academic meetings including general meetings or international meetings

学会名 Conference					
演題 Topic					
開催日 date	年	月	日	開催地 venue	
形式 method	<input type="checkbox"/> 口頭発表 Oral	<input type="checkbox"/> ポスター発表 Poster	言語 Language	<input type="checkbox"/> 日本語	<input type="checkbox"/> 英語 <input type="checkbox"/> 中国語
共同演者名 Co-presenter					
学会名 Conference					
演題 Topic					
開催日 date	年	月	日	開催地 venue	
形式 method	<input type="checkbox"/> 口頭発表 Oral	<input type="checkbox"/> ポスター発表 Poster	言語 Language	<input type="checkbox"/> 日本語	<input type="checkbox"/> 英語 <input type="checkbox"/> 中国語
共同演者名 Co-presenter					
学会名 Conference					
演題 Topic					
開催日 date	年	月	日	開催地 venue	
形式 method	<input type="checkbox"/> 口頭発表 Oral	<input type="checkbox"/> ポスター発表 Poster	言語 Language	<input type="checkbox"/> 日本語	<input type="checkbox"/> 英語 <input type="checkbox"/> 中国語
共同演者名 Co-presenter					
学会名 Conference					
演題 Topic					
開催日 date	年	月	日	開催地 venue	
形式 method	<input type="checkbox"/> 口頭発表 Oral	<input type="checkbox"/> ポスター発表 Poster	言語 Language	<input type="checkbox"/> 日本語	<input type="checkbox"/> 英語 <input type="checkbox"/> 中国語
共同演者名 Co-presenter					

4. 受賞(研究業績) Award (Research achievement)

名称 Award name	国名 Country		受賞年 Year of	年	月
	国名 Country		受賞年 Year of	年	月

5. 本研究テーマに関わる他の研究助成金受給 Other research grants concerned with your research theme

受給実績 Receipt record	<input type="checkbox"/> 有 <input checked="" type="checkbox"/> 無
助成機関名称 Funding agency	
助成金名称 Grant name	
受給期間 Supported period	年 月 ~ 年 月
受給額 Amount received	円
受給実績 Receipt record	<input type="checkbox"/> 有 <input type="checkbox"/> 無
助成機関名称 Funding agency	
助成金名称 Grant name	
受給期間 Supported period	年 月 ~ 年 月
受給額 Amount received	円

6. 他の奨学金受給 Another awarded scholarship

受給実績 Receipt record	<input type="checkbox"/> 有 <input checked="" type="checkbox"/> 無
助成機関名称 Funding agency	
奨学金名称 Scholarship name	
受給期間 Supported period	年 月 ~ 年 月
受給額 Amount received	円

7. 研究活動に関する報道発表 Press release concerned with your research activities

※記載した記事を添付してください。Attach a copy of the article described below

報道発表 Press release	<input type="checkbox"/> 有 <input checked="" type="checkbox"/> 無	発表年月日 Date of release	
発表機関 Released medium			
発表形式 Release method	・新聞 ・雑誌 ・Web site ・記者発表 ・その他()		
発表タイトル Released title			

8. 本研究テーマに関する特許出願予定 Patent application concerned with your research theme

出願予定 Scheduled	<input type="checkbox"/> 有 <input checked="" type="checkbox"/> 無	出願国 Application	
出願内容(概要) Application contents			

9. その他 Others

--

指導責任者(記名) 亀井尚

日中笹川医学奨学金制度<学位取得コース>評価書

課程博士：指導教官用



第 44 期

研究者番号：G4402

作成日：2024年3月1日

氏名	黄璐嬌	HUANG LUJIAO	性別	F	生年月日	1988/09/10
所属機関（役職）	四川省医学科学院・四川省人民医院臨床栄養科（主管技師）					
研究先（指導教官）	筑波大学大学院人間総合科学研究科生命システム医学専攻 国際発達ケア：エンパワメント科学研究室（安梅 勅江 教授）					
研究テーマ	社会資本と生活の質の変化：多民族社会における縦断的研究 Social Capital and Changes in Quality of Life: A Longitudinal Study in Multi-Ethnic Populations					
専攻種別	<input type="checkbox"/> 論文博士			<input checked="" type="checkbox"/> 課程博士		

研究者評価（指導教官記入欄）

成績状況	(優) 良 可 不可 学業成績係数=3.98	取得単位数 34
		取得単位数／取得すべき単位数総数 34/30
学生本人が行った研究の概要	黄璐嬌さんは、博士課程の単位取得において優秀な成績を修めた。研究テーマは、ベースラインの社会資本が、中国の多民族社会における生活の質の変化に影響を与える重要な要因であること、そして社会資本と生活の質の関係は多民族地域では異質性を有することを包括的な視点から捉えようとするものである。ベースラインの社会資本がすでに高いレベルの人々は、生活の質の改善の余地が限られており、天井効果が存在する可能性がある。本研究は、多民族地域における健康増進の指針として示唆深いものである。	
総合評価	【良かった点】 1. 研究仮説が明確で豊富な情報を提供し、適切な研究デザインと調査方法を用い、この分野における研究の方向性を示した。 2. 最先端の集団調査のスキルと方法を習得した。 3. 異分野間のチームワーク能力を身につけた。	
	【改善すべき点】 1. タイムマネジメントをさらに効率的にする。 2. さらに高度な統計スキルを学び、分析の幅を広げる。	
	【今後の展望】 黄璐嬌さんが研究内容をさらに充実・深化させ、学術的価値を高めてくれることを確信している。卒業後も研究に従事し、日中医療交流の架け橋として活躍し、多民族国家の健康増進に貢献することを期待している。	
学位取得見込	博士学位取得見込です。	
		評価者（指導教官名） 安梅勅江

日中笹川医学奨学金制度＜学位取得コース＞報告書 研究者用



第44期

研究者番号: G4402

作成日: 2024年3月 1 日

氏名	黄璐娇	HUANG LUJIAO	性別	F	生年月日 1988/09/10
所属機関(役職)	四川省医学科学院・四川省人民医院臨床栄養科(主管技師)				
研究先(指導教官)	筑波大学大学院人間総合科学研究科生命システム医学専攻 国際発達ケア: エンパワメント科学研究室(安梅 勅江 教授)				
研究テーマ	社会資本と生活の質の変化: 多民族社会における縦断的研究 Social Capital and Changes in Quality of Life: A Longitudinal Study in Multi-Ethnic Populations				
専攻種別	論文博士	<input type="checkbox"/>	課程博士	<input checked="" type="checkbox"/>	

1. 研究概要(1)

1) 目的(Goal)

To explore the association of Social capital with changes in Quality of life in multi-ethnic populations and to clarify the heterogeneity in the effects of Social capital on Quality of life across subgroups in multi-ethnic populations

2) 戦略(Approach)

This longitudinal study was based on the China Multi-Ethnic Cohort (CMEC), five provinces of Southwest China were included. The baseline survey was conducted between May 2018 and September 2019 and a total of 99556 participants were recruited. Data were collected with an electronic questionnaire and face-to-face interviews, medical examinations, and clinical laboratory tests. The repeated survey was conducted between August 2020 and July 2021 involving approximately 10% (11161) of the baseline participants. The on-site survey were mostly the same as the baseline survey, except for an expanded and refined questionnaire.

3) 材料と方法(Materials and methods)

a. Participants

Inclusion criteria:

- ① Adults aged 30–79 years old
- ② Permanent residents who have lived for more than six months

Exclusion criteria:

- ① Inability to provide a unique identity card
- ② Severe physical or mental illness (such as schizophrenia)
- ③ Refusal to comply with study requirements

b. Measurements

Social Capital (SC)

SC was measured using a validated Chinese version of Health-related Social Capital Measurement. According to the purpose and feasibility of this study, 5 items were chosen to measure family SC and community/society SC. The answers consisted of 5-point Likert scales ranging from 1 (strongly disagree) to 5 (strongly agree). A higher total score indicates the stronger SC.

Quality of Life (QoL)

QoL was measured using EQ-5D-5L scale. EQ-5D instrument comprises a short descriptive system questionnaire and a visual analogue scale (EQ VAS). The descriptive system comprises 5 dimensions (Mobility, Self-Care, Usual Activities, Pain/Discomfort, Anxiety/Depression), each dimension has five response levels (no problems, slight problems, moderate problems, severe problems, unable to/extreme problems). The EQ VAS is a 0–100 score scale where participants are asked to indicate their overall health, providing a quantitative measure of the patient's perception of their overall health

Changes in Quality of Life

As continuous variables using QoL index value & VAS score: $\Delta QoL = QoL(\text{Repeated-survey}) - QoL(\text{Baseline-survey})$; As categorical variables according to the Pareto Classification of Health Change (PCHC), there are 4 possibilities: Better, Worse, Unchanged, Mixed (better on one dimension, but worse on another)

c. Statistical analysis

Descriptive statistics: Mean \pm SD, Percentiles (interquartile range) and frequency distributions were conducted to show the demographic characteristics, SC score, QoL index value or QoL VAS score. T-test, ANOVA or Nonparametric tests were used to compare between groups.

Change analysis: Multiple linear regression models and logistic regression models

1. 研究概要(2)

4) 実験結果 (Results)

At baseline, the proportion of participants reporting “no problem”(level 1) in mobility, self-care, pain/discomfort, usual activities, and anxiety/depression were 85.0%, 95.0%, 66.9%, 90.4%, and 87.7%, respectively. By year two, the proportion of participants achieving “no problem”(level 1) in mobility, pain/discomfort, and anxiety/depression had a slightly increase except for “usual activities”. Analysis according to Pareto Classification of Health Change (PCHC) showed that more than a quarter of participants (25.2%) reported improvement(better) in QoL after 2 years. However, there were 19% reported a level below baseline QoL at follow-up. The remaining more than half of the participants either had no change or had a mixed change of the dimensions of EQ-5D.

Taking changes in QoL as a continuous variable, after controlling for potential confounding factors, the Linear regression model indicated a negative association between social capital and changes in QoL. Taking changes in QoL as a categorical variable, after controlling for potential confounding factors, the Multinomial logistic regression model indicated that comparison with “unchanged group”, the higher the social capital at baseline the less likely(OR=0.974) it is to get better QoL. However, No statistically significant associations were found between social capital and “mixed group” or “worse group” when comparison with “unchanged group”.

5) 考察 (Discussion)

This study found better social capital at baseline is associated with less positive improvement in quality of life over 2 years among multi-ethnics in southwest China after adjust for potential confounders. This suggests that those with already higher levels of social capital at baseline have less room for improvement in quality of life. There may be a ceiling effect, wherein social capital has diminishing returns on quality of life, it is difficult for them to significantly improve further. This could relate to theories around social support already being adequate for those starting with better social capital. The stress-buffering hypothesis argues good social support protects against life stressors negatively impacting health and well-being. Those starting with poorer social capital have more uncertainty (a stressor), leaving more room for building networks to improve quality of life.

Heterogeneity exists in the SC-changes in QoL relationships. The marginal returns from SC on QoL may differ between Han majority versus ethnic minority groups due to variances in socioeconomic position, social integration, lifestyles and access to resources.

Urbanization trends have likely disrupted traditional social connections among certain minorities. Those with higher social capital pre-transition may perceive greater subsequent worsening in QoL and wellbeing.

Several limitations exist in this study. First, the study variables were restricted to baseline social capital and changes in quality of life scores. In observational data, where the baseline outcome is a confounder or mediator, change-score analyses evaluate obscure estimates, which may differ in magnitude and direction from the total and direct causal effects. Second, the two-wave data cannot show long-term trajectories. More timepoints are needed to analyze how changes in social capital might shape trajectories in quality of life.

6) 参考文献 (References)

- [1] CDC. Health-Related Quality of Life (HRQOL). 2023. Available from: <https://www.cdc.gov/hrqol/concept.htm>.
- [2] Whoqol Group. The World Health Organization quality of life assessment (WHOQOL): position paper from the World Health Organization. *Soc SciMed*. 1995;41(10):1403-9. [https://doi.org/10.1016/0277-9536\(95\)00112-k](https://doi.org/10.1016/0277-9536(95)00112-k).
- [3] Karimi M, Brazier J. Health, health-related quality of life, and quality of life: what is the difference? *PharmacoEconomics*. 2016;34(7):645-9. <https://doi.org/10.1007/s40273-016-0389-9>
- [4] Development of the World Health Organization WHOQOL-BREF quality of life assessment. The WHOQOL Group. *Psychol Med* 1998; 28:551-8.
- [5] Macran S, Weatherly H, Kind P. Measuring population health: a comparison of three generic health status measures. *Med Care*. 2003;41(2):21831. <https://doi.org/10.1097/01.MLR.0000044901.57067.19>.
- [6] Cunillera O, Tresserras R, Rajmil L, Vilagut G, Brugulat P, Herdman M, et al. Discriminative capacity of the EQ-5D, SF-6D, and SF-12 as measures of health status in population health survey. *Qual Life Res*. 2010;19(6):853-64. <https://doi.org/10.1007/s11136-010-9639-z>
- [7] Wang, D., Xie, S., Wu, J. et al. The trend in quality of life of Chinese population: analysis based on population health surveys from 2008 to 2020. *BMC Public Health* 23, 167 (2023). <https://doi.org/10.1186/s12889-023-15075-2>.
- [8] Reeve BB, Graves KD, Lin L, Potosky AL, Ahn J, Henke DM, Pan W, Fall-Dickson JM. Health-related quality of life by race, ethnicity, and country of origin among cancer survivors. *J Natl Cancer Inst*. 2023 Mar 9;115(3):258-267. doi: 10.1093/jnci/djac230.

2. 執筆論文 Publication of thesis ※記載した論文を添付してください。Attach all of the papers listed below.

論文名 1 Title						
掲載誌名 Published journal						
	年	月	巻(号)	頁 ~	頁	言語 Language
第1著者名 First author			第2著者名 Second author			第3著者名 Third author
その他著者名 Other authors						
論文名 2 Title						
掲載誌名 Published journal						
	年	月	巻(号)	頁 ~	頁	言語 Language
第1著者名 First author			第2著者名 Second author			第3著者名 Third author
その他著者名 Other authors						
論文名 3 Title						
掲載誌名 Published journal						
	年	月	巻(号)	頁 ~	頁	言語 Language
第1著者名 First author			第2著者名 Second author			第3著者名 Third author
その他著者名 Other authors						
論文名 4 Title						
掲載誌名 Published journal						
	年	月	巻(号)	頁 ~	頁	言語 Language
第1著者名 First author			第2著者名 Second author			第3著者名 Third author
その他著者名 Other authors						
論文名 5 Title						
掲載誌名 Published journal						
	年	月	巻(号)	頁 ~	頁	言語 Language
第1著者名 First author			第2著者名 Second author			第3著者名 Third author
その他著者名 Other authors						

3. 学会発表 Conference presentation ※筆頭演者として総会・国際学会を含む主な学会で発表したものを記載してください。

※Describe your presentation as the principal presenter in major academic meetings including general meetings or international meetings

学会名 Conference					
演題 Topic					
開催日 date	年	月	日	開催地 venue	
形式 method	<input type="checkbox"/> 口頭発表 Oral	<input type="checkbox"/> ポスター発表 Poster	言語 Language	<input type="checkbox"/> 日本語	<input type="checkbox"/> 英語 <input type="checkbox"/> 中国語
共同演者名 Co-presenter					
学会名 Conference					
演題 Topic					
開催日 date	年	月	日	開催地 venue	
形式 method	<input type="checkbox"/> 口頭発表 Oral	<input type="checkbox"/> ポスター発表 Poster	言語 Language	<input type="checkbox"/> 日本語	<input type="checkbox"/> 英語 <input type="checkbox"/> 中国語
共同演者名 Co-presenter					
学会名 Conference					
演題 Topic					
開催日 date	年	月	日	開催地 venue	
形式 method	<input type="checkbox"/> 口頭発表 Oral	<input type="checkbox"/> ポスター発表 Poster	言語 Language	<input type="checkbox"/> 日本語	<input type="checkbox"/> 英語 <input type="checkbox"/> 中国語
共同演者名 Co-presenter					
学会名 Conference					
演題 Topic					
開催日 date	年	月	日	開催地 venue	
形式 method	<input type="checkbox"/> 口頭発表 Oral	<input type="checkbox"/> ポスター発表 Poster	言語 Language	<input type="checkbox"/> 日本語	<input type="checkbox"/> 英語 <input type="checkbox"/> 中国語
共同演者名 Co-presenter					

4. 受賞(研究業績) Award (Research achievement)

名称 Award name	国名		受賞年	年	月
	Country name		Year of award		
名称 Award name	国名		受賞年	年	月
	Country name		Year of award		

5. 本研究テーマに関わる他の研究助成金受給 Other research grants concerned with your research theme

受給実績 Receipt record	<input type="checkbox"/> 有 <input checked="" type="checkbox"/> 無
助成機関名称 Funding agency	
助成金名称 Grant name	
受給期間 Supported period	年 月 ~ 年 月
受給額 Amount received	円
受給実績 Receipt record	<input type="checkbox"/> 有 <input checked="" type="checkbox"/> 無
助成機関名称 Funding agency	
助成金名称 Grant name	
受給期間 Supported period	年 月 ~ 年 月
受給額 Amount received	円

6. 他の奨学金受給 Another awarded scholarship

受給実績 Receipt record	<input type="checkbox"/> 有 <input checked="" type="checkbox"/> 無
助成機関名称 Funding agency	
奨学金名称 Scholarship name	
受給期間 Supported period	年 月 ~ 年 月
受給額 Amount received	円

7. 研究活動に関する報道発表 Press release concerned with your research activities

※記載した記事を添付してください。Attach a copy of the article described below

報道発表 Press release	<input type="checkbox"/> 有 <input checked="" type="checkbox"/> 無	発表年月日 Date of release	
発表機関 Released medium			
発表形式 Release method	・新聞 ・雑誌 ・Web site ・記者発表 ・その他()		
発表タイトル Released title			

8. 本研究テーマに関する特許出願予定 Patent application concerned with your research theme

出願予定 Scheduled application	<input type="checkbox"/> 有 <input checked="" type="checkbox"/> 無	出願国 Application country	
出願内容(概要) Application contents			

9. その他 Others

None

指導責任者(記名) 安梅 勅江

日中笹川医学奨学金制度＜学位取得コース＞評価書



課程博士：指導教官用

第 44 期

研究者番号：G4403

作成日：2024年2月21日

氏名	楊 勇	YANG YONG	性別	M	生年月日	1986/07/22
所属機関（役職）	懐化市第一人民医院神経外科（主治医師）					
研究先（指導教官）	千葉大学社会精神保健教育研究センター 病態解析研究部門（橋本 謙二 副センター長・教授）					
研究テーマ	脳疾患の病因解明と新規治療法の開発 Study of brain disorders and development of new therapeutic drugs					
専攻種別	<input type="checkbox"/> 論文博士			<input checked="" type="checkbox"/> 課程博士		

研究者評価（指導教官記入欄）

成績状況	(優) 良 可 不可 学業成績係数=	取得単位数
学生本人が行った研究の概要	楊勇君は、千葉大学大学院在籍中に、うつ病モデルにおける迷走神経や脾臓神経の役割に関する実験を行いました。以前、私の研究室は炎症に重要な役割を果たしている $\alpha 7$ ニコチン受容体遺伝子欠損マウスがうつ様行動を示すことを報告した。楊君は、この遺伝子欠損マウスの横隔膜下の迷走神経の切断あるいは脾臓神経を障害すると、うつ様行動が消失することを見出し、またこの現象に腸内細菌叢や微生物が生成する代謝物が関与している可能性を見出した。このように、うつ病における迷走神経・脾臓神経を介する臓器-脳連関の重要性を明らかにした。さらに、肝障害モデル（肝における虚血再灌流障害モデルと胆管結紮・閉塞性胆汁うっ滞モデル）におけるうつ病との関連を見出し、肝-脳連関の重要性を提唱した。	
総合評価	【良かった点】 上記にあるように、新しい研究成果を発表し、うつ病における臓器-脳連関の重要性を提唱し、これらは国際誌に原著論文（筆頭著者として4本）として掲載された。さらに、原著論文2本を筆頭著者として論文投稿中である。このように、多くの研究成果を発表していることは良かった点である。	
	【改善すべき点】 特に改善する個所は無い。	
	【今後の展望】 現在、貴州省人民病院で脳外科医として勤務しており、臨床研究で益々の活躍を期待している。さらに、日中の医学交流にも尽力すると期待している。	
学位取得見込	楊勇君は、2023年3月末に千葉大学で学位（医学博士）を取得した。	
評価者（指導教官名） 橋本 謙二		

日中笹川医学奨学金制度<学位取得コース>報告書 研究者用



第44期

研究者番号: G4403

作成日: 2024年3月1日

氏名	杨 勇	YANG YONG	性別	M	生年月日	1986/07/22
所属機関(役職)	懐化市第一人民医院神経外科(主治医師)					
研究先(指導教官)	千葉大学社会精神保健教育研究センター病態解析研究部門(橋本 謙二 副センター長・教授)					
研究テーマ	脳疾患の病因解明と新規治療法の開発 Study of brain disorders and development of new therapeutic drugs					
専攻種別	論文博士	<input type="checkbox"/>	課程博士	<input checked="" type="checkbox"/>		
1. 研究概要(1)						
<p>1) 目的(Goal) うつ病は代表的な精神疾患であるが、未だ病因は明らかでなく、現在の治療薬に奏功しない治療抵抗性うつ病患者が存在する。近年、うつ病などの精神疾患の病因に腸-脳相関の異常が寄与している可能性が指摘されている。一方、肝臓疾患患者ではうつ症状を呈するが、その機序は明らかでない。</p> <p>2) 戦略(Approach) 今回、二つの実系を行うことにより、うつ病における臓器-脳連関の役割を調べた。A7ニコチン受容体は炎症に重要な役割を果たしており、この遺伝子欠損マウスはうつ様行動を示すことを報告した(参考文献1-2)。最初の実験は、この遺伝子欠損マウスにおける迷走神経および脾臓神経の役割を調べることである。次に、肝障害患者はうつ症状を呈することが知られているが、その機序は明らかでない。今回、二つの肝障害モデルを用いて、腸-肝-脳連関の役割を調べた。</p> <p>3) 材料と方法(Materials and methods) まずは、A7ニコチン受容体遺伝子欠損マウスおよび野生型マウスを用いた。まずは、横隔膜下の迷走神経切断を行い、うつ様行動、腸内細菌叢や代謝物解析を行った。次に、同様に遺伝子欠損マウスの脾臓神経を傷害させた後、うつ様行動、腸内細菌叢および代謝物解析を行った。次に、肝における虚血再灌流障害モデルと胆管結紮・閉塞性胆汁うっ滞モデルを用いて、うつ様行動における肝-脳連関の役割を調べた。</p> <p>4) 実験結果(Results) A7ニコチン受容体遺伝子欠損マウスのうつ様行動は、横隔膜下の迷走神経切断あるいは脾臓神経障害の前処置により、起きないことを見出した。さらに、腸内細菌叢・代謝物の解析により、これらの効果に、腸内細菌叢や代謝物の関与が示唆された。これらの研究成果は、昨年原著論文として発表し(参考文献3)、もう一つは現在論文投稿中である(参考文献4)。肝における虚血再灌流障害モデルマウスが、うつ様行動を示すことを見出し、この効果は迷走神経切断により生じないことから、迷走神経を介する肝-脳連関が重要であることを明らかにした(参考文献5)。さらに、胆管結紮・閉塞性胆汁うっ滞モデルマウスもうつ様行動を示すことを見出し、迷走神経切断により、うつ様行動が消失することを見出した。迷走神経を介する肝-脳連関の重要性を見出した(論文投稿中)。さらに興味深いことに、千葉大学で開発した新規抗うつ薬アールケタミンは、これらの二つのモデルにおけるうつ様行動を単回投与で改善することを見出した(参考文献4)。</p> <p>5) 考察(Discussion) 本研究により、$\alpha 7$ニコチン受容体はうつ様行動に重要な役割を果たしており、迷走神経および脾臓神経が遺伝子欠損マウスのうつ様行動に重要な役割を果たしていることが分かった。また腸内細菌叢や代謝物を含む腸-脳相関が関与している可能性が示唆された。今後、消化器系だけの受容体遺伝子欠損マウスを用いた研究が重要であると思われる。さらに、二つの肝障害モデルにおいても、迷走神経を介する腸-脳相関がうつ様行動に関与している可能性を見出した。さらに、国内外で臨床試験実施中である新規抗うつ薬アールケタミンが二つのモデルにおいても、即効性の抗うつ化を示したことは特筆すべきことである。うつ症状は、精神疾患だけでなく、様々な内科疾患患者でも観察されることから、適応が広まると考えている。これまでうつ病は、脳の病気であると信じられていたが、今後は末梢臓器を含めた身体疾患であることを知る必要があろう。</p> <p>6) 参考文献(References) (1) Zhang, J.C., Yao, W., Ren, Q., Yang, C., Chao, D., Ma, M., Wu, J., and Hashimoto, K. (2016) Depression-like phenotype by deletion of $\alpha 7$ nicotinic acetylcholine receptor: Role of BDNF-TrkB in nucleus accumbens. <i>Sci. Rep.</i> 6, 36705. (2) Pu, Y., Tan, Y., Qu, Y., Chang, L., Wang, S., Wei, Y., Wang, X., and Hashimoto, K. (2021) A role of the subdiaphragmatic vagus nerve in depression-like phenotypes in mice after fecal microbiota transplantation from Chrna7 knock-out mice with depression-like phenotypes. <i>Brain Behav. Immun.</i> 94, 318-326. (3) Yang, Y., Eguchi, A., Wan, X., Chang, L., Wang, X., Qu, Y., Mori, C. and Hashimoto, K. (2023) A role of gut-microbiota-brain axis via subdiaphragmatic vagus nerve in depression-like phenotypes in Chrna7 gene knock-out mice. <i>Prog. Neuropsychopharmacol. Biol. Psychiatry</i> 120, 110652. (4) Yang, Y., Eguchi, A., Wan, X., Mori, C., and Hashimoto, K. (2024) Depression-like phenotypes in mice with hepatic ischemia/reperfusion injury: A role of gut-microbiota-liver-brain axis via vagus nerve. <i>J. Affect. Disord.</i> 345, 157-167. (5) Yang, Y., Eguchi, A., Mori, C., and Hashimoto, K. (2024) Depression-like phenotypes in mice following common bile duct ligation: Insights into the gut-liver-brain axis via the vagus nerve. <i>Neurobiol. Dis.</i> 192, 106433.</p>						

2. 執筆論文 Publication of thesis ※記載した論文を添付してください。Attach all of the papers listed below.

論文名 1 Title	Abnormalities in gut microbiota composition and short-chain fatty acids in mice after repeated administration of colony stimulating factor 1 receptor inhibitor PLX5622					
掲載誌名 Published journal	Eur. Arch. Psychiatry Clin. Neurosci.					
	2022 年 4 月	272 巻(号)	483 頁 ~	495 頁	言語 Language	English
第1著者名 First author	Yong Yang	第2著者名 Second author	Tamaki Ishima		第3著者名 Third author	Xiayun Wan
その他著者名 Other authors	Yan Wei, Lijia Chang, Jiancheng Zhang, Youge Qu, Kenji Hashimoto					
論文名 2 Title	A role of gut-microbiota-brain axis via subdiaphragmatic vagus nerve in depression-like phenotypes in Chrna7 gene knock-out mice.					
掲載誌名 Published journal	Prog. Neuropsychopharmacol. Biol. Psychiatry					
	2023 年 1 月	120 巻(号)	110652 頁 ~	頁	言語 Language	English
第1著者名 First author	Yong Yang	第2著者名 Second author	Akifumi Eguchi		第3著者名 Third author	Xiayun Wan
その他著者名 Other authors	Lijia Chang, Xingming Wang, Youge Qu, Chisato Mori, Kenji Hashimoto					
論文名 3 Title	Depression-like phenotypes in mice with hepatic ischemia/reperfusion injury: A role of gut-microbiota-liver-brain axis via vagus nerve.					
掲載誌名 Published journal	J. Affect. Disord.					
	2024 年 1 月	345 巻(号)	157 頁 ~	167 頁	言語 Language	English
第1著者名 First author	Yong Yang	第2著者名 Second author	Akifumi Eguchi		第3著者名 Third author	Xiayun Wan
その他著者名 Other authors	Chisato Mori, Kenji Hashimoto					
論文名 4 Title	Depression-like phenotypes in mice following common bile duct ligation: Insights into the gut-liver-brain axis via the vagus nerve.					
掲載誌名 Published journal	Neurobiol. Dis					
	2024 年 2 月	192 巻(号)	106433 頁 ~	頁	言語 Language	English
第1著者名 First author	Yong Yang	第2著者名 Second author	Akifumi Eguchi		第3著者名 Third author	Chisato Mori
その他著者名 Other authors	Kenji Hashimoto					
論文名 5 Title	Key role of the gut-microbiota-brain axis via the subdiaphragmatic vagus nerve in demyelination of the cuprizone-treated mouse brain					
掲載誌名 Published journal	Neurobiol. Dis					
	2023 年 1 月	176 巻(号)	105951 頁 ~	頁	言語 Language	English
第1著者名 First author	Xingming Wang	第2著者名 Second author	Akifumi Eguchi		第3著者名 Third author	Yong Yang
その他著者名 Other authors	Lijia Chang, Xiayun Wan, Jiajing Shan, Youge QU, Li Ma, Chisato Mori, Jianjun Yang, Kenji Hashimoto					

3. 学会発表 Conference presentation ※筆頭演者として総会・国際学会を含む主な学会で発表したものを記載してください。

※Describe your presentation as the principal presenter in major academic meetings including general meetings or international meeting

学会名 Conference	無し				
演題 Topic					
開催日 date	年	月	日	開催地 venue	
形式 method	<input type="checkbox"/> 口頭発表 Oral	<input type="checkbox"/> ポスター発表 Poster	言語 Language	<input type="checkbox"/> 日本語	<input type="checkbox"/> 英語 <input type="checkbox"/> 中国語
共同演者名 Co-presenter					
学会名 Conference					
演題 Topic					
開催日 date	年	月	日	開催地 venue	
形式 method	<input type="checkbox"/> 口頭発表 Oral	<input type="checkbox"/> ポスター発表 Poster	言語 Language	<input type="checkbox"/> 日本語	<input type="checkbox"/> 英語 <input type="checkbox"/> 中国語
共同演者名 Co-presenter					
学会名 Conference					
演題 Topic					
開催日 date	年	月	日	開催地 venue	
形式 method	<input type="checkbox"/> 口頭発表 Oral	<input type="checkbox"/> ポスター発表 Poster	言語 Language	<input type="checkbox"/> 日本語	<input type="checkbox"/> 英語 <input type="checkbox"/> 中国語
共同演者名 Co-presenter					
学会名 Conference					
演題 Topic					
開催日 date	年	月	日	開催地 venue	
形式 method	<input type="checkbox"/> 口頭発表 Oral	<input type="checkbox"/> ポスター発表 Poster	言語 Language	<input type="checkbox"/> 日本語	<input type="checkbox"/> 英語 <input type="checkbox"/> 中国語
共同演者名 Co-presenter					

4. 受賞(研究業績) Award (Research achievement)

名称 Award name	国名 Country		受賞年 Year of award	年	月
	国名 Country		受賞年 Year of award	年	月

5. 本研究テーマに関わる他の研究助成金受給 Other research grants concerned with your research theme

受給実績 Receipt record	<input type="checkbox"/> 有 <input checked="" type="checkbox"/> 無
助成機関名称 Funding agency	
助成金名称 Grant name	
受給期間 Supported period	年 月 ~ 年 月
受給額 Amount received	円
受給実績 Receipt record	<input type="checkbox"/> 有 <input checked="" type="checkbox"/> 無
助成機関名称 Funding agency	
助成金名称 Grant name	
受給期間 Supported period	年 月 ~ 年 月
受給額 Amount received	円

6. 他の奨学金受給 Another awarded scholarship

受給実績 Receipt record	<input checked="" type="checkbox"/> 有 <input type="checkbox"/> 無
助成機関名称 Funding agency	国立大学法人千葉大学
奨学金名称 Scholarship name	千葉大学全方位イノベーション創発博士人材養成プロジェクト
受給期間 Supported period	2022 年 4 月 ~ 2023 年 3 月
受給額 Amount received	2,040,000 円

7. 研究活動に関する報道発表 Press release concerned with your research activities

※記載した記事を添付してください。Attach a copy of the article described below

報道発表 Press release	<input type="checkbox"/> 有 <input checked="" type="checkbox"/> 無	発表年月日 Date of release	
発表機関 Released medium			
発表形式 Release method	・新聞 ・雑誌 ・Web site ・記者発表 ・その他()		
発表タイトル Released title			

8. 本研究テーマに関する特許出願予定 Patent application concerned with your research theme

出願予定 Scheduled	<input type="checkbox"/> 有 <input checked="" type="checkbox"/> 無	出願国 Application	
出願内容(概要) Application contents			

9. その他 Others

特になし

指導責任者(記名) 橋本 謙二



Microglial depletion and abnormalities in gut microbiota composition and short-chain fatty acids in mice after repeated administration of colony stimulating factor 1 receptor inhibitor PLX5622

Yong Yang¹ · Tamaki Ishima¹ · Xiayun Wan¹ · Yan Wei¹ · Lijia Chang¹ · Jiancheng Zhang¹ · Youge Qu¹ · Kenji Hashimoto¹

Received: 7 July 2021 / Accepted: 27 August 2021 / Published online: 4 September 2021
© Springer-Verlag GmbH Germany, part of Springer Nature 2021

Abstract

PLX5622, a brain-penetrant highly specific inhibitor of the colony-stimulating factor 1 receptor (CSF1R), is used to eliminate microglia in the brain. Considering the role of microglia and gut microbiota in the brain homeostasis, this study was undertaken to investigate whether repeated intragastric administration of PLX5622 (65 mg/kg/day for consecutive 7 days) could affect the composition of gut microbiota and the concentration of short-chain fatty acids (SCFAs) in fresh feces of adult mice. Repeated administration of PLX5622 caused significant reductions of the expression of genes and proteins for microglial markers in the prefrontal cortex (PFC) and hippocampus compared to control mice although the elimination of brain's microglia was partial. There was a significant alteration in the β -diversity of intestine microbiota in the PLX5622-treated group. Linear discriminant analysis effect size identified eight significant enriched bacteria as microbial markers for PLX5622-treated group. Repeated administration of PLX5622 affected the relative abundance of several bacteria at the genus and species levels. Furthermore, repeated administration of PLX5622 caused a significant change in lactic acid compared to control group. Interestingly, we found significant correlations between microglial markers in the brain and the relative abundance of several bacteria, suggesting microbiome–microglia crosstalk through the brain–gut axis. These data demonstrate that repeated administration of PLX5622 leads to an abnormal composition of the gut microbiota and lactic acid in adult mice. Therefore, abnormalities in the composition of gut microbiota after repeated treatment of PLX5622 should be considered for behavioral and biological functions in animals treated with CSF1R inhibitors.

Keywords Brain–gut–microbiota axis · CSF1R · Gut microbiota · Microglia

Introduction

Microglia are the mononuclear phagocytes in the natural immune system of the central nervous system (CNS) [1, 2]. Despite the fact that microglia were thought to be mainly in charge of the handling of cellular fragments and answering to neural injury, accumulating evidence suggests that microglia play a role in the pathogenesis of numerous psychiatric and neurological disorders [3–5]. Penetration of myeloid cells into the substantial tissue of brain is very rare in normal healthy CNS conditions following the establishment of

the blood–brain barrier in adult mice [6, 7], indicating that microglia are considered essential macrophages that represent the unique tissue-specificity of the CNS.

Colony stimulating factor 1 receptor (CSF1R) is predominantly expressed on microglia within CNS, and it is necessary for their survival, differentiation and proliferation [3, 8–10]. Microglia were absent in *Csf1r* knock-out (KO) mice [6, 11], suggesting that CSF1R plays a crucial role in the microglia. Interestingly, the extensive treatment of CSF1R inhibitor PLX3397 resulted in probable 99% of microglia in the brain were eliminated, suggesting that microglia in the adult brain are physiologically dependent on CSF1R signaling [12].

PLX5622 is a new inhibitor of CSF1R, which can permeate the brain ($IC_{50} = 0.016 \mu\text{M}$). PLX5622 is selective for CSF1R over the kinase insert domain receptor (KDR), Aurora C, Kit, and FMS-related tyrosine kinase 3 (FLT3)

✉ Kenji Hashimoto
hashimoto@faculty.chiba-u.jp

¹ Division of Clinical Neuroscience, Chiba University Center for Forensic Mental Health, Chiba 260-8670, Japan

($IC_{50s} = 1.1, 1, 0.86$ and $0.39 \mu\text{M}$, respectively), and it is greater than 100-fold selective for CSF1R over a panel of 230 kinases [13, 14]. Thus, CSF1R inhibitors (PLX3397 and PLX5622) have been used widely to eliminate microglia in the CNS without significant effects on peripheral immune cells [3, 15–21]. Although CSF1R is expressed in the microglial cells and macrophages, the role of CSF1R in the gut microbiome is currently unknown.

The brain-gut-microbiota axis is a vital multi-organ two-way signal transduction interaction system between the brain and the host's intestinal microbiota homeostasis [22–27]. An increasing number of preclinical studies have shown a disturbance of intestine microbiota in rodents with depression-like behaviors [28–34]. Short-chain fatty acids (SCFAs), the main metabolic products derived from microbiota in the alimentary canal, play an indispensable role in the metabolic functions in humans and rodents [35–37]. Increasing preclinical findings suggest the role of gut microbiota in the maturation and function of microglia in the CNS [38–40]. Interestingly, clinical trials of small molecule CSF1R inhibitors in patients with cancer are underway [41, 42]. However, there are no reports demonstrating the alterations in the distribution of intestine microbiota and SCFAs in rodents after repeated administration of CSF1R inhibitors such as PLX5622.

The present study was attempted to investigate whether the repeated administration of PLX5622 alters the distribution of the gut microbiota and the concentration of SCFAs in fecal samples of adult mice. In this study, we examined the effects of the repeated intragastric administration of PLX5622 on the composition of gut microbiota and SCFAs in adult mice. Additionally, we examined correlations between microglia markers in the brain, and certain intestine bacteria since brain–gut–microbiota axis plays a key role in the immune system [22, 26].

Methods

Animals

Male adult C57BL/6NCr mice ($n = 16$, 8 weeks old, 21–27 g) were purchased from Japan SLC Inc. (Hamamatsu, Shizuoka, Japan). All the experimental animals were acclimatized to standard laboratory conditions (4/cage), maintain alternating cycles of 12 h of light and 12 h of darkness (7:00–19:00 light), and under controlled conditions for humidity and temperature. Animals were given free admittance to chow and water. The animal protocol was approved by Chiba University of Institutional Animal Care and Use Committee (Permission number was 2–447).

Treatment and sample collection

PLX5622 was purchased from MedChemExpress (Monmouth Junction, NJ, USA). Dietary administration of PLX5622 (1200 ppm in chow) is reported to eliminate approximately 90% of microglia in the brain [14]. It is also shown that dietary administration of PLX5622 (300 ppm in chow) could eliminate the part of the microglia in the brain [13]. The dosage (65 mg/kg/day) by intragastric administration is equal to the 300 ppm in chow daily dosage, eliminating the part of microglia in the brain [13]. The dosage (65 mg/kg/day) of PLX5622 was used in this study.

Briefly, PLX5622 stock solution was dissolved in dimethyl sulfoxide (DMSO) at a concentration of 130 mg/ml; 2% hydroxypropyl methylcellulose (Sigma-Aldrich Co., Ltd, St. Louis, MO, USA), and 25% polysorbate 80 (FUJIFILM Co., Tokyo, Japan) were prepared to make a diluent. The daily intragastric administration, by adding 1 volume of compound stock solution (130 mg/ml) into 19 volumes of diluent, dilutes the PLX5622 stock solution 20 times to make a working solution of 6.5 mg/ml. The vehicle solution was prepared with a mixture of DMSO and diluent. Mice were weighed body weight before intragastric administration every day. According to daily changes in the mice's body weight, animals were treated daily by intragastric administration with 0.1 ml solution (6.5 mg/ml) per 0.01 kg body weight (final dosage at 65 mg/kg body weight) [13].

Mice were treated with either vehicle solution (10 ml/kg/day) or PLX5622 (65 mg/kg/day) for 7 consecutive days (day 1–day 7). Fresh fecal samples were collected in the morning of day 8 (9:00–10:00) to prevent the influence of circadian rhythm effect on the microbiota. Mouse brain was collected by decapitation, subsequently prefrontal cortex (PFC) and hippocampus were dissected on ice. Then, all kinds of samples quickly frozen in liquid nitrogen and stored at -80°C until assays (Fig. 1A).

Quantification of mRNA expression

We measured the gene expression of microglial markers such as Iba1 (or AIF-1), TGF- β 1 and CSF1R in the mouse brain. We used a quantitative RT-PCR system (Step One Plus, Thermo Fisher Scientific, Yokohama, Japan). All specific mRNA transcripts were quantitatively analyzed by TaqManGene Expression assays (Thermo Fisher Scientific, Yokohama, Japan). Expression levels of *Aif1* (Mm00479862_g1), *Tgfb1* (Mm01178820_m1), *Csf1r* (Mm01266652_m1) were measured. Total RNA was extracted using an RNase-Free DNase Set and an RNeasy

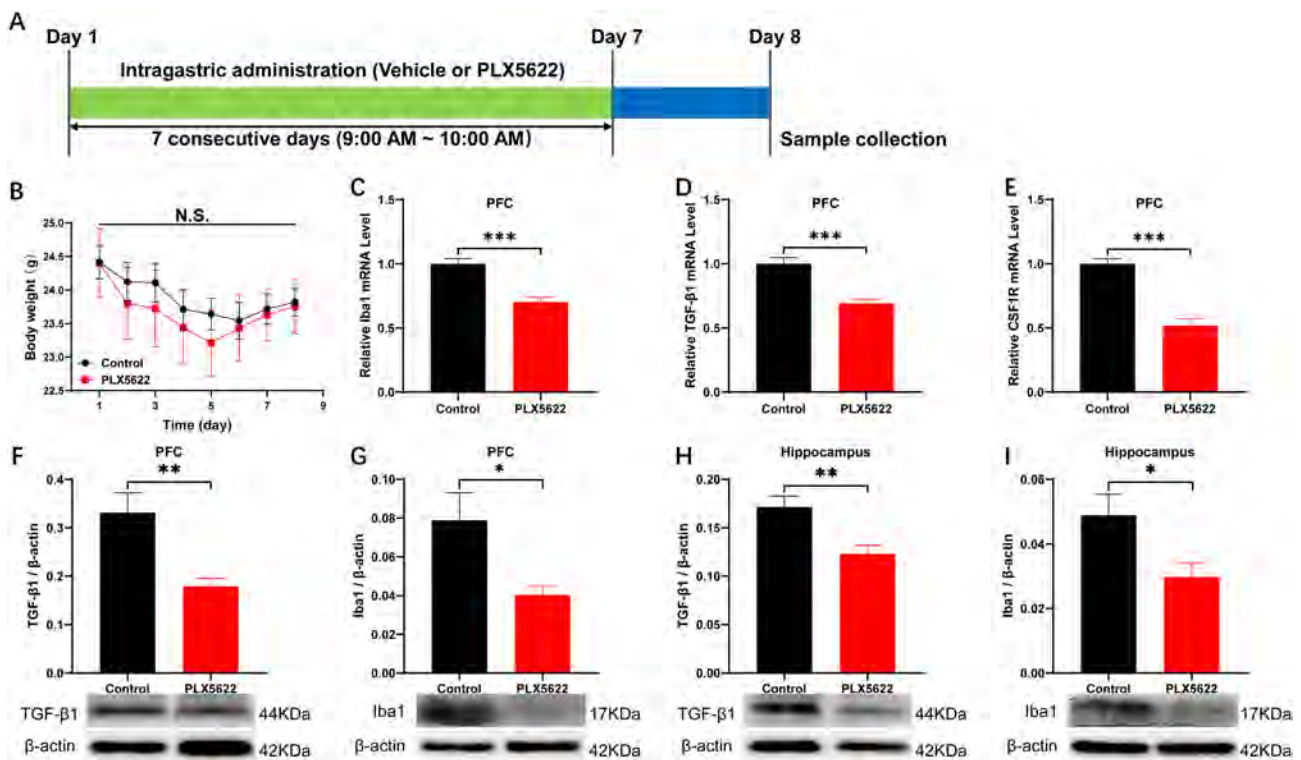


Fig. 1 Experiment design, collection of cerebrum and fecal samples, body weight changes, expression of microglial markers in the brain. **A** Intragastric administration of either vehicle or PLX5622 for consecutive 7 days (day 1—day 7). Collection of feces, prefrontal cortex (PFC) and hippocampus were performed on day 8. **B** Body weighing of two groups from the first day to the eighth day. Repeated measure ANOVA, $F_{(7,14)}=0.166$, $P=0.690$. **C** The level of Iba1 mRNA in the PFC (unpaired t test, $t=5.449$, $df=14$, $P<0.0001$). **D** The level of TGF- β 1 mRNA in the PFC (unpaired t test, $t=5.279$, $df=14$, $P=0.0001$). **E** The level of CSF1R mRNA in the PFC (unpaired t

test, $t=7.183$, $df=14$, $P<0.0001$). **F** Western blot analysis of TGF- β 1 in the PFC (unpaired t test, $t=3.430$, $df=14$, $P=0.0041$). **G** Western blot analysis of Iba1 in the PFC (unpaired t test, $t=2.589$, $df=14$, $P=0.0214$). **H** Western blot analysis of TGF- β 1 in the hippocampus (unpaired t test, $t=3.390$, $df=14$, $P=0.0044$). **I** Western blot analysis of Iba1 in the hippocampus (unpaired t test, $t=2.445$, $df=14$, $P=0.0283$). The data are shown as means \pm SEM ($n=8$). ANOVA: analysis of variance. N.S. not significant; * $P<0.05$; ** $P<0.01$; *** $P<0.001$

Mini Kit (Qiagen, Hilden, Germany). The purity of total RNA was assessed by Bio photometer plus (Eppendorf, Hamburg, Germany). The cDNA libraries were obtained by reverse transcription-PCR using a High-Capacity cDNA Reverse Transcription Kit (#4368813 Thermo Fisher Scientific, Yokohama, Japan). All specimens were detected twice, and arithmetic means were used for quantification. The data of arithmetic mean were normalized to Vic-labeled *Actb* mRNA (#4352341E: pre-developed TaqMan Assay Reagents, Thermo Fisher Scientific, Yokohama, Japan).

Western blot analysis of TGF- β 1 and Iba1

Western blot analysis was performed as previously reported [30, 43]. The tissues were homogenized in freezing Laemmli lysis buffer, each specimen was performed separately, centrifuged at $3000\times g$ (RCF) at 4°C for 5 min to collect the supernatants. Use a DC protein assay kit (Bio-Rad,

Hercules, CA, USA) to measure aliquots (60 μg) of proteins; and boiled at 95°C for 10 min with a quarter volume of 125 mM Tris-HCl, pH 6.8; 0.1% bromophenol blue; 4% sodium dodecyl sulfate; 10% β -mercaptoethanol and 20% glycerol. Proteins were separated using 10% sodium dodecyl sulfate-polyacrylamide gel electrophoresis (SDS-PAGE) (catalog #: 4568125, Mini-PROTEAN TGX™ Stain-Free Gels; Bio-Rad) and then were transferred onto polyvinylidene difluoride membranes using a Trans-Blot Mini Cell apparatus (Bio-Rad).

For immunodetection, the polyvinylidene difluoride membranes were sealed with blocking solution [5% skim milk in TBS + 0.1% Tween-20 (TBST)] at room temperature for 1 h, the membranes for detecting TGF- β 1 were incubated with the appropriate dilution of the primary antibody against TGF- β 1 (1:2000, Catalog No.: ab179695, 1 $\mu\text{g}/\text{mL}$, Abcam, Cambridge, MA, USA), while the membranes for detecting Iba1 were incubated with the appropriate dilution of the primary antibody against Iba1 (1:1000, Cat No.:

016-20001, 1 µg/mL, FUJIFILM, Tokyo, Japan) and β-actin (1:10,000; Cat number: A5441 Sigma-Aldrich Co., Ltd, St Louis, MO, USA) at 4 °C overnight. The next day, wash the polyvinylidene difluoride membranes in three washes of TBST, 10 min each. Then the polyvinylidene difluoride membranes were selectively incubated with a recommended dilution of labeled secondary antibody in 5% blocking buffer in TBST [anti-mouse antibody (1:5000, catalog No.: NA931, GE Healthcare) or a horseradish peroxidase-conjugated anti-rabbit antibody (1:5000, catalog No.: NA934, GE Healthcare)] at room temperature for 1 h. After three final washes in TBST, 10 min each. The bands in the polyvinylidene difluoride membranes were detected using enhanced chemiluminescence plus a Western Blotting Detection system (GE Healthcare Bioscience).

The membranes for detecting TGF-β1 were incubated in elution buffer (62.5 mM Tris-HCl, pH 6.8, 2% sodium dodecyl sulfate, and 100 mM β-mercaptoethanol) at 60 °C for 30 min and then washed three times (10 min at a time) in TBST. The stripped membranes were sealed with blocking solution [5% skim milk in TBS + 0.1% Tween-20 (TBST)] for 1 h and then were incubated with the appropriate dilution of primary antibody directed against β-actin (1:10,000; Cat No.: A5441 Sigma-Aldrich Co., Ltd, St Louis, MO, USA) at 4 °C overnight. The following day, washing the membranes for three times (10 min at a time) in TBST and were incubated with a horseradish peroxidase-conjugated anti-mouse antibody (1:5000, catalog No.: NA931, GE Healthcare) for 1 h at room temperature. After three final washes in TBST, 10 min each. The bands in the polyvinylidene difluoride membranes were detected using enhanced chemiluminescence plus a Western Blotting Detection system (GE Healthcare Bioscience).

Images were produced using a ChemiDoc™ Touch Imaging System (170-01401; Bio-Rad Laboratories, Hercules, CA, USA), and immunoreactive bands were quantified using Image Lab™3.0 software (Bio-Rad Laboratories).

16S ribosome RNA sequencing

DNA extraction from fecal samples and 16S ribosome RNA analysis were performed by MyMetagenome Co., Ltd. (Tokyo, Japan), as previously reported [30, 33, 43–48]. DNA extraction from mouse fecal samples and the 16S ribosome RNA analysis were carried out in reference to the procedure of the previous reports [49, 50]. Briefly, PCR was carried out using 27Fmod 5'-AGRGTGGATYMTGGCTCAG-3' and 338R 5'-TGCTGCCTCCCGTAGGAGT-3' to amplify the V1–V2 region of the bacterial 16S ribosome RNA gene. The 16S amplicons were then sequenced using MiSeq reference to the Illumina protocol. Use the GLSEARCH program to search for similarities between the Ribosome Database Project and the genome database of the National Center for

Biotechnology Information (NCBI) and classify and identify OTUs. The 16S rRNA sequencing data have been deposited to the NCBI Sequence Read Archive and are available at the accession number PRJNA746230.

The abundance and diversity of the microbial community are reflected by α-diversity analyses, including Observed_otus, Chao1, Ace, Shannon, and Shannon_e. β-diversity analysis including principal components analysis (PCA) was used to access similarity or dissimilarity of two communities.

Linear discriminant analysis (LDA) effect size (LEfSe) was used to identify microbiota as a biomarker discovery. Microbiota-based biomarker discoveries were performed with LEfSe using the online galaxy platform [51]. The LDA scores (LDA > 3.5) derived from LEfSe analysis were considered significantly to be increased or decreased bacterial taxa in the gut microbiota between the two groups.

Measurement of the concentration of SCFAs in fresh fecal samples

SCFAs are the primary metabolites produced by bacterial fermentation of dietary fiber in the gastrointestinal tract. As previously reported, SCFAs (i.e., acetic acid, propionic acid, n-butyric acid, lactic acid, and succinic acid) in fresh fecal samples were measured at Techno Suruga Laboratory, Co., Ltd. (Shizuoka, Japan) [30, 34, 46, 47]. The concentration of the SCFAs was measured by gas chromatography with a flame ionization detector. The concentration of SCFAs were displayed as milligrams per gram of feces.

Statistical analysis

The data are shown as the mean ± standard error of the mean (S.E.M.). Statistical analysis was performed using SPSS version 20.0 software (SPSS, Tokyo, Japan). The data of body weight were analyzed using repeated measure analysis of variance (ANOVA), followed by Fisher's least significant difference (LSD) test. The gut microbiota data for α-diversity and the relative abundance at different levels in this study were analyzed using the Mann–Whitney *U* test. The results of Western blot analyses, RT-PCR and the concentration of the SCFAs were statistically analyzed using the unpaired Student's *t* test. Correlations between bacterial relative abundance and SCFAs, correlations between bacterial relative abundance and the expression of microglial markers, and correlations between bacterial relative abundance and mRNA levels of Iba1, TGF-β1, and CSF1R in the brain were all statistically analyzed using Spearman's correlation analysis. *P* values under 0.05 were considered statistically significant.

Results

Effects of PLX5622 on the body weight and the expression of gene and protein for microglial markers in the brain

It is well known that Iba1 and CSF1R are specific markers for microglia in the CNS. In the CNS, TGF- β 1 is also indispensable for the maturation of microglia, the maintenance of homeostasis of adult microglia and the control of microglia activation [52–54]. Repeated measure ANOVA identified significant changes of body weight which declined slowly over time and then increased gradually in two groups; however, there were no changes between the two groups at each time point (Fig. 1B). The levels of *Aif1* mRNA ($P < 0.001$), *Tgfb1* mRNA ($P = 0.001$), and *Csf1r* mRNA ($P < 0.001$) in the PFC of mice treated with PLX5622 were significantly lower than those of the control group (Fig. 1C–E). The reduction of mRNA for *Aif1*, *Tgfb1*, and *Csf1r* in the PFC of mice treated with PLX5622 were ~70%, ~69% and ~51% of control group, respectively.

Western blot statistical analysis showed that the expressions of TGF- β 1 and Iba1 in the PFC and hippocampus of the mice treated with PLX5622 were significantly lower than that of the control group. (Fig. 1F–I). These findings indicated that elimination of microglia in the PFC and hippocampus after repeated intragastric administration of PLX5622 (65 mg/kg/day for 7 consecutive days) was partial.

Effects of PLX5622 on the composition diversity of gut microbiota

The intestinal microbiota composition between PLX5622-treated mice and control mice was analyzed using both α -diversity and β -diversity. Mann–Whitney U test revealed no differences in the Observed_OTUs, Chao1, Ace, Shannon, and Shannon_e indices between PLX5622-treated mice and control mice (Fig. 2A–E). Regarding β -diversity, the bacterial population composition of intestine microbiota between the two groups was analyzed by PCA. Based on the OTU level, PCA analysis showed a significant separation in the bacterial population composition ($R = 0.2009$, $P = 0.022$) (Fig. 2F).

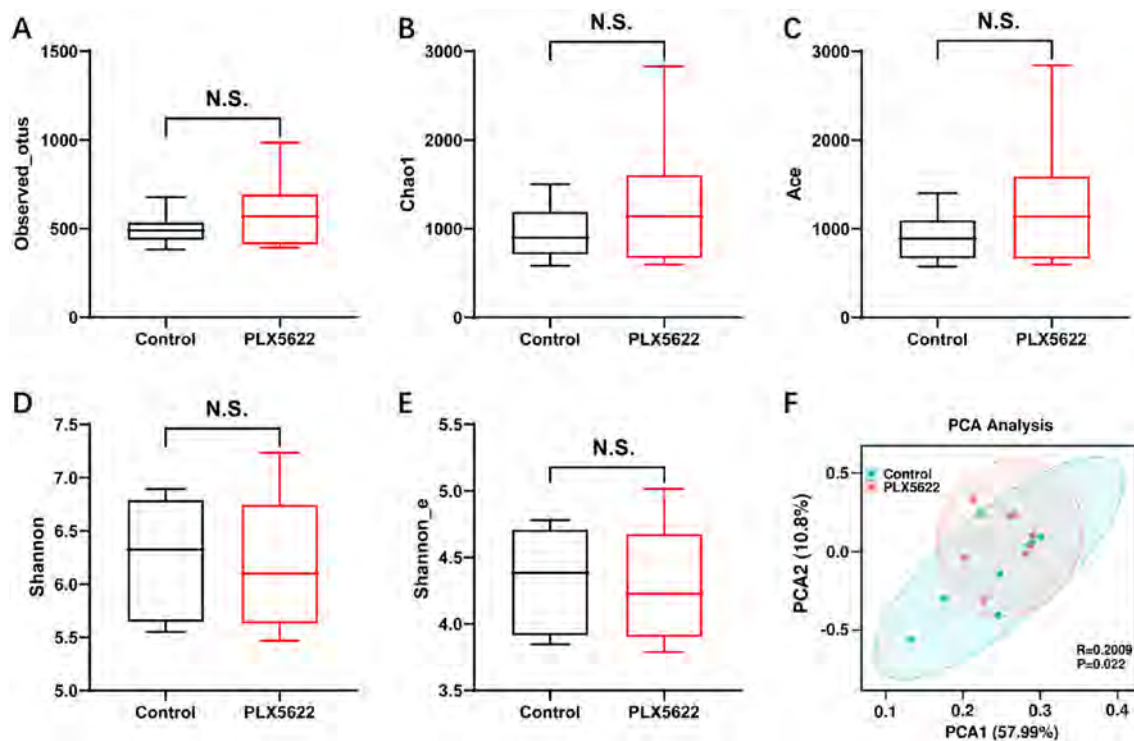


Fig. 2 Effects of PLX5622 on the composition diversity of gut microbiota. **A** α -diversity index of observed_otu (Mann–Whitney U test, $U = 24$, $P = 0.4418$). **B** α -diversity index of Chao1 (Mann–Whitney U test, $U = 26$, $P = 0.5737$). **C** α -diversity index of Ace (Mann–Whitney U test, $U = 22$, $P = 0.3282$). **D** α -diversity index of Shannon (Mann–Whitney U test, $U = 29$, $P = 0.7984$). **E** α -diversity index of

Shannon_e (Mann–Whitney U test, $U = 29$, $P = 0.7984$). **F** PCA based on OTU level ($R = 0.2009$, $P = 0.022$). For all box plots, the middle line in the box addresses the median, the box addresses the interquartile range, and the whisker addresses the most extreme and least values. The number of each group was 8. *N.S.* not significant

Effects of PLX5622 on the LEfSe algorithm of gut microbiota

Cladogram presented the relationship between biomarker taxa (layers of the cladogram represent different levels, with phyla, class, order, family, and genera from inside to outside) generated by LEfSe analysis (Fig. 3A). Furthermore, we identified eight taxonomic biomarkers, the species *Clostridium disporicum*, the genus *Clostridium*, the species *Barnesiella viscericola*, the genus *Barnesiella*, the family *Barnesiellaceae*, the species *Gabonibacter massiliensis*, the genus *Gabonibacter*, and the species *Lactobacillus intestinalis* were statistically significantly enriched in PLX5622-treated group compared to control group (Fig. 3B).

Effects of PLX5622 on the composition of the gut microbiota at the levels of genus and species

At the genus level, the composition of the gut microbiota was altered after repeated intragastric administration of PLX5622 (Fig. 4A). Both *Clostridium* and *Enterorhabdus* in the PLX5622-treated group were significantly higher in abundance than in the control group (Fig. 4B, D). By contrast, the relative abundance of *Anaerotignum* in the PLX5622-treated group was significantly lower than in the control group (Fig. 4C).

At the species level, repeated intragastric administration of PLX5622 also altered the composition of the gut microbiota. The relative abundance of *Lactobacillus intestinalis*, *Clostridium disporicum*, and *Enterorhabdus caecimuris* were higher in the PLX5622-treated group than that of control group. Whereas, compared with the control group, the

relative abundance of *Bacteroides acidifaciens* and *Bacteroides caecimuris* were lower in the PLX5622-treated group (Fig. 5A–F).

Measurement of SCFAs content in fecal samples

The concentration of lactic acid in the PLX5622-treated group was significantly higher than those in the control group (Table 1). In contrast, there were no changes in succinic acid, acetic acid, propionic acid, and n-butyric acid (Table 1).

Correlations between the bacterial relative abundance and lactic acid or microglia markers

There was a significant negative correlation between the concentration of lactic acid and the relative abundance of the genus *Anaerotignum* between the PLX5622-treated group and the control group (Fig. 6A). A negative correlation was determined between the concentration of lactic acid and the relative abundance of the species *Bacteroides acidifaciens* between the PLX5622-treated group and control group (Fig. 6B).

Next, we used the heat maps to show correlations between microglial markers in PFC and hippocampal tissues and the relative abundance of bacteria that differed significantly at the genus and species levels. A heat map showed the correlations between the data of RT-PCR and Western Blot of *Aif1* or *Tgfb1* expression in the PFC and hippocampus and the relative bacterial abundance that differ significantly at

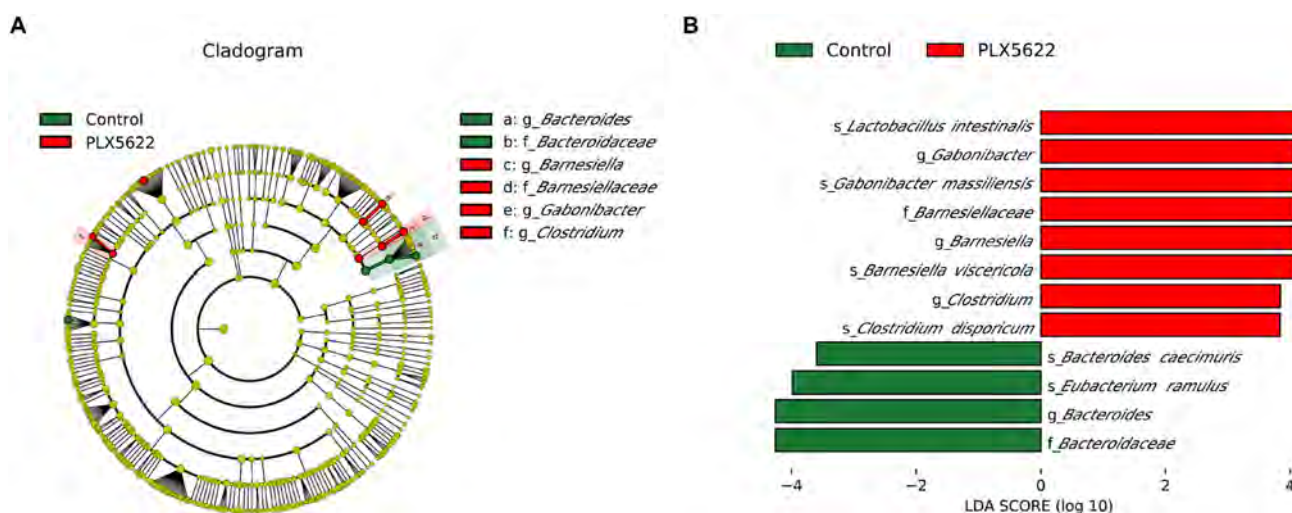


Fig. 3 LEfSe determined bacteria biomarkers of gut microbiota in two groups. **A** Functional branching diagram generated from LEfSe (LDA score > 3.5, $P < 0.05$) showed differences between the two

groups at taxonomic level. **B** Histogram represents enriched taxa with LDA score more than 3.5 and $P < 0.05$ obtained from LEfSe between two groups

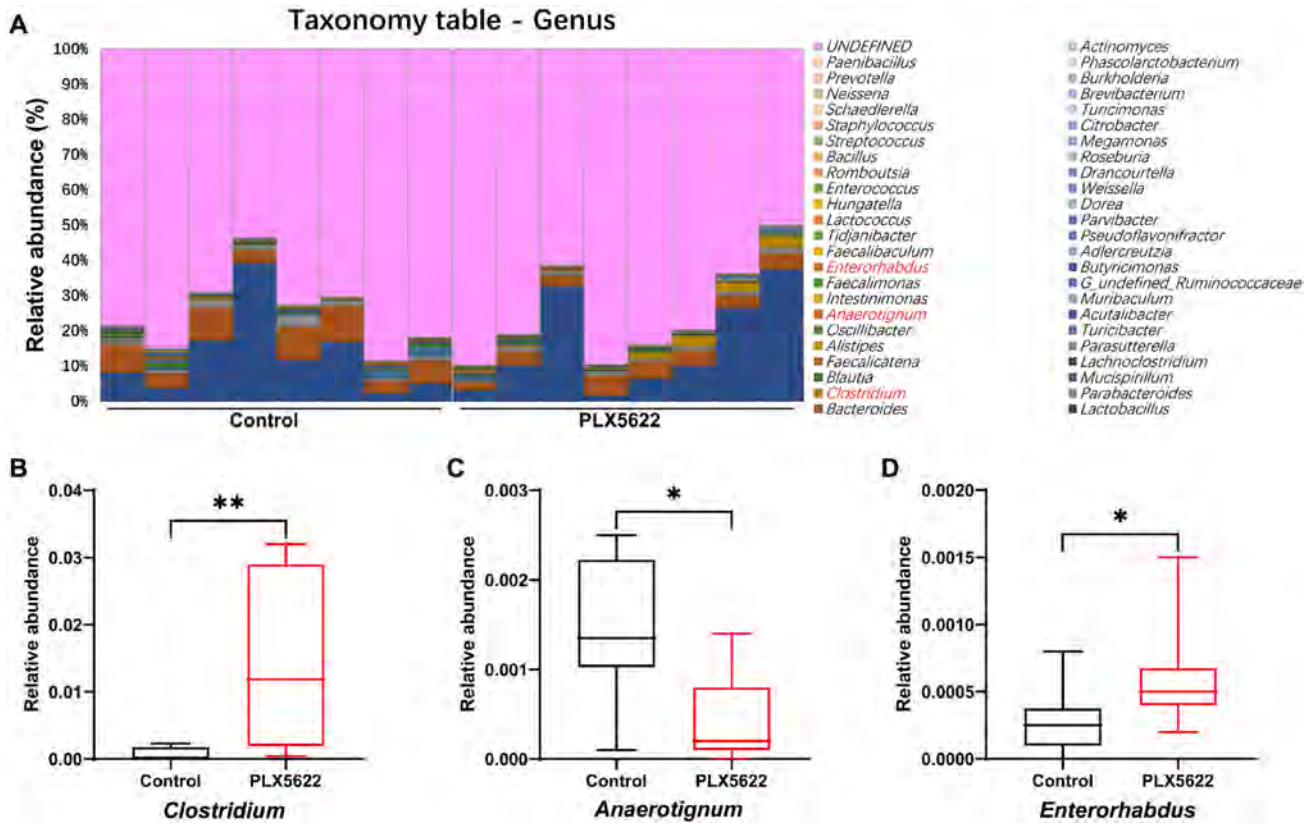


Fig. 4 PLX5622 altered the composition of mice gut microbiota at the genus levels. **A** Gut bacteria composition at the genus level in the two groups. **B** Relative abundance of genus *Clostridium* in two groups. (Mann–Whitney U test, $U=6$, $P=0.0037$). **C** Relative abundance of genus *Anaerotignum* in two groups (Mann–Whitney U test, $U=9$, $P=0.0131$). **D** Relative abundance of genus *Enterorhabdus* in

two groups (Mann–Whitney U test, $U=11.50$, $P=0.0284$). For all box plots, the middle line in the box addresses the median, the box addresses the interquartile range, and the whisker addresses the most extreme and least values. The number of each group was 8. * $P < 0.05$; ** $P < 0.01$

the genus and species levels (Fig. 6C). There were significant positive correlations between *Tgfb1* mRNA levels in the PFC and the relative abundance of the species *Bacteroides caecimuris*. There were significant negative correlations between *Tgfb1* mRNA levels in the PFC and the relative abundance of the genus *Clostridium* (or the species *Clostridium disporicum*) (Fig. 6C).

There were significant positive correlations between *Aif1* mRNA levels in the PFC and the relative abundance of the species *Bacteroides acidifaciens* (or the species *Bacteroides caecimuris*). There were significant negative correlations between *Aif1* mRNA levels in the PFC and the relative abundance of the genus *Clostridium*, the genus *Enterorhabdus*, the species *Clostridium disporicum*, and the species *Enterorhabdus caecimuris* (Fig. 6C).

A positive correlation was identified between *Csflr* mRNA levels in the PFC and the relative abundance of the species *Bacteroides caecimuris*. Furthermore, *Csflr* mRNA levels in the PFC were significant negatively correlated with the relative abundance of the genus *Clostridium*,

the genus *Enterorhabdus*, and the species *Clostridium disporicum* (Fig. 6C).

We found that the abundance of genus *Anaerotignum* and species *Bacteroides caecimuris* were positively correlated with TGF- β 1 expression in the PFC at the protein level. Negative correlations were determined between the abundance of the genus *Clostridium*, the genus *Enterorhabdus*, the species *Lactobacillus intestinalis*, the species *Clostridium disporicum*, or the species *Enterorhabdus caecimuris* and TGF- β 1 protein expression in the PFC. The plentitude of the species *Bacteroides acidifaciens* was positively correlated with Iba1 expression in the PFC (Fig. 6C).

Negative correlations were determined between the plentitude of the genus *Clostridium*, the genus *Enterorhabdus*, or the species *Lactobacillus intestinalis*, the species *Enterorhabdus caecimuris*, and TGF- β 1 protein expression in the hippocampal tissues. The abundance of the genus *Anaerotignum* was positively correlated with Iba1 protein expression in the hippocampal tissues (Fig. 6C).

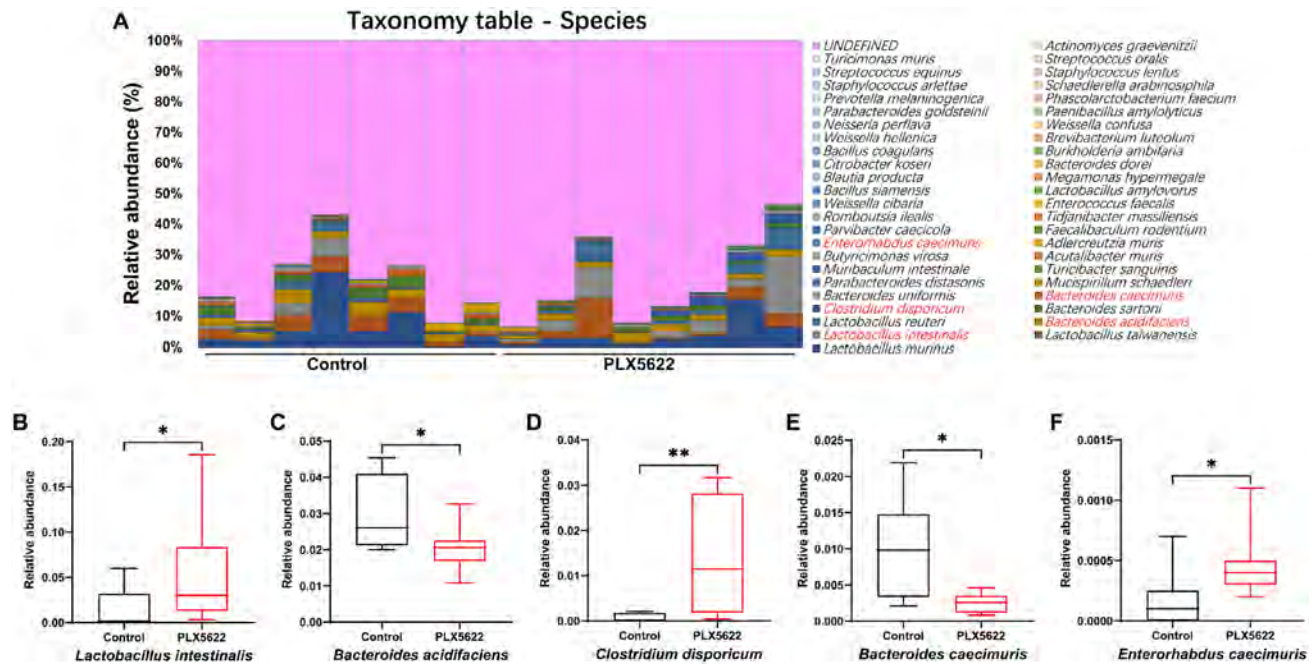


Fig. 5 Effects of PLX5622 on the composition of mice gut microbiota at the species level. **A** Gut bacteria composition at the species level in the two groups. **B** Relative abundance of species *Lactobacillus intestinalis* in two groups (Mann–Whitney *U* test, $U=13$, $P=0.0499$). **C** Relative abundance of species *Bacteroides acidifaciens* (Mann–Whitney *U* test, $U=12.50$, $P=0.0409$). **D** Relative abundance of species *Clostridium disporicum* in two groups (Mann–Whitney *U* test, $U=6$, $P=0.0042$). **E** Relative abundance

of species *Bacteroides caecimuris* in two groups (Mann–Whitney *U* test, $U=8.50$, $P=0.0115$). **F** Relative abundance of species *Enterorhabdus caecimuris* in two groups (Mann–Whitney *U* test, $U=9$, $P=0.0109$). For all box plots, the middle line in the box addresses the median, the box addresses the interquartile range, and the whisker addresses the most extreme and least values. The number of each group was 8. * $P < 0.05$; ** $P < 0.01$

Table 1 The concentration of short-chain fatty acids (SCFAs) in the feces

SCFAs (mg/g)	Control	PLX5622	Student's <i>t</i> test
Lactic acid	0.228 ± 0.026	0.424 ± 0.073	$t = 2.537$, $df = 14$, $P = 0.024$
Succinic acid	0.235 ± 0.031	0.387 ± 0.101*	$t = 1.533$, $df = 13$, $P = 0.149$
Propionic acid	0.370 ± 0.026	0.428 ± 0.043	$t = 1.142$, $df = 14$, $P = 0.273$
Acetic acid	1.629 ± 0.178	1.424 ± 0.161	$t = 0.853$, $df = 14$, $P = 0.408$
n-butyric acid	0.453 ± 0.057	0.494 ± 0.134	$t = 0.284$, $df = 14$, $P = 0.781$

The values represent as the mean ± SEM ($n=8$)

Bold was statistically significant

*One sample from PLX5622-treated group was under the limitation of detection for succinic acid

Discussion

In this study, we demonstrated the partial elimination of microglia in the brain after repeated oral administration of PLX5622 (65 mg/kg/day for consecutive 7 days), consistent with a previous report [13]. We found that repeated administration to PLX5622 in adult mice caused a significant change in the β -diversity of the gut microbiota. Furthermore, the LEfSe algorithm identified the species *Clostridium disporicum*, the genus *Clostridium*, the species *Barnesiella viscericola*, the genus *Barnesiella*, the

family *Barnesiellaceae*, the species *Gabonibacter massiliensis*, the genus *Gabonibacter*, and the species *Lactobacillus intestinalis* as specific microbial biomarkers in the PLX5622-treated group. Repeated administration of PLX5622 caused the alteration of the relative abundance of several microbes at distinct taxa such as genus and species. Moreover, we found higher levels of lactic acid in the feces' samples from the PLX5622-treated group, although levels of other SCFAs were not altered. We found significant negative correlations between lactic acid levels and the relative abundance of *Anaerostignum* (or *Bacteroides acidifaciens*) in feces from the two groups. Very

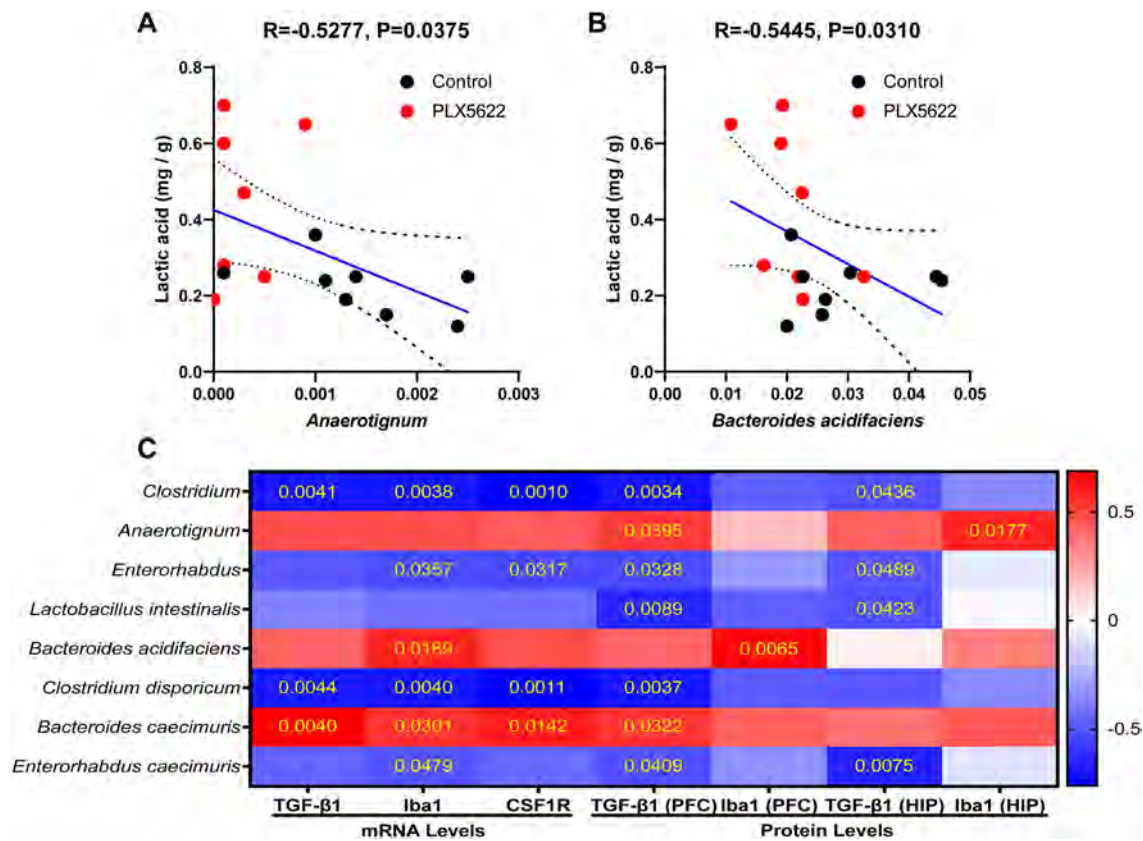


Fig. 6 Correlations between the relative abundance of bacteria and the results of SCFA or the expression of microglial markers. **A** A negative correlation was determined between the genus *Anaerotignum* abundance and lactic acid level of feces in two groups. **B** A negative correlation was found between the species *Bacteroides*

acidifaciens abundance and lactic acid level of feces in two groups. **C** The heat map displayed the correlation coefficient between bacterial abundance and the western blot and RT-PCR results in the PFC and hippocampus. The data are shown as means ± SEM (n = 8). *P < 0.05; **P < 0.01; ***P < 0.001. HIP hippocampus

interestingly, we found significant correlations between microglial markers in the brain and the relative abundance of the microbiome in the two groups, suggesting a possible connection between gut bacteria and microglia functions in the brain. Taken together, the present data suggest that repeated administration of PLX5622 could alter the gut microbiota constitution and SCFAs such as lactic acid in the host, despite the elimination of microglia in the brain by PLX5622 injection was partial.

In the current study, we determined alterations in the relative abundance of specific bacteria at the species level. We found a more abundant *Lactobacillus intestinalis*, *Clostridium disporicum*, and *Enterorhabdus caecimuris* in the PLX5622-treated group compared with the control group. Previously, we demonstrated that the species *Lactobacillus intestinalis* might be accountable for the depression-like phenotype in mice subjected to fecal microbiota transplantation (FMT) from mice with depression-like phenotypes [30]. It seems that a high abundance of *Lactobacillus intestinalis* in PLX5622-treated mice may lead to depression-like behaviors in adult mice, although further study is needed.

Clostridium disporicum is a Gram-positive, rod-shaped, and anaerobic bacterium [55]. A case report shows an orthopedic hardware infection with *Clostridium disporicum* [56]. *Enterorhabdus caecimuris* were isolated from a spontaneous colitis mouse model, suggesting a possible role of this bacteria in inflammatory bowel colitis [57]. Although the precise functions of *Clostridium disporicum* and *Enterorhabdus caecimuris* are currently unknown, it seems that PLX5622 could increase the relative abundance of the above microbes in the host. Further study is required to explore how alterations in the abundance of these three bacteria after repeated administration of PLX5622 can influence biochemical and behavioral functions in rodents.

Here, we found lower abundances of the species *Bacteroides acidifaciens* and *Bacteroides caecimuris* in PLX5622-treated mice than control mice. *Bacteroides acidifaciens* is known to be one of the dominating commensal microbes that facilitate IgA antibody creation in the digestive organ [58]. Interestingly, *Bacteroides acidifaciens* significantly increased in the excrement of Atg7ΔCD11c mice that had alleviated insulin resistance and reduced body weight and

fat mass, suggesting that *Bacteroides acidifaciens* may be a microbiome for regulating metabolic functions such as diabetes and obesity [59]. A recent study revealed that *Bacteroides acidifaciens* may assume a part in the gut–liver axis in rodents [60]. Furthermore, a recent study in healthy control subjects showed a significant decline in *Bacteroides acidifaciens* in non-responder to Vitamin D supplementation [61]. It is also reported that *Bacteroides caecimuris* were enriched in the gut of mice with retinal disease [62] and that higher exposure to 24-h O₃ was related to higher *Bacteroides caecimuris* in youthful grown-ups dwelling in Southern California [63]. Although the exact mechanism by which repeated administration of PLX5622 results in a reduction of relative abundance of these two *Bacteroides* microbes remains unclear, the abnormal composition of these microbes may likely affect biochemical and behavioral outcomes in PLX5622-treated mice.

In this study, we found higher levels of lactic acid in mice treated with PLX5622, although other SCFA did not alter. Interestingly, we found that lactic acid level was negatively correlated with the *Bacteroides acidifaciens* abundance. The detailed mechanisms underlying the negative correlation between lactic acid and *Bacteroides acidifaciens* remain unclear. Given the role of SCFAs in energy sources for the host, it seems that higher levels of lactic acid and lower levels of *Bacteroides acidifaciens* may contribute to abnormal metabolic system in the host. Further study is required to verify the role of *Bacteroides acidifaciens* in the metabolic system.

Importantly, we found significant correlations between several bacterial abundances in feces and microglial markers in the brain. Recent preclinical findings showed the crucial role of gut microbe in the regulations of microglial maturation and function [38–40]. A recent study showed that gut commensal-derived butyrate reversed obesity-induced social deficits and anxiety-like behaviors through regulation of microglial homeostasis [64]. Although the precise mechanisms underlying connections between the bacterial abundance and microglial markers in the brain are unknown, it is possible that the gut microbiota might play a vital role in the physiological functions of microglia in the CNS through the brain–gut–microbiota axis. We recently reported the critical role of the subdiaphragmatic vagus nerve on the brain–gut–microbiota axis in depression-like behaviors [30, 33, 44, 47]. Further study on the role of vagus nerve on the association between the gut microbiota and microglial functions in the CNS would be of interest.

In this study, we used the dosage (65 mg/kg/day for consecutive 7 days) of PLX5622, although the elimination of microglia by this dosage was partial, consistent with the previous report using PLX5622 (300 ppm in chow) [13]. It is noteworthy that elimination of microglia by PLX5622 could cause abnormal composition of gut microbe and SCFAs

alterations in the host's feces. Notably, dietary administration of PLX5622 (1200 ppm in chow) is reported to reduce approximately 90% of the brain's microglia [14, 65]. Given the important role of microglia in the brain–gut–microbiota axis in CNS functions, it is possible that repeated administration of CSF1R inhibitors such as PLX5622 could cause the marked elimination of microglia in the brain, as well as abnormal composition of gut microbe and SCFAs of the host, resulting in alterations in behavioral and physiological functions in the host. A recent study demonstrated that repeated treatment with PLX5622 (1200 ppm for 3 weeks) produced long-lasting alterations in the myeloid and lymphoid compartments of the bone marrow [66], indicating that CSF1R inhibition by PLX5622 is not microglia specific. Given the substantial and long-term effects on circulating and tissue macrophages by PLX5622, it is likely that these changes could affect the experimental data using PLX5622. Future detailed studies are necessary to ascertain the effects of PLX5622 on non-microglia cells.

As aforementioned in the introduction, clinical trials of small molecule CSF1R inhibitors in patients with cancer are underway [41, 42]. In this study, we found that CSF1R inhibitor could affect the composition of gut microbiota and SCFAs in the host. Therefore, abnormalities in the composition of gut microbiota and SCFAs after administration of CSF1R inhibitors should be taken into consideration for clinical outcomes in patients treated with CSF1R inhibitors.

In conclusion, the present study shows that repeated administration of PLX5622 caused abnormal composition of the gut microbiota in adult mice, and that the certain gut microbiota were correlated with expression of microglial markers in the brain. Given the role of the brain–gut–microbiota axis in host homeostasis, we propose that abnormalities in the composition of gut microbiota and SCFAs by CSF1R inhibitors such as PLX5622 should be considered to investigate biochemical and behavioral tests in animals treated with CSF1R inhibitors.

Acknowledgements This study was supported by Japan Society for the Promotion of Science (JSPS) (to K.H., 21H00184 and 21H02846).

Declarations

Conflict of interest The authors report no biomedical financial interests or potential conflicts of interest.

References

1. Glezer I, Simard AR, Rivest S (2007) Neuroprotective role of the innate immune system by microglia. *Neuroscience* 147:867–883. <https://doi.org/10.1016/j.neuroscience.2007.02.055>
2. Gogoleva VS, Drutskaya MS, Atratkhany KS (2019) The role of microglia in the homeostasis of the central nervous system and

- neuroinflammation. *Mol Biol (Mosk)* 53:790–798. <https://doi.org/10.1134/S0026898419050057>
3. Rosin JM, Vora SR, Kurrasch DM (2018) Depletion of embryonic microglia using the CSF1R inhibitor PLX5622 has adverse sex-specific effects on mice, including accelerated weight gain, hyperactivity and anxiolytic-like behaviour. *Brain Behav Immun* 73:682–697. <https://doi.org/10.1016/j.bbi.2018.07.023>
 4. Spangenberg EE, Green KN (2017) Inflammation in Alzheimer's disease: lessons learned from microglia-depletion models. *Brain Behav Immun* 61:1–11. <https://doi.org/10.1016/j.bbi.2016.07.003>
 5. Wolf SA, Boddeke HW, Kettenmann H (2017) Microglia in physiology and disease. *Annu Rev Physiol* 79:619–643. <https://doi.org/10.1146/annurev-physiol-022516-034406>
 6. Ginhoux F, Greter M, Leboeuf M, Nandi S, See P, Gokhan S, Mehler MF, Conway SJ, Ng LG, Stanley ER, Samokhvalov IM, Merad M (2010) Fate mapping analysis reveals that adult microglia derive from primitive macrophages. *Science* 330:841–845. <https://doi.org/10.1126/science.1194637>
 7. Mildner A, Schmidt H, Nitsche M, Merkler D, Hanisch UK, Mack M, Heikenwalder M, Brück W, Priller J, Prinz M (2007) Microglia in the adult brain arise from Ly-6ChiCCR2⁺ monocytes only under defined host conditions. *Nat Neurosci* 10:1544–1553. <https://doi.org/10.1038/nn2015>
 8. Chitu V, Gokhan S, Nandi S, Mehler MF, Stanley ER (2016) Emerging roles for CSF-1 receptor and its ligands in the nervous system. *Trends Neurosci* 39:378–393. <https://doi.org/10.1016/j.tins.2016.03.005>
 9. Li J, Chen K, Zhu L, Pollard JW (2006) Conditional deletion of the colony stimulating factor-1 receptor (c-fms proto-oncogene) in mice. *Genesis* 44:328–335. <https://doi.org/10.1002/dvg.20219>
 10. Patel S, Player MR (2009) Colony-stimulating factor-1 receptor inhibitors for the treatment of cancer and inflammatory disease. *Curr Top Med Chem* 9:599–610. <https://doi.org/10.2174/156802609789007327>
 11. Erblich B, Zhu L, Etgen AM, Dobrenis K, Pollard JW (2011) Absence of colony stimulation factor-1 receptor results in loss of microglia, disrupted brain development and olfactory deficits. *PLoS ONE* 6:e26317. <https://doi.org/10.1371/journal.pone.0026317>
 12. Elmore MR, Najafi AR, Koike MA, Dagher NN, Spangenberg EE, Rice RA, Kitazawa M, Matusow B, Nguyen H, West BL, Green KN (2014) Colony-stimulating factor 1 receptor signaling is necessary for microglia viability, unmasking a microglia progenitor cell in the adult brain. *Neuron* 82:380–397. <https://doi.org/10.1016/j.neuron.2014.02.040>
 13. Lee S, Shi XQ, Fan A, West B, Zhang J (2018) Targeting macrophage and microglia activation with colony stimulating factor 1 receptor inhibitor is an effective strategy to treat injury-triggered neuropathic pain. *Mol Pain* 14:1744806918764979. <https://doi.org/10.1177/1744806918764979>
 14. Spangenberg E, Severson PL, Hohsfield LA, Crapser J, Zhang J, Burton EA, Zhang Y, Spevak W, Lin J, Phan NY, Habets G, Rymar A, Tsang G, Walters J, Nespi M, Singh P, Broome S, Ibrahim P, Zhang C, Bollag G, West BL, Green KN (2019) Sustained microglial depletion with CSF1R inhibitor impairs parenchymal plaque development in an Alzheimer's disease model. *Nat Commun* 10:3758. <https://doi.org/10.1038/s41467-019-11674-z>
 15. Cavnar MJ, Zeng S, Kim TS, Sorenson EC, Ocuin LM, Balachandran VP, Seifert AM, Greer JB, Popow R, Crawley MH, Cohen NA, Green BL, Rossi F, Besmer P, Antonescu CR, DeMatteo RP (2013) KIT oncogene inhibition drives intratumoral macrophage M2 polarization. *J Exp Med* 210:2873–2886. <https://doi.org/10.1084/jem.20130875>
 16. Coniglio SJ, Eugenin E, Dobrenis K, Stanley ER, West BL, Symons MH, Segall JE (2012) Microglial stimulation of glioblastoma invasion involves epidermal growth factor receptor (EGFR) and colony stimulating factor 1 receptor (CSF-1R) signaling. *Mol Med* 18:519–527. <https://doi.org/10.2119/molmed.2011.00217>
 17. Dagher NN, Najafi AR, Kayala KM, Elmore MR, White TE, Medeiros R, West BL, Green KN (2015) Colony-stimulating factor 1 receptor inhibition prevents microglial plaque association and improves cognition in 3xTg-AD mice. *J Neuroinflammation* 12:139. <https://doi.org/10.1186/s12974-015-0366-9>
 18. Green KN, Crapser JD, Hohsfield LA (2020) To kill a microglia: a case for CSF1R inhibitors. *Trends Immunol* 41:771–784. <https://doi.org/10.1016/j.it.2020.07.001>
 19. Janova H, Arinrad S, Balmuth E, Mitjans M, Hertel J, Habes M, Bittner RA, Pan H, Goebbels S, Begemann M, Gerwig UC, Langner S, Werner HB, Kittel-Schneider S, Homuth G, Davatzikos C, Völzke H, West BL, Reif A, Grabe HJ, Boretius S, Ehrenreich H, Nave KA (2018) Microglia ablation alleviates myelin-associated catatonic signs in mice. *J Clin Invest* 128:734–745. <https://doi.org/10.1172/JCI97032>
 20. Walzl I, Käufer C, Gerhauser I, Chhatbar C, Ghita L, Kalinke U, Löscher W (2018) Microglia have a protective role in viral encephalitis-induced seizure development and hippocampal damage. *Brain Behav Immun* 74:186–204. <https://doi.org/10.1016/j.bbi.2018.09.006>
 21. Zhang K, Yang C, Chang L, Sakamoto A, Suzuki T, Fujita Y, Qu Y, Wang S, Pu Y, Tan Y, Wang X, Ishima T, Shirayama Y, Hatano M, Tanaka KF, Hashimoto K (2020) Essential role of microglial transforming growth factor- β 1 in antidepressant actions of (R)-ketamine and the novel antidepressant TGF- β 1. *Transl Psychiatry* 10:32. <https://doi.org/10.1038/s41398-020-0733-x>
 22. Cryan JF, O'Riordan KJ, Cowan CSM, Sandhu KV, Bastiaanssen TFS, Boehme M, Codagnone MG, Cussotto S, Fulling C, Golubeva AV, Guzzetta KE, Jaggar M, Long-Smith CM, Lyte JM, Martin JA, Molinero-Perez A, Moloney G, Morelli E, Morillas E, O'Connor R, Cruz-Pereira JS, Peterson VL, Rea K, Ritz NL, Sherwin E, Spichak S, Teichman EM, van de Wouw M, Ventura-Silva AP, Wallace-Fitzsimons SE, Hyland N, Clarke G, Dinan TG (2019) The microbiota-gut-brain axis. *Physiol Rev* 99:1877–2013. <https://doi.org/10.1152/physrev.00018.2018>
 23. Cussotto S, Sandhu KV, Dinan TG, Cryan JF (2018) The neuroendocrinology of the microbiota-gut-brain axis: a behavioural perspective. *Front Neuroendocrinol* 51:80–101. <https://doi.org/10.1016/j.yfrne.2018.04.002>
 24. Dinan TG, Cryan JF (2017) Brain-gut-microbiota axis and mental health. *Psychosom Med* 79:920–926. <https://doi.org/10.1097/PSY.0000000000000519>
 25. Fung TC, Olson CA, Hsiao EY (2017) Interactions between the microbiota, immune and nervous systems in health and disease. *Nat Neurosci* 20:145–155. <https://doi.org/10.1038/nn.4476>
 26. Long-Smith C, O'Riordan KJ, Clarke G, Stanton C, Dinan TG, Cryan JF (2020) Microbiota-gut-brain axis: new therapeutic opportunities. *Annu Rev Pharmacol Toxicol* 60:477–502. <https://doi.org/10.1146/annurev-pharmtox-010919-023628>
 27. Wei Y, Chang L, Hashimoto K (2021) Molecular mechanisms underlying the antidepressant actions of arketamine: beyond the NMDA receptor. *Mol Psychiatry*. <https://doi.org/10.1038/s41380-021-01121-1>
 28. Jianguo L, Xueyang J, Cui W, Changxin W, Xuemei Q (2019) Altered gut metabolome contributes to depression-like behaviors in rats exposed to chronic unpredictable mild stress. *Transl Psychiatry* 9:40. <https://doi.org/10.1038/s41398-019-0391-z>
 29. Szyzkowicz JK, Wong A, Anisman H, Merali Z, Audet MC (2017) Implications of the gut microbiota in vulnerability to the social avoidance effects of chronic social defeat in male mice. *Brain Behav Immun* 66:45–55. <https://doi.org/10.1016/j.bbi.2017.06.009>
 30. Wang S, Ishima T, Zhang J, Qu Y, Chang L, Pu Y, Fujita Y, Tan Y, Wang X, Hashimoto K (2020) Ingestion of *Lactobacillus*

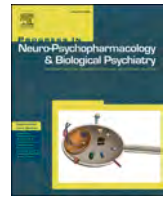
- intestinalis* and *Lactobacillus reuteri* causes depression- and anhedonia-like phenotypes in antibiotic-treated mice via the vagus nerve. *J Neuroinflammation* 17:241. <https://doi.org/10.1186/s12974-020-01916-z>
31. Yang C, Fang X, Zhan G, Huang N, Li S, Bi J, Jiang R, Yang L, Miao L, Zhu B, Luo A, Hashimoto K (2019) Key role of gut microbiota in anhedonia-like phenotype in rodents with neuropathic pain. *Transl Psychiatry* 9:57. <https://doi.org/10.1038/s41398-019-0379-8>
 32. Yang C, Fujita Y, Ren Q, Ma M, Dong C, Hashimoto K (2017) *Bifidobacterium* in the gut microbiota confer resilience to chronic social defeat stress in mice. *Sci Rep* 7:45942. <https://doi.org/10.1038/srep45942>
 33. Zhang J, Ma L, Chang L, Pu Y, Qu Y, Hashimoto K (2020) A key role of the subdiaphragmatic vagus nerve in the depression-like phenotype and abnormal composition of gut microbiota in mice after lipopolysaccharide administration. *Transl Psychiatry* 10:186. <https://doi.org/10.1038/s41398-020-00878-3>
 34. Zhang K, Fujita Y, Chang L, Qu Y, Pu Y, Wang S, Shirayama Y, Hashimoto K (2019) Abnormal composition of gut microbiota is associated with resilience versus susceptibility to inescapable electric stress. *Transl Psychiatry* 9:231. <https://doi.org/10.1038/s41398-019-0571-x>
 35. Dalile B, Van Oudenhove L, Vervliet B, Verbeke K (2019) The role of short-chain fatty acids in microbiota-gut-brain communication. *Nat Rev Gastroenterol Hepatol* 16:461–478. <https://doi.org/10.1038/s41575-019-0157-3>
 36. den Besten G, van Eunen K, Groen AK, Venema K, Reijngoud DJ, Bakker BM (2013) The role of short-chain fatty acids in the interplay between diet, gut microbiota, and host energy metabolism. *J Lipid Res* 54:2325–2340. <https://doi.org/10.1194/jlr.R036012>
 37. Morrison DJ, Preston T (2016) Formation of short chain fatty acids by the gut microbiota and their impact on human metabolism. *Gut Microbes* 7:189–200. <https://doi.org/10.1080/19490976.2015.1134082>
 38. Abdel-Haq R, Schlachetzki J, Glass CK, Mazmanian SK (2019) Microbiome-microglia connections via the gut–brain axis. *J Exp Med* 216:41–59. <https://doi.org/10.1084/jem.20180794>
 39. Ma Q, Xing C, Long W, Wang HY, Liu Q, Wang RF (2019) Impact of microbiota on central nervous system and neurological diseases: the gut–brain axis. *J Neuroinflammation* 16:53. <https://doi.org/10.1186/s12974-019-1434-3>
 40. Wang Y, Wang Z, Wang Y, Li F, Jia J, Song X, Qin S, Wang R, Jin F, Kitazato K, Wang Y (2018) The gut–microglia connection: implications for central nervous system diseases. *Front Immunol* 9:2325. <https://doi.org/10.3389/fimmu.2018.02325>
 41. Cannarile MA, Weisser M, Jacob W, Jegg AM, Ries CH, Rüttinger D (2017) Colony-stimulating factor 1 receptor (CSF1R) inhibitors in cancer therapy. *J Immunother Cancer* 5:53. <https://doi.org/10.1186/s40425-017-0257-y>
 42. Denny WA, Flanagan JU (2021) Small-molecule CSF1R kinase inhibitors; review of patents 2015–present. *Expert Opin Ther Pat* 31:107–117. <https://doi.org/10.1080/13543776.2021.1839414>
 43. Wang S, Qu Y, Chang L, Pu Y, Zhang K, Hashimoto K (2020) Antibiotic-induced microbiome depletion is associated with resilience in mice after chronic social defeat stress. *J Affect Disord* 260:448–457. <https://doi.org/10.1016/j.jad.2019.09.064>
 44. Pu Y, Tan Y, Qu Y, Chang L, Wang S, Wei Y, Wang X, Hashimoto K (2021) A role of the subdiaphragmatic vagus nerve in depression-like phenotypes in mice after fecal microbiota transplantation from *Chrna7* knock-out mice with depression-like phenotypes. *Brain Behav Immun* 94:318–326. <https://doi.org/10.1016/j.bbi.2020.12.032>
 45. Qu Y, Zhang K, Pu Y, Chang L, Wang S, Tan Y, Wang X, Zhang J, Ohnishi T, Yoshikawa T, Hashimoto K (2020) Betaine supplementation is associated with the resilience in mice after chronic social defeat stress: a role of brain–gut–microbiota axis. *J Affect Disord* 272:66–76. <https://doi.org/10.1016/j.jad.2020.03.095>
 46. Shinno-Hashimoto H, Hashimoto Y, Wei Y, Chang L, Fujita Y, Ishima T, Matsue H, Hashimoto K (2021) Abnormal composition of microbiota in the gut and skin of imiquimod-treated mice. *Sci Rep* 11:11265. <https://doi.org/10.1038/s41598-021-90480-4>
 47. Wang S, Ishima T, Qu Y, Shan J, Chang L, Wei Y, Zhang J, Pu Y, Fujita Y, Tan Y, Wang X, Ma L, Wan X, Hammock BD, Hashimoto K (2021) Ingestion of *Faecalibaculum rodentium* causes depression-like phenotypes in resilient *Ephx2* knock-out mice: a role of brain-gut-microbiota axis via the subdiaphragmatic vagus nerve. *J Affect Disord* 292:565–573. <https://doi.org/10.1016/j.jad.2021.06.006>
 48. Pu Y, Yang J, Chang L, Qu Y, Wang S, Zhang K, Xiong Z, Zhang J, Tan Y, Wang X, Fujita Y, Ishima T, Wang D, Hwang SH, Hammock BD, Hashimoto K (2020) Maternal glyphosate exposure causes autism-like behaviors in offspring through increased expression of soluble epoxide hydrolase. *Proc Natl Acad Sci U S A* 117:11753–11759. <https://doi.org/10.1073/pnas.1922287117>
 49. Kim SW, Suda W, Kim S, Oshima K, Fukuda S, Ohno H, Morita H, Hattori M (2013) Robustness of gut microbiota of healthy adults in response to probiotic intervention revealed by high-throughput pyrosequencing. *DNA Res* 20:241–253. <https://doi.org/10.1093/dnares/dst006>
 50. Shibagaki N, Suda W, Clavaud C, Bastien P, Takayasu I, Iioka E, Kurokawa R, Yamashita N, Hattori Y, Shindo C, Breton L, Hattori M (2017) Aging-related changes in the diversity of women's skin microbiomes associated with oral bacteria. *Sci Rep* 7:10567. <https://doi.org/10.1038/s41598-017-10834-9>
 51. Segata N, Izard J, Waldron L, Gevers D, Miropolsky L, Garrett WS, Huttenhower C (2011) Metagenomic biomarker discovery and explanation. *Genome Biol* 12:R60. <https://doi.org/10.1186/gb-2011-12-6-r60>
 52. Priller J, Prinz M (2019) Targeting microglia in brain disorders. *Science* 365:32–33. <https://doi.org/10.1126/science.aau9100>
 53. Spittau B, Dokalis N, Prinz M (2020) The role of TGF- β signaling in microglia maturation and activation. *Trends Immunol* 41:836–848. <https://doi.org/10.1016/j.it.2020.07.003>
 54. Zöller T, Schneider A, Kleimeyer C, Masuda T, Potru PS, Pfeifer D, Blank T, Prinz M, Spittau B (2018) Silencing of TGF β signaling in microglia results in impaired homeostasis. *Nat Commun* 9:4011. <https://doi.org/10.1038/s41467-018-06224-y>
 55. Horn N (1987) *Clostridium disporicum* sp. nov., a Saccharolytic species able to form two spores per cell, isolated from a rat cecum. *Int J Syst Bacteriol* 37:398–401. <https://doi.org/10.1099/00207713-37-4-398>
 56. McBride JA, Sterkel AK, Rehrauer WM, Smith JA (2017) First described case of prosthetic joint infection with *Clostridium disporicum*. *Anaerobe* 48:56–58. <https://doi.org/10.1016/j.anaerobe.2017.06.022>
 57. Clavel T, Duck W, Charrier C, Wenning M, Elson C, Haller D (2010) *Enterorhabdus caecimuris* sp. nov., a member of the family *Coriobacteriaceae* isolated from a mouse model of spontaneous colitis, and emended description of the genus *Enterorhabdus*. *Int J Syst Evol Microbiol* 60:1527–1531. <https://doi.org/10.1099/ijs.0.015016-0>
 58. Yanagibashi T, Hosono A, Oyama A, Tsuda M, Suzuki A, Hachimura S, Takahashi Y, Momose Y, Itoh K, Hirayama K, Takahashi K, Kaminogawa S (2013) IgA production in the large intestine is modulated by a different mechanism than in the small intestine: *Bacteroides acidifaciens* promotes IgA production in the large intestine by inducing germinal center formation and increasing the number of IgA⁺ B cells. *Immunobiology* 218:645–651. <https://doi.org/10.1016/j.imbio.2012.07.033>
 59. Yang JY, Lee YS, Kim Y, Lee SH, Ryu S, Fukuda S, Hase K, Yang CS, Lim HS, Kim MS, Kim HM, Ahn SH, Kwon BE, Ko

- HJ, Kweon MN (2017) Gut commensal *Bacteroides acidifaciens* prevents obesity and improves insulin sensitivity in mice. *Mucosal Immunol* 10:104–116. <https://doi.org/10.1038/mi.2016.42>
60. Wu L, Yan Q, Chen F, Cao C, Wang S (2021) *Bupleuri radix* extract ameliorates impaired lipid metabolism in high-fat diet-induced obese mice via gut microbiota-mediated regulation of FGF21 signaling pathway. *Biomed Pharmacother* 135:111187. <https://doi.org/10.1016/j.biopha.2020.111187>
61. Singh P, Rawat A, Alwakeel M, Sharif E, Al Khodor S (2020) The potential role of vitamin D supplementation as a gut microbiota modifier in healthy individuals. *Sci Rep* 10:21641. <https://doi.org/10.1038/s41598-020-77806-4>
62. Kutsyr O, Maestre-Carballa L, Lluesma-Gomez M, Martinez-Garcia M, Cuenca N, Lax P (2021) Retinitis pigmentosa is associated with shifts in the gut microbiome. *Sci Rep* 11:6692. <https://doi.org/10.1038/s41598-021-86052-1>
63. Fouladi F, Bailey MJ, Patterson WB, Sioda M, Blakley IC, Fodor AA, Jones RB, Chen Z, Kim JS, Lurmann F, Martino C, Knight R, Gilliland FD, Alderete TL (2020) Air pollution exposure is associated with the gut microbiome as revealed by shotgun metagenomic sequencing. *Environ Int* 138:105604. <https://doi.org/10.1016/j.envint.2020.105604>
64. Duan C, Huang L, Zhang C, Zhang L, Xia X, Zhong Z, Wang B, Wang Y, Man Hoi MP, Ding W, Yang Y (2021) Gut commensal-derived butyrate reverses obesity-induced social deficits and anxiety-like behaviors via regulation of microglial homeostasis. *Eur J Pharmacol* 908:174338. <https://doi.org/10.1016/j.ejphar.2021.174338>
65. Clayton K, Delpech JC, Herron S, Iwahara N, Ericsson M, Saito T, Saido TC, Ikezu S, Ikezu T (2021) Plaque associated microglia hyper-secrete extracellular vesicles and accelerate tau propagation in a humanized APP mouse model. *Mol Neurodegener* 16:18. <https://doi.org/10.1186/s13024-021-00440-9>
66. Lei F, Cui N, Zhou C, Chodosh J, Vavvas DG, Paschalis EI (2020) CSF1R inhibition by a small-molecule inhibitor is not microglia specific; affecting hematopoiesis and the function of macrophages. *Proc Natl Acad Sci U S A* 117:23336–23338. <https://doi.org/10.1073/pnas.1922788117>



Contents lists available at ScienceDirect

Progress in Neuropsychopharmacology & Biological Psychiatry

journal homepage: www.elsevier.com/locate/pnp

A role of gut–microbiota–brain axis via subdiaphragmatic vagus nerve in depression-like phenotypes in *Chrna7* knock-out mice

Yong Yang^a, Akifumi Eguchi^b, Xiayun Wan^a, Lijia Chang^a, Xingming Wang^a, Youge Qu^a, Chisato Mori^{b,c}, Kenji Hashimoto^{a,*}

^a Division of Clinical Neuroscience, Chiba University Center for Forensic Mental Health, Chiba 260-8670, Japan

^b Department of Sustainable Health Science, Chiba University Center for Preventive Medical Sciences, Chiba 263-8522, Japan

^c Department of Bioenvironmental Medicine, Graduate School of Medicine, Chiba University, Chiba 260-8670, Japan

ARTICLE INFO

Keywords:

$\alpha 7$ nAChR
Brain-gut axis
Gut microbiota
Metabolites
Vagus nerve

ABSTRACT

The $\alpha 7$ subtype of the nicotinic acetylcholine receptor ($\alpha 7$ nAChR; coded by *Chrna7*) is known to regulate the cholinergic ascending anti-inflammatory pathway. We previously reported that *Chrna7* knock-out (KO) mice show depression-like behaviors through abnormal composition of gut microbiota and systemic inflammation. Given the role of subdiaphragmatic vagus nerve in gut–microbiota–brain axis, we investigated whether subdiaphragmatic vagotomy (SDV) could affect depression-like behaviors, abnormal composition of gut microbiota, and microbes-derived metabolites in *Chrna7* KO mice. SDV blocked depression-like behaviors and reduced expression of synaptic proteins in the medial prefrontal cortex (mPFC) of *Chrna7* KO mice. LEfSe (linear discriminant analysis effect size) analysis revealed that the species *Lactobacillus* sp. *BL302*, the species *Lactobacillus hominis*, and the species *Lactobacillus reuteri*, were identified as potential microbial markers in the KO + SDV group. There were several genus and species altered among the three groups [wild-type (WT) + sham group, KO + sham group, KO + SDV group]. Furthermore, there were several plasma metabolites altered among the three groups. Moreover, there were correlations between relative abundance of several microbiome and behavioral data (or synaptic proteins). Network analysis showed correlations between relative abundance of several microbiome and plasma metabolites (or behavioral data). These data suggest that *Chrna7* KO mice produce depression-like behaviors and reduced expression of synaptic proteins in the mPFC through gut–microbiota–brain axis via subdiaphragmatic vagus nerve.

1. Introduction

Depression is the most prevalent mental disorder with an estimated 5.0% of adults and 5.7% of elderly adults (>60 years old) worldwide. Furthermore, depression is a leading cause of disability worldwide, and it is a major contributor to the overall global burden of disease (WHO, 2021). Although the precise neurobiology underlying depression remains unclear, inflammation is known to play an important role in depression (Brydges et al., 2022; Haroon et al., 2012; Hashimoto, 2009; Hashimoto, 2015; Liu et al., 2020; Lucido et al., 2021; Mac Giollabhui et al., 2021; Miller and Raison, 2016; Shan and Hashimoto, 2022; Toenders et al., 2022; Zhang et al., 2016a).

Nicotinic acetylcholine receptor (nAChR) is a kind of ionotropic

ligand-gated ion channels widely distributed in various cells of the central nervous system (CNS), peripheral nervous system (PNS), enteric nervous system, neuromuscular junction and immune system, which consist of pentameric combinations of α and/or β subunits (Dani, 2015; Dani and Bertrand, 2007). Among its many subtypes, $\alpha 7$ nAChRs, encoded by the *Chrna7* gene, mediates systemic inflammatory homeostasis between the CNS and the immune system through a vagus nerve mediated way known as the “cholinergic anti-inflammatory pathway” (Andersson and Tracey, 2012; Lei and Duan, 2021; Martelli et al., 2014; Olofsson et al., 2012; Piovesana et al., 2021; Ulloa, 2005; Wang et al., 2003; Wu et al., 2021). We previously reported that *Chrna7* KO mice show depression-like phenotypes through systemic inflammation (Pu et al., 2021b; Zhang et al., 2016b).

Abbreviations: *Chrna7*, $\alpha 7$ subtype of the nicotinic acetylcholine receptor; CNS, central nervous system; FMT, fecal microbiota transplantation; FST, forced swimming test; LPS, lipopolysaccharide; mPFC, medial prefrontal cortex; SDV, subdiaphragmatic vagotomy; SPT, sucrose preference test.

* Corresponding author.

E-mail address: hashimoto@faculty.chiba-u.jp (K. Hashimoto).

<https://doi.org/10.1016/j.pnpbp.2022.110652>

Received 13 June 2022; Received in revised form 26 September 2022; Accepted 27 September 2022

Available online 30 September 2022

0278-5846/© 2022 Elsevier Inc. All rights reserved.

Increasing evidence suggests altered composition of intestinal microbiota in rodents with depressive-like phenotypes (Chang et al., 2022; Hashimoto, 2020; Huang et al., 2019; Park et al., 2013; Qu et al., 2017; Wang et al., 2020a, 2020b; Wong et al., 2016; Yang et al., 2017, 2019; Zhang et al., 2017; Zhang et al., 2019), and patients with depression (Caso et al., 2021; Jiang et al., 2015; Li et al., 2022; Nikolova et al., 2021; Sanada et al., 2020; Wei et al., 2022a, 2022b; Wong et al., 2016; Zheng et al., 2016). Fecal microbiota transplantation (FMT) of certain intestinal microbiota from depressed patients or rodents with depressive-like phenotypes causes depression-like phenotypes in mice (Kelly et al., 2016; Pu et al., 2021b; Pu et al., 2022; Wang et al., 2020a; Yang et al., 2019; Zheng et al., 2016). Furthermore, microbial-derived metabolites, including short-chain fatty acids (SCFAs), tryptophan-derived metabolites, bile acids and D-amino acids, could regulate a number of physiological functions such as behaviors (Bartoli et al., 2021; Chang et al., 2022; Hashimoto, 2022; Li et al., 2022; Pu et al., 2021a; Tran and Mohajeri, 2021; Wan et al., 2022a, 2022b). Vagus nerve is known to play a key role in the bi-directional communication between the gut microbiota and the brain (Bonaz et al., 2018; Cawthon and de La Serre, 2018; Chang et al., 2022; Cryan et al., 2019; Forsythe et al., 2014). We reported that subdiaphragmatic vagotomy (SDV) blocked the onset of depression-like behavior and altered composition of intestinal microbiota in mice after lipopolysaccharide (LPS) administration (Zhang et al., 2020). Subsequently, we reported that SDV blocked the onset of depression-like behaviors in mice after FMT from mice with depression-like behaviors (Pu et al., 2021a; Wang et al., 2020a; Wang et al., 2021). Collectively, it is likely that subdiaphragmatic vagus nerve plays a key role in depression-like behaviors (Chang et al., 2022; Wei et al., 2022b). However, there are no reports showing the role of subdiaphragmatic vagus nerve in depression-like phenotypes in *Chrna7* KO mice.

The aim of present study was to evaluate whether SDV could affect depression-like phenotypes and reduced expression of synaptic proteins in the medial prefrontal cortex (mPFC) of *Chrna7* KO mice. Furthermore, we performed 16S rRNA analysis for gut microbiota composition and untargeted metabolomics analysis of plasma samples.

2. Materials and methods

2.1. Animals

Mice deficient in $\alpha 7$ nAChR (coded by *Chrna7* gene, C57BL/6 background) were purchased from the Jackson Laboratory (Bar Harbor, ME, USA) (Zhang et al., 2016b). Adult male wild-type (WT) and *Chrna7* KO mice used in this study were littermates. All the experimental mice were aged 9 weeks, body weight 21–27 g. All the experimental mice were acclimatized to standard laboratory conditions (3 or 4/ cage), maintain alternating cycles of 12 h of light and 12 h of darkness (lights on from 7:00–19:00), and under constant room temperature of 23 ± 1 °C and controlled humidity of $55 \pm 5\%$. Animals were given free admittance to chow and water. The experimental protocol of present study was approved by the Chiba University Institutional Animal Care and Use Committee (Permission number 3–399). The experimental mice were all firstly deeply anesthetized with inhaled isoflurane and then rapidly sacrificed by cervical dislocation. All efforts were made to minimize animals suffering.

2.2. Bilateral subdiaphragmatic vagotomy (SDV)

Bilateral SDV or sham surgery was performed under continuous inhalation anesthesia with 4–5% isoflurane by using an inhalation small animal anesthesia apparatus (KN-1071 NARCOBIT-E; Natsume Seisakusho, Tokyo, Japan), as previously method (Pu et al., 2021a; Wang et al., 2020a, 2021; Zhang et al., 2020) with a slight modification. Briefly, each mouse was placed in the right-side decubitus position, the skin is disinfected with iodophor disinfectant and sterile tissue is laid.

Starting from the midline alba of the abdomen, about 1 cm incision parallel to the costal arch was made at 0.5 cm below the left costal arch. The incision was gently opened with Mini incision spreader to expose the underlying liver tissue. The liver tissue was carefully pushed upward using a small sterilized cotton ball moistened with physiological saline solution and with the aid of an animal surgical microscope (Leica, Heidelberg, Germany), the fascia between the caudate lobe and the left lobe of the liver was sharply cut to fully expose the esophagus and the surrounding surgical field of view. In this case, the dorsal and ventral branches running along the esophagus under the diaphragm of the vagus nerve can be clearly identified and can be severed after careful separation. After that, no bleeding was detected, and no additional injury of esophagus, liver and other organs was checked, the liver tissue was returned to its original normal position, and 0.5 ml physiological saline solution was injected into the abdominal cavity. Then 5–0 surgical silk sutures were used to suture the abdominal incision muscle and skin layers layer by layer, ensuring aseptic operation throughout the operation. The successful implementation of SDV was confirmed by a significant increase in stomach volume on the 14th postoperative day due to loss of vagus nerve innervation.

During the sham operation, the abdominal wall incision of the same size was made in the same way at the same site. After the dorsal and ventral branches of the subdiaphragmatic vagus nerve were also softly exposed but not cut off, no bleeding and no additional damage of other organs was checked. After the abdominal organs were restored to their normal positions, 0.5 ml normal saline was also injected into the abdominal cavity, then the incision was sutured layer by layer using the same method.

2.3. Behavioral tests

Male WT and *Chrna7* KO mice born in the same litter were subjected to behavioral tests, as previously method (Pu et al., 2021a; Wang et al., 2020a, 2021). Behavioral tests including locomotion test (LMT), forced swimming test (FST), and 1% sucrose preference test (1% SPT) (Fig. 1A).

In order to monitor the locomotor activity of the mice, we adopted an automatic animal movement analysis system (SCANET MV-40; MEL-QUEST Co., Ltd., Toyama, Japan). The cumulative ambulatory activity counts were automatic document continuously over a total stage of 60 min (10 min \times 6 times) after the mice were placed into the experimental cube boxes [33 cm (height) \times 56 cm (width) \times 56 cm (length)]. To avoid experimental interference, the cube boxes were cleaned up during the test interval.

A mouse automated forced-swim apparatus (SCANET MV-40; MEL-QUEST Co., Ltd., Toyama, Japan) was used to perform FST. Mice were placed into an inescapable transparent tank [31 cm (height) \times 23 cm (diameter)] that is filled with tap water at a temperature of 23 ± 1 °C and a depth of 15 cm. Then their escape related mobility behavior was measured immediately. The immobility times were automatic document and calculated using the analytical software of the apparatus over a total stage of 6 min (1 min \times 6 times).

For 1% SPT, which was carried out in the separate animal's home cage. Each mouse was presented with two dual bearing sipper bottles, one bottle contained tap water, and the second contained a 1% sucrose solution. After 24 h of every mouse exposed to the respective two bottles containing different solution, replaced the positions of two bottles for each other to lower any confound produced by a side bias. After another 24 h, all food and bottles were deprived lasting 4 h, then performed 1 h exposure to two identical bottles (containing tap water and 1% sucrose solution), which were weighed before and after the exposure period. The 1% sucrose preference was calculated as a percentage of 1% sucrose solution intake weight over the total liquid intake weight.

2.4. Western blotting analysis of synaptic proteins (PSD-95 and GluA1)

Western blotting analysis was performed as previously method (Pu

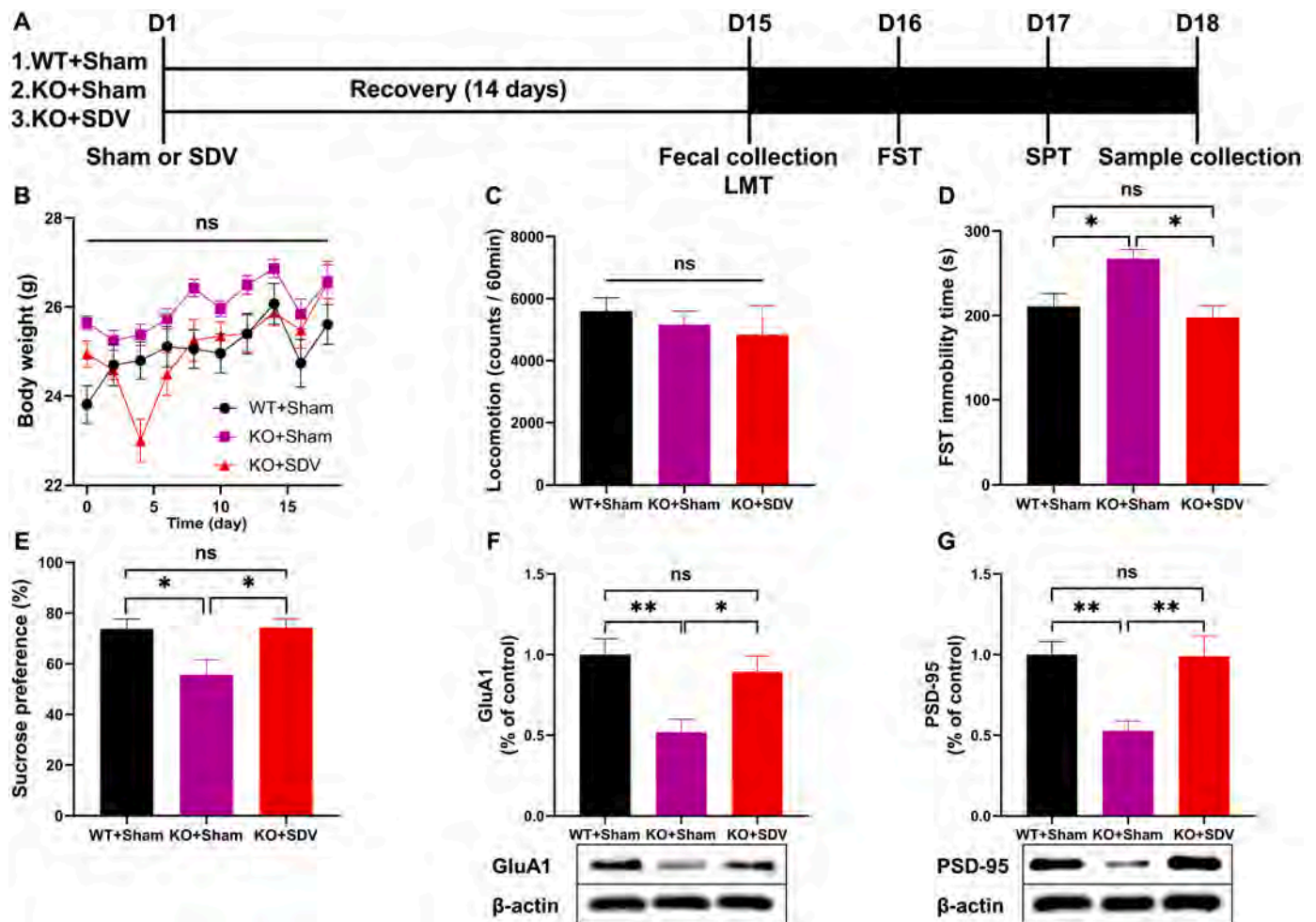


Fig. 1. Effects of bilateral SDV on depression-like phenotypes and reduced expression of synaptic proteins in *Chrna7* KO mice.

(A): Experimental schedule. On day 1, bilateral SDV or sham was performed, and they were recovered 14 days. On day 15, fresh feces samples were collected, and subsequently LMT was performed. FST and SPT were performed on day 16 and day 17, respectively. On day 18, medial prefrontal cortex (mPFC) and plasma samples were collected. (B): Body weight (repeated measure ANOVA, $F_{(2, 21)} = 2.424$, $P = 0.1129$). (C): LMT (one-way ANOVA, $F_{(2,21)} = 0.4278$, $P = 0.6575$). (D): FST (one-way ANOVA, $F_{(2, 21)} = 6.050$, $P = 0.0084$). (E): SPT (one-way ANOVA, $F_{(2, 21)} = 5.312$, $P = 0.0136$). (F): Western blot analysis of GluA1 in the mPFC (one-way ANOVA, $F_{(2, 21)} = 6.805$, $P = 0.0053$) and the representative bands. (G): Western blot analysis of PSD-95 in the mPFC (one-way ANOVA, $F_{(2, 21)} = 8.191$, $P = 0.0023$) and the representative bands. The data are shown as means \pm S.E.M (WT + sham group: $n = 10$, KO + sham group: $n = 7$, KO + SDV group: $n = 7$). ANOVA: analysis of variance. ns: not significant; * $P < 0.05$; ** $P < 0.01$; *** $P < 0.001$.

et al., 2021a; Wang et al., 2020a, 2021; Yang et al., 2022b). The mPFC tissues were mechanically homogenized just right in ice-cold Laemmli lysis buffer. To avoid cross-contamination, each specimen was prepared separately, liquid supernatants were collected after centrifugation at $3000 \times g$ (RCF) at 4°C for 5 min. The total protein concentration extracted from each sample was detected on a spectrophotometer (Molecular Devices Emax Precision Microplate Reader; Molecular Devices., San Jose, CA, USA) using a DC protein assay kit (Bio-Rad, Hercules, CA, USA). By adding a quarter volume of sample buffer (125 mM Tris-HCl, pH 6.8; 0.1% bromophenol blue; 4% sodium dodecyl sulfate; and 10% β -mercaptoethanol and 20% glycerol) and Laemmli Lysis buffer in appropriate proportions to balance the total protein concentration of each sample, then incubate them at 95°C for 10 min.

Considering the size of target protein, we chose 10% sodium dodecyl sulfate-polyacrylamide gel electrophoresis (SDS-PAGE) (catalog #: 4568125, Mini-PROTEAN TGX™ Stain-Free Gels; Bio-Rad, USA) separated the proteins by gel electrophoresis. Then a Trans-Blot Mini Cell apparatus (Bio-Rad) was used to electrotransfer the target protein onto polyvinylidene difluoride membranes.

For immunodetection, the polyvinylidene difluoride membranes were blocked with blocker [5% skim milk in TBS + 0.1% Tween-20

(TBST)] at room temperature for 1 h, the membranes for detecting postsynaptic density protein 95 (PSD-95) were incubated with the recommended dilution of the primary antibody against PSD-95 (1:1000, Catalog No.: 51-6,900, 1 $\mu\text{g}/\text{mL}$, Invitrogen, Camarillo, CA, USA) and β -actin (1:10,000; Cat number: A5441 Sigma-Aldrich Co., Ltd., St Louis, MO, USA) at 4°C overnight. The next day, wash the polyvinylidene difluoride membranes in three washes of TBST, 10 min each. Then the polyvinylidene difluoride membranes were selectively incubated with a recommended dilution of labeled secondary antibody [anti-mouse antibody (1:5000, catalog No.: NA931, GE Healthcare) or a horseradish peroxidase-conjugated anti-rabbit antibody (1:5000, catalog No.: NA934, GE Healthcare)] in 5% blocking buffer in TBST at room temperature for 1 h. After three final washes in TBST, 10 min each. The bands in the polyvinylidene difluoride membranes were detected using enhanced chemiluminescence plus a Western Blotting Detection system (GE Healthcare Bioscience).

The membranes for detecting anti-glutamate receptor 1 (AMPA subtype: GluA1) were incubated in elution buffer (62.5 mM Tris-HCl, pH 6.8, 2% sodium dodecyl sulfate, and 100 mM β -mercaptoethanol) (preheat in incubator at 60°C for 10 min, shake 50 times /min) at 60°C for 30 min and then washed three times (10 min at a time) in TBST. The

stripped membranes were blocked with blocker [5% skim milk in TBS + 0.1% Tween-20 (TBST)] at room temperature for 1 h and then were incubated with the recommended dilution of primary antibody directed against GluA1 (1:1,000; Cat No.: ab31232, Abcam, Cambridge, MA, USA) at 4 °C overnight. The following day, washing the membranes for three times (10 min at a time) in TBST and were incubated with a recommended dilution of horseradish peroxidase-conjugated anti-rabbit antibody (1:5000, catalog No.: NA934, GE Healthcare) for 1 h at room temperature. After three final washes in TBST, 10 min each. The bands in the polyvinylidene difluoride membranes were detected using enhanced chemiluminescence plus a Western Blotting Detection system (GE Healthcare Bioscience). Images were produced using a ChemiDoc™ Touch Imaging System (170-01401; Bio-Rad Laboratories, Hercules, CA, USA), and immunoreactive bands were quantified using Image Lab™ 3.0 software (Bio-Rad Laboratories).

2.5. Collection of fresh fecal samples and 16S ribosome RNA sequencing

We collected fresh fecal samples from mice before behavioral test LMT (Fig. 1A). To avoid cross-contamination, fecal samples from each mouse were collected separately. After the mice defecated, fresh fecal samples were collected immediately and were quickly intromitted into individual sterilized screw cap microtubes and then were stored at -80 °C until use.

Extraction of total DNA from mouse feces samples and subsequent 16S rRNA analysis were performed at MyMetagenome Co., Ltd. (Tokyo, Japan). The specific operation scheme can be carried out according to the procedure previously reported (Pu et al., 2021b; Wang et al., 2020a, 2021; Yang et al., 2022b). In brief, in order to amplify the V1-V2 hypervariable region of the bacterial 16S ribosome RNA gene, the universal primers 27F-mod (5'-AGRGTGATYMTGGCTCAG-3') and 338R (5'-TGCTGCTCCCGTAGGAGT-3') have been used in the process of PCR. Then used an Illumina MiSeq Platform to sequence the 16S amplicons. The similarities between the genome database of the National Center for Biotechnology Information (NCBI) and the Ribosome Database Project were searched by using the GLSEARCH program. Finally, OTUs were classified and identified.

α -diversity analysis such as Observed_otus, Chao1, Ace, Shannon, and Shannon_e was used to reflect the abundance and diversity of intestinal microbial communities. β -diversity analysis including Principal Co-ordinates Analysis (PCoA) was used to access similarity or dissimilarity of the three intestinal microbial communities. Linear discriminant analysis (LDA) effect size (LEfSe) was used for identifying certain bacteria as potential microbial biomarkers discovery. Microbiota-based potential biomarker discoveries were performed with LEfSe using the online galaxy platform (Segata et al., 2011). The LDA scores (LDA > 4.0 and $P < 0.05$) derived from LEfSe analysis were considered significantly to be enriched or deficient bacterial taxa in the intestinal microbiota among the three groups.

2.6. Untargeted metabolomics analysis of plasma samples and data preprocessing

Untargeted metabolomics profiles from plasma samples were analysis by using ultra-performance liquid chromatography-tandem quadrupole time-of-flight mass spectrometry (UPLC-QTOF/MS) technique. The acquisition was operated on an ExionLC™ AD system (SCIEX, Tokyo, Japan) coupled to a X500R QTOF system (SCIEX, Tokyo, Japan), as previously reported (Wan et al., 2022a, 2022b). With the help of R statistical environment Ver 4.0.5. and Mass Spectrometry-Data Independent AnaLysis (MS-DIAL) software version 4.60 (Tsugawa et al., 2015), metabolomics profiles data was analyzed. Metabolites were detected at least 50% from the analyzed samples and the coefficient of variation (CV) values of 30% of metabolites in pooled quality control (QC) samples, and annotation level 2 proposed by Schymanski et al. (2014) were used for data analysis.

2.7. Statistical analysis

Statistical analysis of the data was performed using SPSS version 20.0 software (SPSS, Tokyo, Japan). The data were shown as the mean \pm standard error of the mean (S.E.M.). Data for behavioral tests and the expression levels of synaptic proteins were analyzed using one-way analysis of variance (ANOVA), followed by Fisher's least significant difference (LSD) test. The data of body weight were analyzed using repeated measure ANOVA, followed by Fisher's LSD test. Metabolites, the α -diversity of intestinal microbiota, and the abundance of gut microbiota at the phylum level, genus level, and species level among the three groups were analyzed using the Kruskal-Wallis test, followed by the Dunn's test for post-hoc analysis. Pairwise comparison of metabolomics data among the three groups were analyzed by Wilcoxon rank sum test. Bioinformatic analysis of PCoA, LEfSe algorithm of intestinal microbiota, Volcanic plot analysis of metabolomics and Correlation networks were all performed by using the OmicStudio tools (<https://www.omicstudio.cn/tool>).

Correlations between the plasma metabolites and the intestinal microbiota at species level, depression-like phenotypes and the expression of synaptic proteins in the brain, and correlations between the relative abundance of species bacteria and the expression levels of synaptic proteins in the mPFC and depression-like phenotypes were analyzed using Spearman's correlation analysis. P -value for comparison <0.05 was regarded as significant.

3. Results

3.1. Effects of bilateral SDV on depression-like phenotypes, and the expression of synaptic proteins in the brain

Effects of bilateral SDV in depression-like phenotypes in *Chrna7* KO mice were investigated (Fig. 1A). Body weight after surgery was not different among the three groups (Fig. 1B). There were no changes in locomotion among the three groups (Fig. 1C). The immobility time of FST in the KO + sham group was significantly higher than that of WT + sham group and KO + SDV group (Fig. 1D). In the SPT, sucrose preference of KO + sham group was significantly lower than that of WT + sham and KO + SDV groups (Fig. 1E). There were no differences in FST immobility time and sucrose preference of SPT between WT + sham group and KO + SDV group (Fig. 1D and E).

It is well known that synaptic proteins such as PSD-95 and GluA1 are decreased in the mPFC of rodents with depression-like phenotypes (Pu et al., 2021b; Wang et al., 2020a, 2020b, 2021; Yang et al., 2015; Zhang et al., 2014). Western blotting analysis showed that the expressions of PSD-95 and GluA1 in the mPFC of the KO + sham group were significantly lower than those of WT + sham group and KO + SDV group (Fig. 1F and G). There were no differences in expressions of GluA1 and PSD-95 in the mPFC between WT + sham group and KO + SDV group (Fig. 1F and G).

These data suggest that bilateral SDV significantly blocked depression-like phenotypes and reduced expression of synaptic proteins in the mPFC of *Chrna7* KO mice.

3.2. Effects of bilateral SDV on the composition diversity of intestinal microbiota

For α -diversity, Kruskal-Wallis test revealed no statistically significant differences in the Observed_otus, Chao1, Ace, Shannon, and Shannon_e indices among the three group (Fig. 2A-E). Regarding β -diversity, the bacterial population composition of intestine microbiota in the three groups was analyzed by PCoA. Based on the OUT level, PCoA analysis showed a significant separation in the bacterial population composition through Analysis of similarities (ANOSIM) assessment ($R = 0.3500$, $P = 0.001$) (Fig. 2F).

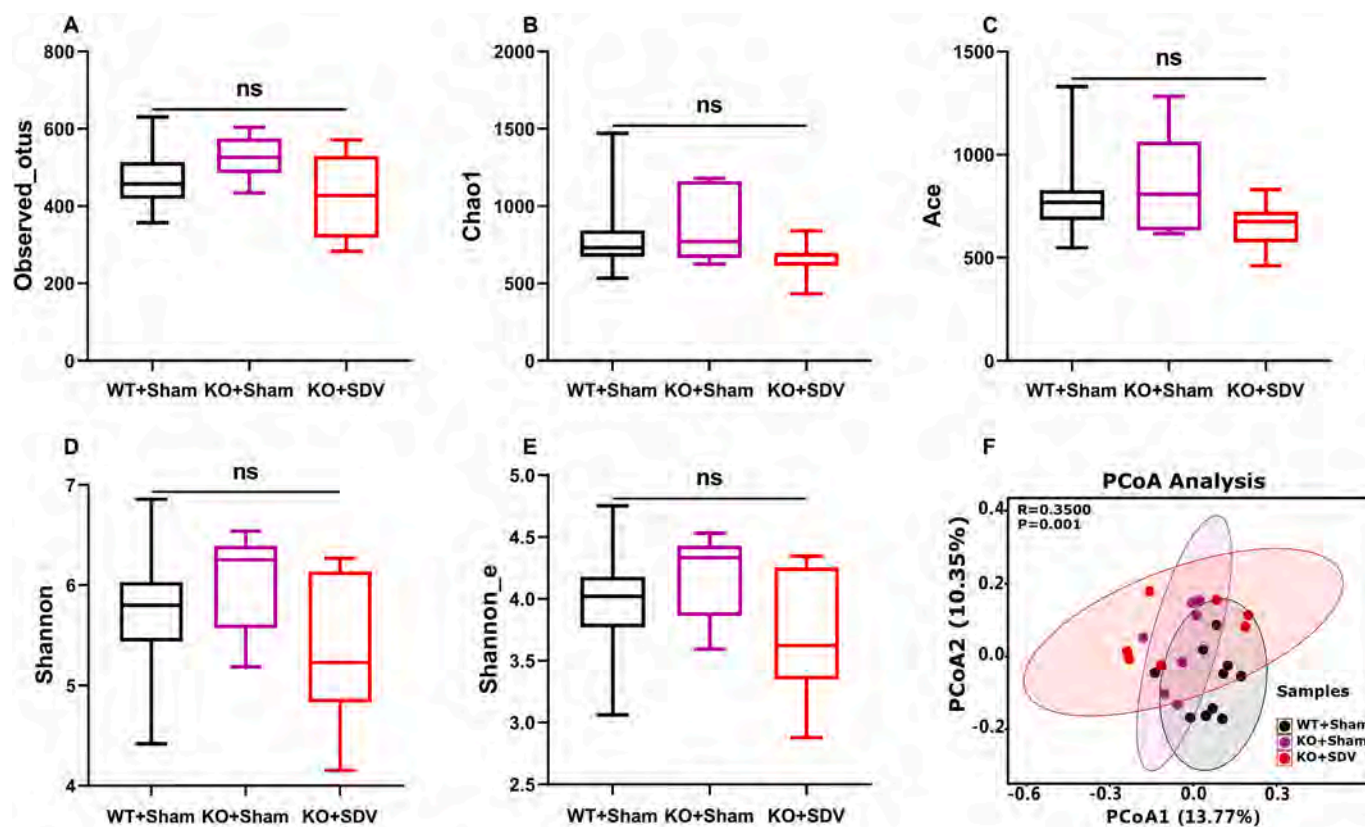


Fig. 2. Effects of bilateral SDV on the diversity of gut microbiota composition.

(A): Observed_otus (Kruskal-Wallis test, $P = 0.2028$). (B): Chao1 (Kruskal-Wallis test, $P = 0.1920$). (C): Ace (Kruskal-Wallis test, $P = 0.2305$). (D): Shannon (Kruskal-Wallis test, $P = 0.1941$). (E): Shannon_e (Kruskal-Wallis test, $P = 0.1941$). (F): PCoA based on OTU level (ANOSIM, Bray-Curtis dissimilarity matrix) ($R = 0.3500$, $P = 0.001$). For all box plots, the middle line in the box addresses the median, the box addresses the interquartile range, and the whisker addresses the most extreme and least values. ns: not significant.

3.3. Effects of bilateral SDV on the LEfSe algorithm of intestinal microbiota

Cladogram presented the relationship between biomarker taxa (layers of the cladogram represent different levels, with phylum, class, order, family, genus, and species from inside to outside) generated by LEfSe analysis (Fig. 3A). Furthermore, we identified 5 taxonomic biomarkers, the species *Porphyromonadaceae bacterium C941*, the genus *G_undefined_Porphyromonadaceae*, the species *Gabonibacter massiliensis*, the genus *Gabonibacter*, and the species *Prevotella sp. oral taxon 317* for the WT + sham group. Furthermore, we identified 6 taxonomic biomarkers, the species *Gabonia massiliensis*, the genus *Gabonia*, the family *Porphyromonadaceae*, the order *Bacteroidales*, the class *Bacteroidia*, and the phylum *Bacteroidetes* for the KO + sham group. Moreover, we identified 8 taxonomic biomarkers, the species *Lactobacillus hominis*, the species *Lactobacillus reuteri*, the species *Lactobacillus sp. BL302*, the genus *Lactobacillus*, the family *Lactobacillaceae*, the order *Lactobacillales*, the class *Bacilli*, and the phylum *Firmicutes* for the KO + SDV group (Fig. 3B).

3.4. Effects of bilateral SDV on the intestinal microbiota at the levels of phylum, genus, and species

At the phylum level, the composition of the intestinal microbiota in *Chrna7* KO mice was altered after SDV (Fig. 4A). Compared with WT + sham group and KO + sham group, the relative abundance of *Firmicutes* in the KO + SDV group were significantly higher, although there were no significant differences between WT + sham group and KO + sham group (Fig. 4B). Although there were no significant differences in the relative

abundance of *Tenericutes* between KO + SDV group and KO + sham group, the relative abundance of *Tenericutes* in the KO + SDV group were significantly lower than that in the WT + sham group (Fig. 4C).

At the genus level, the composition of the gut microbiota in *Chrna7* KO mice was altered after SDV (Fig. 5A). The relative abundance of *Faecalibaculum* in the KO + SDV group were statistically significantly lower than in the WT + sham group and KO + sham group (Fig. 5B). The relative abundance of *Candidatus Arthromitus*, *Bifidobacterium*, *G_undefined_Burkholderiales*, and *Muribaculum* in the KO + SDV group was lower than that in the WT + sham group, whereas the relative abundance of *Ihubacter* in the KO + SDV group was higher than that in the WT + sham group (Fig. 5C, F, and I-5J). The relative abundance of *Turicibacter* in the KO + SDV group were lower than in the KO + sham group (Fig. 5D). The relative abundance of *Lactobacillus* in the KO + SDV group were higher than in the KO + sham group (Fig. 5G). The relative abundance of *Lactococcus* in the KO + sham group and the KO + SDV group were lower than that in the WT + sham group (Fig. 5E).

At the species level, we screened out 15 bacteria with statistical differences based on their relative abundance (Fig. 6A). There were significant differences in the relative abundance of *Lactobacillus intestinalis*, *Lactobacillus hominis*, *Faecalibaculum rodentium*, *Lactobacillus sp. BL302*, *Bacteroides sp. TP-5*, *Candidatus Arthromitus sp. SFB-mouse*, *Turicibacter sp. LA62*, *Lactobacillus reuteri*, *Lactococcus lactis*, *Lactobacillus sp. NBRC 14512*, *Clostridium sp. Culture Jar-56*, *Lachnospiraceae bacterium 607*, *Clostridiales bacterium CIEAF 030*, *Bifidobacterium pseudolongum* and *Muribaculum intestinale* (Fig. 6B-6P). Among these microbes, the relative abundance of three microbiome (*Lactobacillus intestinalis*, *Lactobacillus sp. BL302*, *Turicibacter sp. LA62*) was significantly different between KO + sham group and KO + SDV group (Fig. 6B, E, and H).

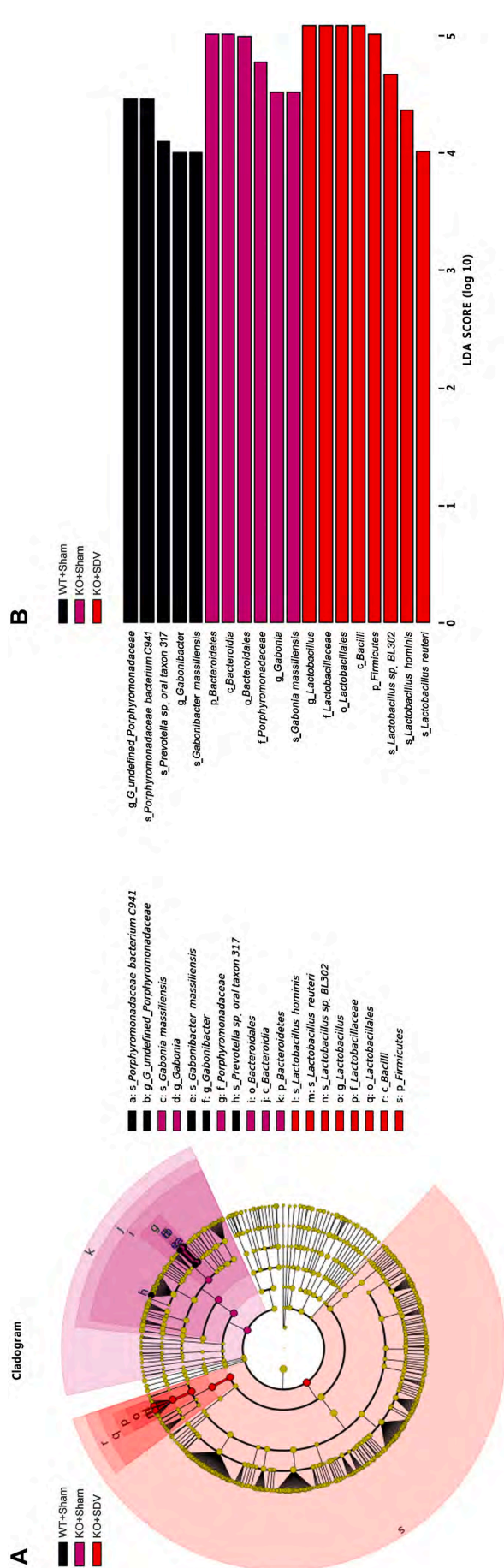


Fig. 3. LEfSe analysis for potential bacteria biomarkers of gut microbiota. (A): Functional branching diagram generated from LEfSe showing the differences of the three groups at different taxonomic levels. (B): Histogram representing the enriched taxa with LDA score > 4.0 and $P < 0.05$ obtained from LEfSe of the three groups.

3.5. Untargeted metabolomic profiles analysis of plasma samples

Considering the close interaction between intestinal microbiome and host metabolism, we conducted untargeted metabolomics profiles analysis from plasma samples. After the quality control and removal of low-abundance peaks, a subset of 175 metabolites was annotated. After log10 transformation of the concentration of metabolomics data, Kruskal-Wallis test was performed among the three groups. We identified 24 metabolites with statistical differences (Fig. 7A-D).

Then we conducted pairwise comparison of metabolomics data among the three groups, and screened out the metabolites with significant up-regulation and down-regulation obtained in each two groups through the form of Volcano plot [the threshold was set as: $P < 0.05$ and fold change (FC) > 2]. When comparing the WT + sham group with the KO + sham group, we confirmed that 3 annotation metabolites were significantly up-regulated and 7 annotation metabolites were significantly down-regulated (Fig. 8A). When comparing the WT + sham group with the KO + SDV group, we confirmed that 9 annotation metabolites were significantly up-regulated and 8 annotation metabolites were significantly down-regulated (Fig. 8B). When the KO + sham group compared with the KO + SDV group, we confirmed 9 significantly up-regulated annotated metabolites and 4 significantly down-regulated metabolites (Fig. 8C).

Finally, we further used UpSet plot listed out that there were 11 kinds of annotated metabolites with statistical differences between WT + sham group and KO + sham group, 17 kinds of annotated metabolites with statistical differences between the KO + sham group and KO + SDV group, and 27 kinds of annotated metabolites with statistical differences between WT + sham group and KO + SDV group. In addition, 6 kinds of annotated metabolites showed significant differences between the WT + sham group and the KO + sham group, and between the WT + sham group and the KO + SDV group. Furthermore, 9 kinds of annotated metabolites showed significant differences between the KO + sham group and the KO + SDV group, and between the WT + sham group and the KO + SDV group (Fig. 8D).

3.6. Correlations between the gut microbiota and plasma metabolites (or FST, synapse proteins)

There was a widely correlation between the plasma metabolites and the gut microbiota of the three groups, indicating the existence of a close relationship between the plasma metabolites and the gut microbiota. Furthermore, we evaluated the association between plasma metabolites and the gut microbiota at the species level. After screening the data by setting the threshold of $P < 0.05$ and the absolute value of $R \geq 0.5$, a Correlation Network was developed to indicate the correlation between the plasma metabolites and the intestinal microbiota at species level, depression-like phenotypes and the expression of synaptic proteins in the brain, all of which significantly differences among the three groups in the present study (Fig. 9A).

Two differentially relative abundant of gut bacteria (*Lactobacillus intestinalis* and *Bacteroides* sp. TP-5) were positively correlated with 1,5-anhydro-D-sorbitol (Fig. 9A). Three differentially relative abundant of gut bacteria (*Faecalibaculum rodentium*, *Turcibacter* sp. LA62 and *Muribaculum intestinale*) were negatively correlated with 1,5-anhydro-D-sorbitol (Fig. 9A). There were positive correlations between the relative abundance of species *Lactobacillus intestinalis*, *Lactobacillus hominis*, *Lactobacillus* sp. BL302, *Lactobacillus* sp. NBRC 14512, and *Clostridiales bacterium CIEAF 030* and L-citrulline. In contrast, there were negative correlations between the relative abundance of species *Faecalibaculum rodentium* and L-citrulline (Fig. 9A).

The relative abundance of species *Lachnospiraceae bacterium 607* was positively correlated with succinic anhydride while the relative abundances of species *Lactobacillus hominis*, *Lactobacillus* sp. BL302, *Bacteroides* sp. TP-5, *Lactobacillus reuteri*, and *Clostridiales bacterium CIEAF 030* were negatively correlated with succinic anhydride (Fig. 9A). The

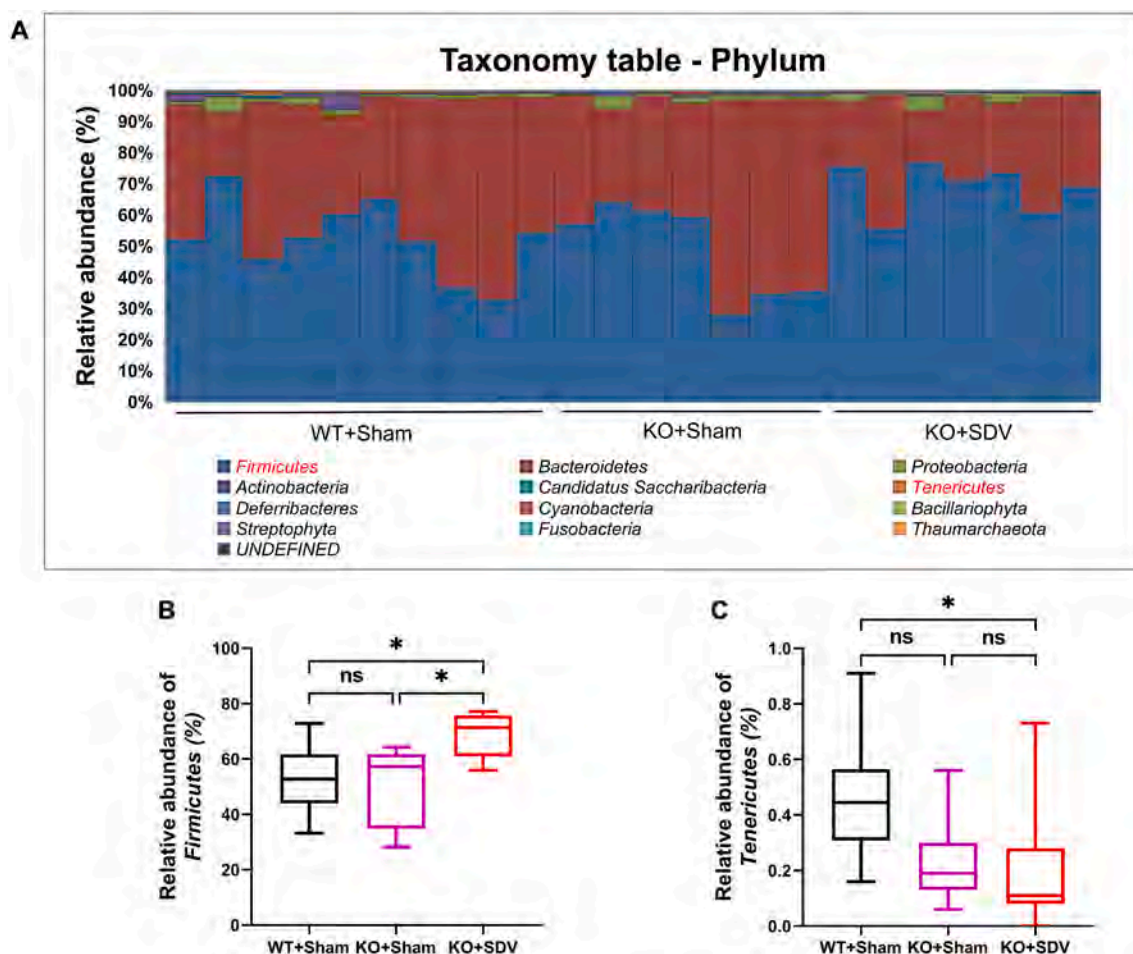


Fig. 4. Effects of bilateral SDV on gut microbiota at the phylum levels.

(A): Gut bacteria composition at the phylum level in the three groups. (B): Relative abundance of the phylum *Firmicutes* (Kruskal-Wallis test, $P = 0.0126$). (C): Relative abundance of the phylum *Tenericutes* (Kruskal-Wallis test, $P = 0.0258$). For all box plots, the middle line in the box addresses the median, the box addresses the interquartile range, and the whisker addresses the most extreme and least values. $*P < 0.05$. ns: not significant.

species *Lactobacillus intestinalis*, *Lactobacillus hominis*, *Lactobacillus* sp. BL302, *Lactobacillus reuteri* and *Lactobacillus* sp. NBRC 14512 were positively correlated with taurocholic acid. In contrast, the species *Faecalibaculum rodentium* and *Turicibacter* sp. LA62 were negatively correlated with taurocholic acid (Fig. 9A).

There was only a significant positive correlation between the FST data and the concentration of ethyl hydrogen sulfate (Fig. 9A). There was no correlation between changes in SPT and changes in metabolite concentration (data not shown). There was a positive correlation between GluA1 expression levels in mPFC and the concentration of 2-oxindole (Fig. 9A). Furthermore, there were positive correlations between PSD-95 expression levels in mPFC and the concentration of L-citrulline, D-ornithine, 2,6-dihydroxybenzoic acid or resorcinol. In contrast, there were no negative correlations between expressions of GluA1 and PSD-95 in the mPFC and plasma metabolites (Fig. 9A).

Similarly, we used a Correlation Network to investigate correlations between the relative abundance of the gut bacteria that differed significantly at the species levels among the three groups and depression-like phenotypes or the expression of synaptic proteins (Fig. 9B). After screening the data by setting the threshold of $P < 0.05$ and the absolute value of $R \geq 0.5$. There were significant negative correlations between the FST data and the relative abundance of the species *Lactobacillus intestinalis*, *Lactobacillus* sp. BL302, *Bacteroides* sp. TP-5, and *Lactobacillus* sp. NBRC 14512 in the three groups (Fig. 9B), suggesting a role of these species in behavioral despair. There were statistically significant positive correlations between the SPT data and the relative abundance of

species *Bacteroides* sp. TP-5 in the three experimental groups (Fig. 9B), suggesting a role of *Bacteroides* sp. TP-5 in anhedonia-like behavior. Furthermore, there were positive or negative correlation between expression levels of synaptic proteins in the mPFC and the relative abundance of species bacteria (Fig. 9B).

4. Discussion

The major findings of this study are as follows: First, SDV blocked depression-like behaviors and reduced expression of synaptic proteins (i. e., GluA1 and PSD-95) in the mPFC of *Chrna7* KO mice. Second, there were no changes in α -diversity among the three groups. However, there was a significant difference in β -diversity among the three groups. LEfSe analysis revealed that the species *Lactobacillus* sp. BL302, the species *Lactobacillus hominis*, and the species *Lactobacillus reuteri*, were identified as potential microbial markers in the KO + SDV group. Furthermore, there were several genus and species altered among the three groups. Third, there were several metabolites altered among the three groups. Fourth, there were correlations between relative abundance of several microbiome and behavioral data (or synaptic proteins). Network analysis showed correlations between several microbiome and blood metabolites or behavioral data. Collectively, these data suggest that subdiaphragmatic vagus nerve plays a crucial role in depression-like phenotypes in *Chrna7* KO mice through gut-microbiota-brain axis including microbiome-derived metabolites.

β -diversity data among the three groups suggest that SDV is a driving

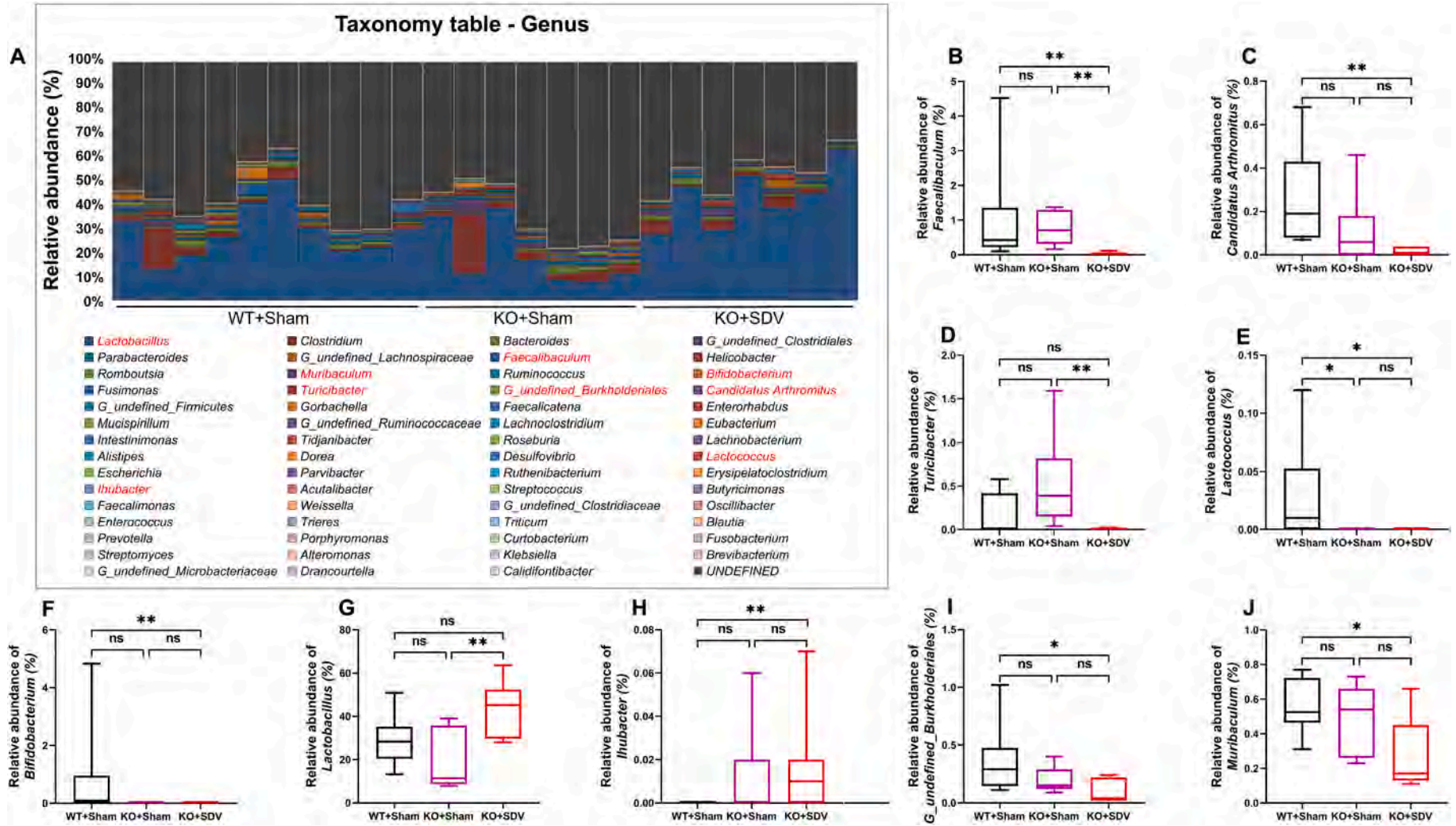


Fig. 5. Effects of bilateral SDV on gut microbiota at the genus levels.

(A): Gut bacteria composition at the genus level in the three groups. (B): Relative abundance of the genus *Faecalibacterium* (Kruskal-Wallis test, $P = 0.0009$). (C): Relative abundance of the genus *Candidatus Arthromitus* (Kruskal-Wallis test, $P = 0.0021$). (D): Relative abundance of the genus *Turicibacter* (Kruskal-Wallis test, $P = 0.0030$). (E): Relative abundance of the genus *Lactococcus* (Kruskal-Wallis test, $P = 0.0053$). (F): Relative abundance of the genus *Bifidobacterium* (Kruskal-Wallis test, $P = 0.0086$). (G): Relative abundance of the genus *Lactobacillus* (Kruskal-Wallis test, $P = 0.0102$). (H): Relative abundance of the genus *Ihubacter* (Kruskal-Wallis test, $P = 0.0131$). (I): Relative abundance of the genus *G_undefined_Burkholderiales* (Kruskal-Wallis test, $P = 0.0132$). (J): Relative abundance of the genus *Muribaculum* (Kruskal-Wallis test, $P = 0.0395$). For all box plots, the middle line in the box addresses the median, the box addresses the interquartile range, and the whisker addresses the most extreme and least values. * $P < 0.05$; ** $P < 0.01$. ns: not significant.

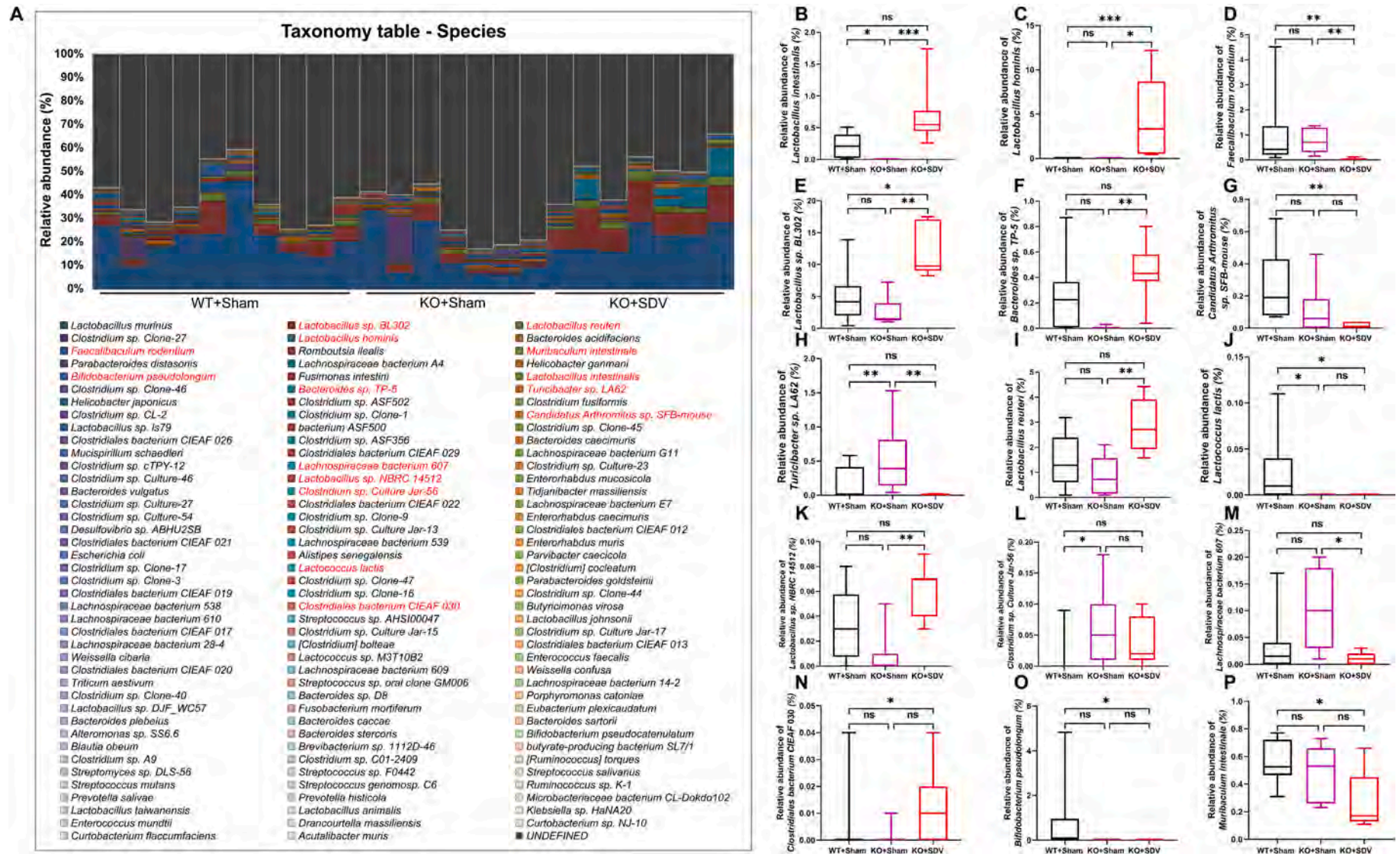


Fig. 6. Effects of bilateral SDV on gut microbiota at the species levels.

(A): Gut bacteria composition at the species level in the three groups. (B): Relative abundance of the species *Lactobacillus intestinalis* (Kruskal-Wallis test, $P = 0.0001$). (C): Relative abundance of the species *Lactobacillus hominis* (Kruskal-Wallis test, $P = 0.0002$). (D): Relative abundance of the species *Faecalibacterium rodentium* (Kruskal-Wallis test, $P = 0.0009$). (E): Relative abundance of the species *Lactobacillus sp. BL302* (Kruskal-Wallis test, $P = 0.0012$). (F): Relative abundance of the species *Bacteroides sp. TP-5* (Kruskal-Wallis test, $P = 0.0018$). (G): Relative abundance of the species *Candidatus Arthromitus sp. SFB-mouse* (Kruskal-Wallis test, $P = 0.0023$). (H): Relative abundance of the species *Turicibacter sp. LA62* (Kruskal-Wallis test, $P = 0.0030$). (I): Relative abundance of the species *Lactobacillus reuteri* (Kruskal-Wallis test, $P = 0.0047$). (J): Relative abundance of the species *Lactococcus lactis* (Kruskal-Wallis test, $P = 0.0053$). (K): Relative abundance of the species *Lactobacillus sp. NBRC 14512* (Kruskal-Wallis test, $P = 0.0088$). (L): Relative abundance of the species *Clostridium sp. Culture Jar-56* (Kruskal-Wallis test, $P = 0.0155$). (M): Relative abundance of the species *Lachnospiraceae bacterium 607* (Kruskal-Wallis test, $P = 0.0155$). (N): Relative abundance of the species *Clostridiales bacterium CIEAF 030* (Kruskal-Wallis test, $P = 0.0214$). (O): Relative abundance of the species *Bifidobacterium pseudolongum* (Kruskal-Wallis test, $P = 0.0245$). (P): Relative abundance of the species *Muribaculum intestinale* (Kruskal-Wallis test, $P = 0.0395$). For all box plots, the middle line in the box addresses the median, the box addresses the interquartile range, and the whisker addresses the most extreme and least values. * $P < 0.05$; ** $P < 0.01$; *** $P < 0.001$. ns: not significant.

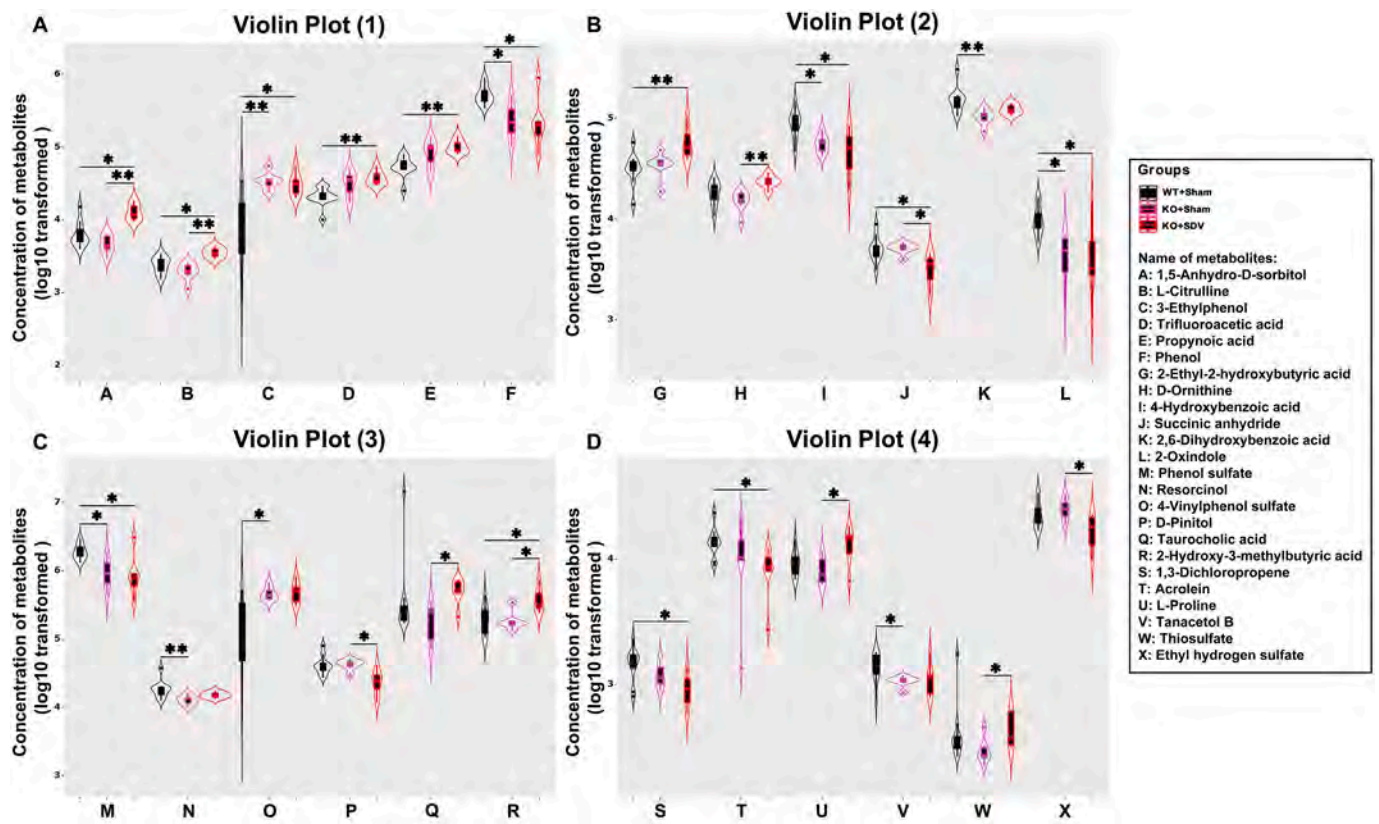


Fig. 7. Effect of bilateral SDV on plasma metabolites.

(A): Violin plot showing the changes of 6 kinds of metabolites [1,5-anhydro-D-sorbitol (Kruskal-Wallis test, $P = 0.0016$), L-citrulline (Kruskal-Wallis test, $P = 0.0018$), 3-ethylphenol (Kruskal-Wallis test, $P = 0.0019$), trifluoroacetic acid (Kruskal-Wallis test, $P = 0.0046$), propynoic acid (Kruskal-Wallis test, $P = 0.0046$), phenol (Kruskal-Wallis test, $P = 0.0055$)] among the three groups. (B): Violin plot showing the changes of 6 kinds of metabolites [2-ethyl-2-hydroxybutyric acid (Kruskal-Wallis test, $P = 0.0059$), D-ornithine (Kruskal-Wallis test, $P = 0.0065$), 4-hydroxybenzoic acid (Kruskal-Wallis test, $P = 0.0077$), succinic anhydride (Kruskal-Wallis test, $P = 0.0078$), 2,6-dihydroxybenzoic acid (Kruskal-Wallis test, $P = 0.0080$), 2-oxindole (Kruskal-Wallis test, $P = 0.0080$)] among the three groups. (C): Violin plot showing the changes of 6 kinds of metabolites [phenol sulfate (Kruskal-Wallis test, $P = 0.0080$), resorcinol (Kruskal-Wallis test, $P = 0.0111$), 4-vinylphenol sulfate (Kruskal-Wallis test, $P = 0.0113$), D-pinitol (Kruskal-Wallis test, $P = 0.0122$), taurocholic acid (Kruskal-Wallis test, $P = 0.0129$), 2-hydroxy-3-methylbutyric acid (Kruskal-Wallis test, $P = 0.0145$)] among the three groups. (D): Violin plot showing the changes of 6 kinds of metabolites [1,3-dichloropropene (Kruskal-Wallis test, $P = 0.0203$), acrolein (Kruskal-Wallis test, $P = 0.0209$), L-proline (Kruskal-Wallis test, $P = 0.0245$), tanacetol B (Kruskal-Wallis test, $P = 0.0321$), thiosulfate (Kruskal-Wallis test, $P = 0.0436$), ethyl hydrogen sulfate (Kruskal-Wallis test, $P = 0.0460$)] among the three groups. The X-axis using the letter symbol representing the names of different plasma metabolites, and the Y-axis represents the concentration of various plasma metabolites after log10 transformation. * $P < 0.05$; ** $P < 0.01$; Different colors of violin plots represent the corresponding groups.

factor for the differential expression of structural similarity in microbial communities. We reported that LPS significantly decreased α -diversity and relative abundance of gut microbiota in mice, and that SDV did not cause LPS-induced alterations in α -diversity and relative abundance of gut microbiota in mice (Zhang et al., 2020), suggesting that LPS could cause depression-like behaviors in mice through gut–microbiota–brain axis via subdiaphragmatic vagus nerve. Furthermore, SDV blocked depression-like behaviors in mice after FMT from mice with depression-like behaviors (Pu et al., 2021b; Wang et al., 2020a; Wang et al., 2021). McVey Neufeld et al. (2019) reported that oral treatment with selective serotonin reuptake inhibitor (SSRI: fluoxetine or sertraline) leads to a significant increase in vagal fiber activity, and that blocking vagal signaling from the gut to the brain via SDV abolished antidepressant-like effect of SSRI, suggesting the role of vagus nerve dependent gut–brain axis in the antidepressant effects of SSRIs. From the current data, it is unclear whether subdiaphragmatic vagus nerve is responsible for depression-like phenotypes of *Chrna7* KO mice. A recent study demonstrated that SDV or genetic knock-out of $\alpha 7$ nAChRs abolished the anti-inflammatory actions of famotidine (a histamine 2 receptor antagonist) in mice with LPS-treated cytokine stream (Yang et al., 2022a), suggesting a role of vagus nerve anti-inflammation via $\alpha 7$ nAChRs. Given the crucial role of $\alpha 7$ nAChRs on vagus nerve inflammatory actions

(O'Mahony et al., 2009; Yang et al., 2022a), it is possible that subdiaphragmatic vagus nerve may be responsible for depression-like phenotypes of *Chrna7* KO mice. Taken together, it is likely that gut–microbiota–brain axis via subdiaphragmatic vagus nerve plays an important role in depression-like phenotypes of *Chrna7* KO mice.

At the phylum level, the most abundant phylum *Firmicutes* was significantly increased in KO + SDV group compared to other two groups, suggesting that subdiaphragmatic vagus nerve may affect relative abundance of *Firmicutes* in gastrointestinal tract. At the species level, the relative abundance of *Lactobacillus intestinalis* and *Lactobacillus* sp. BL302 in KO + SDV group was higher than that of KO + sham group. Furthermore, network analysis showed that these two bacteria were correlated with depression-like phenotypes and reduced synaptic proteins, suggesting a role of these two bacteria in depression. In contrast, the relative abundance of *Turicibacter* sp. LA62 in KO + SDV group was lower than that of KO + sham group. A network analysis showed that *Turicibacter* sp. LA62 was also correlated with depression-like phenotypes and reduced synaptic proteins. Collectively, it seems that *Lactobacillus intestinalis*, *Lactobacillus* sp. BL302, and *Turicibacter* sp. LA62 might be associated with depression-like phenotypes although further study is needed.

Using untargeted metabolomics analysis, we found that plasma

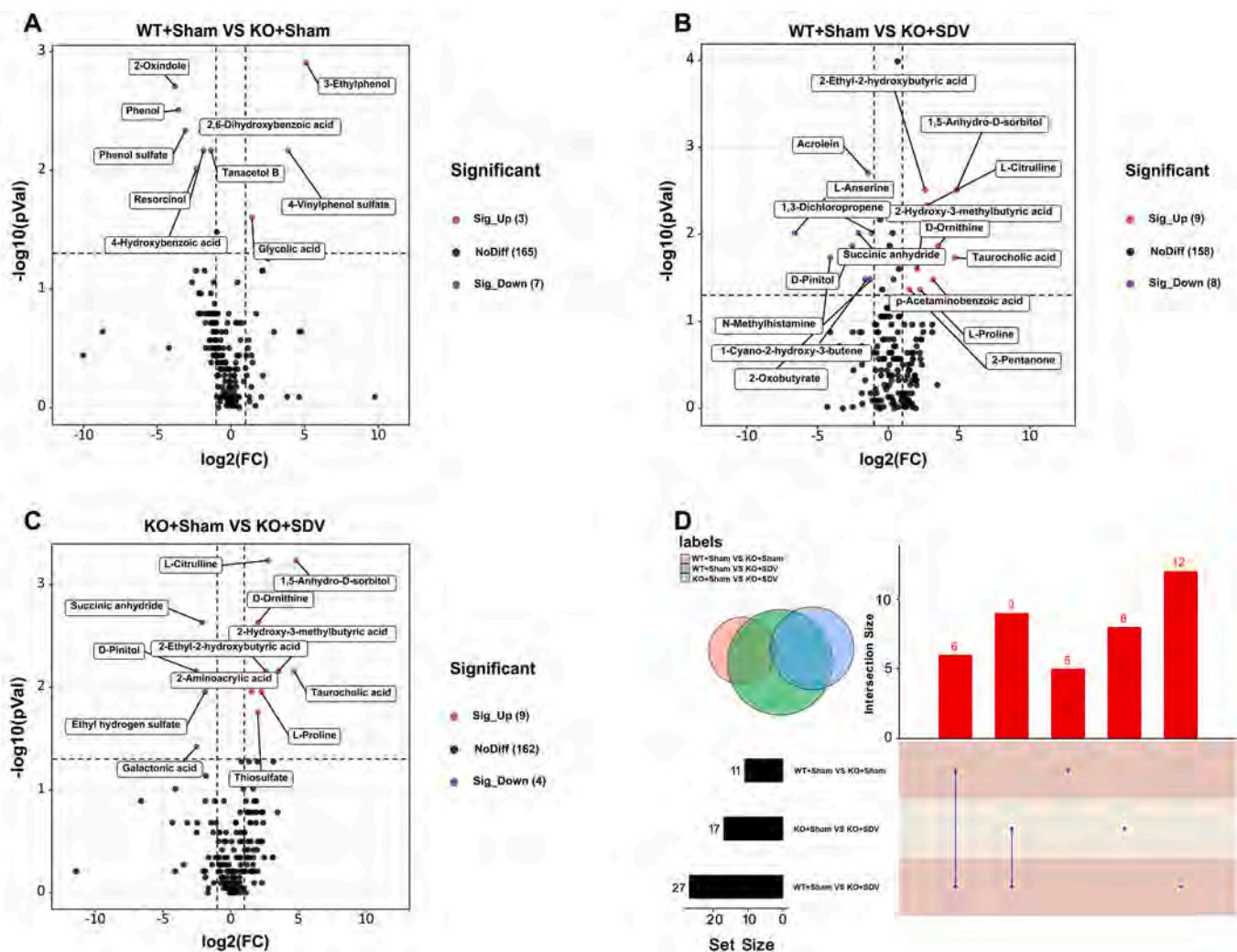


Fig. 8. Differences of plasma metabolites between different experimental groups.

(A): Volcano plot indicating that 3 annotation metabolites were significantly up-regulated, 7 annotation metabolites were significantly down-regulated and 165 annotation metabolites were no differences when comparing the WT + sham group with the KO + sham group. (B): Volcano plot indicating that 9 annotation metabolites were significantly up-regulated, 8 annotation metabolites were significantly down-regulated and 158 annotation metabolites were no differences when comparing the WT + sham group with the KO + SDV group. (C): Volcano plot indicating that 9 annotation metabolites were significantly up-regulated, 4 annotation metabolites were significantly down-regulated and 162 annotation metabolites were no differences when comparing the KO + sham group with the KO + SDV group. The X-axis represents the log₂-transformed values of the FC of plasma metabolite concentration, and the Y-axis represents the -log₁₀-transformed values of P value using the Wilcoxon rank sum test. The horizontal dotted line indicates P = 0.05 and the vertical dotted line indicates FC = ± 2. Metabolites with up-regulated, down-regulated, and no difference were marked in red, purple, and black respectively. (D): UpSet plot listed out that there were 11 kinds of annotated metabolites with statistical differences between the KO + sham group and the KO + SDV group, and 27 kinds of annotated metabolites with statistical differences between the WT + sham group and the KO + SDV group by using the Wilcoxon rank sum test (P < 0.05). In addition, 6 kinds of annotated metabolites showed significant differences between the WT + Sham group and the KO + sham group and between the WT + sham group and the KO + SDV group, and 9 kinds of annotated metabolites showed significant differences between the KO + sham group and the KO + SDV group and between the WT + sham group and the KO + SDV group. Besides, 5 kinds of annotated metabolites showed significant differences only between the WT + sham group and the KO + sham group, 8 kinds of annotated metabolites showed significant differences only between the KO + sham group and the KO + SDV group, 12 kinds of annotated metabolites showed significant differences only between the WT + sham group and the KO + SDV group. (For interpretation of the references to colour in this figure legend, the reader is referred to the web version of this article.)

levels of 1,5-anhydro-D-sorbitol (also known as 1,5-anhydro-D-glucitol), L-citrulline, and taurocholic acid in the KO + SDV group were higher than those of KO + sham group. A network analysis showed that 1,5-anhydro-D-sorbitol was negatively correlated with *Faecalibaculum rodentium*, suggesting that *Faecalibaculum rodentium* may be involved in the synthesis of 1,5-anhydro-D-sorbitol. A report showed that low plasma levels of 1,5-anhydro-D-sorbitol are closely associated with impaired peripheral nerve function and diabetic peripheral neuropathy in patients with type 2 diabetes (Xu et al., 2022), suggesting that lower plasma levels of 1,5-anhydro-D-sorbitol may be a risk factor for diabetic

peripheral neuropathy. L-citrulline is a nitrogen end product produced from glutamine through urea cycle. Blood levels of L-citrulline and L-arginine in unmedicated patients with major depressive disorder (MDD) were significantly lower than healthy controls (Hess et al., 2017). MDD patients had a lower NOS (nitric oxide synthase) activity (L-citrulline/L-arginine ratio) than healthy controls at baseline (Loeb et al., 2020). NOS activity in MDD patients increased significantly after antidepressant treatment (Loeb et al., 2020), suggesting a state biomarker for depression. Furthermore, taurocholic acid (conjugation of cholic acid with taurine) was positively correlated with several bacteria including

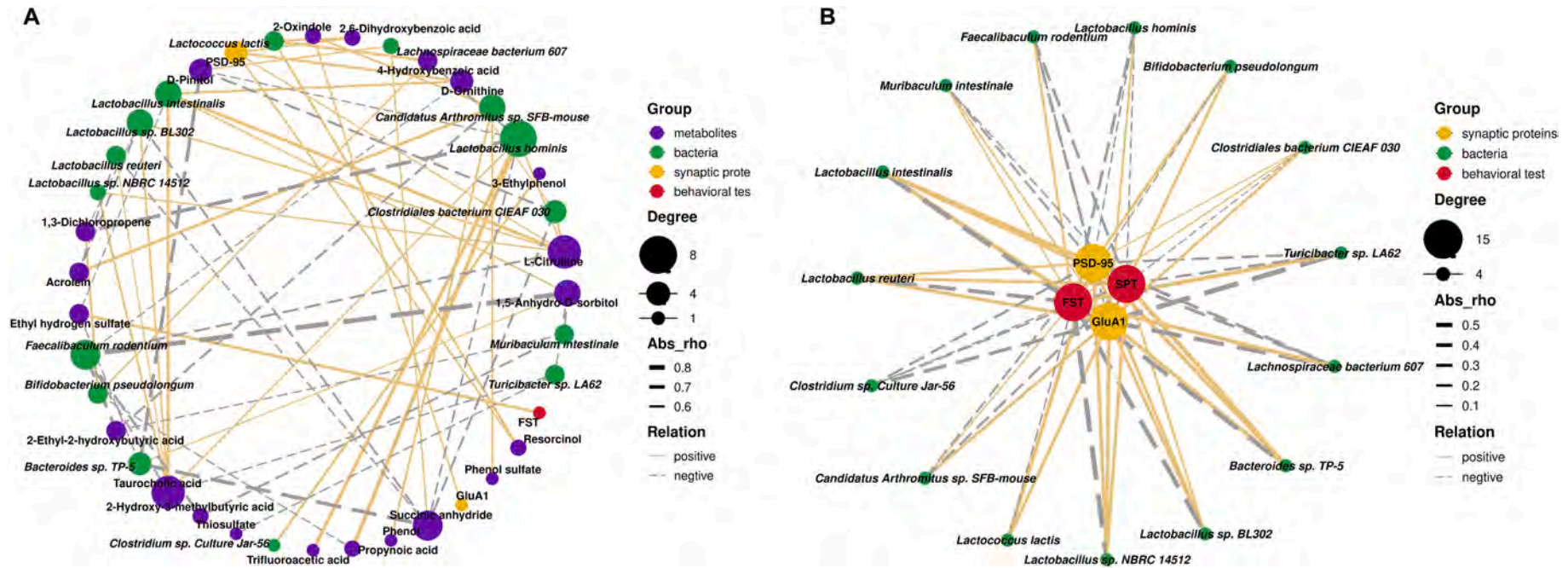


Fig. 9. Correlation network between behavioral data (or synaptic proteins) and microbiota (or metabolites).

(A): A Correlation Network indicating the correlations between the concentrations of plasma metabolites and the gut microbiota at the species level, the results of the behavioral test and the expression of synaptic proteins of mPFC (The threshold was set as $P < 0.05$ and the absolute value of $R \geq 0.5$). The different colors of nodes represent different groups. The sizes of node gradients represent varying degrees of correlation. The thickness of the line represents the absolute value of the correlation coefficient. Solid lines represent positive correlations, dotted lines represent negative correlations). (B): A Correlation Network showed correlations between the relative abundance of gut bacteria at the species level and the results of the behavioral test and the expression of synaptic proteins of mPFC (The threshold was set as $P < 0.05$. The different colors of nodes represent different groups. The sizes of node gradients represent varying degrees of correlation. The thickness of the line represents the absolute value of the correlation coefficient. Solid lines represent positive correlations, dotted lines represent negative correlations).

Lactobacillus intestinalis, suggesting that these bacteria may play a role in the production of taurocholic acid, major bile acid. Interestingly, there was a significant difference in blood levels of taurocholic acid between MDD patients and healthy controls (Bai et al., 2021). Given anti-inflammatory role of taurocholic acid, it is possible that higher levels of taurocholic acid may play a role in antidepressant-like effects of SDV in *Chrna7* KO mice. Succinic anhydride was negatively correlated with *Bacteroides* sp. TP-5 which were associated with depression-like phenotypes. Collectively, it is likely that microbes-derived metabolites may play a role in the antidepressant-like effects of SDV in *Chrna7* KO mice.

A network analysis showed that *Lactobacillus intestinalis*, *Lactobacillus reuteri*, *Turicibacter* sp. LA62, and *Bacteroides* sp. TP-5 were correlated with depression-like behaviors. There are no reports showing the role of *Turicibacter* sp. LA62, and *Bacteroides* sp. TP-5 in depression. We reported that oral ingestion of *Lactobacillus intestinalis* and *Lactobacillus reuteri* caused depression-like phenotypes in antibiotic-treated mice through gut–microbiota–brain axis via subdiaphragmatic vagus nerve (Wang et al., 2020a). Furthermore, we reported that oral ingestion of *Faecalibaculum rodentium* caused depression-like phenotypes in resilient *Ephx2* KO mice through gut–microbiota–brain axis via subdiaphragmatic vagus nerve (Wang et al., 2021). Furthermore, *Faecalibaculum rodentium* was positively correlated with FST data, and negatively correlated with SPT data. These data suggest that *Faecalibaculum rodentium* might play a role in depression-like phenotypes. Collectively, it is likely that these bacteria might play a role in the antidepressant-like effects of SDV in *Chrna7* KO mice although further study is needed.

This study has the one limitation. The current data of this study do not show a direct role of gut microbiota in depression-like phenotypes of *Chrna7* KO mice although a previous study suggests a role of gut microbiota in depression-like phenotypes of *Chrna7* KO mice (Pu et al., 2021b). Further study to identify specific microbiomes which contribute to depression-like phenotypes of *Chrna7* KO mice is needed.

In conclusion, the current data show that SDV blocked depression-like behaviors and reduced synaptic proteins in the mPFC of *Chrna7* KO mice. Therefore, gut–microbiota–brain axis via subdiaphragmatic vagus nerve plays a role in depression-like phenotypes in *Chrna7* KO mice.

Data and code availability

The 16S rRNA sequencing data has been uploaded and saved in the NCBI Sequence Read Archive and is available at the accession number PRJNA845101.

Ethical statement

The experimental protocol of present study was approved by the Chiba University Institutional Animal Care and Use Committee (Permission number 3-399). The experimental mice were all firstly deeply anesthetized with inhaled isoflurane and then rapidly sacrificed by cervical dislocation. All efforts were made to minimize animals suffering.

CRediT authorship contribution statement

Yong Yang: Investigation, Data curation, Formal analysis, Writing – original draft, Writing – review & editing. **Akifumi Eguchi:** Investigation, Data curation, Formal analysis, Writing – review & editing. **Xiayun Wan:** Investigation, Writing – review & editing. **Lijia Chang:** Investigation, Writing – review & editing. **Xingming Wang:** Investigation, Writing – review & editing. **Younge Qu:** Investigation, Writing – review & editing. **Chisato Mori:** Investigation, Funding acquisition, Writing – review & editing. **Kenji Hashimoto:** Conceptualization, Funding acquisition, Writing – original draft, Writing – review & editing.

Declaration of Competing Interest

Dr. Hashimoto is the inventor of filed patent applications on “The use of *R*-ketamine in the treatment of psychiatric diseases”, “(*S*)-norketamine and salt thereof as pharmaceutical”, “*R*-ketamine and derivative thereof as prophylactic or therapeutic agent for neurodegeneration disease or recognition function disorder”, “Preventive or therapeutic agent and pharmaceutical composition for inflammatory diseases or bone diseases”, and “*R*-ketamine and its derivatives as a preventive or therapeutic agent for a neurodevelopmental disorder” by the Chiba University. Dr. Hashimoto has also received speakers' honoraria, consultant fee, or research support from Abbott, Boehringer Ingelheim, Daiichi-Sankyo, Meiji Seika Pharma, Seikagaku Corporation, Dainippon-Sumitomo, Taisho, Otsuka, Murakami Farm and Perception Neuroscience. Other authors declare no conflict of interest.

Data availability

Data will be made available on request.

Acknowledgements

This study was supported by the grant from Japan Society for the Promotion of Science (to K.H., 21H00184, 21H05612), JST OPERA Program Japan (to C.M JPMJOP1831) and unrestricted grant of Yamada Bee Company, Japan (to C.M). Dr. Yong Yang was supported by the Japan China Sasakawa Medical Fellowship (Tokyo, Japan). Dr. Yong Yang and Ms. Xiayun Wan were supported by the Academic Research & Innovation Management Organization of Chiba University (Chiba, Japan).

References

- Andersson, U., Tracey, K.J., 2012. Reflex principles of immunological homeostasis. *Annu. Rev. Immunol.* 30, 313–335. <https://doi.org/10.1146/annurev-immunol-020711-075015>.
- Bai, S., Xie, J., Bai, H., Tian, T., Zou, T., Chen, J.J., 2021. Gut microbiota-derived inflammation-related serum metabolites as potential biomarkers for major depressive disorder. *J. Inflamm. Res.* 14, 3755–3766. <https://doi.org/10.2147/JIR.S324922>.
- Bartoli, F., Misiak, B., Callovini, T., Cavaleri, D., Cioni, R.M., Crocarno, C., Savitz, J.B., Carrà, G., 2021. The kynurenine pathway in bipolar disorder: a meta-analysis on the peripheral blood levels of tryptophan and related metabolites. *Mol. Psychiatry* 26 (7), 3419–3429. <https://doi.org/10.1038/s41380-020-00913-1>.
- Bonaz, B., Bazin, T., Pellissier, S., 2018. The vagus nerve at the interface of the microbiota-gut-brain axis. *Front. Neurosci.* 12, 49. <https://doi.org/10.3389/fnins.2018.00049>.
- Brydges, C.R., Bhattacharyya, S., Dehkordi, S.M., Milanese, Y., Penninx, B., Jansen, R., Kristal, B.S., Han, X., Arnold, M., Kastenmüller, G., Bekhbat, M., Mayberg, H.S., Craighead, W.E., Rush, A.J., Fiehn, O., Dunlop, B.W., Kaddurah-Daouk, R., Mood Disorders Precision Medicine Consortium, 2022. Metabolomic and inflammatory signatures of symptom dimensions in major depression. *Brain Behav. Immun.* 102, 42–52. <https://doi.org/10.1016/j.bbi.2022.02.003>.
- Caso, J.R., MacDowell, K.S., González-Pinto, A., García, S., de Diego-Adeliño, J., Carceller-Sindreu, M., Sarramea, F., Caballero-Villarraso, J., Gracia-García, P., De la Cámara, C., Agüera, L., Gómez-Lus, M.L., Alba, C., Rodríguez, J.M., Leza, J.C., 2021. Gut microbiota, innate immune pathways, and inflammatory control mechanisms in patients with major depressive disorder. *Transl. Psychiatry* 11 (1), 645. <https://doi.org/10.1038/s41398-021-01755-3>.
- Cawthon, C.R., de La Serre, C.B., 2018. Gut bacteria interaction with vagal afferents. *Brain Res.* 1693, 134–139. <https://doi.org/10.1016/j.brainres.2018.01.012>.
- Chang, L., Wei, Y., Hashimoto, K., 2022. Brain-gut-microbiota axis in depression: a historical overview and future directions. *Brain Res. Bull.* 182, 44–56. <https://doi.org/10.1016/j.brainresbull.2022.02.004>.
- Cryan, J.F., O'Riordan, K.J., Cowan, C.S.M., Sandhu, K.V., Bastiaansen, T.F.S., Boehme, M., Codagnone, M.G., Cusotto, S., Fulling, C., Golubeva, A.V., Guzzetta, K. E., Jaggard, M., Long-Smith, C.M., Lyte, J.M., Martin, J.A., Molinero-Perez, A., Moloney, G., Morelli, E., Morillas, E., O'Connor, R., Cruz-Pereira, J.S., Peterson, V.L., Rea, K., Ritz, N.L., Sherwin, E., Spichak, S., Teichman, E.M., van de Wouw, M., Ventura-Silva, A.P., Wallace-Fitzsimons, S.E., Hyland, N., Clarke, G., Dinan, T.G., 2019. The microbiota-gut-brain axis. *Physiol. Rev.* 99 (4), 1877–2013. <https://doi.org/10.1152/physrev.00018.2018>.
- Dani, J.A., 2015. Neuronal nicotinic acetylcholine receptor structure and function and response to nicotine. *Int. Rev. Neurobiol.* 124, 3–19. <https://doi.org/10.1016/bs.inr.2015.07.001>.

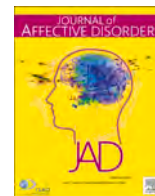
- Dani, J.A., Bertrand, D., 2007. Nicotinic acetylcholine receptors and nicotinic cholinergic mechanisms of the central nervous system. *Annu. Rev. Pharmacol. Toxicol.* 47, 699–729. <https://doi.org/10.1146/annurev.pharmtox.47.120505.105214>.
- Forsythe, P., Bienenstock, J., Kunze, W.A., 2014. Vagal pathways for microbiome-brain-gut axis communication. *Adv. Exp. Med. Biol.* 817, 115–133. https://doi.org/10.1007/978-1-4939-0897-4_5.
- Haroon, E., Raison, C.L., Miller, A.H., 2012. Psychoneuroimmunology meets neuropsychopharmacology: translational implications of the impact of inflammation on behavior. *Neuropsychopharmacology*. 37 (1), 137–162. <https://doi.org/10.1038/npp.2011.205>.
- Hashimoto, K., 2009. Emerging role of glutamate in the pathophysiology of major depressive disorder. *Brain Res. Rev.* 61 (2), 105–123. <https://doi.org/10.1016/j.brainresrev.2009.05.005>.
- Hashimoto, K., 2015. Inflammatory biomarkers as differential predictors of antidepressant response. *Int. J. Mol. Sci.* 16 (4), 7796–7801. <https://doi.org/10.3390/ijms16047796>.
- Hashimoto, K., 2020. Molecular mechanisms of the rapid-acting and long-lasting antidepressant actions of (R)-ketamine. *Biochem. Pharmacol.* 177, 113935 <https://doi.org/10.1016/j.bcp.2020.113935>.
- Hashimoto, K., 2022. Gut–microbiota–brain by bile acids in depression. *Psychiatry Clin. Neurosci.* 76 (7), 281. <https://doi.org/10.1111/pcn.13370>.
- Hess, S., Baker, G., Gyenes, G., Tsuyuki, R., Newman, S., Le Melleo, J.M., 2017. Decreased serum L-arginine and L-citrulline levels in major depression. *Psychopharmacology* 234 (21), 3241–3247. <https://doi.org/10.1007/s00213-017-4712-8>.
- Huang, N., Hua, D., Zhan, G., Li, S., Zhu, B., Jiang, R., Yang, L., Bi, J., Xu, H., Hashimoto, K., Luo, A., Yang, C., 2019. Role of *Actinobacteria* and *Coriobacteriia* in the antidepressant effects of ketamine in an inflammation model of depression. *Pharmacol. Biochem. Behav.* 176, 93–100. <https://doi.org/10.1016/j.pbb.2018.12.001>.
- Jiang, H., Ling, Z., Zhang, Y., Mao, H., Ma, Z., Yin, Y., Wang, W., Tang, W., Tan, Z., Shi, J., Li, L., Ruan, B., 2015. Altered fecal microbiota composition in patients with major depressive disorder. *Brain Behav. Immun.* 48, 186–194. <https://doi.org/10.1016/j.bbi.2015.03.016>.
- Kelly, J.R., Borre, Y., O'Brien, C., Patterson, E., El Aidy, S., Deane, J., Kennedy, P.J., Beers, S., Scott, K., Moloney, G., Hoban, A.E., Scott, L., Fitzgerald, P., Ross, P., Stanton, C., Clarke, G., Cryan, J.F., Dinan, T.G., 2016. Transferring the blues: depression-associated gut microbiota induces neurobehavioural changes in the rat. *J. Psychiatr. Res.* 82, 109–118. <https://doi.org/10.1016/j.jpsychires.2016.07.019>.
- Lei, W., Duan, Z., 2021. Advances in the treatment of cholinergic anti-inflammatory pathways in gastrointestinal diseases by electrical stimulation of vagus nerve. *Digestion* 102 (2), 128–138. <https://doi.org/10.1159/000504474>.
- Li, Z., Lai, J., Zhang, P., Ding, J., Jiang, J., Liu, C., Huang, H., Zhen, H., Xi, C., Sun, Y., Wu, L., Wang, L., Gao, X., Li, Y., Fu, Y., Jie, Z., Li, S., Zhang, D., Chen, Y., Zhu, Y., Lu, S., Lu, J., Wang, D., Zhou, H., Yuan, X., Li, X., Pang, L., Huang, M., Yang, H., Zhang, W., Brix, S., Kristiansen, K., Song, X., Nie, C., Hu, S., 2022. Multi-omics analyses of serum metabolome, gut microbiome and brain function reveal dysregulated microbiota-gut-brain axis in bipolar depression. *Mol. Psychiatry*. <https://doi.org/10.1038/s41380-022-01569-9>.
- Liu, J.J., Wei, Y.B., Strawbridge, R., Bao, Y., Chang, S., Shi, L., Que, J., Gadad, B.S., Trivedi, M.H., Kelseo, J.R., Lu, L., 2020. Peripheral cytokine levels and response to antidepressant treatment in depression: a systematic review and meta-analysis. *Mol. Psychiatry* 25 (2), 339–350. <https://doi.org/10.1038/s41380-019-0474-5>.
- Loeb, E., El Asmar, K., Trabado, S., Gressier, F., Colle, R., Rigal, A., Martin, S., Verstuylt, C., Fève, B., Chanson, P., Becquomont, L., Corruble, E., 2020. Nitric oxide synthase activity in major depressive episodes before and after antidepressant treatment: results of a large case-control treatment study. *Psychol. Med.* 1–10. <https://doi.org/10.1017/S0033291720001749>.
- Lucido, M.J., Bekhbat, M., Goldsmith, D.R., Treadway, M.T., Haroon, E., Felger, J.C., Miller, A.H., 2021. Aiding and abetting anhedonia: impact of inflammation on the brain and pharmacological implications. *Pharmacol. Rev.* 73 (3), 1084–1117. <https://doi.org/10.1124/pharmrev.120.000043>.
- Mac Giollabhui, N., Ng, T.H., Ellman, L.M., Alloy, L.B., 2021. The longitudinal associations of inflammatory biomarkers and depression revisited: systematic review, meta-analysis, and meta-regression. *Mol. Psychiatry* 26 (7), 3302–3314. <https://doi.org/10.1038/s41380-020-00867-4>.
- Martelli, D., McKinley, M.J., McAllen, R.M., 2014. The cholinergic anti-inflammatory pathway: a critical review. *Auton. Neurosci.* 182, 65–69. <https://doi.org/10.1016/j.autneu.2013.12.007>.
- McVey Neufeld, K.A., Bienenstock, J., Bharwani, A., Champagne-Jorgensen, K., Mao, Y., West, C., Liu, Y., Surette, M.G., Kunze, W., Forsythe, P., 2019. Oral selective serotonin reuptake inhibitors activate vagus nerve dependent gut-brain signalling. *Sci. Rep.* 9 (1), 14290. <https://doi.org/10.1038/s41598-019-50807-8>.
- Miller, A.H., Raison, C.L., 2016. The role of inflammation in depression: from evolutionary imperative to modern treatment target. *Nat. Rev. Immunol.* 16 (1), 22–34. <https://doi.org/10.1038/nri.2015.5>.
- Nikolova, V.L., Hall, M.R.B., Hall, L.J., Cleare, A.J., Stone, J.M., Young, A.H., 2021. Perturbations in gut microbiota composition in psychiatric disorders: a review and meta-analysis. *JAMA Psychiatry* 78 (12), 1343–1354. <https://doi.org/10.1001/jamapsychiatry.2021.2573>.
- Olofsson, P.S., Rosas-Ballina, M., Levine, Y.A., Tracey, K.J., 2012. Rethinking inflammation: neural circuits in the regulation of immunity. *Immunol. Rev.* 248 (1), 188–204. <https://doi.org/10.1111/j.1600-065X.2012.01138.x>.
- O'Mahony, C., van der Kleij, H., Bienenstock, J., Shanahan, F., O'Mahony, L., 2009. Loss of vagal anti-inflammatory effect: in vivo visualization and adoptive transfer. *Am. J. Physiol. Regul. Integr. Comp. Physiol.* 297 (4), R1118–R1126. <https://doi.org/10.1152/ajpregu.90904.2008>.
- Park, A.J., Collins, J., Blennerhassett, P.A., Ghia, J.E., Verdu, E.F., Bercik, P., Collins, S.M., 2013. Altered colonic function and microbiota profile in a mouse model of chronic depression. *Neurogastroenterol. Motil.* 25 (9), 733–e575. <https://doi.org/10.1111/nmo.12153>.
- Piovesana, R., Salazar Intriago, M.S., Dini, L., Tata, A.M., 2021. Cholinergic modulation of neuroinflammation: focus on $\alpha 7$ nicotinic receptor. *Int. J. Mol. Sci.* 22 (9), 4912. <https://doi.org/10.3390/ijms22094912>.
- Pu, J., Liu, Y., Zhang, H., Tian, L., Gui, S., Yu, Y., Chen, X., Chen, Y., Yang, L., Ran, Y., Zhong, X., Xu, S., Song, X., Liu, L., Zheng, P., Wang, H., Xie, P., 2021a. An integrated meta-analysis of peripheral blood metabolites and biological functions in major depressive disorder. *Mol. Psychiatry* 26 (8), 4265–4276. <https://doi.org/10.1038/s41380-020-0645-4>.
- Pu, Y., Tan, Y., Qu, Y., Chang, L., Wang, S., Wei, Y., Wang, X., Hashimoto, K., 2021b. A role of the subdiaphragmatic vagus nerve in depression-like phenotypes in mice after fecal microbiota transplantation from *Chrm7* knock-out mice with depression-like phenotypes. *Brain Behav. Immun.* 94, 318–326. <https://doi.org/10.1016/j.bbi.2020.12.032>.
- Pu, Y., Zhang, Q., Tang, Z., Lu, C., Wu, L., Zhong, Y., Chen, Y., Hashimoto, K., Luo, Y., Liu, Y., 2022. Fecal microbiota transplantation from patients with rheumatoid arthritis causes depression-like behaviors in mice through abnormal T cells activation. *Transl. Psychiatry* 12 (1), 223. <https://doi.org/10.1038/s41398-022-01993-z>.
- Qu, Y., Yang, C., Ren, Q., Ma, M., Dong, C., Hashimoto, K., 2017. Comparison of (R)-ketamine and lanicemine on depression-like phenotype and abnormal composition of gut microbiota in a social defeat stress model. *Sci. Rep.* 7 (1), 15725. <https://doi.org/10.1038/s41598-017-16060-7>.
- Sanada, K., Nakajima, S., Kurokawa, S., Barceló-Soler, A., Ikuse, D., Hirata, A., Yoshizawa, A., Tomizawa, Y., Salas-Valero, M., Noda, Y., Mimura, M., Iwanami, A., Kishimoto, T., 2020. Gut microbiota and major depressive disorder: a systematic review and meta-analysis. *J. Affect. Disord.* 266, 1–13. <https://doi.org/10.1016/j.jad.2020.01.102>.
- Schymanski, E.L., Jeon, J., Gulde, R., Fenner, K., Ruff, M., Singer, H.P., Hollender, J., 2014. Identifying small molecules via high resolution mass spectrometry: communicating confidence. *Environ. Sci. Technol.* 48 (4), 2097–2098. <https://doi.org/10.1021/es5002105>.
- Segata, N., Izard, J., Waldron, L., Gevers, D., Miropolsky, L., Garrett, W.S., Huttenhower, C., 2011. Metagenomic biomarker discovery and explanation. *Genome Biol.* 12 (6), R60. <https://doi.org/10.1186/gb-2011-12-6-r60>.
- Shan, J., Hashimoto, K., 2022. Soluble epoxide hydrolase as a therapeutic target for neuropsychiatric disorders. *Int. J. Mol. Sci.* 23 (9), 4951. <https://doi.org/10.3390/ijms23094951>.
- Toenders, Y.J., Laskaris, L., Davey, C.G., Berk, M., Milanese, Y., Lamers, F., Penninx, B.W.J.H., Schmaal, L., 2022. Inflammation and depression in young people: a systematic review and proposed inflammatory pathways. *Mol. Psychiatry* 27 (1), 315–327. <https://doi.org/10.1038/s41380-021-01306-8>.
- Tran, S.M., Mohajeri, M.H., 2021. The role of gut bacterial metabolites in brain development, aging and disease. *Nutrients* 13 (3), 732. <https://doi.org/10.3390/nu13030732>.
- Tsugawa, H., Cajka, T., Kind, T., Ma, Y., Higgins, B., Ikeda, K., Kanazawa, M., VanderGheynst, J., Fiehn, O., Arita, M., 2015. MS-DIAL: data-independent MS/MS deconvolution for comprehensive metabolome analysis. *Nat. Methods* 12 (6), 523–526. <https://doi.org/10.1038/nmeth.3393>.
- Ulloa, L., 2005. The vagus nerve and the nicotinic anti-inflammatory pathway. *Nat. Rev. Drug Discov.* 4 (8), 673–684. <https://doi.org/10.1038/nrd1797>.
- Wan, X., Eguchi, A., Fujita, Y., Ma, L., Wang, X., Yang, Y., Qu, Y., Chang, L., Zhang, J., Mori, C., Hashimoto, K., 2022a. Effects of (R)-ketamine on reduced bone mineral density in ovariectomized mice: a role of gut microbiota. *Neuropharmacol.* 213, 109139. <https://doi.org/10.1016/j.neuropharm.2022.109139>.
- Wan, X., Eguchi, A., Qu, Y., Yang, Y., Chang, L., Shan, J., Mori, C., Hashimoto, K., 2022b. Gut–microbiota–brain axis in the vulnerability to psychosis in adulthood after repeated cannabis exposure during adolescence. *Eur. Arch. Psychiatry Clin. Neurosci.* 272 (7), 1297–1309. <https://doi.org/10.1007/s00406-022-01437-1>.
- Wang, H., Yu, M., Ochani, M., Amella, C.A., Tanovic, M., Susarla, S., Li, J.H., Wang, H., Yang, H., Ulloa, L., Al-Abed, Y., Czura, C.J., Tracey, K.J., 2003. Nicotinic acetylcholine receptor $\alpha 7$ subunit is an essential regulator of inflammation. *Nature*. 421 (6921), 384–388. <https://doi.org/10.1038/nature01339>.
- Wang, S., Ishima, T., Zhang, J., Qu, Y., Chang, L., Pu, Y., Fujita, Y., Tan, Y., Wang, X., Hashimoto, K., 2020a. Ingestion of *Lactobacillus intestinalis* and *Lactobacillus reuteri* causes depression- and anhedonia-like phenotypes in antibiotic-treated mice via the vagus nerve. *J. Neuroinflammation* 17 (1), 241. <https://doi.org/10.1186/s12974-020-01916-z>.
- Wang, S., Qu, Y., Chang, L., Pu, Y., Zhang, K., Hashimoto, K., 2020b. Antibiotic-induced microbiome depletion is associated with resilience in mice after chronic social defeat stress. *J. Affect. Disord.* 260, 448–457. <https://doi.org/10.1016/j.jad.2019.09.064>.
- Wang, S., Ishima, T., Qu, Y., Shan, J., Chang, L., Wei, Y., Zhang, J., Pu, Y., Fujita, Y., Tan, Y., Wang, X., Ma, L., Wan, X., Hammock, B.D., Hashimoto, K., 2021. Ingestion of *Faecalibaculum rodentium* causes depression-like phenotypes in resilient *Ephx2* knock-out mice: a role of brain-gut-microbiota axis via the subdiaphragmatic vagus nerve. *J. Affect. Disord.* 292, 565–573. <https://doi.org/10.1016/j.jad.2021.06.006>.
- Wei, Y., Chang, L., Hashimoto, K., 2022a. Molecular mechanisms underlying the antidepressant actions of arketamine: beyond the NMDA receptor. *Mol. Psychiatry* 27 (1), 559–573. <https://doi.org/10.1038/s41380-021-01121-1>.

- Wei, Y., Wang, T., Liao, L., Fan, X., Chang, L., Hashimoto, K., 2022b. Brain-spleen axis in health and diseases: a review and future perspective. *Brain Res. Bull.* 182, 130–140. <https://doi.org/10.1016/j.brainresbull.2022.02.008>.
- WHO, 2021. Depression. <https://www.who.int/news-room/fact-sheets/default/depression>.
- Wong, M.L., Inserra, A., Lewis, M.D., Mastronardi, C.A., Leong, L., Choo, J., Kentish, S., Xie, P., Morrison, M., Wesselingh, S.L., Rogers, G.B., Licinio, J., 2016. Inflammasome signaling affects anxiety- and depressive-like behavior and gut microbiome composition. *Mol. Psychiatry* 21 (6), 797–805. <https://doi.org/10.1038/mp.2016.46>.
- Wu, Y.J., Wang, L., Ji, C.F., Gu, S.F., Yin, Q., Zuo, J., 2021. The role of $\alpha 7$ nAChR-mediated cholinergic anti-inflammatory pathway in immune cells. *Inflammation*. 44 (3), 821–834. <https://doi.org/10.1007/s10753-020-01396-6>.
- Xu, F., Zhao, L.H., Wang, X.H., Wang, C.H., Yu, C., Zhang, X.L., Ning, L.Y., Huang, H.Y., Su, J.B., Wang, X.Q., 2022. Plasma 1,5-anhydro-D-glucitol is associated with peripheral nerve function and diabetic peripheral neuropathy in patients with type 2 diabetes and mild-to-moderate hyperglycemia. *Diabetol. Metab. Syndr.* 14 (1), 24. <https://doi.org/10.1186/s13098-022-00795-z>.
- Yang, C., Shirayama, Y., Zhang, J.C., Ren, Q., Yao, W., Ma, M., Dong, C., Hashimoto, K., 2015. R-ketamine: a rapid-onset and sustained antidepressant without psychotomimetic side effects. *Transl. Psychiatry* 5 (9), e632. <https://doi.org/10.1038/tp.2015.136>.
- Yang, C., Qu, Y., Fujita, Y., Ren, Q., Ma, M., Dong, C., Hashimoto, K., 2017. Possible role of the gut microbiota-brain axis in the antidepressant effects of (R)-ketamine in a social defeat stress model. *Transl. Psychiatry* 7 (12), 1294. <https://doi.org/10.1038/s41398-017-0031-4>.
- Yang, C., Fang, X., Zhan, G., Huang, N., Li, S., Bi, J., Jiang, R., Yang, L., Miao, L., Zhu, B., Luo, A., Hashimoto, K., 2019. Key role of gut microbiota in anhedonia-like phenotype in rodents with neuropathic pain. *Transl. Psychiatry* 9 (1), 57. <https://doi.org/10.1038/s41398-019-0379-8>.
- Yang, H., George, S.J., Thompson, D.A., Silverman, H.A., Tsaava, T., Tynan, A., Pavlov, V.A., Chang, E.H., Andersson, U., Brines, M., Chavan, S.S., Tracey, K.J., 2022a. Famotidine activates the vagus nerve inflammatory reflex to attenuate cytokine storm. *Mol. Med.* 28 (1), 57. <https://doi.org/10.1186/s10020-022-00483-8>.
- Yang, Y., Ishima, T., Wan, X., Wei, Y., Chang, L., Zhang, J., Qu, Y., Hashimoto, K., 2022b. Microglial depletion and abnormalities in gut microbiota composition and short-chain fatty acids in mice after repeated administration of colony stimulating factor 1 receptor inhibitor PLX5622. *Eur. Arch. Psychiatry Clin. Neurosci.* 272 (3), 483–495. <https://doi.org/10.1007/s00406-021-01325-0>.
- Zhang, J.C., Wu, J., Fujita, Y., Yao, W., Ren, Q., Yang, C., Li, S.X., Shirayama, Y., Hashimoto, K., 2014. Antidepressant effects of TrkB ligands on depression-like behavior and dendritic changes in mice after inflammation. *Int. J. Neuropsychopharmacol.* 18 (4), pyu077. <https://doi.org/10.1093/ijnp/pyu077>.
- Zhang, J.C., Yao, W., Hashimoto, K., 2016a. Brain-derived neurotrophic factor (BDNF)-TrkB signaling in inflammation-related depression and potential therapeutic targets. *Curr. Neuropharmacol.* 14 (7), 721–731. <https://doi.org/10.2174/1570159x146666160119094646>.
- Zhang, J.C., Yao, W., Ren, Q., Yang, C., Dong, C., Ma, M., Wu, J., Hashimoto, K., 2016b. Depression-like phenotype by deletion of $\alpha 7$ nicotinic acetylcholine receptor: role of BDNF-TrkB in nucleus accumbens. *Sci. Rep.* 6, 36705. <https://doi.org/10.1038/srep36705>.
- Zhang, J.C., Yao, W., Dong, C., Ren, Q., Ma, M., Hashimoto, K., 2017. Blockade of interleukin-6 receptor in the periphery promotes rapid and sustained antidepressant actions: a possible role of gut-microbiota-brain axis. *Transl. Psychiatry* 7 (5), e1138. <https://doi.org/10.1038/tp.2017.112>.
- Zhang, K., Fujita, Y., Chang, L., Qu, Y., Pu, Y., Wang, S., Shirayama, Y., Hashimoto, K., 2019. Abnormal composition of gut microbiota is associated with resilience versus susceptibility to inescapable electric stress. *Transl. Psychiatry* 9 (1), 231. <https://doi.org/10.1038/s41398-019-0571-x>.
- Zhang, J., Ma, L., Chang, L., Pu, Y., Qu, Y., Hashimoto, K., 2020. A key role of the subdiaphragmatic vagus nerve in the depression-like phenotype and abnormal composition of gut microbiota in mice after lipopolysaccharide administration. *Transl. Psychiatry* 10 (1), 186. <https://doi.org/10.1038/s41398-020-00878-3>.
- Zheng, P., Zeng, B., Zhou, C., Liu, M., Fang, Z., Xu, X., Zeng, L., Chen, J., Fan, S., Du, X., Zhang, X., Yang, D., Yang, Y., Meng, H., Li, W., Melgiri, N.D., Licinio, J., Wei, H., Xie, P., 2016. Gut microbiome remodeling induces depressive-like behaviors through a pathway mediated by the host's metabolism. *Mol. Psychiatry* 21 (6), 786–796. <https://doi.org/10.1038/mp.2016.44>.



Contents lists available at ScienceDirect

Journal of Affective Disorders

journal homepage: www.elsevier.com/locate/jad

Research paper

Depression-like phenotypes in mice with hepatic ischemia/reperfusion injury: A role of gut–microbiota–liver–brain axis via vagus nerve

Yong Yang^{a,b}, Akifumi Eguchi^c, Xiayun Wan^a, Chisato Mori^{c,d}, Kenji Hashimoto^{a,*}^a Division of Clinical Neuroscience, Chiba University Center for Forensic Mental Health, Chiba 260-8670, Japan^b Department of Neurosurgery, Guizhou Provincial People's Hospital, Guiyang 550002, China^c Department of Sustainable Health Science, Chiba University Center for Preventive Medical Sciences, Chiba 263-8522, Japan^d Department of Bioenvironmental Medicine, Graduate School of Medicine, Chiba University, Chiba 260-8670, Japan

ARTICLE INFO

Keywords:

Arketamine
Depression
Gut microbiota
Liver
Metabolites
Vagus nerve

ABSTRACT

Depression is a frequent symptom in patients with chronic liver disease; however, the mechanisms underlying this association remain unclear. Dysbiosis of gut microbiota plays a critical role in depression through the gut–brain axis via the vagus nerve. In this study, we investigated whether the gut–microbiota–liver–brain axis plays a role in depression-like phenotypes in mice with hepatic ischemia/reperfusion (HI/R) injury via the vagus nerve. Behavioral tests for depression-like behaviors were performed 7 days after sham or HI/R injury surgery. Mice with HI/R injury exhibited splenomegaly, systemic inflammation, depression-like behaviors, reduced expression of synaptic proteins in the prefrontal cortex (PFC), abnormal composition of gut microbiota, and altered blood metabolites and lipids. Furthermore, there were positive or negative correlations between the relative abundance of microbiome and behavioral data or blood metabolites (or lipids). Moreover, subdiaphragmatic vagotomy significantly blocked these changes in mice with HI/R injury. Notably, depression-like phenotypes in mice with HI/R injury were ameliorated after subsequent single injection of the new antidepressant arketamine. The current findings suggest that HI/R injury induces depression-like phenotypes in mice through the gut–microbiota–liver–brain axis via the subdiaphragmatic vagus nerve. Furthermore, arketamine may have therapeutic potential in the treatment of depression in patients with chronic liver disease.

1. Introduction

Chronic liver disease (CLD) is a progressive disorder characterized by the degeneration and regeneration of the liver parenchyma, leading to fibrosis and cirrhosis. The prevalence of depression is higher in patients with CLD than in the general population, suggesting a link between the two disorders (Gutteling et al., 2006; Kronsten et al., 2022; Mullish et al., 2014; Patten et al., 2008). A recent review revealed a high prevalence of depression in patients with CLD, including chronic hepatitis B, chronic hepatitis, alcoholic liver disease, and non-alcoholic fatty liver disease (Huang et al., 2017). Interestingly, signs of psychological distress and depression in patients with cirrhosis are associated with the severity of liver disease (Bianchi et al., 2005). Although depression is a common psychiatric symptom in patients with CLD, the pathogenetic mechanisms underlying this association are not well understood.

Multiple lines of evidence from clinical and pre-clinical studies suggest a role of the gut–microbiota–brain axis in depression (Chang

et al., 2022; Cryan et al., 2019; Jiang et al., 2015; Liu et al., 2023; Sanada et al., 2020; Wei et al., 2022a; Zheng et al., 2016). Notably, the vagus nerve plays an important role in the bidirectional communication between the gut microbiota and the brain (Bonaz et al., 2018; Chang et al., 2022; Forsythe et al., 2014; Hashimoto, 2023a; Wei et al., 2022a). Interestingly, subdiaphragmatic vagotomy (SDV) prevents the onset of depression-like behaviors and changes in the composition of the gut microbiota in mice caused by injection of lipopolysaccharide (LPS) (Zhang et al., 2020) and fecal microbiota transplantation from mice with depression-like phenotypes (Pu et al., 2021; Wang et al., 2020, 2021). Furthermore, SDV blocks depression-like behaviors in *Chrna7* knock-out mice (Yang et al., 2023) and working memory impairment in mice with chronic inflammatory pain (Yue et al., 2023). Taken together, these observations suggest that the gut microbiota–brain axis plays a critical role in depression via the subdiaphragmatic vagus nerve (Chang et al., 2022; Hashimoto, 2023a; Wei et al., 2022a). Kronsten et al. (2022) proposed that gut-mediated systemic inflammation might contribute to

* Corresponding author.

E-mail address: hashimoto@faculty.chiba-u.jp (K. Hashimoto).<https://doi.org/10.1016/j.jad.2023.10.142>

Received 26 May 2023; Received in revised form 14 October 2023; Accepted 22 October 2023

Available online 24 October 2023

0165-0327/© 2023 Elsevier B.V. All rights reserved.

the close relationship between depression and CLD, suggesting abnormalities in the gut–liver–brain axis.

Hepatic ischemia/reperfusion (HI/R) injury causes damage to the liver parenchyma. HI/R injury is a major complication of liver surgery, including liver resection, and liver transplantation (Hirao et al., 2022; Konishi and Lentsch, 2017). Despite technological advances over the last decade, the mechanisms of HI/R injury remain unclear because of the complexity of the underlying pathogenetic processes (Rampes and Ma, 2019). Rodent models of HI/R injury have been widely used; however, there are no reports showing depression-like phenotypes in rodents with HI/R injury. There are also no reports on the role of the gut–liver–brain axis, via the vagus nerve, in rodents with HI/R injury.

Here, we investigated the link between depression and CLD. We evaluated depression-like behaviors in mice with HI/R injury, and we measured blood inflammation, and synaptic proteins in the brain. We also performed 16 s rRNA analysis of feces samples, as well as untargeted metabolomics and lipidomic analyses of plasma samples to examine the role of the gut microbiota–brain axis in the depression-like behaviors. Additionally, we examined the role of the subdiaphragmatic vagus nerve on these depression-like phenotypes by performing SDV. Furthermore, we investigated the effects of the new antidepressant arketamine in mice with HI/R injury since a single dose showed rapid-acting antidepressant-like effects in rodents with depression-like phenotypes (Hashimoto, 2020, 2023a, 2023b; Wei et al., 2022b; Yang et al., 2015, 2019; Zhang et al., 2014, 2022a; Zhang et al., 2023).

2. Materials and methods

2.1. Animals

Male adult C57BL/6Ncr mice were purchased from the Japan SLC Co., Ltd. (Hamamatsu, Shizuoka, Japan). All the experimental mice were aged 9 weeks, body weight 18–28 g. All the experimental mice were acclimatized to standard laboratory conditions (4 or 5/cage), maintain alternating cycles of 12 h of light and 12 h of darkness (lights on from 7:00–19:00), and under constant room temperature of 23 ± 1 °C and controlled humidity of 55 ± 5 %. Animals were given free admittance to chow and water. The experimental protocol of this study was approved by the Chiba University Institutional Animal Care and Use Committee (Permission number: 4–314, 4–375 and 4–438). The experimental mice were deeply anesthetized with inhaled isoflurane and then rapidly sacrificed by cervical dislocation. All efforts were made to minimize animals suffering.

2.2. Reagents

Arketamine [or (R)-ketamine] hydrochloride was prepared as reported previously (Zhang et al., 2014). The dose (10 mg/kg as hydrochloride salt) of arketamine was dissolved in the saline as reported previously (Yang et al., 2015; Zhang et al., 2014). Other reagents were purchased commercially.

2.3. Hepatic ischemia-reperfusion (HI/R) injury

Sham surgery or 70 % HI/R was performed under continuous inhalation anesthesia with 4–5 % isoflurane by using an inhalation small animal anesthesia apparatus (KN-1071 NARCOBIT-E; Natsume Seisakusho, Tokyo, Japan), according to the previous method (Ji et al., 2010, 2013) with a slight modification. Briefly, the arterial/portal vessels to the left and middle lobes of the liver were clamped for 1 h, while preserving blood flow to the right and caudate lobes. There was no vascular occlusion in sham group mice.

2.4. Bilateral subdiaphragmatic vagotomy (SDV)

Bilateral SDV or sham surgery was performed under continuous

inhalation anesthesia with 4–5 % isoflurane using an inhalation small animal anesthesia apparatus (KN-1071 NARCOBIT-E; Natsume Seisakusho, Tokyo, Japan) according to previous methods (Pu et al., 2021; Wang et al., 2020, 2021; Yang et al., 2023; Zhang et al., 2020). During the sham operation, the abdominal wall incision of the same size was made in the same way at the same site. After the dorsal and ventral branches of the subdiaphragmatic vagus nerve were also softly exposed but not cut off. When the HI/R + SDV procedure was performed, the SDV was performed first through the same abdominal approach, followed by the HI/R procedure.

2.5. Behavioral tests

Behavioral tests, including locomotion test (LMT), forced swimming test (FST), and 1 % sucrose preference test (SPT) were performed as reported previously (Pu et al., 2021; Yang et al., 2023).

2.6. Enzyme-linked immunosorbent assay (ELISA)

ELISA kits for the measurement of interleukin-6 (IL-6) (cat number: 88-7064, Invitrogen, Camarillo, CA, USA), and tumor necrosis factor- α (TNF- α) (cat number: 88-7324, Invitrogen, Camarillo, CA, USA) were used.

2.7. Western blotting analysis

Western blotting analysis was performed as previously reported (Yang et al., 2022, 2023). The PFC tissues were homogenized in ice-cold Laemmli lysis buffer. To avoid cross-contamination, each specimen was prepared separately. Then liquid supernatants were collected after centrifugation at $3000 \times g$ (RCF) at 4 °C for 20 min. The total protein concentration extracted from each sample was detected on a spectrophotometer (Molecular Devices Emax Precision Microplate Reader; Molecular Devices., San Jose, CA, USA) using a DC protein assay kit (Bio-Rad, Hercules, CA, USA). By adding a quarter volume of sample buffer (125 mM Tris-HCl, pH 6.8; 0.1 % bromophenol blue; 4 % sodium dodecyl sulfate; and 10 % β -mercaptoethanol and 20 % glycerol) and Laemmli Lysis buffer in appropriate proportions to balance the total protein concentration of each sample, then incubate them at 95 °C for 10 min.

Considering the size of target protein, we chose 10 % sodium dodecyl sulfate–polyacrylamide gel electrophoresis (SDS-PAGE) (catalog #: 4568125, Mini-PROTEAN TGX™ Stain-Free Gels; Bio-Rad, USA) separated the proteins by gel electrophoresis. Then a Trans-Blot Mini Cell apparatus (Bio-Rad) was used to electrotransfer the target protein onto polyvinylidene difluoride membranes.

Synaptic proteins such as glutamate receptor 1 (AMPA subtype: GluA1: [the α -amino-3-hydroxy-5-methyl-4-isoxazolepropionic acid receptor A1]) and postsynaptic density protein 95 (PSD-95) were decreased in the PFC of mice with depression-like phenotypes (Pu et al., 2021; Wang et al., 2020, 2021; Yang et al., 2023). Ionized calcium-binding adapter molecule 1 (Iba1) is a specific marker for microglia in the brain. For immunodetection, the polyvinylidene difluoride membranes were blocked with blocker [5 % skim milk in TBS + 0.1 % Tween-20 (TBST)] at room temperature for 1 h, the membranes for detecting PSD-95 were incubated with the recommended dilution of the primary antibody against PSD-95 (1:1000, catalog number: 51-6900695, 1 μ g/mL, Invitrogen, Camarillo, CA, USA), while the membranes for detecting Iba1 and β -actin were incubated with the appropriate dilution of the primary antibody against Iba1 (1:1000, catalog number: 016-20001, 1 μ g/mL, FUJIFILM, Tokyo, Japan) and β -actin (1:10,000; catalog number: A5441 Sigma-Aldrich Co., Ltd., St Louis, MO, USA) at 4 °C overnight. The next day, wash the polyvinylidene difluoride membranes in three washes of TBST, 10 min each. Then the polyvinylidene difluoride membranes were selectively incubated with a recommended dilution of labeled secondary antibody [anti-mouse antibody (1:5000, catalog

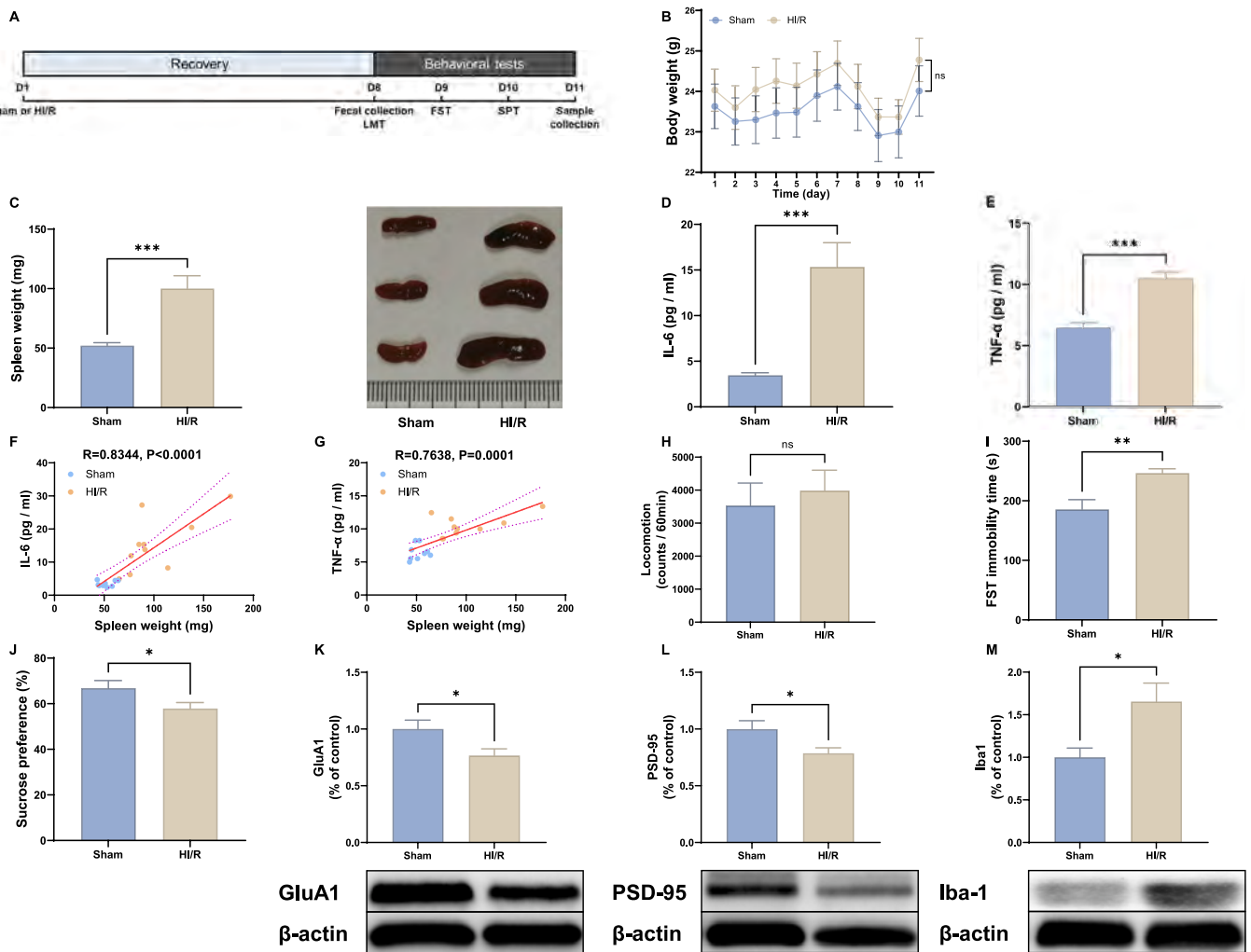


Fig. 1. Depression-like phenotypes in mice with HI/R injury.

(A): Experimental schedule. On day 1, sham or HI/R surgery was performed, and they were recovered 7 days. On day 8, fresh feces samples were collected, and subsequently LMT was performed. FST and 1 % SPT were performed on day 9 and day 10, respectively. On day 11, prefrontal cortex (PFC) and plasma samples were collected. (B): Body weight (repeated measure ANOVA, $F_{(1, 17)} = 0.5576, P = 0.4654$). (C): Spleen weight (unpaired t-test, $t = 4.131, df = 17, P = 0.0007$) and representative photograph of spleen in the two groups. (D): Plasma levels of IL-6 (unpaired t-test, $t = 4.207, df = 17, P = 0.0006$). (E): Plasma levels of TNF- α (unpaired t-test, $t = 6.232, df = 17, P < 0.0001$). (F): There was a positive correlation ($R = 0.8344, P < 0.0001$) between the spleen weight and plasma levels of IL-6 in two groups. (G): There was a positive correlation ($R = 0.7638, P = 0.0001$) between the spleen weight and plasma levels of TNF- α in two groups. (H): locomotion (LMT) (unpaired t-test, $t = 0.4923, df = 17, P = 0.6288$). (I): FST (unpaired t-test, $t = 3.543, df = 17, P = 0.0025$). (J): SPT (unpaired t-test, $t = 2.158, df = 17, P = 0.0455$). (K) Western blot analysis of GluA1 in the PFC (unpaired t-test, $t = 2.403, df = 17, P = 0.0279$) and the representative bands. (L): Western blot analysis of PSD-95 in the PFC (unpaired t-test, $t = 2.473, df = 17, P = 0.0243$) and the representative bands. (M): Western blot analysis of Iba1 in the PFC (unpaired t-test, $t = 2.612, df = 17, P = 0.0182$) and the representative bands. The data are shown as means \pm S.E.M (sham group: $n = 9$, HI/R group: $n = 10$). ANOVA: analysis of variance. ns: not significant; * $P < 0.05$; ** $P < 0.01$; *** $P < 0.001$.

number: NA931, GE Healthcare) or a horseradish peroxidase-conjugated anti-rabbit antibody (1:5000, catalog number: NA934, GE Healthcare)] in 5 % blocking buffer in TBST at room temperature for 1 h. After three final washes in TBST, 10 min each. The bands in the polyvinylidene difluoride membranes were detected using enhanced chemiluminescence plus a Western Blotting Detection system (GE Healthcare Bioscience).

The membranes for detecting GluA1 were incubated in elution buffer (62.5 mM Tris-HCl, pH 6.8, 2 % sodium dodecyl sulfate, and 100 mM β -mercaptoethanol) (preheat in incubator at 60 °C for 10 min, shake 50 times/min) at 60 °C for 30 min and then washed three times (10 min at a time) in TBST. The stripped membranes were incubated with the recommended dilution of primary antibody directed against GluA1 (1:10,000; catalog number: ab31232, Abcam, Cambridge, MA, USA) at 4 °C overnight. The following day, washing the membranes for three times (10 min at a time) in TBST and were incubated with a

recommended dilution of horseradish peroxidase-conjugated anti-rabbit antibody (1:5000, catalog number: NA934, GE Healthcare) for 1 h at room temperature. After three final washes in TBST, 10 min each. The bands in the polyvinylidene difluoride membranes were detected using enhanced chemiluminescence plus a Western Blotting Detection system (GE Healthcare Bioscience). Images were produced using a ChemiDoc™ Touch Imaging System (170-01401; Bio-Rad Laboratories, Hercules, CA, USA), and immunoreactive bands were quantified using Image Lab™3.0 software (Bio-Rad Laboratories).

2.8. Collection of fresh fecal samples and 16S ribosome RNA sequencing

We collected fresh fecal samples from mice before the behavioral test LMT. Subsequently, the experimental workflow including the microbial community DNA extraction, DNA quality control, PCR, product purification, library quality control, sequencing and bioinformatics analysis

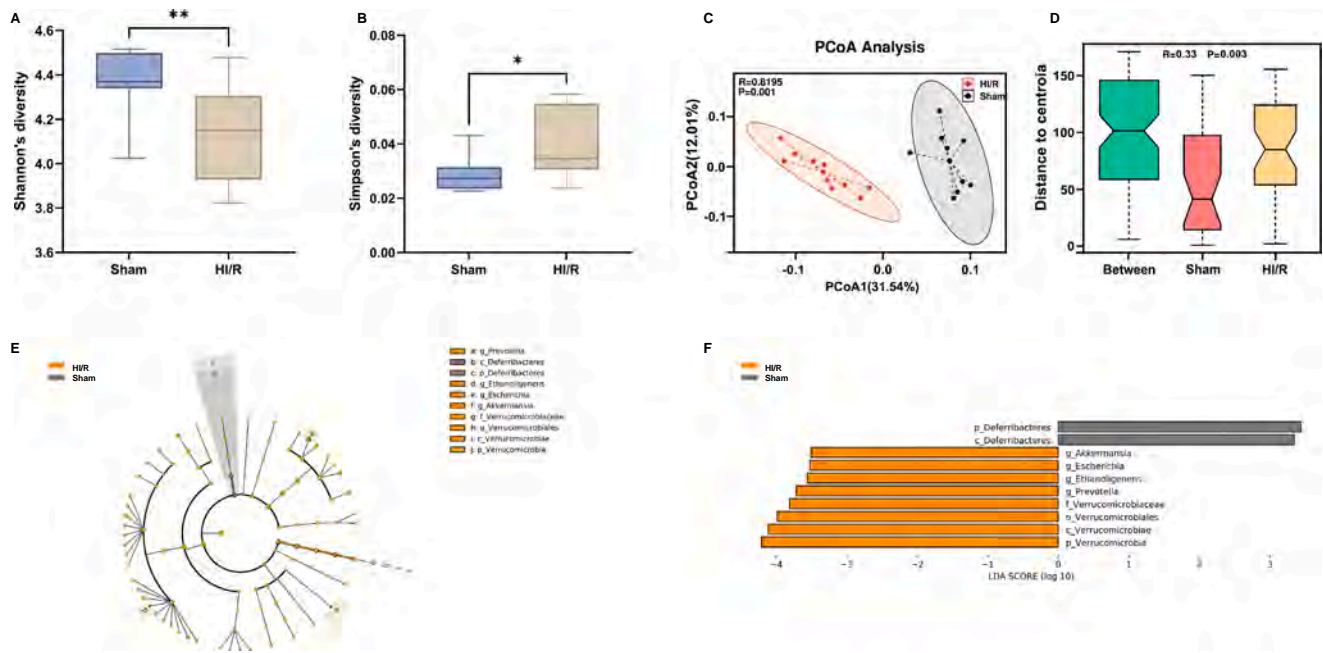


Fig. 2. Abnormal composition of gut microbiota and the LEfSe algorithm in the mice with HI/R injury.

(A): Shannon's diversity (Mann-Whitney test, $P = 0.008$). (B): Simpson's diversity (Mann-Whitney test, $P = 0.022$). (C): PCoA based on OTU level (ANOSIM, Bray-Curtis dissimilarity matrix) ($R = 0.8195$, $P = 0.001$). (D): OTU ANOSIM analysis ($R = 0.33$, $P = 0.003$) ("Between" indicates the difference between groups, and others indicate the difference within each group. R value represents the degree of difference between groups and within groups, ranged from -1 to 1 ; R value >0 indicates that the difference between groups is greater than the difference within the group; R value <0 indicates that the difference between groups is greater than the difference within the group; the larger the absolute value of R value, the greater the relative difference. The lower the P value, the more significant the effect of this difference test. P value <0.05 indicates a significant difference). (E): Functional branching diagram generated from LEfSe showing the differences of the two groups at different taxonomic levels. (F): Histogram representing the enriched taxa with LDA score > 3.3 and $P < 0.05$ obtained from LEfSe of the two groups (p: phylum, c: class, o: order, f: family, g: genus). For all boxplots, the middle line in the box addresses the median, the box addresses the interquartile range, and the whisker addresses the most extreme and least values. * $P < 0.05$; ** $P < 0.01$.

was performed as our previously method (Yang et al., 2023). The 16S ribosome RNA sequencing data has been uploaded and saved in the NCBI Sequence Read Archive and is available at the accession number PRJNA929656.

2.9. Untargeted metabolomic and lipidomic analyses of plasma samples

Untargeted metabolomics profiles from plasma samples were analyzed using ultra-performance liquid chromatography-tandem quadruple time-of-flight mass spectrometry (UPLC-QTOF/MS) technique. The acquisition was operated on an ExionLC™ AD system (SCIEX, Tokyo, Japan) coupled to a X500R QTOF system (SCIEX, Tokyo, Japan), then the metabolomics profiles data was annotated and analyzed as our previously reported (Yang et al., 2023). Untargeted lipidomic analysis of plasma samples were performed using an X500R QTOF system (SCIEX, Tokyo, Japan) operated in positive and negative electrospray mode (AB Sciex, Foster City, CA) coupled with a ExionLC™ AD system (SCIEX, Tokyo, Japan). The lipidomic data processing and analysis were performed as previously reported (Tsugawa et al., 2020).

2.10. Statistical analysis

Statistical analysis of the data was performed using SPSS version 20.0 software (SPSS, Tokyo, Japan). The data were shown as the mean \pm standard error of the mean (S.E.M.). The data of body weight were analyzed using repeated measure analysis of variance (ANOVA), followed by Fisher's least significant difference (LSD) test. The data of spleen weight were analyzed using unpaired *t*-test (for two groups) or two-way ANOVA (for four groups). Data of behavioral tests, pro-inflammatory cytokines, synaptic proteins and microglial marker were analyzed using unpaired *t*-test (for two groups), one-way ANOVA (for

three groups), or two-way ANOVA (for four groups), followed by Fisher's LSD test. The α -diversity of gut microbiota, the abundance of gut microbiota at the species level, metabolites and lipids between the two groups were analyzed using Mann-Whitney test. Bioinformatic analysis of PCoA, LEfSe algorithm of intestinal microbiota, boxplot analysis of metabolomics and correlation networks were all performed by using the OmicStudio tools (<https://www.omicstudio.cn/tool>).

Correlations between spleen weight and the concentrations of pro-inflammatory cytokines were analyzed by using Pearson's correlation analysis. Correlations between the plasma metabolites (or lipids), the intestinal microbiota at species level, depression-like phenotypes, the concentrations of pro-inflammatory cytokines and synaptic proteins (or microglial marker) in the PFC were analyzed using Spearman's correlation analysis. P-value for comparison <0.05 was regarded as significant.

3. Results

3.1. Depression-like phenotypes in mice with HI/R injury

Behavioral tests were performed 7 days after surgery (Fig. 1A). There were no changes in body weight between the two groups (Fig. 1B). The HI/R group showed splenomegaly compared with the sham group (Fig. 1C). Plasma levels of pro-inflammatory cytokines such as interleukin-6 (IL-6) and tumor necrosis factor- α (TNF- α) were higher in the HI/R group than in the sham group (Fig. 1D, E). There were positive correlations between spleen weight and plasma levels of IL-6 and TNF- α (Fig. 1F, G). In the behavioral tests, there were no changes in locomotor activity between the two groups (Fig. 1H). However, the HI/R group showed increased immobility time in the forced swimming test (FST) (Fig. 1I) and reduced sucrose preference in the sucrose preference test

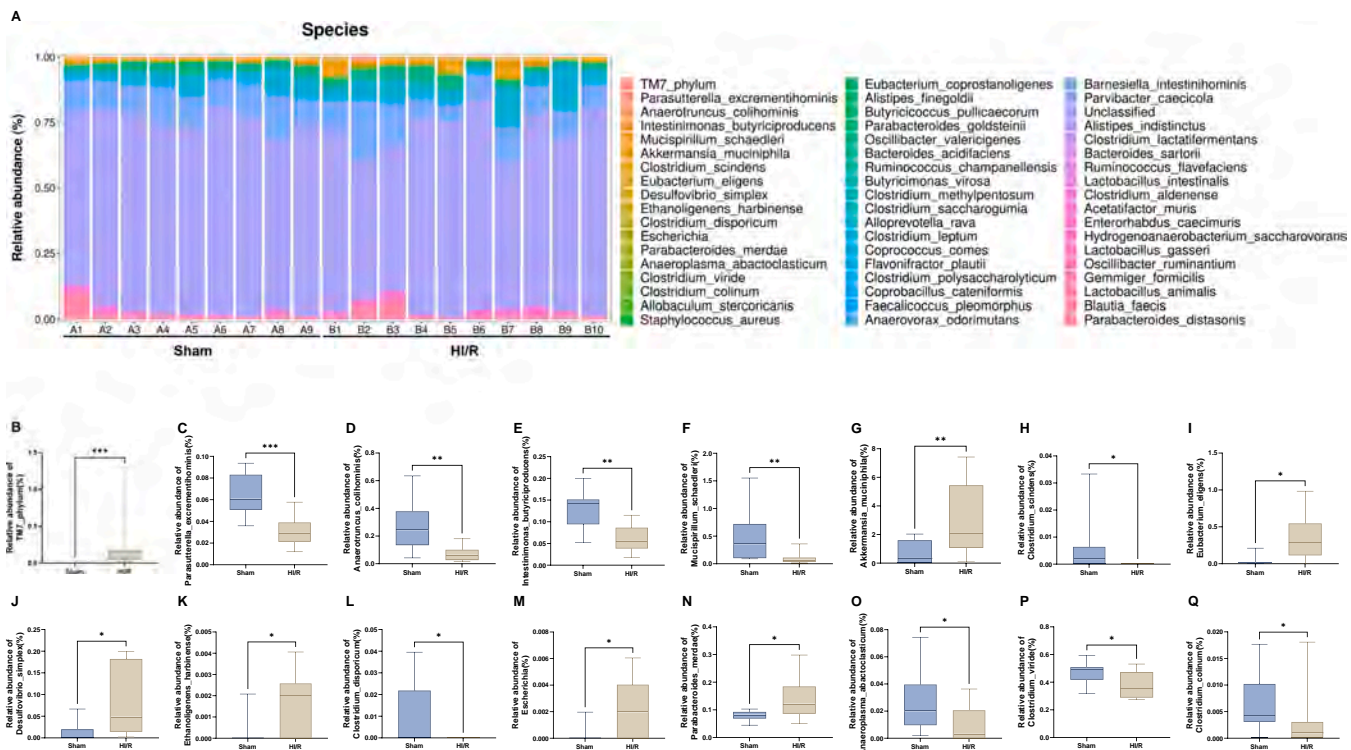


Fig. 3. Effects of HI/R on the gut microbiota at the level of species.

(A): Gut bacteria composition at the species level in the two groups. (B): Relative abundance of the species *TM7_phylum* (Mann-Whitney test, $P < 0.0001$). (C): Relative abundance of the species *Parasutterella_excrementihominis* (Mann-Whitney test, $P = 0.0004$). (D): Relative abundance of the species *Anaerotruncus_colihominis* (Mann-Whitney test, $P = 0.0015$). (E): Relative abundance of the species *Intestinimonas_butyrificiproducens* (Mann-Whitney test, $P = 0.0030$). (F): Relative abundance of the species *Mucispirillum_schaedleri* (Mann-Whitney test, $P = 0.0057$). (G): Relative abundance of the species *Akkermansia_muciniphila* (Mann-Whitney test, $P = 0.0108$). (H): Relative abundance of the species *Clostridium_scindens* (Mann-Whitney test, $P = 0.0101$). (I): Relative abundance of the species *Eubacterium_eligens* (Mann-Whitney test, $P = 0.0126$). (J): Relative abundance of the species *Desulfovibrio_simplex* (Mann-Whitney test, $P = 0.0162$). (K): Relative abundance of the species *Ethanoligenens_harbinense* (Mann-Whitney test, $P = 0.0162$). (L): Relative abundance of the species *Clostridium_disporicum* (Mann-Whitney test, $P = 0.0325$). (M): Relative abundance of the species *Escherichia* (Mann-Whitney test, $P = 0.0257$). (N): Relative abundance of the species *Parabacteroides_merdae* (Mann-Whitney test, $P = 0.0279$). (O): Relative abundance of the species *Anaeroplasmabactoclasticum* (Mann-Whitney test, $P = 0.0267$). (P): Relative abundance of the species *Clostridium_viride* (Mann-Whitney test, $P = 0.0350$). (Q): Relative abundance of the species *Clostridium_colinum* (Mann-Whitney test, $P = 0.0347$). For all boxplots, the middle line in the box addresses the median, the box addresses the interquartile range, and the whisker addresses the most extreme and least values. * $P < 0.05$; ** $P < 0.01$; *** $P < 0.001$.

(SPT) compared with the sham group (Fig. 1J). Furthermore, expression of synaptic proteins (GluA1 and PSD-95) in the prefrontal cortex (PFC) was lower in the HI/R group than in the sham group (Fig. 1K, L). In contrast, levels of Iba1 in the PFC were significantly higher in the HI/R group compared with the sham group (Fig. 1M). These data suggest that mice with HI/R injury have systemic inflammation, reduced expression of synaptic proteins, and microglial activation in the PFC, resulting in depression-like phenotypes.

3.2. Composition of gut microbiota and LEfSe analysis

Examination of α -diversity revealed significant differences in Shannon's diversity and Simpson's diversity indices between the two groups (Fig. 2A, B). The β -diversity of the gut microbiota in the two groups was analyzed by Principal Coordinate Analysis (PCoA). At the operational taxonomic unit (OTU) level, PCoA analysis revealed a significant difference in composition through analysis of similarities (ANOSIM) assessment ($R = 0.8195$, $P = 0.001$) (Fig. 2C). ANOSIM analysis at the OTU level indicated that the difference between the two groups was greater than the differences within the groups ($R = 0.33$, $P = 0.003$) (Fig. 2D).

A cladogram was used to depict the relationship between the biomarker taxa (layers of the cladogram representing different levels, with phylum, class, order, family and genus from inside to outside) generated by LEfSe (linear discrimination analysis effect size) analysis

(Fig. 2E). We identified eight taxonomic biomarkers for the following microbes in the HI/R group: the genus *Akkermansia*, the genus *Escherichia*, the genus *Ethanoligenens*, the genus *Prevotella*, the family *Verrucomicrobiaceae*, the order *Verrucomicrobiales*, the class *Verrucomicrobiae*, and the phylum *Verrucomicrobia* (Fig. 2F). Furthermore, we identified two taxonomic biomarkers, for the class and the phylum *Deferritbacteres* in the sham group (Fig. 2F).

3.3. Gut microbiota at the species level

At the species level, the screen identified 16 bacteria that significantly differed in relative abundance (Fig. 3A). The relative abundances of *TM7_phylum*, *Akkermansia_muciniphila*, *Eubacterium_eligens*, *Desulfovibrio_simplex*, *Ethanoligenens_harbinense*, *Escherichia* and *Parabacteroides_merdae* were significantly higher in the HI/R group compared with the sham group, whereas the relative abundances of *Parasutterella_excrementihominis*, *Anaerotruncus_colihominis*, *Intestinimonas_butyrificiproducens*, *Mucispirillum_schaedleri*, *Clostridium_scindens*, *Clostridium_disporicum*, *Anaeroplasmabactoclasticum*, *Clostridium_viride* and *Clostridium_colinum* were significantly lower in the HI/R group compared with the sham group (Fig. 3B–Q).

3.4. Untargeted metabolomic and lipidomic analyses of plasma samples

To examine the interaction between the gut microbiome and host

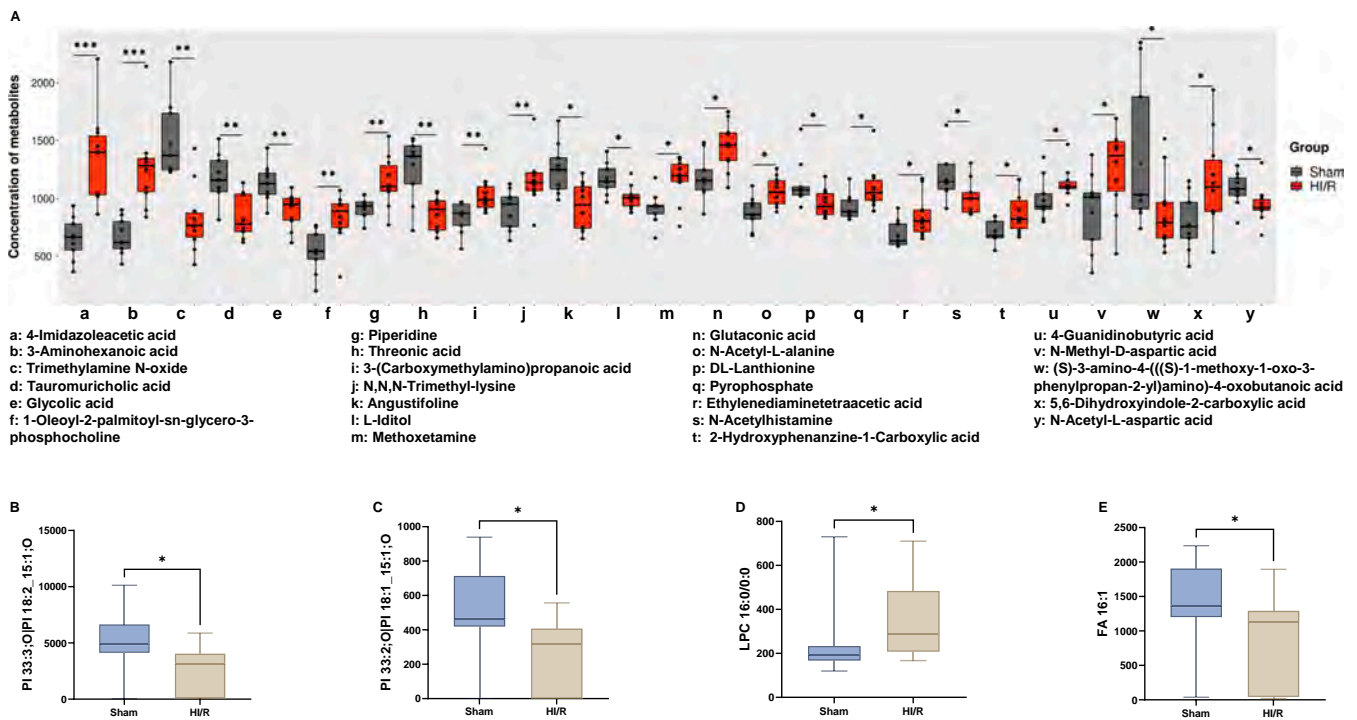


Fig. 4. Untargeted metabolomic and lipidomic analyses of plasma samples in mice with HI/R injury.

(A): Boxplots showing the changes of 25 kinds of metabolites between the two groups. They are listed as follows: 4-imidazoleacetic acid (Mann-Whitney test, $P < 0.0001$), 3-aminohexanoic acid (Mann-Whitney test, $P = 0.0002$), trimethylamine *N*-oxide (Mann-Whitney test, $P = 0.0004$), taurumuricholic acid (Mann-Whitney test, $P = 0.0010$), glycolic acid (Mann-Whitney test, $P = 0.0030$), 1-oleoyl-2-palmitoyl-sn-glycero-3-phosphocholine (Mann-Whitney test, $P = 0.0057$), piperidine (Mann-Whitney test, $P = 0.0057$), threonic acid (Mann-Whitney test, $P = 0.0057$), 3-(carboxymethylamino) propanoic acid (Mann-Whitney test, $P = 0.0076$), *N,N,N*-trimethyl-lysine (Mann-Whitney test, $P = 0.0076$), angustifoline (Mann-Whitney test, $P = 0.0101$), *L*-iditol (Mann-Whitney test, $P = 0.0133$), methoxetamine (Mann-Whitney test, $P = 0.0133$), glutaconic acid (Mann-Whitney test, $P = 0.0172$), *N*-acetyl-*L*-alanine (Mann-Whitney test, $P = 0.0172$), *DL*-lanthionine (Mann-Whitney test, $P = 0.0220$), pyrophosphate (Mann-Whitney test, $P = 0.0220$), ethylenediaminetetraacetic acid (Mann-Whitney test, $P = 0.0279$), *N*-acetylhistamine (Mann-Whitney test, $P = 0.0279$), 2-hydroxyphenazine-1-carboxylic acid (Mann-Whitney test, $P = 0.0350$), 4-guanidinobutyric acid (Mann-Whitney test, $P = 0.0350$), *N*-methyl-*D*-aspartic acid (Mann-Whitney test, $P = 0.0350$), (*S*)-3-amino-4-(((*S*)-1-methoxy-1-oxo-3-phenylpropan-2-yl)amino)-4-oxobutanoic acid (Mann-Whitney test, $P = 0.0435$), 5,6-dihydroxyindole-2-carboxylic acid (Mann-Whitney test, $P = 0.0435$), *N*-acetyl-*L*-aspartic acid (Mann-Whitney test, $P = 0.0435$). The X-axis using the lowercase letter symbol representing the names of different plasma metabolites, and the Y-axis represents the concentration of various plasma metabolites. Different colors of boxplots represent the corresponding groups.

(B) PI 33:3; O|PI 18:2_15:1; O (Mann-Whitney test, $P = 0.0172$). (C) PI 33:2; O|PI 18:1_15:1; O (Mann-Whitney test, $P = 0.0291$). (D) LPC 16:0/0:0 (Mann-Whitney test, $P = 0.035$). (E) FA 16:1 (Mann-Whitney test, $P = 0.0435$). * $P < 0.05$; ** $P < 0.01$; *** $P < 0.001$.

metabolism, we conducted untargeted metabolomic and lipidomic analyses of plasma samples. After quality control and removal of low-abundance peaks, a subset of 214 metabolites was annotated. We identified 25 metabolites that differed significantly between the two groups (Fig. 4A). Furthermore, a subset of 55 lipids was annotated after data processing. We identified 4 significantly different lipids between the two groups (Fig. 4B–E).

3.5. Correlations among the gut microbiota, plasma metabolites/lipids, depression-like phenotypes, plasma pro-inflammatory cytokines, synaptic proteins and Iba1

There were correlations between the plasma metabolites/lipids and the relative abundance of gut microbiota in the two groups, suggesting a close relationship between the two. After screening the data, with a threshold of $P < 0.05$ and an absolute *R*-value of ≥ 0.5 , a Correlation Network was constructed to indicate the relationship between the plasma metabolites/lipids and gut microbiome at the species level, depression-like behaviors, plasma pro-inflammatory cytokines, synaptic proteins and the microglial marker Iba1 in the PFC, all of which significantly differed between the two groups (Fig. 5A). The relative abundance of several microbes was positively or negatively correlated with plasma metabolites such as 4-imidazoleacetic acid, 3-aminohexanoic acid, trimethylamine *N*-oxide, taurumuricholic acid, and glycolic

acid (Fig. 5A). In addition, there were correlations between the plasma metabolites/lipids and the FST data, plasma levels of pro-inflammatory cytokines, synaptic proteins and the microglial marker Iba1 in the PFC (Fig. 5A).

Using the Correlation Network, we investigated correlations between the relative abundance of the gut bacteria and depression-like phenotypes, plasma cytokines, synaptic proteins and Iba1 in the PFC (Fig. 5B). There were also positive or negative correlations between plasma IL-6 or TNF- α and the relative abundance of several species (Fig. 5B). Furthermore, there were positive (or negative) correlations between the FST data and the relative abundance of several species (Fig. 5B). Moreover, there were positive (or negative) correlations between the relative abundance of the species and the levels of synaptic proteins or Iba1 in the PFC (Fig. 5B). These data suggest that several microbiota and metabolites may contribute to systemic inflammation, resulting in microglial activation in the brain and depression-like phenotypes.

3.6. Effects of bilateral SDV in depression-like phenotypes in the HI/R mouse model

Prior research suggests that the subdiaphragmatic vagus nerve could be implicated in depression-like phenotypes in mice (Pu et al., 2021; Wang et al., 2020, 2021; Yang et al., 2023; Zhang et al., 2020). To examine the role of the subdiaphragmatic vagus nerve in the depression-

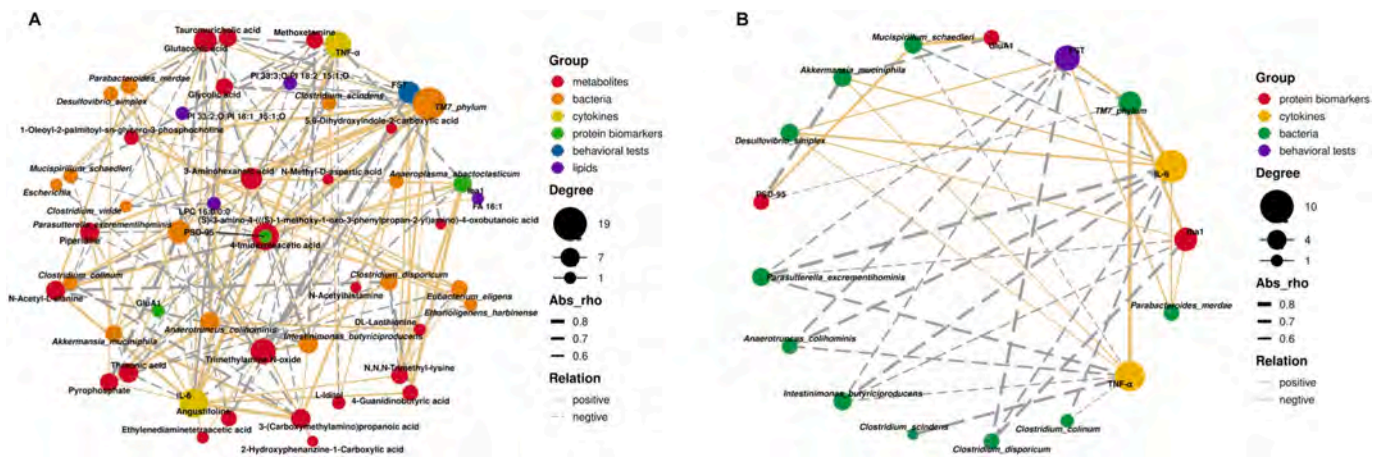


Fig. 5. Correlation network between behavioral data (or synaptic proteins, microglial marker, and pro-inflammatory cytokine) and microbiota (or metabolites and lipids).

(A): A Correlation Network indicating the correlations between the concentrations of plasma metabolites (or lipids) and the gut microbiota at the species level, the results of the behavioral test, the concentrations of pro-inflammatory cytokines, synaptic proteins and microglial marker Iba1 in the PFC. (B): A Correlation Network showed correlations between the relative abundance of gut bacteria at the species level and the results of the behavioral test, the concentrations of pro-inflammatory cytokines, synaptic proteins and microglial marker Iba1 in the PFC. Both the threshold of correlation networks above were set as $P < 0.05$ and the absolute value of $R \geq 0.5$. The different colors of nodes represent different groups. The sizes of node gradients represent varying degrees of correlation. The thickness of the line represents the absolute value of the correlation coefficient. Solid lines represent positive correlations, dotted lines represent negative correlations.

like phenotypes in mice with HI/R injury, we investigated the effects of bilateral SDV (Fig. 6A). Body weights after surgery were significantly changed among the four groups (Fig. 6B). The spleen weights in the HI/R + SDV group were significantly lower than those in the HI/R + sham group (Fig. 6C). Furthermore, plasma levels of IL-6 and TNF- α in the HI/R + SDV group were significantly lower than those in the HI/R + sham group (Fig. 6D, E). There were positive correlations between spleen weight and the plasma concentration of IL-6 or TNF- α among the four groups (Fig. 6F, G).

There were no differences in locomotor activity among the four groups (Fig. 6H). The immobility time in the FST in the HI/R + SDV group was significantly lower than that in the HI/R + sham group (Fig. 6I). In the SPT, sucrose preference in the HI/R + SDV group was significantly higher than that in the HI/R + sham group (Fig. 6J). Furthermore, the expression levels of synaptic proteins (e.g., GluA1 and PSD-95) in the PFC were significantly higher in the HI/R + SDV group compared with the HI/R + sham group (Fig. 6K, L). The expression of Iba1 in the PFC was significantly lower in the HI/R + SDV group than in the HI/R + sham group (Fig. 6M). These data suggest that bilateral SDV blocks depression-like behaviors, increased plasma levels of pro-inflammatory cytokines, altered expressions of synaptic proteins and Iba1 in the PFC of mice with HI/R injury.

3.7. Effects of arketamine on depression-like phenotypes in mice with HI/R injury

We have demonstrated that arketamine could be a rapid-acting antidepressant, devoid of the side effects associated with ketamine (Wei et al., 2022b; Zhang et al., 2022a; Zhang et al., 2023). Here, we examined the effects of a single dose of the new antidepressant arketamine (10 mg/kg, i.p.) in the HI/R model (Fig. 7A). There were no changes in body weight (Fig. 7B) or locomotor activity (Fig. 7C) among the three groups. The immobility time in the FST was significantly greater in the HI/R + saline group compared with the other two groups (Fig. 7D). In the SPT, sucrose preference was significantly lower in the HI/R + saline group compared with the other two groups (Fig. 7E). Arketamine also attenuated the reduced levels of GluA1 and PSD-95 in the PFC of mice with HI/R injury (Fig. 7F, G). A single injection of arketamine significantly attenuated the increase in expression of Iba1 in the PFC of mice with HI/R injury (Fig. 7H). These results suggest that depression-like

phenotypes in mice with HI/R injury are ameliorated by a single dose of arketamine.

4. Discussion

There are a number of major findings of this study. First, mice with HI/R injury had higher blood levels of pro-inflammatory cytokines, reduced expression of synaptic proteins (i.e., GluA1 and PSD-95) and increased expression of Iba1 (indicative of microglial activation) in the PFC, resulting in depression-like phenotypes. Second, there were significant changes in α -diversity and β -diversity in gut microbiota between the two groups. LEfSe analysis identified the genera *Akkermansia*, *Escherichia*, *Ethanoligenens* and *Prevotella* as potential microbial markers in the HI/R group. Furthermore, several species and metabolites/lipids were altered between the two groups. There were also correlations between the relative abundance of several microbes and blood cytokines, depression-like behaviors, or synaptic proteins and the microglia marker in the PFC. Network analysis showed correlations between several microbes and blood metabolites or behavioral indices. Third, SDV prevented splenomegaly, systemic inflammation (the increases in IL-6 and TNF- α), and altered expression of synaptic proteins and Iba1 in the PFC of mice with HI/R injury. Finally, depression-like phenotypes, and altered expressions of GluA1, PSD-95 and Iba1 in the PFC of mice with HI/R injury were improved after a single injection of arketamine. Taken together, these findings suggest that the gut microbiota–liver–brain axis plays a key role in depression-like phenotypes in mice with HI/R injury via the subdiaphragmatic vagus nerve, and that arketamine exhibits a rapid-acting antidepressant-like action in mice with HI/R injury.

It has been reported that LPS-induced splenomegaly is associated with blood levels of pro-inflammatory cytokines (Ma et al., 2022, 2023; Zhang et al., 2020, 2021a, 2021b). In this study, we found a positive correlation between spleen weight and blood levels of pro-inflammatory cytokines in mice. Collectively, these results suggest that HI/R-induced liver injury contributes to systemic inflammation, resulting in splenomegaly and depression-like phenotypes.

Analysis of gut microbiota shows that HI/R injury is a driving factor for the differential expression of microbial communities. At the species level, there were differences in the relative abundance of several microbiota between the two groups. Using untargeted metabolomic and lipidomic analyses, we found that several metabolites/lipids were

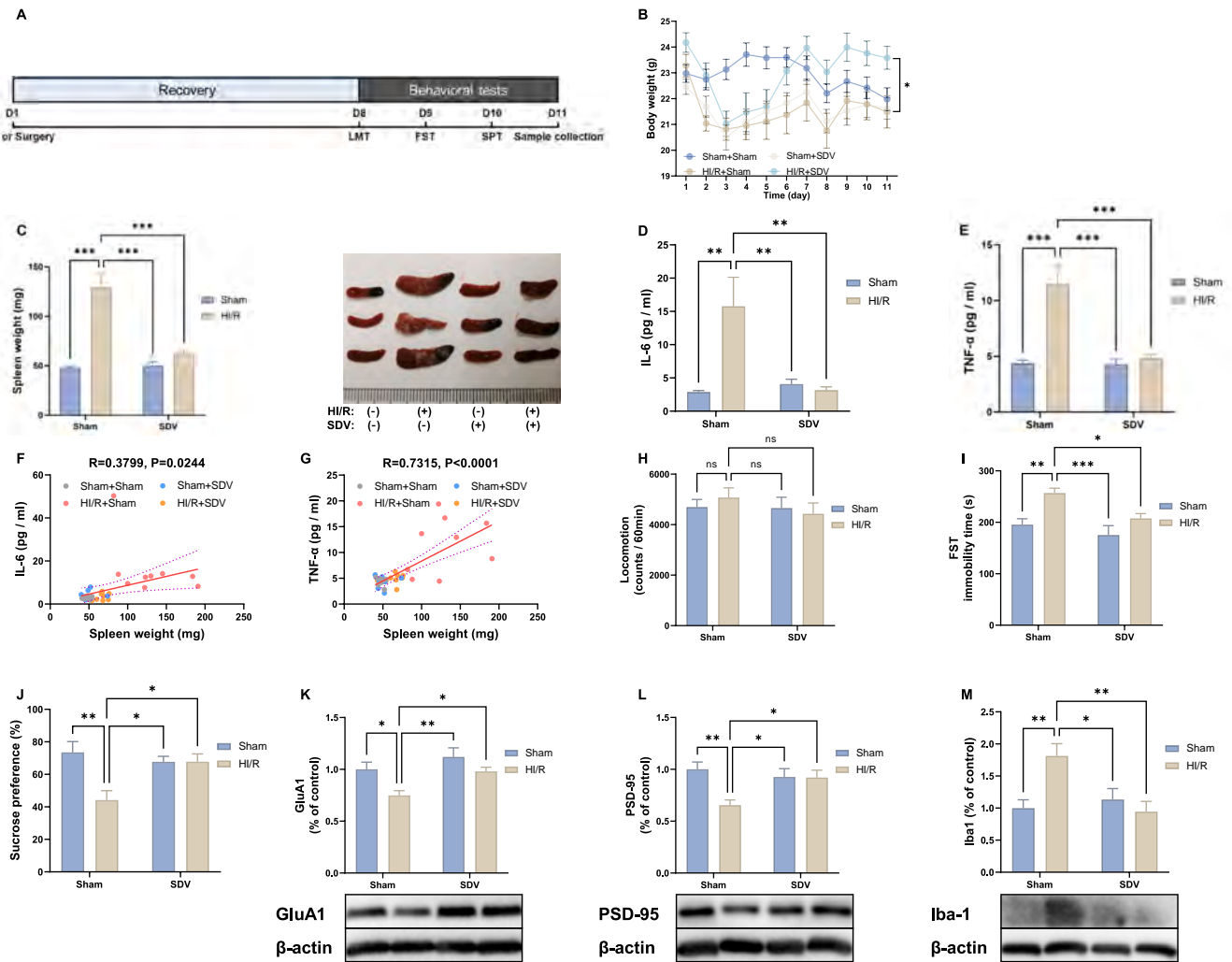


Fig. 6. Effects of bilateral SDV in depression-like phenotypes of mice with HI/R injury. (A): Experimental schedule. On day 1, surgery (HI/R and/or SDV) or sham surgery was performed, and they were recovered 7 days. On day 11, PFC and plasma samples were collected. (B): Body weight (repeated measure two-way ANOVA, time: $F_{(3,481, 107.9)} = 23.84, P < 0.0001$; group: $F_{(3,31)} = 2.987, P = 0.0461$; interaction: $F_{(30,310)} = 9.574, P < 0.0001$). (C): Spleen weight (two-way ANOVA, HI/R: $F_{(1,31)} = 20.06, P < 0.0001$; SDV: $F_{(1,31)} = 42.52, P < 0.0001$; Interaction: $F_{(1,31)} = 22.97, P < 0.0001$) and representative photograph of spleen in the four group. (D): Plasma levels of IL-6 (two-way ANOVA, HI/R: $F_{(1,31)} = 6.074, P = 0.0195$; SDV: $F_{(1,31)} = 6.689, P = 0.0146$; Interaction: $F_{(1,31)} = 8.886, P = 0.0056$). (E): Plasma levels of TNF- α (two-way ANOVA, HI/R: $F_{(1,31)} = 11.58, P = 0.0019$; SDV: $F_{(1,31)} = 14.94, P = 0.0005$; Interaction: $F_{(1,31)} = 11.06, P = 0.0023$). (F): There was a positive correlation ($R = 0.3799, P = 0.0244$) between the spleen weight and plasma levels of IL-6 in the four groups. (G): There was a positive correlation ($R = 0.7315, P < 0.0001$) between the spleen weight and plasma levels of TNF- α in the four groups. (H): Locomotion (LMT) (two-way ANOVA, HI/R: $F_{(1,31)} = 0.7289, P = 0.3998$; SDV: $F_{(1,31)} = 0.03425, P = 0.8544$; Interaction: $F_{(1,31)} = 0.5760, P = 0.4536$). (I): FST (two-way ANOVA, HI/R: $F_{(1,31)} = 8.150, P = 0.0076$; SDV: $F_{(1,31)} = 14.68, P = 0.0006$; Interaction: $F_{(1,31)} = 1.430, P = 0.2408$). (J): SPT (two-way ANOVA, HI/R: $F_{(1,31)} = 2.776, P = 0.1058$; SDV: $F_{(1,31)} = 7.544, P = 0.0099$; Interaction: $F_{(1,31)} = 7.634, P = 0.0095$). (K): Western blot analysis of GluA1 in the PFC (two-way ANOVA, HI/R: $F_{(1,31)} = 8.269, P = 0.0072$; SDV: $F_{(1,31)} = 10.23, P = 0.0032$; Interaction: $F_{(1,31)} = 0.8455, P = 0.3649$) and the representative bands. (L): Western blot analysis of PSD-95 in the PFC (two-way ANOVA, HI/R: $F_{(1,31)} = 1.958, P = 0.1716$; SDV: $F_{(1,31)} = 6.524, P = 0.0158$; Interaction: $F_{(1,31)} = 6.101, P = 0.0192$) and the representative bands. (M): Western blot analysis of Iba1 in the PFC (two-way ANOVA, HI/R: $F_{(1,31)} = 4.846, P = 0.0353$; SDV: $F_{(1,31)} = 3.468, P = 0.0721$; Interaction: $F_{(1,31)} = 9.057, P = 0.0052$) and the representative bands. The data are shown as means \pm S.E.M (sham + sham group: $n = 8$, HI/R + sham group: $n = 9$, sham + SDV group: $n = 8$, HI/R + SDV group: $n = 10$). ANOVA: analysis of variance. ns: not significant; * $P < 0.05$; ** $P < 0.01$; *** $P < 0.001$.

altered between the two groups. Network analysis showed that blood levels of metabolites/lipids were correlated with the relative abundance of microbiota, suggesting a role of the microbiome in the synthesis of these metabolites/lipids. Notably, we found correlations between depression-like behaviors and the relative abundances of microbiota, suggesting a role of the gut microbiome in depression. A recent study demonstrated that gut microbiota-derived metabolites play a role in HI/R injury through the modulation of macrophage metabolic reprogramming (Lu et al., 2023). Given the role of gut microbiota in depression (Chang et al., 2022; Liu et al., 2023), it is likely that alterations in the gut microbiota–brain axis, including metabolites and lipids, may play a role

in the depression-like behaviors in mice with HI/R injury.

Previous studies demonstrated that SDV blocks the onset of depression-like behaviors in mice caused by LPS administration (Zhang et al., 2020) or fecal microbiota transplantation from mice with depression-like behaviors (Pu et al., 2021; Wang et al., 2020, 2021). Furthermore, SDV blocks the onset of depression-like behaviors in *Chrna7* knockout mice (Yang et al., 2023) and demyelination in the brain of cuprizone-treated mice (Wang et al., 2023). A study showed a role of the gut–spleen axis, via the subdiaphragmatic vagus nerve, in sleep deprivation-induced aggravation of systemic inflammation in mice after LPS injection (Zhang et al., 2021b). In this study, we found that

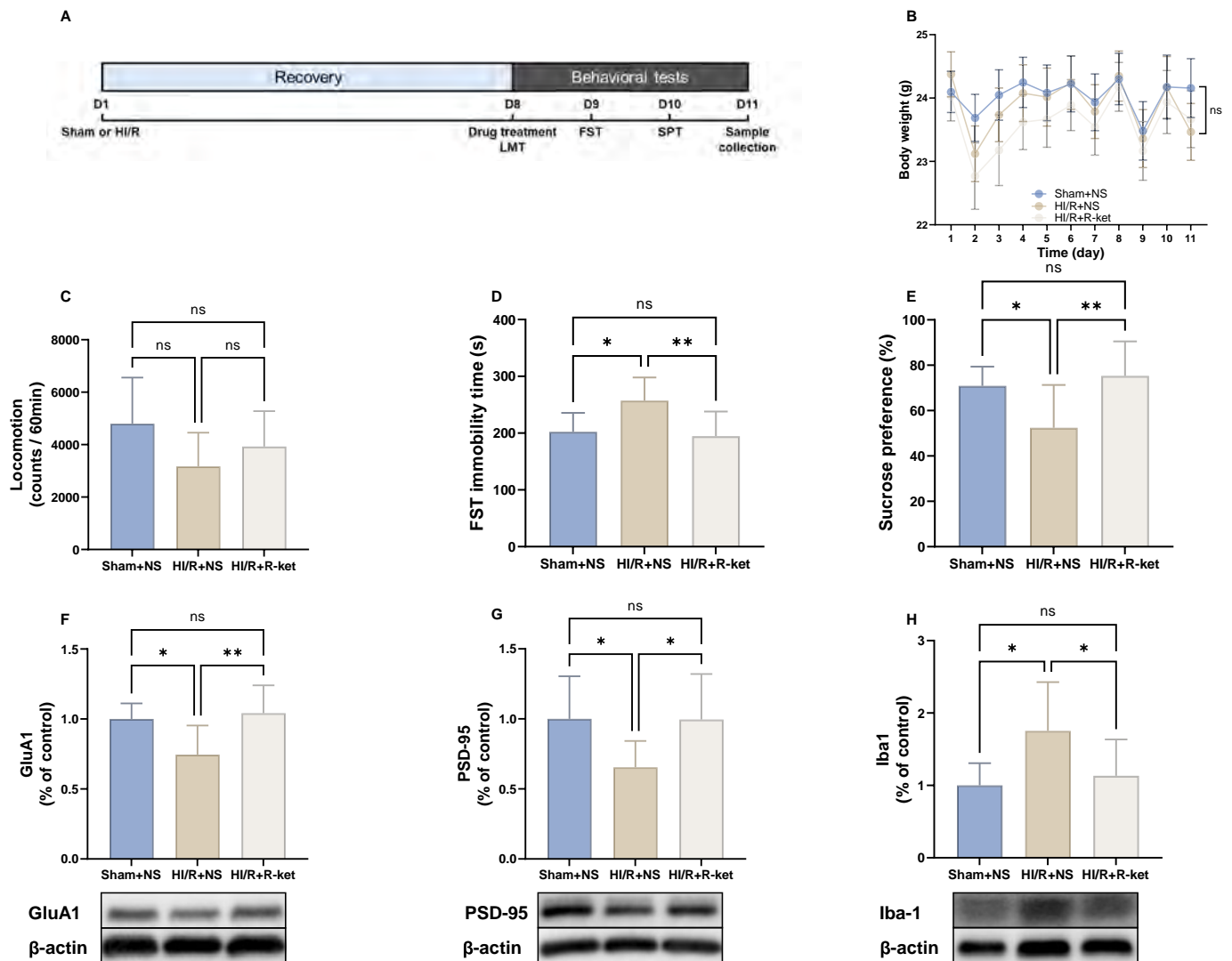


Fig. 7. Effect of new antidepressant arketamine in depression-like phenotypes of mice with HI/R injury.

(A): Experimental schedule. On day 1, sham or HI/R was performed, and they were recovered 7 days. On day 8, normal saline (NS) (10 ml/kg) or arketamine (R-ket) (10 mg/kg) was administered intraperitoneally and subsequently LMT was performed. FST and SPT were performed on day 9 and day 10, respectively. On day 11, prefrontal cortex (PFC) and plasma samples were collected. (B): Body weight (repeated measure ANOVA, $F_{(2, 24)} = 0.2773$, $P = 0.7603$). (C): LMT (one-way ANOVA, $F_{(2, 24)} = 2.728$, $P = 0.0856$). (D): FST (one-way ANOVA, $F_{(2, 24)} = 6.770$, $P = 0.0047$). (E): SPT (one-way ANOVA, $F_{(2, 24)} = 6.034$, $P = 0.0075$). (F): Western blot analysis of GluA1 in the PFC (one-way ANOVA, $F_{(2, 24)} = 7.317$, $P = 0.0033$) and the representative bands. (G): Western blot analysis of PSD-95 in the PFC (one-way ANOVA, $F_{(2, 24)} = 4.538$, $P = 0.0213$) and the representative bands. (H): Western blot analysis of Iba1 in the PFC (one-way ANOVA, $F_{(2, 24)} = 5.422$, $P = 0.0114$) and the representative bands. The data are shown as means \pm S.E.M (Sham + NS group: $n = 9$, HI/R + NS group: $n = 9$, HI/R + arketamine group: $n = 9$). ANOVA: analysis of variance. NS: normal saline. R-ket: Arketamine. ns: not significant; * $P < 0.05$; ** $P < 0.01$.

SDV notably reduced depression-like phenotypes and splenomegaly in mice with HI/R injury by exerting anti-inflammatory effects. Given the role of the gut–liver axis in liver diseases (Albillos et al., 2020; Schwabe and Greten, 2020; Wiest et al., 2017; Zhang et al., 2022b), it is likely that the gut–liver–brain axis, via the subdiaphragmatic vagus nerve, plays a critical role in depression-like phenotypes in mice with HI/R injury. A study underscored the role of the vagus nerve in regulating the systemic inflammatory response to the endotoxin LPS (Borovikova et al., 2000). Given this, SDV might effectively reduce systemic inflammation in this model. Because vagus nerve stimulation (VNS) has potent anti-inflammatory actions (Hashimoto, 2023a, 2023c; Wang et al., 2022), it is likely that VNS might be a potential therapeutic option for patients with CLD.

The robust antidepressant action of the anesthetic ketamine was a serendipitous discovery in the field of psychiatric disorders, producing rapid-acting and sustained antidepressant actions in treatment-resistant patients with depression (Hashimoto, 2022). Accumulating preclinical

data suggest that arketamine, the (*R*)-enantiomer of ketamine, is a safer antidepressant than ketamine or esketamine, the (*S*)-enantiomer of ketamine (Hashimoto, 2020; Wei et al., 2022b; Zhang et al., 2022a; Zhang et al., 2023). Previous studies have reported that arketamine improves depression-like behaviors and altered composition of the gut microbiota in mice with depression-like behaviors (Qu et al., 2017; Wan et al., 2023; Yang et al., 2017), suggesting a role of the gut microbiota–brain axis in the beneficial effects of arketamine (Hashimoto, 2020, 2023b; Hua et al., 2022; Wei et al., 2022b). In this study, we found that arketamine improved depression-like phenotypes in mice with HI/R injury. It is noteworthy that these changes in mice with HI/R injury were ameliorated by a single post-injection of arketamine. Although the mechanisms underlying the effects of arketamine in the HI/R model are currently unclear, it is likely that anti-inflammatory actions via the gut–liver–brain axis may play a role in its beneficial effects. A phase II trial of arketamine (PCN-101) by Perception Neuroscience is currently underway (Zhang et al., 2022a). Therefore, it is of interest to investigate

whether arketamine can improve depression in patients with CLD.

This study has some limitations. First, we did not evaluate the blood levels of alanine aminotransferase (ALT) and aspartate aminotransferase (AST), nor did we conduct H&E staining of the liver 7 days post-surgery. This is because ALT and AST levels typically return to baseline 24 h after surgery (Wu et al., 2011). Second, we focused on the PFC for assessing synaptic protein expression, even though other brain regions, such as hippocampus, are implicated in depression. Third, we did not investigate the effects of fecal microbiota transplantation (FMT) from mice with HI/R injury, which would have provided insights into the role of gut microbiota in depression-like phenotypes. This necessitates future exploration using FMT from mice with HI/R injury. Fourth, the study did not examine the impact of an antibiotic cocktail designed to delete host microbiota, leaving room to further determine the influence of host microbiota in this model. A future study using an antibiotic cocktail is recommended. Finally, we have yet to explore the relationship between the microbiome or metabolites and depression-like phenotypes in mice with HI/R injury. Future research should delve into how these factors potentially influence depression-like phenotypes in this model.

In summary, our findings suggest that the gut microbiota–liver–brain axis, via the subdiaphragmatic vagus nerve, plays a key role in depression-like phenotypes in the HI/R mouse model. Arketamine may have therapeutic potential for depression in patients with CLD.

Financial support

This study was supported by the grant from Japan Society for the Promotion of Science (to K.H., 21H02846, 21H00184, 21H05612), JST OPERA Program Japan (to C.M. JPMJOP1831) and unrestricted grant of Yamada Bee Company, Japan (to C.M.). Dr. Yong Yang was supported by the Japan China Sasakawa Medical Fellowship (Tokyo, Japan). Dr. Yong Yang and Ms. Xiayun Wan were supported by the Academic Research & Innovation Management Organization of Chiba University (Chiba, Japan).

Author statement

YY and KH designed the study. YY, and XW performed the experiments. AE and CM performed metabolomics analysis. YY analyzed the data. YY and KH wrote the manuscript. All authors have read and approved the final manuscript.

CRediT authorship contribution statement

YY and KH performed study concept/design; YY and XW performed animal experiments and data acquisition; AE and CM performed metabolomic and lipidomic analyses; YY and KH drafted manuscript; CM and KH obtained funding; all authors have read/edited the manuscript.

Declaration of competing interest

Dr. Hashimoto is the inventor of filed patent applications on “The use of R-Ketamine in the treatment of psychiatric diseases”, “(S)-norketamine and salt thereof as pharmaceutical”, “R-Ketamine and derivative thereof as prophylactic or therapeutic agent for neurodegeneration disease or recognition function disorder”, “Preventive or therapeutic agent and pharmaceutical composition for inflammatory diseases or bone diseases”, “R-Ketamine and its derivatives as a preventive or therapeutic agent for a neurodevelopmental disorder”, and “Preventive or therapeutic agent and pharmaceutical composition for inflammatory diseases” by the Chiba University. Dr. Hashimoto also declares that he has received research support and consultant from Abbott, Boehringer Ingelheim, Daiichi-Sankyo, Meiji Seika Pharma, Seikagaku Corporation, Sumitomo-Pharma, Taisho, Otsuka, Murakami Farm and Perception Neuroscience. The other authors have no conflict of interest.

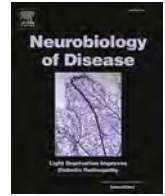
Acknowledgment

We thank Edanz (<https://jp.edanz.com/ac>) for editing a draft of this manuscript.

References

- Albillos, A., de Gottardi, A., Rescigno, M., 2020. The gut-liver axis in liver disease: pathophysiological basis for therapy. *J. Hepatol.* 72 (3), 558–577. <https://doi.org/10.1016/j.jhep.2019.10.003>.
- Bianchi, G., Marchesini, G., Nicolino, F., Graziani, R., Sgarbi, D., Loguercio, C., Abbiati, R., Zoli, M., 2005. Psychological status and depression in patients with liver cirrhosis. *Dig. Liver Dis.* 37 (8), 593–600. <https://doi.org/10.1016/j.dld.2005.01.020>.
- Bonaz, B., Bazin, T., Pellissier, S., 2018. The vagus nerve at the interface of the microbiota-gut-brain axis. *Front. Neurosci.* 12, 49. <https://doi.org/10.3389/fnins.2018.00049>.
- Borovikova, L.V., Ivanova, S., Zhang, M., Yang, H., Botchkina, G.I., Watkins, L.R., Wang, H., Abumrad, N., Eaton, J.W., Tracey, K.J., 2000. Vagus nerve stimulation attenuates the systemic inflammatory response to endotoxin. *Nature* 405 (6785), 458–462. <https://doi.org/10.1038/35013070>.
- Chang, L., Wei, Y., Hashimoto, K., 2022. Brain-gut-microbiota axis in depression: a historical overview and future directions. *Brain Res. Bull.* 182, 44–56. <https://doi.org/10.1016/j.brainresbull.2022.02.004>.
- Cryan, J.F., O’Riordan, K.J., Cowan, C.S.M., Sandhu, K.V., Bastiaansen, T.F.S., Boehme, M., Codagnone, M.G., Cussotto, S., Fulling, C., Golubeva, A.V., Guzzetta, K. E., Jaggar, M., Long-Smith, C.M., Lyte, J.M., Martin, J.A., Molinero-Perez, A., Moloney, G., Morelli, E., Morillas, E., O’Connor, R., Cruz-Pereira, J.S., Peterson, V.L., Rea, K., Ritz, N.L., Sherwin, E., Spichak, S., Teichman, E.M., van de Wouw, M., Ventura-Silva, A.P., Wallace-Fitzsimons, S.E., Hyland, N., Clarke, G., Dinan, T.G., 2019. The microbiota-gut-brain axis. *Physiol. Rev.* 99 (4), 1877–2013. <https://doi.org/10.1152/physrev.00018.2018>.
- Forsythe, P., Bienenstock, J., Kunze, W.A., 2014. Vagal pathways for microbiome-brain-gut axis communication. *Adv. Exp. Med. Biol.* 817, 115–133. https://doi.org/10.1007/978-1-4939-0897-4_5.
- Gutteling, J.J., de Man, R.A., van der Plas, S.M., Schalm, S.W., Busschbach, J.J.V., Darlington, A.S.E., 2006. Determinants of quality of life in chronic liver patients. *Aliment. Pharmacol. Ther.* 23 (11), 1629–1635. <https://doi.org/10.1111/j.1365-2036.2006.02934.x>.
- Hashimoto, K., 2020. Molecular mechanisms of the rapid-acting and long-lasting antidepressant actions of (R)-ketamine. *Biochem. Pharmacol.* 177, 113935. <https://doi.org/10.1016/j.bcp.2020.113935>.
- Hashimoto, K., 2022. Ketamine: anesthetic, psychotomimetic, antidepressant, or anthelmintic? *Mol. Psychiatry* 27 (8), 3116–3118.
- Hashimoto, K., 2023a. Neuroinflammation through the vagus nerve-dependent gut–microbiota–brain axis in treatment-resistant depression. *Prog. Brain Res.* 278, 61–77. <https://doi.org/10.1016/bs.pbr.2023.01.003>.
- Hashimoto, K., 2023b. Arketamine for cognitive impairment in psychiatric disorders. *Eur. Arch. Psychiatry Clin. Neurosci.* 273 (7), 1513–1525. <https://doi.org/10.1007/s00406-023-01570-5>.
- Hashimoto, K., 2023c. Detrimental effects of COVID-19 in the brain and therapeutic options for long COVID: the role of Epstein-Barr virus and the gut-brain axis. *Mol. Psychiatry* (2023 Jul 4). <https://doi.org/10.1038/s41380-023-02161-5>.
- Hirao, H., Nakamura, K., Kupiec-Weglinski, J.W., 2022. Liver ischaemia-reperfusion injury: a new understanding of the role of innate immunity. *Nat. Rev. Gastroenterol. Hepatol.* 19 (4), 239–256. <https://doi.org/10.1038/s41575-021-00549-8>.
- Hua, H., Huang, C., Liu, H., Xu, X., Xu, X., Wu, Z., Liu, C., Wang, Y., Yang, C., 2022. Depression and antidepressant effects of ketamine and its metabolites: the pivotal role of gut microbiota. *Neuropharmacology* 220, 109272. <https://doi.org/10.1016/j.neuropharm.2022.109272>.
- Huang, X., Liu, X., Yu, Y., 2017. Depression and chronic liver diseases: are there shared underlying mechanisms? *Front. Mol. Neurosci.* 10, 134. <https://doi.org/10.3389/fnmol.2017.00134>.
- Ji, H., Shen, X., Gao, F., Ke, B., Freitas, M.C., Uchida, Y., Busuttill, R.W., Zhai, Y., Kupiec-Weglinski, J.W., 2010. Programmed death-1/B7-H1 negative costimulation protects mouse liver against ischemia and reperfusion injury. *Hepatology* 52 (4), 1380–1389. <https://doi.org/10.1002/hep.23843>.
- Ji, H., Zhang, Y., Liu, Y., Shen, X.D., Gao, F., Nguyen, T.T., Busuttill, R.W., Waschek, J.A., Kupiec-Weglinski, J.W., 2013. Vasoactive intestinal peptide attenuates liver ischemia/reperfusion injury in mice via the cyclic adenosine monophosphate-protein kinase a pathway. *Liver Transpl.* 19 (9), 945–956. <https://doi.org/10.1002/lt.23681>.
- Jiang, H., Ling, Z., Zhang, Y., Mao, H., Ma, Z., Yin, Y., Wang, W., Tang, W., Tan, Z., Shi, J., Li, L., Ruan, B., 2015. Altered fecal microbiota composition in patients with major depressive disorder. *Brain Behav. Immun.* 48, 186–194. <https://doi.org/10.1016/j.bbi.2015.03.016>.
- Konishi, T., Lentsch, A.B., 2017. Hepatic ischemia/reperfusion: mechanisms of tissue injury, repair, and regeneration. *Gene Expr.* 17 (4), 277–287. <https://doi.org/10.3727/105221617X15042750874156>.
- Kronsten, V.T., Tranah, T.H., Pariante, C., Shawcross, D.L., 2022. Gut-derived systemic inflammation as a driver of depression in chronic liver disease. *J. Hepatol.* 76 (3), 665–680. <https://doi.org/10.1016/j.jhep.2021.11.008>.

- Liu, L., Wang, H., Chen, X., Zhang, Y., Zhang, H., Xie, P., 2023. Gut microbiota and its metabolites in depression: from pathogenesis to treatment. *EBioMedicine* 90, 104527. <https://doi.org/10.1016/j.ebiom.2023.104527>.
- Lu, T., Li, Q., Lin, W., Zhao, X., Li, F., Ji, J., Zhang, Y., Xu, N., 2023. Gut microbiota-derived glutamine attenuates liver ischemia/reperfusion injury via macrophage metabolic reprogramming. *Cell. Mol. Gastroenterol. Hepatol.* 15 (5), 1255–1275. <https://doi.org/10.1016/j.jcmgh.2023.01.004>.
- Ma, L., Zhang, J., Fujita, Y., Qu, Y., Shan, J., Wan, X., Wang, X., Ishima, T., Kobayashi, K., Wang, L., Hashimoto, K., 2022. Nuclear factor of activated T cells 4 in the prefrontal cortex is required for prophylactic actions of (R)-ketamine. *Transl. Psychiatry* 12 (1), 27. <https://doi.org/10.1038/s41398-022-01803-6>.
- Ma, L., Wang, L., Qu, Y., Wan, X., Hashimoto, K., 2023. A role of splenic heme biosynthesis pathway in the persistent prophylactic actions of arketamine in lipopolysaccharide-treated mice. *Transl. Psychiatry* 13 (1), 269. <https://doi.org/10.1038/s41398-023-02564-6>.
- Mullish, B.H., Kabir, M.S., Thursz, M.R., Dhar, A., 2014. Review article: depression and the use of antidepressants in patients with chronic liver disease or liver transplantation. *Aliment. Pharmacol. Ther.* 40 (8), 880–892. <https://doi.org/10.1111/apt.12925>.
- Patten, S.B., Williams, J.V., Lavorato, D.H., Modgill, G., Jette, N., Eliasziw, M., 2008. Major depression as a risk factor for chronic disease incidence: longitudinal analysis in a general population cohort. *Gen. Hosp. Psychiatry* 30 (5), 407–413. <https://doi.org/10.1016/j.genhosppsych.2008.05.001>.
- Pu, Y., Tan, Y., Qu, Y., Chang, L., Wang, S., Wei, Y., Wang, X., Hashimoto, K., 2021. A role of the subdiaphragmatic vagus nerve in depression-like phenotypes in mice after fecal microbiota transplantation from *Chrna7* knock-out mice with depression-like phenotypes. *Brain Behav. Immun.* 94, 318–326. <https://doi.org/10.1016/j.bbi.2020.12.032>.
- Qu, Y., Yang, C., Ren, Q., Ma, M., Dong, C., Hashimoto, K., 2017. Comparison of (R)-ketamine and lanicemine on depression-like phenotype and abnormal composition of gut microbiota in a social defeat stress model. *Sci. Rep.* 7 (1), 15725. <https://doi.org/10.1038/s41598-017-16060-7>.
- Rampes, S., Ma, D., 2019. Hepatic ischemia-reperfusion injury in liver transplant setting: mechanisms and protective strategies. *J. Biomed. Res.* 33 (4), 221–234. <https://doi.org/10.7555/JBR.32.20180087>.
- Sanada, K., Nakajima, S., Kurokawa, S., Barceló-Soler, A., Ikuse, D., Hirata, A., Yoshizawa, A., Tomizawa, Y., Salas-Valero, M., Noda, Y., Mimura, M., Iwanami, A., Kishimoto, T., 2020. Gut microbiota and major depressive disorder: a systematic review and meta-analysis. *J. Affect. Disord.* 266, 1–13. <https://doi.org/10.1016/j.jpsy.2021.05.009>.
- Schwabe, R.F., Greden, T.F., 2020. Gut microbiome in HCC—mechanisms, diagnosis and therapy. *J. Hepatol.* 72 (2), 230–238. <https://doi.org/10.1016/j.jhep.2019.08.016>.
- Tsugawa, H., Ikeda, K., Takahashi, M., Satoh, A., Mori, Y., Uchino, H., Okahashi, N., Yamada, Y., Tada, I., Bonini, P., Higashi, Y., Okazaki, Y., Zhou, Z., Zhu, Z.J., Koelmel, J., Cajka, T., Fiehn, O., Saito, K., Arita, M., Arita, M., 2020. A lipidome atlas in MS-DIAL 4. *Nat. Biotechnol.* 38 (10), 1159–1163. <https://doi.org/10.1038/s41587-020-0531-2>.
- Wan, X., Eguchi, A., Chang, L., Mori, C., Hashimoto, K., 2023. Beneficial effects of arketamine on the reduced bone mineral density in susceptible mice after chronic social defeat stress: role of the gut-microbiota-bone-brain axis. *Neuropharmacology* 228, 109466. <https://doi.org/10.1016/j.neuropharm.2023.109466>.
- Wang, S., Ishima, T., Zhang, J., Qu, Y., Chang, L., Pu, Y., Fujita, Y., Tan, Y., Wang, X., Hashimoto, K., 2020. Ingestion of *Lactobacillus intestinalis* and *Lactobacillus reuteri* causes depression- and anhedonia-like phenotypes in antibiotic-treated mice via the vagus nerve. *J. Neuroinflammation* 17 (1), 241. <https://doi.org/10.1186/s12974-020-01916-z>.
- Wang, S., Ishima, T., Qu, Y., Shan, J., Chang, L., Wei, Y., Zhang, J., Pu, Y., Fujita, Y., Tan, Y., Wang, X., Ma, L., Wan, X., Hammock, B.D., Hashimoto, K., 2021. Ingestion of *Faecalibaculum rodentium* causes depression-like phenotypes in resilient *Ephx2* knock-out mice: a role of brain-gut-microbiota axis via the subdiaphragmatic vagus nerve. *J. Affect. Disord.* 292, 565–573. <https://doi.org/10.1016/j.jad.2021.06.006>.
- Wang, X., Yang, J., Hashimoto, K., 2022. (R)-ketamine as prophylactic and therapeutic drug for neurological disorders: beyond depression. *Neurosci. Biobehav. Rev.* 139, 104762. <https://doi.org/10.1016/j.neubiorev.2022.104762>.
- Wang, X., Eguchi, A., Yang, Y., Chang, L., Wan, X., Shan, J., Qu, Y., Ma, L., Mori, C., Yang, J., Hashimoto, K., 2023. Key role of the gut-microbiota-brain axis via the subdiaphragmatic vagus nerve in demyelination of the cuprizone-treated mouse brain. *Neurobiol. Dis.* 176, 105951. <https://doi.org/10.1016/j.nbd.2022.105951>.
- Wei, Y., Chang, L., Hashimoto, K., 2022a. Molecular mechanisms underlying the antidepressant actions of arketamine: beyond the NMDA receptor. *Mol. Psychiatry* 27 (1), 559–573. <https://doi.org/10.1038/s41380-021-01121-1>.
- Wei, Y., Wang, T., Liao, L., Fan, X., Chang, L., Hashimoto, K., 2022b. Brain-spleen axis in health and diseases: a review and future perspective. *Brain Res. Bull.* 182, 130–140. <https://doi.org/10.1016/j.brainresbull.2022.02.008>.
- Wiest, R., Albillos, A., Trauner, M., Bajaj, J.S., Jalan, R., 2017. Targeting the gut-liver axis in liver disease. *J. Hepatol.* 67 (5), 1084–1103. <https://doi.org/10.1016/j.jhep.2017.05.007>.
- Wu, C., Xia, Y., Wang, P., Lu, L., Zhang, F., 2011. Triptolide protects mice from ischemia/reperfusion injury by inhibition of IL-17 production. *Int. Immunopharmacol.* 11 (10), 1564–1572. <https://doi.org/10.1016/j.intimp.2011.05.015>.
- Yang, C., Shirayama, Y., Zhang, J.C., Ren, Q., Yao, W., Ma, M., Dong, C., Hashimoto, K., 2015. R-ketamine: a rapid-onset and sustained antidepressant without psychotomimetic side effects. *Transl. Psychiatry* 5 (9), e632. <https://doi.org/10.1038/tp.2015.136>.
- Yang, C., Qu, Y., Fujita, Y., Ren, Q., Ma, M., Dong, C., Hashimoto, K., 2017. Possible role of the gut microbiota-brain axis in the antidepressant effects of (R)-ketamine in a social defeat stress model. *Transl. Psychiatry* 7 (12), 1294. <https://doi.org/10.1038/s41398-017-0031-4>.
- Yang, C., Yang, J., Luo, A., Hashimoto, K., 2019. Molecular and cellular mechanisms underlying the antidepressant effects of ketamine enantiomers and its metabolites. *Transl. Psychiatry* 9 (1), 280. <https://doi.org/10.1038/s41398-019-0624-1>.
- Yang, Y., Ishima, T., Wan, X., Wei, Y., Chang, L., Zhang, J., Qu, Y., Hashimoto, K., 2022. Microglial depletion and abnormalities in gut microbiota composition and short-chain fatty acids in mice after repeated administration of colony stimulating factor 1 receptor inhibitor PLX5622. *Eur. Arch. Psychiatry Clin. Neurosci.* 272 (3), 483–495. <https://doi.org/10.1007/s00406-021-01325-0>.
- Yang, Y., Eguchi, A., Wan, X., Chang, L., Wang, X., Qu, Y., Mori, C., Hashimoto, K., 2023. A role of gut-microbiota-brain axis via subdiaphragmatic vagus nerve in depression-like phenotypes in *Chrna7* knock-out mice. *Prog. Neuropsychopharmacol. Biol. Psychiatry* 120, 110652. <https://doi.org/10.1016/j.pnpbp.2022.110652>.
- Yue, C., Luan, W., Gu, H., Qiu, D., Ding, X., Liu, P., Wang, X., Hashimoto, K., Yang, J.J., 2023. The role of the gut-microbiota-brain axis via the subdiaphragmatic vagus nerve in chronic inflammatory pain and comorbid spatial working memory impairment in complete Freund's adjuvant mice. *J. Psychiatr. Res.* 166, 61–73. <https://doi.org/10.1016/j.jpsy.2023.09.003>.
- Zhang, J.C., Li, S.X., Hashimoto, K., 2014. R (-)-ketamine shows greater potency and longer lasting antidepressant effects than S (+)-ketamine. *Pharmacol. Biochem. Behav.* 116, 137–141. <https://doi.org/10.1016/j.pbb.2013.11.033>.
- Zhang, J., Ma, L., Chang, L., Pu, Y., Qu, Y., Hashimoto, K., 2020. A key role of the subdiaphragmatic vagus nerve in the depression-like phenotype and abnormal composition of gut microbiota in mice after lipopolysaccharide administration. *Transl. Psychiatry* 10 (1), 186. <https://doi.org/10.1038/s41398-020-00878-3>.
- Zhang, J., Ma, L., Wan, X., Shan, J., Qu, Y., Hashimoto, K., 2021a. (R)-ketamine attenuates LPS-induced endotoxin-derived delirium through inhibition of neuroinflammation. *Psychopharmacology (Berl)* 238 (10), 2743–2753. <https://doi.org/10.1007/s00213-021-05889-6>.
- Zhang, Y., Xie, B., Chen, X., Zhang, J., Yuan, S., 2021b. A key role of gut microbiota-vagus nerve/spleen axis in sleep deprivation-mediated aggravation of systemic inflammation after LPS administration. *Life Sci.* 265, 118736. <https://doi.org/10.1016/j.lfs.2020.118736>.
- Zhang, J.C., Yao, W., Hashimoto, K., 2022a. Arketamine, a new rapid-acting antidepressant: a historical review and future directions. *Neuropharmacology* 218, 109219. <https://doi.org/10.1016/j.neuropharm.2022.109219>.
- Zhang, X., Liu, H., Hashimoto, K., Yuan, S., Zhang, J., 2022b. The gut–liver axis in sepsis: interaction mechanisms and therapeutic potential. *Crit. Care* 26 (1), 213. <https://doi.org/10.1186/s13054-022-04090-1>.
- Zhang, K., Yao, Y., Hashimoto, K., 2023. Ketamine and its metabolites: potential as novel treatments for depression. *Neuropharmacology* 222, 109305. <https://doi.org/10.1016/j.neuropharm.2022.109305>.
- Zheng, P., Zeng, B., Zhou, C., Liu, M., Fang, Z., Xu, X., Zeng, L., Chen, J., Fan, S., Du, X., Zhang, X., Yang, D., Wang, Y., Meng, H., Li, W., Melgiri, N.D., Licinio, J., Wei, H., Xie, P., 2016. Gut microbiome remodeling induces depressive-like behaviors through a pathway mediated by the host's metabolism. *Mol. Psychiatry* 21 (6), 786–796. <https://doi.org/10.1038/mp.2016.44>.



Depression-like phenotypes in mice following common bile duct ligation: Insights into the gut–liver–brain axis via the vagus nerve

Yong Yang^{a,b}, Akifumi Eguchi^c, Chisato Mori^{c,d}, Kenji Hashimoto^{a,*}

^a Division of Clinical Neuroscience, Chiba University Center for Forensic Mental Health, Chiba 260-8670, Japan

^b Department of Neurosurgery, Guizhou Provincial People's Hospital, Guiyang 550002, China

^c Department of Sustainable Health Science, Chiba University Center for Preventive Medical Sciences, Chiba 263-8522, Japan

^d Department of Bioenvironmental Medicine, Graduate School of Medicine, Chiba University, Chiba 260-8670, Japan

ARTICLE INFO

Keywords:

Arketamine
Depression
Gut microbiota
Liver cirrhosis
Metabolites
Vagus nerve

ABSTRACT

Depression frequently occurs in patients with liver cirrhosis, yet the reasons for this correlation are not fully understood. Dysbiosis of gut microbiota has been implicated in depression through the gut–brain axis via the vagus nerve. This study explored the potential role of the gut–liver–brain axis via the vagus nerve in depression-like phenotypes in mice with liver cirrhosis. These mice underwent common bile duct ligation (CBDL), a method used to stimulate liver cirrhosis. To assess depression-like behaviors, behavioral tests were conducted 10 days following either sham or CBDL surgeries. The mice with CBDL displayed symptoms such as splenomegaly, elevated plasma levels of interleukin-6 and tumor necrosis factor- α , depression-like behaviors, decreased levels of synaptic proteins in the prefrontal cortex (PFC), disrupted gut microbiota balance, and changes in blood metabolites (or lipids). Additionally, there were positive or negative correlations between the relative abundance of microbiome and behavioral data or blood metabolites (or lipids). Significantly, these changes were reversed in CBDL mice by performing a subdiaphragmatic vagotomy. Intriguingly, depression-like phenotypes in mice with CBDL were improved after a single injection of arketamine, a new antidepressant. These results suggest that CBDL-induced depression-like phenotypes in mice are mediated through the gut–liver–brain axis via the subdiaphragmatic vagus nerve, and that arketamine might offer a new treatment approach for depression in liver cirrhosis patients.

1. Introduction

Liver cirrhosis, characterized by the overaccumulation of extracellular matrix proteins like collagen, is common in most chronic liver diseases (CLDs) (Ginès et al., 2021; Tapper and Parikh, 2023). Depression is frequently observed in liver cirrhosis patients, with its prevalence notably higher than in the general populations, indicating a possible connection between these conditions (Bianchi et al., 2005; Nardelli et al., 2013; Singh et al., 1997). A substantial U.S. population-based study (56,197,690 adults) found a significant association between liver cirrhosis and an increased risk of depression (Abureesh et al., 2022). The exact biological mechanisms linking depression and liver cirrhosis remain elusive. However, liver cirrhosis can induce various physiological changes that might contribute to depression, including hormonal imbalances, immune system dysfunction, and the build-up of neurotoxins that the damaged liver fails to filter effectively (Bonnel

et al., 2011; Kur et al., 2020; Zhou et al., 2014). Notably, the severity of liver disease in patients with cirrhosis correlates with signs of psychological distress and depression (Bianchi et al., 2005). Depression in liver cirrhosis patients is more than a comorbidity; it can influence the liver disease's progression, affecting treatment adherence, lifestyle choices, and overall prognosis. Therefore, treating depression in these patients is essential. Although the interaction between liver cirrhosis and depression is complex and bidirectional, the precise underlying mechanisms are still not fully understood (Huang et al., 2017).

Numerous clinical and pre-clinical studies indicate a significant role of the gut–brain axis, including gut microbiota, in depression (Chang et al., 2022; Cryan et al., 2019; Hashimoto, 2023a, 2023b; Hua et al., 2022; Liu et al., 2023; Sanada et al., 2020; Wei et al., 2022a, 2022b; Zheng et al., 2016). The vagus nerve is key in the two-way communication between the gut microbiota and the brain (Bonaz et al., 2018; Chang et al., 2022; Forsythe et al., 2014; Hashimoto, 2023b, 2023c; Wei

* Corresponding author.

E-mail address: hashimoto@faculty.chiba-u.jp (K. Hashimoto).

<https://doi.org/10.1016/j.nbd.2024.106433>

Received 13 January 2024; Received in revised form 6 February 2024; Accepted 6 February 2024

Available online 7 February 2024

0969-9961/© 2024 The Authors. Published by Elsevier Inc. This is an open access article under the CC BY-NC-ND license (<http://creativecommons.org/licenses/by-nc-nd/4.0/>).

et al., 2022b). Interestingly, subdiaphragmatic vagotomy (SDV) has been shown to prevent depression-like behaviors and alterations in gut microbiota composition in mice following lipopolysaccharide (LPS) administration (Zhang et al., 2020) and fecal microbiota transplantation (FMT) from mice with depression-like phenotypes (Pu et al., 2021; Wang et al., 2020, 2021). Additionally, SDV blocks depression-like behaviors in *Chrna7* knock-out mice (Yang et al., 2023) and in mice with hepatic ischemia/reperfusion (HI/R) injury (Yang et al., 2024), as well as working memory impairment in mice with chronic inflammatory pain (Yue et al., 2023). SDV also blocks the resilience-enhancing effects of the entactogen 3,4-methylenedioxymetamphetamine in mice subjected to chronic restraint stress (Qu et al., 2023a, 2023b), and prevents demyelination in the mouse brain treated with cuprizone (Wang et al., 2023). These studies support the crucial role of the gut–brain axis via the subdiaphragmatic vagus nerve in depression (Chang et al., 2022; Hashimoto, 2023b; Wei et al., 2022a). Kronsten et al. (2022) hypothesized that gut-mediated systemic inflammation might link depression and CLD, indicating potential abnormalities in the gut–liver–brain axis. Furthermore, clinical data highlight significant patterns of gut microbiota dysbiosis in liver cirrhosis patients, which may lead to cognitive impairments and mood disorders (Smith et al., 2023).

Common bile duct ligation (CBDL), a well-established model for studying secondary biliary fibrosis, triggers the proliferation of biliary epithelial cells and oval cells. This proliferation leads to an increase in bile ductules, portal inflammation, and fibrosis, and ultimately results in liver cirrhosis and liver failure (Geerts et al., 2008; Tag et al., 2015; Van Campenhout et al., 2019). While rodent models of CBDL are extensively utilized in research, there have been no studies reported to date that demonstrate depression-like phenotypes in rodents subjected to CBDL. Similarly, the potential role of the gut–liver–brain axis, specifically through the vagus nerve, in rodents with CBDL has not been reported in the literature.

This study aimed to explore the connection between depression and liver cirrhosis. Initially, we assessed depression-like behaviors in mice with CBDL, alongside measuring blood inflammation markers and synaptic proteins in the brain. Secondly, to delve into the gut–liver–brain axis's role in these depression-like behaviors, we conducted 16 s rRNA analysis of feces samples and untargeted metabolomic and lipidomic analyses of plasma samples. Thirdly, we explored the role of the subdiaphragmatic vagus nerve on these depression-like phenotypes by performing SDV. Lastly, we investigated the impact of the novel antidepressant arketamine in mice with CBDL since a single dose showed rapid-acting antidepressant-like effects in rodents with depression-like phenotypes (Hashimoto, 2020, 2022, 2023d; Wei et al., 2022a; Yang et al., 2015, 2019; Zhang et al., 2014, 2022a; Zhang et al., 2023).

2. Materials and methods

2.1. Animals

Male adult C57BL/6Ncr mice, sourced from the Japan SLC Co., Ltd. (Hamamatsu, Shizuoka, Japan), were used in this study. All the experimental mice were aged 9 weeks, body weight 21.5–26.5 g. All the experimental mice were acclimatized to standard laboratory conditions (4 or 5/ cage), maintained alternating cycles of 12 h of light and 12 h of darkness (lights on from 7:00–19:00), and under constant room temperature of 23 ± 1 °C and controlled humidity of $55 \pm 5\%$. Animals were given free admittance to chow and water. The experimental protocol of present study was approved by the Chiba University Institutional Animal Care and Use Committee (Permission numbers 4–312, 4–405 and 4–441). The mice were all firstly deeply anesthetized with inhaled isoflurane and then rapidly sacrificed by cervical dislocation. All efforts were made to minimize animal's suffering.

2.2. Reagents

Arketamine [or (*R*)-ketamine] hydrochloride was prepared as reported previously (Zhang et al., 2014). The dose (10 mg/kg as hydrochloride salt) of arketamine was dissolved in the saline as reported previously (Yang et al., 2015; Yang et al., 2024; Yao et al., 2022). Other reagents were purchased commercially.

2.3. Common bile duct ligation (CBDL)

Sham or CBDL surgeries were performed under continuous inhalation anesthesia with 4–5% isoflurane using an inhalation small animal anesthesia apparatus (KN-1071 NARCOBIT-E; Natsume Seisakusho, Tokyo, Japan), with minor modifications from previous reports (Tag et al., 2015). Briefly, mice were placed in a supine position and, once fully anesthetized, the abdominal operation area was prepared. The skin was disinfected with iodophor. A 1.5 cm median incision was made along the abdominal midline, starting 0.5 cm below the xiphoid process. This incision was gently opened using a Mini incision spreader to expose the liver. The liver tissue was carefully maneuvered upwards with a small cotton ball moistened in saline, aided by a surgical microscope (Leica, Heidelberg, Germany), positioning the ventral side against the diaphragm and making the hilum visible. The small intestine was gently separated to expose the common bile duct. The bile duct was carefully isolated from the adjacent portal vein and hepatic artery using microserrations forceps. A 5–0 suture was placed around the bile duct and secured with two surgical knots, applying increasing traction to ensure effective obstruction without severing the duct. A second ligation was added in the same manner but did not dissect the bile duct in-between. Post-operation, no bleeding or no additional injury was noted. The peritoneal cavity was rinsed with 0.9% NaCl solution, and abdominal organs were gently repositioned. The abdominal incision was sutured in layers using 5–0 surgical silk, maintaining aseptic conditions throughout.

During sham surgeries, an identical abdominal incision was made, and the common bile duct was exposed, but not ligated. All other steps mirrored those of the surgery group.

2.4. Bilateral subdiaphragmatic vagotomy (SDV)

Bilateral SDV or sham surgeries were conducted under continuous inhalation anesthesia with 4–5% isoflurane, using a small animal anesthesia apparatus (KN-1071 NARCOBIT-E; Natsume Seisakusho, Tokyo, Japan), following methods described in previous studies (Pu et al., 2021; Yang et al., 2023, 2024; Zhang et al., 2020). Briefly, mice were placed in a right-side decubitus position. The skin was disinfected with iodophor disinfectant, and sterile tissue was laid down. An incision about 1 cm in length, parallel to the costal arch, was made at 0.5 cm below the left costal arch, starting from the midline alba of abdomen. The incision was gently opened with a Mini incision spreader to expose the underlying liver tissue. The liver was cautiously elevated using a sterilized cotton ball moistened with saline, and under guidance of a surgical microscope (Leica, Heidelberg, Germany), the fascia between the caudate and left lobes of the liver was sharply incised to fully expose the esophagus and surrounding area. The dorsal and ventral branches of the vagus nerve running along the esophagus under the diaphragm were identified and carefully severed. Post-procedure, no bleeding or additional injury to the esophagus, liver, or other organs was observed. The liver tissue was repositioned, and 0.5 ml saline solution was injected into the abdominal cavity. The incision was then sutured in layers using 5–0 surgical silk, ensuring aseptic technique throughout. SDV success was verified by a significant increase in stomach volume on the 14th postoperative day, indicative of vagus nerve innervation loss.

During sham surgeries, an identical abdominal incision was made. The dorsal and ventral branches of the subdiaphragmatic vagus nerve were gently exposed but not severed. No bleeding or additional organ

damage was noted. After repositioning the abdominal organs, 0.5 ml normal saline was injected into the abdominal cavity, and the incision was closed using the same layered suture technique. When combining CBDL + SDV procedures, SDV was performed first via the same abdominal approach, followed by the CBDL procedure.

2.5. Behavioral tests

Behavioral tests, including locomotion test (LMT), forced swimming test (FST), and 1% sucrose preference test (SPT) were performed as reported previously (Yang et al., 2023, 2024) (Fig. 1A).

In order to monitor the locomotor activity of the mice, we adopted an automatic animal movement analysis system (SCANET MV-40; MEL-QUEST Co., Ltd., Toyama, Japan). The cumulative ambulatory activity counts were automatic document continuously over a total stage of 60 min (10 min \times 6 times) after the mice were placed into the experimental cube boxes [33 cm (height) \times 56 cm (width) \times 56 cm (length)]. To avoid experimental interference, the cube boxes were cleaned up during the test interval.

A mouse automated forced-swim apparatus (SCANET MV-40; MEL-QUEST Co., Ltd., Toyama, Japan) was used to perform FST. Mice were placed into an inescapable transparent tank [31 cm (height) \times 23 cm (diameter)] that was filled with tap water at a temperature of $23 \pm 1^\circ\text{C}$ and a depth of 15 cm. Then their escape related mobility behavior was measured immediately. The immobility times were automatic document

and calculated using the analytical software of the apparatus over a total stage of 6 min (1 min \times 6 times).

For 1% SPT, which was carried out in the separate animal's home cage. Each mouse was presented with two dual bearing sipper bottles, one bottle contained tap water, and the second contained a 1% sucrose solution. After 24 h of every mouse exposed to the respective two bottles containing different solutions, replaced the positions of two bottles for each other to lower any confound produced by a side bias. After another 24 h, all food and bottles were deprived lasting 4 h, then performed 1 h exposure to two identical bottles (containing tap water and 1% sucrose solution), which were weighed before and after the exposure period. The 1% sucrose preference was calculated as a percentage of 1% sucrose solution intake weight over the total liquid intake weight.

2.6. Enzyme-linked immunosorbent assay (ELISA)

ELISA kits for the detection of interleukin-6 (IL-6) (cat Number: 88-7064, Invitrogen, Camarillo, CA, USA), and tumor necrosis factor- α (TNF- α) (cat Number: 88-7324, Invitrogen, Camarillo, CA, USA) were used as reported previously (Yang et al., 2024).

2.7. Western blot analysis

Western blot analysis was conducted following the methods described in previous studies (Yang et al., 2022, 2023, 2024). Prefrontal

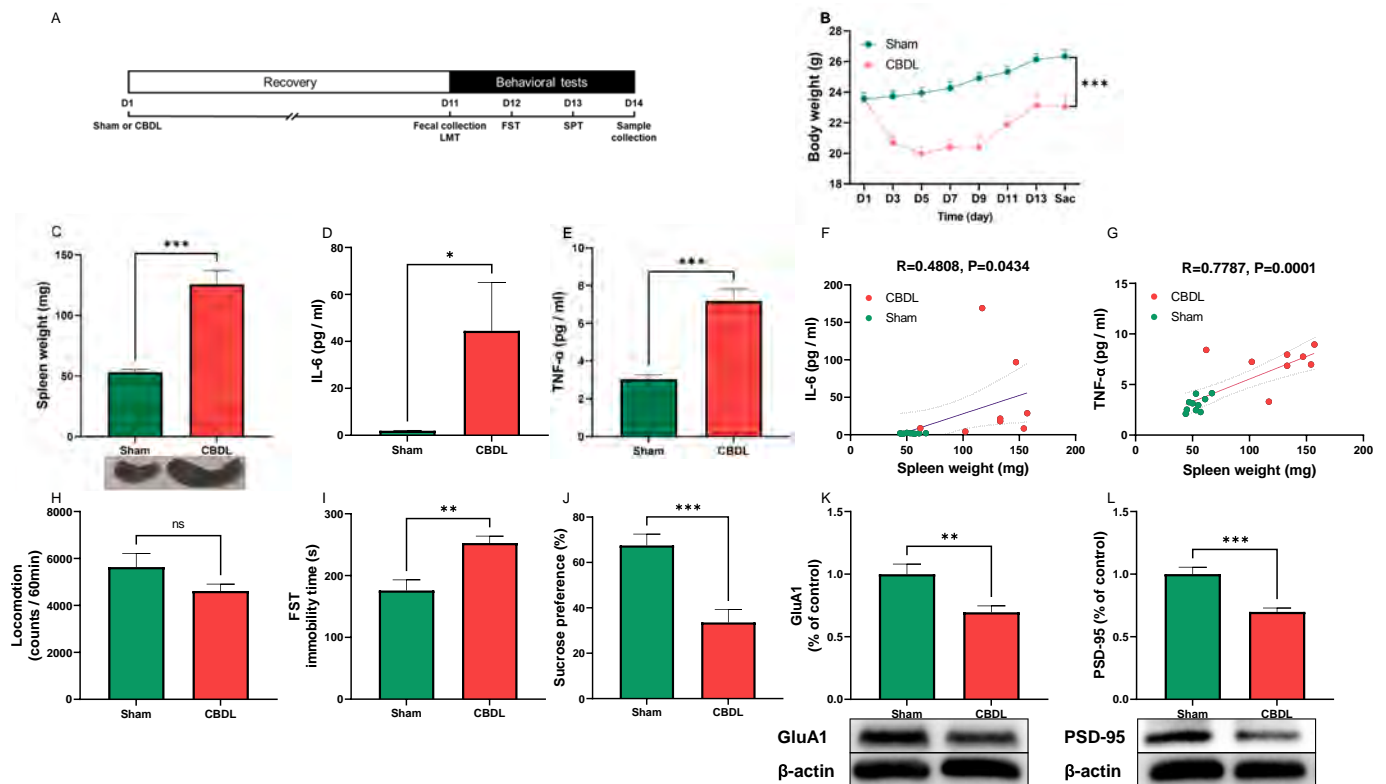


Fig. 1. Depression-like phenotypes in mice with CBDL.

(A): Experimental schedule. On day 1, mice underwent either sham or CBDL surgery. A 10-day recovery period followed. Fresh fecal samples were collected on day 11, and subsequently LMT was performed. FST and 1% SPT were performed on day 12 and day 13, respectively. Prefrontal cortex (PFC) and plasma samples were collected on day 14. (B): Body weight (repeated measure ANOVA, $F_{(1,16)} = 33.08$, $P < 0.001$). (C): Spleen weight (unpaired t -test, $t = 7.050$, $df = 16$, $P < 0.001$) and representative photograph of spleen in the two groups. (D): Plasma levels of IL-6 (unpaired t -test, $t = 2.320$, $df = 16$, $P = 0.0339$). (E): Plasma levels of TNF- α (unpaired t -test, $t = 6.895$, $df = 16$, $P < 0.001$). (F): There was a positive correlation ($R = 0.4808$, $P = 0.0434$) between the spleen weight and plasma levels of IL-6 in two groups. (G): There was a positive correlation ($R = 0.7787$, $P = 0.0001$) between the spleen weight and plasma levels of TNF- α in two groups. (H): locomotion (LMT) (unpaired t -test, $t = 1.446$, $df = 16$, $P = 0.1675$). (I): FST (unpaired t -test, $t = 3.522$, $df = 16$, $P = 0.0028$). (J): SPT (unpaired t -test, $t = 4.495$, $df = 16$, $P = 0.0004$). (K) Western blot analysis of GluA1 in the PFC (unpaired t -test, $t = 2.996$, $df = 16$, $P = 0.0086$) and the representative bands. (L): Western blot analysis of PSD-95 in the PFC (unpaired t -test, $t = 4.396$, $df = 16$, $P = 0.0005$) and the representative bands. The data are shown as means \pm S.E.M (sham group: $n = 10$, CBDL group: $n = 8$). ANOVA: analysis of variance. ns: not significant; * $P < 0.05$; ** $P < 0.01$; *** $P < 0.001$.

cortex (PFC) tissues were homogenized in ice-cold Laemmli lysis buffer, with each specimen processed separately to prevent cross-contamination. After centrifugation at 3000 ×g (RCF) at 4 °C for 20 min, liquid supernatants were collected. The total protein concentration in each sample was measured using a DC protein assay kit (Bio-Rad, Hercules, CA, USA) on a spectrophotometer (Molecular Devices Emax Precision Microplate Reader; Molecular Devices., San Jose, CA, USA). To prepare the samples for electrophoresis, a quarter volume of sample buffer (125 mM Tris-HCl, pH 6.8; 0.1% bromophenol blue; 4% sodium dodecyl sulfate; and 10% β-mercaptoethanol and 20% glycerol) was added to the Laemmli Lysis buffer. The proportions were adjusted to equalize the total protein concentration across samples. These mixtures were then incubated at 95 °C for 10 min. For electrophoresis, we employed 10% sodium dodecyl sulfate–polyacrylamide gel electrophoresis (SDS-PAGE) (catalog #: 4568125, Mini-PROTEAN TGX™ Stain-Free Gels; Bio-Rad, USA), selected based on the size of the target protein. The separated proteins were then transferred onto polyvinylidene difluoride membranes using a trans-Blot Mini Cell apparatus (Bio-Rad).

Synaptic proteins such as glutamate receptor 1 (AMPA subtype: GluA1: [the α-amino-3-hydroxy-5-methyl-4-isoxazolepropionic acid receptor A1]) and postsynaptic density protein 95 (PSD-95) were decreased in the PFC of mice with depression-like phenotypes (Yang et al., 2022, 2023, 2024). For immunodetection, the polyvinylidene difluoride membranes were blocked with blocker [5% skim milk in TBS + 0.1% Tween-20 (TBST)] at room temperature for 1 h, the membranes for detecting PSD-95 were incubated with the recommended dilution of the primary antibody against PSD-95 (1:1000, catalog number: 51–6,900,695, 1 μg/mL, Invitrogen, Camarillo, CA, USA), while the membranes for detecting β-actin were incubated with the appropriate dilution of the primary antibody against β-actin (1:10,000; catalog number: A5441 Sigma-Aldrich Co., Ltd., St Louis, MO, USA) at 4 °C overnight. The next day, wash the polyvinylidene difluoride membranes in three washes of TBST, 10 min each. Then the polyvinylidene difluoride membranes were selectively incubated with a recommended dilution of labeled secondary antibody [anti-mouse antibody (1:5000, catalog number: NA931, GE Healthcare) or a horseradish peroxidase-conjugated anti-rabbit antibody (1:5000, catalog number: NA934, GE Healthcare)] in 5% blocking buffer in TBST at room temperature for 1 h. After three final washes in TBST, 10 min each. The bands in the polyvinylidene difluoride membranes were detected using enhanced chemiluminescence plus a Western Blotting Detection system (GE Healthcare Bioscience).

The membranes for detecting GluA1 were incubated in elution buffer (62.5 mM Tris-HCl, pH 6.8, 2% sodium dodecyl sulfate, and 100 mM β-mercaptoethanol) (preheat in incubator at 60 °C for 10 min, shake 50 times/min) at 60 °C for 30 min and then washed three times (10 min at a time) in TBST. The stripped membranes were incubated with the recommended dilution of primary antibody directed against GluA1 (1:10,000; catalog number: ab31232, Abcam, Cambridge, MA, USA) at 4 °C overnight. The following day, washing the membranes for three times (10 min at a time) in TBST and were incubated with a recommended dilution of horseradish peroxidase-conjugated anti-rabbit antibody (1:5000, catalog number: NA934, GE Healthcare) for 1 h at room temperature. After three final washes in TBST, 10 min each. The bands in the polyvinylidene difluoride membranes were detected using enhanced chemiluminescence plus a Western Blotting Detection system (GE Healthcare Bioscience). Images were produced using a ChemiDoc™ Touch Imaging System (170–01401; Bio-Rad Laboratories, Hercules, CA, USA), and immunoreactive bands were quantified using Image Lab™3.0 software (Bio-Rad Laboratories).

2.8. Collection of fresh fecal samples and 16S ribosome RNA sequencing

We collected fresh fecal samples from mice before the behavioral test of LMT. The subsequent experimental workflow, which included microbial community DNA extraction, DNA quality control, PCR

amplification, product purification, library quality control, sequencing, and bioinformatics analysis, was carried out in accordance with our previously reported methods (Yang et al., 2023, 2024). The 16S ribosome RNA sequencing data has been uploaded to and stored in the NCBI Sequence Read Archive, and can be accessed using the accession number PRJNA929668.

2.9. Untargeted metabolomic and lipidomic analyses of plasma samples

Untargeted metabolomics profiling of plasma samples was conducted using ultra-performance liquid chromatography–tandem quadrupole time-of-flight mass spectrometry (UPLC-QTOF/MS) technique. This process involved an ExionLC™ AD system (SCIEX, Tokyo, Japan) coupled with a X500R QTOF system (SCIEX, Tokyo, Japan). The metabolomics profile data were subsequently annotated and analyzed according to the methods we previously reported (Yang et al., 2024). In parallel, untargeted lipidomic analysis of plasma samples were carried out using an X500R QTOF system (SCIEX, Tokyo, Japan), operated in both positive and negative electrospray ionization modes (AB Sciex, Foster City, CA). This system was also coupled with an ExionLC™ AD system (SCIEX, Tokyo, Japan). The data processing and analysis for this lipidomic study were performed in line with previously established protocols (Tsugawa et al., 2020; Yang et al., 2024).

2.10. Statistical analysis

Statistical analysis of the data was performed using the SPSS version 20.0 software (SPSS, Tokyo, Japan). The data were shown as the mean ± standard error of the mean (S.E.M.). The data of body weight were analyzed using repeated measure analysis of variance (ANOVA), followed by Fisher's least significant difference (LSD) test. The data of spleen weight were analyzed using an unpaired *t*-test (for two groups) or two-way ANOVA (for four groups). Data of behavioral tests, pro-inflammatory cytokines and synaptic proteins were analyzed using unpaired *t*-test (for two groups), one-way ANOVA (for three groups), or two-way ANOVA (for four groups), followed by Fisher's LSD test. The α-diversity of gut microbiota, the abundance of gut microbiota at the species level, metabolites and lipids between the two groups were analyzed using Mann-Whitney test. Bioinformatic analysis of PCoA, LEfSe algorithm of intestinal microbiota, boxplot analysis of metabolomics/lipids and correlation networks were all performed by using the OmicStudio tools (<https://www.omicstudio.cn/tool>).

Correlations between spleen weight and the concentrations of pro-inflammatory cytokines were analyzed by using Pearson's correlation analysis. Correlations between the plasma metabolites (or lipids), the intestinal microbiota at species level, depression-like phenotypes, the concentrations of pro-inflammatory cytokines and synaptic proteins in the PFC were analyzed using Spearman's correlation analysis. *P*-value for comparison <0.05 was regarded as significant.

3. Results

3.1. Depression-like phenotypes in mice with CBDL

Behavioral tests were conducted 11 days post-surgery (Fig. 1A). The CBDL group exhibited a reduction in body weight relative to the sham-operated group (Fig. 1B). The CBDL group presented splenomegaly compared to the sham group (Fig. 1C). In the CBDL group, plasma levels of pro-inflammatory cytokines, including IL-6 and TNF-α, were elevated compared to those in the sham group (Fig. 1D, E). Positive correlations were observed between the weight of the spleen and the plasma levels of IL-6 and TNF-α (Fig. 1F, G). In behavioral tests, no significant differences in locomotor activity were noted between the two groups (Fig. 1H). However, the CBDL group demonstrated increased immobility time in the FST (Fig. 1I) and a decreased sucrose preference in the SPT (Fig. 1J) compared to the sham group. Additionally, levels of synaptic proteins

(GluA1 and PSD-95) in the PFC were lower in the CBDL group than in the sham group (Fig. 1K, L). These findings indicate that mice with CBDL exhibit reduced body weight, splenomegaly, heightened systemic inflammation, and diminished synaptic protein expression in the PFC, which collectively contribute to depression-like phenotypes.

3.2. Effects of CBDL on the composition diversity of gut microbiota

The composition of the intestinal microbiota in both the CBDL group and sham group was examined using both α -diversity and β -diversity metrics. The Mann–Whitney U test showed no significant differences in Observed_otus, Chao, Ace, Shannon's diversity, Simpson's diversity, and Good's coverage between the CBDL and sham groups (Fig. 2A–F). β -diversity in the intestinal microbiota of the two groups was assessed using Principal Coordinate Analysis (PCoA). At the operational taxonomic unit (OTU) level, the PCoA analysis indicated a marked difference in microbiota composition, as shown by analysis of similarities (ANOSIM) ($R = 0.6971$, $P = 0.001$) (Fig. 2G). The ANOSIM at the OTU level suggested that the inter-group differences in microbiota composition were more pronounced than the intra-group variations ($R = 0.691$, $P = 0.001$) (Fig. 2H).

3.3. Effects of CBDL on the LEfSe algorithm of intestinal microbiota

A cladogram was utilized to illustrate the relationship among biomarker taxa identified by LEfSe. This cladogram is structured in layers representing different taxonomic levels: phylum, class, order, family and genus, arranged from the innermost to the outermost layer (Fig. 3A). In the CBDL group, LEfSe analysis identified five taxonomic biomarkers: the phylum *Firmicutes*, the class *Clostridia*, the order *Clostridiales*, the family *Lachnospiraceae* and the genus *Clostridium_XIVa*

(Fig. 3B). Conversely, six taxonomic biomarkers were identified in the sham group, including the phylum *Bacteroidetes*, the class *Bacteroidia*, the order *Bacteroidales*, the family *Porphyromonadaceae* and *Prevotellaceae*, and the genus *Barnesiella* (Fig. 3B).

3.4. Gut microbiota at the species level

At the species level, the analysis revealed 21 bacterial species with significant differences in relative abundance between the groups (Fig. 4A). In the CBDL group, the species *Alistipes_finegoldii*, *Akkermansia_muciniphila*, *Lactobacillus_intestinalis*, *Clostridium_aldenense*, *Allobaculum_stercoricanis*, *Clostridium_methylpentosum*, *Parabacteroides_goldsteini*, *Gemmiger_formicilis*, *Bacteroides_acidifaciens*, *Parabacteroides_distasonii*, and *Clostridium_cocleatum* exhibited significantly higher relative the sham group. Conversely, the species *Alloprevotella_rava*, *Bacteroides_sartorii*, *Parvibacter_caecicola*, *Barnesiella_intestinihominis*, *Butyrivibrio_pullicaeorum*, *Enterorhabdus_caecimuris*, *Leptotrichia_shahii*, *Escherichia*, *Eubacterium_coprostanoligenes* and *Prevotella_baroniae* showed significantly lower relative to the sham group (Fig. 4B–V).

3.5. Untargeted metabolomic and lipidomic analyses of plasma samples

To examine the interaction between the gut microbiome and host metabolic processes, untargeted metabolomic and lipidomic analyses were performed on plasma samples. Following quality control measures and the exclusion of low-abundance peaks, 131 metabolites were successfully annotated. Among these, 29 metabolites were found to have significant differences in abundance between the two groups (Fig. 5A). Additionally, after thorough data processing, 92 lipids were annotated. Of these, 50 lipids showed significant variations in abundance between the two groups (Fig. 5B).

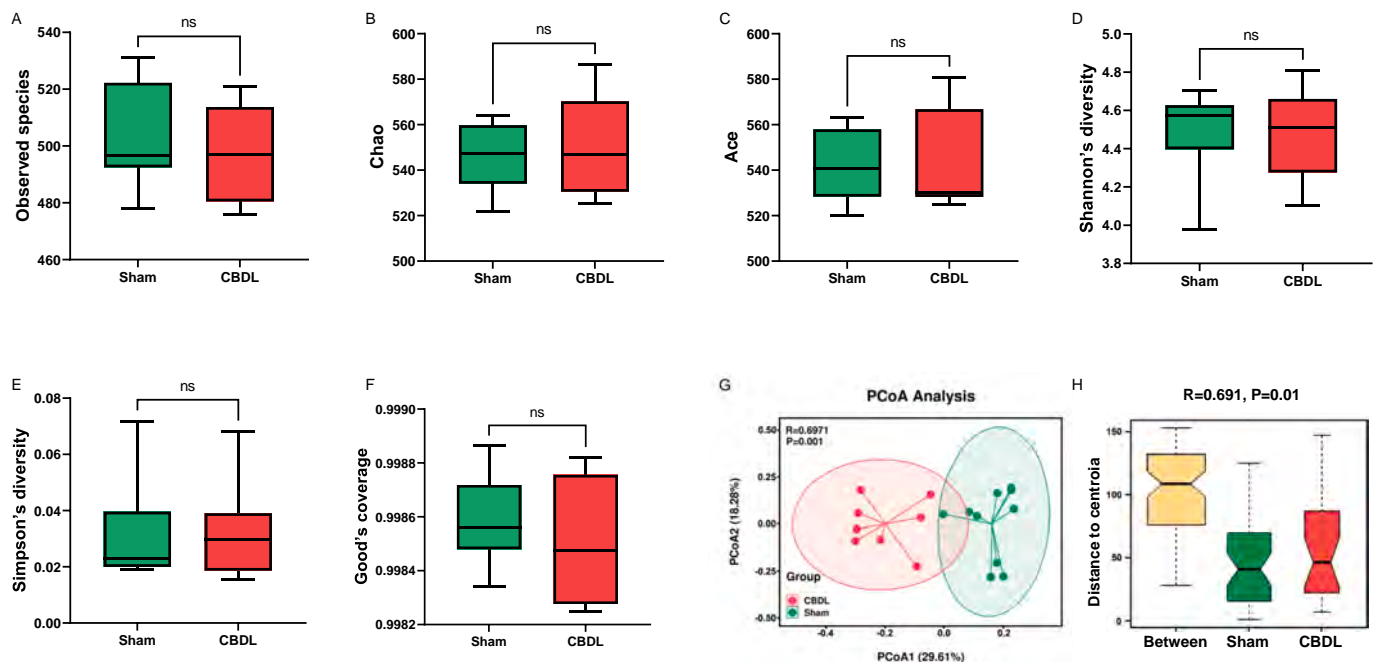


Fig. 2. Effects of CBDL on the diversity of gut microbiota composition.

(A): Observed_species (Mann-Whitney test, $P = 0.594$). (B): Chao (Mann-Whitney test, $P = 0.829$). (C): Ace (Mann-Whitney test, $P = 0.829$). (D): Shannon's diversity (Mann-Whitney test, $P = 0.762$). (E): Simpson's diversity (Mann-Whitney test, $P = 0.897$). (F): Good's coverage (Mann-Whitney test, $P = 0.450$). (G): PCoA based on OTU level (ANOSIM, bray methods) ($R = 0.6971$, $P = 0.001$). (H): OTU ANOSIM analysis ($R = 0.691$, $P = 0.001$). ("Between" indicates the difference between groups, and others indicate the difference within each group. R value represents the degree of difference between groups and within groups, ranged from -1 to 1 ; R value >0 indicates that the difference between groups is greater than the difference within the group; R value <0 indicates that the difference within the group is greater than the difference between groups; the larger the absolute value of R value, the greater the relative difference. The lower the P value, the more significant the effect of this difference test. P value <0.05 indicates a significant difference). For all box plots, the middle line in the box addresses the median, the box addresses the interquartile range, and the whisker addresses the most extreme and least values. ns: not significant.

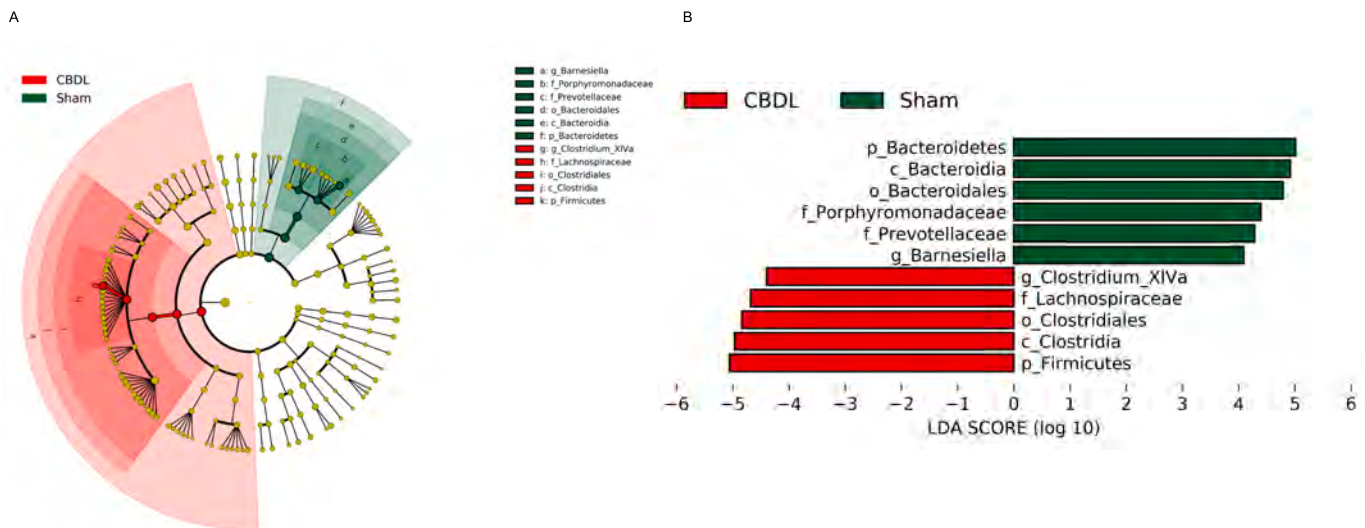


Fig. 3. LefSe analysis for potential bacteria biomarkers of gut microbiota.

(A): Functional branching diagram generated from LefSe showing the differences of the two groups at different taxonomic levels. (B): Histogram representing the enriched taxa with LDA score > 4.0 and $P < 0.05$ obtained from LefSe of the two groups (p: phylum. c: class. o: order. f: family. g: genus).

3.6. Correlations among the gut microbiota, plasma metabolites/lipids, depression-like phenotypes, plasma pro-inflammatory cytokines, and synaptic proteins

Correlations were observed between the plasma metabolites/lipids and the relative abundance of gut microbiota in the two groups, indicating a significant association between them. Through data screening with a threshold of $P < 0.05$ and an absolute R-value of ≥ 0.5 , a Correlation Network was established. This network highlights the connections between the plasma metabolites, gut microbiome at the species level, depression-like behaviors, plasma pro-inflammatory cytokines, and synaptic proteins in the PFC, all of which showed significant differences between the groups (Fig. 6A). The relative abundance of various microbial species was found to be either positively or negatively correlated with 29 plasma metabolites that exhibited significant differences between the groups (Fig. 6A). Moreover, there were notable correlations between plasma metabolites and the behavioral outcomes (SPT and FST), plasma levels of pro-inflammatory cytokines, and synaptic protein concentrations in the PFC (Fig. 6A).

A Correlation Network was developed to illustrate the connections between plasma lipids, gut microbiome at the species level, depression-like behaviors, plasma pro-inflammatory cytokines, and synaptic proteins in the PFC, all of which exhibited significant variations between the two groups (Fig. 6B). Several microbial species demonstrated either positive or negative correlations with various types of plasma lipids (Fig. 6B). Additionally, associations were observed between plasma lipids and the behavioral outcomes (SPT and FST), plasma levels of pro-inflammatory cytokines, and synaptic protein concentrations in the PFC (Fig. 6B).

Using the Correlation Network, the study also explored the relationships between the relative abundance of the gut bacteria and depression-like phenotypes, plasma cytokines, and synaptic proteins in the PFC (Fig. 6C). Notable positive or negative correlations were identified between plasma IL-6 or TNF- α levels and the relative abundance of several bacterial species (Fig. 6C). Furthermore, both positive and negative correlations between the SPT/FST data and the relative abundance of various microbial species (Fig. 6C). Likewise, correlations, either positive or negative, were observed between the abundance of certain species and the levels of synaptic proteins in the PFC (Fig. 6C). These findings suggest a potential role of various microbiota and metabolites in contributing to systemic inflammation, which may lead to

the development of depression-like phenotypes.

3.7. Effects of bilateral SDV in depression-like phenotypes in mice with CBDL

Previous studies indicate a potential role of the subdiaphragmatic vagus nerve in the development of depression-like phenotypes in mice (Pu et al., 2021; Wang et al., 2020, 2021; Yang et al., 2023, 2024; Zhang et al., 2020). To explore the role of the subdiaphragmatic vagus nerve in the depression-like phenotypes in mice with CBDL, we assessed the effects of bilateral SDV (Fig. 7A). Significant variations in body weight were observed among the four groups (Fig. 7B). In the CBDL + SDV group, plasma concentrations of IL-6 and TNF- α were significantly lower than those in the CBDL + sham group (Fig. 7C, D). Locomotor activity did not show any significant differences across the four groups (Fig. 7E). The immobility time in the FST in the CBDL + SDV group was significantly lower than that in the CBDL + sham group (Fig. 7F). In the SPT, sucrose preference was significantly higher in the CBDL + SDV group than that in the CBDL + sham group (Fig. 7G). Additionally, the expression levels of synaptic proteins (e.g., GluA1 and PSD-95) in the PFC were significantly increased in the CBDL + SDV group compared to the CBDL + sham group (Fig. 7H, I). These findings suggest that bilateral SDV may mitigate depression-like behaviors, decrease elevated plasma levels of pro-inflammatory cytokines, normalize altered expressions of synaptic proteins in the PFC of mice subjected to CBDL.

3.8. Effects of arketamine on depression-like phenotypes in mice with CBDL

Arketamine has been proposed as a rapid-acting antidepressant, potentially without the adverse effects commonly associated with ketamine (Wei et al., 2022a; Zhang et al., 2022a, 2022b; Zhang et al., 2023). In this study, we examined the effects of a single dose of arketamine (10 mg/kg, i.p.) in the CBDL model (Fig. 8A). Significant differences in body weight were observed among the three groups (Fig. 8B). The spleen weights in the CBDL + normal saline (NS) group were significantly higher compared to the other two groups (Fig. 8C). No changes in locomotor activity were detected across the three groups (Fig. 8D). The immobility time in the FST was significantly longer in the CBDL + NS group than in the other two groups (Fig. 8E). In the SPT, the sucrose preference was significantly reduced in the CBDL + NS group

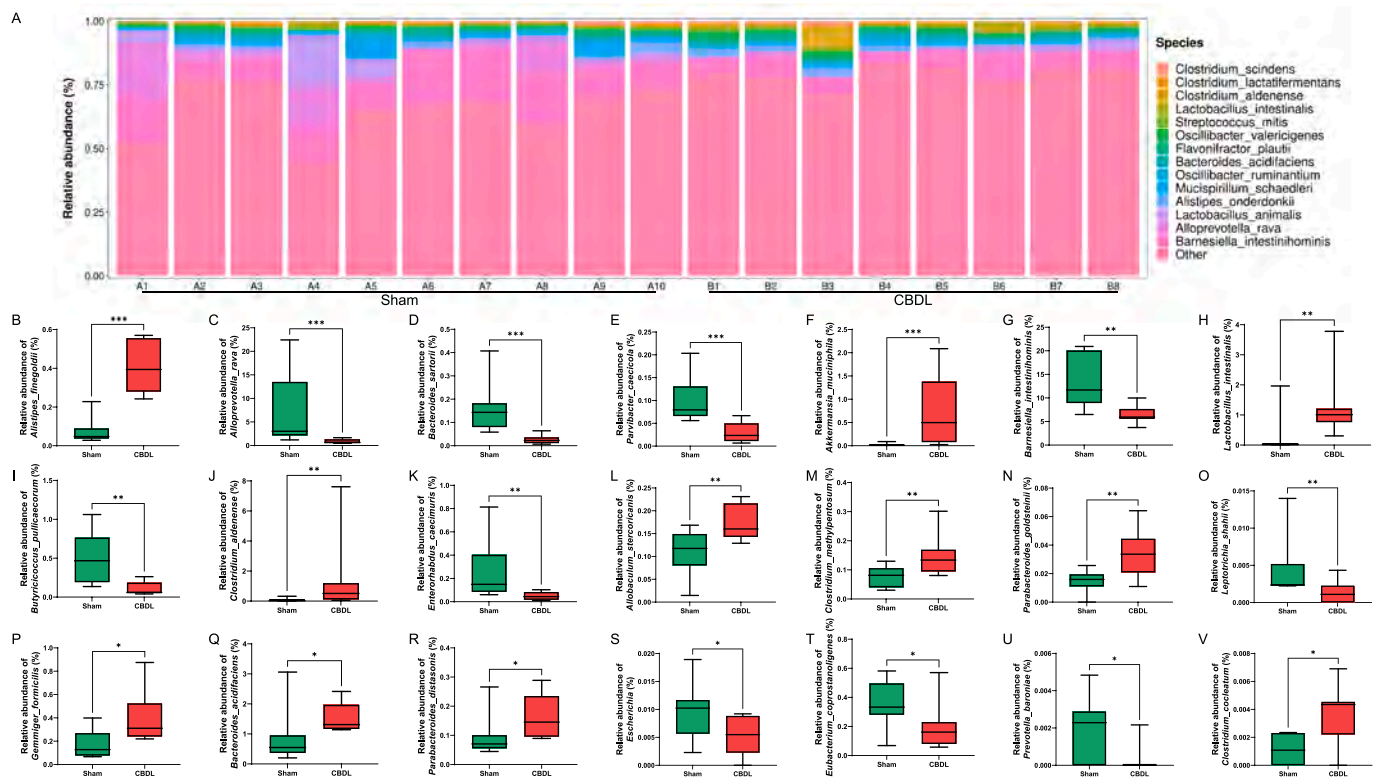


Fig. 4. Effects of CBDL on gut microbiota at the species levels. (A): Gut bacteria composition at the species level in the two groups. (B): Relative abundance of the species *Alistipes finegoldii* (Mann-Whitney test, $P < 0.0001$). (C): Relative abundance of the species *Alloprevotella rava* (Mann-Whitney test, $P = 0.0002$). (D): Relative abundance of the species *Bacteroides sartorii* (Mann-Whitney test, $P = 0.0002$). (E): Relative abundance of the species *Parvibacter caecicola* (Mann-Whitney test, $P = 0.0002$). (F): Relative abundance of the species *Akkermansia muciniphila* (Mann-Whitney test, $P = 0.0005$). (G): Relative abundance of the species *Barnesiella intestinihominis* (Mann-Whitney test, $P = 0.0014$). (H): Relative abundance of the species *Lactobacillus intestinalis* (Mann-Whitney test, $P = 0.0021$). (I): Relative abundance of the species *Butyrivibrio furiosus* (Mann-Whitney test, $P = 0.0031$). (J): Relative abundance of the species *Clostridium aldense* (Mann-Whitney test, $P = 0.0044$). (K): Relative abundance of the species *Enterorhabdus caecimuris* (Mann-Whitney test, $P = 0.0044$). (L): Relative abundance of the species *Alloaculum stercoricans* (Mann-Whitney test, $P = 0.0085$). (M): Relative abundance of the species *Clostridium methylpentosum* (Mann-Whitney test, $P = 0.0085$). (N): Relative abundance of the species *Parabacteroides goldsteinii* (Mann-Whitney test, $P = 0.0085$). (O): Relative abundance of the species *Leptotrichia shahii* (Mann-Whitney test, $P = 0.0079$). (P): Relative abundance of the species *Gemmiger fornicilis* (Mann-Whitney test, $P = 0.0117$). (Q): Relative abundance of the species *Bacteroides acidifaciens* (Mann-Whitney test, $P = 0.0155$). (R): Relative abundance of the species *Parabacteroides distasonis* (Mann-Whitney test, $P = 0.0205$). (S): Relative abundance of the species *Escherichia* (Mann-Whitney test, $P = 0.0266$). (T): Relative abundance of the species *Eubacterium coprostanoligenes* (Mann-Whitney test, $P = 0.0266$). (U): Relative abundance of the species *Prevotella baroniae* (Mann-Whitney test, $P = 0.0241$). (V): Relative abundance of the species *Clostridium cocleatum* (Mann-Whitney test, $P = 0.0261$). For all box plots, the middle line in the box addresses the median, the box addresses the interquartile range, and the whisker addresses the most extreme and least values. * $P < 0.05$; ** $P < 0.01$; *** $P < 0.001$.

compared to the other groups (Fig. 8F). Arketamine also counteracted the decreased levels of GluA1 and PSD-95 in the PFC of mice with CBDL (Fig. 8G, H). These findings indicate that a single administration of arketamine can effectively alleviate depression-like phenotypes in mice subjected to CBDL.

4. Discussion

The major findings of this study are summarized as follows: Firstly, mice subjected to CBDL demonstrated a loss of body weight, splenomegaly, elevated blood levels of pro-inflammatory cytokines, and a reduction in synaptic protein expression (i.e., GluA1 and PSD-95) in the PFC, which contributed to depression-like phenotypes (increased immobility time of FST and decreased sucrose preference of SPT). Secondly, significant alterations in the β -diversity of gut microbiota were observed between the two groups. LEfSe analysis pinpointed the genus *Clostridium_X1a* as a potential microbial marker in the CBDL group. Additionally, notable changes in various species and metabolites were detected between the two groups, with correlations found between the relative abundance of certain microbes and blood cytokines, depression-like behaviors, and synaptic proteins in the PFC. Network analysis

revealed associations between specific microbes, blood metabolites (or lipids), and behavioral indices. Thirdly, SDV effectively prevented splenomegaly, systemic inflammation (characterized by increased IL-6 and TNF- α levels), and alterations in synaptic protein expression in the PFC of CBDL mice. Finally, the administration of a single dose of arketamine ameliorated depression-like phenotypes and reversed the decreased expressions of GluA1 and PSD-95 in the PFC of mice with CBDL. Collectively, these findings suggest a crucial role for the gut–liver–brain axis mediated by the subdiaphragmatic vagus nerve in the development of depression-like phenotypes in mice with CBDL. Additionally, arketamine demonstrated rapid-acting antidepressant-like properties in this model.

Recent studies have indicated a link between LPS-induced splenomegaly and elevated blood levels of pro-inflammatory cytokines such as IL-6 and TNF- α (Ma et al., 2022a, 2022b, 2023; Zhang et al., 2020; Zhang et al., 2021a, 2021b). In this study, we observed a positive correlation between the weight of spleen and the levels of pro-inflammatory cytokines in the blood of mice. Taken together, these findings imply that CBDL surgery may lead to systemic inflammation, which in turn contribute to the development of splenomegaly and depression-like phenotypes.

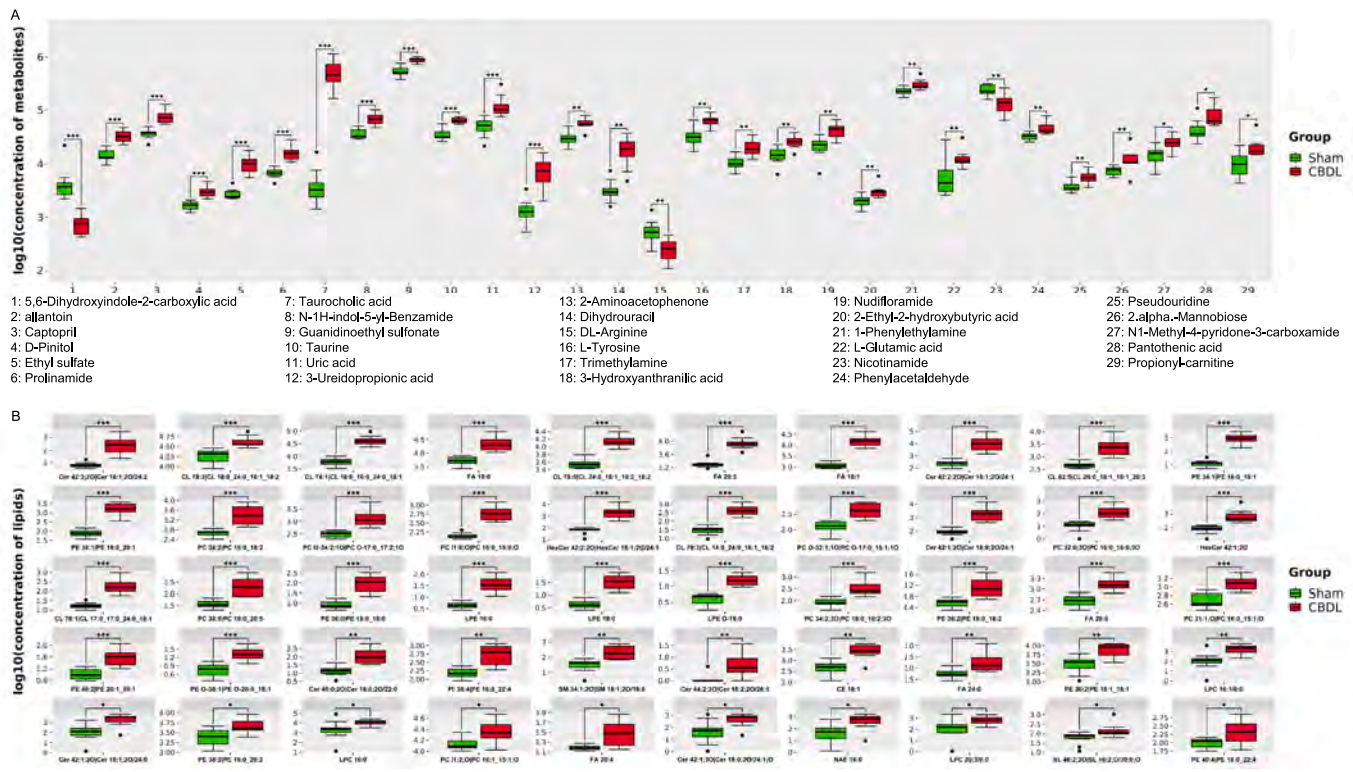


Fig. 5. Untargeted metabolomic and lipidomic analyses of plasma samples in mice with CBDL. (A) Boxplots showing the changes of 29 kinds of metabolites between the two groups. They are listed as follows: 5,6-dihydroxyindole-2-carboxylic acid (Mann-Whitney test, $P < 0.001$), allantoin (Mann-Whitney test, $P < 0.001$), captopril (Mann-Whitney test, $P < 0.001$), D-pinitol (Mann-Whitney test, $P < 0.001$), ethyl sulfate (Mann-Whitney test, $P < 0.001$), prolinamide (Mann-Whitney test, $P < 0.001$), taurocholic acid (Mann-Whitney test, $P < 0.001$), N-1H-indol-5-yl-benzamide (Mann-Whitney test, $P < 0.001$), guanidinoethyl sulfonate (Mann-Whitney test, $P < 0.001$), taurine (Mann-Whitney test, $P < 0.001$), uric acid (Mann-Whitney test, $P < 0.001$), 3-ureidopropionic acid (Mann-Whitney test, $P < 0.001$), 2-aminoacetophenone (Mann-Whitney test, $P = 0.0010$), dihydrouracil (Mann-Whitney test, $P = 0.0010$), DL-arginine (Mann-Whitney test, $P = 0.0014$), L-tyrosine (Mann-Whitney test, $P = 0.0019$), trimethylamine (Mann-Whitney test, $P = 0.0025$), 3-hydroxyanthranilic acid (Mann-Whitney test, $P = 0.0034$), nudifloramide (Mann-Whitney test, $P = 0.0034$), 2-ethyl-2-hydroxybutyric acid (Mann-Whitney test, $P = 0.0045$), 1-phenylethylamine (Mann-Whitney test, $P = 0.0059$), L-glutamic acid (Mann-Whitney test, $P = 0.0059$), pseudouridine (Mann-Whitney test, $P = 0.0059$), phenylacetaldehyde (Mann-Whitney test, $P = 0.0059$), 2.alpha.-mannobiose (Mann-Whitney test, $P = 0.0077$), N1-methyl-4-pyridone-3-carboxamide (Mann-Whitney test, $P = 0.0100$), pantothenic acid (Mann-Whitney test, $P = 0.0100$), propionyl-carnitine (Mann-Whitney test, $P = 0.0100$). The X-axis using the Arabic numerals representing the names of different plasma metabolites, and the Y-axis represents the concentration of various plasma metabolites. Different colors of boxplots represent the corresponding groups. (B) Boxplots showing the changes of 50 kinds of lipids between the two groups. They are listed as follows: Cer 42:3|20|Cer 18:1;20/24:2 (Mann-Whitney test, $P < 0.001$), CL 78:3|CL 18:0 24:0 18:1 18:2 (Mann-Whitney test, $P < 0.001$), CL 74:1|CL 16:0 16:0 24:0 18:1 (Mann-Whitney test, $P < 0.001$), FA 18:0 (Mann-Whitney test, $P < 0.001$), CL 78:5|CL 24:0 18:1 18:2 18:2 (Mann-Whitney test, $P < 0.001$), FA 20:3 (Mann-Whitney test, $P < 0.001$), FA 18:1 (Mann-Whitney test, $P < 0.001$), Cer 42:2|20|Cer 18:1;20/24:1 (Mann-Whitney test, $P < 0.001$), CL 82:5|CL 26:0 18:1 18:1 20:3 (Mann-Whitney test, $P < 0.001$), PE 34:1|PE 16:0 18:1 (Mann-Whitney test, $P < 0.001$), PE 38:1|PE 18:0 20:1 (Mann-Whitney test, $P < 0.001$), PC 36:2|PC 18:0 18:2 (Mann-Whitney test, $P < 0.001$), PC O-34:2;10|PC O-17:0 17:2;10 (Mann-Whitney test, $P < 0.001$), PC 31:0;O|PC 16:0 15:0;O (Mann-Whitney test, $P < 0.001$), HexCer 42:2;20|HexCer 18:1;20/24:1 (Mann-Whitney test, $P < 0.001$), CL 70:3|CL 14:0 24:0 16:1 16:2 (Mann-Whitney test, $P < 0.001$), Cer 42:1;20|Cer 18:0;20/24:1 (Mann-Whitney test, $P < 0.001$), PC 32:0;30|PC 16:0 16:0;30 (Mann-Whitney test, $P < 0.001$), HexCer 42:1;20 (Mann-Whitney test, $P < 0.001$), CL 76:1|CL 17:0 17:0 24:0 18:1 (Mann-Whitney test, $P < 0.001$), PC 38:5|PC 18:0 20:5 (Mann-Whitney test, $P < 0.001$), PE 36:0|PE 18:0 18:0 (Mann-Whitney test, $P < 0.001$), LPE 16:0 (Mann-Whitney test, $P < 0.001$), LPE 18:0 (Mann-Whitney test, $P < 0.001$), LPE O-18:0 (Mann-Whitney test, $P < 0.001$), PC 34:2;30|PC 18:0 16:2;30 (Mann-Whitney test, $P < 0.001$), PE 36:2|PE 18:0 18:2 (Mann-Whitney test, $P < 0.001$), FA 20:5 (Mann-Whitney test, $P < 0.001$), PC 31:1;O|PC 16:0 15:1;O (Mann-Whitney test, $P < 0.001$), PE 40:2|PE 20:1 20:1 (Mann-Whitney test, $P < 0.001$), PE O-38:1|PE O-20:0 18:1 (Mann-Whitney test, $P < 0.001$), Cer 40:0;20|Cer 18:0;20/22:0 (Mann-Whitney test, $P = 0.0010$), PE 38:4|PE 16:0 22:4 (Mann-Whitney test, $P = 0.0014$), SM 34:1;20|SM 18:1;20/16:0 (Mann-Whitney test, $P = 0.0014$), Cer 44:2;20|Cer 18:2;20/26:0 (Mann-Whitney test, $P = 0.0021$), CE 18:1 (Mann-Whitney test, $P = 0.0025$), FA 24:0 (Mann-Whitney test, $P = 0.0045$), PE 36:2|PE 18:1 18:1 (Mann-Whitney test, $P = 0.0059$), LPC 16:1/0:0 (Mann-Whitney test, $P = 0.0059$), Cer 42:1;20|Cer 18:1;20/24:0 (Mann-Whitney test, $P = 0.0100$), PE 38:2|PE 18:0 20:2 (Mann-Whitney test, $P = 0.0129$), LPC 16:0 (Mann-Whitney test, $P = 0.0164$), PC 31:2;O|PC 16:1 15:1;O (Mann-Whitney test, $P = 0.0209$), FA 20:4 (Mann-Whitney test, $P = 0.0209$), Cer 42:1;30|Cer 18:0;20/24:1;O (Mann-Whitney test, $P = 0.0209$), NAE 16:0 (Mann-Whitney test, $P = 0.0209$), LPC 20:3/0:0 (Mann-Whitney test, $P = 0.0330$), SL 46:2;20|SL 16:2;O/30:0;O (Mann-Whitney test, $P = 0.0367$), PE 40:4|PE 18:0 22:4 (Mann-Whitney test, $P = 0.0410$). * $P < 0.05$; ** $P < 0.01$; *** $P < 0.001$.

Analysis of gut microbiota revealed that CBDL significantly influences the variations in microbial community expression. Specifically, at the species level, notable differences in the relative abundance of various microbiota were observed between the two groups. Through comprehensive untargeted metabolomic and lipidomic analyses, we identified distinct changes in several metabolites and lipids across these groups. Network analysis further indicated that the blood levels of these metabolites and lipids are associated with the relative abundance of

certain microbiota, hinting at the microbiome's involvement in their synthesis. Importantly, our findings also include correlations between depression-like behaviors and specific microbiota abundances, underscoring the potential role of the gut microbiome in depression. A previous study reported dysbiosis in gut microbiota and changes in tight junction proteins (i.e., claudin-1, ZO-1) in mice following CBDL (Alaish et al., 2013). Considering the established link between gut microbiota and depression (Chang et al., 2022; Liu et al., 2023), it seems plausible

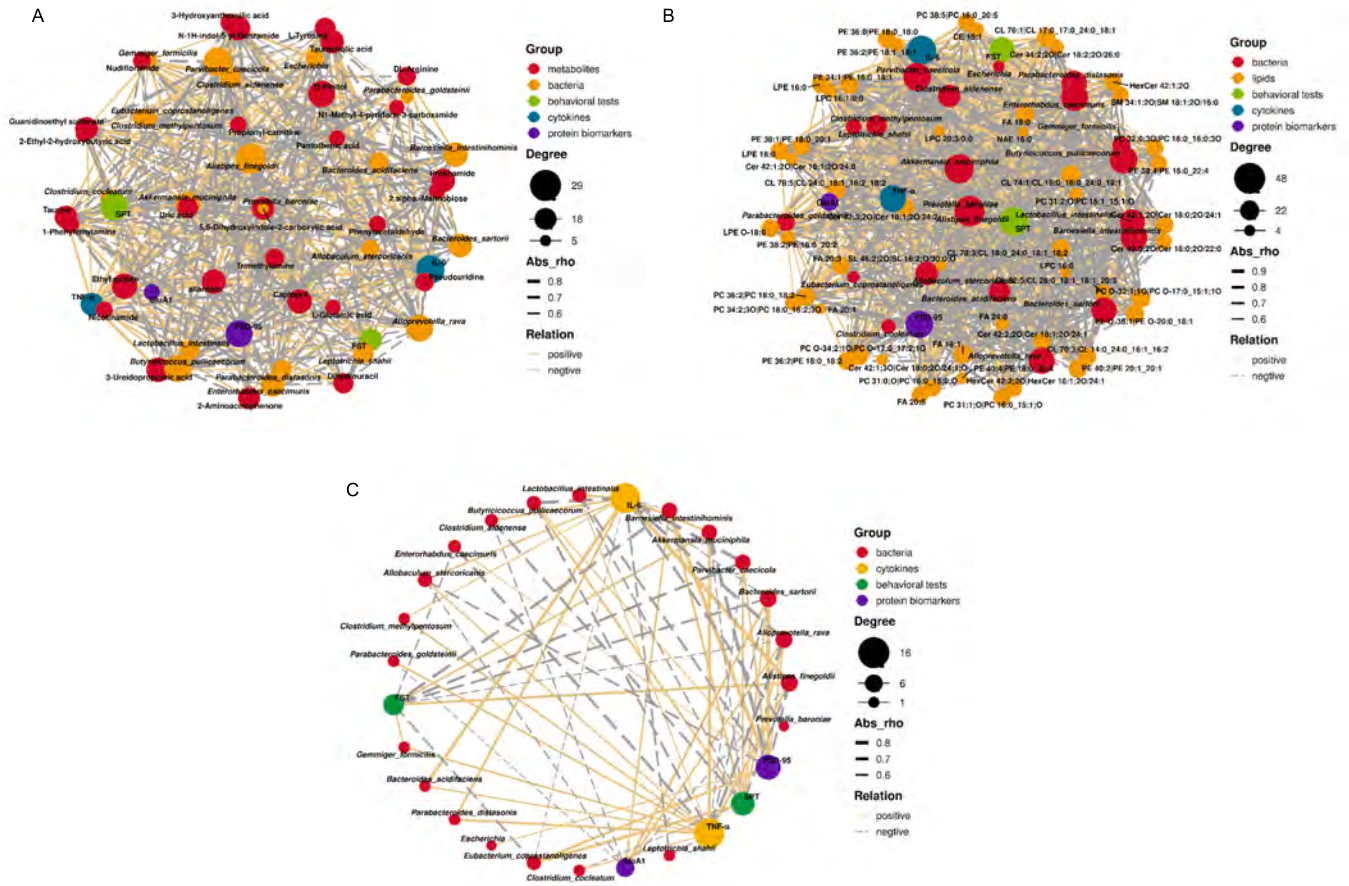


Fig. 6. Correlation network between behavioral data (or synaptic proteins, microglial marker, and pro-inflammatory cytokine) and microbiota (or metabolites and lipids).

(A): A Correlation Network indicating the correlations between the concentrations of plasma metabolites and the gut microbiota at the species level, the results of the behavioral test, the concentrations of pro-inflammatory cytokines and synaptic proteins in the PFC. (B): A Correlation Network indicating the correlations between the concentrations of plasma lipids and the gut microbiota at the species level, the results of the behavioral test, the concentrations of pro-inflammatory cytokines and synaptic proteins in the PFC. (C): A Correlation Network showed correlations between the relative abundance of gut bacteria at the species level and the results of the behavioral test, the concentrations of pro-inflammatory cytokines and synaptic proteins in the PFC. Both the threshold of correlation networks above were set as $P < 0.05$ and the absolute value of $R \geq 0.5$. The different colors of nodes represent different groups. The sizes of node gradients represent varying degrees of correlation. The thickness of the line represents the absolute value of the correlation coefficient. Solid lines represent positive correlations, dotted lines represent negative correlations.

that alterations in the gut–brain axis, including changes in metabolites and lipids, might contribute to the depression-like behaviors in CBDL mice.

Prior research has established that SDV can prevent the onset of depression-like behaviors in mice. This effect was observed following LPS administration (Zhang et al., 2020), as well as after FMT from mice with depression-like behaviors (Pu et al., 2021; Wang et al., 2020, 2021). Additionally, SDV has been effective in preventing depression-like behaviors in *Chrna7* knockout mice (Yang et al., 2023), in mice with HI/R injury (Yang et al., 2024), and in alleviating demyelination in the brains of cuprizone-treated mice (Wang et al., 2023). Another study highlighted the role of the gut–spleen axis, specifically through the subdiaphragmatic vagus nerve, in exacerbating systemic inflammation in mice under sleep deprivation following LPS administration (Zhang et al., 2021b). In our study, we found that SDV effectively alleviated both depression-like phenotypes and splenomegaly in mice with CBDL, indicating a role of the subdiaphragmatic vagus nerve in depression-like behaviors and splenomegaly in these mice. Considering the significance of the gut–liver axis in liver diseases (Albillos et al., 2020; Schwabe and Greten, 2020; Wiest et al., 2017; Zhang et al., 2022b), the

gut–liver–brain axis, likely mediated through the subdiaphragmatic vagus nerve, appears to be crucial in the development of depression-like phenotypes in mice with CBDL. The role of the vagus nerve in modulating the systemic inflammatory response to LPS was also underscored (Borovikova et al., 2000). Given the vagus nerve's role on systemic inflammation, SDV might be an effective strategy in reducing inflammation in this model. Moreover, with vagus nerve stimulation (VNS) known for its potent anti-inflammatory actions (Hashimoto, 2023b, 2023c; Wang et al., 2022), VNS could potentially be a therapeutic option for patients suffering from liver cirrhosis.

The discovery of ketamine's robust antidepressant properties was an unexpected milestone in the treatment of psychiatric disorders, offering rapid and sustained antidepressant actions for treatment-resistant patients with depression (Hashimoto, 2022). Preclinical studies indicate that arketamine, the (R)-enantiomer of ketamine, may be a safer antidepressant alternative compared to ketamine or esketamine, the (S)-enantiomer of ketamine (Hashimoto, 2020, 2023b, 2023d, 2024; Wei et al., 2022a; Zhang et al., 2022a; Zhang et al., 2023). Our earlier research demonstrated that arketamine not only alleviates depression-like behaviors in mice but also modifies the gut microbiota

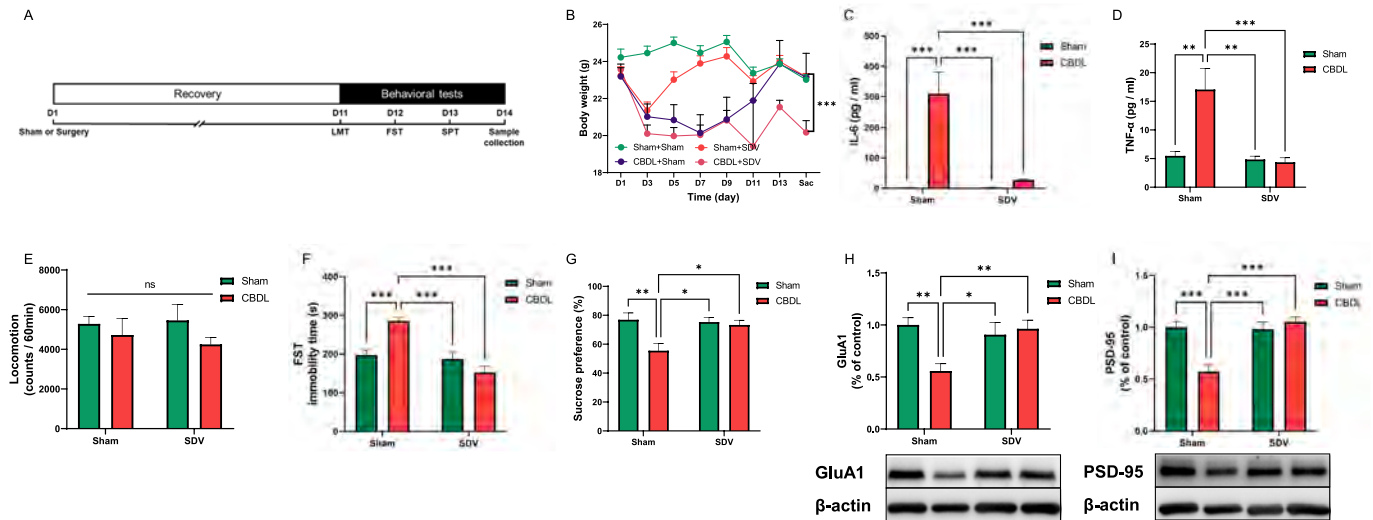


Fig. 7. Effects of bilateral SDV in depression-like phenotypes of mice with CBDL.

(A): Experimental schedule. On day 1, surgery (CBDL and/or SDV) or sham surgery was performed, and they were recovered 10 days. On day 11, LMT was performed. FST and SPT were performed on day 12 and day 13, respectively. On day 14, PFC and plasma samples were collected. (B): Body weight (repeated measure two-way ANOVA, time: $F_{(2,135, 53.37)} = 4.169, P = 0.0187$; group: $F_{(3, 25)} = 10.68, P = 0.0001$; interaction: $F_{(21, 175)} = 2.654, P = 0.0003$). (C): Plasma levels of IL-6 (two-way ANOVA, CBDL: $F_{(1, 25)} = 16.44, P = 0.0004$; SDV: $F_{(1, 25)} = 22.86, P < 0.0001$; Interaction: $F_{(1, 25)} = 16.44, P = 0.0004$). (D): Plasma levels of TNF- α (two-way ANOVA, CBDL: $F_{(1, 25)} = 12.01, P = 0.0019$; SDV: $F_{(1, 25)} = 8.348, P = 0.0079$; Interaction: $F_{(1, 25)} = 9.862, P = 0.0043$). (E): Locomotion (LMT) (two-way ANOVA, CBDL: $F_{(1, 25)} = 0.06112, P = 0.8068$; SDV: $F_{(1, 25)} = 2.205, P = 0.1501$; Interaction: $F_{(1, 25)} = 0.2991, P = 0.5893$). (F): FST (two-way ANOVA, CBDL: $F_{(1, 25)} = 25.91, P < 0.0001$; SDV: $F_{(1, 25)} = 3.552, P = 0.0712$; Interaction: $F_{(1, 25)} = 18.73, P = 0.0002$). (G): SPT (two-way ANOVA, CBDL: $F_{(1, 25)} = 3.752, P = 0.0641$; SDV: $F_{(1, 25)} = 7.740, P = 0.0101$; Interaction: $F_{(1, 25)} = 5.314, P = 0.0297$). (H): Western blot analysis of GluA1 in the PFC (two-way ANOVA, CBDL: $F_{(1, 25)} = 3.411, P = 0.0766$; SDV: $F_{(1, 25)} = 5.223, P = 0.0310$; Interaction: $F_{(1, 25)} = 8.779, P = 0.0066$) and the representative bands. (I): Western blot analysis of PSD-95 in the PFC (two-way ANOVA, CBDL: $F_{(1, 25)} = 15.78, P = 0.0005$; SDV: $F_{(1, 25)} = 9.410, P = 0.0051$; Interaction: $F_{(1, 25)} = 18.27, P = 0.0002$) and the representative bands. The data are shown as means \pm S.E.M (sham + sham group: $n = 8$, CBDL + sham group: $n = 7$, sham + SDV group: $n = 6$, CBDL + SDV group: $n = 8$). ANOVA: analysis of variance. ns: not significant; * $P < 0.05$; ** $P < 0.01$; *** $P < 0.001$.

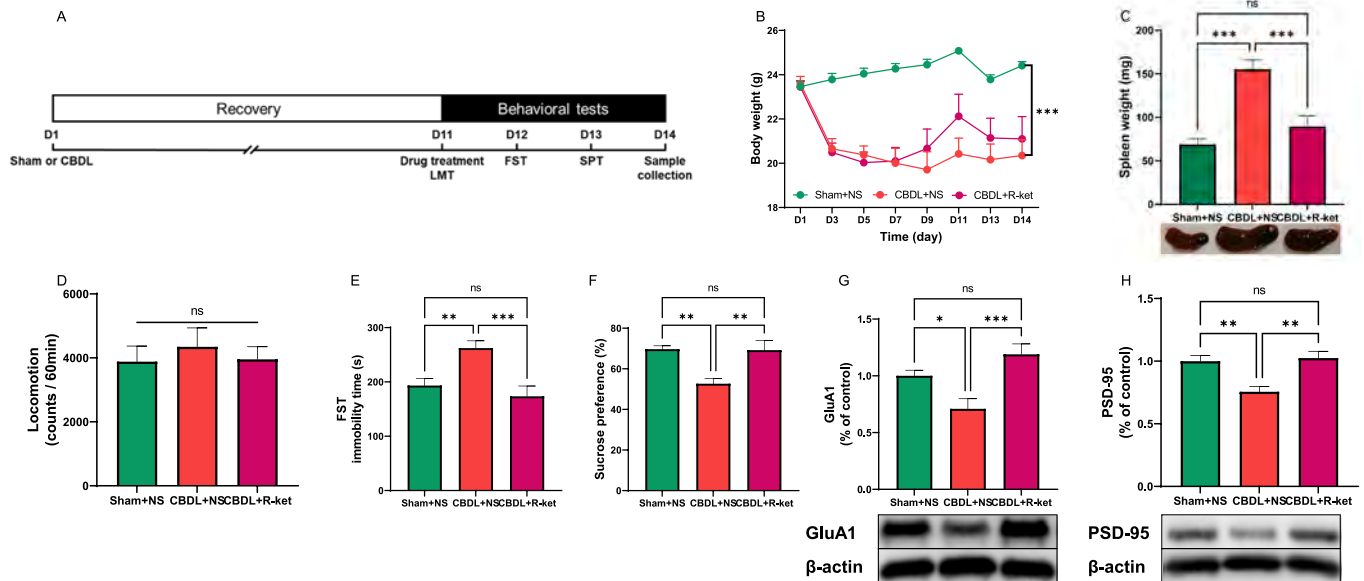


Fig. 8. Effect of new antidepressant arketamine in depression-like phenotypes of mice with CBDL.

(A): Experimental schedule. On day 1, sham or CBDL was performed, and they were recovered 10 days. On day 11, normal saline (NS) (10 ml/kg) or arketamine (R-ket) (10 mg/kg) was administered intraperitoneally and subsequently LMT was performed. FST and SPT were performed on day 12 and day 13, respectively. On day 14, prefrontal cortex (PFC) and plasma samples were collected. (B): Body weight (repeated measure ANOVA, $F_{(2, 26)} = 16.89, P < 0.001$). (C): Spleen weight (one-way ANOVA, $F_{(2, 26)} = 20.42, P < 0.001$). (D): LMT (one-way ANOVA, $F_{(2, 26)} = 0.2491, P = 0.7813$). (E): FST (one-way ANOVA, $F_{(2, 26)} = 9.660, P = 0.0007$). (F): SPT (one-way ANOVA, $F_{(2, 26)} = 9.743, P = 0.0007$). (G): Western blot analysis of GluA1 in the PFC (one-way ANOVA, $F_{(2, 26)} = 9.429, P = 0.0008$) and the representative bands. (H): Western blot analysis of PSD-95 in the PFC (one-way ANOVA, $F_{(2, 26)} = 10.26, P = 0.0005$) and the representative bands. The data are shown as means \pm S.E.M (Sham + NS group: $n = 10$, CBDL + NS group: $n = 10$, CBDL + R-ket group: $n = 9$). ANOVA: analysis of variance. NS: normal saline. R-ket: Arketamine. ns: not significant; * $P < 0.05$; ** $P < 0.01$; *** $P < 0.001$.

composition in these models (Qu et al., 2017; Yang et al., 2017). Additionally, we found that arketamine can reverse reduced bone mineral density in mice exposed to stress (Wan et al., 2023) and ovariectomized mice (Wan et al., 2022), acting through the gut-microbiota-bone axis. Considering the crucial role of gut microbiota on bone mineral density (Chen et al., 2023; Ohlsson and Sjögren, 2015), it seems plausible that the gut microbiota–bone axis may play a pivotal role in arketamine's beneficial effects on bone mineral density (Wan et al., 2022, 2023; Wei et al., 2022a). More recently, our studies have shown that a single dose of arketamine can improve depression-like phenotypes in mice with HI/R injury (Yang et al., 2024), as well as in mice with CBDL (this study). Remarkably, these beneficial effects on HI/R injury or CBDL models are attainable with just one post-injection of arketamine. While the precise mechanisms of arketamine's action in the HI/R or CBDL models remain to be fully understood, it is plausible that its anti-inflammatory actions, potentially mediated via the gut–liver–brain axis, play a significant role. The association between depressive symptoms and cognitive decline in patients with liver cirrhosis is well-documented (Pantiga et al., 2003; San Martín-Valenzuela et al., 2020; Stewart et al., 2011). Given the influence of depression and cognitive function on the progression of liver cirrhosis (Mullish et al., 2014; Patten et al., 2008), exploring whether arketamine can alleviate depression in patients with liver cirrhosis presents a compelling area of research.

This study has several limitations. Initially, we were unable to measure the blood levels of alanine aminotransferase and aspartate aminotransferase, as the plasma samples were allocated for metabolomic and lipidomic analyses. Additionally, our research did not include behavioral assessments for cognitive deficits, although a previous study has shown that rats with bile duct ligation can exhibit spatial memory deficits (Huang et al., 2009). Another limitation is our focus solely on the PFC for evaluating synaptic protein expression, despite the known relevance of other brain regions, like the hippocampus, in depression. Furthermore, the study did not examine the potential effects of FMT from mice with CBDL, which could have provided further understanding of the gut microbiota's role in depression-like phenotypes. This area warrants future investigations using FMT from CBDL mice. Lastly, the current research has not yet investigated the connections between the microbiome or metabolites and depression-like phenotypes in CBDL mice. Future studies should aim to elucidate how these factors may contribute to depression-like phenotypes in this model.

In conclusion, our findings indicate that the gut–liver–brain axis, particularly through the subdiaphragmatic vagus nerve, is crucial in the development of depression-like phenotypes in mice following CBDL. Considering the significant role that depression plays in the progression of liver cirrhosis, arketamine emerges as a promising therapeutic candidate for treating depression in patients with this condition.

CRedit authorship contribution statement

Yong Yang: Writing – review & editing, Writing – original draft, Methodology, Investigation, Formal analysis, Data curation, Conceptualization. **Akifumi Eguchi:** Writing – review & editing, Validation, Resources, Methodology, Investigation, Data curation. **Chisato Mori:** Writing – review & editing, Supervision, Resources, Funding acquisition. **Kenji Hashimoto:** Writing – review & editing, Writing – original draft, Supervision, Funding acquisition, Conceptualization.

Declaration of competing interest

Dr. Hashimoto is the inventor of filed patent applications on “The use of R-ketamine in the treatment of psychiatric diseases”, “(S)-norketamine and salt thereof as pharmaceutical”, “R-ketamine and derivative thereof as prophylactic or therapeutic agent for neurodegeneration disease or recognition function disorder”, “Preventive or therapeutic agent and pharmaceutical composition for inflammatory diseases or bone diseases”, and “R-ketamine and its derivatives as a preventive or

therapeutic agent for a neurodevelopmental disorder” by the Chiba University. Dr. Hashimoto has also received speakers' honoraria, consultant fee, or research support from Abbott, Daiichi-Sankyo, Meiji Seika Pharma, Seikagaku Corporation, Dainippon-Sumitomo, Taisho, Otsuka, Murakami Farm and Perception Neuroscience. Other authors declare no conflict of interest.

Data availability

Data will be made available on request.

Acknowledgements

This study was supported by the grants from Japan Society for the Promotion of Science (to K.H., 21H00184, 21H05612, 23 K17634), JST OPERA Program Japan (to C.M. JPMJOP1831) and unrestricted grant of Yamada Bee Company, Japan (to C.M.). Dr. Yong Yang was supported by the Japan China Sasakawa Medical Fellowship (Tokyo, Japan) and JST SPRING (JPMJSP2109).

References

- Abureesh, M., Alkhayyat, M., Abualnadi, I., Badran, R., Henneberry, J.D., Sadiq, W., Novakovic, V., Barkin, R., Barkin, S., Deeb, L.S., 2022. Epidemiology of depressive disorders in patients with liver cirrhosis: a population-based study in the United States. *Prim. Care Compan. CNS Disord.* 24 (1), 20m02889. <https://doi.org/10.4088/PCC.20m02889>.
- Alaish, S.M., Smith, A.D., Timmons, J., Greenspon, J., Eyvazzadeh, D., Murphy, E., Shea-Donahue, T., Cirimotich, S., Mongodin, E., Zhao, A., Fasano, A., Nataro, J.P., Cross, A., 2013. Gut microbiota, tight junction protein expression, intestinal resistance, bacterial translocation and mortality following cholestasis depend on the genetic background of the host. *Gut Microbes* 4 (4), 292–305. <https://doi.org/10.4161/gmic.24706>.
- Albillos, A., de Gottardi, A., Rescigno, M., 2020. The gut-liver axis in liver disease: pathophysiological basis for therapy. *J. Hepatol.* 72 (3), 558–577. <https://doi.org/10.1016/j.jhep.2019.10.003>.
- Bianchi, G., Marchesini, G., Nicolino, F., Graziani, R., Sgarbi, D., Loguercio, C., Abbati, R., Zoli, M., 2005. Psychological status and depression in patients with liver cirrhosis. *Dig. Liver Dis.* 37 (8), 593–600. <https://doi.org/10.1016/j.dld.2005.01.020>.
- Bonaz, B., Bazin, T., Pellissier, S., 2018. The vagus nerve at the interface of the microbiota-gut-brain axis. *Front. Neurosci.* 12, 49. <https://doi.org/10.3389/fnins.2018.00049>.
- Bonnell, A.R., Bunchorntavakul, C., Reddy, K.R., 2011. Immune dysfunction and infections in patients with cirrhosis. *Clin. Gastroenterol. Hepatol.* 9 (9), 727–738. <https://doi.org/10.1016/j.cgh.2011.02.031>.
- Borovikova, L.V., Ivanova, S., Zhang, M., Yang, H., Botchkina, G.I., Watkins, L.R., Wang, H., Abumrad, N., Eaton, J.W., Tracey, K.J., 2000. Vagus nerve stimulation attenuates the systemic inflammatory response to endotoxin. *Nature* 405 (6785), 458–462. <https://doi.org/10.1038/35013070>.
- Chang, L., Wei, Y., Hashimoto, K., 2022. Brain-gut-microbiota axis in depression: a historical overview and future directions. *Brain Res. Bull.* 182, 44–56. <https://doi.org/10.1016/j.brainresbull.2022.02.004>.
- Chen, S., Zhou, G., Han, H., Jin, J., Li, Z., 2023. Causal effects of specific gut microbiota on bone mineral density: a two-sample Mendelian randomization study. *Front. Endocrinol. (Lausanne)* 14, 1178831. <https://doi.org/10.3389/fendo.2023.1178831>.
- Cryan, J.F., O'Riordan, K.J., Cowan, C.S.M., Sandhu, K.V., Bastiaansen, T.F.S., Boehme, M., Codagnone, M.G., Cusotto, S., Furling, C., Golubeva, A.V., Guzzetta, K. E., Jaggar, M., Long-Smith, C.M., Lyte, J.M., Martin, J.A., Molinero-Perez, A., Moloney, G., Morelli, E., Morillas, E., O'Connor, R., Cruz-Pereira, J.S., Peterson, V.L., Rea, K., Ritz, N.L., Sherwin, E., Spichak, S., Teichman, E.M., van de Wouw, M., Ventura-Silva, A.P., Wallace-Fitzsimons, S.E., Hyland, N., Clarke, G., Dinan, T.G., 2019. The microbiota-gut-brain axis. *Physiol. Rev.* 99 (4), 1877–2013. <https://doi.org/10.1152/physrev.00018.2018>.
- Forsythe, P., Bienenstock, J., Kunze, W.A., 2014. Vagal pathways for microbiome-brain-gut axis communication. *Adv. Exp. Med. Biol.* 817, 115–133. https://doi.org/10.1007/978-1-4939-0897-4_5.
- Geerts, A.M., Vanheule, E., Praet, M., Van Vlierberghe, H., De Vos, M., Colle, I., 2008. Comparison of three research models of portal hypertension in mice: macroscopic, histological and portal pressure evaluation. *Int. J. Exp. Pathol.* 89 (4), 251–263. <https://doi.org/10.1111/j.1365-2613.2008.00597.x>.
- Ginès, P., Krag, A., Abaldas, J.G., Solà, E., Fabrellas, N., Kamath, P.S., 2021. Liver cirrhosis. *Lancet* 398 (10308), 1359–1376. [https://doi.org/10.1016/S0140-6736\(21\)01374-X](https://doi.org/10.1016/S0140-6736(21)01374-X).
- Hashimoto, K., 2020. Molecular mechanisms of the rapid-acting and long-lasting antidepressant actions of (R)-ketamine. *Biochem. Pharmacol.* 177, 113935. <https://doi.org/10.1016/j.bcp.2020.113935>.

- Hashimoto, K., 2022. Ketamine: anesthetic, psychotomimetic, antidepressant, or anthelmintic? *Mol. Psychiatry* 27 (8), 3116–3118.
- Hashimoto, K., 2023a. Emerging role of the host microbiome in neuropsychiatric disorders: overview and future directions. *Mol. Psychiatry* 28 (9), 3625–3637. <https://doi.org/10.1038/s41380-023-02287-6>.
- Hashimoto, K., 2023b. Neuroinflammation through the vagus nerve-dependent gut-microbiota-brain axis in treatment-resistant depression. *Prog. Brain Res.* 278, 61–77. <https://doi.org/10.1016/bs.pbr.2023.01.003>.
- Hashimoto, K., 2023c. Detrimental effects of COVID-19 in the brain and therapeutic options for long COVID: the role of Epstein-Barr virus and the gut-brain axis. *Mol. Psychiatry*. <https://doi.org/10.1038/s41380-023-02161-5>, 2023 Jul 4.
- Hashimoto, K., 2023d. Arketamine for cognitive impairment in psychiatric disorders. *Eur. Arch. Psychiatry Clin. Neurosci.* 273 (7), 1513–1525. <https://doi.org/10.1007/s00406-023-01570-5>.
- Hashimoto, K., 2024. Are “mystical experiences” essential for antidepressant actions of ketamine and the classic psychedelics? *Eur. Arch. Psychiatry Clin. Neurosci.* (in press).
- Hua, H., Huang, C., Liu, H., Xu, X., Xu, X., Wu, Z., Liu, C., Wang, Y., Yang, C., 2022. Depression and antidepressant effects of ketamine and its metabolites: the pivotal role of gut microbiota. *Neuropharmacology* 220, 109272. <https://doi.org/10.1016/j.neuropharm.2022.109272>.
- Huang, L.T., Tiao, M.M., Tain, Y.L., Chen, C.C., Hsieh, C.S., 2009. Melatonin ameliorates bile duct ligation-induced systemic oxidative stress and spatial memory deficits in developing rats. *Pediatr. Res.* 65 (2), 176–180. <https://doi.org/10.1203/PDR.0b013e31818d5bc7>.
- Huang, X., Liu, X., Yu, Y., 2017. Depression and chronic liver diseases: are there shared underlying mechanisms? *Front. Mol. Neurosci.* 10, 134. <https://doi.org/10.3389/fnmol.2017.00134>.
- Kronsten, V.T., Tranah, T.H., Pariante, C., Sawcross, D.L., 2022. Gut-derived systemic inflammation as a driver of depression in chronic liver disease. *J. Hepatol.* 76 (3), 665–680. <https://doi.org/10.1016/j.jhep.2021.11.008>.
- Kur, P., Kolasa-Wolosiuk, A., Misiakiewicz-Has, K., Wiszniewska, B., 2020. Sex hormone-dependent physiology and diseases of liver. *Int. J. Environ. Res. Public Health* 17 (8), 2620. <https://doi.org/10.3390/ijerph17082620>.
- Liu, L., Wang, H., Chen, X., Zhang, Y., Zhang, H., Xie, P., 2023. Gut microbiota and its metabolites in depression: from pathogenesis to treatment. *EBioMedicine* 90, 104527. <https://doi.org/10.1016/j.ebiom.2023.104527>.
- Ma, L., Zhang, J., Fujita, Y., Qu, Y., Shan, J., Wan, X., Wang, X., Ishima, T., Kobayashi, K., Wang, L., Hashimoto, K., 2022a. Nuclear factor of activated T cells 4 in the prefrontal cortex is required for prophylactic actions of (R)-ketamine. *Transl. Psychiatry* 12 (1), 27. <https://doi.org/10.1038/s41398-022-01803-6>.
- Ma, L., Zhang, J., Fujita, Y., Shinno-Hashimoto, H., Shan, J., Wan, X., Qu, Y., Chang, L., Wang, X., Hashimoto, K., 2022b. Effects of spleen nerve denervation on depression-like phenotype, systemic inflammation, and abnormal composition of gut microbiota in mice after administration of lipopolysaccharide: a role of brain-spleen axis. *J. Affect. Disord.* 317, 156–165. <https://doi.org/10.1016/j.jad.2022.08.087>.
- Ma, L., Wang, L., Qu, Y., Wan, X., Hashimoto, K., 2023. A role of splenic heme biosynthesis pathway in the persistent prophylactic actions of arketamine in lipopolysaccharide-treated mice. *Transl. Psychiatry* 13 (1), 269. <https://doi.org/10.1038/s41398-023-02564-6>.
- Mullish, B.H., Kabir, M.S., Thurst, M.R., Dhar, A., 2014. Review article: depression and the use of antidepressants in patients with chronic liver disease or liver transplantation. *Aliment. Pharmacol. Ther.* 40 (8), 880–892. <https://doi.org/10.1111/apt.12925>.
- Nardelli, S., Pentassuglio, I., Pasquale, C., Ridola, L., Moscucci, F., Merli, M., Mina, C., Marianetti, M., Frattino, M., Izzo, C., Merkel, C., Riggio, O., 2013. Depression, anxiety and alexithymia symptoms are major determinants of health related quality of life (HRQoL) in cirrhotic patients. *Metab. Brain Dis.* 28 (2), 239–243. <https://doi.org/10.1007/s11011-012-9364-0>.
- Ohlsson, C., Sjögren, K., 2015. Effects of the gut microbiota on bone mass. *Trends Endocrinol. Metab.* 26 (2), 69–74. <https://doi.org/10.1016/j.tem.2014.11.004>.
- Pantiga, C., Rodrigo, L.R., Cuesta, M., Lopez, L., Arias, J.L., 2003. Cognitive deficits in patients with hepatic cirrhosis and in liver transplant recipients. *J. Neuropsychiatr. Clin. Neurosci.* 15 (1), 84–89. <https://doi.org/10.1176/jnp.15.1.84>.
- Patten, S.B., Williams, J.V., Lavorato, D.H., Modgill, G., Jette, N., Eliasziw, M., 2008. Major depression as a risk factor for chronic disease incidence: longitudinal analysis in a general population cohort. *Gen. Hosp. Psychiatry* 30 (5), 407–413. <https://doi.org/10.1016/j.genhosppsych.2008.05.001>.
- Pu, Y., Tan, Y., Qu, Y., Chang, L., Wang, S., Wei, Y., Wang, X., Hashimoto, K., 2021. A role of the subdiaphragmatic vagus nerve in depression-like phenotypes in mice after fecal microbiota transplantation from *Chrna7* knock-out mice with depression-like phenotypes. *Brain Behav. Immun.* 94, 318–326. <https://doi.org/10.1016/j.bbi.2020.12.032>.
- Qu, Y., Yang, C., Ren, Q., Ma, M., Dong, C., Hashimoto, K., 2017. Comparison of (R)-ketamine and lanicemine on depression-like phenotype and abnormal composition of gut microbiota in a social defeat stress model. *Sci. Rep.* 7 (1), 15725. <https://doi.org/10.1038/s41598-017-16060-7>.
- Qu, Y., Eguchi, A., Wan, X., Ma, L., Chang, L., Shan, J., Yang, Y., Mori, C., Hashimoto, K., 2023a. Repeated use of 3,4-methylenedioxymethamphetamine is associated with the resilience in mice after chronic social defeat stress: a role of gut-microbiota-brain axis. *Psychiatry Res.* 320, 115020. <https://doi.org/10.1016/j.psychres.2022.115020>.
- Qu, Y., Eguchi, A., Ma, L., Wan, X., Mori, C., Hashimoto, K., 2023b. Role of the gut-brain axis via the subdiaphragmatic vagus nerve in stress resilience of 3,4-methylenedioxymethamphetamine in mice exposed to chronic restraint stress. *Neurobiol. Dis.* 189, 106348. <https://doi.org/10.1016/j.nbd.2023.106348>.
- San Martín-Valenzuela, C., Borrás-Barrachina, A., Gallego, J.J., Urios, A., Mestre-Salvador, V., Correa-Ghisays, P., Ballester, M.P., Escudero-García, D., Tosca, J., Montón, C., Ríos, M.P., Kosenko, E., Felipe, V., Tabares-Seisdedos, R., Selva-Verá, G., Montoliu, C., 2020. Motor and cognitive performance in patients with liver cirrhosis with minimal hepatic encephalopathy. *J. Clin. Med.* 9 (7), 2154. <https://doi.org/10.3390/jcm9072154>.
- Sanada, K., Nakajima, S., Kurokawa, S., Barceló-Soler, A., Ikuse, D., Hirata, A., Yoshizawa, A., Tomizawa, Y., Salas-Valero, M., Noda, Y., Mimura, M., Iwanami, A., Kishimoto, T., 2020. Gut microbiota and major depressive disorder: a systematic review and meta-analysis. *J. Affect. Disord.* 266, 1–13. <https://doi.org/10.1016/j.jpsy.2021.05.009>.
- Schwabe, R.F., Greten, T.F., 2020. Gut microbiome in HCC—mechanisms, diagnosis and therapy. *J. Hepatol.* 72 (2), 230–238. <https://doi.org/10.1016/j.jhep.2019.08.016>.
- Singh, N., Gayowski, T., Wagener, M.M., Marino, I.R., 1997. Depression in patients with cirrhosis. Impact on outcome. *Dig. Dis. Sci.* 42 (7), 1421–1427. <https://doi.org/10.1023/a:1018898106656>.
- Smith, M.L., Wade, J.B., Wolstenholme, J., Bajaj, J.S., 2023. Gut microbiota-brain-cirrhosis axis. *Hepatology*. <https://doi.org/10.1097/HEP.0000000000000344>, 2023 Mar 6.
- Stewart, C.A., Enders, F.T., Mitchell, M.M., Felmlee-Devine, D., Smith, G.E., 2011. The cognitive profile of depressed patients with cirrhosis. *Prim. Care Compan. CNS Disord.* 13 (3). <https://doi.org/10.4088/PCC.10m01090>. PCC.10m01090.
- Tag, C.G., Sauer-Lehnen, S., Weiskirchen, S., Borkham-Kamphorst, E., Tolba, R.H., Tacke, F., Weiskirchen, R., 2015. Bile duct ligation in mice: induction of inflammatory liver injury and fibrosis by obstructive cholestasis. *J. Vis. Exp.* 96, e52438. <https://doi.org/10.3791/52438>.
- Tapper, E.B., Parikh, N.D., 2023. Diagnosis and management of cirrhosis and its complications: a review. *JAMA* 329 (18), 1589–1602. <https://doi.org/10.1001/jama.2023.5997>.
- Tsugawa, H., Ikeda, K., Takahashi, M., Satoh, A., Mori, Y., Uchino, H., Okahashi, N., Yamada, Y., Tada, I., Bonini, P., Higashi, Y., Okazaki, Y., Zhou, Z., Zhu, Z.J., Koelme, J., Cajka, T., Fiehn, O., Saito, K., Arita, M., Arita, M., 2020. A lipidome atlas in MS-DIAL 4. *Nat. Biotechnol.* 38 (10), 1159–1163. <https://doi.org/10.1038/s41587-020-0531-2>.
- Van Campenhout, S., Van Vlierberghe, H., Devisscher, L., 2019. Common bile duct ligation as model for secondary biliary cirrhosis. *Methods Mol. Biol.* 1981, 237–247. https://doi.org/10.1007/978-1-4939-9420-5_15.
- Wan, X., Eguchi, A., Fujita, Y., Ma, L., Wang, X., Yang, Y., Qu, Y., Chang, L., Zhang, J., Mori, C., Hashimoto, K., 2022. Effects of (R)-ketamine on reduced bone mineral density in ovarietomized mice: a role of gut microbiota. *Neuropharmacology* 213, 109139. <https://doi.org/10.1016/j.neuropharm.2022.109139>.
- Wan, X., Eguchi, A., Chang, L., Mori, C., Hashimoto, K., 2023. Beneficial effects of arketamine on the reduced bone mineral density in susceptible mice after chronic social defeat stress: role of the gut-microbiota-brain axis. *Neuropharmacology* 228, 109466. <https://doi.org/10.1016/j.neuropharm.2023.109466>.
- Wang, S., Ishima, T., Zhang, J., Qu, Y., Chang, L., Pu, Y., Fujita, Y., Tan, Y., Wang, X., Hashimoto, K., 2020. Ingestion of *Lactobacillus intestinalis* and *Lactobacillus reuteri* causes depression- and anhedonia-like phenotypes in antibiotic-treated mice via the vagus nerve. *J. Neuroinflammation* 17 (1), 241. <https://doi.org/10.1186/s12974-020-01916-z>.
- Wang, S., Ishima, T., Qu, Y., Shan, J., Chang, L., Wei, Y., Zhang, J., Pu, Y., Fujita, Y., Tan, Y., Wang, X., Ma, L., Wan, X., Hammock, B.D., Hashimoto, K., 2021. Ingestion of *Faecalibaculum rodentium* causes depression-like phenotypes in resilient *Ephx2* knock-out mice: a role of brain-gut-microbiota axis via the subdiaphragmatic vagus nerve. *J. Affect. Disord.* 292, 565–573. <https://doi.org/10.1016/j.jad.2021.06.006>.
- Wang, X., Yang, J., Hashimoto, K., 2022. (R)-ketamine as prophylactic and therapeutic drug for neurological disorders: beyond depression. *Neurosci. Biobehav. Rev.* 139, 104762. <https://doi.org/10.1016/j.neubiorev.2022.104762>.
- Wang, X., Eguchi, A., Yang, Y., Chang, L., Wan, X., Shan, J., Qu, Y., Ma, L., Mori, C., Yang, J., Hashimoto, K., 2023. Key role of the gut-microbiota-brain axis via the subdiaphragmatic vagus nerve in demyelination of the cuprizone-treated mouse brain. *Neurobiol. Dis.* 176, 105951. <https://doi.org/10.1016/j.nbd.2022.105951>.
- Wei, Y., Chang, L., Hashimoto, K., 2022a. Molecular mechanisms underlying the antidepressant actions of arketamine: beyond the NMDA receptor. *Mol. Psychiatry* 27 (1), 559–573. <https://doi.org/10.1038/s41380-021-01121-1>.
- Wei, Y., Wang, T., Liao, L., Fan, X., Chang, L., Hashimoto, K., 2022b. Brain-spleen axis in health and diseases: a review and future perspective. *Brain Res. Bull.* 182, 130–140. <https://doi.org/10.1016/j.brainresbull.2022.02.008>.
- Wiest, R., Albillos, A., Trauner, M., Bajaj, J.S., Jalan, R., 2017. Targeting the gut-liver axis in liver disease. *J. Hepatol.* 67 (5), 1084–1103. <https://doi.org/10.1016/j.jhep.2017.05.007>.
- Yang, C., Shirayama, Y., Zhang, J.C., Ren, Q., Yao, W., Ma, M., Dong, C., Hashimoto, K., 2015. R-ketamine: a rapid-onset and sustained antidepressant without psychotomimetic side effects. *Transl. Psychiatry* 5 (9), e632. <https://doi.org/10.1038/tp.2015.136>.
- Yang, C., Qu, Y., Fujita, Y., Ren, Q., Ma, M., Dong, C., Hashimoto, K., 2017. Possible role of the gut microbiota-brain axis in the antidepressant effects of (R)-ketamine in a social defeat stress model. *Transl. Psychiatry* 7 (12), 1294. <https://doi.org/10.1038/s41398-017-0031-4>.
- Yang, C., Yang, J., Luo, A., Hashimoto, K., 2019. Molecular and cellular mechanisms underlying the antidepressant effects of ketamine enantiomers and its metabolites. *Transl. Psychiatry* 9 (1), 280. <https://doi.org/10.1038/s41398-019-0624-1>.
- Yang, Y., Ishima, T., Wan, X., Wei, Y., Chang, L., Zhang, J., Qu, Y., Hashimoto, K., 2022. Microglial depletion and abnormalities in gut microbiota composition and short-chain fatty acids in mice after repeated administration of colony stimulating factor 1

- receptor inhibitor PLX5622. *Eur. Arch. Psychiatry Clin. Neurosci.* 272 (3), 483–495. <https://doi.org/10.1007/s00406-021-01325-0>.
- Yang, Y., Eguchi, A., Wan, X., Chang, L., Wang, X., Qu, Y., Mori, C., Hashimoto, K., 2023. A role of gut-microbiota-brain axis via subdiaphragmatic vagus nerve in depression-like phenotypes in *Chrna7* knock-out mice. *Prog. Neuro-Psychopharmacol. Biol. Psychiatry* 120, 110652. <https://doi.org/10.1016/j.pnpbp.2022.110652>.
- Yang, Y., Eguchi, A., Wan, X., Mori, C., Hashimoto, K., 2024. Depression-like phenotypes in mice with hepatic ischemia/reperfusion injury: a role of gut-microbiota-liver-brain axis via vagus nerve. *J. Affect. Disord.* 345, 157–167. <https://doi.org/10.1016/j.jad.2023.10.142>.
- Yao, W., Cao, Q., Luo, S., He, L., Yang, C., Chen, J., Qi, Q., Hashimoto, K., Zhang, J.C., 2022. Microglial ERK-NRBP1-CREB-BDNF signaling in sustained antidepressant actions of (R)-ketamine. *Mol. Psychiatry* 27 (3), 1618–1629. <https://doi.org/10.1038/s41380-021-01377-7>.
- Yue, C., Luan, W., Gu, H., Qiu, D., Ding, X., Liu, P., Wang, X., Hashimoto, K., Yang, J.J., 2023. The role of the gut-microbiota-brain axis via the subdiaphragmatic vagus nerve in chronic inflammatory pain and comorbid spatial working memory impairment in complete Freund's adjuvant mice. *J. Psychiatr. Res.* 166, 61–73. <https://doi.org/10.1016/j.jpsychires.2023.09.003>.
- Zhang, J., Ma, L., Chang, L., Pu, Y., Qu, Y., Hashimoto, K., 2020. A key role of the subdiaphragmatic vagus nerve in the depression-like phenotype and abnormal composition of gut microbiota in mice after lipopolysaccharide administration. *Transl. Psychiatry* 10 (1), 186. <https://doi.org/10.1038/s41398-020-00878-3>.
- Zhang, J., Ma, L., Wan, X., Shan, J., Qu, Y., Hashimoto, K., 2021a. (R)-ketamine attenuates LPS-induced endotoxin-derived delirium through inhibition of neuroinflammation. *Psychopharmacology* 238 (10), 2743–2753. <https://doi.org/10.1007/s00213-021-05889-6>.
- Zhang, J.C., Li, S.X., Hashimoto, K., 2014. R (–)-ketamine shows greater potency and longer lasting antidepressant effects than S (+)-ketamine. *Pharmacol. Biochem. Behav.* 116, 137–141. <https://doi.org/10.1016/j.pbb.2013.11.033>.
- Zhang, J.C., Yao, W., Hashimoto, K., 2022a. Arketamine, a new rapid-acting antidepressant: a historical review and future directions. *Neuropharmacology* 218, 109219. <https://doi.org/10.1016/j.neuropharm.2022.109219>.
- Zhang, K., Yao, Y., Hashimoto, K., 2023. Ketamine and its metabolites: potential as novel treatments for depression. *Neuropharmacology* 222, 109305. <https://doi.org/10.1016/j.neuropharm.2022.109305>.
- Zhang, X., Liu, H., Hashimoto, K., Yuan, S., Zhang, J., 2022b. The gut–liver axis in sepsis: interaction mechanisms and therapeutic potential. *Crit. Care* 26 (1), 213. <https://doi.org/10.1186/s13054-022-04090-1>.
- Zhang, Y., Xie, B., Chen, X., Zhang, J., Yuan, S., 2021b. A key role of gut microbiota–vagus nerve/spleen axis in sleep deprivation-mediated aggravation of systemic inflammation after LPS administration. *Life Sci.* 265, 118736. <https://doi.org/10.1016/j.lfs.2020.118736>.
- Zheng, P., Zeng, B., Zhou, C., Liu, M., Fang, Z., Xu, X., Zeng, L., Chen, J., Fan, S., Du, X., Zhang, X., Yang, D., Yang, Y., Meng, H., Li, W., Melgiri, N.D., Licinio, J., Wei, H., Xie, P., 2016. Gut microbiome remodeling induces depressive-like behaviors through a pathway mediated by the host's metabolism. *Mol. Psychiatry* 21 (6), 786–796. <https://doi.org/10.1038/mp.2016.44>.
- Zhou, W.C., Zhang, Q.B., Qiao, L., 2014. Pathogenesis of liver cirrhosis. *World J. Gastroenterol.* 20 (23), 7312–7324. <https://doi.org/10.3748/wjg.v20.i23.7312>.

日中笹川医学奨学金制度<学位取得コース>評価書

課程博士：指導教官用



第 44 期

研究者番号：G4404

作成日：2024年3月10日

氏名	蔣 夢恬	JIANG MENG TIAN	性別	F	生年月日	1996/03/15
所属機関（役職）	東京医科歯科大学大学院医歯学総合研究科（大学院生）					
研究先（指導教官）	東京医科歯科大学大学院医歯学総合研究科 口腔機能再構築学講座生体補綴歯科学分野（若林 則幸 教授）					
研究テーマ	暗条件下での血清及び唾液中の二酸化チタンの殺菌効果に及ぼす3種類のイオン性抗菌剤の影響に関する研究 Development of antibacterial dental materials using cation-doped TiO ₂ nanosheet in dark condition					
専攻種別	<input type="checkbox"/> 論文博士			<input checked="" type="checkbox"/> 課程博士		

研究者評価（指導教官記入欄）

成績状況	優 学業成績係数=	取得単位数
		30/30
学生本人が行った研究の概要	研究課題では、優れた抗菌活性を有する新規歯科補綴装置用材料の創製のため、光析出法にて金属ナノ粒子を担持させたチタニアナノシートを開発することを目的としている。本年度は、作製した金属固溶チタニアナノシートのキャラクタリゼーションを、走査型電子顕微鏡、透過型電子顕微鏡、X線回折により解析した。また、電子線散乱による評価を継続している。また、う蝕原性細菌である Streptococcus mutans を用いた抗菌活性を評価した。その結果、銅を固溶したチタニアナノシートの抗菌活性が最も優れていることが明らかとなり、本成果を、国際学会である The 3rd International Symposium on Design & Engineering by Joint Inverse Innovation for Materials Architecture (DEJI2MA-3) と 2024 International Association for Dental, Oral, and Craniofacial Research にて発表を行った。次年度に論文を投稿予定である。	
総合評価	【良かった点】 本年度は、作製した金属固溶チタニアナノシートのキャラクタリゼーションと抗菌活性評価までを行い、十分な研究活動を行ったと評価できる。特に、水熱化学合成法と光析出法を用いた金属固溶チタニアナノシートの合成方法に習熟し、今後、本法を応用した材料開発を遂行できるようになった。また、細菌を用いた抗菌活性評価を独立して遂行可能となった。研究室のチームとも協調性をもって活動することができた。	
	【改善すべき点】 今後、自立した研究者として活躍するためには、得られた実験結果の解釈とその意味を理解することが重要である。また、その結果から今後の検討課題を吟味することが必要であるが、問題点の抽出とその解決策の提案が不十分であることが見受けられた。改善の傾向が見受けられるが、独立した研究者として活躍するためには、今後一層の研鑽が必要である。	
	【今後の展望】 作製した金属ナノ粒子は数 nm サイズのため、学内機器では詳細な解析を行うことができない。そこで次年度は、東京都立産業技術センターにてキャラクタリゼーションを行う予定である。また、歯科材料への応用のため、光触媒活性と抗菌活性の評価を行う予定である。	

学位取得見込	研究は順調に進捗しており、本学が定める学位取得の単位も到達している。次年度は論文の執筆にとりかかり、学術雑誌への投稿を予定しており、十分に学位取得の要件を満たすと考える。
評価者（指導教官名） 若林 則幸	

日中笹川医学奨学金制度(学位取得コース)中間報告書 研究者用



第44期

研究者番号: G4404

作成日: 2024年3月 5 日

氏名	蒋 梦恬	JIANG MENG TIAN	性別	F	生年月日	1996/03/15
所属機関(役職)	東京医科歯科大学大学院医歯学総合研究科(大学院生)					
研究先(指導教官)	東京医科歯科大学大学院医歯学総合研究科 口腔機能再構築学講座生体補綴歯科学分野(若林 則幸 教授)					
研究テーマ	暗条件下での血清及び唾液中の二酸化チタンの殺菌効果に及ぼす3種類のイオン性抗菌剤の影響に関する研究 Development of antibacterial dental materials using cation-doped TiO ₂ nanosheet in dark condition					
専攻種別	論文博士	<input type="checkbox"/>	課程博士	<input checked="" type="checkbox"/>		

1. 研究概要(1)

1) 目的(Goal)

Titania (TiO₂) has antibacterial effects due to its photocatalytic activity and has been applied not only in the industrial field but also in the medical and dental fields. To improve the functions of TiO₂, we have prepared highly-ordered TiO₂ nanosheets (TiO₂ NS) exposing the {001} planes and have shown that they have superior photocatalytic activity compared to conventional titania nanoparticles. In this study, we made silver, copper, and cerium-doped titania nanosheets (Ag/TiO₂ NS, Cu/TiO₂ NS, and Ce/TiO₂ NS) and performed antibacterial tests of these 3 kinds of metal-doped TiO₂ NS to explore the antibacterial effect against *Streptococcus mutans*.

2) 戦略(Approach)

The photodeposition method is based on the photocatalytic property of semiconductor materials afforded by their band gap. Several conditions are needed to enable the photodeposition method. First, the photon energy of the exposure light should be larger than the energy band gap of the semiconductor. When light that has the proper energy level for the band gap of the semiconductor is absorbed, electrons from the valence band can be excited. Second, the reduction potential of the metal ion should be more positive than the conduction band energy level of the semiconductor. Third, the efficient separation and migration of photo-generated electron-hole pairs is necessary. Finally, the semiconductor should act as a template for active sites of metal deposition and have a large surface area. If these four conditions are met, the synthesis of metal/semiconductor nanocomposite by photodeposition method is possible, since nanoscale semiconductor materials have many active sites that have large surface energy due to their morphology. Also, this is a simple and green method since it does not require the addition of chemical reagents or any conditions other than light exposure[1].

3) 材料と方法(Materials and methods)

1. Synthesis of F-TiO₂ NS

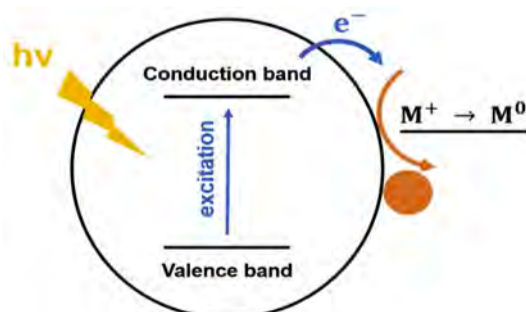
Dissolve 1 g Ammonium hexafluorotitanate into 5 ml of hydrochloric acid (5 M). Add a controlled amount titanium (IV) butoxide to the above solution to make that the total F/Ti molar ratio is 1.0 under strong stirring and white gels formed. The gels are placed into a 50 ml Teflon tube for a 6-hour hydrothermal reaction at 180° C. The products of the hydrothermal reaction are washed with ultrapure water three times and by methanol once, all with subsequent centrifugal separation. The obtained TiO₂ NS were then freeze dried[2,3].

2. Removal of the fluorides from F-TiO₂ NS to produce TiO₂ NS

To attain the removal of the fluorides from the surface, the as-prepared F-TiO₂ NS was washed with 0.1M NaOH (10 mg TiO₂/ml, 2 h under stirring at ~300K). The suspension was then centrifuged (4000rpm, 15min). The paste of TiO₂ NS was recovered by centrifugation and washed by water 3 times (1500mg, 40 ml, 4000 rpm, 15 min) to remove Na⁺ ions from the surface.

Preparation of metal doped TiO₂ NS by photodeposition

For preparation of metal-modified TiO₂ NS, silver nitrate, copper sulfate pentahydrate and cerium nitrate hexahydrate are used as metal precursors. The amount of each metal doped on 1500mg TiO₂ NS is 1.2*10⁻⁴mol, which means that the quantity of silver nitrate, copper sulfate and cerium nitrate is 20.40mg, 30.00mg and 52.08mg respectively.



Schematic diagram of photodeposition method. When light is absorbed in the band gap, electrons from valence band are excited and migrate to reduce metal ions to metal. hv, light energy; e⁻, photoexcited electron; M⁺, metal ion; M⁰, metal.

1. 研究概要 (2)

The weighted TiO₂ NS powder is put into a Pyrex glass tube equipped with a magnetic stirrer, to which 75ml of methanol(99.5%) aqueous solution(50vol%, distilled water) is added. Then, the aqueous solution of metal salt is slowly dropped while being stirred(75ml distilled water). The suspension is gas-sparged (N₂) for 15 min. The tube is photoirradiated for 3 hours for Ag/TiO₂, Cu/TiO₂ and Ce/TiO₂ with magnetic stirring (500rpm) by a 121-W high-pressure mercury lamp under thermostatic control at 298K. The thus-obtained photocatalysts is centrifuged (4000rpm for 30 min), washed three times with methanol and three times with distilled water, and freeze-dried, and then the product is collected for further study[4].

3. Characterization of three composite materials

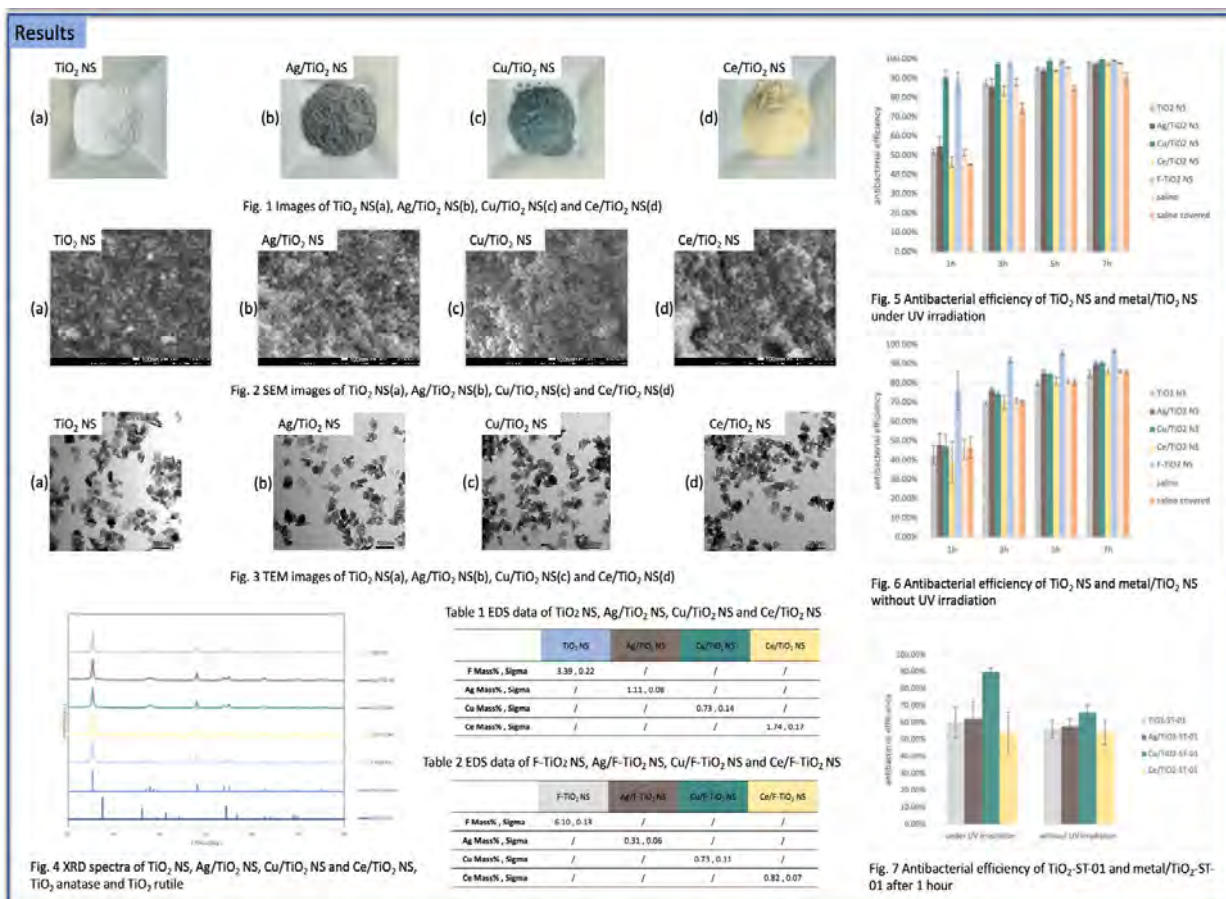
Use X-ray diffractometer, scanning electron microscope, transmittance electron microscope and energy-dispersive X-ray spectrometer to show the crystal structure, morphology and chemical composition of the precipitates. The length and thickness are measured from TEM images.

4. Antibacterial tests against S. mutans

Precultures of S. mutans was grown in ATCC Medium:44 Brain-Heart Infusion (BHI) Broth at 37°C anaerobically (180 rpm). After 18 h, cells are harvested by centrifugation (2200 rpm, 19°C, 5 min), washed twice with 5 ml of saline and resuspended in saline. The density is standardized and adjusted to 0.5 McFarland concentration using a turbidity meter. 9 ml of S. mutans' suspension is poured into the glass bottle with 1 ml metal/TiO₂ or metal/TiO₂-ST-01 or metal/TiO₂-ST-41 saline solution. In addition, two controls were set as 9 ml of S. mutans's suspension with 1 ml saline and one of the glass bottles was covered with aluminum foil.

All experiments are carried out in glass bottles with and without UV irradiation (2.5 mW/cm², 315nm-400nm, 27W) with magnetic stirring (speed 300rpm). At proposed time intervals luminescence was recorded.

4) 実験結果 (Results)



5) 考察 (Discussion)

Ag, Cu and Ce could be doped on titanium dioxide by photodeposition. Ag, Cu and Ce doping by photodeposition could affect the antibacterial efficiency of TiO₂ nanosheets and TiO₂ nanoparticles against Streptococcus mutans.

6) 参考文献 (References)

[1].Lee, Y. et al. Photodeposited metal-semiconductor nanocomposites and their applications. J. Materiomics 4, 83-94 (2018).
 [2].Hayashi, K. et al. Enhanced Antibacterial Property of Facet-Engineered TiO₂ Nanosheet in Presence and Absence of Ultraviolet Irradiation. Materials 13, 78 (2019).
 [3].Tan, Z. et al. Particle size for photocatalytic activity of anatase TiO₂ nanosheets with highly exposed {001} facets. RSC Adv. 3, 19268 (2013).
 [4].Wei, Z. et al. Noble metal-modified octahedral anatase titania particles with enhanced activity for decomposition of chemical and microbiological pollutants. Chem. Eng. J. 318, 121-134 (2017).
 [5].Effects of catalyst preparation method and reaction parameters on the ultrasound assisted Photocatalytic oxidation of reactive yellow 84 dye.

2. 執筆論文 Publication of thesis ※記載した論文を添付してください。Attach all of the papers listed below.

論文名 1 Title	Enhanced Photocatalysis of Electrically Polarized Titania Nanosheets					
掲載誌名 Published journal	nanomaterials					
	2024 年 1 月	14 巻(号)	171 頁 ~	181 頁	言語 Language	English
第1著者名 First author	Tomoyuki Mihara	第2著者名 Second author	Kosuke Nozaki		第3著者名 Third author	Yasuyuki Kowaka
その他著者名 Other authors	Mengtian Jiang , Kimihiro Yamashita, Hiroyuki Miura and Satoshi Ohara					
論文名 2 Title						
掲載誌名 Published journal						
	年 月	巻(号)	頁 ~	頁	言語 Language	
第1著者名 First author		第2著者名 Second author			第3著者名 Third author	
その他著者名 Other authors						
論文名 3 Title						
掲載誌名 Published journal						
	年 月	巻(号)	頁 ~	頁	言語 Language	
第1著者名 First author		第2著者名 Second author			第3著者名 Third author	
その他著者名 Other authors						
論文名 4 Title						
掲載誌名 Published journal						
	年 月	巻(号)	頁 ~	頁	言語 Language	
第1著者名 First author		第2著者名 Second author			第3著者名 Third author	
その他著者名 Other authors						
論文名 5 Title						
掲載誌名 Published journal						
	年 月	巻(号)	頁 ~	頁	言語 Language	
第1著者名 First author		第2著者名 Second author			第3著者名 Third author	
その他著者名 Other authors						

3. 学会発表 Conference presentation ※筆頭演者として総会・国際学会を含む主な学会で発表したものを記載してください
 ※Describe your presentation as the principal presenter in major academic meetings including general meetings or international meetings

学会名 Conference	International Summer Program 2023, Tokyo Medical and Dental University		
演題 Topic	Development of metal nanoparticle-modified titanium dioxide nanosheets through photodeposition		
開催日 date	2023 年 8 月 1 日	開催地 venue	Tokyo
形式 method	<input type="checkbox"/> 口頭発表 Oral <input checked="" type="checkbox"/> ポスター発表 Poster	言語 Language	<input type="checkbox"/> 日本語 <input checked="" type="checkbox"/> 英語 <input type="checkbox"/> 中国語
共同演者名 Co-presenter	Kosuke Nozaki, Takeshi Ueno, Noriyuki Wakabayashi		
学会名 Conference	The 3rd International Symposium on Design & Engineering by Joint Inverse Innovation for Materials Architecture (DEJI2MA-3)		
演題 Topic	Influence of three kinds of ionic antibacterial agents on the antibacterial effect of titania		
開催日 date	2023 年 10 月 20 日	開催地 venue	Tokyo
形式 method	<input type="checkbox"/> 口頭発表 Oral <input checked="" type="checkbox"/> ポスター発表 Poster	言語 Language	<input type="checkbox"/> 日本語 <input checked="" type="checkbox"/> 英語 <input type="checkbox"/> 中国語
共同演者名 Co-presenter	Kosuke Nozaki, Takeshi Ueno, Satoshi Ohara, Takayuki Mokudai, Noriyuki Wakabayashi		
学会名 Conference			
演題 Topic			
開催日 date	年 月 日	開催地 venue	
形式 method	<input type="checkbox"/> 口頭発表 Oral <input type="checkbox"/> ポスター発表 Poster	言語 Language	<input type="checkbox"/> 日本語 <input type="checkbox"/> 英語 <input type="checkbox"/> 中国語
共同演者名 Co-presenter			
学会名 Conference			
演題 Topic			
開催日 date	年 月 日	開催地 venue	
形式 method	<input type="checkbox"/> 口頭発表 Oral <input type="checkbox"/> ポスター発表 Poster	言語 Language	<input type="checkbox"/> 日本語 <input type="checkbox"/> 英語 <input type="checkbox"/> 中国語
共同演者名 Co-presenter			

4. 受賞(研究業績) Award (Research achievement)

名称 Award name	国名 Country	受賞年 Year of	年 月
名称 Award name	国名 Country	受賞年 Year of	年 月

5. 本研究テーマに関わる他の研究助成金受給 Other research grants concerned with your research theme

受給実績 Receipt record	<input checked="" type="checkbox"/> 有 <input type="checkbox"/> 無
助成機関名称 Funding agency	国立研究開発法人科学技術振興機構次世代研究者挑戦的研究プログラム
助成金名称 Grant name	東京医科歯科大学卓越大学院生制度(II)
受給期間 Supported period	2022 年 4 月 ~ 2025 年 3 月
受給額 Amount received	50万/年 円
受給実績 Receipt record	<input type="checkbox"/> 有 <input type="checkbox"/> 無
助成機関名称 Funding agency	
助成金名称 Grant name	
受給期間 Supported period	年 月 ~ 年 月
受給額 Amount received	円

6. 他の奨学金受給 Another awarded scholarship

受給実績 Receipt record	<input checked="" type="checkbox"/> 有 <input type="checkbox"/> 無
助成機関名称 Funding agency	国立研究開発法人科学技術振興機構次世代研究者挑戦的研究プログラム
奨学金名称 Scholarship name	東京医科歯科大学卓越大学院生制度(II)
受給期間 Supported period	2022 年 4 月 ~ 2025 年 3 月
受給額 Amount received	16万/月 円

7. 研究活動に関する報道発表 Press release concerned with your research activities

※記載した記事を添付してください。Attach a copy of the article described below

報道発表 Press release	<input type="checkbox"/> 有 <input type="checkbox"/> 無	発表年月日 Date of release	
発表機関 Released medium			
発表形式 Release method	・新聞 ・雑誌 ・Web site ・記者発表 ・その他()		
発表タイトル Released title			

8. 本研究テーマに関する特許出願予定 Patent application concerned with your research theme

出願予定 Scheduled	<input type="checkbox"/> 有 <input type="checkbox"/> 無	出願国 Application	
出願内容(概要) Application contents			

9. その他 Others

--

指導責任者(記名) 若林 則幸

Article

Enhanced Photocatalysis of Electrically Polarized Titania Nanosheets

Tomoyuki Mihara ¹, Kosuke Nozaki ^{1,*}, Yasuyuki Kowaka ¹, Mengtian Jiang ¹, Kimihiro Yamashita ¹, Hiroyuki Miura ¹ and Satoshi Ohara ²

¹ Graduate School of Medical and Dental Sciences, Tokyo Medical and Dental University, Bunkyo-ku, Tokyo 113-8549, Japan; t.mihara.fpro@tmd.ac.jp (T.M.); y.kowaka.fpro@tmd.ac.jp (Y.K.); jiang.mt.fpro@tmd.ac.jp (M.J.); yama-k.bcr@tmd.ac.jp (K.Y.); h.miura.fpro@tmd.ac.jp (H.M.)

² New Industry Creation Hatchery Center, Tohoku University, Aoba, Sendai 980-8579, Japan; s.ohara@super-nano.com

* Correspondence: k.nozaki.fpro@tmd.ac.jp; Tel.: +83-5803-5516

Abstract: Titania (TiO₂) nanosheets are crystals with controlled, highly ordered structures that improve the functionality of conventional TiO₂ nanoparticles. Various surface modification methods have been studied to enhance the effectiveness of these materials as photocatalysts. Surface modifications using electrical polarization have attracted considerable attention in recent years because they can improve the function of titania without changing its composition. However, the combination of facet engineering and electrical polarization has not been shown to improve the functionality of TiO₂ nanosheets. In the present study, the dye-degradation performance of polarized TiO₂ nanosheets was evaluated. TiO₂ nanosheets with a F/Ti ratio of 0.3 were synthesized via a hydrothermal method. The crystal morphology and structure were evaluated using transmission electron microscopy and X-ray diffraction. Then, electrical polarization was performed under a DC electric field of 300 V at 300 °C. The polarized material was evaluated using thermally stimulated current measurements. A dye-degradation assay was performed using a methylene blue solution under ultraviolet irradiation. The polarized TiO₂ nanosheets exhibited a dense surface charge and accelerated decolorization. These results indicate that electrical polarization can be used to enhance the photocatalytic activity of TiO₂.

Keywords: TiO₂; surface charge; electrical polarization; photocatalytic activity; dye decolorization



Citation: Mihara, T.; Nozaki, K.; Kowaka, Y.; Jiang, M.; Yamashita, K.; Miura, H.; Ohara, S. Enhanced Photocatalysis of Electrically Polarized Titania Nanosheets. *Nanomaterials* **2024**, *14*, 171. <https://doi.org/10.3390/nano14020171>

Academic Editor: Antonino Gulino

Received: 1 December 2023

Revised: 5 January 2024

Accepted: 5 January 2024

Published: 12 January 2024



Copyright: © 2024 by the authors. Licensee MDPI, Basel, Switzerland. This article is an open access article distributed under the terms and conditions of the Creative Commons Attribution (CC BY) license (<https://creativecommons.org/licenses/by/4.0/>).

1. Introduction

Titania (TiO₂) has been used in industrial applications as well as in the dental field as a denture cleaner and for tooth bleaching because it causes a reduction–oxidation (redox) reaction through photocatalytic activity on its surface [1]. Ultraviolet (UV) irradiation generates electrons and holes on the surface of titania, resulting in the generation of reactive oxygen species (ROS) such as superoxide anions (O₂^{•−}) and hydroxyl radicals (•OH) in the presence of water and oxygen [2]. These oxidizing substances can decompose organic dyes with a higher efficiency than common oxygen molecules [3]. However, the generated electrons and holes recombine within 50 ns, indicating that carriers have a longer lifetime on their surfaces [4].

The photocatalytic activity of titania has been improved using various methods, such as facet engineering [5,6], structure regulation [7], and metal doping [8]. These methods aim to enhance the photocatalytic activity by delaying electron–hole recombination. Especially enhanced photocatalysis has been obtained by designing compact heterojunctions [9]. We previously reported a highly ordered, facet-controlled, anatase-type titania nanosheet (NS) with several {001} planes and found that it had superior photocatalytic activity and antibacterial capability compared to conventional titania nanoparticles [10,11]. Titania NSs with side lengths of 29 nm were synthesized using ammonium hexafluorotitanate

((NH₄)₂TiF₆) and titanium butoxide (Ti(OBu)₄). Fluoride from ammonium hexafluorotitanate inhibits crystal growth of the {001} facet by adhering to its facet, which has a high surface energy. The {001} surface has also been reported to have a higher reactivity site against UV irradiation than the {101} surface, which causes redox reactions on both the {001} and {101} surfaces [12]. These results suggest that facet-engineered titania is crucial for the design of photocatalyst-containing biomaterials. However, decolorization was achieved through decomposition via photocatalytic activity as well as by adsorbing dyes on the titania surface [13].

Dye adsorption is typically regulated by physical forces such as van der Waals forces, hydrogen bonds, polarity, and dipole–dipole interactions [14]. The surface charge also plays a critical role in dye adsorption [15]. Electrical polarization has attracted considerable attention as a promising surface modification method [16–18]. We previously reported the surface modification of bioceramics, including hydroxyapatite, carbonated apatite, β -tricalcium phosphate (TCP), zirconia, bioglasses, and glass ceramics, through the electrical polarization process, which can induce surface charges without any doped elements or coating [19–23]. Although the strong ferroelectric polarization of TiO₂ can be achieved through the conjunction of perovskite-based material layers [24], such as BaTiO₃ and SrTiO₃, for applications in the medical and dental fields, surface modifications without any other impurities are highly recommended.

Electrical polarization also regulates titania's electrical dipole orientation under DC electric fields and a high temperature of approximately 300 to 400 °C and maintains its orientation at room temperature [25]. Electrically polarized titania has been reported to enhance osteoblast-like cell proliferation and differentiation and osteoconductivity [23,25,26]. In previous studies, polarized titania was fabricated using the micro-arc oxidation method, which incorporates calcium and phosphate ions. However, it is unclear whether the dipole orientation of titania without doped elements can be induced using electrical polarization. Concerning metal Ti-oxidated titania, we electrically polarized a thick titania layer on a titanium substrate. Bandyopadhyay et al. also reported that titania nanotubes on Ti can be polarized by electrothermal polarization and are supposed to be a novel biomaterial to promote in vivo osseointegration at an early stage in vivo [27]. It is still unclear whether titania powder can be electrically polarized.

The purpose of this study was to attempt the surface modification of NSs by electrical polarization and evaluate the dye-degradation capability of polarized titania NSs to clarify their functions. TiO₂ NSs with a fluorine-to-titanium molar ratio of 0.3 were hydrothermally synthesized. The crystal structure was characterized using transmission electron microscopy (TEM) and X-ray diffraction (XRD). Subsequently, electrical polarization was performed, and the surface charges were evaluated using thermally stimulated current (TSDC) measurements. The dye-degradation performance of the polarized NS was evaluated using a methylene blue (MB) dye-degradation test. The null hypothesis was that electrical polarization does not enhance the decolorizing performance of TiO₂.

2. Materials and Methods

2.1. Synthesis of Titania Nanosheets

The details of the fabrication process for the titania NSs have been described previously [10]. Briefly, titanium butoxide (Sigma-Aldrich, St. Louis, MO, USA) was added dropwise with stirring to 37% hydrochloric acid (FUJIFILM Wako Pure Chemical Corp., Osaka, Japan) and ammonium hexafluorotitanate (Sigma-Aldrich, St. Louis, MO, USA) at a F/Ti ratio of 0.3. The precursor was transferred to a high-pressure reaction vessel and hydrothermally synthesized at 180 °C for 6 h. The precipitates were sonicated thrice with methanol and twice with distilled water. The precipitates were then freeze-dried to obtain a titania NS using a freeze dryer (FDS-1000, Tokyo Rikakikai Co., Ltd., Tokyo, Japan). Titania nanoparticles (NPs, FUJIFILM Wako Pure Chemical Corp. Osaka, Japan) were used as control materials.

Japan). Titania nanoparticles (NPs, FUJIFILM Wako Pure Chemical Corp. Osaka, Japan) were used as control materials.

2.2. Electrical Polarization

2.2.1. Electrical Polarization

NS and NP powders were poured into an alumina ring with an inner diameter of 10 mm and a depth of 2 mm, sandwiched between platinum foil electrodes, and then electrically polarized under a DC electric field at 300 V/mm and 300 °C for 1 h (P-NS, P-NP) (Figure 1). As the control group, NSs and NPs were subjected to the same process of heating at 300 °C under 0 V/mm (H-NS, H-NP).

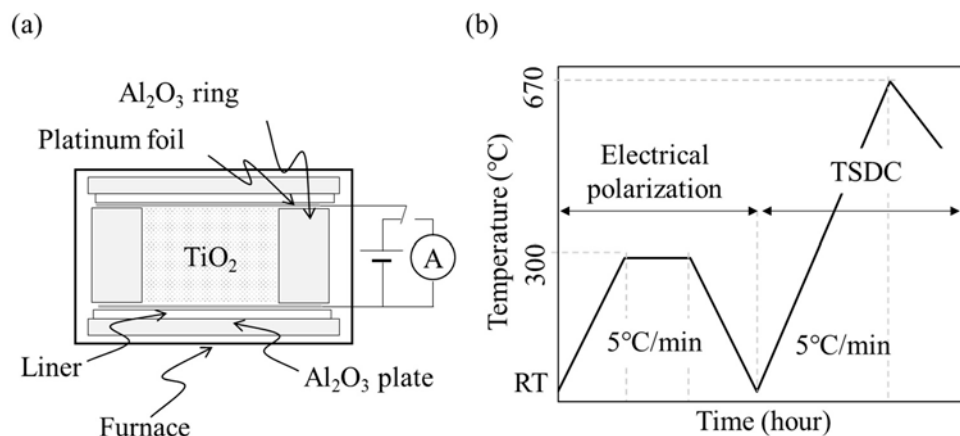


Figure 1. (a) Schematic diagram of sample preparation for electrical polarization. For the thermally polarized sample, a current (J) was prepared for electrical polarization. For the galvanostatic (G) temperature program for TSDC polarization and TSDC measurement, the temperature was increased to a galvanometer. (b) Temperature program for electrical polarization and TSDC measurement procedure.

2.3. Characterization

The crystal morphology and structure of each sample were observed using TEM (JEOL-2100/HR2300, JEOL Ltd., Tokyo, Japan) (JEM-1400Flash, JEOL Ltd., Tokyo, Japan). In addition, the phase composition of the sample surface was analyzed in the 2 θ range of 20° to 80° using XRD (D8 advance, Bruker AXS GmbH, Karlsruhe, Germany) (JEM-1400Flash, JEOL Ltd., Tokyo, Japan). In addition, polarized and non-polarized samples were evaluated using TSDC at a temperature increase rate of 5.0 °C/min from room temperature to 670 °C in air after polarization with a galvanometer (6514/J, Tektronix Inc., Tokyo, Japan) (Figure 1) [20–22,26,27]. The stored charge (Q) was calculated from the TSDC spectra using the following equation:

$$Q = \frac{1}{\beta} \int J(T) dT$$

where Q is the stored charge (C/cm²), β is the ramp rate of the temperature (K/s), and J(T) is the depolarized current density (A/cm).

The optical properties of the heated and polarized samples were characterized using UV-visible (UV-vis) spectrophotometer (Jasco M-550, JASCO International Co. Ltd., Tokyo, Japan). The optical bandgap energies (E_g) of the polarized and non-polarized samples were calculated using Tauc plots as previously described [28].

2.4. Dye-Degradation Assay

The dye-degradation test using the redox reaction was conducted using a 0.3 mM MB solution. Each sample was mixed with MB at a concentration of 10 mg/mL. The mixed samples were irradiated at 20 °C (NCP2215, Nissinrika Corp., Tokyo, Japan) for 1, 10, 30, 60, 120, 180, 240, or 480 min under UV light (HL100G, Sen special light Source, SEN LIGHTS CORP., Osaka, Japan) at 2.5 mW/cm² (Figure 2). The samples were centrifuged (20,000 × g, 10 min) the supernatant was diluted 10-fold, and the absorbance was measured at 630 nm using a microplate reader (Model680, Bio-Rad Laboratories Inc., Hercules, Berkeley, CA, USA). For the non-irradiated group, the absorbance was measured in the same manner after UV irradiation under the same conditions, shielded with aluminum foil. After obtaining

at 630 nm using a microplate reader (Model680, Bio-Rad Laboratories Berkeley, CA, USA). For the non-irradiated group, the absorbance was measured in the same manner after UV irradiation under the same conditions, shielded with a foil. After obtaining the absorbance at each time point, the rate constant of MB was calculated using the following equation:

the absorbance at each time point, the rate constant of MB degradation was calculated using the following equation:

$$\ln \frac{A_0}{A_t} = k_a t$$

where k_a is a rate constant, A_t is the absorbance of the MB solution at each time point, A_0 is the absorbance of the MB solution at each time, and A_0 is the absorbance after 1 min.

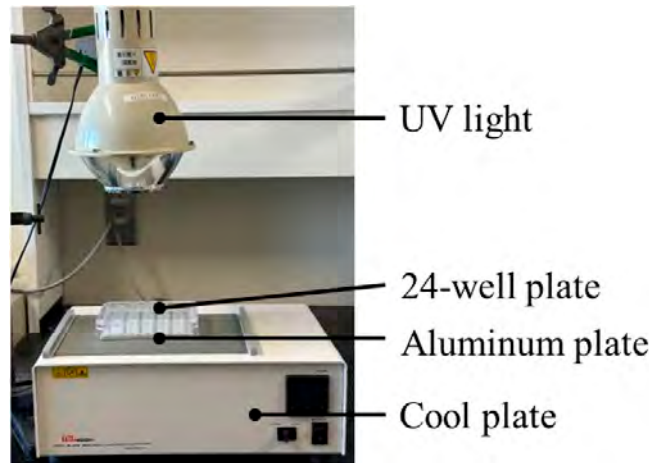


Figure 2. Experimental setup for dye degradation assay. The temperature of the 24-well plate was regulated by a cool plate via an aluminum plate.

2.5. Measurement of ROS

2.5.1. Measurement of ROS
 To measure the ROS generated from the titania samples (P-NS, P-NP, H-NS, and H-NP) and their reactions under UV irradiation, disodium terephthalate (DTA, Tokyo Kasei Kogyo, Tokyo, Japan) and nitro blue tetrazolium (NBT, Tokyo Kasei Kogyo, Tokyo, Japan) assays were performed. NBT and DTA react with superoxide anions and convert them to formazan and 2-hydroxy terephthalic acid (HTA), respectively [10,29].

The NBT solution was mixed with 4 mg/mL of TiO₂ and irradiated with UV light at 2.5 mW/cm² for 2 h. After irradiation, the solution was centrifuged at 13,000 rpm for 5 min, and the supernatant was discarded. The precipitates were dissolved in dimethyl sulfoxide (DMSO, Fujifilm Wako Pure Chemicals Corporation, Osaka, Japan) and stirred for 10 min. The absorbance was measured at 570 nm using a spectrophotometer.

The NBT solution was mixed with 4 mg/mL of TiO₂ and irradiated with UV light at 2.5 mW/cm² for 2 h. After irradiation, the solution was centrifuged at 13,000 rpm for 5 min, and the supernatant was discarded. The precipitates were dissolved in dimethyl sulfoxide (DMSO, Fujifilm Wako Pure Chemicals Corporation, MA, USA) and stirred for 10 min. The absorbance and fluorescence intensity were measured at 570 nm using a spectrophotometer.

As previously reported [10], the absorbance and fluorescence intensity were converted to the concentrations of superoxide anions and hydroxyl radicals, respectively [30,31].

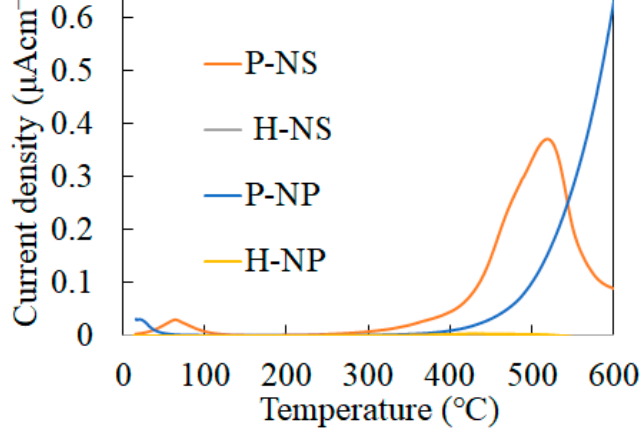
Briefly, a reaction mixture containing riboflavin, methionine, and NBT in potassium phosphate buffer was incubated for 1 h at room temperature. The purple precipitates were dissolved in DMSO and diluted up to the representative concentrations.

Then, 2-hydroxy terephthalic acid (2-HTA) was dissolved in distilled water up to the representative concentrations. The fluorescence intensity of the supernatant was measured using a fluorescence microplate reader (Wallac Arvo MX; Perkin Elmer, Waltham, MA, USA).

As previously reported [10], the absorbance and fluorescence intensity were converted to the concentrations of superoxide anions and hydroxyl radicals and 2-HTA. Briefly, a reaction mixture containing riboflavin, methionine, potassium phosphate buffer was incubated for 1 h at room temperature. The purple precipitates were dissolved in DMSO and diluted up to the representative concentrations.

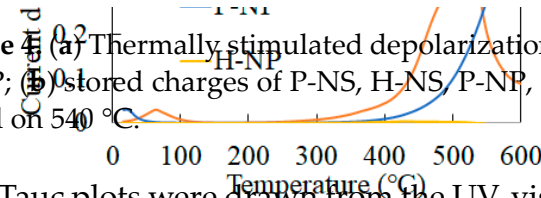
Then, 2-hydroxy terephthalic acid (2-HTA) was dissolved in distilled water up to the representative concentrations. The concentration of the hydroxyl radical can be estimated using the following reaction:

As previously reported [10], the absorbance and fluorescence intensity were converted to the concentrations of superoxide anions and hydroxyl radicals and 2-HTA. Briefly, a reaction mixture containing riboflavin, methionine, potassium phosphate buffer was incubated for 1 h at room temperature. The purple precipitates were dissolved in DMSO and diluted up to the representative concentrations. Then, 2-hydroxy terephthalic acid (2-HTA) was dissolved in distilled water up to the representative concentrations. The concentration of the hydroxyl radical can be estimated using the following reaction:



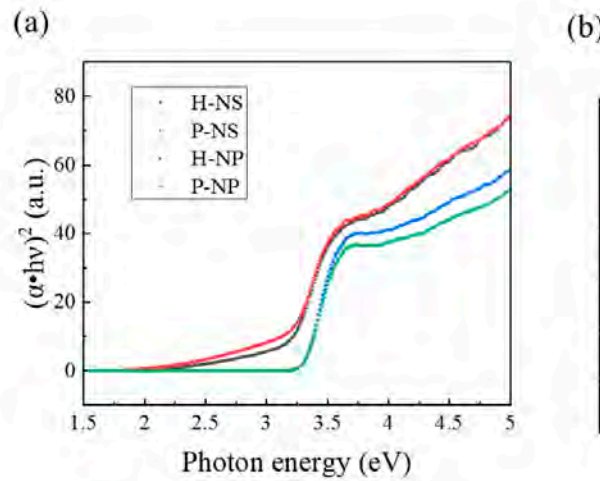
	Stored charges (µCcm ⁻²)
P-NS	315.4
H-NS	3.2
P-NP	106.4
H-NP	0.9

Figure 4. (a) Thermally stimulated depolarization current (TSDC) spectra of P-NS, H-NS, P-NP, and H-NP; (b) stored charges of P-NS, H-NS, P-NP, and H-NP. The spectra were cut off and calculated based on 540 °C.



	Stored charges (µCcm ⁻²)
P-NS	315.4
H-NS	3.2
P-NP	106.4
H-NP	0.9

Figure 5. (a) Tauc plots and (b) optical bandgap energy of heated and polarized TiO₂ NSs (H-NS and P-NS) and NPs (H-NP and P-NP).



	Optical bandgap energy (eV)
P-NS	3.14
H-NS	3.13
P-NP	3.31
H-NP	3.31

Figure 5. (a) Tauc plots and (b) optical bandgap energy of heated and polarized TiO₂ NSs (H-NS and P-NS) and NPs (H-NP and P-NP).

3.3. Effects of Electrical Polarization on Photocatalytic Properties of Titania Nanosheet

Figure 5. (a) Tauc plots and (b) optical bandgap energy of heated and polarized TiO₂ NSs (H-NS and P-NS) and NPs (H-NP and P-NP).

3.3.1. Production of Hydroxyl Radical and Superoxide Anion under UV Irradiation

The generation of superoxide anions and hydroxyl radicals was evaluated using nitro blue tetrazolium and DTA assays. Because the amount of converted formalin and 2-HTA standard curves, as shown in Figure 6, P-NP showed the highest efficiency in generating superoxide and hydroxyl radicals. The polarized titania also generated more ROS than non-polarized titania.

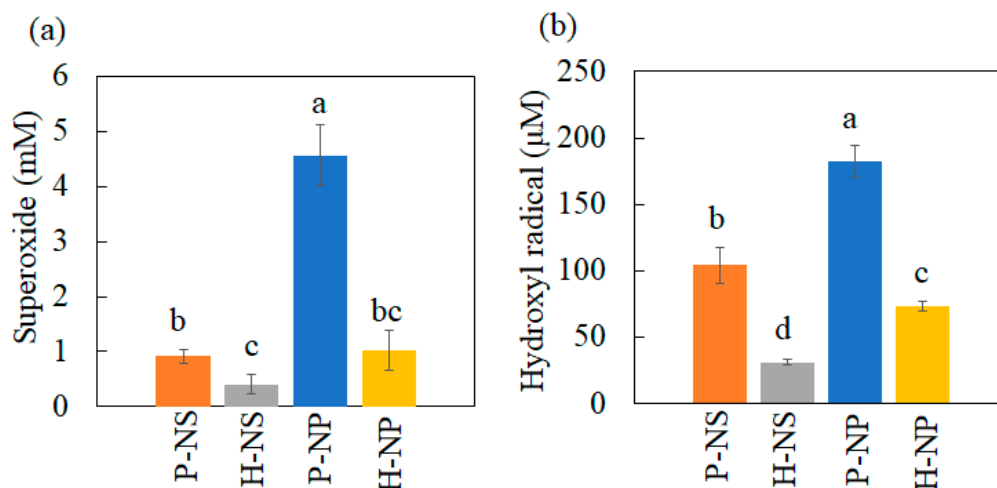


Figure 6. ROS production under UV irradiation. (a) Superoxide anion production and (b) hydroxyl radical production. The different letters show significant differences at $\alpha = 0.05$.

3.3.2. Decolorization Experimental Results

The decolorization of the MB solution with titania without UV irradiation was evaluated at regular intervals. Under UV irradiation, MB decomposed in a time-dependent manner (Figure 7a). P-NS showed the highest dye degradation efficiency after 480 min

evaluated at regular intervals. Under UV irradiation, MB decomposed in a time-dependent manner (Figure 7a). P-NS showed the highest dye degradation efficiency after 480 min (Figure 7a). Electrical polarization enhanced dye degradation in the NS group, but no effect was observed in the NP group. The decolorization of MB without UV irradiation showed no time-dependent changes after 30 min (Figure 7b). However, as significant differences of P-NS, H-NP, and P-NP (Figure 7b). Polarized titania showed the significantly enhanced decolorization compared to non-polarized titania. The calculated rate constant of P-NS was higher than those of H-NS, H-NP, and P-NP (Figure 8). The electrical polarization of the NS significantly enhanced the decolorization compared to non-polarized titania. The calculated rate constant of P-NS was higher than those of H-NS, H-NP, and P-NP (Figure 8). The

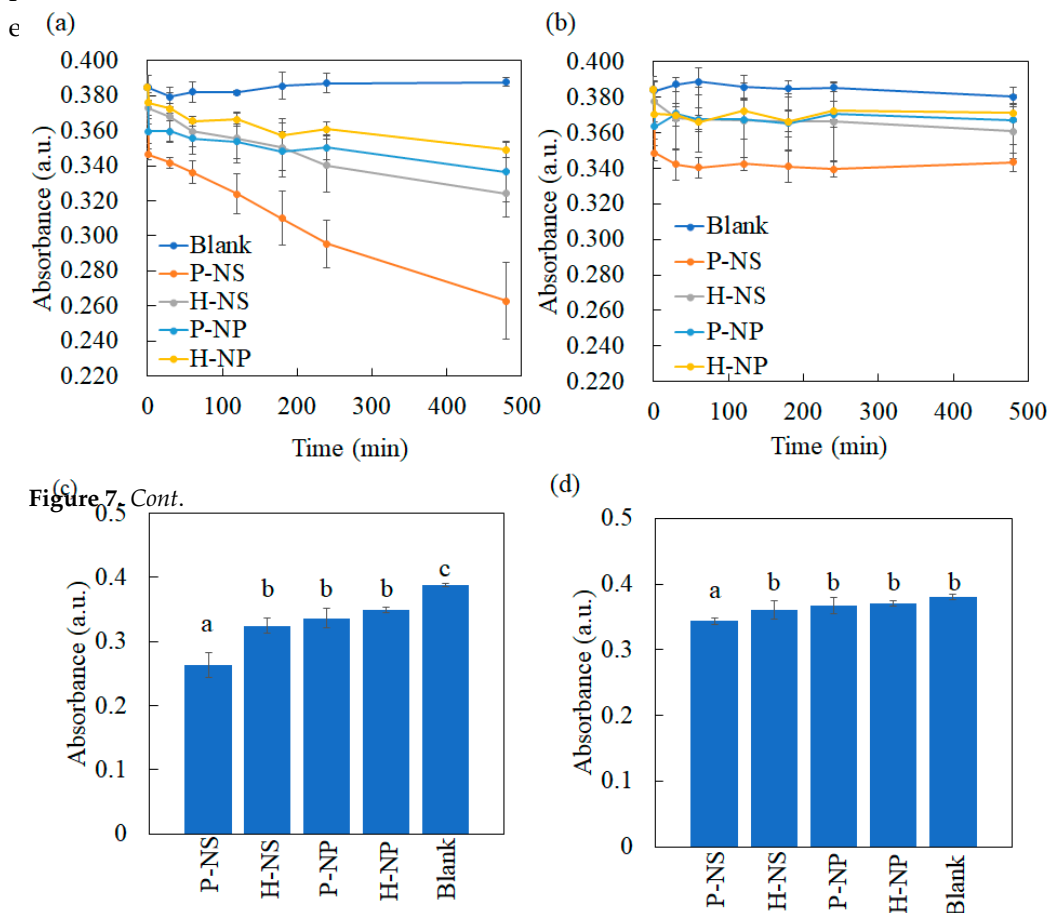


Figure 7. Cont.

Figure 7. Time course plot of the MB decolorization reaction using the prepared titania samples (a) under UV irradiation and (b) in the dark. Multiple comparisons of MB absorbance after 480 min (c)

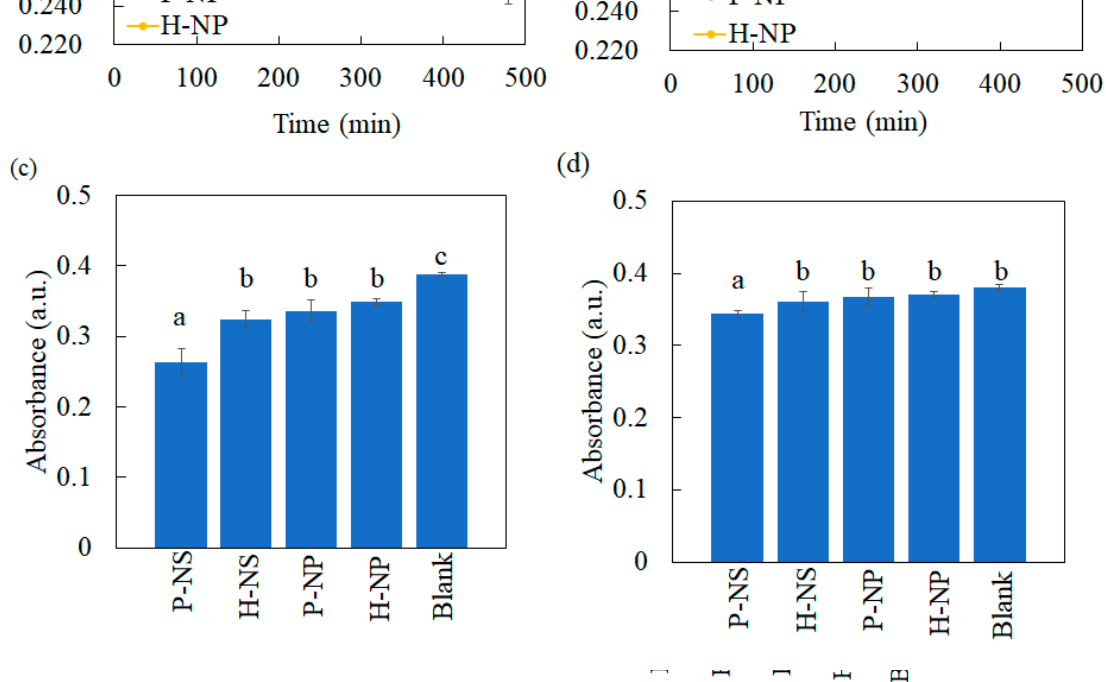


Figure 7. Time course plot of the MB decolorization reaction using the prepared titania samples (a) under UV irradiation and (b) in the dark. Multiple comparisons of MB absorbance after 480 min (c) under UV irradiation and (d) in the dark. Multiple comparisons of MB absorbance after 480 min (c) under UV irradiation and (d) in the dark. The different letters show significant differences at $\alpha = 0.05$.

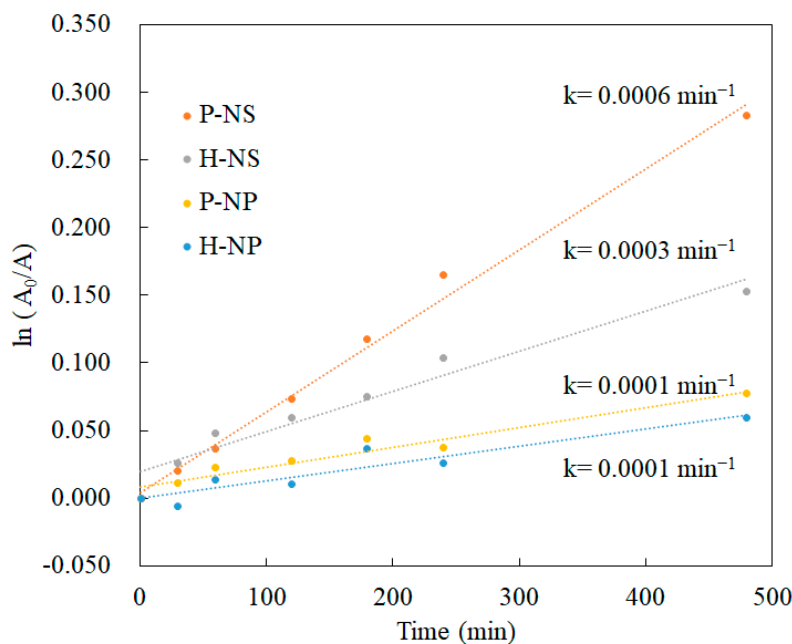


Figure 8. Reaction rate of $\ln(A_0/A)$ of MB under UV irradiation.

4. Discussion

This is the first study to regulate the surface charges of TiO₂ NPs and NSs using the electrical polarization method. We showed enhanced dye-degradation activity of polarized TiO₂ NSs. To modify the degradation performance of TiO₂, the crystal growth was regulated by supplying F ions during the hydrothermal synthesis using ammonium hexafluorotitanate and titanium butoxide as starting materials with a F/Ti ratio of 0.3. Anatase-type TiO₂ NSs as small as 6.3 nm were obtained. The TiO₂ powder was then electrically polarized by a DC electric field at 300 V/mm and 300 °C for 1 h to control the surface charges. The TSDC results showed that polarized TiO₂ NSs were successfully prepared. Accelerated dye degradation was achieved by P-NS, but not by polarized P-NP. However, superoxide anion and hydroxyl radical generation, detected using NBT and DTA assays, was enhanced by both P-NS and P-NP. From these results, the null hypothesis, which states that electrical polarization does not enhance the decolorizing performance of TiO₂, was rejected, as P-NS accelerated MB degradation compared to H-NS.

Titania NSs have been reported to have high photocatalytic activity because of the heterojunctions of the {101}/{001} plane, and they are considered an alternative for titania nanoparticles [32]. We previously synthesized titania NSs with a side length of 6.3 to 445 nm and clarified that the best photocatalytic activity was achieved by titania NSs with a side length of 6.3 nm [28]. In this study, a titania NS with a side length of 6.3 nm was used as a representative substrate for electrical polarization because the single-nanometer-sized titania NS showed the highest dye-degradation performance compared to the other NSs and NPs.

Dipole formation in a crystal structure originates from the orientation of the positive and negative ions. Electrical polarization enables the reorientation of ions at room temperature to be fixed by a constant DC electric field from high to low temperatures without substituting ions. TSDC measurements can evaluate the surface charges as an electric current induced by the relaxation of dipoles through a heating process. The surface charges of TiO₂ NPs and NSs were estimated to be induced by the reorientation of oxygen vacancies and Ti³⁺ because regularly synthesized TiO₂ contains 1% oxygen vacancies [33]. Furthermore, the TiO₂ NSs contained F⁻, not only at the surface, but also in the lattice, substituting for O²⁻ and inducing the reduction of Ti⁴⁺ to Ti³⁺ to compensate for the charges [34]. Hence, P-NS dipoles may be induced by reorienting the oxygen vacancy and F⁻.

In the decolorization experiment, P-NS showed the strongest decolorizing power after 480 min compared with H-NS, P-NP, and H-NP. These results agree with the trend in our previous report showing the better decolorizing capability of NSs compared to that of NPs. Furthermore, electrical polarization accelerated the decolorization of MB by P-NS. The TSDC measurements confirmed that the surface charges of P-NS and P-NP were successfully induced by electrical polarization. Azeez et al. reported that the MB adsorption by TiO₂ NPs was enhanced by the higher surface charges originating from the rich hydroxyl groups [13]. However, this study showed that the adsorption of the MB dye was also enhanced by electrical polarization, inducing surface charges without adding any elements to the surfaces. This study also demonstrated that polarized NSs and NPs induced the production of more superoxide anions and hydroxyl radicals under UV irradiation compared to the non-polarized samples. Although ROS generation can be enhanced by accelerated redox reactions on the surface of TiO₂ by UV irradiation, the optical bandgap energy results indicated that electrical polarization had no influence on the reactivity against UV irradiation. ROS are usually detected by indirect methods using scavengers such as DTA and NBT because of the rapid reactions and decomposition during UV irradiation [2]. This indicates that the polarized TiO₂ accelerated the reaction of DTA and NBT through redox reactions, following the enhanced adsorption of scavengers.

Despite the greater generation of ROS by P-NP and H-NP, the decolorizing effects of P-NS and H-NS were greater than those of P-NP and H-NP. This is because the formation of ROS has been reported to be enhanced by the mixed phase of rutile and anatase [35]. The commercially available NPs used in this study showed a mixed phase of anatase and rutile phases, whereas the NSs showed a single anatase phase. A previous study indicated that the adsorption of MB was enhanced by TiO₂ NSs compared to that by TiO₂ NPs [36], which resulted in accelerated dye degradation by the P-NS.

From the above results, the dye-degradation process by polarized TiO₂ NSs under aqueous conditions was proposed as follows. The adsorption of efficient photons by TiO₂ NSs generated electrons and holes, which resulted in the generation of superoxide anions and hydroxyl radicals. The polarized TiO₂ NSs absorbed more MB dye compared to the polarized TiO₂ NPs, heated TiO₂ NSs, or heated TiO₂ NPs. Oxidation by the generated ROS and direct oxidation by the reaction with holes degraded the MB solution.

5. Conclusions

A facile preparation of TiO₂ NSs using a hydrothermal synthesis with a fluorine/titanium ratio of 0.3 and the modification of surface charges by electrical polarization methods was reported. The synthesized TiO₂ NSs formed a flattened crystal structure with an average side length and thickness of 6.3 nm and 4.9 nm, respectively. TSDC measurements showed a dense surface charge of P-NS and P-NP without changing their morphology or optical properties. The MB degradation assay using P-NS showed an increase in the dye-degradation rate and adsorption efficiency. Furthermore, P-NS and P-NP accelerated the generation of hydroxyl and superoxide anions, respectively. This simple and robust technique can be applied to various ceramic nanocatalysts to manipulate their surface charge and enhance their photocatalytic activity. Considering the enhanced photocatalytic activity of polarized TiO₂ NSs, the band structure of heated and polarized TiO₂ will be further investigated to clarify the mechanisms of enhanced dye degradation.

Author Contributions: Conceptualization, K.N., K.Y. and S.O.; formal analysis, K.N. and T.M.; funding acquisition, K.N., K.Y. and S.O.; investigation, K.N., Y.K. and T.M.; methodology, K.N.; project administration, H.M. and K.N.; resources, S.O.; supervision, K.N., K.Y. and S.O.; validation, K.N., M.J., Y.K. and T.M.; visualization, K.N., T.M., Y.K. and M.J.; writing—original draft, K.N. and T.M.; writing—review and editing, K.Y., K.N., and S.O. All authors have read and agreed to the published version of the manuscript.

Funding: This research was partially funded by the Ministry of Education, Culture, Sports, Science, and Technology of Japan (grant numbers 20K10049, 20K09990, and 23K09269). Part of this research was supported by a Grant-in-Aid for the Cooperative Research Project of Creation of Life Innovation Materials for Interdisciplinary and International Researcher Development from the Ministry of Education, Culture, Sports, Science, and Technology of Japan (MEXT), the Cooperative Research Project of the Research Center for Biomedical Engineering, the Nippon Sheet Glass Foundation for Materials Science and Engineering, and the Iketani Science and Technology Foundation (0311049-A).

Data Availability Statement: Data is contained within the article.

Conflicts of Interest: The authors declare no conflicts of interest.

References

1. Nam, Y.; Lim, J.H.; Ko, K.C.; Lee, J.Y. Photocatalytic activity of TiO₂ nanoparticles: A theoretical aspect. *J. Mater. Chem. A* **2019**, *7*, 13833–13859. [[CrossRef](#)]
2. Nosaka, Y.; Nosaka, A.Y. Generation and detection of reactive oxygen species in photocatalysis. *Chem. Rev.* **2017**, *117*, 11302–11336. [[CrossRef](#)] [[PubMed](#)]
3. Wang, J.; Zhang, Y.Y.; Guo, Y.; Zhang, L.; Xu, R.; Xing, Z.Q.; Wang, S.; Zhang, X. Interaction of bovine serum albumin with acridine orange (CI Basic Orange 14) and its sonodynamic damage under ultrasonic irradiation. *Dye. Pigment.* **2009**, *80*, 271–278. [[CrossRef](#)]
4. Ozawa, K.; Emori, M.; Yamamoto, S.; Yukawa, R.; Yamamoto, S.; Hobara, R.; Fujikawa, K.; Sakama, H.; Matsuda, I. Electron-hole recombination time at TiO₂ single-crystal surfaces: Influence of surface band bending. *J. Phys. Chem. Lett.* **2014**, *5*, 1953–1957. [[CrossRef](#)]
5. Yang, H.G.; Sun, C.H.; Qiao, S.Z.; Zou, J.; Liu, G.; Smith, S.C.; Cheng, H.M.; Lu, G.Q. Anatase TiO₂ single crystals with a large percentage of reactive facets. *Nature* **2008**, *453*, 638–641. [[CrossRef](#)]
6. Liu, X.G.; Dong, G.J.; Li, S.P.; Lu, G.X.; Bi, Y.P. Direct observation of charge separation on anatase TiO₂ crystals with selectively etched {001} facets. *J. Am. Chem. Soc.* **2016**, *138*, 2917–2920. [[CrossRef](#)] [[PubMed](#)]
7. Zhang, C.; Zhou, Y.M.; Bao, J.H.; Fang, J.S.; Zhao, S.; Zhang, Y.W.; Sheng, X.; Chen, W. Structure regulation of ZnS@g-C₃N₄/TiO₂ nanospheres for efficient photocatalytic H₂ production under visible-light irradiation. *Chem. Eng. J.* **2018**, *346*, 226–237. [[CrossRef](#)]
8. Basavarajappa, P.S.; Patil, S.B.; Ganganagappa, N.; Reddy, K.R.; Raghu, A.V.; Reddy, C.V. Recent progress in metal-doped TiO₂, non-metal doped/codoped TiO₂ and TiO₂ nanostructured hybrids for enhanced photocatalysis. *Int. J. Hydrog. Energy* **2020**, *45*, 7764–7778. [[CrossRef](#)]
9. Zhu, X.; Xu, H.; Liu, J.; Bi, C.; Tian, J.; Zong, K.; Wang, B.; Ding, P.; Wang, X.; Chu, P.K.; et al. Stacking Engineering of Heterojunctions in Half-Metallic Carbon Nitride for Efficient CO₂ Photoreduction. *Adv. Sci.* **2023**, *10*, 2307192. [[CrossRef](#)]
10. Tan, Z.Q.; Sato, K.; Takami, S.; Numako, C.; Umetsu, M.; Soga, K.; Nakayama, M.; Sasaki, R.; Tanaka, T.; Ogino, C.; et al. Particle size for photocatalytic activity of anatase TiO₂ nanosheets with highly exposed {001} facets. *RSC Adv.* **2013**, *3*, 19268–19271. [[CrossRef](#)]

11. Hayashi, K.; Nozaki, K.; Tan, Z.Q.; Fujita, K.; Nemoto, R.; Yamashita, K.; Miura, H.; Itaka, K.; Ohara, S. Enhanced antibacterial property of facet-engineered TiO₂ nanosheet in presence and absence of ultraviolet irradiation. *Materials* **2020**, *13*, 78. [[CrossRef](#)]
12. Tachikawa, T.; Yamashita, S.; Majima, T. Evidence for crystal-face-dependent TiO₂ photocatalysis from single-molecule imaging and kinetic analysis. *J. Am. Chem. Soc.* **2011**, *133*, 7197–7204. [[CrossRef](#)] [[PubMed](#)]
13. Azeez, F.; Al-Hetlani, E.; Arafa, M.; Abdelmonem, Y.; Nazeer, A.A.; Amin, M.O.; Madkour, M. The effect of surface charge on photocatalytic degradation of methylene blue dye using chargeable titania nanoparticles. *Sci. Rep.* **2018**, *8*, 7104. [[CrossRef](#)]
14. Yagub, M.T.; Sen, T.K.; Afroze, S.; Ang, H.M. Dye and its removal from aqueous solution by adsorption: A review. *Adv. Colloid Interface Sci.* **2014**, *209*, 172–184. [[CrossRef](#)] [[PubMed](#)]
15. Zhang, R.Z.; Quan, S.; Xia, M.; Wang, Q.; Zhang, W.; Yang, J.M. Effect of surface charge status of amorphous porous coordination polymer particles on the adsorption of organic dyes from an aqueous solution. *J. Colloid Interface Sci.* **2018**, *525*, 54–61. [[CrossRef](#)] [[PubMed](#)]
16. Das, A.; Pamu, D. A comprehensive review on electrical properties of hydroxyapatite based ceramic composites. *Mater. Sci. Eng. C Mater. Biol. Appl.* **2019**, *101*, 539–563. [[CrossRef](#)]
17. Saxena, A.; Kakimoto, K.; Dubey, A.K. Polarization induced dielectric and electrical response of electrovector hydroxyapatite and ferroelectric sodium potassium niobate ceramics. *J. Phys. D* **2020**, *53*, 395402. [[CrossRef](#)]
18. Sans, J.; Arnau, M.; Fontana-Escartín, A.; Turon, P.; Alemán, C. Permanently polarized materials: An approach for designing materials with customized electrical properties. *Chem. Mater.* **2023**, *35*, 3765–3780. [[CrossRef](#)]
19. Yamashita, K.; Oikawa, N.; Umegaki, T. Acceleration and deceleration of bone-like crystal growth on ceramic hydroxyapatite by electric poling. *Chem. Mater.* **1996**, *8*, 2697–2700. [[CrossRef](#)]
20. Ubele-Kalnina, D.; Nakamura, M.; Gross, K.A. Inter-Laboratory Study on Measuring the Surface Charge of Electrically Polarized Hydroxyapatite. *J. Funct. Biomater.* **2023**, *14*, 100. [[CrossRef](#)]
21. Belik, A.A.; Morozov, V.A.; Deyneko, D.V.; Savon, A.E.; Baryshnikova, O.V.; Zhukovskaya, E.S.; Dorbakov, N.G.; Katsuya, Y.; Tanaka, M.; Stefanovich, S.Y.; et al. Antiferroelectric properties and site occupations of R³⁺ cations in Ca₈MgR(PO₄)₇ luminescent host materials. *J. Alloys Compd.* **2017**, *699*, 928–937. [[CrossRef](#)]
22. Metwally, S.; Stachewicz, U. Surface potential and charges impact on cell responses on biomaterials interfaces for medical applications. *Mat. Sci. Eng. C-Mat.* **2019**, *104*, 109883. [[CrossRef](#)] [[PubMed](#)]
23. Verma, A.S.; Singh, A.; Kumar, D.; Dubey, A.K. Electro-mechanical and Polarization-Induced Antibacterial Response of 45S5 Bioglass-Sodium Potassium Niobate Piezoelectric Ceramic Composites. *ACS Biomater. Sci. Eng.* **2020**, *6*, 3055–3069. [[CrossRef](#)] [[PubMed](#)]
24. Li, Y.; Li, J.; Yang, W.; Wang, X. Implementation of ferroelectric materials in photocatalytic and photoelectrochemical water splitting. *Nanoscale Horiz.* **2020**, *5*, 1174–1187. [[CrossRef](#)]
25. Nagai, A.; Yamazaki, Y.; Ma, C.F.; Nozaki, K.; Toyama, T.; Yamashita, K. Response of osteoblast-like MG63 cells to TiO₂ layer prepared by micro-arc oxidation and electric polarization. *J. Eur. Ceram. Soc.* **2012**, *32*, 2647–2652. [[CrossRef](#)]
26. Ma, C.F.; Xiong, X.B.; Li, H.J.; Huang, J.F.; Lu, J.H.; Hu, Z.B. Response of osteoblast to CVIC/C and HA coating on CVIC/C in vitro. *Rare Met. Mater. Eng.* **2004**, *33*, 1274–1277.
27. Bandyopadhyay, A.; Shivaram, A.; Mitra, I.; Bose, S. Electrically polarized TiO₂ nanotubes on Ti implants to enhance early-stage osseointegration. *Acta Biomater.* **2019**, *96*, 686–693. [[CrossRef](#)]
28. Kowaka, Y.; Nozaki, K.; Mihara, T.; Yamashita, K.; Miura, H.; Tan, Z.; Ohara, S. Development of TiO₂ nanosheets with high dye degradation performance by regulating crystal growth. *Materials* **2023**, *16*, 1229. [[CrossRef](#)]
29. Sahni, M.; Locke, B.R. Quantification of hydroxyl radicals produced in aqueous phase pulsed electrical discharge reactors. *Ind. Eng. Chem. Res.* **2006**, *45*, 5819–5825. [[CrossRef](#)]
30. Ishibashi, K.; Fujishima, A.; Watanabe, T.; Hashimoto, K. Quantum yields of active oxidative species formed on TiO₂ photocatalyst. *J. Photochem. Photobiol. A* **2000**, *134*, 139–142. [[CrossRef](#)]
31. Bournonville, C.F.; Díaz-Ricci, J.C. Quantitative determination of superoxide in plant leaves using a modified NBT staining method. *Phytochem. Anal.* **2011**, *22*, 268–271. [[CrossRef](#)] [[PubMed](#)]
32. Masudy, P.S.; Tanhaei, M.; Farahani, H.D.A.M.; Jianguyong, H. A review on the synthesis of the various types of anatase TiO₂ facets and their applications for photocatalysis. *Katal R. Chem. Eng. J.* **2020**, *384*, 123384.
33. Bi, X.; Du, G.; Kalam, A.; Sun, D.; Yu, Y.; Su, Q.; Xu, B.; Al-Sehemi, A.G. Tuning oxygen vacancy content in TiO₂ nanoparticles to enhance the photocatalytic performance. *Chem. Eng. Sci.* **2021**, *234*, 116440. [[CrossRef](#)]
34. Fu, R.; Wu, Z.; Pan, Z.; Gao, Z.; Li, Z.; Kong, X.; Li, L. Fluorine-Induced Surface Metallization for ammonia Synthesis under Photoexcitation up to 1550 nm. *Angew. Chem. Int. Ed. Engl.* **2021**, *60*, 11173–11179. [[CrossRef](#)]
35. Nosaka, Y.; Nosaka, A. Understanding hydroxyl radical (•OH) generation processes in photocatalysis. *ACS Energy Lett.* **2016**, *1*, 356–359. [[CrossRef](#)]
36. Nakamura, S.; Takeda, H.; Yamashita, K. Proton transport polarization and depolarization of hydroxyapatite ceramics. *J. Appl. Phys.* **2001**, *89*, 5386–5392. [[CrossRef](#)]

Disclaimer/Publisher’s Note: The statements, opinions and data contained in all publications are solely those of the individual author(s) and contributor(s) and not of MDPI and/or the editor(s). MDPI and/or the editor(s) disclaim responsibility for any injury to people or property resulting from any ideas, methods, instructions or products referred to in the content.

日中笹川医学奨学金制度<学位取得コース>評価書

課程博士：指導教官用



第 44 期

研究者番号：G4405

作成日：2024年3月10日

氏名	陳曹傑	CHEN CAOJIE	性別	M	生年月日	1984/01/23
所属機関（役職）	慶應義塾大学医学部（大学院生）					
研究先（指導教官）	慶應義塾大学医学部形成外科学教室（貴志 和生 教授）					
研究テーマ	創傷治癒とオートファジーの関係 The relationship between autophagy and wound healing					
専攻種別	<input type="checkbox"/> 論文博士			<input checked="" type="checkbox"/> 課程博士		

研究者評価（指導教官記入欄）

成績状況	良 学業成績係数=	取得単位数
		100%
学生本人が行った研究の概要	オートファジーと創傷治癒、YAP,En-1,mTOR の関係について、in vitro 並びに in vivo のマウスを用いた動物実験を行い、それぞれの関係性について調べた。	
総合評価	【良かった点】 一生懸命研究を行い、解らないところのトラブルシューティングができていた。	
	【改善すべき点】 試問での質疑、応答能力。	
	【今後の展望】 中国に帰り、本研究成果を生かした医師の仕事を行う。	
学位取得見込	あり	
評価者（指導教官名） 貴志和生		

日中笹川医学奨学金制度<学位取得コース>報告書 研究者用



第44期

研究者番号: G4405

作成日: 2024年3月10日

氏名	陈 曹杰	CHEN CAOJIE	性別	M	生年月日 1984/01/23
所属機関(役職)	慶應義塾大学医学部(大学院生)				
研究先(指導教官)	慶應義塾大学医学部形成外科学教室(貴志 和生 教授)				
研究テーマ	創傷治癒とオートファジーの関係 The relationship between autophagy and wound healing				
専攻種別	論文博士	<input type="checkbox"/>	課程博士	<input checked="" type="checkbox"/>	

1. 研究概要(1)

1) 目的(Goal)

Wound repair dysfunction is becoming a major public health issue worldwide. Yes-associated protein (YAP) has previously been reported to be closely related to wound healing, while how YAP accelerates wound healing via regulating autophagy needs to be further probed.

2) 戦略(Approach)

A series of comparative experiments were conducted on skin trauma models to investigate the mechanisms of autophagy and other roles in the trauma healing process.

3) 材料と方法(Materials and methods)

ICR male mice were involved in two independent animal experiments; the mice were randomly allocated into control, autophagy inhibitor (3-MA) (injection), and 3-MA (drip) group or control, si-NC, si-YAP group (8 mice for each). Full-thickness excisional wounds (8 mm) in mice were created by punch to construct an in vivo wound model to observe the effects of autophagy inhibitor (3-MA) (by injection and drip) and si-YAP by electrotransfection.

4) 実験結果(Results)

Firstly, we found that the autophagy inhibitor (3-MA) accelerated wound closure in vivo. Loss-of-function experiments subsequently revealed that YAP knockdown led to increased proliferation and migration of fibroblasts as well as reduced autophagy, resulting in accelerated wound healing. In addition, our results revealed that YAP could positively regulate Engrailed-1 (En1) expression in fibroblasts. En1 knockdown also promoted the proliferation and migration of fibroblasts, meanwhile resulting in increased mammalian target of rapamycin (mTOR) levels and reduced autophagy in fibroblasts.

5) 考察(Discussion)

YAP knockdown repressed autophagy in fibroblasts to accelerate wound closure by regulating the En1/mTOR axis.

6) 参考文献(References)

1. Singer AJ, Clark RA. Cutaneous wound healing. *N Engl J Med* 1999; 341: 738-46.
2. Eming SA, Martin P, Tomic-Canic M. Wound repair and regeneration: mechanisms, signaling, and translation. *Sci Transl Med* 2014; 6: 265sr6.
3. Reed BR, Clark RA. Cutaneous tissue repair: practical implications of current knowledge. II. *J Am Acad Dermatol* 1985; 13: 919-41.
4. Brem H, Tomic-Canic M. Cellular and molecular basis of wound healing in diabetes. *J Clin Invest* 2007; 117: 1219-22.
5. Klionsky DJ. Autophagy: from phenomenology to molecular understanding in less than a decade. *Nat Rev Mol Cell Biol* 2007; 8: 931-7.
6. Ren H, Zhao F, Zhang Q, Huang X, Wang Z. Autophagy and skin wound healing. *Burns Trauma* 2022; 10: tkac003.
7. Qiang L, Yang S, Cui YH, He YY. Keratinocyte autophagy enables the activation of keratinocytes and fibroblasts and facilitates wound healing. *Autophagy* 2021; 17: 2128-43.
8. Mijaljica D, Spada F, Klionsky DJ, Harrison IP. Autophagy is the key to making chronic wounds acute in skin wound healing. *Autophagy* 2023: 1-7.
9. Dey A, Varelas X, Guan KL. Targeting the Hippo pathway in cancer, fibrosis, wound healing and regenerative medicine. *Nat Rev Drug Discov* 2020; 19: 480-94.
10. Wei F, Wang A, Wang Q, Han W, Rong R, Wang L. Plasma endothelial cells-derived extracellular vesicles promote wound healing in diabetes through YAP and the PI3K/Akt/mTOR pathway. *Aging (Albany NY)* 2020; 12: 12002-18.
11. Mascharak S, desJardins-Park HE, Davitt MF, Griffin M, Borrelli MR, Moore AL, Chen K, Duoto B, Chinta M, Foster DS, Shen AH, Januszyk M, Kwon SH, Wernig G, Wan DC, Lorenz HP, Gurtner GC, Longaker MT. Preventing Engrailed-1 activation in fibroblasts yields wound regeneration without scarring. *Science* 2021; 372: eaba2374.

1. 研究概要(2)

12. Györfi AH, Matei AE, Fuchs M, Liang C, Rigau AR, Hong X, Zhu H, Lubner M, Bergmann C, Dees C, Ludolph I, Horch RE, Distler O, Wang J, Bengsch B, Schett G, Kunz M, Distler JHW. Engrailed 1 coordinates cytoskeletal reorganization to induce myofibroblast differentiation. *J Exp Med* 2021; 218: e20201916.
13. Gao Y, Luo C, Rui T, Fan Y, Yao Y, Shen H, Gao C, Wang T, Wang H, Chen X, Zhang J, Li D, Xia C, Li LL, Wang Z, Zhang M, Chen X, Tao L. Autophagy inhibition facilitates wound closure partially dependent on the YAP/IL-33 signaling in a mouse model of skin wound healing. *FASEB J* 2021; 35: e21920.
14. Huo JF, Chen XB. Long noncoding RNA growth arrest-specific 5 facilitates glioma cell sensitivity to cisplatin by suppressing excessive autophagy in an mTOR-dependent manner. *J Cell Biochem* 2019; 120: 6127-36.
15. Qiang L, Sample A, Liu H, Wu X, He YY. Epidermal SIRT1 regulates inflammation, cell migration, and wound healing. *Sci Rep* 2017; 7: 14110.
16. Spiekstra SW, Breetveld M, Rustemeyer T, Scheper RJ, Gibbs S. Wound-healing factors secreted by epidermal keratinocytes and dermal fibroblasts in skin substitutes. *Wound Repair Regen* 2007; 15: 708-17.
17. van Zanten MC, Mistry RM, Suami H, Campbell-Lloyd A, Finkemeyer JP, Piller NB, et al. The Lymphatic Response to Injury with Soft-Tissue Reconstruction in High-Energy Open Tibial Fractures of the Lower Extremity. *Plast Reconstr Surg* 2017; 139: 483-91.
18. Ban E, Jeong S, Park M, Kwon H, Park J, Song EJ, Kim A. Accelerated wound healing in diabetic mice by miRNA-497 and its anti-inflammatory activity. *Biomed Pharmacother* 2020; 121: 109613.
19. Wang F, Zhang C, Dai L, Zhang Y, Wang Y, Hao Y, Ji S, Xu Z, Han N, Chen H, Zhang Q, Nan W. Bafilomycin A1 Accelerates Chronic Refractory Wound Healing in db/db Mice. *Biomed Res Int* 2020; 2020: 6265701.
20. Lawrence J, Nho R. The Role of the Mammalian Target of Rapamycin (mTOR) in Pulmonary Fibrosis. *Int J Mol Sci* 2018; 19: 778.
21. Guo Y, Lin C, Xu P, Wu S, Fu X, Xia W, Yao M. AGEs Induced Autophagy Impairs Cutaneous Wound Healing via Stimulating Macrophage Polarization to M1 in Diabetes. *Sci Rep* 2016; 6: 36416.
22. Shi W, Wu Y, Bian D. p75NTR silencing inhibits proliferation, migration, and extracellular matrix deposition of hypertrophic scar fibroblasts by activating autophagy through inhibiting the PI3K/Akt/mTOR pathway. *Can J Physiol Pharmacol* 2021; 99: 349-59.
23. Schlegelmilch K, Mohseni M, Kirak O, Pruszek J, Rodriguez JR, Zhou D, Kreger BT, Vasioukhin V, Avruch J, Brummelkamp TR, Camargo FD. Yap1 acts downstream of α -catenin to control epidermal proliferation. *Cell* 2011; 144: 782-95.
24. Silvis MR, Kreger BT, Lien WH, Klezovitch O, Rudakova GM, Camargo FD, Lantz DM, Seykora JT, Vasioukhin V. α -catenin is a tumor suppressor that controls cell accumulation by regulating the localization and activity of the transcriptional coactivator Yap1. *Sci Signal* 2011; 4: ra33.
25. Jiang D, Correa-Gallegos D, Christ S, Stefanska A, Liu J, Ramesh P, Rajendran V, De Santis MM, Wagner DE, Rinkevich Y. Two succeeding fibroblastic lineages drive dermal development and the transition from regeneration to scarring. *Nat Cell Biol* 2018; 20: 422-431.
26. Kim YC, Guan KL. mTOR: a pharmacologic target for autophagy regulation. *J Clin Invest* 2015; 125: 25-32.

2. 執筆論文 Publication of thesis ※記載した論文を添付してください。Attach all of the papers listed below.

論文名 1 Title	YAP knockdown repressed autophagy in fibroblasts to accelerate wound healing through regulating En1/mTOR axis					
掲載誌名 Published journal	European Review for Medical and phamacological Sciences					
	2024 年 2 月	28 巻(号)	949 頁 ~	958 頁	言語 Language	English
第1著者名 First author	Chen Caojie	第2著者名 Second author	Kishi Kazuo		第3著者名 Third author	
その他著者名 Other authors						
論文名 2 Title	Single-Cell RNA-seq Analysis Reveals Cellular Functional Heterogeneity in Dermis Between Fibrotic and Regenerative Wound Healing Fates					
掲載誌名 Published journal	Frontiers in Immunology					
	2022 年 5 月	875407 巻(号)	頁 ~	頁	言語 Language	English
第1著者名 First author	Chen Caojie	第2著者名 Second author	Hiroki Kajita		第3著者名 Third author	Kento Takaya
その他著者名 Other authors	Noriko Aramaki-Hattori , Shigeki Sakai , Toru Asou , Kazuo Kishi					
論文名 3 Title						
掲載誌名 Published journal						
	年 月	巻(号)	頁 ~	頁	言語 Language	English
第1著者名 First author		第2著者名 Second author			第3著者名 Third author	
その他著者名 Other authors						
論文名 4 Title						
掲載誌名 Published journal						
	年 月	巻(号)	頁 ~	頁	言語 Language	
第1著者名 First author		第2著者名 Second author			第3著者名 Third author	
その他著者名 Other authors						
論文名 5 Title						
掲載誌名 Published journal						
	年 月	巻(号)	頁 ~	頁	言語 Language	
第1著者名 First author		第2著者名 Second author			第3著者名 Third author	
その他著者名 Other authors						

3. 学会発表 Conference presentation ※筆頭演者として総会・国際学会を含む主な学会で発表したものを記載してください

※Describe your presentation as the principal presenter in major academic meetings including general meetings or international meetin

学会名 Conference					
演題 Topic	オートファジーと創傷治癒の関係				
開催日 date	年	月	日	開催地 venue	Tokyo
形式 method	<input type="checkbox"/> 口頭発表 Oral	<input type="checkbox"/> ポスター発表 Poster	言語 Language	<input type="checkbox"/> 日本語	<input type="checkbox"/> 英語 <input type="checkbox"/> 中国語
共同演者名 Co-presenter					
学会名 Conference					
演題 Topic					
開催日 date	年	月	日	開催地 venue	Tokyo
形式 method	<input type="checkbox"/> 口頭発表 Oral	<input type="checkbox"/> ポスター発表 Poster	言語 Language	<input type="checkbox"/> 日本語 <input checked="" type="checkbox"/> 英語	<input type="checkbox"/> 中国語
共同演者名 Co-presenter					
学会名 Conference					
演題 Topic					
開催日 date	年	月	日	開催地 venue	
形式 method	<input type="checkbox"/> 口頭発表 Oral	<input type="checkbox"/> ポスター発表 Poster	言語 Language	<input type="checkbox"/> 日本語 <input type="checkbox"/> 英語	<input type="checkbox"/> 中国語
共同演者名 Co-presenter					
学会名 Conference					
演題 Topic					
開催日 date	年	月	日	開催地 venue	
形式 method	<input type="checkbox"/> 口頭発表 Oral	<input type="checkbox"/> ポスター発表 Poster	言語 Language	<input type="checkbox"/> 日本語 <input type="checkbox"/> 英語	<input type="checkbox"/> 中国語
共同演者名 Co-presenter					

4. 受賞(研究業績) Award (Research achievement)

名称 Award name	国名 Country		受賞年 Year of award	年	月
	国名 Country		受賞年 Year of award	年	月

5. 本研究テーマに関わる他の研究助成金受給 Other research grants concerned with your research theme

受給実績 Receipt record	<input type="checkbox"/> 有 <input type="checkbox"/> 無
助成機関名称 Funding agency	
助成金名称 Grant name	
受給期間 Supported period	年 月 ~ 年 月
受給額 Amount received	円
受給実績 Receipt record	<input type="checkbox"/> 有 <input type="checkbox"/> 無
助成機関名称 Funding agency	
助成金名称 Grant name	
受給期間 Supported period	年 月 ~ 年 月
受給額 Amount received	円

6. 他の奨学金受給 Another awarded scholarship

受給実績 Receipt record	<input type="checkbox"/> 有 <input type="checkbox"/> 無
助成機関名称 Funding agency	
奨学金名称 Scholarship name	
受給期間 Supported period	年 月 ~ 年 月
受給額 Amount received	円

7. 研究活動に関する報道発表 Press release concerned with your research activities

※記載した記事を添付してください。Attach a copy of the article described below

報道発表 Press release	<input type="checkbox"/> 有 <input type="checkbox"/> 無	発表年月日 Date of release	
発表機関 Released medium			
発表形式 Release method	・新聞 ・雑誌 ・Web site ・記者発表 ・その他()		
発表タイトル Released title			

8. 本研究テーマに関する特許出願予定 Patent application concerned with your research theme

出願予定 Scheduled	<input type="checkbox"/> 有 <input type="checkbox"/> 無	出願国 Application	
出願内容(概要) Application contents			

9. その他 Others

--

指導責任者(記名) 貴志 和生

YAP knockdown repressed autophagy in fibroblasts to accelerate wound healing through regulating En1/mTOR axis

C.-J. CHEN, K. KISHI

Department of Plastic and Reconstructive Surgery, Keio University School of Medicine, Tokyo, Japan

Abstract. – OBJECTIVE: Wound repair dysfunction is becoming a major public health issue worldwide. Yes-associated protein (YAP) has previously been reported to be closely related to wound healing, while how YAP accelerates wound healing *via* regulating autophagy needs to be further probed.

MATERIALS AND METHODS: ICR male mice were involved in two independent animal experiments; the mice were randomly allocated into control, autophagy inhibitor (3-MA) (injection), and 3-MA (drip) group or control, si-NC, si-YAP group (8 mice for each). Full-thickness excisional wounds (8 mm) in mice were created by punch to construct an *in vivo* wound model to observe the effects of autophagy inhibitor (3-MA) (by injection and drip) and si-YAP by electrotransfection.

RESULTS: Firstly, we found that the autophagy inhibitor (3-MA) accelerated wound closure *in vivo*. Loss-of-function experiments subsequently revealed that YAP knockdown led to increased proliferation and migration of fibroblasts as well as reduced autophagy, resulting in accelerated wound healing. In addition, our results revealed that YAP could positively regulate Engrailed-1 (En1) expression in fibroblasts. En1 knockdown also promoted the proliferation and migration of fibroblasts, meanwhile resulting in increased mammalian target of rapamycin (mTOR) levels and reduced autophagy in fibroblasts.

CONCLUSIONS: YAP knockdown repressed autophagy in fibroblasts to accelerate wound closure by regulating the En1/mTOR axis.

Key Words:

Wound healing, Autophagy, YAP, Engrailed-1, mTOR.

Abbreviations

Yes-associated protein (YAP); Engrailed-1 (En1); Mammalian target of rapamycin (mTOR); 3-(4, 5-Dimethylthiazolyl)-2, 5-diphenyltetrazolium bromide (MTT); Immunohistochemistry (IHC); Quantitative real-time

polymerase chain reaction (RT-qPCR); Standard deviation, (SD); Analysis of variance (ANOVA); Dulbecco's Modified Eagle Medium (DMEM).

Introduction

Mammalian skin wound healing refers to an evolutionarily conserved process that includes three separated but overlapping stages: hemostasis/inflammatory, proliferative, and remodeling stages to rebuild the skin's barrier function¹. Various cells in the skin, including keratinocytes and fibroblasts, work together to respond rapidly after acute skin injury to restore damaged skin function². Currently, many people, including the elderly, diabetic patients, and patients undergoing chemotherapy or radiotherapy, suffer from wound repair dysfunction, which imposes a huge burden on their lives and health^{3,4}. Therefore, it is urgent and necessary to explore the pathogenesis of wound healing dysfunction. Autophagy, a cellular self-decomposing process for degrading and recycling excess components⁵, is involved in the regulation of wound healing^{6,7}. Autophagy is finely modulated in different stages of wound healing at a precise extent of activity to meet the stage-specific requirements. However, the role of autophagic activity in facilitating wound healing is still controversial. Autophagy, under appropriate conditions, operates as a modulator to monitor and promote timely and proper healing processes. However, any alterations in regulating autophagy can lead to improper activity, resulting in imperfect wound healing, such as persistent chronic wounds and hypertrophic scarring⁸. Importantly, inhibition of autophagy was reported in the literature to facilitate wound healing, of which the underlying mechanism remains largely unknown.

Yes-associated protein (YAP), a transcriptional co-activator of Hippo signaling, functions in tissue regeneration, wound healing and immune regulation⁹. Much evidence^{9,10} has emphasized its function in epidermal development and skin wound repair. As proof, Mascharak et al¹¹ revealed that YAP knockdown could promote fibroblast-induced wound regeneration by repressing engrailed-1 (En1) activation. En1 is a neural-specific transcription factor that functions in regulating the development of many tissues and organs¹². However, the specific mechanism of the YAP/En1 axis in regulating wound healing needs to be revealed. Notably, YAP inhibition was reported¹³ to repress autophagy and accelerate skin wound closure, and the downstream target of En1, the mammalian target of rapamycin (mTOR), is also the core regulator of autophagy^{12,14}. All this evidence suggests that the YAP/En1/mTOR axis is a risk factor affecting wound healing, while its role in regulating autophagy during wound healing is largely unknown.

Based on the above evidence, we speculated that YAP knockdown repressed autophagy in wound healing by regulating the En1/mTOR axis, thereby ameliorating wound healing dysfunction. Our research provided potential therapeutic targets for wound healing dysfunction.

Materials and Methods

Construction of In Vivo Wound Model

The study was carried out between 2021.12 and 2023.8. The ICR male mice (8-10 weeks of age, Sankyo, Tokyo, Japan) were purchased and fed in separate cages. A full-thickness excisional wound (8 mm) in mice was created as previously reported¹⁵. Two independent animal experiments were conducted, and the mice were randomly allocated into the control, 3-MA (injection), and 3-MA (drip) group or control, si-NC, and si-YAP group (8 mice for each). Mice in 3-MA (injection) group, 3-MA (drip) group, and control group were intraperitoneally injected with 3-MA (10 mg/kg, AdipoGen, San Diego, CA, USA), drip 3-MA (10 mM) and drip Phosphate-buffered saline (PBS), respectively, every day after skin injury. For si-YAP experiment, 10 μ L PBS, 10 μ L si-NC and si-YAP (Horizon Discovery, London, UK) with a concentration of 5 mM were mixed with 40 μ L green fluorescent protein (GFP) reporter plasmid with a concentration of 500 mg/L, and then the mixture

was dripped onto the wound edges of mice for electrotransfection by NEPA21 electroporator (NEPA GENE Co. Ltd. Chiba, Japan) using electrodes for *in vivo* experiments. The number of GFP-positive cells on the wound edges was observed and calculated one day after electrotransfection to confirm successful transfection. Wound images were acquired after wounding on days 0, 4, 7, 10 and 14. The wound healing rate was calculated as the percentage of the original wound size using the following formula: (initial area – final area)/initial area \times 100%. On day 10 after the wound injury in the 3-MA experiment, three wound samples were randomly selected from the wounds of three mice in each group. Half of the samples were subjected to western blot experiments, and the other half to immunostaining experiments. On day 10 after the wound injury in the si-YAP experiment, three wound samples were randomly selected from three mice in each group. Half of the samples were subjected to immunostaining experiments, 1/4 of the samples were subjected to RT-qPCR experiments, and the rest 1/4 were subjected to western blot experiments. These mice were sacrificed by cervical dislocation after anesthesia. Then, wound samples were collected from these mice. Our study was approved by the Animal Ethics Committee of Keio University School of Medicine [A2022-128].

Immunohistochemistry (IHC)

The sections (4 μ m in thickness) were prepared. After deparaffinization and antigen retrieval, sections were then blocked and incubated with antibodies against LC3A/B (CST, Danvers, MA, USA, 1:100, 12741), YAP (CST, Danvers, MA, USA, 1:100, 14074) and En1 (Bioss, Woburn, MA, USA, 1:100, bs-11744R-HRP) overnight. The staining of LC3 and YAP was followed by the incubation with the secondary antibody biotinylated goat anti-rabbit (Vector Laboratories, Newark, NJ, USA, 1:500, BA1000) for 1 h. A secondary antibody was not used for staining En1. We used the ABC kit (Vector Laboratories, Newark, NJ, USA) for staining except for En1. The sections were stained with DAB and then counterstained with hematoxylin, dehydrated, and mounted. The images were taken using a microscope. Then, we calculated the proportion of positive cells in the dermis of skin tissue (excluding the epidermis) in the 3 separate fields of view using ImageJ software.

Quantitative Real-Time Polymerase Chain Reaction (RT-qPCR)

Total RNA was extracted with Isogen (Nippongene, Tokyo, Japan). The cDNA was synthesized using the cDNA Synthesis System (BioRad, Hercules, CA, USA). Then, SYBR Qpcr Mix (Toyobo, Tokyo, Japan) was employed for the RT-qPCR assay. *GAPDH* was used as the reference gene for mRNA.

The data was analyzed with $2^{-\Delta\Delta CT}$ method. The primers used in the study were listed as follows (5'-3'):

YAP (F): ACCCTCGTTTTGCCATGAAC
YAP (R): TGTGCTGGGATTGATATTCCGTA
En1 (F): GCACACGTTATTCGGATCG
En1 (R): GCTTGTCTCCTTCTCGTTCT
GAPDH (F): AGGTCGGTGTGAACGGATTTG
GAPDH (R): GGGGTCGTTGATGGCAACA

Western Blot

Total proteins were extracted using Ristocetin-induced platelet aggregation (RIPA). Qubit Protein Assay Kit (Invitrogen, Carlsbad, CA, USA) was used to quantify the concentration. Proteins were separated using the 10% sodium dodecyl-sulfate polyacrylamide gel electrophoresis (SDS-PAGE) TGX mini gel and further transferred into a Polyvinylidene fluoride (PVDF) membrane (Transblot Turbo, Bio-Rad, Hercules, CA, USA). The membranes were subsequently incubated overnight with antibodies against LC3A/B (CST, Danvers, MA, USA, 1:1000, 12741), YAP (CST, Danvers, MA, USA, 1:1000, 14074), mTOR (Abcam, Waltham, MA, USA, 1:1000, ab134903), β -actin (Abcam, Waltham, MA, USA, 1:5000, ab8226) and En1 (Bioss Inc., Woburn, MA, USA, 1:1000, bs-11744R-HRP). After being washed with PBS-T, membranes were then incubated with the corresponding secondary antibody goat anti-rabbit HRP-linked (CST, Danvers, MA, USA, 1:5000, 7074), goat anti-rabbit HRP-linked (CST, Danvers, MA, USA, 1:5000, 7074), goat anti-rabbit HRP-linked (CST, Danvers, MA, USA, 1:5000, 7074), goat anti-mouse pAb-HRP (MBL, Chiba, Japan, 1:5000, 330) respectively for 60 min. A secondary antibody was not used for the western blot of En1. Protein bands were analyzed by an ECL detection kit (WBULS0100, Millipore, Billerica, MA, USA). Pictures were taken by ImageQuant LAS 4000mini (Cytiva, MA, USA) and then analyzed by ImageJ.

Isolation and Culture of Fibroblasts

ICR male mice (8-10 weeks old) were sacrificed by cervical dislocation after anesthesia. The trunk skin was separated and cut into small pieces in the ultra-clean bench after disinfection with 75% ethanol. After removing blood by rinsing with PBS, the tissues were transferred evenly to cell culture flasks. DMEM complete medium was added to submerge the tissue block in a constant temperature incubator to fully cultivate. After 24 h, DMEM complete medium was added, which was replaced every 3 days. The purified mouse skin fibroblasts were used for subsequent experiments.

Cell Transfection

siRNA of YAP, En1 (si-YAP, si-En1 – Horizon Discovery, London, UK), and their negative controls were transfected into cells using the TransIT-TKO Transfection Reagent (Mirus Bio, Madison, Wisconsin, United States).

3-(4, 5-Dimethylthiazolyl)2, 5-Diphenyltetrazolium Bromide (MTT) Assay

Cells were seeded in a 96-well plate (2×10^3 cells/well) for 24 h and incubated in 5 mg/mL MTT (MTT Cell Count kit, Nacalai Tesque Inc., Nakagyo-ku, Kyoto, Japan) for 4 h. Then the absorbance at 490 nm was analyzed with a microplate reader (SpectraMax, Molecular Devices, San Jose, CA, USA) after DMSO supplement.

Scratch Assay

Mouse fibroblasts were plated into 6-well plates supplemented with DMEM. An artificial wound was created in the confluent cell monolayer using a 200 μ L pipette tip. Cells were cultured after the removal of the medium. The images were taken at 0 h and 24 h using a microscope. The area was measured without cells in the middle, respectively, by ImageJ, and then the change rate of the area from 0 to 24 hours was calculated using the following formula: (initial area – final area)/initial area \times 100%.

Statistical Analysis

Statistical data was analyzed by SPSS 19.0 (IBM Corp., Armonk, NY, USA) and expressed as means \pm standard deviation (SD). The differences between the two groups were analyzed using Student's *t*-tests. One-way analysis of variance (ANOVA) was performed to assess the differences among multiple groups. *p*-values lower than 0.05 were considered significant.

Results

Autophagy Inhibition Accelerated Wound Closure *In Vivo*

As previously reported¹³, autophagy inhibitor treatment accelerated wound healing *in vivo*. In the current study, it was also observed that the wound healing rate of a skin injury mouse model was significantly increased by 3-MA (autophagy inhibitor) treatment on day 10 (Figure 1A-B). The increased autophagy marker (LC3II/I), YAP, and En1 levels were observed in the skin of control mice, while these changes were partially reversed by 3-MA treatment, resulting in accelerated wound closure and reduced expression of YAP, EN1, and autophagy marker (LC3A/B) in the skin 10 days after injury (Figure 1C-D). Collectively, our results suggested that autophagy inhibition contributed to wound closure *in vivo*.

YAP Knockdown Facilitated Wound Closure *In Vivo*

To probe the role of YAP in wound healing, we induced the knockdown of YAP in the wounds of model mice. It was observed that the wound healing rate was significantly higher in the si-YAP group than in the si-NC group (Figure 2A-B). In addition, YAP knockdown led to reduced YAP and En1 mRNA levels in the skin of model mice 10 days after injury (Figure 2C). Moreover, it was observed that si-YAP transfection resulted in reduced LC3II/I, YAP and En1 levels (Figure 2D). Taken together, YAP knockdown increased the wound healing rate by repressing autophagy.

YAP Knockdown Promoted the Proliferation and Migration of Fibroblasts

Fibroblasts are commonly used cells to study wound healing *in vitro*¹⁶. Herein, we aimed to explore the role of YAP in regulating the proliferation and migration of fibroblasts isolated from mouse skin. Firstly, we induced YAP knockdown in fibroblasts (Figure 3A). As revealed in Figure 3B, cell proliferation of fibroblasts was increased by YAP knockdown (Figure 3C). In addition, it was observed that YAP knockdown led to increased cell migration of fibroblasts (Figure 3D). Moreover, YAP knockdown resulted in reduced protein level of LC3II/I in fibroblasts. In conclusion, YAP knockdown promoted the proliferation and migration of fibroblasts.

YAP Regulated mTOR-Mediated Autophagy in Fibroblasts by Regulation of En1

We first observed that the YAP knockdown resulted in reduced En1 level and increased mTOR level in mouse fibroblasts (Figure 4A). In order to probe the role of En1 in regulating mTOR and autophagy in wound healing, we induced En1 knockdown in fibroblasts by transfecting si-En1 into cells. As demonstrated in Figure 4B, si-En1 transfection resulted in reduced En1 level and increased mTOR level in fibroblasts. Functional experiments subsequently demonstrated that the proliferation (Figure 4C) and migration (Figure 4D) of fibroblasts were promoted by En1 silencing. Additionally, En1 knockdown resulted in reduced LC3II/I level in fibroblasts (Figure 4E). In summary, En1 served as the target of YAP in regulating mTOR-mediated autophagy in fibroblasts, thereby regulating cell proliferation and migration.

Discussion

Skin injury is a common event after accidental trauma¹⁷. Delayed wound healing has always been an important health problem worldwide, especially among diabetic patients and the elderly¹⁸. Wound healing is a complicated process, the specific mechanism of which has not been fully understood. In the current study, it was found that autophagy inhibition promoted wound closure *in vivo*. We subsequently investigated the regulatory mechanisms of autophagy during wound healing *in vitro*; our results revealed that YAP promoted autophagy in fibroblasts and facilitated their migration and proliferation in wound healing by regulating the En1/mTOR axis, providing a potential therapeutic target for wound healing dysfunction.

Autophagy refers to a catabolic process that removes unwanted components *via* lysosomal degradation pathways. Autophagy has been largely reported to be involved in various diseases such as heart disease, cancer, and neurodegeneration, and the function of autophagy in tissue regeneration is intriguing. Our study found that autophagy inhibition could accelerate wound closure *in vivo*, making it a promising target for chronic wound healing. Consistently, several other studies^{13,19,20} also pointed out that autophagy inhibitors accelerated wound healing in normal mice or diabetic wounds. For example, advanced glycation end-

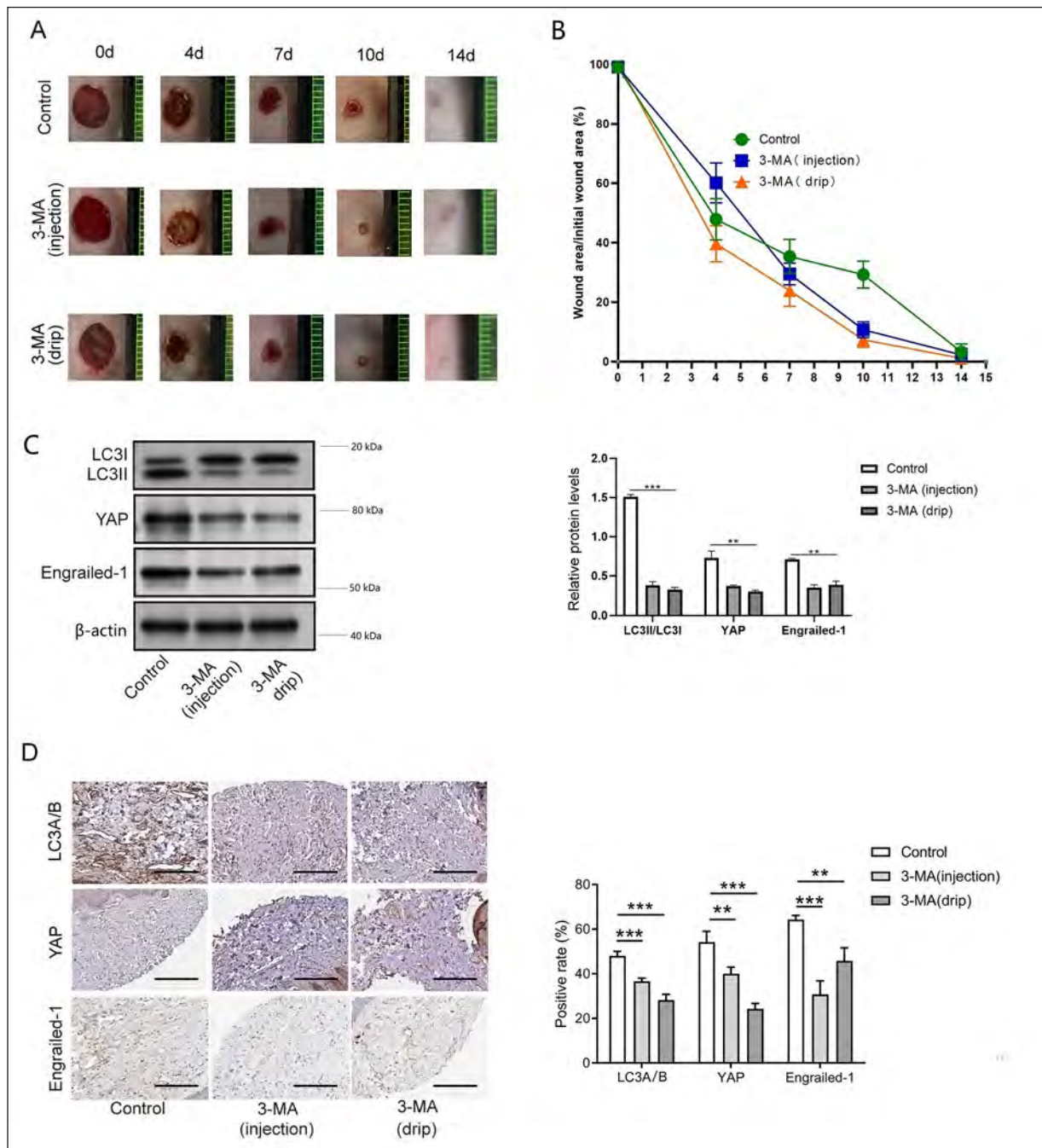


Figure 1. Autophagy inhibition accelerated wound closure *in vivo*. Mice after the skin was injured were subjected to 3-MA. **A-B**, Representative wound healing images, and the wound closures were quantified. **C**, Western blot was employed to evaluate LC3II/I, YAP and En1 levels in skin tissues. **D**, The protein levels of LC3A/B, En1, and YAP in the dermis of skin tissues were detected by IHC (magnification 200×). The solid line represents 100 μm. The measurement data were presented as mean ± SD. N = 5. ***p* < 0.01, ****p* < 0.001.

products (AGEs) can elicit autophagy, modulating macrophage polarization to M1 and impairing wound healing²¹. In addition, excessive autophagy impairs the healing process of diabetic wounds and leads to the formation of hypertrophic scars²². However, some studies^{7,8} also demonstrated that

autophagy may have a positive impact on wound healing. Appropriate hydration can contribute to rapid and efficient wound closure by promoting cell proliferation and migration and extracellular matrix reorganization *via* inducing autophagy⁸. Moreover, autophagy in various types of cells

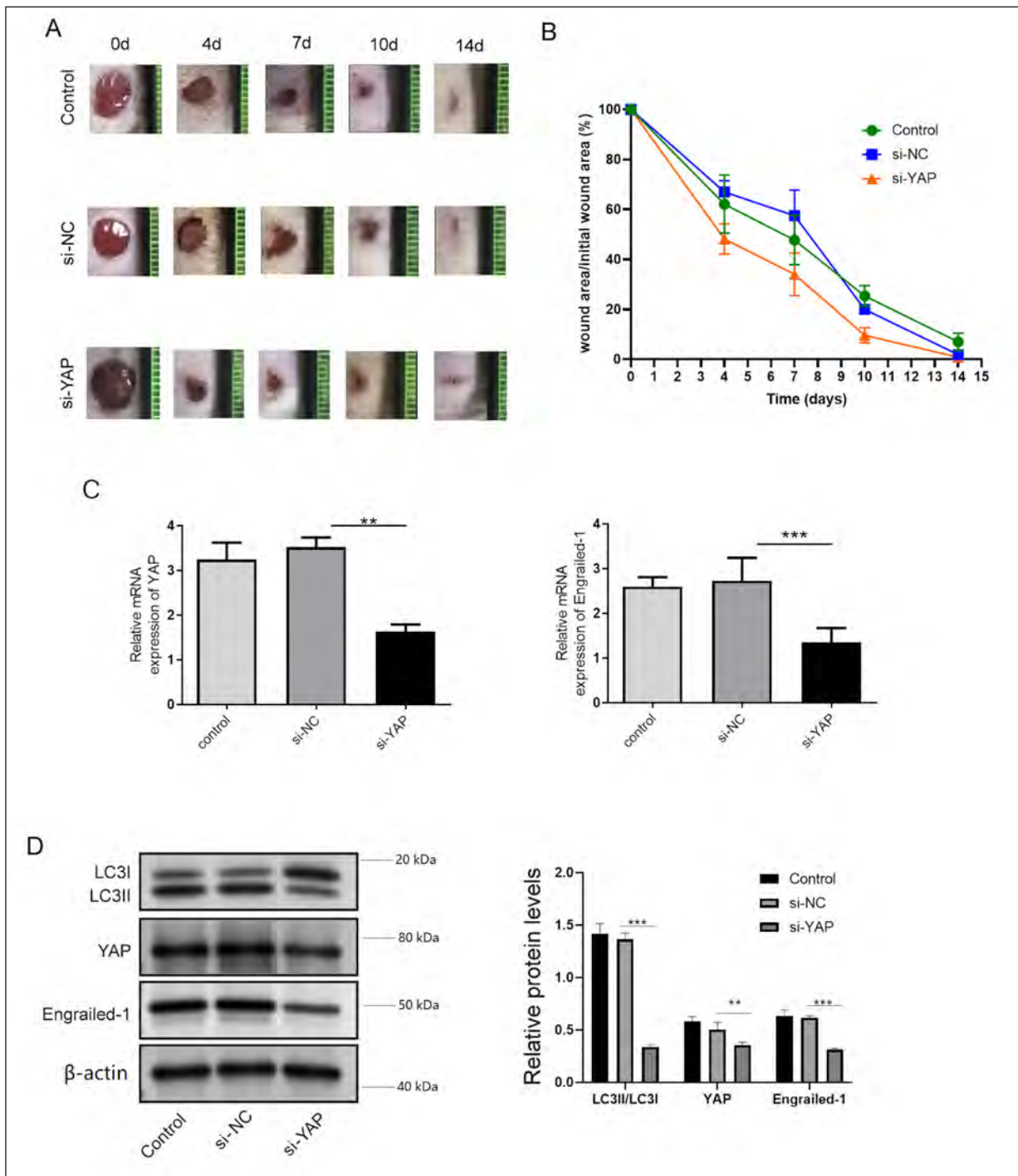


Figure 2. YAP knockdown facilitated wound closure *in vivo*. We electrotransfected si-YAP or si-NC into the wound edges of mice after the skin was injured. **A-B**, Representative wound healing images, and the wound closures were quantified. **C**, RT-qPCR was carried out to determine the mRNA levels of YAP and En1 in skin tissues. **D**, The protein levels of LC3II/I, YAP and En1 levels in skin tissues were detected using western blot. The measurement data were presented as mean \pm SD. N = 5. ** p < 0.01, *** p < 0.001.

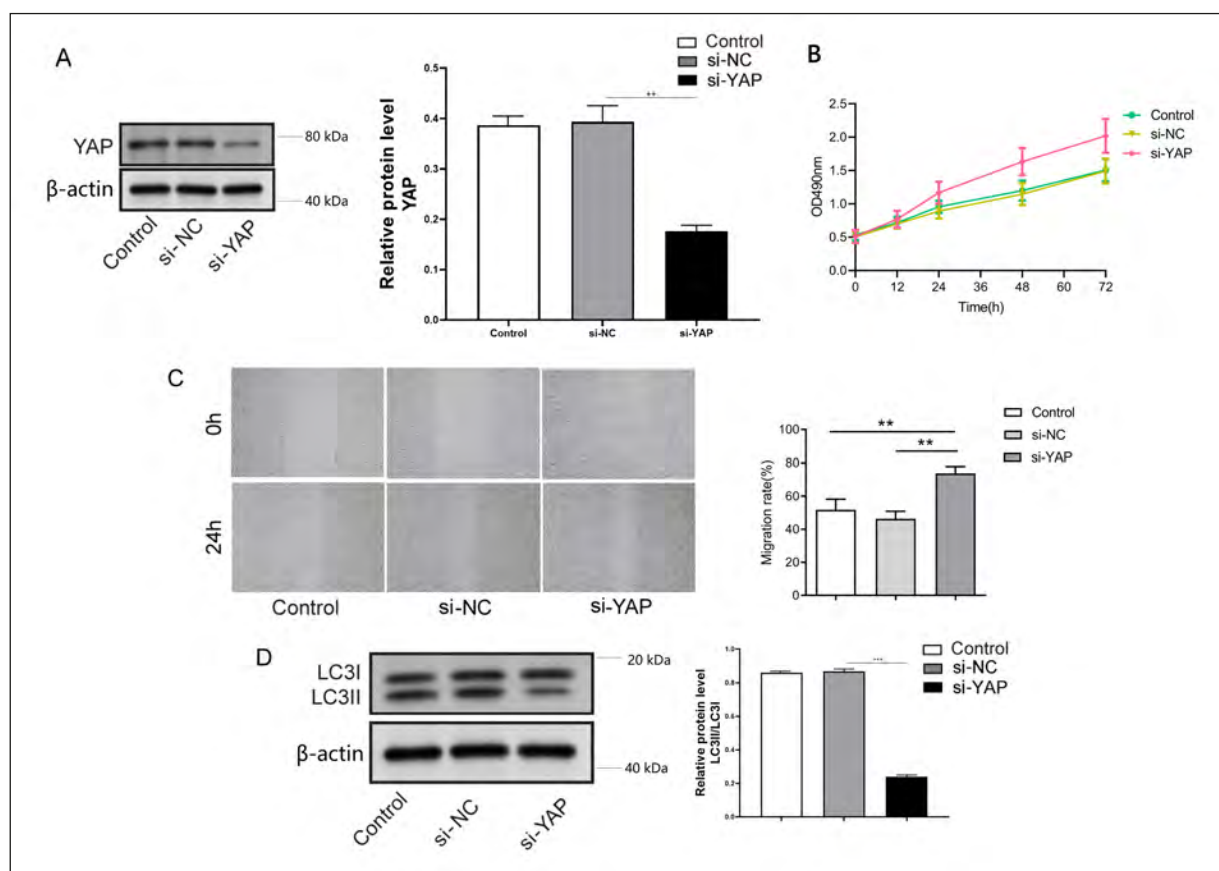


Figure 3. YAP knockdown promoted the proliferation and migration of fibroblasts. We induced YAP knockdown in fibroblasts. **A**, YAP expression was examined by RT-qPCR and western blot. **B**, Cell proliferation was analyzed by MTT assay. **C**, Cell migration was analyzed by scratch assay. **D**, Western blot was employed to evaluate LC3II/I levels. The measurement data were presented as mean \pm SD. All data was obtained from at least three replicate experiments. * $p < 0.05$, ** $p < 0.01$, *** $p < 0.001$.

may cause different results. Qiang et al⁷ showed that epidermal autophagy can facilitate the activation of keratinocytes and fibroblasts and coordinate their interactions, thus enhancing skin repair, whereas we found that autophagy in fibroblasts is a risk factor for wound healing. Hence, autophagy has a dual role in regulating wound healing and can determine different clinical outcomes depending on the tissue or cell in which it occurs⁶. Therefore, future studies should further clarify the exact role of autophagy in different stages of wound healing and develop cell-specific autophagy drugs to promote wound healing.

As above, autophagy is a crucial process for wound healing. However, its underlying molecular mechanism needs to be further elucidated. We found that the YAP/En1/mTOR axis is essential to regulate autophagy in skin wound healing. YAP knockdown repressed autophagy in fibroblasts in wound healing to promote their migration and

proliferation, accelerating wound closure through modulating En/mTOR pathway. As widely described, YAP, as a transcriptional coactivator of the Hippo signaling, plays a critical role in skin wound repair⁹. As proof, ectopic expression of activated YAP mutants or deregulation of upstream regulators of YAP localization resulted in an uncontrolled epidermal injury response^{23,24}. More importantly, it was also previously reported¹¹ that verteporfin (YAP inhibitor) or YAP knockdown could promote wound regeneration with restoration of skin attachment, ultrastructure, and mechanical strength. In agreement with previous results, our study suggested that YAP is a risk factor affecting wound healing, and loss-of-function experiments revealed that YAP knockdown promoted the proliferation and migration of fibroblasts, leading to accelerated wound closure *in vivo* as well as reduced autophagy in wounds. Therefore, the conclusion drawn was that YAP

knockdown accelerated wound healing *in vitro* and *in vivo* by suppressing autophagy in fibroblasts.

As previously described¹¹, YAP inhibition promoted wound regeneration by suppressing En1 activation, indicating that En1 might function as the target of YAP in regulating wound healing. The current study also illustrated that En1 was the downstream target of YAP in regulating wound healing and autophagy. En1 is crucial for tissue regeneration. For instance, in the fetal stage, En1-history-positive fibroblasts possess scarring abilities. Conversely, En1-history-naive fibroblasts drive dermal development and regeneration²⁵. As expected, En1 knockdown can also reduce autophagy in fibroblasts and promote the proliferation and migration of fibroblasts through activation of the mTOR pathway. mTOR, a serine/threonine kinase, is a master regulator of autophagy²⁶. Previous studies²⁶ showed that mTOR activation results in inhibition of autophagy. Col-

lectively, YAP knockdown increased mTOR level by inhibiting En1 expression, thereby repressing autophagy in fibroblasts during wound healing. As a result, YAP can be chosen as a therapeutic target for skin regeneration, and inhibition of YAP can accelerate wound healing.

The major limitation of the present study was lack of clinical validations. The effect of autophagy inhibitor on wound healing needs to be further verified. In addition, the mechanisms underlying how YAP regulates En1/mTOR axis should be further clarified in future studies.

Conclusions

Taken together, YAP knockdown repressed autophagy in fibroblasts and accelerated wound healing by regulating the En1/mTOR axis. Our research provided a hopeful strategy for wound repair dysfunction.

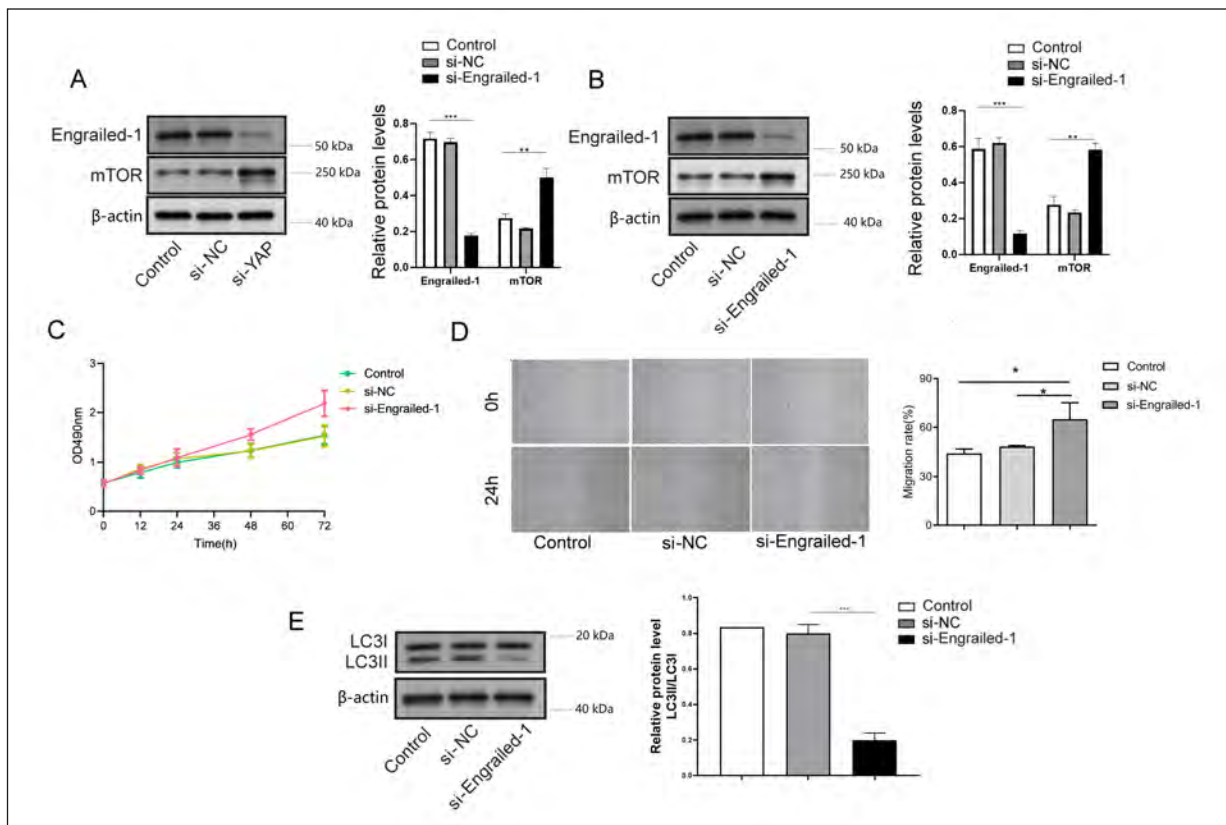


Figure 4. YAP regulated mTOR-mediated autophagy in fibroblasts by regulation of En1. **A**, En1 and mTOR levels in fibroblasts following YAP knockdown were assessed by western blot. We induced En1 knockdown in fibroblasts. **B**, Western blot was conducted to detect En1 and mTOR levels in cells. **C**, MTT assay was carried out to examine cell proliferation. **D**, Cell migration was analyzed by scratch assay. **E**, Western blot was employed to evaluate LC3II/I levels. The measurement data were presented as mean \pm SD. All data was obtained from at least three replicate experiments. * $p < 0.05$, ** $p < 0.01$, *** $p < 0.001$.

Conflict of Interest

All authors agree with the presented findings, have contributed to the work, and declare no conflict of interest.

Funding

This work was supported in part by Japan China Sasakawa Medical Fellowship (2017816).

Ethics Approval

Our study was approved by the Animal Ethics Committee of Keio University School of Medicine [A2022-128].

Data Availability

Data will be made available on request to the corresponding author.

Authors' Contribution

CJC: Conceptualization, Methodology, Software, Data curation, Writing- Original draft preparation, Visualization, Investigation. KK: Conceptualization, Supervision, Writing- Reviewing and Editing.

References

- 1) Singer AJ, Clark RA. Cutaneous wound healing. *N Engl J Med* 1999; 341: 738-746.
- 2) Eming SA, Martin P, Tomic-Canic M. Wound repair and regeneration: mechanisms, signaling, and translation. *Sci Transl Med* 2014; 6: 265sr6.
- 3) Reed BR, Clark RA. Cutaneous tissue repair: practical implications of current knowledge. II. *J Am Acad Dermatol* 1985; 13: 919-941.
- 4) Brem H, Tomic-Canic M. Cellular and molecular basis of wound healing in diabetes. *J Clin Invest* 2007; 117: 1219-1222.
- 5) Klionsky DJ. Autophagy: from phenomenology to molecular understanding in less than a decade. *Nat Rev Mol Cell Biol* 2007; 8: 931-937.
- 6) Ren H, Zhao F, Zhang Q, Huang X, Wang Z. Autophagy and skin wound healing. *Burns Trauma* 2022; 10: tkac003.
- 7) Qiang L, Yang S, Cui YH, He YY. Keratinocyte autophagy enables the activation of keratinocytes and fibroblasts and facilitates wound healing. *Autophagy* 2021; 17: 2128-2143.
- 8) Mijaljica D, Spada F, Klionsky DJ, Harrison IP. Autophagy is the key to making chronic wounds acute in skin wound healing. *Autophagy* 2023; 19: 2578-2584.
- 9) Dey A, Varelas X, Guan KL. Targeting the Hippo pathway in cancer, fibrosis, wound healing and regenerative medicine. *Nat Rev Drug Discov* 2020; 19: 480-494.
- 10) Wei F, Wang A, Wang Q, Han W, Rong R, Wang L. Plasma endothelial cells-derived extracellular vesicles promote wound healing in diabetes through YAP and the PI3K/Akt/mTOR pathway. *Aging (Albany NY)* 2020; 12: 12002-12018.
- 11) Mascharak S, desJardins-Park HE, Davitt MF, Griffin M, Borrelli MR, Moore AL, Chen K, Duoto B, Chinta M, Foster DS, Shen AH, Januszyk M, Kwon SH, Wernig G, Wan DC, Lorenz HP, Gurtner GC, Longaker MT. Preventing Engrailed-1 activation in fibroblasts yields wound regeneration without scarring. *Science* 2021; 372: eaba2374.
- 12) Györfi AH, Matei AE, Fuchs M, Liang C, Rigau AR, Hong X, Zhu H, Lubner M, Bergmann C, Dees C, Ludolph I, Horch RE, Distler O, Wang J, Bengsch B, Schett G, Kunz M, Distler JHW. Engrailed 1 coordinates cytoskeletal reorganization to induce myofibroblast differentiation. *J Exp Med* 2021; 218: e20201916.
- 13) Gao Y, Luo C, Rui T, Fan Y, Yao Y, Shen H, Gao C, Wang T, Wang H, Chen X, Zhang J, Li D, Xia C, Li LL, Wang Z, Zhang M, Chen X, Tao L. Autophagy inhibition facilitates wound closure partially dependent on the YAP/IL-33 signaling in a mouse model of skin wound healing. *FASEB J* 2021; 35: e21920.
- 14) Huo JF, Chen XB. Long noncoding RNA growth arrest-specific 5 facilitates glioma cell sensitivity to cisplatin by suppressing excessive autophagy in an mTOR-dependent manner. *J Cell Biochem* 2019; 120: 6127-6136.
- 15) Qiang L, Sample A, Liu H, Wu X, He YY. Epidermal SIRT1 regulates inflammation, cell migration, and wound healing. *Sci Rep* 2017; 7: 14110.
- 16) Spiekstra SW, Breetveld M, Rustemeyer T, Scheper RJ, Gibbs S. Wound-healing factors secreted by epidermal keratinocytes and dermal fibroblasts in skin substitutes. *Wound Repair Regen* 2007; 15: 708-717.
- 17) van Zanten MC, Mistry RM, Suami H, Campbell-Lloyd A, Finkemeyer JP, Piller NB, Caplash Y. The Lymphatic Response to Injury with Soft-Tissue Reconstruction in High-Energy Open Tibial Fractures of the Lower Extremity. *Plast Reconstr Surg* 2017; 139: 483-491.
- 18) Ban E, Jeong S, Park M, Kwon H, Park J, Song EJ, Kim A. Accelerated wound healing in diabetic mice by miRNA-497 and its anti-inflammatory activity. *Biomed Pharmacother* 2020; 121: 109613.
- 19) Wang F, Zhang C, Dai L, Zhang Y, Wang Y, Hao Y, Ji S, Xu Z, Han N, Chen H, Zhang Q, Nan W. Bafilomycin A1 Accelerates Chronic Refractory Wound Healing in db/db Mice. *Biomed Res Int* 2020; 2020: 6265701.
- 20) Lawrence J, Nho R. The Role of the Mammalian Target of Rapamycin (mTOR) in Pulmonary Fibrosis. *Int J Mol Sci* 2018; 19: 778.
- 21) Guo Y, Lin C, Xu P, Wu S, Fu X, Xia W, Yao M. AGEs Induced Autophagy Impairs Cutaneous Wound Healing via Stimulating Macrophage Polarization to M1 in Diabetes. *Sci Rep* 2016; 6: 36416.

- 22) Shi W, Wu Y, Bian D. p75NTR silencing inhibits proliferation, migration, and extracellular matrix deposition of hypertrophic scar fibroblasts by activating autophagy through inhibiting the PI3K/Akt/mTOR pathway. *Can J Physiol Pharmacol* 2021; 99: 349-359.
- 23) Schlegelmilch K, Mohseni M, Kirak O, Pruszek J, Rodriguez JR, Zhou D, Kreger BT, Vasioukhin V, Avruch J, Brummelkamp TR, Camargo FD. Yap1 acts downstream of α -catenin to control epidermal proliferation. *Cell* 2011; 144: 782-795.
- 24) Silvis MR, Kreger BT, Lien WH, Klezovitch O, Rudakova GM, Camargo FD, Lantz DM, Seykora JT, Vasioukhin V. α -catenin is a tumor suppressor that controls cell accumulation by regulating the localization and activity of the transcriptional coactivator Yap1. *Sci Signal* 2011; 4: ra33.
- 25) Jiang D, Correa-Gallegos D, Christ S, Stefanska A, Liu J, Ramesh P, Rajendran V, De Santis MM, Wagner DE, Rinkevich Y. Two succeeding fibroblastic lineages drive dermal development and the transition from regeneration to scarring. *Nat Cell Biol* 2018; 20: 422-431.
- 26) Kim YC, Guan KL. mTOR: a pharmacologic target for autophagy regulation. *J Clin Invest* 2015; 125: 25-32.



Single-Cell RNA-seq Analysis Reveals Cellular Functional Heterogeneity in Dermis Between Fibrotic and Regenerative Wound Healing Fates

Cao-Jie Chen¹, Hiroki Kajita¹, Kento Takaya¹, Noriko Aramaki-Hattori¹, Shigeki Sakai¹, Toru Asou^{2*} and Kazuo Kishi^{1*}

¹ Department of Plastic and Reconstructive Surgery, Keio University School of Medicine, Tokyo, Japan, ² Department of Plastic Surgery, Tokyo Cosmetic Surgery Clinic, Tokyo, Japan

OPEN ACCESS

Edited by:

Tian Li,
Independent Researcher, Xi'an, China

Reviewed by:

Li-xin Tang,
Chongqing Public Health Medical
Center, China
Zi-chao Li,
Fourth Military Medical University,
China

*Correspondence:

Kazuo Kishi
kkishi@a7.keio.jp
Toru Asou
mori@ideajapan.com

Specialty section:

This article was submitted to
Cancer Immunity
and Immunotherapy,
a section of the journal
Frontiers in Immunology

Received: 14 February 2022

Accepted: 04 April 2022

Published: 17 May 2022

Citation:

Chen C-J, Kajita H, Takaya K,
Aramaki-Hattori N, Sakai S, Asou T
and Kishi K (2022) Single-Cell RNA-
seq Analysis Reveals Cellular
Functional Heterogeneity in Dermis
Between Fibrotic and Regenerative
Wound Healing Fates.
Front. Immunol. 13:875407.
doi: 10.3389/fimmu.2022.875407

Background: Fibrotic scars are common in both human and mouse skin wounds. However, wound-induced hair neogenesis in the murine wounding models often results in regenerative repair response. Herein, we aimed to uncover cellular functional heterogeneity in dermis between fibrotic and regenerative wound healing fates.

Methods: The expression matrix of single-cell RNA sequencing (scRNA-seq) data of fibrotic and regenerative wound dermal cells was filtered, normalized, and scaled; underwent principal components analysis; and further analyzed by Uniform Manifold Approximation and Projection (UMAP) for dimension reduction with the Seurat package. Cell types were annotated, and cell-cell communications were analyzed. The core cell population myofibroblast was identified and the biological functions of ligand and receptor genes between myofibroblast and macrophage were evaluated. Specific genes between fibrotic and regenerative myofibroblast and macrophage were identified. Temporal dynamics of myofibroblast and macrophage were reconstructed with the Monocle tool.

Results: Across dermal cells, there were six cell types, namely, EN1-negative myofibroblasts, EN1-positive myofibroblasts, hematopoietic cells, macrophages, pericytes, and endothelial cells. Ligand and receptor genes between myofibroblasts and macrophages mainly modulated cell proliferation and migration, tube development, and the TGF- β pathway. Specific genes that were differentially expressed in fibrotic compared to regenerative myofibroblasts or macrophages were separately identified. Specific genes between fibrotic and regenerative myofibroblasts were involved in the mRNA metabolic process and organelle organization. Specific genes between fibrotic and regenerative macrophages participated in regulating immunity and phagocytosis. We then observed the underlying evolution of myofibroblasts or macrophages.

Conclusion: Collectively, our findings reveal that myofibroblasts and macrophages may alter the skin wound healing fate through modulating critical signaling pathways.

Keywords: skin wound healing, fibrosis, regeneration, myofibroblast, macrophage, single-cell RNA sequencing

INTRODUCTION

The skin is the organ with the largest surface area in the human body that provides an efficient protective barrier against mechanical injury, microbial pathogens, and trauma (1). The skin's immune system is divided into two structural compartments: epidermis and dermis, both of which contain a plethora of immunocompetent cell types (2). The epidermis is home to the main skin-resident immune cells, Langerhans cells, and melanocytes. Meanwhile, immune-specialized cells like dendritic cells, macrophages, and T cells reside in the dermis (3). The communications within immune populations and the skin environment are critical to the effectiveness of the skin immune system (4). Wound healing is a complex process in the human body, where numerous cell populations with different functions are involved in the stages of hemostasis, inflammatory response, growth, re-epithelialization, and remodeling (5). It is essential to repair the skin after damage (6). Skin wound healing involves three primary phases: inflammation, re-epithelialization, and tissue remodeling (7). Nevertheless, effective therapeutic strategies of accelerating healing and decreasing scarring remain lacking. Single-cell RNA sequencing (scRNA-seq) technology has emerged as an indispensable tool for elucidating cellular phenotype and functional heterogeneity (8). Deciphering the role of each cell type and interactions within cells is of importance to understand the mechanism of normal wound closure (9). Alterations in the microenvironment may influence cellular recruitment or activation, resulting in damaged states of wound healing. ScRNA-seq can be applied for deciphering the cellular changes in chronic wounds and hypertrophic scarring, thereby promoting the development of more effective therapeutic solutions for healing wounds (10). Moreover, in-depth understanding of the differences between fibrotic and regenerative wound healing fates is a prerequisite for developing more effective therapeutic interventions (2). Here, the purpose of this study was to reveal cellular functional heterogeneity in the dermis between fibrotic and regenerative wound healing fates.

MATERIALS AND METHODS

Acquisition of scRNA-seq Profiles

10× genomics scRNA-seq data of regenerative [GSM4213633; large full-thickness excision (1 cm²) allows *de novo* follicle regeneration] and fibrotic (GSM4213632; large wounds lead to hairless scars) wound-induced hair neogenesis (WIHN) wounds of adult 6- or 7-week-old C57Bl/6j mice were curated from the Gene Expression Omnibus (GEO) repository (<https://www.ncbi.nlm.nih.gov/gds/>). The accession number was GSE141814 (11). Regenerative wounds were defined as hair neogenesis, decreased contraction, decreased Wnt and TGF- β signaling activity, and decreased collagen production, while fibrotic wounds were defined as decreased hair neogenesis, increased contraction, increased Wnt and TGF- β signaling activity, and increased collagen production. This dataset was based on the platform of GPL21103 Illumina HiSeq 4000 (*Mus musculus*).

Quality Control

The DropletUtils package (v 3.13) was adopted to read unique molecular identifiers (UMI) count matrix, identify cells from empty droplets, remove barcode-swapped pseudo-cells, and downsample the count matrix (12). The calculateQCMetrics function of the Scater package was used for counting the expression of genes in cells (13). Cells with proportions of mitochondrial genes $\leq 10\%$ and ribosomal genes $\geq 10\%$ were determined for further analysis.

Data Preprocessing and Principal Component Analysis

The expression matrix was normalized with the NormalizeData function of the Seurat package (14). The top 2,000 highly variable genes were screened by the FindVariableFeatures function. Then, expression data were linearly scaled utilizing the ScaleData function. Finally, principal component analysis (PCA) was performed with the RunPCA function based on the 2,000 genes.

Cell Cluster and Annotation

The principal components with large standard deviations were selected. Then, cell clustering analysis was performed using the FindNeighbors and FindClusters function of the Seurat package. With the RunUMAP function, Uniform Manifold Approximation and Projection (UMAP) was carried out for dimension reduction. Cell types were annotated on the basis of the known marker genes.

Identification of Novel Marker Genes

To calculate the differentially expressed genes between each cluster and all other cells, the FindAllMarkers function of the Seurat package was used and novel marker genes were identified according to the following criteria: $|\log$ fold change (FC) ≥ 0.1 , the minimum expression ratio of cell population = 0.25, and p -value ≤ 0.05 .

Ligand–Receptor Network Analysis

Based on the ligand–receptor pairs from the previous literature (15), the relationship pairs of receptors and ligands were analyzed based on the marker genes of various cells. Then, a cell–cell communication network was conducted and visualized with the Cytoscape software (16). The core cell population was identified according to the largest number of receptor–ligand pairs in the network. Moreover, the receptor and ligand genes were extracted.

Function Enrichment Analysis

Function enrichment analysis of the indicated genes was carried out utilizing the clusterProfiler package, including Gene Ontology (GO) and Kyoto Encyclopedia of Genes and Genomes (KEGG) pathway analysis (17). GO categories contain biological process, cellular component, and molecular function. Terms with $p < 0.05$ were considered significantly enriched.

Protein–Protein Interaction Analysis

The Search Tool for the Retrieval of Interacting Genes (STRING) database (version 11.0; <https://string-db.org/>) was utilized for

exploring the functional interactions between marker gene-encoded proteins (18). Then, PPI networks were constructed and the top 20 hub genes were identified.

Pseudotime Analysis

Pseudotime analysis was carried out with the Monocle 3 tool (19). Firstly, genes that were expressed in at least 5% of the cells were selected. Then, the `reduceDimension` function was utilized to perform dimensionality reduction analysis, followed by cell cluster with the `clusterCells` function. Afterwards, the `differentialGeneTest` function was adopted to determine candidate genes with differences between the clusters with $p < 0.05$. The dimensionality reduction analysis of the cells was carried out using the `DDRTree` approach and the `reduceDimension` function based on the candidate genes. Through the `orderCells` function, the cells along the quasi-chronological trajectory were sorted and visualized.

Gene Set Variation Analysis

The single-sample gene set enrichment analysis (ssGSEA) function of the Gene Set Variation Analysis (GSVA) package was utilized for comparisons of the differences in GO and KEGG terms between groups (20).

Isolation and Culture of Fibroblasts

C57BL/6 male mice (8–10 weeks old; Sankyo) were used for fibroblast isolation. Briefly, mice were sacrificed by cervical dislocation. The trunk skin was separated in the ultra-clean bench, immersed in 75% ethanol for disinfection, and then cut into small pieces. Blood was removed by rinsing with PBS buffer and transferred evenly to cell culture dishes. DMEM complete medium (Wako) was added to submerge the tissue block that was placed in a constant temperature incubator to fully cultivate. After 24 h, DMEM complete medium was added, which was replaced every 3 days. The mouse skin fibroblasts were purified by the differential adhesion method and were used for subsequent experiments. Our study was approved by the Animal Ethics Committee of Keio University School of Medicine [12090(5)].

Transfection

Using the TransIT-TKO Transfection Reagent (Mirus), siRNA-Engrailed-1 (horizon) and siRNA-control were transfected into fibroblasts in a constant-temperature incubator. Forty-eight hours later, the knockdown effect of siRNA was confirmed by real-time quantitative polymerase-chain reaction (RT-qPCR).

RT-qPCR

Total RNA was extracted from fibroblasts using the Isogen reagent (Nippon Gene) following the manufacturer's instructions. cDNA synthesis was achieved based on the cDNA Synthesis System (Bio-Rad). RT-qPCR was carried out utilizing SYBR Qpcr Mix (Toyobo) on a 7500 Real-Time PCR system (Applied Biosystems). The primer sequences were as follows: EN1, 5'-ACACAACCTGCGATCC TACT-3'(forward) and 5'-GGACGGTCCGAATAGCGTG-3' (reverse); ACTB, 5'-GGC TGTATTCCCCTCCATCG-3'(forward) and 5'-CCAGTTGGTAACAATGCCATGT-3' (reverse). The relative expressions were calculated with the $2^{-\Delta\Delta Ct}$ method.

Wound Healing Assay

Fibroblasts were plated onto a 6-well plate (about 3×10^5 cells/well). When the confluence reached 100%, the fibroblast monolayer was scratched with a 1000- μ l pipette tip. Additionally, detached fibroblasts were removed with serum-free medium. At 0 h and 24 h, the wounded area was photographed.

Statistical Analysis

All statistical analysis was performed using the R language (version 3.6.1) and R Bioconductor packages. $p < 0.05$ indicated statistical significance.

RESULTS

Quality Control of scRNA-seq Data of Fibrotic and Regenerative Wound Dermal Cells

Herein, we collected scRNA data of dermal cells from large skin wounds on day 18 with two distinct healing fates (fibrosis: GSM4213632 or regeneration: GSM4213633) from the GSE141814 dataset. Before analysis, we presented quality control of scRNA data. Barcode rank plots separately depicted the distribution of barcodes in total UMI count for fibrotic and regenerative wound dermal cells (**Supplementary Figures 1A, B**). Knee and inflection points in the barcode rank plots indicated the transition of the total UMI count distribution, which reflected the difference between empty droplets and cell droplets. After filtrating empty droplets, we counted the expression of genes in each cell (**Supplementary Figures 1C, D**). Afterwards, we filtrated out cells with proportions of mitochondrial genes $> 10\%$ and ribosomal genes $< 10\%$ (**Supplementary Figures 1E, F**).

Cell Cluster of Fibrotic and Regenerative Wound Dermal Cells

After normalizing scRNA data, we screened the top 2,000 highly variable genes across fibrotic and regenerative wound dermal cells (**Figure 1A**). Then, scRNA data were linearly scaled and analyzed by dimensionality reduction with PCA. Here, we screened the top two principal components for subsequent analysis (**Figure 1B**). PCA results uncovered the prominent difference between fibrotic and regenerative wound dermal cells (**Figure 1C**). According to the elbow point, we identified the optimal principal components as 8 (**Figure 1D**). Heatmaps depicted the top 20 marker genes in each principal component (**Figure 1E**). With the UMAP method, dermal cells were clustered into 15 clusters (**Figure 1F**). The top ten marker genes of each cell cluster are presented in **Figure 1G**.

Identification of Cell Types and Their Marker Genes Across Fibrotic and Regenerative Wound Dermal Cells

This study attempted to identify cell types across fibrotic and regenerative wound dermal cells. Based on the known marker genes, six cell types were annotated, as follows: EN1-negative

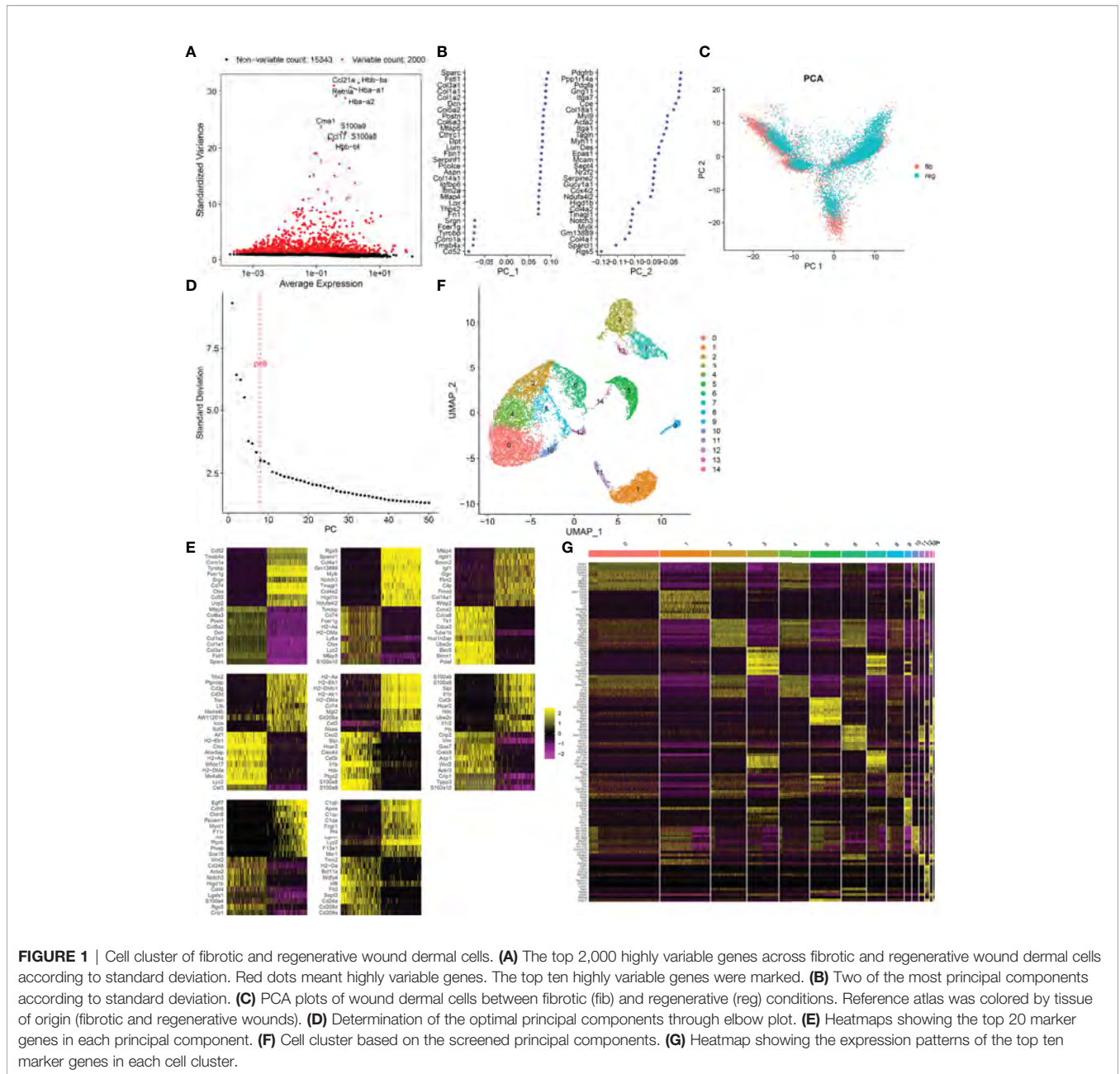


FIGURE 1 | Cell cluster of fibrotic and regenerative wound dermal cells. **(A)** The top 2,000 highly variable genes across fibrotic and regenerative wound dermal cells according to standard deviation. Red dots meant highly variable genes. The top ten highly variable genes were marked. **(B)** Two of the most principal components according to standard deviation. **(C)** PCA plots of wound dermal cells between fibrotic (fib) and regenerative (reg) conditions. Reference atlas was colored by tissue of origin (fibrotic and regenerative wounds). **(D)** Determination of the optimal principal components through elbow plot. **(E)** Heatmaps showing the top 20 marker genes in each principal component. **(F)** Cell cluster based on the screened principal components. **(G)** Heatmap showing the expression patterns of the top ten marker genes in each cell cluster.

myofibroblasts ($n = 6,392$), EN1-positive myofibroblasts ($n = 2,219$), hematopoietic cells ($n = 3,774$), macrophages ($n = 1,461$), pericytes ($n = 1,493$), and endothelial cells ($n = 303$; **Figure 2A**). **Table 1** lists the cell ratio of each cell type. In particular, we noticed the differences in ratios of EN1-negative and -positive myofibroblasts between fibrotic and regenerative wound dermal cells (**Figure 2B**). With $|\log_{2}FC| \geq 0.1$, the minimum expression ratio of cell population = 0.25, and $p\text{-value} \leq 0.05$, we identified novel marker genes in each cell type (**Supplementary Table 1**). The top ten marker genes in each cell type were visualized, as follows: EN1-negative myofibroblasts (Aebp1, Col1a1, Col1a2, Col3a1, Col8a1, Dcn, Eln, Mfap2, Mfap4, and Sparc),

hematopoietic cells (AW112010, Cd3d, Cd3g, Cd52, Hcst, Ltb, Ptpcrap, Rac2, Srgn, and Trbc2), macrophages (Apoe, C1qb, Ccl9, Cd74, Ctss, Fcer1g, H2-Eb1, Lyz2, Ms4a6c, and Tyrobp), pericytes (Acta2, Col4a1, Col4a2, Gm13889, Higd1b, Myl9, Mylk, Rgs5, Sparcl1, and Tagln), EN1-positive myofibroblasts (Birc5, Pclaf, Stnm1, Ube2c, Hist1h2ap, Col5a3, Cks2, Aqp1, Tnfrsf10b, and Timp1), and endothelial cells (Egfl7, Cldn5, Cdh5, Ramp2, Ecsr, Pecam1, Cd200, Ltbp4, Aqp1, and Hist1h2ap) (**Figure 2C**). Furthermore, we detected the expression levels of the known marker genes that were used for annotating cell types, as follows: endothelial cells (Cldn5, Pecam1, and Cd74), EN1-negative and -positive myofibroblasts (En1, Col1a1, Dcn, Sfrp4,

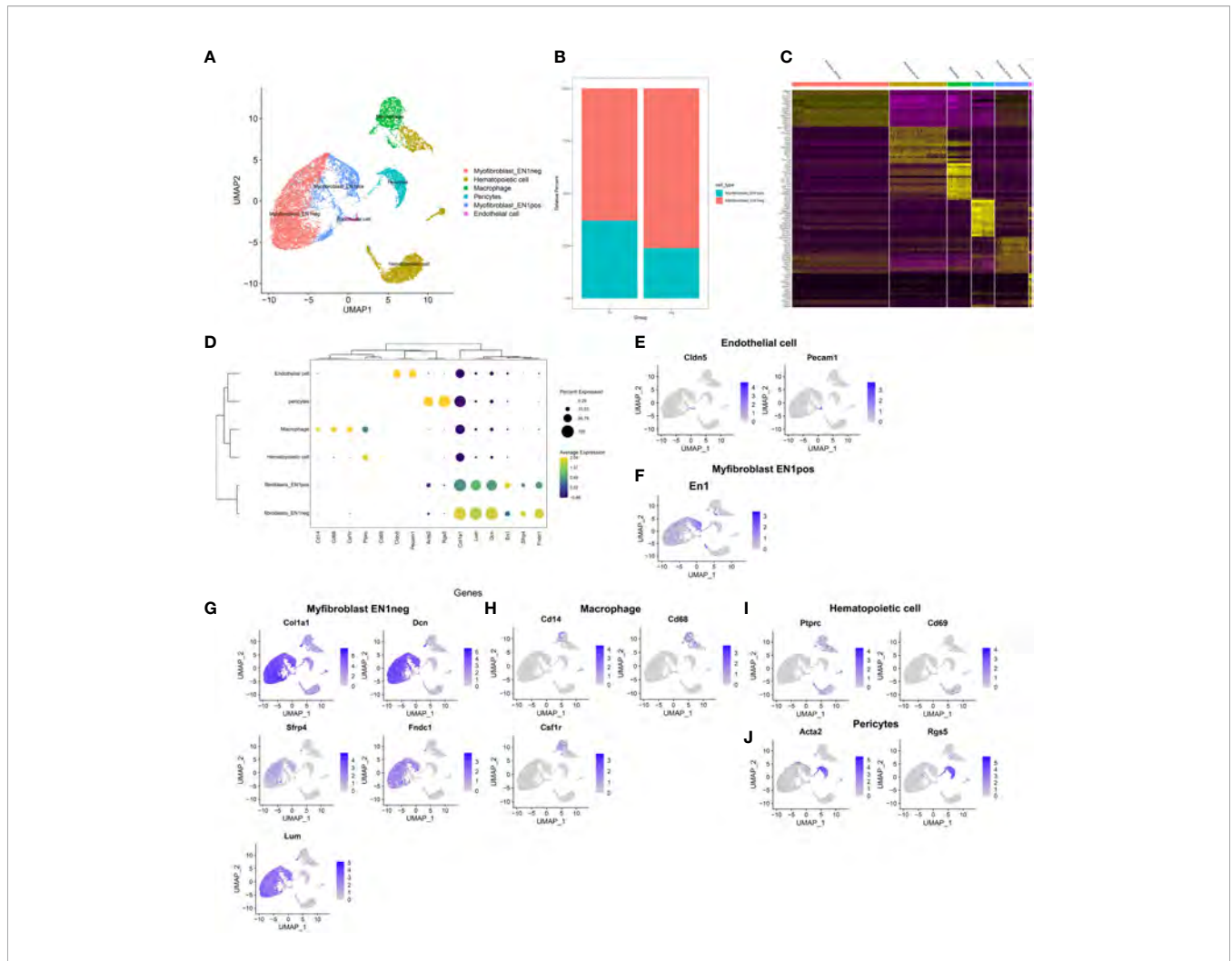


FIGURE 2 | Identification of cell types and their marker genes across fibrotic and regenerative wound dermal cells. **(A)** UMAP plots showing cell types identified by marker genes. Each cell type was colored by a unique color. **(B)** The cell ratio of EN1-negative and -positive myfibroblasts among fibrotic and regenerative wound dermal cells. **(C)** Heatmap visualizing cell-type-specific gene expression patterns. Each column represented the average expression after cells were grouped. **(D)** Integrated analysis showing marker genes across cell types. The size of each circle reflected the percentage of cells in each cell type where the gene was detected, and the color shadow reflected the average expression level within each cell type. **(E–J)** UMAP plots of expression of the marker genes for endothelial cells, EN1-negative and -positive myfibroblasts, macrophages, hematopoietic cells, and pericytes.

TABLE 1 | Cell ratio of each cell type.

Cell type	Group	Count	Total	Ratio
Endothelial cell	Fibrotic	76	5,130	0.014815
Endothelial cell	Regenerative	112	10,512	0.010654
EN1-negative myfibroblasts	Fibrotic	772	5,130	0.150487
EN1-negative myfibroblasts	Regenerative	5,620	10,512	0.534627
EN1-positive myfibroblasts	Fibrotic	454	5,130	0.088499
EN1-positive myfibroblasts	Regenerative	1,765	10,512	0.167903
Hematopoietic cell	Fibrotic	2,439	5,130	0.475439
Hematopoietic cell	Regenerative	1,335	10,512	0.126998
Macrophage	Fibrotic	725	5,130	0.141326
Macrophage	Regenerative	851	10,512	0.080955
Pericytes	Fibrotic	664	5,130	0.129435
Pericytes	Regenerative	829	10,512	0.078862

Fndc1, and Lum), macrophages (Cd14, Cd68, and Csf1r), and hematopoietic cells (Ptpcr, Cd69, Acta2, and Rgs5) (Figures 2D–J).

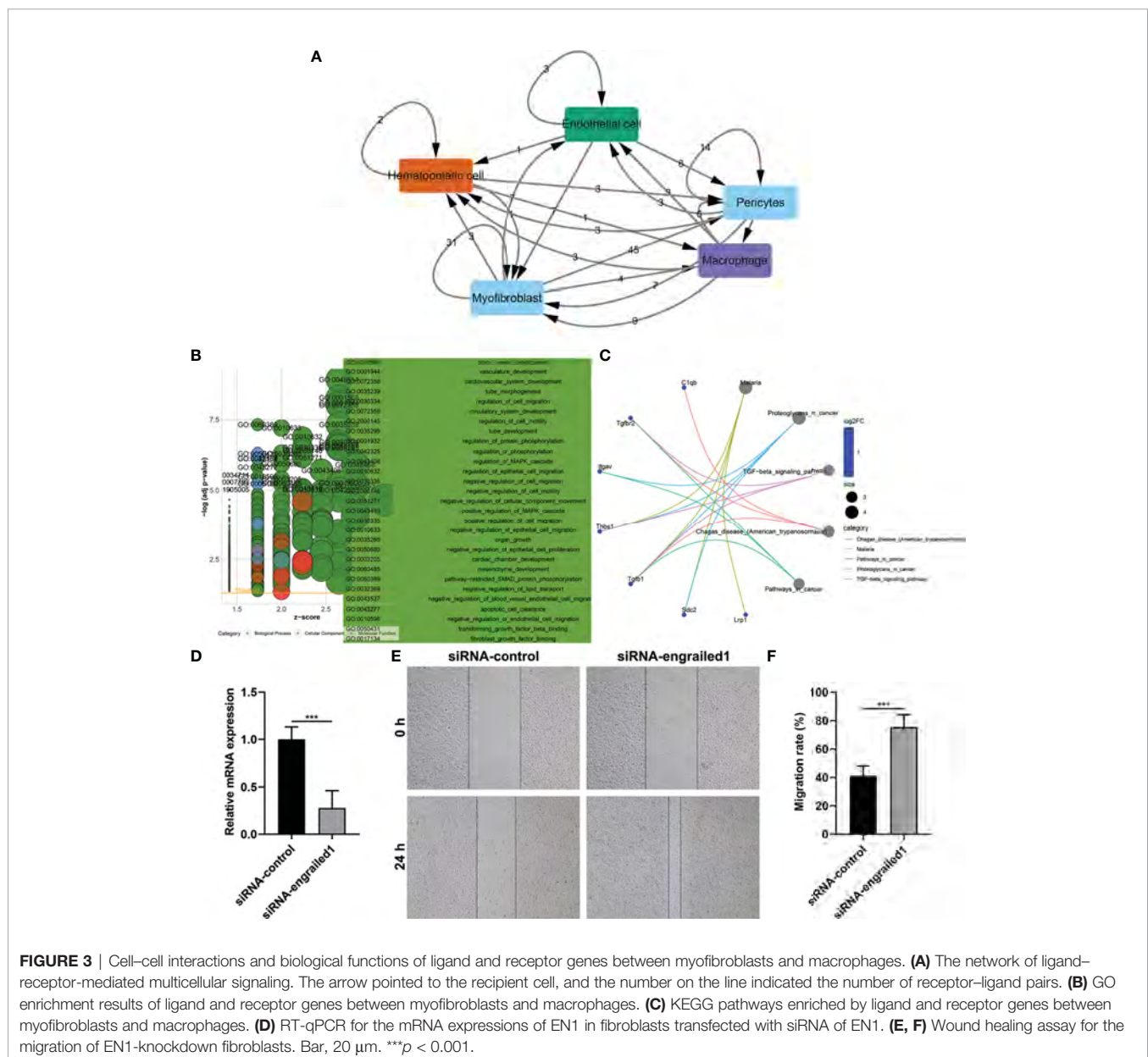
Cell–Cell Interactions Based on Ligand–Receptor Interactions

Wound healing is a complex process that necessitates the collaborative efforts of diverse cell lineages (21). Cell-to-cell communications across diverse cell types thoroughly govern appropriate functions of metazoans as well as widely rely on interactions between secreted ligands and cell-surface receptors. Based on the marker genes, ligand–receptor interactions were matched. The number of ligands/receptors for myofibroblasts, pericytes, endothelial cells, macrophages, and hematopoietic cells

was 114, 91, 32, 28 and 17, respectively (Figure 3A). According to the number of intercellular receptor–ligand pairs, we screened out myofibroblasts as the core cell population.

Biological Functions of Ligand and Receptor Genes Between Myofibroblasts and Macrophages

We further evaluated the biological functions of ligand and receptor genes between myofibroblasts and macrophages. Our results demonstrated that ligand and receptor genes between myofibroblasts and macrophages were mainly involved in tube morphogenesis and development, regulation of cell migration, and motility (Figure 3B). Moreover, we found that the TGF- β signaling pathway was markedly enriched by these



ligand and receptor genes between myfibroblasts and macrophages (Figure 3C).

Knockdown of EN1 Facilitates Fibroblast Migration

We further verified the effects of EN1 on the migration of fibroblasts. Firstly, siRNA against EN1 was designed and transected into fibroblasts. RT-qPCR demonstrated that EN1 mRNA expression was distinctly reduced following siRNA-EN1 transfection (Figure 3D). According to wound healing results, EN1-knockout fibroblasts displayed significantly enhanced migration capacity (Figures 3E, F). Hence, EN1 suppression enabled to facilitate fibroblast migration.

Identification of Specific Genes Between Fibrotic and Regenerative Myfibroblasts and Their Biological Functions

With the cutoffs of $|FC| > 1.2$ and $p < 0.05$, we identified 546 up- and 481 downregulated specific genes in regenerative compared to fibrotic myfibroblasts (Figures 4A–C). Table 2 lists the first 20 up- and downregulated specific genes between regenerative and fibrotic myfibroblasts. As depicted in Figure 4D, we observed that the specific genes markedly participated in

collagen-containing extracellular matrix, posttranscriptional regulation of gene expression, positive regulation of cell migration, mRNA metabolic process, and apoptotic signaling pathway. Moreover, ribosome and thermogenesis were prominently enriched by the specific genes (Figure 4E).

Identification of Specific Genes Between Fibrotic and Regenerative Macrophages and Their Biological Functions

With the cutoffs of $|FC| > 1.2$ and $p < 0.05$, we found that 100 specific genes were significantly upregulated while 197 specific genes were significantly downregulated in regenerative compared to fibrotic macrophages (Figures 5A–C). Table 3 lists the first 20 up- and downregulated specific genes between fibrotic and regenerative macrophages. GO enrichment analysis uncovered that the specific genes were markedly involved in the negative regulation of programmed cell death, the regulation of cell migration, innate immune response and apoptotic signaling pathway, collagen-containing extracellular matrix, the positive regulation of T cell activation, and response to interferon γ (Figure 5D). Moreover, we observed that antigen processing and presentation, pathways in cancer, phagosome, ribosome, and tuberculosis were prominently enriched by the specific genes (Figure 5E).

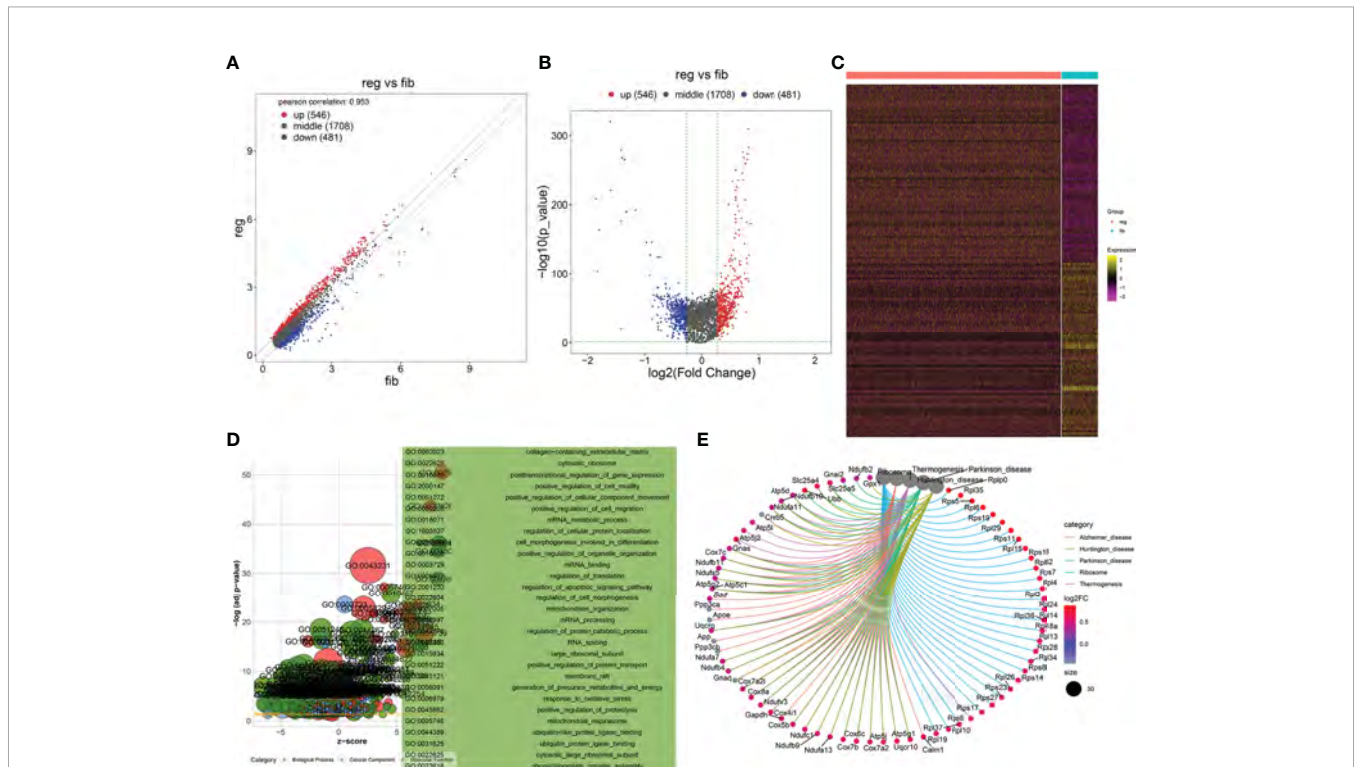


FIGURE 4 | Identification of specific genes between fibrotic and regenerative myfibroblasts and their biological functions. (A, B) Scatter plots and volcano diagram for the up- and downregulated specific genes in regenerative (reg) compared to fibrotic (fib) myfibroblasts. Red dots meant upregulated genes while blue dots meant downregulated genes. (C) Heatmap visualizing the expression patterns of the specific genes in fibrotic and regenerative myfibroblasts. Yellow represented upregulation and purple represented downregulation. (D) GO enrichment results of specific genes that were abnormally expressed between fibrotic and regenerative myfibroblasts. (E) KEGG pathways involved in specific genes that were abnormally expressed between fibrotic and regenerative myfibroblasts.

TABLE 2 | The first 20 up- and downregulated specific genes between fibrotic and regenerative myofibroblasts.

Gene	log2FC	p-value	Q-value	Regenerative	Fibrotic
Rplp0	0.870992	0	0	5.166991	4.295999
Ifitm2	0.843781	1.12E-173	1.94E-169	3.837826	2.994046
Mfap5	0.826158	5.93E-128	1.03E-123	4.591184	3.765026
Lgals1	0.820706	4.86E-284	8.43E-280	6.19352	5.372813
Hist1h2bc	0.81979	4.50E-90	7.81E-86	2.042755	1.222965
Serf2	0.805752	1.37E-310	2.39E-306	4.973459	4.167707
Rpl35	0.801322	0	0	5.164454	4.363133
Rps5	0.795055	5.07E-274	8.79E-270	4.725084	3.930029
Basp1	0.794315	1.55E-93	2.69E-89	2.268422	1.474106
Rpl6	0.792999	4.84E-266	8.40E-262	4.489802	3.696803
Ybx1	0.791379	6.39E-117	1.11E-112	2.98192	2.19054
Rps19	0.790084	0	0	5.198609	4.408525
Ost4	0.782118	2.55E-123	4.42E-119	3.079057	2.296939
Rpl29	0.780779	1.14E-175	1.98E-171	3.875578	3.094799
H19	0.767949	8.58E-45	1.49E-40	3.185378	2.417429
Rps11	0.763653	3.10E-260	5.37E-256	4.655295	3.891641
Rpl15	0.760256	2.28E-207	3.96E-203	4.262648	3.502392
Ifi20	0.758	1.47E-93	2.55E-89	2.397842	1.639842
Ssr4	0.745387	2.11E-101	3.67E-97	2.89302	2.147633
Ubb	0.744921	1.14E-144	1.97E-140	4.529784	3.784862
mt-Nd4l	-2.08112	0	0	0.883721	2.964844
mt-Atp6	-1.85976	0	0	5.349053	7.20881
Hspa1b	-1.85125	4.49E-209	7.79E-205	0.611879	2.463132
mt-Co2	-1.84169	0	0	4.106449	5.948142
AC160336.1	-1.81875	4.98E-104	8.63E-100	0.763221	2.58197
Hspa1a	-1.79337	2.08E-164	3.61E-160	1.385872	3.179244
mt-Nd4	-1.60147	3.51E-321	6.08E-317	3.543676	5.145146
mt-Nd5	-1.59322	2.78E-221	4.83E-217	1.144946	2.738165
mt-Cytb	-1.57454	0	0	4.565919	6.140456
Igfbp2	-1.4162	1.28E-20	2.21E-16	2.045862	3.462061
mt-Nd3	-1.41514	1.13E-177	1.96E-173	1.403288	2.818428
mt-Nd1	-1.4142	4.61E-280	8.00E-276	4.509633	5.923829
mt-Co3	-1.39259	1.24E-268	2.15E-264	5.529273	6.921861
mt-Co1	-1.35374	1.30E-265	2.26E-261	5.598606	6.952347
mt-Nd2	-1.32088	1.81E-190	3.14E-186	2.765453	4.086338
Gm26917	-1.31863	7.03E-191	1.22E-186	0.653702	1.972335
Cd74	-1.15624	2.79E-193	4.84E-189	0.624805	1.781046
Lars2	-0.96874	2.21E-146	3.83E-142	0.232192	1.200933
Luc7l2	-0.91132	1.16E-98	2.01E-94	1.18695	2.098275
Hspg2	-0.90368	3.60E-128	6.24E-124	2.381196	3.284878

PPI Network Analysis of Specific Genes Between Fibrotic and Regenerative Myofibroblasts or Macrophages

With the STRING tool, we probed the interactions between myofibroblast- or macrophage-specific gene-encoded proteins. In **Figure 6A**, there were 616 nodes in the PPI network of myofibroblasts, reflecting the close interactions of myofibroblast-specific gene-encoded proteins. According to degree, the top 20 nodes were identified as hub genes, including Rps27a, Rps11, Rps23, Rps3, Rps5, Rps15a, Rps6, Rps9, Rps13, Rps14, Rps25, Rps3a1, Rps27, Rps8, Rps19, Rps28, Rps7, Rpl8, Rps18, Rpl26, Rpl32, and Rps16, indicating that the above genes were the core of the network. **Figure 6B** depicts the interactions between macrophage-specific gene-encoded proteins. The 20 hub genes were as follows: Uba52, Rps9, Gnb2l1, Rpl27, Rpl38, Rps13, Rps15a, Fau, Rpl18, Rpl30, Rpl35a, Rpl7, Rpl2, Rps24, Rpl13a, Rpl4, Rps10, Rps12, Rps27rt, and Rps2. The above genes deserve in-depth explorations.

Reconstruction of the Temporal Dynamics of Myofibroblast and Macrophage

To investigate the underlying evolution among myofibroblasts and macrophages, this study adopted the Monocle tool to reveal a pseudotemporal ordering for the similarity of cell clusters with developmental lineages. For myofibroblasts, the results clearly demonstrated the uniform development of myofibroblasts from cluster 6 to cluster 10 (**Figure 7A**). The trends of pseudotime-dependent genes along the pseudo-timeline were divided into six cell clusters of myofibroblasts with diverse expression dynamics. Furthermore, we observed that macrophage under fibrotic conditions was in the beginning position of the differentiation process and was sequentially transformed into macrophage under regenerative conditions (**Figure 7B**).

GSVA Between Clusters 6 and 10 of Fibrotic and Regenerative Myofibroblasts

According to the results of pseudotime analysis of myofibroblasts, we carried out GSVA between the initially differentiated cluster 6

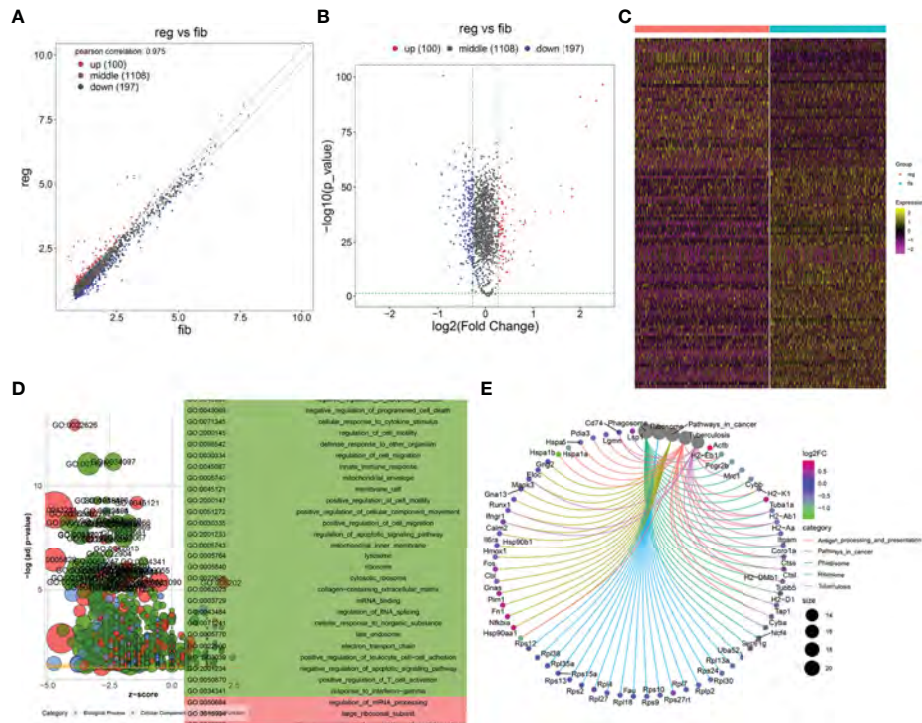


FIGURE 5 | Identification of specific genes between fibrotic and regenerative macrophages and their biological functions. **(A, B)** Scatter plots and volcano diagram showing the up- and downregulated specific genes in regenerative (reg) compared to fibrotic (fib) macrophages. Red dots meant upregulated genes while blue dots meant downregulated genes. **(C)** Heatmap visualizing the expression patterns of the specific genes in fibrotic and regenerative macrophages. Yellow represented upregulation and purple represented downregulation. **(D)** GO enrichment results of specific genes that were abnormally expressed between fibrotic and regenerative macrophages. **(E)** KEGG pathways involved in specific genes that were abnormally expressed between fibrotic and regenerative macrophages.

and the final differentiated cluster 10. Compared with cluster 10 of myofibroblasts in fibrotic and regenerative dermal cells, biological processes such as the metabolic process significantly activated cluster 6 of myofibroblasts in fibrotic and regenerative dermal cells (**Figure 8A**). As depicted in **Figure 8B**, we noticed the prominent activation of cellular components such as mitochondria in cluster 6 of fibrotic and regenerative myofibroblasts in comparison to those in cluster 10. Moreover, we observed that fibrotic and regenerative myofibroblasts in cluster 6 had significantly activated molecular functions like oxidoreductase activity compared with fibrotic and regenerative myofibroblasts in cluster 10 (**Figure 8C**). We also compared the differences in KEGG pathways between clusters. Diverse signaling pathways like metabolic pathways, RNA transport, spliceosome, thermogenesis, oxidative phosphorylation, carbon metabolism, ribosome, cell cycle, protein processing in the endoplasmic reticulum, and biosynthesis of amino acids were prominently activated in fibrotic and regenerative myofibroblasts in cluster 6 compared to those in cluster 10 (**Figure 8D**).

GSVA Between Fibrotic and Regenerative Macrophages

GSVA was also presented between fibrotic and regenerative macrophages. In **Figure 9A**, we determined that biological processes such as the metabolic process and immune response

were markedly activated in fibrotic macrophages compared to regenerative macrophages. The significantly activated cellular components such as the spliceosomal complex, catalytic complex, ribonucleoprotein complex, nuclear lumen, nucleoplasm, nucleolus, cytosol, nucleus, catalytic step 2 spliceosome, chromosome, and protein-containing complex were found in fibrotic macrophages compared with regenerative macrophages (**Figure 9B**). As shown in **Figure 9C**, we investigated the marked activation of molecular functions like RNA binding, ATP binding, mRNA binding, adenylyl ribonucleotide binding, adenylyl nucleotide binding, drug binding, nucleic acid binding, heterocyclic compound binding, organic cyclic compound binding, and ATPase activity in fibrotic macrophages in comparison to regenerative macrophages. Moreover, our results showed that KEGG pathways such as spliceosome, NOD-like receptor signaling pathway, Fc gamma R-mediated phagocytosis, antigen processing and presentation, endocytosis, necroptosis, and natural killer cell-mediated cytotoxicity displayed marked activation in fibrotic macrophages compared to regenerative macrophages (**Figure 9D**).

DISCUSSION

Skin wound healing involves complicated coordinated interactions within cells. Through scRNA-seq data, this study identified six cell

TABLE 3 | The first 20 up- and downregulated specific genes between fibrotic and regenerative macrophages.

Gene name	log2FC	p-value	Q-value	Regenerative	Fibrotic
Sparc	2.474022	3.60E-97	6.24E-93	5.010571	2.536548
Col1a1	2.33817	6.49E-90	1.13E-85	5.266303	2.928133
Col1a2	2.13485	3.01E-78	5.21E-74	5.327119	3.192269
Col3a1	2.005563	1.16E-91	2.01E-87	5.223726	3.218163
Dcn	1.836106	2.30E-46	3.98E-42	2.785851	0.949745
Bgn	1.83586	5.99E-50	1.04E-45	2.600128	0.764269
Fstl1	1.648779	1.28E-39	2.22E-35	2.200177	0.551399
Postn	1.572566	2.54E-51	4.40E-47	2.775437	1.202871
Mfap5	1.370976	2.18E-39	3.79E-35	2.023966	0.65299
Hbb-bs	1.031846	1.21E-39	2.10E-35	2.844128	1.812282
Cxcl2	1.004274	2.60E-15	4.51E-11	3.268016	2.263742
Actb	0.934603	1.46E-21	2.53E-17	7.663418	6.728815
Klf2	0.828223	1.34E-34	2.33E-30	2.497856	1.669632
Timp2	0.824526	1.09E-35	1.89E-31	1.978589	1.154062
Neat1	0.789153	1.13E-33	1.96E-29	2.328203	1.53905
Nfkbia	0.718421	2.88E-35	4.99E-31	2.761737	2.043317
Lgals1	0.61418	3.23E-47	5.60E-43	4.783109	4.168928
Fn1	0.610899	5.21E-31	9.03E-27	3.726565	3.115666
Pim1	0.59329	1.34E-26	2.32E-22	2.966403	2.373113
Cd63	0.592092	2.84E-21	4.92E-17	2.447508	1.855417
Hspa1b	-1.44863	2.08E-61	3.60E-57	1.266466	2.715092
Hsp90aa1	-0.957	1.59E-41	2.76E-37	2.518111	3.475109
Gm26917	-0.91834	3.81E-57	6.61E-53	0.782974	1.701314
Gm42418	-0.91626	1.85E-56	3.20E-52	1.082872	1.999131
Tpt1	-0.89005	3.21E-101	5.57E-97	4.517284	5.40733
mt-Nd5	-0.87923	1.13E-46	1.96E-42	0.858755	1.737986
Hspa1a	-0.83491	4.80E-34	8.32E-30	3.320621	4.155527
mt-Co2	-0.78506	1.59E-46	2.76E-42	3.967573	4.752638
mt-Atp6	-0.77046	5.82E-42	1.01E-37	4.934988	5.70545
Mycbp2	-0.75645	1.65E-49	2.86E-45	0.967289	1.723739
H2-Eb1	-0.75235	6.73E-15	1.17E-10	5.220528	5.972878
Fcgr2b	-0.75221	7.44E-61	1.29E-56	1.801335	2.553547
Mrc1	-0.72837	6.62E-26	1.15E-21	1.012111	1.740482
mt-Nd4l	-0.67023	7.15E-38	1.24E-33	0.682842	1.35307
AC160336.1	-0.65981	5.00E-25	8.66E-21	1.805651	2.465465
Prkcd	-0.6507	2.95E-59	5.12E-55	1.387319	2.038016
Cybb	-0.64225	8.79E-67	1.52E-62	1.99459	2.636836
Tgfb1	-0.63629	6.10E-51	1.06E-46	2.746255	3.382547
H2-K1	-0.62809	3.72E-45	6.44E-41	2.787025	3.415118
Irf5	-0.61724	5.52E-41	9.58E-37	2.037704	2.654947

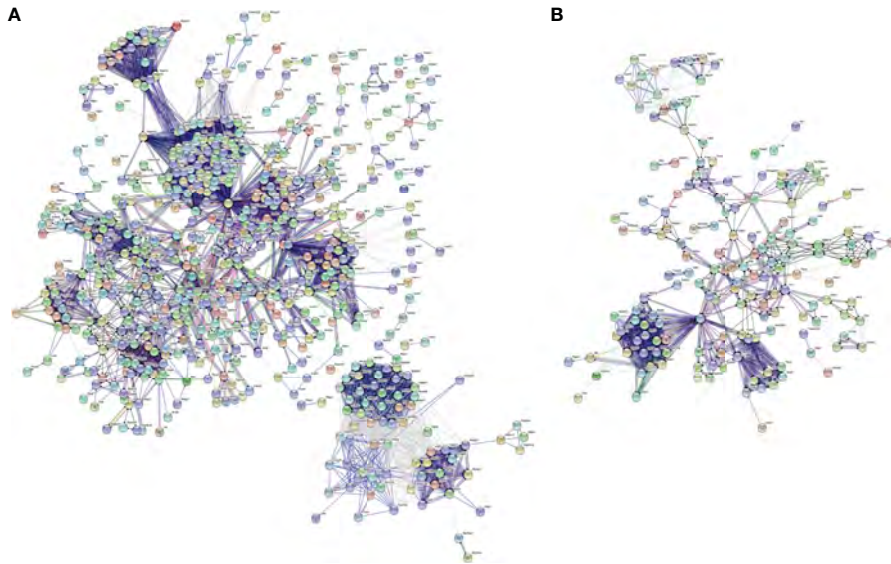


FIGURE 6 | PPI network analysis of specific genes between fibrotic and regenerative myfibroblasts or macrophages. **(A)** The PPI network of specific genes between fibrotic and regenerative myfibroblasts. **(B)** The PPI network of specific genes between fibrotic and regenerative macrophages.

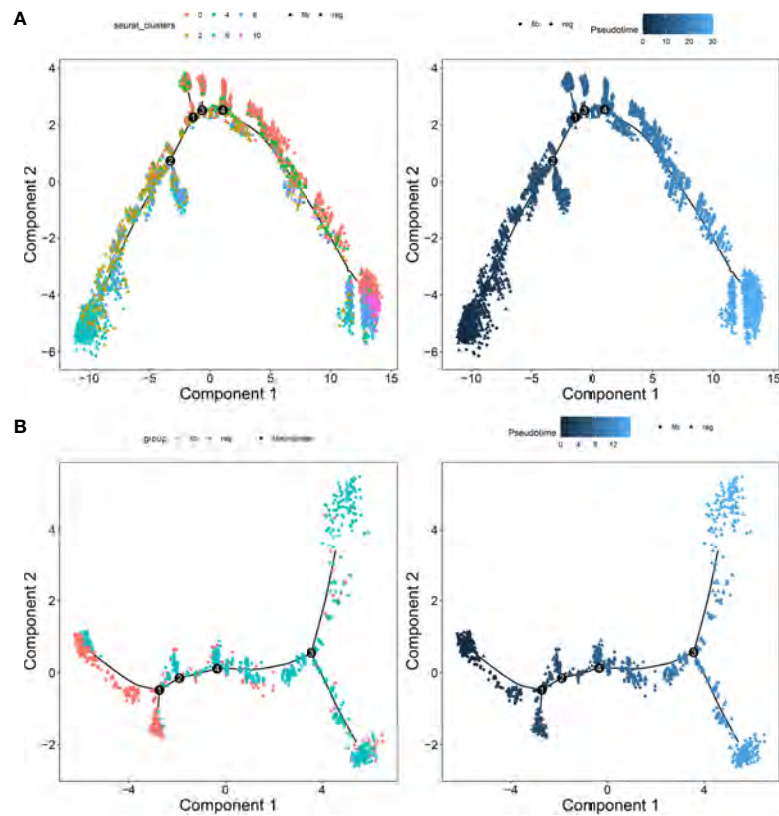


FIGURE 7 | Pseudotime ordering of myfibroblasts and macrophages. **(A)** Myfibroblasts and **(B)** macrophages. Each dot represented one cell and each branch represented one cell state. The left plot was labeled with cell states and the right plot was labeled with developmental time.

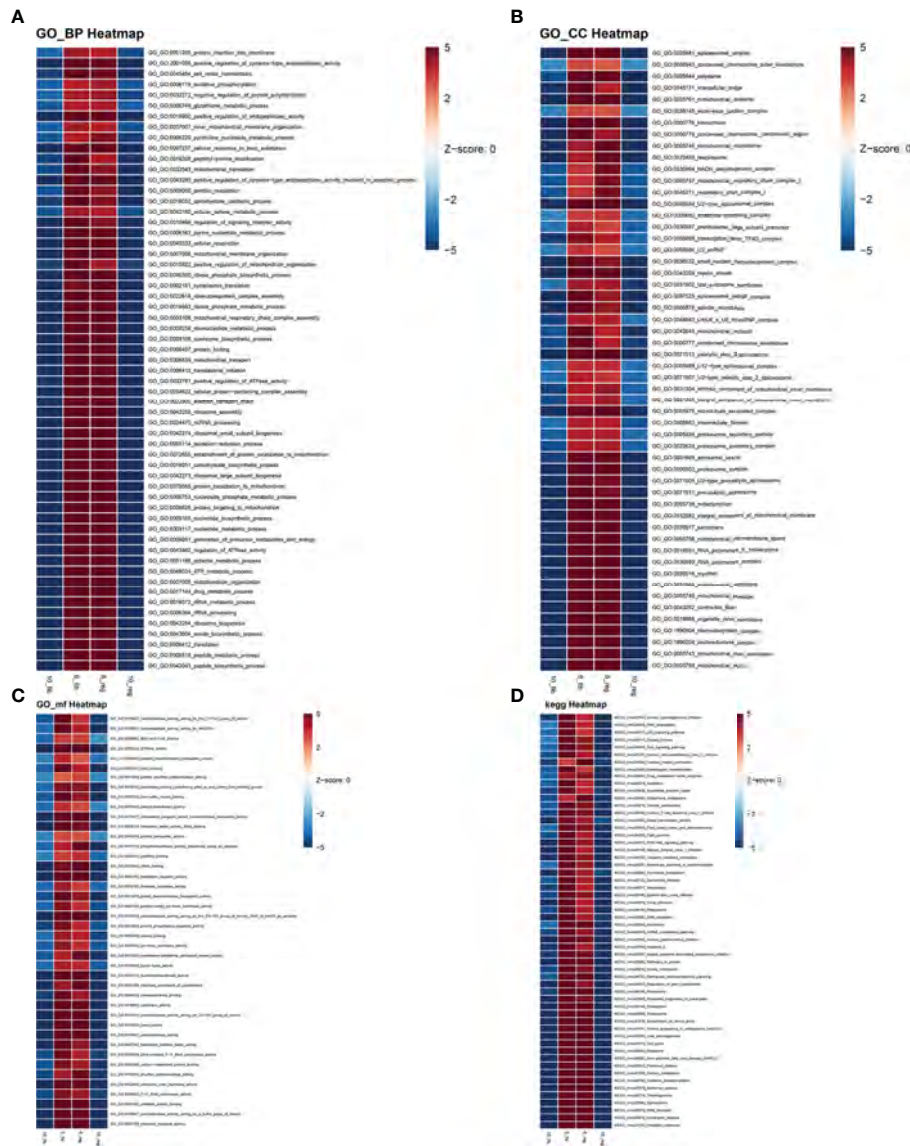


FIGURE 8 | GSEA between clusters 6 and 10 of fibrotic and regenerative myfibroblasts. **(A–D)** Heatmaps showing the differences in activation of biological processes, cellular components, molecular functions, and KEGG pathways between clusters 6 and 10 of fibrotic (fib) and regenerative (reg) myfibroblasts.

populations, namely, EN1-negative myfibroblasts, EN1-positive myfibroblasts, hematopoietic cells, macrophages, pericytes, and endothelial cells, across the dermis. Evidence suggests that EN1-positive fibroblasts are known to function in scarring, and EN1-negative fibroblasts yield wound regeneration. Thus, we used EN1 as a marker to divide the subgroups. Dynamic cellular events after skin injury rely on bidirectional cell–cell communications against effective wound healing (22). Our results demonstrated the cross-talks between myfibroblasts, hematopoietic cells, macrophages, pericytes, and endothelial cells in the dermis based on the ligand–receptor interactions. As per previous studies, CX3CR1 may mediate the recruitment of bone marrow-derived monocytes or macrophages in skin wound healing, thereby releasing profibrotic

as well as angiogenic mediators (23). Moreover, macrophages support proliferation and heterogeneity of myfibroblasts in skin repair (24). Serum endothelial cell-derived extracellular vesicles facilitate diabetic wound healing *via* enhancing myfibroblast proliferation and decreasing senescence (25). Intradermal adipocytes modulate the recruitment of myfibroblasts in skin wound healing (26). Fibroblasts promote NG²⁺ pericyte populations in murine skin development as well as repair (27). On the basis of the above lines of evidence, there were remarkable interplays between diverse cell types during dermis progression. According to the number of ligands and receptors, we identified myfibroblasts as the core cell population. Our function enrichment analyses uncovered that the ligand and receptor

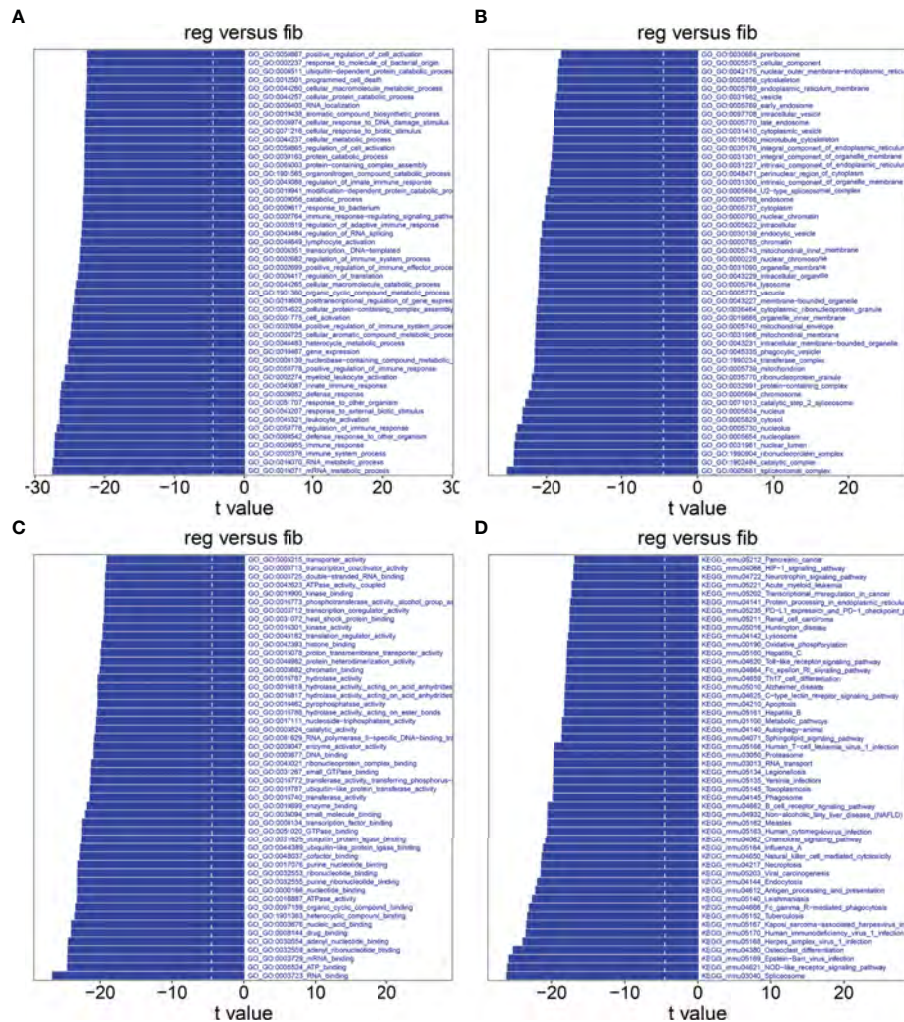


FIGURE 9 | GSVA between fibrotic and regenerative macrophages. (A–D) Heatmaps visualizing the differences in activation of biological processes, cellular components, molecular functions, and KEGG pathways between fibrotic (fib) and regenerative (reg) macrophages.

genes between myfibroblasts and macrophages were mainly involved in regulating cell proliferation and migration, tube development, and the TGF- β pathway. The TGF- β signaling pathway plays an important role in the formation of collagen in fibroblasts and myfibroblasts (28). Cytokine TGF- β may induce dermal dendritic cells to express IL-31, thereby activating sensory neurons as well as stimulating wound itching during skin wound healing (29). Hence, targeting the TGF- β pathway is the promising therapeutic intervention to reduce abnormal skin scar formation.

To explore the differences in molecular mechanisms involving myfibroblasts between fibrotic and regenerative wound healing fates, we identified 546 up- and 481 downregulated specific genes in regenerative compared to fibrotic myfibroblasts. This revealed the heterogeneity of myfibroblasts between fibrotic and regenerative wound healing. Our GO and KEGG enrichment analysis uncovered the key biological functions involving the specific genes between fibrotic and regenerative myfibroblasts. As a

result, these specific genes between fibrotic and regenerative myfibroblasts prominently participated in the mRNA metabolic process and organelle organization. Extracellular matrix of connective tissues is synthesized by myfibroblasts that play a critical role in sustaining the structural integrity of various tissues (30).

Skin wound macrophage is an important regulator of skin repair, and its dysfunction may cause chronic and non-healing skin wounds (31). Further analysis identified that 100 specific genes were significantly upregulated while 197 specific genes were significantly downregulated in regenerative compared to fibrotic macrophages. Functional enrichment analysis uncovered that these specific genes between fibrotic and regenerative macrophages primarily participated in regulating inflammatory response, immunity, and phagocytosis. Immunity is the most important function of the skin, which can prevent harmful exposure from the external and internal environment (32).

Furthermore, late wound macrophage phagocytosis of the Wnt inhibitor may induce chronic Wnt activity during fibrotic skin healing (11). Collectively, our findings revealed that the heterogeneity of myofibroblasts or macrophages might determine wound healing fate as regenerative or fibrotic.

CONCLUSION

Taken together, this study uncovered cellular functional heterogeneity in dermis between fibrotic and regenerative wound healing fates. Moreover, myofibroblasts and macrophages may change the skin wound healing fates by modulating critical signaling pathways. Therefore, our data provided an insight into the development of more effective therapeutic interventions for improving healing fates.

DATA AVAILABILITY STATEMENT

The datasets presented in this study can be found in online repositories. The names of the repository/repositories and accession number(s) can be found at: <https://www.ncbi.nlm.nih.gov/>, GSM4213633; <https://www.ncbi.nlm.nih.gov/>, GSM4213632; <https://www.ncbi.nlm.nih.gov/>, GSE141814.

ETHICS STATEMENT

Ethical review and approval were not required for the study on human participants in accordance with the local legislation and institutional requirements. Written informed consent for participation was not required for this study in accordance with the national legislation and the institutional requirements. The animal study was reviewed and approved by Keio University

REFERENCES

- Rajesh A, Stuart G, Real N, Tschirley A, Ahn J, Wise L, et al. Skin Antigen-Presenting Cells and Wound Healing: New Knowledge Gained and Challenges Encountered Using Mouse Depletion Models. *Immunology* (2021) 163(1):98–104. doi: 10.1111/imm.13311
- Griffin DR, Archang MM, Kuan C-H, Weaver WM, Weinstein JS, Feng AC, et al. Activating an Adaptive Immune Response From a Hydrogel Scaffold Imparts Regenerative Wound Healing. *Nat Mater* (2021) 20(4):560–9. doi: 10.1038/s41563-020-00844-w
- Yamaguchi K, Kanno E, Tanno H, Sasaki A, Kitai Y, Miura T, et al. Distinct Roles for Dectin-1 and Dectin-2 in Skin Wound Healing and Neutrophilic Inflammatory Responses. *J Invest Dermatol* (2021) 141(1):164–76.e8. doi: 10.1016/j.jid.2020.04.030
- Chen T-Y, Wen T-K, Dai N-T, Hsu S-H. Cryogel/hydrogel Biomaterials and Acupuncture Combined to Promote Diabetic Skin Wound Healing Through Immunomodulation. *Biomaterials* (2021) 269:120608. doi: 10.1016/j.biomaterials.2020.120608
- Rodrigues M, Kosaric N, Bonham CA, Gurtner GC. Wound Healing: A Cellular Perspective. *Physiol Rev* (2019) 99(1):665–706. doi: 10.1152/physrev.00067.2017

School of Medicine. Written informed consent was not obtained from the individual(s) for the publication of any potentially identifiable images or data included in this article.

AUTHOR CONTRIBUTIONS

C-JC, HK, and KT: conception or design of the work. C-JC, HK, KT, NA-H, SS, TA, and KK: acquisition, analysis, or interpretation of data. C-JC, HK, KT, NA-H, SS, TA, and KK: drafting the manuscript or revising it critically for important intellectual content. All authors contributed to the article and approved the submitted version.

FUNDING

This work was supported in part by Japan China Sasakawa Medical Fellowship (2017816).

SUPPLEMENTARY MATERIAL

The Supplementary Material for this article can be found online at: <https://www.frontiersin.org/articles/10.3389/fimmu.2022.875407/full#supplementary-material>

Supplementary Figure 1 | Quality control of scRNA-seq data of fibrotic and regenerative wound dermal cells. **(A, B)** Barcode rank plots separately showing the detected knee and inflection points for fibrotic and regenerative wound dermal cells. **(C, D)** The expression of all genes, ribosomal genes, and mitochondrial genes in each cell was shown for fibrotic and regenerative wound dermal cells. **(E, F)** The proportions of mitochondrial and ribosomal genes expressed in each cell were counted for fibrotic and regenerative wound dermal cells.

Supplementary Table 1 | The list of novel marker genes identified in each cell type.

- Aragona M, Dekoninck S, Rulands S, Lenglez S, Mascré G, Simons BD, et al. Defining Stem Cell Dynamics and Migration During Wound Healing in Mouse Skin Epidermis. *Nat Commun* (2017) 8:14684. doi: 10.1038/ncomms14684
- Govindaraju P, Todd L, Shetye S, Monslow J, Puré E. CD44-Dependent Inflammation, Fibrogenesis, and Collagenolysis Regulates Extracellular Matrix Remodeling and Tensile Strength During Cutaneous Wound Healing. *Matrix Biol* (2019) 75–6:314–30. doi: 10.1016/j.matbio.2018.06.004
- Haensel D, Jin S, Sun P, Cinco R, Dragan M, Nguyen Q, et al. Defining Epidermal Basal Cell States During Skin Homeostasis and Wound Healing Using Single-Cell Transcriptomics. *Cell Rep* (2020) 30(11):3932–47.e6. doi: 10.1016/j.celrep.2020.02.091
- Theocharidis G, Baltzis D, Roustit M, Tellechea A, Dangwal S, Khetani RS, et al. Integrated Skin Transcriptomics and Serum Multiplex Assays Reveal Novel Mechanisms of Wound Healing in Diabetic Foot Ulcers. *Diabetes* (2020) 69(10):2157–69. doi: 10.2337/db20-0188
- Guerrero-Juarez CF, Dedhia PH, Jin S, Ruiz-Vega R, Ma D, Liu Y, et al. Single-Cell Analysis Reveals Fibroblast Heterogeneity and Myeloid-Derived Adipocyte Progenitors in Murine Skin Wounds. *Nat Commun* (2019) 10(1):650. doi: 10.1038/s41467-018-08247-x
- Gay D, Ghinatti G, Guerrero-Juarez CF, Ferrer RA, Ferri F, Lim CH, et al. Phagocytosis of Wnt Inhibitor SFRP4 by Late Wound Macrophages Drives

- Chronic Wnt Activity for Fibrotic Skin Healing. *Sci Adv* (2020) 6(12): eay3704. doi: 10.1126/sciadv.aay3704
12. Lun ATL, Riesenfeld S, Andrews T, Dao TP, Gomes T, Marioni JC. EmptyDrops: Distinguishing Cells From Empty Droplets in Droplet-Based Single-Cell RNA Sequencing Data. *Genome Biol* (2019) 20(1):63. doi: 10.1186/s13059-019-1662-y
 13. McCarthy DJ, Campbell KR, Lun ATL, Wills QF. Scater: Pre-Processing, Quality Control, Normalization and Visualization of Single-Cell RNA-Seq Data in R. *Bioinformatics* (2017) 33(8):1179–86. doi: 10.1093/bioinformatics/btw777
 14. Butler A, Hoffman P, Smibert P, Papalexi E, Satija R. Integrating Single-Cell Transcriptomic Data Across Different Conditions, Technologies, and Species. *Nat Biotechnol* (2018) 36(5):411–20. doi: 10.1038/nbt.4096
 15. Ramiłowski JA, Goldberg T, Harshbarger J, Kloppmann E, Lizio M, Satagopam VP, et al. A Draft Network of Ligand-Receptor-Mediated Multicellular Signalling in Human. *Nat Commun* (2015) 6:7866. doi: 10.1038/ncomms8866
 16. Doncheva NT, Morris JH, Gorodkin J, Jensen LJ. Cytoscape StringApp: Network Analysis and Visualization of Proteomics Data. *J Proteome Res* (2019) 18(2):623–32. doi: 10.1021/acs.jproteome.8b00702
 17. Yu G, Wang L-G, Han Y, He Q-Y. ClusterProfiler: An R Package for Comparing Biological Themes Among Gene Clusters. *OMICS* (2012) 16(5):284–7. doi: 10.1089/omi.2011.0118
 18. Szklarczyk D, Gable AL, Lyon D, Junge A, Wyder S, Huerta-Cepas J, et al. STRING V11: Protein-Protein Association Networks With Increased Coverage, Supporting Functional Discovery in Genome-Wide Experimental Datasets. *Nucleic Acids Res* (2019) 47(D1):D607–13. doi: 10.1093/nar/gky1131
 19. Cao J, Spielmann M, Qiu X, Huang X, Ibrahim DM, Hill AJ, et al. The Single-Cell Transcriptional Landscape of Mammalian Organogenesis. *Nature* (2019) 566(7745):496–502. doi: 10.1038/s41586-019-0969-x
 20. Hänzelmann S, Castelo R, Guinney J. GSVA: Gene Set Variation Analysis for Microarray and RNA-Seq Data. *BMC Bioinf* (2013) 14:7. doi: 10.1186/1471-2105-14-7
 21. Sorkin M, Huber AK, Hwang C, Carson WF4, Menon R, Li J, et al. Regulation of Heterotopic Ossification by Monocytes in a Mouse Model of Aberrant Wound Healing. *Nat Commun* (2020) 11(1):722. doi: 10.1038/s41467-019-14172-4
 22. Zhou X, Brown BA, Siegel AP, El Masry MS, Zeng X, Song W, et al. Exosome-Mediated Crosstalk Between Keratinocytes and Macrophages in Cutaneous Wound Healing. *ACS Nano* (2020) 14(10):12732–48. doi: 10.1021/acsnano.0c03064
 23. Ishida Y, Gao J-L, Murphy PM. Chemokine Receptor CX3CR1 Mediates Skin Wound Healing by Promoting Macrophage and Fibroblast Accumulation and Function. *J Immunol* (2008) 180(1):569–79. doi: 10.4049/jimmunol.180.1.569
 24. Shook BA, Wasko RR, Rivera-Gonzalez GC, Salazar-Gatzimas E, López-Giráldez F, Dash BC, et al. Myofibroblast Proliferation and Heterogeneity are Supported by Macrophages During Skin Repair. *Science* (2018) 362(6417). doi: 10.1126/science.aar2971
 25. Wei F, Wang A, Wang Q, Han W, Rong R, Wang L, et al. Plasma Endothelial Cells-Derived Extracellular Vesicles Promote Wound Healing in Diabetes Through YAP and the PI3K/Akt/mTOR Pathway. *Aging (Albany NY)* (2020) 12(12):12002–18. doi: 10.18632/aging.103366
 26. Schmidt BA, Horsley V. Intradermal Adipocytes Mediate Fibroblast Recruitment During Skin Wound Healing. *Development* (2013) 140(7):1517–27. doi: 10.1242/dev.087593
 27. Goss G, Rognoni E, Salameti V, Watt FM. Distinct Fibroblast Lineages Give Rise to NG2+ Pericyte Populations in Mouse Skin Development and Repair. *Front Cell Dev Biol* (2021) 9:675080. doi: 10.3389/fcell.2021.675080
 28. Zhang T, Wang X-F, Wang Z-C, Lou D, Fang Q-Q, Hu Y-Y, et al. Current Potential Therapeutic Strategies Targeting the TGF- β /Smad Signaling Pathway To Attenuate Keloid and Hypertrophic Scar Formation. *BioMed Pharmacother* (2020) 129:110287. doi: 10.1016/j.biopha.2020.110287
 29. Xu J, Zanvit P, Hu L, Tseng P-Y, Liu N, Wang F, et al. The Cytokine TGF- β Induces Interleukin-31 Expression From Dermal Dendritic Cells to Activate Sensory Neurons and Stimulate Wound Itching. *Immunity* (2020) 53(2):371–83.e5. doi: 10.1016/j.immuni.2020.06.023
 30. Lynch MD, Watt FM. Fibroblast Heterogeneity: Implications for Human Disease. *J Clin Invest* (2018) 128(1):26–35. doi: 10.1172/JCI93555
 31. Chen H, Shi R, Luo B, Yang X, Qiu L, Xiong J, et al. Macrophage Peroxisome Proliferator-Activated Receptor γ Deficiency Delays Skin Wound Healing Through Impairing Apoptotic Cell Clearance in Mice. *Cell Death Dis* (2015) 6(1):e1597. doi: 10.1038/cddis.2014.544
 32. Matejuk A. Skin Immunity. *Arch Immunol Ther Exp (Warsz)* (2018) 66(1):45–54. doi: 10.1007/s00005-017-0477-3

Conflict of Interest: The authors declare that the research was conducted in the absence of any commercial or financial relationships that could be construed as a potential conflict of interest.

Publisher's Note: All claims expressed in this article are solely those of the authors and do not necessarily represent those of their affiliated organizations, or those of the publisher, the editors and the reviewers. Any product that may be evaluated in this article, or claim that may be made by its manufacturer, is not guaranteed or endorsed by the publisher.

Copyright © 2022 Chen, Kajita, Takaya, Aramaki-Hattori, Sakai, Asou and Kishi. This is an open-access article distributed under the terms of the Creative Commons Attribution License (CC BY). The use, distribution or reproduction in other forums is permitted, provided the original author(s) and the copyright owner(s) are credited and that the original publication in this journal is cited, in accordance with accepted academic practice. No use, distribution or reproduction is permitted which does not comply with these terms.

日中笹川医学奨学金制度<学位取得コース>評価書

論文博士：指導教官用



第 44 期

研究者番号：G4406

作成日：2024年3月10日

氏名	趙 宏波	ZHAO HONGBO	性別	M	生年月日	1980/10/11
所属機関（役職）	中国医学科学院肿瘤医院深圳医院胸外科（副主任醫師）					
研究先（指導教官）	東海大学医学部消化器外科上部消化管グループ（小柳 和夫 教授）					
研究テーマ	食道癌術後縫合不全に対する ICG 蛍光イメージング法の有用性の検討 To investigate the value of Indocyanine Green Fluorescence Imaging (ICGFI) in preventing postoperative anastomotic leakage after esophagectomy					
専攻種別	<input checked="" type="checkbox"/> 論文博士			<input type="checkbox"/> 課程博士		

研究者評価（指導教官記入欄）

成績状況	(優) 良 可 不可	取得単位数
		取得単位数 / 取得すべき単位数総数
学生本人が行った研究の概要	タイトル：食道癌術後縫合不全に対する ICG 蛍光イメージング法の有用性の検討 概要：食道癌再建胃管血流は縫合不全に関与する因子の一つである。われわれはこれまでに胃管血流速度の遅延が縫合不全に関与することを報告してきた。本研究では胃管作成時の切離線の違いが血流速度と縫合不全に関連するかどうかを検討した。結果として、右胃大網動静脈を温存することにより血流速度が速くなり、術後の縫合不全が減少することが分かった。現在、論文を作成し投稿中である。	
総合評価	【良かった点】 研究を熱心に行い論文作成まで終了した。 消化器外科グループのスタッフとも良好なコミュニケーションを図り、病棟回診や手術見学なども積極的に行った。	
	【改善すべき点】 コロナ感染症の影響もあったと考えるが、もう少し交流の輪が広がるとさらに有意義であったと考えられる。	
	【今後の展望】 本研究は食道癌術後の合併症回避において汎用性が高い。今後も研究継続が可能であるので、さらに研究を深めて後進の指導にもあたってほしい。	
学位取得見込	論文作成は済み現在、投稿中である。 Accept が得られたところで学位申請を行う見込みである。	
評価者（指導教官名） 小柳 和夫		

日中笹川医学奨学金制度<学位取得コース>報告書

研究者用



第44期

研究者番号: G4406

作成日: 2024年2月 18 日

氏名	赵宏波	ZHAO HONGBO	性別	M	生年月日	1980/10/11
所属機関(役職)	中国医学科学院肿瘤医院深圳医院胸外科(副主任醫師)					
研究先(指導教官)	東海大学医学部消化器外科上部消化管グループ(小柳 和夫 教授)					
研究テーマ	食道癌術後縫合不全に対するICG蛍光イメージング法の有用性の検討 To investigate the value of Indocyanine Green Fluorescence Imaging (ICGFI) in preventing postoperative anastomotic leakage after esophagectomy					
専攻種別	論文博士	<input checked="" type="checkbox"/>	課程博士	<input type="checkbox"/>		

1. 研究概要(1)

1) 目的 (Goal) This study aimed to investigate the effectiveness of a modified incision line on the lesser curvature for gastric conduit formation during esophagectomy in enhancing the perfusion of gastric conduit as determined by indocyanine green fluorescence imaging, and reducing the incidence of anastomotic leakage.

2) 戦略 (Approach) & 3) 材料と方法 (Materials and methods) 272 patients who underwent esophagectomy at our institute between 2014 and 2022 were enrolled in this study. These patients were divided based on two different types of cutlines on lesser curvature: Conventional group (n = 141) followed the traditional cutline, and Current group (n = 131) adopted a modified cutline. Gastric conduit perfusion was assessed by ICG fluorescence imaging and clinical outcomes after esophagectomy were evaluated.

4) 実験結果 (Results): The distance from pylorus to the cutline was significantly longer in Current group compared with Conventional group (median: 9.0 cm vs. 5.0 cm, $p < 0.001$). The blood flow speed in gastric conduit wall was significantly higher in Current group than in Conventional group (median: 2.81 cm/sec vs. 2.54 cm/sec, $p = 0.001$). Furthermore, anastomotic leakage was significantly lower ($p = 0.024$) and hospital stay was significantly shorter ($p < 0.001$) in Current group compared with Conventional group. Multivariate analysis identified blood flow speed in the gastric conduit wall as the only variable significantly associated with anastomotic leakage. Conclusions: ICG fluorescence imaging is a feasible, reliable method for assessment of gastric conduit perfusion. Modified lesser curvature cutline could enhance gastric conduit perfusion, promote blood circulation around anastomotic site, and reduce the risk of anastomotic leakage after esophagectomy.

5) 考察 (Discussion) In this study, we investigated the effectiveness of using a modified cutline on the gastric lesser curvature during esophagectomy to reduce the incidence of postoperative anastomotic leakage. The blood flow speed in the gastric conduit wall increased significantly with the use of the modified cutline on the gastric lesser curvature to preserve the entire RGA, thus, our proposed modification of the cutline resulted in improved perfusion of the gastric conduit. Furthermore, our findings revealed a significant reduction of anastomotic leakage for patients in which the modified cutline was performed. These findings further indicate the feasibility and reliability of ICG fluorescence imaging for intraoperative assessment of gastric conduit perfusion and suggest that modifying the lesser curvature cutline to preserve the entire RGA could be a promising strategy to minimize the risk of anastomotic leakage after esophagectomy.

Ischemia of the gastric conduit at the anastomotic site is widely acknowledged as a significant predisposing factor for anastomotic leakage. Early endoscopic assessments after esophagectomy have indicated that anastomotic defects predominantly occur in the region between the remaining esophagus and the proximal end of the longitudinal gastric staple line. In addition, unlike the greater curvature, which receives relatively higher blood flow from the right gastroepiploic artery, the lesser curvature side of the formed gastric conduit often lacks adequate arterial supply. These findings are also in accordance with clinical observations and prompt us to consider strategies to enhance blood perfusion in the gastric wall with the use of ICG fluorescence imaging.

The importance of preserving the right gastroepiploic artery for forming the gastric conduit is widely recognized in surgical practice, while handling of the RGA is currently not standardized and is mostly based on individual surgeons' preferences. In general, the fully intact stomach and wider gastric tube exhibit adequate vascularization, whereas a narrow gastric tube tends to show poor vascularization, particularly at the anastomosis site. In narrow gastric tubes, the right gastroepiploic artery is the only feeding artery (23,24). Furthermore, narrower gastric tubes may be associated with a wide disruption of the broad microscopic network of capillaries and arterioles in the submucosa of the lesser curvature. A larger width of the gastric conduit has been demonstrated as being significantly associated with improved gastric conduit perfusion and reduced risk of anastomotic leaks. Assuming that the length of the gastric conduit allows for sufficient anastomosis, preserving the RGA, which also allows retention of the right gastric vein, may be essential for maintaining adequate blood supply and improving the venous drainage for the gastric conduit wall based on its anatomical distribution and microvascular connections.

We adopted the strategy of preserving the entire RGA with a 3.5 cm width gastric conduit and verified its potential impact on the perfusion of the gastric conduit assessed by intraoperative ICG fluorescence imaging and the clinical outcomes. Our results revealed that adoption of a modified cutline on the gastric lesser curvature resulted in a significant increase in the distance from the pylorus to the cutline and a significantly shorter length of the gastric conduit as compared with that of the conventional cutline. However, we found that all of the preserved gastric conduits were sufficiently long to be pulled up to the neck for completion of the standard anastomosis in the area of ICG fluorescence imaging. We also found that preservation of the entire RGA led to a significantly improved blood flow speed within the gastric conduit, especially in the gastric wall. Furthermore, there was a positive correlation between improvement of the blood flow speed in the gastroepiploic artery and that in the gastric conduit wall. Some studies have demonstrated the existence of a correlation between the inflow and outflow of blood in the gastric conduit. For example, severe venous congestion in the gastric conduit could lead to a reduction in the inflow. We concluded from the above results that adoption of the modified strategy for gastric conduit formation led to significantly improved blood perfusion throughout the gastric conduit. Notably, preservation of the entire RGA resulted in a significantly lower incidence of anastomotic leakage and shorter hospital stays. We also found a significant negative correlation between anastomotic leakage and the blood flow speed in the gastric conduit wall. This is consistent with the theoretical expectation of a reduced incidence of anastomotic leakage after esophagectomy and shorter hospital stays with improved gastric conduit perfusion.

1. 研究概要(2)

Multivariable logistic regression analysis using data from the entire cohort identified the blood flow speed in the gastric conduit wall as the only variable showing a significant association with the risk of postoperative anastomotic leakage. A blood flow speed of ≤ 2.19 cm/s in the gastric conduit was found as a significant independent predictor for anastomotic leakage. This cutoff value for the blood flow speed in the gastric conduit was consistent with that reported from a previous study conducted in 2023, but higher than the cutoff values determined in two previous studies. In the first study, conducted in 2016, we determined a cutoff value of 1.76 cm/s, while in the second study, conducted in 2020, we determined a cutoff value of 2.07 cm/s. We speculate that in the first study, the small sample size could have limited our determination of the cutoff value, while in the second study, in which a significant number of patients with systemic atherosclerosis were included, systemic atherosclerosis could have impacted the microvascular perfusion of the capillary vessels of the gastric conduit, resulting in a lower calculated cutoff value. We propose to further explore the appropriate cutoff value for the blood flow speed in the gastric conduit wall to reduce the risk of anastomotic leakage in future studies.

There were several limitations of our study. First, the study was a retrospective investigation conducted at a single center, which may limit the generalizability of the results. Second, the difference in the periods in which the surgeries were performed could have introduced some bias. All patients who underwent surgery by the conventional method were operated before 2019, while all patients who underwent surgery by the modified method were operated after 2019. Third, a significant portion of anastomoses in our patient cohort were hand-sewn, and it has been found that a relatively short gastric conduit is sufficient when manual anastomosis is performed as compared with other anastomosis methods. Therefore, surgeons who prefer using other anastomosis methods than the manual method should interpret the results of our present study with caution.

In conclusion, it is feasible and reliable to assess gastric conduit perfusion intraoperatively by ICG fluorescence imaging with appropriate parameter settings. Moreover, preservation of the entire RGA during gastric conduit formation led to significantly improved vascular perfusion and reduced risk of anastomotic leakage after esophagectomy. Thus, this modified strategy for lesser curvature incision should be considered as the standard for handling the lesser curvature during esophagectomy with gastric conduit reconstruction.

6)参考文献(References)

1. Moody S, Senkin S, Islam SMA, Wang J, Nasrollahzadeh D, Cortez Cardoso Penha R, et al. Mutational signatures in esophageal squamous cell carcinoma from eight countries with varying incidence. *Nat Genet.* 2021 Nov;53(11):1553-63.
2. Kitagawa Y, Uno T, Oyama T, Kato K, Kato H, Kawakubo H, et al. Esophageal cancer practice guidelines 2017 edited by the Japan Esophageal Society: part 1. *Esophagus.* 2019 Jan;16(1):1-24.
3. Fabbi M, Hagens ERC, van Berge Henegouwen MI, Gisbertz SS. Anastomotic leakage after esophagectomy for esophageal cancer: definitions, diagnostics, and treatment. *Dis Esophagus.* 2021 Jan 11;34(1).
4. Takeuchi H, Miyata H, Gotoh M, Kitagawa Y, Baba H, Kimura W, et al. A risk model for esophagectomy using data of 5354 patients included in a Japanese nationwide web-based database. *Ann Surg.* 2014;260(2):259-66.
5. Koyanagi K, Ozawa S, Ninomiya Y, Oguma J, Kazuno A, Yatabe K, et al. Association between indocyanine green fluorescence blood flow speed in the gastric conduit wall and superior mesenteric artery calcification: predictive significance for anastomotic leakage after esophagectomy. *Esophagus.* 2021 Apr 1;18(2):248-57.
6. Ninomiya Y, Koyanagi K, Ozawa S, Oguma J, Kazuno A, Yatabe K, et al. Predictive impact of the thoracic inlet space on ICG fluorescence blood flow speed in the gastric conduit wall and anastomotic leakage after esophagectomy. *Esophagus.* 2023 Jan 1;20(1):81-8.
7. Koyanagi K, Ozawa S, Ninomiya Y, Yatabe K, Higuchi T, Yamamoto M, et al. Indocyanine green fluorescence imaging for evaluating blood flow in the reconstructed conduit after esophageal cancer surgery. *Vol. 52, Surgery Today.* Springer; 2022. p. 369-76.
8. Koyanagi K, Ozawa S, Oguma J, Kazuno A, Yamazaki Y, Ninomiya Y, et al. Blood flow speed of the gastric conduit assessed by indocyanine green fluorescence: New predictive evaluation of anastomotic leakage after esophagectomy. *Medicine (United States).* 2016 Jul 1;95(30).
9. Ishikawa Y, Breuler C, Chang AC, Lin J, Orringer MB, Lynch WR, et al. Quantitative perfusion assessment of gastric conduit with indocyanine green dye to predict anastomotic leak after esophagectomy. *Diseases of the Esophagus.* 2022 May 1;35(5).
10. Yoshimi F, Asato Y, Ikeda S, Okamoto K, Komuro Y, Imura J, et al. Using the supercharge technique to additionally revascularize the gastric tube after a subtotal esophagectomy for esophageal cancer. *Am J Surg.* 2006 Feb;191(2):284-7.
11. Ikeda Y, Niimi M, Kan S, Shatari T, Takami H, Kodaira S. Clinical significance of tissue blood flow during esophagectomy by laser doppler flowmetry. *J Thorac Cardiovasc Surg.* 2001 Dec;122(6):1101-6.
12. Ladak F, Dang JT, Switzer N, Mocanu V, Tian C, Birch D, et al. Indocyanine green for the prevention of anastomotic leaks following esophagectomy: a meta-analysis. *Vol. 33, Surgical Endoscopy.* Springer New York LLC; 2019. p. 384-94.
13. Polom K, Murawa D, Rho YS, Nowaczyk P, Hünerbein M, Murawa P. Current trends and emerging future of indocyanine green usage in surgery and oncology: a literature review. *Cancer.* 2011 Nov 1;117(21):4812-22.
14. Nishikawa K, Fujita T, Yuda M, Tanaka Y, Matsumoto A, Tanishima Y, et al. Quantitative assessment of blood flow in the gastric conduit with thermal imaging for esophageal reconstruction. *Ann Surg.* 2020 Jun 1;271(6):1087-94.
15. Thammineedi SR, Patnaik SC, Saksena AR, Ramalingam PR, Nusrath S. The utility of indocyanine green angiography in the assessment of perfusion of gastric conduit and proximal esophageal stump against visual assessment in patients undergoing esophagectomy: a prospective study. *Indian J Surg Oncol.* 2020 Dec 1;11(4):684-91.
16. Ng CSH, Ong BH, Chao YK, Wright GM, Sekine Y, Wong I, et al. Use of indocyanine green fluorescence imaging in thoracic and esophageal surgery. *Ann Thorac Surg.* 2023 Apr;115(4):1068-76.

1. 研究概要(3)

17. Kitagawa H, Namikawa T, Iwabu J, Yokota K, Uemura S, Munekage M, et al. Correlation between indocyanine green visualization time in the gastric tube and postoperative endoscopic assessment of the anastomosis after esophageal surgery. *Surg Today*. 2020 Nov 1;50(11):1375–82.
18. Jansen SM, de Bruin DM, van Berge Henegouwen MI, Strackee SD, Veelo DP, van Leeuwen TG, et al. Optical techniques for perfusion monitoring of the gastric tube after esophagectomy: a review of technologies and thresholds. *Dis Esophagus*. 2018 Jun 1;31(6).
19. Åkesson O, Heyman I, Johansson J, Rissler P, Falkenback D. Early endoscopic assessment after esophagectomy can predict anastomotic complications: a novel scoring system. *Surg Endosc*. 2022 Mar 1;36(3):1903–9.
20. Page RD, Asmat A, McShane J, Russell GN, Pennefather SH. Routine endoscopy to detect anastomotic leakage after esophagectomy. *Annals of Thoracic Surgery*. 2013 Jan;95(1):292–8.
21. Fujiwara H, Nakajima Y, Kawada K, Tokairin Y, Miyawaki Y, Okada T, et al. Endoscopic assessment 1 day after esophagectomy for predicting cervical esophagogastric anastomosis-relating complications. *Surg Endosc*. 2016 Apr 1;30(4):1564–71.
22. Kobayashi S, Kanetaka K, Yoneda A, Yamaguchi N, Kobayashi K, Nagata Y, et al. Endoscopic mucosal ischemic index for predicting anastomotic complications after esophagectomy: a prospective cohort study. *Langenbecks Arch Surg*. 2023 Jan 17;408(1):37.
23. Pierie JPEN, De Graaf PW, Van Vroonhoven TJM V, Obertopf H. The vascularization of a gastric tube as a substitute for the esophagus is affected by its diameter.
24. Liebermann-Meffert DM, Meier R, Siewert JR. Vascular anatomy of the gastric tube used for esophageal reconstruction. *Ann Thorac Surg*. 1992 Dec;54(6):1110–5.
25. Mingol-Navarro F, Ballester-Pla N, Jimenez-Rosellon R. Ischaemic conditioning of the stomach previous to esophageal surgery. *J Thorac Dis*. 2019 Apr;11(Suppl 5):S663–74.
26. Pather K, Deladisma AM, Guerrier C, Kriley IR, Awad ZT. Indocyanine green perfusion assessment of the gastric conduit in minimally invasive Ivor Lewis esophagectomy. *Surg Endosc*. 2022 Feb 1;36(2):896–903.

Esophageal squamous cell carcinoma (ESCC) is a serious health concern, particularly in regions like Japan and China where incidence rates are notably high. One of the most perilous complications that can arise after surgical removal of the esophagus, known as esophagectomy, is anastomotic leakage. This complication occurs when the connection between the remaining esophagus and the newly created gastric conduit fails to seal properly, leading to leakage of digestive fluids and potentially severe infections. Preventing such leaks is vital and has thus become a focal point in the field of esophageal surgery research.

To address this issue, surgeons have turned to the use of Indocyanine green (ICG) fluorescence during surgery. ICG is a fluorescent dye that, when injected into the bloodstream, emits light that can be detected by special cameras. This technology allows surgeons to evaluate the blood supply at the anastomosis site—a crucial factor in successful healing and prevention of leaks. By ensuring adequate blood flow to the area, surgical techniques can be refined to enhance the perfusion of the gastric conduit, which is the section of the stomach that is connected to the esophagus during reconstruction.

ICG fluorescence-guided surgeries have demonstrated promising results in reducing anastomotic leakage rates. Building on this potential, the study in question explored the effectiveness of a specific surgical modification: altering the incision line on the lesser curvature during the formation of the gastric conduit. The rationale behind this modification is that by changing the angle or position of the cut, one might improve blood flow to the area, thereby boosting the overall perfusion.

The study involved a retrospective analysis of 272 patients who underwent esophagectomy procedures between 2014 and 2022. These patients were divided into two groups based on the type of cutline used for their gastric conduit formation: the conventional group, which followed traditional surgical guidelines, and the current group, which implemented the modified cutline approach.

Using ICG fluorescence imaging, the researchers assessed the perfusion of the gastric conduit in both groups. They also monitored postoperative outcomes, including the rate of anastomotic leakage and the duration of hospital stays. The data revealed that the current group, with the modified cutline, had several advantages over the conventional group. Notably, this group exhibited a longer distance from the pylorus to the cutline, which was associated with significantly higher blood flow speeds within the wall of the gastric conduit. Furthermore, the rate of anastomotic leakage was significantly reduced, and patients in this group tended to have shorter hospital stays compared to those in the conventional group.

Multivariate analysis confirmed that increased blood flow speed in the gastric conduit wall was significantly linked to a reduced risk of leakage. This finding underscores the importance of adequate blood supply in preventing anastomotic leaks and suggests that the modified cutline technique could play a pivotal role in enhancing surgical outcomes.

In conclusion, the study provides evidence that ICG fluorescence imaging is a reliable method for assessing perfusion during esophageal surgeries. The modified cutline technique on the lesser curvature for gastric conduit formation appears to improve perfusion, enhance blood circulation around the anastomosis site, and reduce the likelihood of postoperative leaks. Such findings could lead to changes in surgical practices aimed at minimizing the risk of anastomotic leakage and improving patient recovery times.

2. 執筆論文 Publication of thesis ※記載した論文を添付してください。Attach all of the papers listed below.

論文名 1 Title	Modification of the Lesser Curvature Incision Line Enhanced Gastric Conduit Perfusion as Determined by Indocyanine Green Fluorescence Imaging and Decreased the Incidence of Anastomotic Leakage Following Esophagectomy(Under review).					
掲載誌名 Published journal						
	年	月	巻(号)	頁 ~	頁	言語 Language
第1著者名 First author	Hongbo Zhao		第2著者名 Second author	Kazuo Koyanagi1, MD, PhD		第3著者名 Third author
第3著者名 Third author	Yamato Ninomiya					
その他著者名 Other authors	Akihito Kazuno MD, PhD, Miho Yamamoto, MD, PhD, Yoshiaki Shoji, MD, PhD, Kentaro Yatabe, MD, PhD, Kohei Kanamori MD, PhD, Kohei Tajima, MD, Masaki Mori					
論文名 2 Title	Effective Postoperative Surveillance Protocol after Thoracoscopic Esophagectomy Focusing on Symptoms in Patients with Esophageal Cancer.					
掲載誌名 Published journal	Journal of the American College of Surgeons					
	2023 年	Nov 月	237(5) 巻(号)	771 頁 ~	778 頁	言語 Language
第1著者名 First author	Kohei Tajima1, MD		第2著者名 Second author	uo Koyanagi1, MD, PhD, FA		第3著者名 Third author
第3著者名 Third author	Shoji Ozawa1, MD, PhD, FAC					
その他著者名 Other authors	Akihito Kazuno1, MD, PhD, Miho Yamamoto, MD, PhD, Yoshiaki Shoji, MD, PhD, Kentaro Yatabe, MD, PhD, Kohei Kanamori, MD, PhD, Hongbo Zhao, MD, PhD, Masaki					
論文名 3 Title	Perioperative outcomes of neoadjuvant chemotherapy plus camrelizumab compared with chemotherapy alone and chemoradiotherapy for locally advanced esophageal squamous cell cancer. Front Immunol.					
掲載誌名 Published journal	Frontiers in Immunology					
	2023 年	Feb 月	7;14:1066527 巻(号)	頁 ~	頁	言語 Language
第1著者名 First author	Baihua Zhang,Hongbo Zhao		第2著者名 Second author	Xun Wu		第3著者名 Third author
第3著者名 Third author	Lianghui Gong					
その他著者名 Other authors	Desong Yang1,XuLi, Xiaoyan Chen, Jigang Li, Wenxiang Wang, Jie Wu1 and Qin Xiao					
論文名 4 Title						
掲載誌名 Published journal						
	年	月	巻(号)	頁 ~	頁	言語 Language
第1著者名 First author			第2著者名 Second author			第3著者名 Third author
第3著者名 Third author						
その他著者名 Other authors						
論文名 5 Title						
掲載誌名 Published journal						
	年	月	巻(号)	頁 ~	頁	言語 Language
第1著者名 First author			第2著者名 Second author			第3著者名 Third author
第3著者名 Third author						
その他著者名 Other authors						

3. 学会発表 Conference presentation ※筆頭演者として総会・国際学会を含む主な学会で発表したものを記載してください

※Describe your presentation as the principal presenter in major academic meetings including general meetings or international meetin

学会名 Conference					
演題 Topic					
開催日 date	年	月	日	開催地 venue	
形式 method	<input type="checkbox"/> 口頭発表 Oral	<input type="checkbox"/> ポスター発表 Poster	言語 Language	<input type="checkbox"/> 日本語	<input type="checkbox"/> 英語 <input type="checkbox"/> 中国語
共同演者名 Co-presenter					
学会名 Conference					
演題 Topic					
開催日 date	年	月	日	開催地 venue	
形式 method	<input type="checkbox"/> 口頭発表 Oral	<input type="checkbox"/> ポスター発表 Poster	言語 Language	<input type="checkbox"/> 日本語	<input type="checkbox"/> 英語 <input type="checkbox"/> 中国語
共同演者名 Co-presenter					
学会名 Conference					
演題 Topic					
開催日 date	年	月	日	開催地 venue	
形式 method	<input type="checkbox"/> 口頭発表 Oral	<input type="checkbox"/> ポスター発表 Poster	言語 Language	<input type="checkbox"/> 日本語	<input type="checkbox"/> 英語 <input type="checkbox"/> 中国語
共同演者名 Co-presenter					
学会名 Conference					
演題 Topic					
開催日 date	年	月	日	開催地 venue	
形式 method	<input type="checkbox"/> 口頭発表 Oral	<input type="checkbox"/> ポスター発表 Poster	言語 Language	<input type="checkbox"/> 日本語	<input type="checkbox"/> 英語 <input type="checkbox"/> 中国語
共同演者名 Co-presenter					

4. 受賞(研究業績) Award (Research achievement)

名称 Award name	国名 Country		受賞年 Year of award	年	月
	国名 Country		受賞年 Year of award	年	月

5. 本研究テーマに関わる他の研究助成金受給 Other research grants concerned with your research theme

受給実績 Receipt record	<input type="checkbox"/> 有 <input type="checkbox"/> 無
助成機関名称 Funding agency	
助成金名称 Grant name	
受給期間 Supported period	年 月 ~ 年 月
受給額 Amount received	円
受給実績 Receipt record	<input type="checkbox"/> 有 <input type="checkbox"/> 無
助成機関名称 Funding agency	
助成金名称 Grant name	
受給期間 Supported period	年 月 ~ 年 月
受給額 Amount received	円

6. 他の奨学金受給 Another awarded scholarship

受給実績 Receipt record	<input type="checkbox"/> 有 <input type="checkbox"/> 無
助成機関名称 Funding agency	
奨学金名称 Scholarship name	
受給期間 Supported period	年 月 ~ 年 月
受給額 Amount received	円

7. 研究活動に関する報道発表 Press release concerned with your research activities

※記載した記事を添付してください。Attach a copy of the article described below

報道発表 Press release	<input type="checkbox"/> 有 <input type="checkbox"/> 無	発表年月日 Date of release	
発表機関 Released medium			
発表形式 Release method	・新聞 ・雑誌 ・Web site ・記者発表 ・その他()		
発表タイトル Released title			

8. 本研究テーマに関する特許出願予定 Patent application concerned with your research theme

出願予定 Scheduled	<input type="checkbox"/> 有 <input type="checkbox"/> 無	出願国 Application	
出願内容(概要) Application contents			

9. その他 Others

--

指導責任者(記名) 小柳 和夫



OPEN ACCESS

EDITED BY

Zhihao Lu,
Beijing Cancer Hospital, Peking University,
China

REVIEWED BY

Kezhou Zhu,
Life Sciences Institute, University of
Michigan, United States
Tong Wu,
Purdue University Indianapolis,
United States

*CORRESPONDENCE

Jie Wu

✉ wujie@hnca.org.cn

Qin Xiao

✉ xiaoqin2501@hnca.org.cn

[†]These authors have contributed
equally to this work and share
first authorship

SPECIALTY SECTION

This article was submitted to
Cancer Immunity
and Immunotherapy,
a section of the journal
Frontiers in Immunology

RECEIVED 11 October 2022

ACCEPTED 25 January 2023

PUBLISHED 07 February 2023

CITATION

Zhang B, Zhao H, Wu X, Gong L, Yang D,
Li X, Chen X, Li J, Wang W, Wu J and
Xiao Q (2023) Perioperative outcomes of
neoadjuvant chemotherapy plus
camrelizumab compared with
chemotherapy alone and
chemoradiotherapy for locally advanced
esophageal squamous cell cancer.
Front. Immunol. 14:1066527.
doi: 10.3389/fimmu.2023.1066527

COPYRIGHT

© 2023 Zhang, Zhao, Wu, Gong, Yang, Li,
Chen, Li, Wang, Wu and Xiao. This is an
open-access article distributed under the
terms of the [Creative Commons Attribution
License \(CC BY\)](https://creativecommons.org/licenses/by/4.0/). The use, distribution or
reproduction in other forums is permitted,
provided the original author(s) and the
copyright owner(s) are credited and that
the original publication in this journal is
cited, in accordance with accepted
academic practice. No use, distribution or
reproduction is permitted which does not
comply with these terms.

Perioperative outcomes of neoadjuvant chemotherapy plus camrelizumab compared with chemotherapy alone and chemoradiotherapy for locally advanced esophageal squamous cell cancer

Baihua Zhang^{1†}, Hongbo Zhao^{2†}, Xun Wu¹, Lianghai Gong¹,
Desong Yang¹, Xu Li¹, Xiaoyan Chen³, Jigang Li³,
Wenxiang Wang¹, Jie Wu^{1*} and Qin Xiao^{4*}

¹The Second Department of Thoracic Surgery, Hunan Clinical Medical Research Center of Accurate Diagnosis and Treatment for Esophageal Carcinoma, Hunan Cancer Hospital and The Affiliated Cancer Hospital of Xiangya School of Medicine, Central South University, Changsha, China, ²Department of Thoracic Surgery, National Cancer Center/National Clinical Research Center for Cancer/Cancer Hospital and Shenzhen Hospital, Chinese Academy of Medical Sciences and Peking Union Medical College, Shenzhen, China, ³Department of Pathology, Hunan Cancer Hospital and The Affiliated Cancer Hospital of Xiangya School of Medicine, Central South University, Changsha, China, ⁴Key Laboratory of Translational Radiation Oncology, Hunan Province, The First Department of Thoracic Radiation Oncology, Hunan Cancer Hospital, The Affiliated Cancer Hospital of Xiangya School of Medicine, Central South University, Changsha, Hunan, China

Purpose: Neoadjuvant chemoimmunotherapy (nCIT) is becoming a new therapeutic frontier for resectable esophageal squamous cell carcinoma (ESCC); however, crucial details and technical know-how regarding surgical techniques and the perioperative challenges following nCIT remain poorly understood. The study investigated and compared the advantages and disadvantages of esophagectomy following nCIT with neoadjuvant chemotherapy (nCT) and chemoradiotherapy (nCRT).

Methods: We retrospectively analyzed data of patients initially diagnosed with resectable ESCC at clinical stage T2-4N+ and received neoadjuvant therapy followed by esophagectomy at the Hunan Cancer Hospital between October 2014 and February 2021. Patients were divided into three groups according to neoadjuvant treatment: (i) nCIT; (ii) nCT; and (iii) nCRT.

Results: There were 34 patients in the nCIT group, 97 in the nCT group, and 31 in the nCRT group. Compared with nCT, nCIT followed by esophagectomy achieved higher pathological complete response (pCR; 29.0% versus 4.1%, $p < 0.001$) and major pathological response (MPR; 52.9% versus 16.5%, $p < 0.001$) rates, more resected lymph nodes during surgery (25.06 ± 7.62 versus 20.64 ± 9.68 , $p = 0.009$), less intraoperative blood loss (200.00 ± 73.86 versus 266.49 ± 176.29 mL, $p = 0.035$), and comparable results in other perioperative parameters. Compared with nCRT, nCIT achieved similar pCR (29.0% versus 25.8%) and MPR (52.9% versus 51.6%, $p = 0.862$) rates, with significantly more lymph nodes resected

during surgery (25.06 ± 7.62 versus 16.94 ± 7.24 , $p < 0.001$), shorter operation time (267.79 ± 50.67 versus 306.32 ± 79.92 min, $p = 0.022$), less intraoperative blood loss (200.00 ± 73.86 versus 264.53 ± 139.76 mL, $p = 0.022$), and fewer ICU admissions after surgery (29.4% versus 80.6%, $p < 0.001$). Regarding perioperative adverse events and complications, no significant statistical differences were detected between the nCIT and the nCT or nCRT groups. The 3-year overall survival rate after nCIT was 73.3%, slightly higher than 46.1% after nCT and 39.7% after nCRT, with no statistically significant differences ($p = 0.883$).

Conclusions: This clinical analysis showed that nCIT is safe and feasible, with satisfactory pCR and MPR rates. Esophagectomy following nCIT has several perioperative advantages over nCT and nCRT, with comparable perioperative morbidity and mortality. The long-term survival benefits after nCIT still requires further investigation.

KEYWORDS

neoadjuvant therapy, programmed cell death protein-1 inhibitors, immunotherapy, esophagectomy, neoadjuvant chemoradiotherapy, esophageal squamous cell carcinoma

Introduction

In 2020, esophageal carcinoma was the seventh most prevalent cancer and sixth leading cause of cancer-related death worldwide (1). The predominant esophageal cancer subtype in Asia is esophageal squamous cell carcinoma (ESCC) (2). ESCC accounts for over 84% of newly diagnosed esophageal cancers annually (3, 4). Surgical resection remains the gold standard for patients with locally advanced resectable ESCC. However, studies have shown that local recurrence and distant metastasis occur in approximately 33% of patients who receive surgery alone (5, 6). Thus, ESCC treatment is challenging and requires a multidisciplinary approach to improve the surgical therapeutic effect in locally advanced resectable disease.

Following the launch of a new era in immunotherapy (including programmed cell death-ligand 1 [PD-L1] and programmed cell death protein-1 [PD-1] inhibitors), further exploration of neoadjuvant immunotherapy alone or combined with chemotherapy or chemoradiotherapy is expected to further improve the therapeutic effect in locally advanced resectable ESCC. In a recent systematic review including 27 phase 2 or 3 clinical trials with 815 patients, the pooled pathological complete response (pCR) rate was 32.4% in ESCC after neoadjuvant chemoimmunotherapy (nCIT), with the pooled incidence of treatment-related severe adverse events of 26.9% (7). Zhu et al. reported that neoadjuvant immunochemoradiotherapy could not improve the pCR rate than neoadjuvant chemoradiotherapy (nCRT) for ESCC, but significantly increased the risk of severe adverse events (8). Another multicenter retrospective study that included 370 ESCC patients showed that the pCR rates of mono-immunotherapy, nCIT, and nCRT plus immunotherapy were 12.1%, 25.5%, and 42.3%, respectively (9). Hence, neoadjuvant PD-1/PD-L1 inhibitors in combination with chemotherapy or chemoradiotherapy are becoming a new therapeutic frontier for resectable ESCC with promising clinical outcomes. However, long-term follow-up are warranted to validate the survival benefits of nCIT or nCRT plus immunotherapy.

Camrelizumab is a PD-1 inhibitor produced in China by Jiangsu Hengrui Pharmaceuticals Co, Ltd. (Lianyungang, China). The ESCORT-1st study showed that first-line camrelizumab plus chemotherapy could achieve better disease control and long-term survival in advanced ESCC than chemotherapy alone (10). Several prospective phase-II clinical trials have also demonstrated that after neoadjuvant chemotherapy plus camrelizumab (nCIT) for ESCC, pCR rates ranged from 24.1% to 42.5%, with major pathological response (MPR) rates of between 45% and 68.8% (11–14). However, these sample sizes were small, and only a few studies reported survival results. Additionally, crucial details and technical know-how regarding the surgical techniques and perioperative challenges following nCIT are still poorly understood.

In the present study, we retrospectively reviewed the perioperative outcomes of esophagectomy following nCIT to compare it with surgery after nCT and nCRT. This study aimed to investigate the potential advantages and disadvantages of esophagectomy after nCIT.

Patients and methods

Inclusion and exclusion criteria

This is a retrospective, single-center, observational study. Patients initially diagnosed with resectable ESCC at clinical stages T2-4N+ (American Joint Committee on Cancer, 8th edition) and received neoadjuvant therapy followed by curative-intent surgery between October 2014 and February 2021 at the Hunan Cancer Hospital were recruited. The Eastern Cooperative Oncology Group's performance status of all patients was 0 or 1. Patients were included on the basis of the following criteria; (1): only squamous cell carcinoma components; (2); thoracic ESCC; (3); patients who received neoadjuvant chemotherapy (nCT), nCIT (only camrelizumab), or nCRT followed by esophagectomy; and (4) the

chemotherapy regimens only consisted of paclitaxel and platinum. The exclusion criteria were as follows; (1): pathological non-squamous cell carcinoma components; (2); patients with unresectable primary tumors, more than seven lymph node metastases (N3), or distant metastasis (M1) before neoadjuvant treatment; (3); patients with previous cancer type(s) or other concurrent malignant tumors; (4); patients that received other forms of treatment before surgery; and (5) incomplete medical records.

All clinical data were obtained from medical records and retrospectively analyzed. This study was conducted per the Declaration of Helsinki (as revised in 2013). The Ethics Committee of Hunan Cancer Hospital approved this study (No. 2022097), and patients' written informed consent was obtained.

Neoadjuvant treatment modalities

Patients were retrospectively divided into three groups according to the neoadjuvant treatment modality they received; (1): the nCT group, including patients who received one to four cycles of paclitaxel combined with platinum chemotherapy (21 days per cycle); (2); the nCIT group, including patients who received conventional chemotherapy (1–4 cycles of paclitaxel and platinum) and camrelizumab (200 mg) on the first day of each cycle; and (3) the nCRT group, including patients who received concurrent chemotherapy (1–4 cycles of paclitaxel and platinum) and radiotherapy (6-MV X-ray, 39.6–45.0 Gy/1.8–2.0 Gy/f) before esophagectomy.

Surgery and adjuvant therapy

Generally, patients would receive a tumor re-evaluation within 2 to 6 weeks after the last neoadjuvant treatment cycle. Following multidisciplinary discussion, a curative-intent surgical resection was immediately performed when the tumor was considered operable. Overall, esophagectomy with the stomach as the esophageal substitute and cervical or thoracic anastomosis were performed in all patients, while experienced surgeons regularly conducted a standard 2-field lymphadenectomy. Cervical lymphadenectomy (3-field) was performed only when lymph node metastasis was suspected in the neck region.

Adjuvant treatments were then performed on the basis of pathological tumor stage and each patient's recovery condition. After multidisciplinary discussion, postoperative chemoradiotherapy or chemotherapy alone might be recommended for patients with ypN + or palliative resection. In the nCIT group, adjuvant therapy with camrelizumab might be recommended for 1 year after surgery.

Outcome measures and follow-up

As reported in previous studies (15, 16), pCR was defined as no viable tumor cells in the resected specimen. In contrast, MPR was defined as <10% viable residual tumor cells detected in the specimen. Pathological responses were evaluated independently by two

experienced pathologists. Treatment-related adverse events (TRAEs) were graded as per the National Cancer Institute Common Terminology Criteria for Adverse Events (CTCAE) version 5.0. Weight loss at initial diagnosis was defined as weight loss detected within six months before the diagnosis of ESCC. Operation time was calculated from incision to wound closure.

Radiographic evaluations were conducted every 3 months for the first 2 years after surgery, and then every 6 months thereafter. Whenever recurrence was suspected, rebiopsy and/or 18F-FDG positron emission tomography-computed tomography (PET-CT) or both were performed to identify the possible recurrence.

Statistical analysis

The primary endpoint was the MPR rate, and the secondary endpoints were the pCR, perioperative morbidity, and 3-year OS rates. OS was defined as the time (in months) from surgery to the date of death or the last follow-up. Survival analyses were calculated and compared using Kaplan–Meier curves and the log-rank test.

Differences in clinicopathological features between groups were calculated using the chi-square (χ^2) test or *t*-test. SPSS software 23.0 (IBM Corp., Armonk, NY, USA) was used to perform all statistical analyses. A *p*-value <0.05 (two-sided) was considered to be statistically significant.

Results

Overview of patient cohorts

Between October 2014 and February 2021, 194 patients were screened for eligibility. Eventually, 162 patients were enrolled for further analysis (34 patients in the nCIT group, 97 in the nCT group, and 31 in the nCRT group) (Figure 1). All 162 patients in the study finished one to four cycles of neoadjuvant therapy. As summarized in Table 1, the enrolled patients in the nCIT group have a mean age of 60.68 ± 7.44 years old and predominantly consisted of males (91.2%), which were consistent with the nCT and nCRT groups. No significant differences were detected between the nCIT and the nCT or nCRT groups in other baseline characteristics, including cigarette consumption, alcohol abuse, weight loss at initial diagnosis, body mass index, tumor location, tumor length, cN, and pathological differentiation. However, the cT4 percentage in the nCIT group was 35.3%, which was significantly higher than in the nCT group (16.5%, *p*=0.021) but comparable to that in the nCRT group (19.4%, *p*=0.238).

Perioperative outcomes

All patients successfully received esophagectomy and most achieved radical resection with no significant statistical differences (Table 2). The time interval between final neoadjuvant therapy and surgery in the nCIT group was 35.91 ± 6.76 days, which was significantly longer than in the nCT group (32.70 ± 7.56 days, *p*=0.024) but shorter than in the nCRT group (41.87 ± 10.60 days,

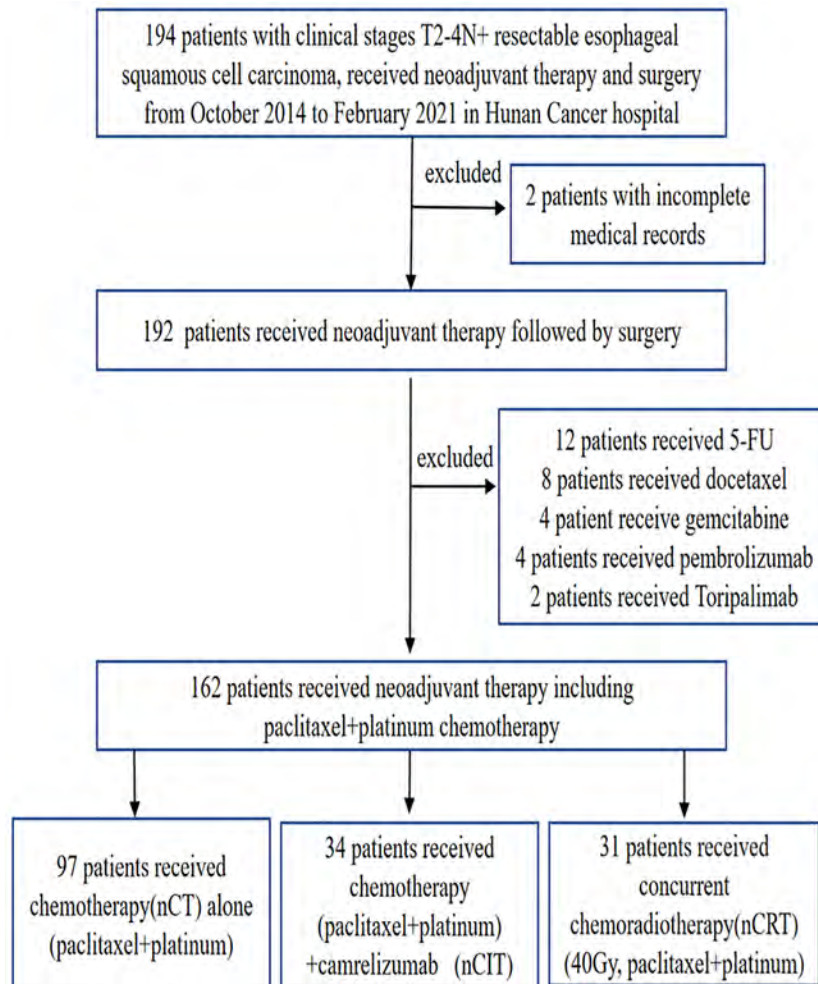


FIGURE 1
Patient selection flowchart.

$p=0.010$). Patients in the nCIT group (267.79 ± 50.67 min) required a shorter operation time than those in the nCRT group (306.32 ± 79.92 min, $p=0.022$). Meanwhile, no significant difference was detected between the nCIT and nCT groups (291.40 ± 71.48 min, $p=0.078$). Additionally, intraoperative blood loss in the nCIT group (200.00 ± 73.86 mL) was less than in the nCT (266.49 ± 176.29 mL, $p=0.035$) and nCRT (264.53 ± 139.76 mL, $p=0.022$) groups. Notably, 2-field lymphadenectomy was the principal method for lymph node resection in all groups. However, the average number of resected lymph nodes in the nCIT group (25.06 ± 7.62) was significantly higher than in the other two groups ($p=0.009$, $p<0.001$, respectively).

Three-incisional esophagectomy with anastomosis in the neck was the principal surgery in all three groups. As summarized in Table 2, no significant differences were detected between the groups in the total drainage after operation, duration of chest tube, and hospital stay after surgery. The frequency of ICU stay after surgery in the nCIT group (29.4%) was comparable with that in the nCT group (32.0%, $p=0.783$) but significantly lower than in the nCRT group (80.6%, $p<0.001$).

Pathological efficacy

In the pathological analysis after surgery, MPR was observed in 18 patients in the nCIT group (52.9%), including nine primary tumor pCRs (26.4%) (8 T0N0 [23.5%], 1 T0N+ [2.9%]), and nine patients (26.5%) had 1% to 10% viable residual tumor cells detected in the specimens. In the nCT group, MPR was achieved in 16 patients (16.5%), including four primary tumor pCRs (4.1%) (3 T0N0 [3.1%], 1 T0N+ [1.0%]), which was significantly lower than in the nCIT group ($p<0.001$). In the nCRT group, 16 patients (51.6%) achieved MPR, including eight primary tumor pCRs (25.8%) (7 T0N0 [22.6%], 1 T0N+ [3.2%]), which was similar to the nCIT group ($p=0.862$).

Accordingly, the ypT0-2 percentage in the nCIT group (67.6%) was also significantly higher than in the nCT group (39.2%, $p=0.004$) but similar to the nCRT group (58.1%, $p=0.424$). No significant differences were detected between the groups for other pathological parameters including ypN stage, ypTNM stage, positive lymph node number, and lymphovascular invasion (LVI), or perineural invasion. After surgery, approximately half of the patients received adjuvant

TABLE 1 Clinical characteristics for ESCC patients received neoadjuvant therapy.

Variables	nCIT (n=34)	nCT (n=97)	P value	nCIT (n=34)	nCRT (n=31)	P value
Age						
Mean \pm SD ^a , y	60.68 \pm 7.44	60.08 \pm 7.78	0.699	60.68 \pm 7.44	57.23 \pm 6.79	0.056
Gender						
Male	31 (91.2)	94 (96.9)	0.169	31 (91.2)	30 (96.8)	0.348
Female	3 (8.8)	3 (3.1)		3 (8.8)	1 (3.2)	
Cigarette consumption						
Former/current	30 (88.2)	86 (88.7)	0.947	30 (88.2)	27 (87.1)	0.889
No	4 (11.8)	11 (11.3)		4 (11.8)	4 (12.9)	
Alcohol abuse						
Former/current	28 (82.4)	78 (80.4)	0.804	28 (82.4)	29 (93.5)	0.170
No	6 (17.6)	19 (19.6)		6 (17.6)	2 (6.5)	
Weight loss at initial diagnosis						
Yes	21 (61.8)	50 (51.5)	0.303	21 (61.8)	15 (48.4)	0.279
No	13 (38.2)	47 (48.5)		13 (38.2)	16 (51.6)	
BMI index						
Mean \pm SD ^a	21.82 \pm 2.74	21.35 \pm 3.17	0.442	21.82 \pm 2.74	21.77 \pm 1.91	0.932
Tumor location						
Upper thoracic	3 (8.8)	10 (10.3)	0.642	3 (8.8)	4 (12.9)	0.169
Middle thoracic	11 (32.4)	39 (40.2)		11 (32.4)	16 (51.6)	
Lower thoracic	20 (58.8)	48 (49.5)		20 (58.8)	11 (35.5)	
Tumor length before treatment						
Mean \pm SD ^a , cm	5.36 \pm 1.81	5.11 \pm 1.89	0.512	5.36 \pm 1.81	5.21 \pm 1.72	0.736
cT						
T2/3	22 (64.7)	81 (83.5)	0.021	22 (64.7)	25 (80.6)	0.151
T4	12 (35.3)	16 (16.5)		12 (35.3)	6 (19.4)	
cN						
N1	17 (50.0)	59 (60.8)	0.271	17 (50.0)	11 (35.5)	0.238
N2	17 (50.0)	38 (39.2)		17 (50.0)	20 (64.5)	
Pathological differentiation						
Poor/moderate	27 (79.4)	70 (72.2)	0.407	27 (79.4)	27 (87.1)	0.409
Well	7 (20.6)	27 (27.8)		7 (20.6)	4 (12.9)	

^aVariables were described by mean (x) and standard deviation (s).

ESCC, esophageal squamous cell carcinoma; cT, clinical T stage before treatment; cN, clinical N stage before treatment; nCT, neoadjuvant chemotherapy; nCIT, neoadjuvant chemotherapy plus Camrelizumab; nCRT, neoadjuvant chemoradiotherapy.

therapy, with no statistically significant difference observed among the three groups.

Perioperative adverse events and complications

The adverse events related to neoadjuvant therapy are summarized in Table 3. The frequency of adverse events in the

nCIT group was 47.1%, which was comparable with the nCT and nCRT groups. Regarding CTCAE grade, the frequency of severe adverse events (grade III/IV) in the nCIT group was 25.0%, which was similar to the 16.2% and 41.1% in the nCT and nCRT groups, respectively. No deaths related to neoadjuvant therapy (CTCAE grade V) were observed in any group. As to the adverse event types, myelosuppression and erythra were the principal events in the nCIT group, which was different from that of myelosuppression and gastrointestinal react in the nCT group ($p=0.002$).

TABLE 2 The perioperative outcomes of esophagectomy after neoadjuvant therapy.

Variables	nCIT (n=34)	nCT (n=97)	P value	nCIT (n=34)	nCRT (n=31)	P value
Interval days						
$x \pm s^a$ (day)	35.91 \pm 6.76	32.70 \pm 7.56	0.024	35.91 \pm 6.76	41.87 \pm 10.60	0.010
Surgical radicality						
Radical	33 (97.1)	89 (91.8)	0.293	33 (97.1)	29 (93.5)	0.500
Palliative	1 (2.9)	8 (8.2)		1 (2.9)	2 (6.5)	
Operation time						
$x \pm s^a$ (min)	267.79 \pm 50.67	291.40 \pm 71.48	0.078	267.79 \pm 50.67	306.32 \pm 79.92	0.022
Intraoperative blood loss						
$x \pm s^a$ (ml)	200.00 \pm 73.86	266.49 \pm 176.29	0.035	200.00 \pm 73.86	264.53 \pm 139.76	0.022
Extent of lymph node resection						
2-field	34 (100.0)	96 (99.0)	0.552	34 (100.0)	30 (96.8)	0.291
3-field	0	1 (1.0)		0	1 (3.2)	
Resected lymph nodes number						
$x \pm s^a$	25.06 \pm 7.62	20.64 \pm 9.68	0.009	25.06 \pm 7.62	16.94 \pm 7.24	< 0.001
Anastomosis position						
Neck	33 (97.1)	90 (92.8)	0.370	33 (97.1)	26 (83.9)	0.067
Thoracic	1 (2.9)	7 (7.2)		1 (2.9)	5 (16.1)	
Total drainage after operation						
$x \pm s^a$ (ml)	1925.29 \pm 2239.05	2476.25 \pm 3335.70	0.285	1925.29 \pm 2239.05	3664.35 \pm 6581.08	0.151
Duration of chest tube						
$x \pm s^a$ (day)	8.00 \pm 4.70	8.78 \pm 3.47	0.378	8.00 \pm 4.70	11.42 \pm 19.98	0.336
ICU stay after surgery						
Yes	10 (29.4)	31 (32.0)	0.783	10 (29.4)	25 (80.6)	< 0.001
No	24 (70.6)	66 (68.0)		24 (70.6)	6 (19.4)	
Hospital stays after surgery						
$x \pm s^a$ (day)	12.76 \pm 7.30	12.27 \pm 4.71	0.713	12.76 \pm 7.30	15.65 \pm 19.38	0.423
Pathological response						
MPR	18 (52.9)	16 (16.5)	< 0.001	18 (52.9)	16 (51.6)	0.862
PR	9 (26.5)	48 (49.5)		9 (26.5)	7 (22.6)	
SD/PD	7 (20.6)	33 (34.0)		7 (20.6)	8 (25.8)	
ypT stage						
T0-2	23 (67.6)	38 (39.2)	0.004	23 (67.6)	18 (58.1)	0.424
T3-4	11 (32.4)	59 (60.8)		11 (32.4)	13 (41.9)	
ypN stage						
N-	20 (58.8)	45 (46.4)	0.212	20 (58.8)	18 (58.1)	0.951
N+	14 (41.2)	52 (53.6)		14 (41.2)	13 (41.9)	
ypTNM stage						

(Continued)

TABLE 2 Continued

Variables	nCIT (n=34)	nCT (n=97)	P value	nCIT (n=34)	nCRT (n=31)	P value
0-II	22 (64.7)	45 (46.4)	0.179	22 (64.7)	20 (64.5)	0.839
III	9 (26.5)	41 (42.3)		9 (26.5)	7 (22.6)	
IVA	3 (8.8)	11 (11.3)		3 (8.8)	4 (12.9)	
Positive lymph nodes number						
$\bar{x} \pm s^a$	1.32 \pm 2.43	1.51 \pm 2.36	0.707	1.32 \pm 2.43	1.06 \pm 1.98	0.642
LVI/perineural invasion						
Yes	6 (17.6)	14 (14.4)	0.654	6 (17.6)	2 (6.5)	0.170
No	28 (82.4)	83 (85.6)		28 (82.4)	29 (93.5)	
Adjuvant therapy						
Yes	20 (58.8)	46 (47.4)	0.253	20 (58.8)	15 (48.4)	0.399
No	14 (41.2)	51 (52.6)		14 (41.2)	16 (51.6)	

^aVariables were described by mean (\bar{x}) and standard deviation (s).

nCIT, neoadjuvant chemotherapy plus Camrelizumab; nCT, neoadjuvant chemotherapy; nCRT, neoadjuvant chemoradiotherapy; Interval days, interval days between final neoadjuvant therapy and surgery; ypT, pathological T stage after neoadjuvant therapy; ypN, pathological N stage after neoadjuvant therapy; ypTNM, pathological TNM stage after neoadjuvant therapy; ICU, intensive care unit; LVI, lymphovascular invasion; MPR, major pathological response; PR, partial response; SD, stable disease; PD, progressive disease.

Postoperative complications related to surgery within 30 days occurred in 17 patients (50.0%) in the nCIT group, approximately 37 patients (38.1%) in the nCT group, and 13 patients (41.9%, $p=0.227$) in the nCRT group ($p=0.515$) (Table 4). The principal complications included pulmonary complications, anastomotic leakage, hoarseness, and cardiac complications, and these were unrelated to the neoadjuvant therapeutic modality. One patient in the nCIT group received

a reoperation within 30 days due to diaphragmatic hernia and chyle, four patients in the nCT group due to anastomotic leakage or tracheostomy, and one patient in the nCRT group due to intrathoracic anastomotic leakage.

Only one patient suffered from sudden death, which was 11 days after surgery, and the patient was in the nCT group. The 90-day mortality rate was 8.8% in the nCIT group, and 7.2% in the nCT group ($p=0.761$), while no deaths within 90 days were observed in the

TABLE 3 The adverse events of neoadjuvant therapy.

Variables	nCIT (n=34)	nCT (n=97)	P value	nCIT (n=34)	nCRT (n=31)	P value
Adverse events						
Yes	16 (47.1)	37 (38.1)	0.362	16 (47.1)	17 (54.8)	0.531
No	18 (52.9)	60 (61.9)		18 (52.9)	14 (45.2)	
CTCAE grade						
Any grade	N=16	N=37		N=16	N=17	
I	6 (37.5)	15 (40.5)	0.765	6 (37.5)	4 (23.5)	0.596
II	6 (37.5)	16 (43.2)	0.877	6 (37.5)	6 (35.3)	0.859
III	2 (12.5)	3 (8.1)	0.465	2 (12.5)	4 (23.5)	0.329
IV	2 (12.5)	3 (8.1)	0.465	2 (12.5)	3 (17.6)	0.566
V	0	0		0	0	
Adverse event types						
Myelosuppression	7 (43.8)	18 (48.6)	0.002	7 (43.8)	12 (70.6)	0.129
Erythra	7 (43.8)	1 (2.7)		7 (43.8)	1 (5.9)	
Hepatic dysfunction	1 (6.3)	4 (10.8)		1 (6.3)	1 (5.9)	
Gastrointestinal react	1 (6.3)	12 (32.4)		1 (6.3)	2 (11.8)	
Renal dysfunction	0	2 (5.49)		0	1 (5.9)	

nCT, neoadjuvant chemotherapy; nCIT, neoadjuvant chemotherapy plus Camrelizumab; nCRT, neoadjuvant chemoradiotherapy; CTCAE, Common Terminology Criteria for Adverse Events (version 5.0).

TABLE 4 Perioperative complications within 30 days after surgery and mortality.

Variables	nCIT (n=34)	nCT (n=97)	P value	nCIT (n=34)	nCRT (n=31)	P value
Postoperative complications						
Yes	17 (50.0)	37 (38.1)	0.227	17 (50.0)	13 (41.9)	0.515
No	17 (50.0)	58 (61.9)		17 (50.0)	18 (58.1)	
Complication types	n=17	n=37		n=17	n=13	
Hoarseness	2 (11.8)	6 (16.2)		2 (11.8)	1 (7.7)	
Pulmonary complications	7 (41.7)	10 (27.0)		7 (41.7)	3 (23.1)	
Cardiac complications	2 (11.8)	1 (2.7)		2 (11.8)	2 (15.4)	
Chyle	1 (5.9)	3 (8.1)		1 (5.9)	0	
Anastomotic leakage	2 (11.8)	8 (21.6)		2 (11.8)	4 (30.8)	
Gastric and intestinal complications	1 (5.9)	3 (8.1)		1 (5.9)	0	
Other complications	2 (11.8)	6 (16.2)		2 (11.8)	3 (23.1)	
Reoperation in 30 days						
No	33 (97.1)	93 (95.9)	0.757	33 (97.1)	30 (96.8)	0.947
Yes	1 (2.9)	4 (4.1)		1 (2.9)	1 (3.2)	
30-day mortality						
No	34 (100.0)	96 (99.0)	0.552	34 (100.0)	31 (100.0)	1.000
Yes	0	1 (1.0)		0	0	
90-day mortality						
No	31 (91.2)	90 (92.8)	0.761	31 (91.2)	31 (100.0)	0.09
Yes	3 (8.8)	7 (7.2)		3 (8.8)	0	

nCT, neoadjuvant chemotherapy; nCIT, neoadjuvant chemotherapy plus Camrelizumab; nCRT, neoadjuvant chemoradiotherapy.

nCRT group. No statistically significant difference was found between the nCIT and nCRT groups ($p=0.09$).

Overall survival and analysis of prognostic factors

Until July 30, 2022, the median follow-up of the entire cohort was 20.45 months, with a range of 0.36 to 84.76 months. In the nCIT group, the 1- and 3-year OS rates were 82.4% and 73.3%, respectively, which were not significantly different from the nCT group (77.3% and 46.1%, respectively) and the nCRT group (83.9% and 39.7%, respectively) (Figure 2A, $p=0.883$). Furthermore, the 3-year OS for patients who achieved MPR was 68.7%, which was significantly higher than 46.3% for partial responders and 23.8% for those with stable/progressive disease (Figure 2B, $p<0.001$). Patients who achieved radical esophagectomy attained a much better 3-year OS rate than those who achieved palliative surgery (49.7% versus 0%, Figure 2C, $p<0.001$). In the analysis of postoperative pathological stage, patients with stage ypN- achieved a 3-year OS of 60.6%, which was longer than the 29.0% for patients with ypN+ (Figure 2D, $p<0.001$). Further analysis showed that patients with earlier ypT0-2 and yp0-II staged disease also had better long-term survival rates (Figures 2E, F, $p<0.001$).

Interestingly, the 3-year OS rate of patients with weight loss at initial diagnosis was 38.7%, which was significantly shorter than the 55.8% for patients without weight loss ($p=0.032$). Additionally, the 3-year OS for patients without LVI/perineural invasion was 48.3%, which was longer than the 33.8% for patients with LVI/perineural invasion ($p=0.022$). However, age, sex, body mass index, tumor length at initial diagnosis, tumor location, pathological differentiation, and adjuvant systemic therapy were not significantly correlated with OS in univariate Cox analysis (Table 5).

In the multivariate analysis, which included significant factors identified by univariate analysis, only surgical radicality (hazard ratio [HR]: 5.882, 95% confidence interval [CI]: 2.799–12.359, $p<0.001$), pathological response (HR: 1.493, 95% CI: 1.040–2.143, $p=0.030$), and ypN stage (HR: 2.100, 95% CI: 1.245–3.542, $p=0.005$) were found to be independent prognostic factors for OS other than neoadjuvant modality (Table 5).

Discussion

This study described potential intraoperative technical challenges after nCIT and compared them with other neoadjuvant treatment modalities including nCT and nCRT. Compared with nCT, nCIT followed by esophagectomy achieved higher pCR and MPR rates,

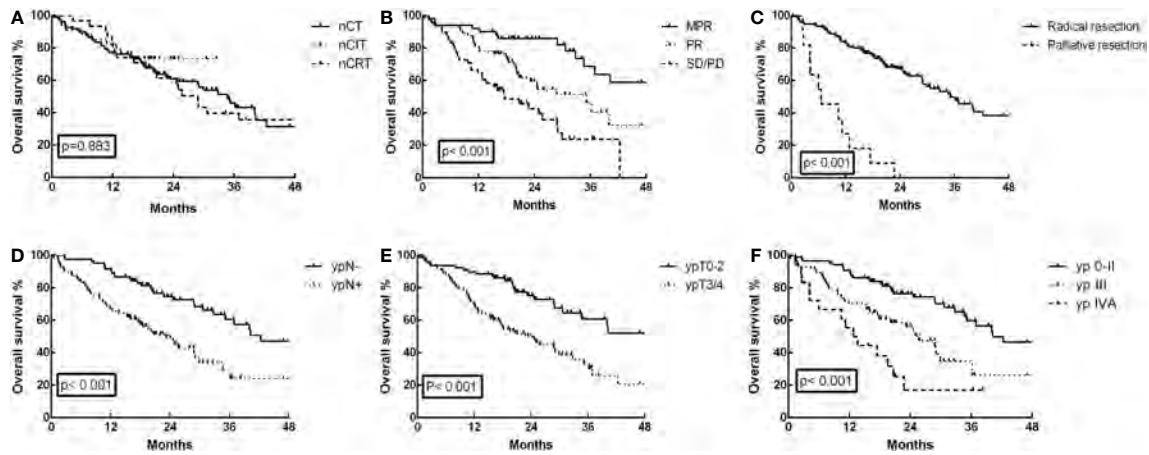


FIGURE 2
Overall survival (OS) curves for the 162 ESCC patients. (A) OS was not significantly different in the neoadjuvant chemoimmunotherapy (nCIT) group compared with the neoadjuvant chemotherapy (nCT) and neoadjuvant chemoradiotherapy (nCRT) groups ($p=0.883$). (B) OS was significantly increased for patients who achieved major pathological response (MPR) compared with those who achieved partial response (PR) and stable disease (SD)/progressive disease (PD) ($p<0.001$). (C) OS was increased for patients who achieved radical esophagectomy compared with those who achieved palliative surgery ($p<0.001$). (D) OS was increased in patients with stage ypN- compared with those who had stage ypN+ ($p<0.001$). (E) OS was increased in patients with stage ypT0-2 compared with those who had stage ypT3/4 ($p<0.001$). (F) OS was increased in patients with stage yp0-II compared with those who had stage ypIII and ypIVA ($p<0.001$).

more resected lymph nodes during surgery, less intraoperative blood loss, and comparable results in other perioperative parameters. Compared with nCRT, nCIT achieved similar pCR and MPR rates, significantly more resected lymph nodes during surgery, shorter operation time, less intraoperative blood loss, and less frequent ICU stays after surgery. Regarding postoperative complications, no

significant statistical difference was detected between the nCIT and the nCT or nCRT groups.

Over the past decade, there have been lingering controversies concerning the effects of neoadjuvant chemotherapy (nCT), chemoradiotherapy (nCRT), and immunotherapy for ESCC. There is still no convincing evidence to prove which neoadjuvant

TABLE 5 Univariate and multivariate analysis of OS for 162 ESCC patients treated with surgery following neoadjuvant therapy.

Characteristics	Univariate		Multivariate	
	HR (95% CI)	P	HR (95% CI)	P
Age (y): < 60 vs ≥ 60	1.039 (0.660-1.634)	0.870		
Gender: Male vs Female	0.564 (0.138-2.299)	0.424		
Weight loss at initial diagnosis: Yes vs No	1.679 (1.047-2.692)	0.032*		
BMI index: < 22 vs ≥ 22	0.870 (0.545-1.390)	0.561		
Tumor length at initial diagnosis: <5 vs ≥ 5 cm	0.981 (0.620-1.553)	0.936		
Tumor location: Lower vs Upper/middle	1.250 (0.793-1.972)	0.337		
Pathological differentiation: Poor/moderate vs Well	1.170 (0.673-2.035)	0.579		
Surgical radicality: Palliative vs Radical	7.415 (3.765-14.605)	<0.001*	5.882 (2.799-12.359)	<0.001
Pathological response: SD(PD) vs PR vs MPR(CR)	2.090 (1.533-2.849)	<0.001*	1.493 (1.040-2.143)	0.030
ypT stage: ypT3-4 vs ypT0-2	2.555 (1.569-4.161)	<0.001*		
ypN stage: ypN+ vs ypN-	2.601 (1.615-4.190)	<0.001*	2.100 (1.245-3.542)	0.005
ypTNM stage: IVA vs III vs 0-II	1.588 (1.300-1.939)	<0.001*		
LVI/perineural invasion: Yes vs No	2.026 (1.105-3.715)	0.022*		
Neoadjuvant therapeutic modality: nCRT vs nCIT vs nCT	0.990 (0.872-1.125)	0.883		
Adjuvant systemic therapy: Yes vs No	0.957(0.606-1.511)	0.849		

*Factors included into multivariate analysis.

ESCC, esophageal squamous cell carcinoma; OS, overall survival; nCIT, neoadjuvant chemotherapy plus Camrelizumab; nCT, neoadjuvant chemotherapy; nCRT, neoadjuvant chemoradiotherapy; ypT, pathological T stage after neoadjuvant therapy; ypN, pathological N stage after neoadjuvant therapy; ypTNM, pathological TNM stage after neoadjuvant therapy; vs, versus; HR, hazard ratio; CI, confidence interval.

therapeutic modality is best for locally advanced resectable ESCC. Pathological responses including pCR and MPR have been considered as principal surrogate endpoints to evaluate the therapeutic efficacy of different neoadjuvant treatments. Previous large-scale randomized clinical trials have reported that nCRT could achieve higher pCR rates (43.2-49%) than nCT (3.8-10.7%) in ESCC, but nCRT might have more postoperative complications and higher postoperative mortality, with no identified overall survival differences (4, 17–24). Therefore, in Western countries, many institutions have adopted nCRT followed by esophagectomy, but globally, many other countries support nCT alone (4, 25).

In this study, the pCR rate for the primary tumor was 26.4%, and the MPR rate was 52.9% after nCIT, consistent with previous reports (9, 11, 12, 26–30). However, after nCT for ESCC, the pCR rate in previous studies is usually between 3.8% and 10.7% (23, 24, 31), which is close to the 4.1% for the primary tumor in this study and significantly lower than the results for nCIT. In contrast, the pCR rate for nCRT has reached approximately 28.9% to 49% in previous studies, which is slightly better than the 25.8% in this study (21, 24, 31–33). Xu et al. demonstrated that the pCR rate was comparable between nCIT and nCRT (29.8% vs 34.0%), with no significant differences in the incidence of postoperative complications and 30-day mortality (34). Thus, this study showed that ESCC might achieve better therapeutic efficacy from nCIT and nCRT on the basis of pCR and MPR results.

Although the pathological efficacy was better for nCIT and nCRT, controversies concerning the long-term survival results remained. Previous prospective trials on esophageal cancer, including JCOG9907, OEO2, CROSS, and NEOCRTEC5010 have demonstrated that nCT or nCRT can achieve better OS results than surgery alone or postoperative chemotherapy (20, 21, 32, 35). Nonetheless, survival differences between different neoadjuvant therapeutic modalities have not been clarified. Klevebro et al. and Wang et al. showed that nCRT could result in a higher pCR rate than nCT, but with no significant survival benefits (24, 31). Another study showed no significant differences in the 5-year OS or the 5-year relapse-free survival (RFS) rates between nCRT and nCT (36). Two separate meta-analyses also reported that nCRT did not show significant long-term survival benefits as nCT (37, 38). In this study, the 1-year OS rate in the nCIT group were 82.4%, consistent with the 1-year OS of between 87.6% and 92.8% in previous reports (29, 39), but not significantly different from nCT (77.3%) and nCRT (83.9%). In a few propensity score matching analyses, the 1-year OS rate in the nCIT group was 94.5-95.7%, slightly better than 84.8% in the nCT group and 86.2% in the nCRT group, but with no significant statistical differences (40, 41). Although no statistically significant difference was observed in our data, the 3-year OS after nCIT was 73.3%, slightly higher than 46.1% after nCT and 39.7% after nCRT. However, the sample size and follow-up time in the present study were too limited to report mature OS results. Therefore, the survival benefit after nCIT in locally advanced resectable ESCC still requires further investigation. Furthermore, as previously reported (4, 36, 42), our further analysis showed that radical esophagectomy, MPR, and ypN0 (no lymph node metastasis) were independent favorable prognostic factors for OS after neoadjuvant therapy. As to adjuvant therapy, approximately half of the patients received adjuvant therapy in each group, and no statistically significant difference was observed

among the three groups. No survival difference was observed between patients received adjuvant therapy or not in our analysis.

This study also highlighted advantages for esophagectomy, as nCIT had more lymph nodes resected and less intraoperative blood loss compared with nCT. During our surgery, tumor and metastatic lymph nodes regression was more significant in the nCIT group than in the nCT group, facilitating lymph node clearance and reducing operation times. Qiao et al. also reported that patients who received nCIT had more lymph nodes cleared during surgery than those who received nCT (34 vs. 30, $p < 0.001$), with comparable incidence of complications (23). Furthermore, when compared with nCRT, esophagectomy after nCIT also achieved more resected lymph nodes, shorter operation times, less intraoperative blood loss, and less frequent ICU stays after surgery. Based on our surgical experience, mild or moderate tissue adhesions were more frequently observed in the nCIT group compared to the nCRT group, which might help reduce the intraoperative difficulties. In certain propensity score matching analyses by Hong et al. and Xiao et al, esophagectomy after nCIT required shorter operative times, and dissected more lymph nodes than after nCRT (41, 43). Cheng et al. also reported that the nCIT group had minimal intraoperative blood loss, shorter operative times, and fewer perioperative complications than the nCRT group (37). However, the extent of lymph node resection and positive lymph node numbers after nCIT were similar to after nCT and nCRT in this study. Regarding other perioperative parameters such as radical resection rate and several postoperative recovery parameters, no significant differences were detected among the three groups.

Perioperative morbidity and mortality are the principal concerns in surgical treatment following neoadjuvant therapy. This study detected no significant statistical differences in the CTCAE grade related to neoadjuvant therapy and postoperative complication types among the three groups. Thus, the addition of camrelizumab to nCT did not increase morbidity or mortality. Additionally, another study by Qiao et al. showed that the total incidence of adverse events during nCIT was lower (77.1%) than nCT (91.7%, $p = 0.003$) (23). As reported in previous studies (26, 30), pneumonia was the most prevalent major 30-day postoperative complication in this study. Other common complications included hoarseness, cardiac complication, and anastomotic leakage. Fortunately, no treatment- or surgery-related deaths were observed within 30 days after esophagectomy in this study, except for one sudden death in the nCT group, proving that esophagectomy following nCIT is safe and feasible.

Some limitations are apparent in this study. First, selection biases were inevitable between groups due to the limited sample size and the retrospective design. For example, the cT4 percentage in the nCIT group was 35.3%, which was significantly higher than in the nCT group. Second, the follow-up and recurrences data are insufficient to report mature OS and disease-free survival results. Third, each neoadjuvant therapy might have specific benefits for patient subgroups. The information on predictive biomarkers for therapeutic efficacy, such as PD-L1 expression, was absent in the present study. Therefore, the problem remains with selecting optimal patients who might benefit from different therapeutic modalities. Hence, more prospective phase III clinical trials with larger sample sizes and multiple centers should be conducted to identify the advantages and disadvantages of each neoadjuvant therapy in locally advanced resectable ESCC.

Conclusion

In conclusion, this real-world analysis showed that nCIT is safe and feasible, with satisfactory pCR and MPR rates. Esophagectomy following nCIT achieved several perioperative advantages over nCT and nCRT, with comparable perioperative morbidity and mortality. Although the 3-year OS after nCIT is slightly higher, the long-term survival benefits still require further investigation.

Data availability statement

The original contributions presented in the study are included in the article/supplementary material. Further inquiries can be directed to the corresponding authors.

Ethics statement

The studies involving human participants were reviewed and approved by The Ethics Committee of Hunan Cancer Hospital (No. 2022097). The patients/participants provided their written informed consent to participate in this study.

Author contributions

(I) Conception and design: BZ, QX, W, JW, XW, HZ. (II) Administrative support: BZ, QX. (III) Provision of study materials or patients: BZ, JW, DY, XL, WW, QX, XW, HZ, LG, XC, JL. (IV) Collection and assembly of data: BZ, JW, QX, XW, HZ, LG. (V) Data analysis and interpretation: BZ, QX. (VI) Manuscript writing: all

References

- Sung H, Ferlay J, Siegel RL, Laversanne M, Soerjomataram I, Jemal A, et al. Global cancer statistics 2020: GLOBOCAN estimates of incidence and mortality worldwide for 36 cancers in 185 countries. *CA: Cancer J Clin* (2021) 71(3):209–49. doi: 10.3322/caac.21660
- Pennathur A, Gibson MK, Jobe BA, Luketich JD. Oesophageal carcinoma. *Lancet* (2013) 381(9864):400–12. doi: 10.1016/S0140-6736(12)60643-6
- Arnold M, Ferlay J, van Berge Henegouwen MI, Soerjomataram I. Global burden of oesophageal and gastric cancer by histology and subsite in 2018. *Gut* (2020) 69(9):1564–71. doi: 10.1136/gutjnl-2020-321600
- Leng XF, Daiko H, Han YT, Mao YS. Optimal preoperative neoadjuvant therapy for resectable locally advanced esophageal squamous cell carcinoma. *Ann New York Acad Sci* (2020) 1482(1):213–24. doi: 10.1111/nyas.14508
- Demarest CT, Chang AC. The landmark series: Multimodal therapy for esophageal cancer. *Ann Surg Oncol* (2021) 28(6):3375–82. doi: 10.1245/s10434-020-09565-5
- Yang H, Liu H, Chen Y, Zhu C, Fang W, Yu Z, et al. Long-term efficacy of neoadjuvant chemoradiotherapy plus surgery for the treatment of locally advanced esophageal squamous cell carcinoma: The NEOCRTEC5010 randomized clinical trial. *JAMA Surg* (2021) 156(8):721–9. doi: 10.1001/jamasurg.2021.2373
- Ge F, Huo Z, Cai X, Hu Q, Chen W, Lin G, et al. Evaluation of clinical and safety outcomes of neoadjuvant immunotherapy combined with chemotherapy for patients with resectable esophageal cancer: A systematic review and meta-analysis. *JAMA Net Open* (2022) 5(11):e2239778. doi: 10.1001/jamanetworkopen.2022.39778
- Zhu J, Leng X, Gao B, Wang B, Zhang H, Wu L, et al. Efficacy and safety of neoadjuvant immunotherapy in resectable esophageal or gastroesophageal junction carcinoma: A pooled analysis of prospective clinical trials. *Front Immunol* (2022) 13:1041233. doi: 10.3389/fimmu.2022.1041233
- Yang Y, Tan L, Hu J, Li Y, Mao Y, Tian Z, et al. Safety and efficacy of neoadjuvant treatment with immune checkpoint inhibitors in esophageal cancer: Real-world multicenter retrospective study in China. *Dis esophagus* (2022) 35(11):doac031. doi: 10.1093/dote/doac031
- Luo H, Lu J, Bai Y, Mao T, Wang J, Fan Q, et al. Effect of camrelizumab vs placebo added to chemotherapy on survival and progression-free survival in patients with advanced or metastatic esophageal squamous cell carcinoma: The ESCORT-1st randomized clinical trial. *Jama* (2021) 326(10):916–25. doi: 10.1001/jama.2021.12836
- Liu J, Yang Y, Liu Z, Fu X, Cai X, Li H, et al. Multicenter, single-arm, phase II trial of camrelizumab and chemotherapy as neoadjuvant treatment for locally advanced esophageal squamous cell carcinoma. *J immunother Cancer* (2022) 10(3):e004291. doi: 10.1136/jitc-2021-004291
- Liu J, Li J, Lin W, Shao D, Depypere L, Zhang Z, et al. Neoadjuvant camrelizumab plus chemotherapy for resectable, locally advanced esophageal squamous cell carcinoma (NIC-ESCC2019): A multicenter, phase 2 study. *Int J cancer*. (2022) 151(1):128–37. doi: 10.1002/ijc.33976
- Yang P, Zhou X, Yang X, Wang Y, Sun T, Feng S, et al. Neoadjuvant camrelizumab plus chemotherapy in treating locally advanced esophageal squamous cell carcinoma patients: a pilot study. *World J Surg Oncol* (2021) 19(1):333. doi: 10.1186/s12957-021-02446-5
- Yang W, Xing X, Yeung SJ, Wang S, Chen W, Bao Y, et al. Neoadjuvant programmed cell death 1 blockade combined with chemotherapy for resectable esophageal squamous cell carcinoma. *J immunother Cancer* (2022) 10(1):e003497. doi: 10.1136/jitc-2021-003497
- Zhang B, Xiao H, Pu X, Zhou C, Yang D, Li X, et al. A real-world comparison between neoadjuvant chemoimmunotherapy and chemotherapy alone for resectable non-small cell lung cancer. *Cancer Med* (2022) 12(1):274–86. doi: 10.1002/cam4.4889

authors. (VII) Final approval of manuscript: all authors. All authors contributed to the article and approved the submitted version.

Funding

This study was supported in part by the Hunan Natural Science Foundation (2021JJ70105), Innovation Guide Program of Medical Technology in Hunan Province (2020SK51111), National Cancer Center Climbing Fund (NCC201918A01), and Changsha Science and Technology Project (kq1901079).

Acknowledgments

We thank James P. Mahaffey, PhD, from Liwen Bianji (Edanz) (www.liwenbianji.cn) for editing the English text of this manuscript.

Conflict of interest

The authors declare that the research was conducted in the absence of any commercial or financial relationships that could be construed as a potential conflict of interest.

Publisher's note

All claims expressed in this article are solely those of the authors and do not necessarily represent those of their affiliated organizations, or those of the publisher, the editors and the reviewers. Any product that may be evaluated in this article, or claim that may be made by its manufacturer, is not guaranteed or endorsed by the publisher.

16. Cottrell TR, Thompson ED, Forde PM, Stein JE, Duffield AS, Anagnostou V, et al. Pathologic features of response to neoadjuvant anti-PD-1 in resected non-small-cell lung carcinoma: A proposal for quantitative immune-related pathologic response criteria (irPRC). *Ann Oncol* (2018) 29(8):1853–60. doi: 10.1093/annonc/mdy218
17. Mariette C, Dahan L, Mornex F, Maillard E, Thomas PA, Meunier B, et al. Surgery alone versus chemoradiotherapy followed by surgery for stage I and II esophageal cancer: Final analysis of randomized controlled phase III trial FFCO 9901. *J Clin Oncol* (2014) 32(23):2416–22. doi: 10.1200/JCO.2013.53.6532
18. Chan KKW, Saluja R, Delos Santos K, Lien K, Shah K, Cramarossa GA, et al. Neoadjuvant treatments for locally advanced, resectable esophageal cancer: A network meta-analysis. *Int J Cancer*. (2018) 143(2):430–7. doi: 10.1002/ijc.31312
19. Zheng Y, Liu XB, Sun HB, Xu J, Shen S, Ba YF, et al. A phase III study on neoadjuvant chemotherapy versus neoadjuvant toripalimab plus chemotherapy for locally advanced esophageal squamous cell carcinoma: Henan cancer hospital thoracic oncology group 1909 (HCHTOG1909). *Ann Trans Med* (2021) 9(1):73. doi: 10.21037/atm-20-5404
20. Ando N, Kato H, Igaki H, Shinoda M, Ozawa S, Shimizu H, et al. A randomized trial comparing postoperative adjuvant chemotherapy with cisplatin and 5-fluorouracil versus preoperative chemotherapy for localized advanced squamous cell carcinoma of the thoracic esophagus (JCOG9907). *Ann Surg Oncol* (2012) 19(1):68–74. doi: 10.1245/s10434-011-2049-9
21. Yang H, Liu H, Chen Y, Zhu C, Fang W, Yu Z, et al. Neoadjuvant chemoradiotherapy followed by surgery versus surgery alone for locally advanced squamous cell carcinoma of the esophagus (NEOCRTEC5010): A phase III multicenter, randomized, open-label clinical trial. *J Clin Oncol* (2018) 36(27):2796–803. doi: 10.1200/JCO.2018.79.1483
22. van Hagen P, Hulshof MC, van Lanschot JJ, Steyerberg EW, van Berge Henegouwen MI, Wijnhoven BP, et al. Preoperative chemoradiotherapy for esophageal or junctional cancer. *New Engl J Med* (2012) 366(22):2074–84. doi: 10.1056/NEJMoa1112088
23. Qiao Y, Zhao C, Li X, Zhao J, Huang Q, Ding Z, et al. Efficacy and safety of camrelizumab in combination with neoadjuvant chemotherapy for ESCC and its impact on esophagectomy. *Front Immunol* (2022) 13:953229. doi: 10.3389/fimmu.2022.953229
24. Wang H, Tang H, Fang Y, Tan L, Yin J, Shen Y, et al. Morbidity and mortality of patients who underwent minimally invasive esophagectomy after neoadjuvant chemoradiotherapy vs neoadjuvant chemotherapy for locally advanced esophageal squamous cell carcinoma: A randomized clinical trial. *JAMA Surg* (2021) 156(5):444–51. doi: 10.1001/jamasurg.2021.0133
25. Shah MA, Kennedy EB, Catenacci DV, Deighton DC, Goodman KA, Malhotra NK, et al. Treatment of locally advanced esophageal carcinoma: ASCO guideline. *J Clin Oncol* (2020) 38(23):2677–94. doi: 10.1200/JCO.20.00866
26. Zhang Z, Hong ZN, Xie S, Lin W, Lin Y, Zhu J, et al. Neoadjuvant sintilimab plus chemotherapy for locally advanced esophageal squamous cell carcinoma: A single-arm, single-center, phase 2 trial (ESONICT-1). *Ann Trans Med* (2021) 9(21):1623. doi: 10.21037/atm-21-5381
27. Xing W, Zhao L, Zheng Y, Liu B, Liu X, Li T, et al. The sequence of chemotherapy and toripalimab might influence the efficacy of neoadjuvant chemioimmunotherapy in locally advanced esophageal squamous cell cancer—a phase II study. *Front Immunol* (2021) 12:772450. doi: 10.3389/fimmu.2021.772450
28. Yan X, Duan H, Ni Y, Zhou Y, Wang X, Qi H, et al. Tislelizumab combined with chemotherapy as neoadjuvant therapy for surgically resectable esophageal cancer: A prospective, single-arm, phase II study (TD-NICE). *Int J Surg (London England)*. (2022) 103:106680. doi: 10.1016/j.ijsu.2022.106680
29. Chen F, Qiu L, Mu Y, Sun S, Yuan Y, Shang P, et al. Neoadjuvant chemoradiotherapy with camrelizumab in patients with locally advanced esophageal squamous cell carcinoma. *Front Surg* (2022) 9:893372. doi: 10.3389/fsurg.2022.893372
30. Gu YM, Shang QX, Zhang HL, Yang YS, Wang WP, Yuan Y, et al. Safety and feasibility of esophagectomy following neoadjuvant immunotherapy combined with chemotherapy for esophageal squamous cell carcinoma. *Front Surg* (2022) 9:851745. doi: 10.3389/fsurg.2022.851745
31. Klevebro F, Alexandersson von Döbeln G, Wang N, Johnsen G, Jacobsen AB, Friesland S, et al. A randomized clinical trial of neoadjuvant chemotherapy versus neoadjuvant chemoradiotherapy for cancer of the oesophagus or gastro-oesophageal junction. *Ann Oncol* (2016) 27(4):660–7. doi: 10.1093/annonc/mdw010
32. Shapiro J, van Lanschot JJB, Hulshof M, van Hagen P, van Berge Henegouwen MI, Wijnhoven BPL, et al. Neoadjuvant chemoradiotherapy plus surgery versus surgery alone for oesophageal or junctional cancer (CROSS): Long-term results of a randomised controlled trial. *Lancet Oncol* (2015) 16(9):1090–8. doi: 10.1016/S1470-2045(15)00040-6
33. Chao YK, Chen HS, Wang BY, Hsu PK, Liu CC, Wu SC. Factors associated with survival in patients with oesophageal cancer who achieve pathological complete response after chemoradiotherapy: A nationwide population-based study. *Eur J cardio-thoracic Surg* (2017) 51(1):155–9. doi: 10.1093/ejcts/ezw246
34. Xu L, Wei XF, Li CJ, Yang ZY, Yu YK, Li HM, et al. Pathologic responses and surgical outcomes after neoadjuvant immunotherapy versus neoadjuvant chemoradiotherapy in patients with locally advanced esophageal squamous cell carcinoma. *Front Immunol* (2022) 13:1052542. doi: 10.3389/fimmu.2022.1052542
35. Allum WH, Stenning SP, Bancewicz J, Clark PI, Langley RE. Long-term results of a randomized trial of surgery with or without preoperative chemotherapy in esophageal cancer. *J Clin Oncol* (2009) 27(30):5062–7. doi: 10.1200/JCO.2009.22.2083
36. Zhang G, Zhang C, Sun N, Xue L, Yang Z, Fang L, et al. Neoadjuvant chemoradiotherapy versus neoadjuvant chemotherapy for the treatment of esophageal squamous cell carcinoma: A propensity score-matched study from the national cancer center in China. *J Cancer Res Clin Oncol* (2022) 148(4):943–54. doi: 10.1007/s00432-021-03659-7
37. Jing SW, Qin JJ, Liu Q, Zhai C, Wu YJ, Cheng YJ, et al. Comparison of neoadjuvant chemoradiotherapy and neoadjuvant chemotherapy for esophageal cancer: A meta-analysis. *Future Oncol (London England)*. (2019) 15(20):2413–22. doi: 10.2217/fon-2019-0024
38. Han J, Wang Z, Liu C. Survival and complications after neoadjuvant chemotherapy or chemoradiotherapy for esophageal cancer: a meta-analysis. *Future Oncol (London England)*. (2021) 17(17):2257–74. doi: 10.2217/fon-2021-0021
39. Yin GQ, Li ZL, Li D. The safety and efficacy of neoadjuvant camrelizumab plus chemotherapy in patients with locally advanced esophageal squamous cell carcinoma: A retrospective study. *Cancer Manage Res* (2022) 14:2133–41. doi: 10.2147/CMAR.S358620
40. Jing SW, Zhai C, Zhang W, He M, Liu QY, Yao JF, et al. Comparison of neoadjuvant immunotherapy plus chemotherapy versus chemotherapy alone for patients with locally advanced esophageal squamous cell carcinoma: A propensity score matching. *Front Immunol* (2022) 13:970534. doi: 10.3389/fimmu.2022.970534
41. Xiao X, Yang YS, Zeng XX, Shang QX, Luan SY, Zhou JF, et al. The comparisons of neoadjuvant chemoimmunotherapy versus chemoradiotherapy for oesophageal squamous cancer. *Eur J cardio-thoracic Surg* (2022) 62(1):ezac341. doi: 10.1093/ejcts/ezac341
42. Leng X, He W, Yang H, Chen Y, Zhu C, Fang W, et al. Prognostic impact of postoperative lymph node metastases after neoadjuvant chemoradiotherapy for locally advanced squamous cell carcinoma of esophagus: From the results of NEOCRTEC5010, a randomized multicenter study. *Ann Surg* (2021) 274(6):e1022–e9. doi: 10.1097/SLA.00000000000003727
43. Hong ZN, Gao L, Weng K, Huang Z, Han W, Kang M. Safety and feasibility of esophagectomy following combined immunotherapy and chemotherapy for locally advanced esophageal squamous cell carcinoma: A propensity score matching analysis. *Front Immunol* (2022) 13:836338. doi: 10.3389/fimmu.2022.836338

Journal of the American College of Surgeons Publish Ahead of Print

DOI: 10.1097/XCS.0000000000000801

**Effective Postoperative Surveillance Protocol after Thoracoscopic Esophagectomy
Focusing on Symptoms in Patients with Esophageal Cancer**

Kohei Tajima¹, MD, Kazuo Koyanagi¹, MD, PhD, FACS, Soji Ozawa¹, MD, PhD, FACS,
Akihito Kazuno¹, MD, PhD, Miho Yamamoto¹, MD, PhD, Yoshiaki Shoji¹, MD, PhD,
Kentaro Yatabe¹, MD, PhD, Kohei Kanamori¹, MD, PhD, Hongbo Zhao¹, MD, PhD, Masaki
Mori¹, MD, PhD, FACS

¹Department of Gastroenterological Surgery, Tokai University School of Medicine, Isehara,
Japan

Disclosure Information: Nothing to disclose.

Presented at the 75th Annual meeting of the Japan Esophageal Society, Tokyo, Japan, July
2021, the 29th Japan Digestive Disease Week Meeting, Kobe, Japan,
November 2021, and the 122nd Annual Congress of the Japan Surgical Society, Kumamoto,
Japan, April 2022.

Correspondence address: Soji Ozawa, MD, FACS, PhD, Department of Gastroenterological
Surgery, Tokai University School of Medicine, 143, Shimokasuya, Isehara, Kanagawa,
Japan, 259-1193, (e-mail: soji888@gmail.com)

Brief title: Surveillance Protocol after Esophagectomy

Abstract

Background: The optimal postoperative surveillance protocol after esophagectomy for patients with esophageal cancer has still not been established. We investigated the risk factors for recurrence of esophageal cancer to devise an appropriate surveillance protocol. Furthermore, we focused on the appearance/worsening of symptoms to determine if additional imaging examinations should be performed.

Methods: We enrolled 416 patients with esophageal and esophagogastric junctional cancer who had undergone thoracoscopic esophagectomy at Tokai University Hospital. Outpatient visits for the patients are usually scheduled at least 4 times per year with CT imaging and blood biochemical examination. We evaluated the time to recurrence after esophagectomy, especially the correlation of this parameter with the appearance/worsening of symptoms during the postoperative outpatient follow-up.

Results: Of the 416 patients, recurrence occurred in 127 patients (30.5%). The median time to recurrence was 6 months after esophagectomy; recurrence occurred within 24 months in 112 patients (88%), and 51 of these patients (40%) developed some new symptom(s) (symptomatic group) prior to the diagnosis of recurrence. The number of patients who developed recurrence within 6 months was significantly higher in the symptomatic group as compared with that in the asymptomatic group (66.7% vs. 46.0%, $p=0.02$). The overall survival in the symptomatic group was significantly shorter than that in the asymptomatic group ($p<0.001$).

Conclusions: We advocate an effective surveillance protocol depending on the appearance/worsening of symptoms to diagnose recurrence of esophageal cancer; we recommend routine imaging examinations every 6 months and clinical outpatient follow-up at even shorter intervals for the first 24 months after esophagectomy.

Abbreviations

MIE = minimally invasive esophagectomy

PET-CT = positron emission tomography-CT

UICC = the Union for International Cancer Control

TNM = Tumor-Node-Metastasis

ICS = intercostal space

OS = overall survival

ASA-PS = Anesthesiologists physical status

ICIs = immune checkpoint inhibitors

Keywords: surveillance, symptom, esophageal cancer, thoracoscopic esophagectomy, recurrence, outpatient

ACCEPTED

Introduction

Esophageal cancer was ranked seventh in terms of the cancer incidence and sixth in terms of the cancer mortality worldwide in 2020¹. The highest regional incidence rates are reported from East Asia for both men and women. The histology in the majority is squamous cell carcinoma. Despite the advances in the diagnostic methods, surgical procedures, and multidisciplinary treatment approaches, the prognosis of esophageal cancer remains unsatisfactory². The reported rate of recurrence of esophageal cancer after radical esophagectomy is 29%-43%³⁻⁵. Moreover, as recurrence after esophagectomy is observed within two years after surgery in almost all cases, an appropriate postoperative clinical surveillance protocol is recommended even for patients undergoing curative esophagectomy.

On the other hand, very few patients develop recurrence later than three years after radical esophagectomy. Follow-up intervals and frequency of imaging examinations after esophagectomy may need to be adjusted depending on the time elapsed after the surgery. According to a nationwide survey conducted in Japan, most hospitals usually require their patients to visit the outpatient department at least four times a year during the first two years after curative resection and at least twice a year in the third and subsequent years; however, no consensus has been established yet⁶. The National Comprehensive Cancer Network Guidelines recommend follow-up at the outpatient clinic for medical history taking and physical examination every 3-6 months for 1-2 years, and every 6-12 months for 3-5 years after curative esophagectomy⁷. However, the frequencies of imaging examinations are not clearly specified, and these are performed as needed. Frequent imaging tests are not recommended for the diagnosis of recurrence, not only owing to a lack evidence of improved prognosis, but may also lead to unnecessary radiation exposure of the patients and increased healthcare costs. On the other hand, outpatient visits enable communication between the patient and physician and establishment of a positive patient-physician relationship, which

improves patient satisfaction and plays an important role in cancer treatment^{8,9}. To date, few studies have discussed establishment of an appropriate surveillance protocol after esophagectomy for esophageal cancer. Therefore, no appropriate postoperative surveillance protocol has been defined yet, and patients are often followed up empirically at each institution.

The purpose of this study was to clarify the risk factors for recurrence for esophageal cancer and the influence of the risk factors on the timing of recurrence, in order to devise an appropriate postoperative surveillance protocol, including the optimal intervals for outpatient visits and frequencies of imaging examinations. We assessed the long-term outcomes in esophageal cancer patients who had undergone minimally invasive esophagectomy (MIE) at our high-volume center (single-institution study). Notably, we focused on the appearance/worsening of symptoms in the patients with recurrence to determine if additional imaging examinations are needed, because the postoperative appearance/worsening of symptoms could be a marker of systemic tumor recurrence and influence the survival.

Methods

Patients

This was a single-center retrospective cohort study of patients with esophageal and esophagogastric junctional cancer conducted at the Tokai University Hospital. We enrolled a total of 416 patients who had undergone thoracoscopic esophagectomy with two- or three-field lymph node dissection for esophageal cancer between January 2010 and December 2019 at our hospital. Patients with R1 or R2 were excluded from the study as cases in which radical curative resection was not possible. The median observation period was 39 months. We conducted this retrospective study with the approval of the Institution Review Board of Tokai University Hospital (20R-346).

Tumor staging

Clinical staging investigations in this study included upper gastrointestinal endoscopy, upper gastrointestinal series, computed tomography (CT) of the neck, chest and abdomen, and positron emission tomography-CT (PET-CT).

Tumor staging was based on the Union for International Cancer Control (UICC) Tumor-Node-Metastasis (TNM) grading system, 8th edition. In principle, preoperative chemotherapy was administered to patients with cStage II or more advanced cancer. Patients with supraclavicular lymph node metastasis were indicated for esophagectomy with lymph node dissection including the supraclavicular lymph nodes. Histopathological diagnosis of the resected tumors was performed according to the Japanese Classification of Esophageal Cancer, 11th Edition¹⁰.

Surgical procedure

MIE was first introduced at our hospital in 2009, and has several advantages over open thoracic esophagectomy¹¹⁻¹⁴. Our standard surgical procedure for patients with esophageal cancer is MIE, except in patients in whom unilateral ventilation is expected to be difficult and those who have intense adhesions within the thoracic cavity.

We performed MIE with the patient in prone position, in which the gravity in the thoracic cavity and the CO₂ pneumothorax push down the organs in the middle mediastinum, affording a wide surgical field¹⁵. It is also beneficial in terms of ergonomics for the surgeon's stance, pulmonary gas exchange in the patient, and avoidance of direct lung injury¹⁶. The patient is placed in a prone position, with the right arm raised over the head. The surgeon, assistant, and endoscopist stand on the right side of the patient and watch the video monitor placed on the opposite side. At first, a 12-mm trocar is inserted into the seventh intercostal space (ICS) between the inferior scapular angle line and posterior axillary line, and a pneumothorax in the right chest is induced using CO₂ gas. The thoracic cavity is examined to

identify any pleural adhesions, and a 12-mm trocar is inserted into the ninth ICS on the inferior scapular angle line for inserting the flexible thoracoscope. Another 12-mm trocar is inserted into the fifth ICS on the posterior axillary line. Five-millimeter trocars are then inserted into the seventh ICS on the middle axillary line, and the third ICS on the middle axillary line. First, the anterior mediastinal pleura of the esophagus is incised, and the trachea and heart are shifted downward, to make the dissection between the esophagus and middle mediastinal organs much easier. Next, dissection is performed between the esophagus and the vertebra or descending aorta. The esophagus is finally mobilized from the thoracic inlet along with the peri-esophageal mediastinal lymph nodes.

Postoperative follow-up

All esophageal cancer patients are followed up after radical esophagectomy at the outpatient gastrointestinal surgical care. Outpatient visits are scheduled at least 4 times a year at first. In principle, blood samples are drawn at each visit, and CT imaging from the neck to the pelvis is performed every 3 months. Further outpatient and imaging examinations are scheduled as needed depending on the appearance/worsening of symptoms in the patients. We evaluated the patients at the postoperative outpatient clinic for the appearance/worsening of symptoms.

Statistical analysis

The overall survival (OS) of the patients overall was calculated by the Kaplan- Meier method, and the difference in the OS between the recurrence group and no- recurrence group was analyzed using the log-rank test. Next, the clinicopathological factors were compared between the recurrence and no-recurrence group, and the risk factors for recurrence were examined. The length of time from the date of esophagectomy to the date of diagnosis of recurrence was defined as the time to recurrence, and the relationship between the time to recurrence and risk factors for recurrence or symptoms at recurrence were also examined.

Differences between the two groups were analyzed using the Mann-Whitney *U* test for continuous variables and the χ^2 test or Fisher's exact test for categorical variables.

Survival curves were drawn using the Kaplan-Meier method. P values of less than 0.05 were considered as denoting significance. All the analyzes were performed using the statistical software package IBM SPSS statistics 26 (IBM Japan, Tokyo, Japan).

Results

Characteristics of the patients

Of the 416 patients, 357 (86%) were male and 59 (14%) were female (Supplemental Digital Content 1, <http://links.lww.com/JACS/A287>). The median age was 68 years, and the median BMI was 21.6. The American Society of Anesthesiologists physical status (ASA-PS) was 2 in 361 patients (87%). The most common frequent tumor location was the middle esophagus (225 patients, 54%), followed by the lower and upper esophagus. The most common histological type was squamous cell carcinoma (365 patients, 88%). According to the TNM classification, the pStage was classified as I in 139 patients (33%), II in 99 patients (24%), and III in 101 patients (24%). Preoperative treatment was administered in 181 patients (43%) and postoperative complications were observed in 239 patients (57%). Of the 416 patients, 127 (31%) were diagnosed as having recurrence.

Comparison between the recurrence and no-recurrence groups

Comparison of characteristics between the recurrence group (127 patients) and no-recurrence group (289 patients) revealed that mean age ($p=0.02$) and BMI ($p=0.008$) were lower in the recurrence group (Supplemental Digital Content 1, <http://links.lww.com/JACS/A287>). The no-recurrence group was more likely to have pT1, pN0, pM0, or pStage I disease as compared with the recurrence group ($p<0.001$). Preoperative treatment was administered more frequently in the recurrence group than in the no-recurrence group ($p<0.001$). The median OS in the overall study cohort was 104 months (Supplemental Digital Content 2,

<http://links.lww.com/JACS/A287>). The median OS in the recurrence group was 24 months. The 5-year OS rate in the recurrence group was 13%, which was shorter than that of 78% in the no-recurrence group ($p < 0.001$), indicating the very poor prognosis in the recurrence group (Supplemental Digital Content 3, <http://links.lww.com/JACS/A287>).

Time to recurrence

The recurrence rate by stage was 0% in patients with pStage 0 disease, 11% in patients with pStage I disease, 22% in patients with pStage II disease, 48% in patients with pStage III disease, and 72% in patients with pStage IV disease. The recurrence rate was lower in patients with Stage I and Stage II disease and higher in patients with Stage III and Stage IV disease. The median time to recurrence in the recurrence groups was 6 months. In 88% of cases with recurrence, the recurrence occurred within 24 months, and in 95% of cases, the recurrence occurred within 36 months after esophagectomy. In all of the cases with recurrence, the recurrence occurred within 60 months after the surgery (Fig. 1a). The median time to recurrence by stage was 18 months in patients with pStage I disease, 7 months in patients with pStage II disease, 5 months in patients with pStage III disease, and 4 months in patients with pStage IV disease (Supplemental Digital content 4, <http://links.lww.com/JACS/A287>). More than 90% of patients with Stage III/Stage IV disease developed recurrence within 24 months after esophagectomy. pStage I patients showed a lower recurrence rate as well as a longer to time to recurrence as compared with pStage III and pStage IV patients.

Sites of recurrence

Among the 127 patients with recurrence, lymph nodes ($n=90$, 70%) were the most common recurrent organ, followed by the lungs ($n=31$, 24%), liver ($n=27$, 21%), and bones ($n=13$, 10%) (include duplicate data). All of the recurrent patients with bone metastasis had simultaneous metastasis in other organs. Rare sites of recurrence were the skin (3%),

cerebellum (0.7%), and adrenal glands (3%). There was no difference in the survival duration after diagnosis of recurrence or in the time to recurrence between patients with and without lymph node recurrence (Supplemental Digital Content 5 a,b, <http://links.lww.com/JACS/A287>). The time to recurrence and survival after diagnosis of recurrence also did not differ significantly between patients with and without lung recurrence (Supplemental Digital Content 5 c,d, <http://links.lww.com/JACS/A287>). Patients with liver recurrence tended to have a shorter time to recurrence than those without liver recurrence ($p=0.05$). Of the patients with liver recurrence, the recurrence developed within 12 months after esophagectomy in 80% of cases and within 24 months in all cases (Supplemental Digital Content 5e, <http://links.lww.com/JACS/A287>). The prognosis of patients with liver recurrence was poor, with a median survival time after recurrence of 9 months ($p=0.002$) (Supplemental Digital Content 5f, <http://links.lww.com/JACS/A287>). The time to recurrence in patients with bone recurrence did not differ significantly as compared with that in patients with non-bone recurrence (Supplemental Digital Content 5g, <http://links.lww.com/JACS/A287>). However, the prognosis of patients with bone recurrence was poor, with a median survival time after recurrence of only 4 months ($p=0.003$) (Supplemental Digital Content 5h, <http://links.lww.com/JACS/A287>).

Number of recurrence sites

Of the 127 patients in the recurrence group, 77 (61%) showed single-organ recurrence (Table 1), while the remaining 39% showed simultaneous recurrence in multiple organs. The higher the number of recurrence sites, the poorer the prognosis of the patients (Supplemental Digital Content 6, <http://links.lww.com/JACS/A287>).

Symptoms at recurrence

Among the 127 patients with recurrence, 51 (40%) complained of some symptom(s) prior to the diagnosis of recurrence. In 66% of the patients with symptoms (symptomatic group), the

recurrence occurred within 6 months after the surgery. On the other hand, recurrence occurred within 6 months after the surgery only in 46.0% ($p=0.02$) of the patients without symptoms (asymptomatic group). The time to recurrence in the symptomatic group tended to be shorter than that in the asymptomatic group (median: 5 months vs. 7 months; $p=0.08$) (Fig. 1b). The main type of symptom at the recurrence was investigated in 51 patients in the symptomatic group. The most common symptom was pain, followed by respiratory symptom, fatigue, lump, and digestive symptom (Table 2). Further, the time to recurrence was significantly longer for the patients with pain compared to the patients with symptoms other than pain such as respiratory symptoms, fatigue, lump, and digestive symptoms (median: 9 months vs. 4 months; $p=0.042$, Fig. 2). In the examination of the relationship between the site of initial recurrence and the presence of symptoms at recurrence, there was no significant difference in the percentage of patients with symptoms among patients with lymph node, liver or lung recurrence, but the percentage of patients with symptoms was higher in the patients with bone recurrence ($p=0.006$) (Table 3). The median OS was 14 months in the symptomatic group and 33 months in the asymptomatic group, with a worse prognosis in the patient group with symptoms at recurrence ($p<0.001$) (Fig. 1c). Patients with symptoms at recurrence had a worse median survival after recurrence than the patients without symptoms at recurrence (median: 5 months vs. 22 months; $p<0.0001$) (Fig. 1d).

Discussion

This study was conducted to devise an appropriate postoperative surveillance protocol for patients with esophageal cancer undergoing radical esophagectomy. Of all the patients who developed recurrence after the surgery, the recurrence occurred within 24 months of the surgery in 88% of patients. The median time to recurrence was 6 months in the recurrence group and 5 months in the patients of this group with symptoms at recurrence. Routine outpatient follow-up with imaging studies is necessary at least every 6 months for up to 24

months after esophagectomy, and additional studies should be considered according to the symptoms of the patients. The frequency of imaging studies could possibly be reduced after 24 months from surgery.

The time to recurrence decreased as the pathological stage of the disease increased. This result was similar to previously published reports by Lindenmann et al. and Hiyoshi et al.^{17,18}. On the other hand, the presence/absence of preoperative treatment had no influence on the time to recurrence. In more than 80% of all patients with recurrence, the recurrence developed within 24 months after the esophagectomy. These results suggest that periodic follow-up is required within 24 months after radical resection, regardless of the tumor stage and treatment administration prior to surgery. As there were no cases of recurrence later than 60 months after esophagectomy, systematic follow-up to detect recurrence may not be necessary in long-term survivors later than 5 years after esophageal cancer surgery.

With regard to the initial site of recurrence, lymph nodes were the most common site of recurrence, consistent with previous reports¹⁹⁻²³. Patients with liver recurrence had a poor prognosis, even if the recurrence was localized within the liver. This may be because multiple intrahepatic recurrences are often detected in patients with liver recurrence and less responsive to any chemotherapy, as previously reported^{19,24}. Bone recurrence often occurs together with recurrences in other organs, which could explain why patients with bone metastases show a relatively poor prognosis.

With regard to the number of organ sites with recurrence, single-organ recurrence was the most common, accounting for 77 cases (61%). Lymph node recurrence accounted for 49 cases (63%) of all the cases with single-organ recurrence. In many of the patients with lymph node recurrence, the recurrence was limited to the local area nodes and to a limited number of nodes. In recent years, oligo-recurrence, in which a small number of metastatic recurrences are found in a limited number of organs, has attracted attention. In this study also, lymph

node recurrence was frequently observed in patients with oligo- recurrence (data not shown), and chemoradiotherapy or surgical resection could possibly be performed as radical treatment in such cases. On the other hand, the prognosis was poorer in patients with simultaneous recurrences in multiple organs, and the greater the number of organ sites of recurrence, the poorer the prognosis. All patients with bone recurrence in this study also had recurrence(s) in other organs, which could explain the poor prognosis in patients with bone recurrence.

In this study to devise an appropriate surveillance protocol for patients with esophageal cancer after MIE, we focused on the occurrence/worsening of symptoms at recurrence. Among all patients with recurrence, 51 patients (40%) complained of some symptom(s) prior to the diagnosis of recurrence. The time to recurrence in the group with symptoms at the time of recurrence was 5 months, which was shorter than in the group that reported no symptoms at the diagnosis of recurrence. The most common symptom at the recurrence was pain, followed by respiratory symptom, fatigue, lump, and digestive symptom. The time to recurrence was 3-4.5 months in the group with symptoms other than pain. These results suggest that it is important to enquire about the presence/absence of new/worsening symptoms and the type of symptoms, particularly respiratory symptoms, fatigue, lump or digestive symptoms, at the time of the outpatient follow-up visits. In patients with symptoms at recurrence, not only the time to recurrence was shorter, but also the survival time after recurrence was shorter. All patients with bone metastasis had simultaneous metastases in other organs, and the symptoms in patients with bone metastases were related to both bone and other organ recurrence. Shortened survival of the patients with bone metastases was caused by multiple organ recurrence.

In this study, we demonstrated the existence of a correlation between a shorter time to recurrence and the development/worsening of symptoms after MIE, therefore, medical examination at the outpatient clinic should be frequently performed in patients with

symptoms. Furthermore, imaging studies should be performed as needed. Additional examinations should be performed promptly for the patients developing respiratory symptoms, fatigue, lump, or digestive symptoms, especially in the early postoperative period. On the other hand, the time to recurrence in the group without any symptom(s) at recurrence was 7 months. Therefore, routine imaging tests should be performed at least every 6 months even in patients without any symptoms. Based on these findings, we propose that a combination of outpatient follow-up at least every 3 months and imaging examinations every 6 months until 24 months after curative esophagectomy for esophageal cancer as an effective surveillance method. It is important to mention that imaging examinations should be promptly performed to check for tumor recurrence in patients reporting symptoms at the time of the outpatient follow-up consultation.

None of the patients included in the present study received immune checkpoint inhibitors (ICIs) as adjuvant therapy. Most of the patients had also not received ICIs as 2nd or further line therapy. ICI therapy has been reported effective as adjuvant therapy after radical resection and also as 1st line treatment in patients with unresectable locally advanced or recurrent esophageal cancer²⁵⁻²⁷. Therefore, further investigation of an effective surveillance protocol for patients who have received adjuvant ICI therapy is warranted.

This study had several advantages and limitations. The first of the advantages was that all of the patients had undergone thoracoscopic esophagectomy, so that there was little bias arising from the technique used for the surgery in the current study. Second, our institution has extensive experience in thoracoscopic esophagectomy and this study was conducted in patients who received treatment with an already established surgical technique. Third, almost all patients with Stage II and Stage III cancer had routinely received neoadjuvant chemotherapy, so that there was little preoperative treatment bias.

The first limitation was that our study was conducted retrospectively at a single institution, and large prospective multicenter studies are needed to establish an optimal postoperative surveillance protocol for patients with esophageal cancer after radical esophagectomy. The second limitation of our study was that squamous cell carcinoma was predominant among the cases enrolled in the study, so that the results may not be extrapolatable to patients with esophageal adenocarcinoma. This is an issue for future study.

Conclusions

We advocate an effective surveillance protocol focused on the occurrence/worsening of patient symptoms for early detection of recurrence in patients with esophageal cancer who have undergone radical resection; we recommend routine imaging examinations every 6 months and outpatient care at even shorter intervals for the first 24 months after esophagectomy. We believe that this surveillance protocol may enable early therapeutic intervention and improvement of the prognosis in esophageal cancer patients with disease recurrence after surgery.

References

1. Sung H, Ferlay J, Siegel RL, Laversanne M, et al. Global cancer statistics 2020: GLOBOCAN estimates of incidence and mortality worldwide for 36 cancers in 185 countries. *CA Cancer J Clin* 2021; **71**: 209-249.
2. Koyanagi K, Kanamori K, Ninomiya Y, et al. Progress in multimodal treatment for advanced esophageal squamous cell carcinoma: Results of multi-institutional trials conducted in Japan. *Cancers* 2021; **13**: 51.
3. Sugiyama M, Morita M, Yoshida R, et al. Patterns and time of recurrence after complete resection of esophageal cancer. *Surg Today* 2012; **42**: 752-758
4. Lou F, Sima CS, Adusumilli PS, Bains MS, et al. Esophageal cancer recurrence patterns and implications for surveillance. *J Thorac Oncol* 2013; **8**: 1558-1562
5. Kunisaki C, Makino H, Takagawa R, et al. Surgical outcomes in esophageal cancer patients with tumor recurrence after curative esophagectomy. *J Gastrointest Surg* 2008; **12**: 802-810
6. Toh Y, Kitagawa Y, Kuwano H, et al. A nation-wide survey of follow-up strategies for esophageal cancer patients after a curative esophagectomy or a complete response by definitive chemoradiotherapy in Japan. *Esophagus* 2016; **13**: 173-181.
7. NCCN clinical practice guidelines in oncology – Esophageal and Esophagogastric Junction Cancers 2022.
<https://www.nccn.org/patients/guidelines/content/PDF/esophageal-patient.pdf>
8. Zachariae R, Pedersen CG, Jensen AB, et al. Association of perceived physician communication style with patient satisfaction, distress, cancer-related self-efficacy, and perceived control over the disease. *Br J Cancer* 2003; **88**: 658-65

9. Bernacki R, Paladino J, Neville BA, et al. Effect of the serious illness care program in outpatient oncology: A cluster randomized clinical trial. *JAMA Intern Med* 2019; **179**: 751-759
10. Japan Esophageal Society. Japanese classification of esophageal cancer, 11th edition: part II and III. *Esophagus* 2017; **14**: 37-65
11. Cushieri A, Shimi S, Banting S. Endoscopic oesophagectomy through a right thoracoscopic approach. *J R Coll Surg Edinb* 1992; **37**: 7-11.
12. Biere SS, van Berge Henegouwen MI, et al. Minimally invasive versus open oesophagectomy for patients with oesophageal cancer: a multicentre, open-label, randomised controlled trial. *Lancet* 2012; **379**: 1887-1892.
13. Straatman J, van der Wielen N, Cuesta MA, et al. Minimally invasive versus open esophageal resection: three-year follow-up of the previously reported randomized controlled trial: the TIME Trial. *Ann Surg* 2017; **266**: 232-236.
14. Osugi H, Takemura M, Higashino M, et al. A comparison of video-assisted thoracoscopic oesophagectomy and radical lymph node dissection for squamous cell cancer of the oesophagus with open operation. *Br J Surg* 2003; **90**: 108- 113.
15. Ozawa S, Ito E, Kazuno A, Chino O, et al. Thoracoscopic esophagectomy while in a prone position for esophageal cancer: a preceding anterior approach method. *Surg Endosc* 2013; **27**: 40–47.
16. Koyanagi K, Ozawa S, Tachimori Y. Minimally invasive esophagectomy performed with performed with the patient in a prone position: a systematic review. *Surg Today* 2016; **46**: 275–284.
17. Lindenmann J, Fediuk M, Fink-Neuboeck N, et al. Hazard curves for tumor recurrence and tumor-related death following esophagectomy for esophageal cancer. *Cancers* 2020; **12**: 2066.

18. Hiyoshi Y, Yoshida N, Watanabe M, et al. Late recurrence after radical resection of esophageal cancer *World J Surg*. 2016; **40**: 913– 920.
19. Miyata H, Yamasaki M, Kurokawa Y, et al. Survival factors in patients with recurrence after curative resection of esophageal squamous cell carcinomas. *Ann Surg Oncol* 2011; **18**: 3353–3361.
20. Bhansali MS, Fujita H, Kakegawa T, et al. Pattern of recurrence after extended radical esophagectomy with three-field lymph node dissection for squamous cell carcinoma in the thoracic esophagus. *World J Surg* 1997; **21**: 275-281.
21. Yamashita K, Watanabe M, Mine S, et al. Patterns and Outcomes of Recurrent Esophageal Cancer After Curative Esophagectomy. *World J Surg* 2017; **41**: 2337-2344.
22. Morinaga T, Iwatsuki M, Yamashita K, et al. Oligometastatic recurrence as a prognostic factor after curative resection of esophageal squamous cell carcinoma. *Surg Today* 2021; **51**: 798-806.
23. Sugiyama M, Morita M, Yoshida R, et al. Patterns and time of recurrence after complete resection of esophageal cancer. *Surg Today* 2012; **42**: 752-758.
24. Nobel TB, Sihag S, Xing X, Eljalby M, et al. Oligometastases after curative esophagectomy are not one size fits all. *Ann Thorac Surg* 2021; **112**: 1775- 1781.
25. Kelly RJ, Ajani JA, Kuzdzal J, et al. Adjuvant nivolumab in resected esophageal or gastroesophageal junction cancer. *N Engl J Med* 2021; **384**: 1191-1203.
26. Doki Y, Ajani JA, Kato K, et al. Nivolumab combination therapy in advanced esophageal squamous-cell carcinoma. *N Engl J Med* 2022; **386**: 449-462.
27. Sun JM, Shen L, Shah MA, et al. Pembrolizumab plus chemotherapy versus chemotherapy alone for first-line treatment of advanced oesophageal cancer (KEYNOTE-590): a randomised, placebo-controlled, phase 3 study. *Lancet* 2021; **398**: 759-771.

Figure legend

Figure 1. Time to recurrence and survival after recurrence in patients with symptom or without symptom. (A) Time to recurrence (all patients with recurrence); (B) time to recurrence; (C) overall survival; (D) survival after recurrence

Figure 2. Time to recurrence in patients with pain or with other symptoms (respiratory symptoms, fatigue, lump or digestive symptoms)

ACCEPTED

Table 1. Number Of Recurrent Organs at Diagnosis of Recurrence

Number of recurrent organs	Patients with recurrence, n (%)
1	77 (61)
2	28 (22)
3	13 (10)
4	7 (6)
5	1 (1)
6	1 (1)
Total	127 (100)

ACCEPTED

Table 2. Type Of Symptoms and Time After Surgery in the Symptomatic Group

Symptom	Data, n (%), (n=51)	Time after surgery, mo
Pain	17 (33)	8
Respiratory	12 (23)	4
Fatigue	9 (18)	4
Lump	7 (14)	3
Digestive	6 (12)	4.5

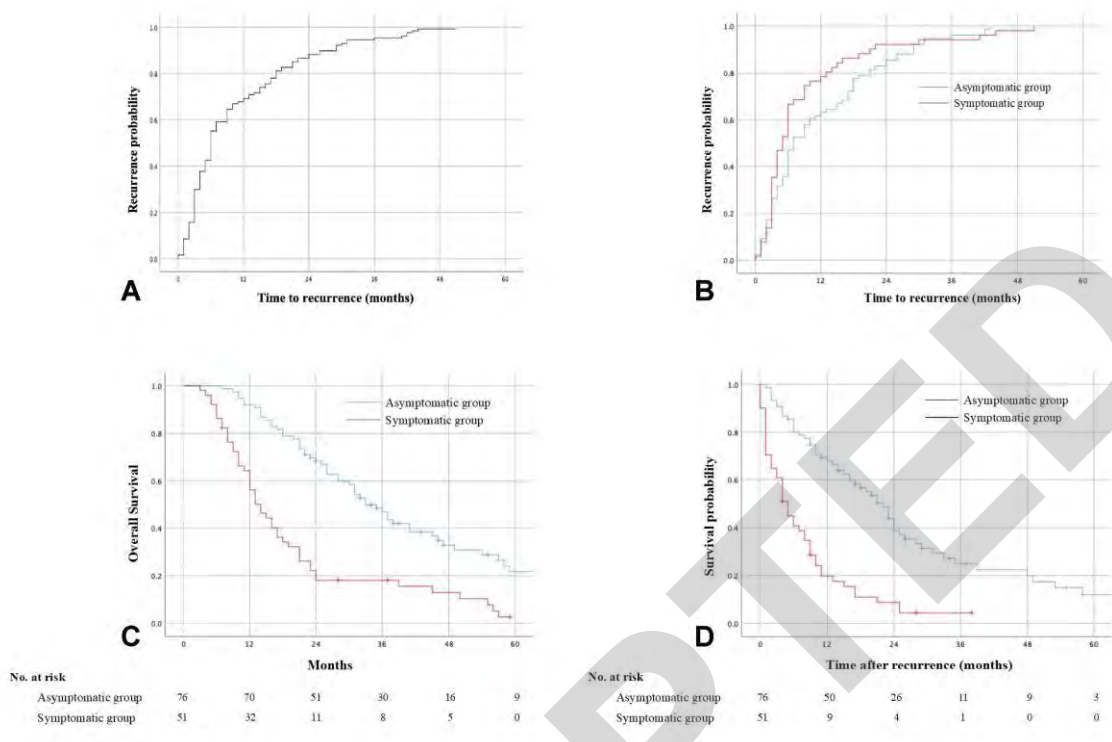
ACCEPTED

Table 3. Comparison of Symptoms at Recurrence According to Organs

Site of recurrence	Symptoms, n (N=51)	No symptom, n (N=76)	p Value*
Lymph node, n			
Yes	39	51	0.320
No	12	25	
Liver, n			
Yes	10	17	0.826
No	41	59	
Lung, n			
Yes	15	16	0.299
No	36	60	
Bone, n			
Yes	10	3	0.006
No	41	73	
Other, n			
Yes	25	14	<0.001
No	26	62	

* χ^2 test or Fisher's exact test

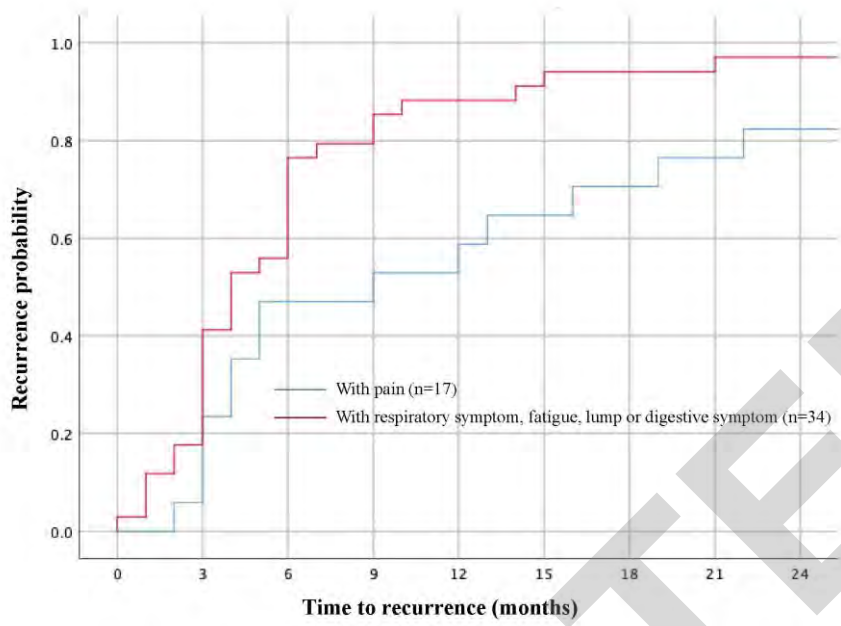
Figure 1



Downloaded from http://journals.lww.com/journals by BHDME5ePHKav1ZEoum1IQNda+kLJLhEZgbsIHod4XMMIOncY WcX1AWmnyQp/ID3I3D00dFy7T7vSF4C3YCA/OAV/pDDa8KKGKv0Ymy+78= on 08/15/2023

ACCEPTED

Figure 2



ACCEPTED

日中笹川医学奨学金制度<学位取得コース>評価書

課程博士：指導教官用



第 44 期

研究者番号：G4407

作成日：2024年3月10日

氏名	周英	ZHOU YING	性別	F	生年月日	1983/11/10
所属機関（役職）	金沢大学大学院人間社会環境研究科（博士後期課程大学院生）					
研究先（指導教官）	金沢大学大学院人間社会環境研究科人間社会環境学専攻（堤敦朗教授）					
研究テーマ	日本における精神科医療通訳者の実態と心理的体験 Actual situation and psychological experiences of psychiatric interpreters in Japan					
専攻種別	<input type="checkbox"/> 論文博士			<input checked="" type="checkbox"/> 課程博士		

研究者評価（指導教官記入欄）

成績状況	<input checked="" type="checkbox"/> 優 <input type="checkbox"/> 良 <input type="checkbox"/> 可 <input type="checkbox"/> 不可 学業成績係数=	取得単位数
		取得単位数=19／取得すべき単位総数=16
学生本人が行った研究の概要	多くの外国人が日本に在留しているが、在日外国人医療に関する病院や診療所における課題は少なくない。その中で、医療通訳者に求められている役割は大きい。しかし、日本では医療通訳が国家資格として確立されておらず、その多くがボランティアベースで取り組まれているのが現実である。医療の現場に医学を修めていない医療通訳者が入ることでその質の担保や危険性が指摘されている。また、医療の現場では死産や癌の告知、余命の説明や抗がん剤による治療など、精神的に負担の大きい内容の通訳を強いられることがある。特に、医療通訳の中でも精神科医療通訳は、一般身体の医療通訳以上に様々な心理的な影響を受けていることが報告されている。したがって、精神科医療通訳を含む医療通訳の受ける心理的体験と心理的影響を究明する必要がある。研究では17人の医療通訳者を対象に、半構造化インタビューを行なった。質的記述的研究法で分析した結果、10の「サブカテゴリー」と4つの「カテゴリー」を抽出した。それぞれ【阻害要因】（[制約]、[困難な経験]、[感情的な疲弊]からなる）、【促進要因】（[保証]、[承認]、[やりがい]からなる）、【医療通訳者の資質】（[情熱と奉仕の精神]、[対処と適応]からなる）と【専門的基盤への追求】（[体制整備への要望]、[医療通訳としての専門性]からなる）である。	
総合評価	【良かった点】 日本の精神科医療通訳者の実態と心理的体験はこれまで研究されなかった。そういう意味では価値のある研究だといえる。医療通訳の背景、歴史、海外と日本の状況などを漏れなく紹介し、精神科医療通訳者の実態の調査を展開するための土台を作った。研究結果を既存理論との比較もあり、自身のオリジナリティを出している。精神科医療通訳者の実態が究明され、医療通訳者への注目、支援、こころのケアなどのニーズも言及され、今後の政策改善につながると期待される。	
	【改善すべき点】 テーマは日本にとどまらないグローバルな課題である。よって、今後は英語での論文執筆および国際誌への投稿に挑戦してほしい	
	【今後の展望】 今後はさらなる大きいサンプルサイズで、量的研究法を用いて、研究結果を検証したり、発展させたりすることを期待される。博士論文執筆の過程で、基本的な研究実施のための素養や能力を身につけており、大いに活躍できると思う。	

学位取得見込	2024年3月に取得が決定している。
評価者（指導教官名） 堤 敦朗	

日中笹川医学奨学金制度<学位取得コース>報告書 研究者用



第44期

研究者番号: G4407

作成日: 2024年3月5日

氏名	周英	ZHOU YING	性別	F	生年月日	1983/11/10
所属機関(役職)	金沢大学大学院人間社会環境研究科(大学院生)					
研究先(指導教官)	金沢大学大学院人間社会環境研究科人間社会環境学専攻(堤 敦朗 教授)					
研究テーマ	日本における精神科医療通訳者の実態と心理的体験 Actual situation and psychological experiences of psychiatric interpreters in Japan					
専攻種別	論文博士	<input type="checkbox"/>	課程博士	<input checked="" type="checkbox"/>		

1. 研究概要(1)

1) 目的 (Goal)

多くの外国人が日本に在留しているが、在日外国人医療に関する病院や診療所における課題は少なくない。その中で、医療通訳者に求められている役割は大きい。しかし、日本では医療通訳が国家資格として確立されておらず、その多くがボランティアベースで取り組まれているのが現実である。医療の現場に医学を修めていない医療通訳者が入ることでその質の担保や危険性が指摘されている。また、医療の現場では死産や癌の告知、余命の説明や抗がん剤による治療など、精神的に負担の大きい内容の通訳を強いられることがある。特に、医療通訳の中でも精神科医療通訳は、一般身体医療通訳以上に様々な心理的影響を受けていることが報告されている。したがって、精神科医療通訳を含む医療通訳の受ける心理的体験と心理的影響を究明する必要がある。

2) 戦略 (Approach)

- 半構造化インタビューによってデータを収集した。「リサーチクエスション」は以下のとおりである。
- ・医療通訳という職業に関連する精神的苦痛、性質、程度とはどういったものか。
 - ・精神科医療通訳は一般身体医療通訳と比べて、通訳によって受ける心理的影響または精神的苦痛は何か特徴があるのか。
 - ・通訳者が実施している対処法は何か。
 - ・支援や監督体制について、どう考えているか。

3) 材料と方法 (Materials and methods)

調査は2022年9月から2023年5月にかけて、複数の通訳派遣団体および医療通訳が配置されている病院の協力を得て実施した。本調査は金沢大学人間社会研究域倫理審査委員会より承認を受けた(承認番号: 2022-31)。日本における精神科医療通訳の実態と心理的体験に関する研究は存在しない。そのため、この主観的体験を明らかにするためには、質的記述的研究デザインが適切だと判断した。作成した逐語録に基づき、文節の意味の内容を検討し、コード化、サブカテゴリー化、カテゴリー化した。

4) 実験結果 (Results)

本研究では、2件以上の精神科医療通訳の経験を持ち、3年以上の医療通訳経験者であることである。または、精神科の経験がなくても、10年以上の医療通訳の経験者の方を対象とした。最終的に17名に半構造化面接を行なった。分析の結果、一次コード600個前後、二次コード97個、サブカテゴリー10個が抽出され、4つのカテゴリーを生成した。

日本における医療通訳者は、社会的に認識されず、守られず、サポートを受けていないなどの【制約】をされながら、暴力などの【困難な経験】をし、ネガティブな感情を抱くなど【感情的な疲弊】を体験する一方、派遣機関や病院の自らの工夫でのサポートとなる【保証】を受け、患者や医療関係者に【承認】をされ、【やりがい】を感じて、医療通訳の仕事に励んでいる。そもそも、日本で活躍している医療通訳者の多くは【情熱と奉仕の精神】を持ち、医療通訳の仕事をしていくうちに、自分磨きを常に行い、【難しい場面への【対処と適応】】を考える。しかし、自分の素質や努力だけでは不足するとも気づき、【体制整備への要望】を持ち、【医療通訳としての専門性】を確立したいとも思っている。

【促進要因】と【医療通訳者の資質】がそれぞれ【阻害要因】と拮抗関係にあった。困難な状況などの【阻害要因】は重圧のようなものだが、情熱と奉仕の精神を持つ【医療通訳者の素質】や、やりがいなどの【促進要因】が基盤となっており、バランスが取れるように支えている。特に【医療通訳者の資質】がバランスを保持するための基盤の中核に存在していた。すなわち、困難な状況がありながらも、【促進要因】と【医療通訳者の資質】がパワーとなり、重圧である【阻害要因】に対抗している。しかし、このバランスが取れている状態が決して丈夫なものや持続可能なものではない。これに気づいている医療通訳者たちはより確固たるバランスを求めめるために、【専門的基盤への追求】をする。この三者が拮抗している関係の切り口が【専門的基盤への追求】であると考えられる。

5) 考察 (Discussion)

・制約

医療通訳者たちは、暴力などの【困難な経験】をし、ネガティブな感情を抱くなど【感情的な疲弊】を体験し、全体的にみて、日本における医療通訳者が未だに社会的に認識されず、守られず、サポートを受けていないなどの【制約】を受けている。これは日本の外国人政策および外国人の地位に関係するものではないかと考える。

日本はアメリカなどと比較して移民の数が少なく、移民に対する姿勢が消極的であると言える。移民政策には外国人の出入国を扱う「出入国管理政策」と入国した外国人を生活者として社会に受け入れる「社会統合政策」がある。日本は移民に消極的であるから、外国人の社会統合を任されたのは地方自治体で、実際に現場で外国人の生活支援を担っているのはNPOやボランティアの市民である。このように医療通訳のような外国人の生活支援を担う専門職へのサポートを担うのもNPOやボランティアであることが現状である。

さらに、(医療通訳者を含む)コミュニティ通訳者はマイナーな言語を扱うことが多く、サービス提供の対象者もマイノリティの人たちで、社会の辺縁に置かれる外国人たちである。どの言語を使い、誰のために通訳するかによって、通訳者のステータスが決まる。このような背景で、(医療通訳者を含む)コミュニティ通訳者の社会的ステータスが低く認識されているのである。

・体験

本研究では、精神科医療通訳者を含む医療通訳者の悲しみ、辛さ、不安、心配、動揺などのネガティブな感情と二次的トラウマ体験が確認された。これは先行研究と一致している。また、難民への対応の特段の難しさと心情の複雑さを確認でき、難民への対応が日本や海外に関わらず医療通訳者にとって困難な体験になりやすいことが示唆された。さらに、日本における医療通訳者が感じる苦痛の多くは時間が経つに連れ、気分転換などにより軽減をしていくことが確認でき、先行研究と一致した。

ネガティブな感情以外に、本研究では医療通訳者の達成感、感謝の気持ちなどのポジティブな感情も確認できた。これは海外のプロフェッショナルの医療通訳者と対照的に、日本の医療通訳者のほとんどはボランティアで活動している。ボランティアでも一つの専門分野を成り立たせるパワーとエネルギーは日本における医療通訳者の身で確認できた。

・精神科

本研究で精神科の通訳は困難であると調査で確認できた。場面的に、「暴力（言語的または身体的）をふるう患者の通訳」、「自殺行為のあった患者の通訳」、「患者が拘束される保護室に入る必要」、「強制入院の患者への対応」、「患者と家族が敵対し、通訳をそれぞれの味方にさせようとする板挟み状態」、「通訳によって、自分のキャラクターを変える患者」、「急に連絡が途切れる患者」などがあり、通訳者たちは身構えたり、気を使ったり、戸惑ったりする。内容的には、精神科は「患者が支離滅裂な内容を話す」、「主訴が診断基準で、難しい」、「抽象的な内容で、伝わるかどうか心配」、「ブライバシーが特に重視される領域で、事前に資料がもらえず、準備しにくい」など、対応の難しさが伺えた。通訳者たちの心理に関して、「怖い」、「自分を責める」、「動揺」、「戸惑い」、「共感しすぎて二次受傷を受ける」などが確認でき、さらに「患者への配慮」も確認できた。例えば、「患者は鬱で通訳依頼をするのも精一杯で、他は望まない」とか、「精神科患者を社会全体でサポートすべき」とか、「母語で自分の心情を語れない患者は大変だ」とかである。また、精神科で医療通訳をする際に、特に気をつけなければならないのは「距離感（頼りにされすぎ問題）」、「言葉の加減、ニュアンス」などがある。精神科対応として、「傾聴」、「安心させる態度」、「優しい言葉」、「患者の言葉を真に受けない」、「割り切る」、「言葉尻を取られないようにする」、「言葉のやり取りを意識して訳す」、「補って訳す」、「ありえない話をありえないまま訳す」、「精神科にはアドホック通訳が厳禁」、「患者に寄り添い、患者の立場にたつ」などが確認できた。また、精神科医療通訳をやって、肯定的な側面もあった。「精神科に興味がある」、「勉強になって、役に立った」、「知ることで、動揺や怖さを克服する」、「医者が患者の行動を見ているので、それほど言葉が必要でない時もある」、「精神的な病気の患者さんを病院が待たせないで、待ち時間が少ない」などがあった。

・レジリエンス理論との照合

ネガティブな経験をした人が必ずしもネガティブな影響を受けるとは限らない。[制約]を受け、[困難な経験]をし、[感情的な疲弊]があるが、回復して適応できるようになるパワーとエネルギーが医療通訳者の身に見られた。または、回復でき適応できる医療通訳者しか残れない現実があるとも言えよう。

レジリエンスは多くの分野で研究されるが、統一された定義はない。平野によると、「レジリエンスとは心理的な傷つきや落ち込みから立ち直る回復力のこと」であり、持って生まれた気質と関連の強い「資質的レジリエンス要因」と、後天的に身につけていきやすい「獲得的レジリエンス要因」に分けた。

レジリエンスに関する記述は医療通訳者の身でも確認できた。【阻害要因】の状況下で、【医療通訳者の資質】（「情熱と奉仕の精神」と「対処と適応」）を発揮して、「逆境」を乗り越えた。レジリエンス研究における「逆境」とは「困難・不幸・トラウマに結びつくひどい苦難や苦悩」、あるいは広範に「日常生活の中に埋め込まれた些末な混乱を含む」である。本研究での【阻害要因】となる「制約」、「困難な経験」、「感情的な疲弊」を医療通訳者にとっての「逆境」とみなすことができる。このような「逆境」を医療通訳者たちは乗り越え、心理的社会的良好な状態を維持でき適応的に生活している。彼らのこのような適応する過程・能力・結果のことをレジリエンスとすることができる。

・提案

医療通訳の市場という点では、通訳者は不利な状況に置かれる。しかも、医療通訳者利用サービスの財源が不安定で、外国人患者自身が支払う受益者負担、地方自治体や医療機関が負担する、各種助成金によるなど、ケースバイケースである。このように市場原理がうまく働かない分野においては、政府が介入すべきだと思われる。中村によると、医療通訳サービスをどのように組み込むかという課題に取り組む必要がある。健康保険法の診療報酬算定方法に医療通訳者加算などの形で医療通訳サービスを組み込むことにより、医療通訳者という存在を制度化することが可能になるという。

また、医療通訳を対象にする研修に関して、厚労省は「医療通訳育成カリキュラム基準」や「テキスト」を作成して提示するが、研修時間や具体的な研修内容は自治体や各NPO団体に任せているのが現状である。今後、国家レベルの統一研修、統一教材および統一の試験ができれば、医療通訳者の質の確保が可能になるだろう。

最後に、医療通訳者は医療通訳の仕事によって、[困難な経験]をし、[感情的な疲弊]になることが本研究で確認された。医療通訳者へのフォローアップは一部の派遣団体NPOや病院機関で見られるが、全ての医療通訳者がフォローされ、精神的なケアを受けられるとは言い難い。医療通訳者向けのカウンセリング制度の確立も必要であると思われる。これは医療通訳者たちへのエンパワーメントにもなると思われる。

・限界と課題

本研究の限界について述べる。1点目として、対象者に偏りがある可能性がある。本研究は、研究目的に賛同してインタビューに答えてくださった方の体験から分析した結果であり、インタビューを拒否した者とは違った体験をしている可能性がある。2点目として、本研究の対象者の選定に、年齢、言語、性別に関して多様性に限界がある。3点目として、本研究では精神科クリニックなど精神科に特化する医療通訳の方へのインタビューができなかった。

しかし、日本では、医療通訳者、精神科医療通訳者の実態や心理的体験に関する研究は極めて少ないため、医療通訳者たちの語りは、今後の体制整備、研修、支援への示唆を得る上で、重要な意義があったと考えられる。

今後の課題について述べる。本研究では、対象者の偏りがあったため、今後は若い世代の医療通訳者、少数言語の医療通訳者、男性の医療通訳者、および精神科クリニックに所属する精神科に特化した医療通訳者の方へアクセスをすることが必要である。また、本研究は、質的研究でベースとなるモデル図を作成したが、今後は量的研究を用いて、日本全国にいる医療通訳者を対象に、結果の検証をより大きいサンプルサイズでしていくことが求められる。

6) 参考文献 (References)

・中村安秀：医療通訳士の必要性と重要性 ―外国人に対する保健医療の現状と課題―。(中村安秀, 南谷かおり編) 医

療通訳という仕事 ―ことばと文化の壁を超えて―, 3-19, 大阪大学出版会, 大阪 (2013) など多数。

(紙面の関係で詳細を省略、添付ファイルの博士論文をご参考に)

2. 執筆論文 Publication of thesis ※記載した論文を添付してください。Attach all of the papers listed below.

論文名 1 Title	精神科医療通訳の「患者擁護」について					
掲載誌名 Published journal	日中医学					
	2022 年 11 月	Vol.37 No.3 巻(号)	29/59 頁 ~	33/62 頁	言語 Language	日本語/中国語
第1著者名 First author	周英	第2著者名 Second author	堤敦朗		第3著者名 Third author	
その他著者名 Other authors						
論文名 2 Title						
掲載誌名 Published journal						
	年 月	巻(号)	頁 ~	頁	言語 Language	
第1著者名 First author		第2著者名 Second author			第3著者名 Third author	
その他著者名 Other authors						
論文名 3 Title						
掲載誌名 Published journal						
	年 月	巻(号)	頁 ~	頁	言語 Language	
第1著者名 First author		第2著者名 Second author			第3著者名 Third author	
その他著者名 Other authors						
論文名 4 Title						
掲載誌名 Published journal						
	年 月	巻(号)	頁 ~	頁	言語 Language	
第1著者名 First author		第2著者名 Second author			第3著者名 Third author	
その他著者名 Other authors						
論文名 5 Title						
掲載誌名 Published journal						
	年 月	巻(号)	頁 ~	頁	言語 Language	
第1著者名 First author		第2著者名 Second author			第3著者名 Third author	
その他著者名 Other authors						

3. 学会発表 Conference presentation ※筆頭演者として総会・国際学会を含む主な学会で発表したものを記載してくだ

※Describe your presentation as the principal presenter in major academic meetings including general meetings or international me

学会名 Conference	第29回多文化間精神医学会学術総会			
演題 Topic	日本における医療通訳(特に精神科医療通訳)が受ける心理的影響に関する研究:質的研究			
開催日 date	2023 年 1 月 20 日	開催地 venue	滋賀県大津市	
形式 method	<input checked="" type="checkbox"/> 口頭発表 Oral <input type="checkbox"/> ポスター発表 Poster	言語 Language	<input checked="" type="checkbox"/> 日本語 <input type="checkbox"/> 英語 <input type="checkbox"/> 中国語	
共同演者名 Co-presenter	堤敦朗			
学会名 Conference				
演題 Topic				
開催日 date	年 月 日	開催地 venue		
形式 method	<input type="checkbox"/> 口頭発表 Oral <input type="checkbox"/> ポスター発表 Poster	言語 Language	<input type="checkbox"/> 日本語 <input type="checkbox"/> 英語 <input type="checkbox"/> 中国語	
共同演者名 Co-presenter				
学会名 Conference				
演題 Topic				
開催日 date	年 月 日	開催地 venue		
形式 method	<input type="checkbox"/> 口頭発表 Oral <input type="checkbox"/> ポスター発表 Poster	言語 Language	<input type="checkbox"/> 日本語 <input type="checkbox"/> 英語 <input type="checkbox"/> 中国語	
共同演者名 Co-presenter				
学会名 Conference				
演題 Topic				
開催日 date	年 月 日	開催地 venue		
形式 method	<input type="checkbox"/> 口頭発表 Oral <input type="checkbox"/> ポスター発表 Poster	言語 Language	<input type="checkbox"/> 日本語 <input type="checkbox"/> 英語 <input type="checkbox"/> 中国語	
共同演者名 Co-presenter				

4. 受賞(研究業績) Award (Research achievement)

名称 Award name	国名 Country	受賞年 Year of	年 月
名称 Award name	国名 Country	受賞年 Year of	年 月

5. 本研究テーマに関わる他の研究助成金受給 Other research grants concerned with your research theme

受給実績 Receipt record	<input type="checkbox"/> 有 <input checked="" type="checkbox"/> 無
助成機関名称 Funding agency	
助成金名称 Grant name	
受給期間 Supported period	年 月 ~ 年 月
受給額 Amount received	円
受給実績 Receipt record	<input type="checkbox"/> 有 <input checked="" type="checkbox"/> 無
助成機関名称 Funding agency	
助成金名称 Grant name	
受給期間 Supported period	年 月 ~ 年 月
受給額 Amount received	円

6. 他の奨学金受給 Another awarded scholarship

受給実績 Receipt record	<input type="checkbox"/> 有 <input checked="" type="checkbox"/> 無
助成機関名称 Funding agency	
奨学金名称 Scholarship name	
受給期間 Supported period	年 月 ~ 年 月
受給額 Amount received	円

7. 研究活動に関する報道発表 Press release concerned with your research activities

※記載した記事を添付してください。Attach a copy of the article described below

報道発表 Press release	<input type="checkbox"/> 有 <input checked="" type="checkbox"/> 無	発表年月日 Date of release	
発表機関 Released medium			
発表形式 Release method	・新聞 ・雑誌 ・Web site ・記者発表 ・その他()		
発表タイトル Released title			

8. 本研究テーマに関する特許出願予定 Patent application concerned with your research theme

出願予定 Scheduled	<input type="checkbox"/> 有 <input checked="" type="checkbox"/> 無	出願国 Application	
出願内容(概要) Application contents			

9. その他 Others

--

指導責任者(記名) 堤 敦朗

精神科医療通訳の「患者擁護」について

“Patient Advocacy” for Psychiatric Interpreters

金沢大学人間社会環境研究科 博士後期課程

周 英
堤 敦朗

金沢大学融合研究域 教授

【Abstract】

Globalization has facilitated international travel, and the number of non-native patients receiving psychiatric services in Japan is increasing. Consequently, differences in language and culture have become the biggest issues faced by psychiatric institutions. Therefore, psychiatric interpreters are expected to play a major role. Studies have indicated that medical interpreters require advocacy, especially in psychiatric settings. This article clarifies what is meant by the term “advocacy” and why it is required in psychiatric interpretation.

【Key words】

Psychiatric interpreters, Advocacy, Community interpreters

はじめに

世界規模でグローバル化が進み、人々の国境を跨ぐ移動が容易となっている。出入国在留管理庁^[1]によると、2020年6月末に日本における在留外国人数は288万5904人で、日本の総人口のおよそ2%を占めている。

日本全国の精神医療機関に対して実施された「精神医療機関における外国人患者受入の現状と課題把握に関する調査」^[2]（2020年3月）で、精神医療機関を受診する外国人患者の対応には多くの施設が苦慮していて、その背景に「言語面」や「文化的」背景が存在すること、また日本にいる外国人に対応するために「同意書および告知文書」の多言語版の作成や精神保健福祉法の早急な整備など、精神科医療における外国人患者の受け入れ環境の整備の必要性などが認識された。

このような状況下において、医療通訳が大きな役割を担うことができる。「言葉」の問題に関して、「心の病を患うと、外国語能力が極端に落ちる」「母語以外で自分の内面を語ることは難しい」^[3] ことがあるため、医療通訳が間に立つと、患者が母語で病状や心境などを語るができる。さらに「文化」の問題に関しては、両方の文化を知る医療通訳者がいる場合、文化の違いによる理解の差に気づき、適度な範囲内で補足説明をすることで医師と患者の間の意思疎通がよりスムーズになり、医師の病状把握や患者の安心感につながる事が期待できる。

本稿では、精神科の医師と患者の間に立つ医療通訳者のことを「精神科医療通訳」とする。「精神科医療通訳」は「一般身体医療通訳」と区別するために名づけたもので、既存の固有名詞ではない。また、医療通訳は「コミュニティ通訳」の一種であるため、医療通訳を論ずるにあたり、まずコミュニティ通訳について論ずる必要がある。

コミュニティ通訳とは

通訳の種類分類方法には大きく分けて2つある。一つは通訳の手法で分類する方法であり、「同時通訳」「逐次通訳」「ウィスパリング通訳」がある。もう一つは目的によって分類する方法であり、「会議通訳」「エンターテインメント通訳」「ビジネス通訳」「放送通訳」「コミュニティ通訳」「通訳ガイド」などがある¹⁾。

本稿で取り扱う「コミュニティ通訳」とは、在住外国人が専門職と話す時に使う通訳であり、具体的には「医療通訳」「司法通訳」「行政通訳」「教育通訳」などが挙げられる^[4]。これらの異なるタイプの通訳者は異文化の媒介者として意思疎通のための役割を果たす点においては同じだが、通訳者が置かれている環境がそれぞれ異なるため、通訳に求められる「言葉の伝達」以外の要素が異なってくる。例えば、「司法通訳」は中立性が極端に求められる^[5]のに対し、医療通訳は医師と患者のつなぎ役として患者の擁護をする必要がある^[6]。

精神科医療通訳の特殊性

医療通訳の役割を決定するいくつかの要素の一つに「医療科の特質」がある。

精神科医療の特質は、精神科医が患者の「行動・振る舞い」「認知能力」「コミュニケーション能力」を確認して診断をする点にある。これらの要素を判断するために、Turner^[7]は患者の話し方の要素、すなわち「構文」「語順」「語彙の整合性」「言葉の

脱落」「文化や宗教との整合性」「母国語での言語能力」の6つに注目すべきだと述べている。

つまり精神科医療における医療通訳では、患者の話す言葉の構文や語順の自然さ、不自然さを再現し、語彙の選択や整合性に問題があればそれも再現し、患者が話す事柄がその所属する文化や宗教において適切なものであるかも説明し、さらには通訳するだけではわからない患者の母国語での言語能力の評価を行うことまでもが求められるのである。精神科医療において医療通訳は、辻褄の合わないものは辻褄の合わないまま通訳して、その説明も求められる^[8]。例えば、統合失調症の幻覚妄想状態の患者がいるとする。統合失調症患者の最も重要な障害は思考障害で、精神科医が患者の訴えを聞いても、思考に論理の飛躍があるため、話の脈絡がうまくつかめず、理解不能であったりする。構文や語順の崩れ、語彙の整合性の不具合、言葉の脱落、自分自身で新しい言葉を作るという言語新作もみられる^[6]。しかし、通訳者はそのまま通訳し、その内容についても説明しなければならない。

さらに、上述の6つの要素を再現するには「機械的な通訳」では足りないため、事前に医師と通訳者が打ち合わせを行う必要がある。Turnerが診察前の打ち合わせ項目として「患者の医療背景」「患者の文化背景」「医療通訳の役割」「異文化問題への対処法」そして「中断方法」を提起している。さらに診察後の確認項目として、「診断に重要な要素の確認」と「通訳者の精神状態の把握」を指摘している^[7]。

事前の打ち合わせに関して、精神科医の阿部先生は、通訳者と患者が行うことも必要だと指摘する^[6]。診察をスムーズに進めるためには、患者が受

¹⁾ 通訳の分類法は国や地域、ひいては通訳派遣会社などによって違うため、上記の分類法は、状況や場面によって呼称が変わる場合がある。

診に至った背景を通訳者が事前に聞き取っておく必要があり、そのため通訳者は、精神科医療に関する医学的知識をある程度有しておく必要がある。また、医師と通訳者の事前打ち合わせと比較して、患者と通訳者の事前打ち合わせは、患者に通訳者が自分の味方であると感じさせやすいため、患者と通訳者の信頼構築につながる可能性がある。

精神科医療において同じ通訳者が担当することがより良いと考えられている。同じ通訳が継続的に担当すると患者と通訳者の間に個人的な関係が生まれ、「中立的」な立場が取りにくくなる懸念もあるが、他方で同じ通訳者が担当することで、前述した6つの要素に精通しやすくなり、患者との信頼関係の構築が容易になるメリットもある。その結果、診断に必要な要素を効率よく、正確に伝えることが可能になる^[8]。

したがって、精神科医療以外の医療における通訳は主に身体疾患に関わる医学的な知識が求められるが、精神医療における通訳は、精神疾患の症状、診断名や精神医療制度などに関する専門的知識が求められる。また、精神科医と患者の心をつなぐ理解者として位置づけられなければならないため、語学力以外に文化の理解や患者の擁護が求められる^[8]。

精神医療の通訳者に求められる専門性とは、精神疾患名とその疾患の概念、精神症状、診断方法、治療法、薬物の効用と副作用、治療経過、予後と精神医療制度の知識を指す。さらに、診察室で患者と精神科医をつなぐ通訳者として、自分の感情をできるだけ排除し、習得した知識を用いて両者の橋渡しをすることである。そのためには、両者の表情に気を配り、患者の苦悩や文化社会的背景を理解し、それぞれの感情と会話を正確な訳語で適切に伝え、患者と精神科医が通訳内容に対して同じ解釈をしているかを見抜いて、両者のつながりに揺るぎなく位置することが求められる^[6]。

精神科医療通訳の「患者擁護」とは

日本看護協会^[9]によると、「患者擁護」=アドボカシー (advocacy) とは権利擁護や代弁などという意味であり、看護実践において看護職は、患者のアドボケーター (権利擁護者、代弁者) として患者の権利を擁護し、患者の価値や信念に最も近い決定ができるように援助し、さらに患者の人間としての尊厳、プライバシーなどを尊重しなければならないという。

通訳の立場での「患者擁護」の定義について、国際的な規定やアメリカ、日本の規定、また専門家の見解を以下に示す。

- ・ 国際医療通訳者協会^[10] (IMIA: International Medical Interpreters Association) は医療通訳者の行動に関する倫理規定を策定した。倫理規程においては「通訳者は、患者の権利を擁護する役割、および情報伝達のために適切かつ必要な場合に限り、専門的な判断力で、異文化間の仲介者として医療提供者と患者に文化の違いや慣行を説明する役割を担う。」との記述がある。
- ・ 全米医療通訳協議会^[11] (NCIHC) は2004年7月に「全米医療通訳倫理規定」を発表した。この規定で「患者擁護」について「患者の健康、福利、あるいは尊厳が危険にさらされている場合、通訳者は、アドボケーター (擁護者) としてふるまうことを正当化されるかもしれない。アドボカシー (擁護的行為) とは、健康上の良い結果を支援するという意図を伴い、コミュニケーション促進の範囲を超えて、個人のために行われる行為であると理解される。擁護は、状況を慎重に思慮深く分析した後に、そして、他のより介入的でない手段によって問題が解決されなかった場合にのみ、行われるべきである。」

と示している。

- ・ 日本における規程に関して、厚生労働省の「医療通訳」^[12] テキストでは、権利擁護（アドボカシー）に関して「権利擁護（アドボカシー）とは患者が生命の尊厳や危機にさらされている場合には、適切な知識と判断によって権利擁護を果たすことである。」と示している。さらに、「通訳者が権利擁護を行うことは、通訳者の役割を超えており、すべきではないと禁止している国もあるが、本基準では、医療通訳においては、適切な状況分析をした上で、患者の安全や生命が脅かされる、危機にさらされている場合に限り、本来の医療通訳者としての役割から外れて、権利擁護のための行動を取ることができる」と付け加えている。
- ・ 専門家は通訳者の「患者擁護」について、飯田^[13]は「医療通訳士は患者と医療従事者の言葉と文化、置かれる状況を理解するから、全ての人に適切な医療サービスが提供されるよう尽力することが求められ、患者擁護ができる。」、また「権利の擁護は医療通訳士が直接的代理や代行を行うことでなく、患者が自らの権利を確保し回復して行くための支援を行うこと」と述べている。
- ・ エレーラ・ルルデス^[14]は「患者擁護」について、「外国人の患者などが言葉の壁によって自分を語れない（自身を代弁できない）場合、通訳士は「救済者」として手を差し伸べる」、「日本に暮らす外国人の社会的・経済的状況を把握したり、患者のわずかな顔の表情から文化的、家族的、個人的な状況を読み取ったりして必要な擁護を行う」、「通訳士は外国人に対する情報提供者（情報源）の役割を担っている。患者は通訳士に対して色々な期待を寄せているが、通訳者は、いつ直接介入すべきか、いつ他者に援

助を求めるべきかについて判断しなければならない」、「通訳士という仕事は、良心的で粘り強く、過保護にならない程度の暖かさを持った尊敬されるような対人援助である」と述べている。

以上の倫理規定および専門家の観点を踏まえ、通訳者の立場における「患者擁護」は「患者が危険にさらされ、他の介入的な手段がない場合にのみ行って良いという極めて稀な行為だ」と一部に認識されている一方、「通訳者が患者を観察し、患者が危険にさらされている場合には、患者の権利が尊重されるように患者の代弁者になったり、文化の理解者として患者と医者との間の文化的なギャップを埋めたり、情報提供者になったり、患者のために他の人に助けを求めたりして患者の回復を支援することである」と暫定的に定義づけることもできる。

終わりに

精神科医療通訳の特殊性と「患者擁護」の定義について論じた。しかし、実際の現場で精神科医療通訳をしている医療通訳者たちは「患者擁護」をどのように認識・実行しているのか、また実行する際の課題の有無に関して、引き続き研究をしていきたい。

謝辞

本研究は、日中笹川医学奨学金の助成を受けたものです。この奨学金制度により、私は研究活動に専念することができています。ご支援いただいた方々に厚く御礼申し上げます。

引用文献：

- [1] 出入国在留管理庁 在留外国人統計（旧登録外国人統計）統計表 https://www.moj.go.jp/isa/policies/statistics/toukei_ichiran_touroku.html（アクセス日：2022年3月1日）
- [2] 厚生労働省課題 令和元年度障害者総合福祉推進事業精神医療機関における外国人患者受入の現状と課題把握に関する調査 <https://www.mhlw.go.jp/content/12200000/000672477.pdf>（アクセス日：2022年3月1日）
- [3] 阿部裕 多文化精神医療 鹿児島：ラグーナ出版：2019
- [4] 村松紀子 「コミュニティ活動における医療通訳士の役割」『医療通訳士という仕事』大阪：大阪大学出版社：2013：76
- [5] 長尾ひろみ 「医療通訳の職業倫理規定」『医療通訳入門』東京：松柏社：2007 29-46
- [6] 阿部裕 精神医療におけるコミュニティ通訳の必要性 シリーズ多言語・多文化協働実践研究 16 2013：105-113
- [7] Turner G Onsite Mental Health Interpreting A workshop for Professional Interpreters from MMHA's NT forum
- [8] 押見貴之 精神医療における医療通訳 こころと文化 2009：8巻：108-113
- [9] 日本看護協会 看護実践情報 臨床倫理のアプローチ <https://www.nurse.or.jp/nursing/practice/rinri/text/basic/approach/index.html>（アクセス日：2022年3月1日）
- [10] IMIA Code of Ethics <https://www.imiaweb.org/code/default.asp>（アクセス日：2022年3月1日）
IMIA 倫理規定（日本語訳） <https://www.imiaweb.org/uploads/pages/393.pdf>（アクセス日：2022年3月1日）
- [11] 全米医療通訳倫理規定 https://www.migrationpolicy.org/sites/default/files/language_portal/ANationalCodeofEthicsforInterpretersinHealthCareinJapanese_0.pdf（アクセス日：2022年3月1日）
- [12] 厚生労働省 医療通訳に関する資料 テキスト「医療通訳」 <https://www.mhlw.go.jp/content/10800000/000385181.pdf> アクセス日：2022年3月1日
- [13] 飯田奈美子 「医療通訳士倫理規定を読み解く」『医療通訳士という仕事』大阪：大阪大学出版社：2013：33-47
- [14] エレーラ・ルルデス 「外国人患者から見た医療通訳士の役割」『医療通訳士という仕事』大阪：大阪大学出版社：2013：89-97

◆ 著者連絡先 ◆

周 英

金沢大学人間社会環境研究科 博士後期課程

E-mail：11431984@qq.com

精神科医疗口译的“患者拥护”

“Patient Advocacy” for Psychiatric Interpreters

金泽大学人间社会环境研究科 博士后期课程

周 英
堤 敦朗

金泽大学融合研究域 教授

【Abstract】

Globalization has facilitated international travel, and the number of non-native patients receiving psychiatric services in Japan is increasing. Consequently, differences in language and culture have become the biggest issues faced by psychiatric institutions. Therefore, psychiatric interpreters are expected to play a major role. Studies have indicated that medical interpreters require advocacy, especially in psychiatric settings. This article clarifies what is meant by the term “advocacy” and why it is required in psychiatric interpretation.

【Key words】

Psychiatric interpreters, Advocacy, Community interpreters

前 言

全球化正在世界范围进行，人们可以更容易的在世界各地移动。根据日本出入国在留管理厅^[1]的数据显示，截至2020年6月底，在日本的外国人人数为288万5904人，约占日本总人口的2%。

根据以日本全国范围的精神科医疗机构为对象开展的“精神科医疗机构接收外国人患者的现状和问题把握的相关调查”^[2]（2020年3月）显示，许多精神科医疗机构在接诊外国患者时感到困惑，并表示其原因在于“语言”和“文化”的不同。为了更好地应对在日本的外国患者，有必要准备更多种语言版本的“知情同意书和告知文件”，尽早完善精神保健福祉法，以改善对外国患者的接收环境。

在这样的大背景下，医疗口译员可以发挥重要作用。在“语言”的问题上，由于“当一个人患有精神疾病时，他的外语能力会极大降低。”“使用母语之外

的语言来谈论自己内心感受是很困难的”^[3]，所以医疗口译员可以帮助患者使用母语来谈论自己的病情和感受。此外，在“文化”方面，可以预见，了解两种文化的医疗口译员更明白文化差异造成的理解偏差，并能在合理的范围内提供补充说明，从而使医生和患者之间的沟通更加顺畅，使医生更好的了解患者病情并使患者更为放心。

在本文中，将介于精神科医生和患者之间的医疗口译员称为“精神科医疗口译”。它并非固定术语，是为了与“一般身体类医疗口译”区分，才冠以此名。医疗口译是“社区口译”的一种，在探讨医疗口译之前，需要首先认识什么是社区口译。

什么是社区口译

口译主要有两种分类。一种是按照翻译方式，可分为“同声传译”、“交替传译”和“耳语翻译”。另

一种是按照翻译目的划分。主要类别包括“会议口译”、“娱乐口译”、“商务口译”、“广播口译”、“社区口译”和“导游口译”等¹。

而本文所涉及的“社区口译”是指居住在日本的外国居民与专职人员交谈时所使用的口译。具体包括“医疗口译”、“司法口译”、“行政口译”和“教育口译”^[4]。这些不同类型的口译员作为不同文化间的中介，发挥促进沟通的作用方面是相同的，但由于口译员所处的环境不同，所以对他们除了“语言传播”之外的素质要求也不同。比如，“司法口译”被要求必须极为中立^[5]，而与此相对，医疗口译则更需要口译员作为医生与患者之间的纽带，对患者进行拥护^[6]。

精神科医疗口译的特殊性

有几个要素决定了医疗口译的实际作用，其中之一是“医疗部门的特质”。

精神科医学的特殊性在于医生诊断时需要考虑患者的“行动和行为”、“认知能力”以及“沟通能力”。Turner^[7]认为，精神科医生需要关注患者的表达，即“句法”、“词序”、“词汇的一致性”、“单词的遗漏”、“与文化和宗教的一致性”、“母语的语言能力”这六要素。

也就是说，精神科医疗口译，需要在翻译中再现实出患者所表达的语言的句法和词序是否自然，如果词汇的选择和一致性方面出现问题也应将其体现在翻译中，并对患者所说的事由是否与其所属的文化与宗教相契合进行说明。并且，因为仅靠翻译无法评估患者的母语水平，口译员还需要对其母语能力进行评价。也就是说，精神科医疗口译如果遇到患者的话语不合常理不合逻辑，也应该使用不合常理不合逻辑的方式进行翻译^[8]。例如，假设有一位精神分裂症的患者出

现幻觉和妄想。由于精神分裂症患者最严重的问题是思维障碍，所以精神科医生即使倾听了患者的主诉，但由于病人的思维具有跳跃性，无法掌握其言语脉络，从而导致患者的话语无法理解。除了句法和词序的混乱之外，还可能出现词汇的不一致以及单词的遗漏和患者自身创造出新语言的语言创新现象^[6]。但是，出现这样的情况时，口译员必须如实翻译，并对这些情况进行解释说明。

此外，由于“机械翻译”不足以再现上述六个要素，所以需要医生与口译员进行事前沟通确认。Turner提出了“患者的就医经历”、“患者的文化背景”、“医疗口译的作用”、“跨文化问题的处理方法”以及“如何打断”来作为检查前的沟通项目。并认为，就诊后应该“确认诊断过程中的重要要素”和“把握口译员的精神状态”^[7]。

但是，关于事前沟通确认，精神科的阿部医生认为应该由口译员和患者来进行事前沟通^[6]。为使诊疗能够顺利进行，口译员需要事先听取患者的就诊背景，因此，口译员需要具备一定的精神科方面的医学知识。此外，与医生和口译员的事前沟通确认相比，患者与口译员的事前沟通确认能让患者更容易产生口译员是站在自己一方的感觉，从而更容易的建立双方之间的信任关系。

在精神科医疗中由同一位口译员来持续负责被认为是更为理想的。但也有人担心，同一位口译员持续负责会使患者和译员之间形成个人关系，从而很难保持“中立”立场。但另一方面，同一位口译员负责的好处在于更容易把握上述六要素，并更容易与患者建立信任关系，从而能够更高效准确的传递诊断所需的要素信息^[8]。

因此，精神科医疗之外的医疗口译主要需要掌握与身体疾病相关的医学知识。而精神科医疗口译，则需要具备精神疾病的症状、诊断名称和精神保健系统

¹ 由于各国、各地区以及各口译派遣机构对口译员的分类不同，上述分类法在不同的情况和场合下会有不同的叫法。

的专业知识。此外，他们还必须是精神科医生与患者心灵之间的理解纽带。除了语言能力之外，还需要有文化的理解和对患者的拥护^[8]。

精神科医疗口译需要具备的专业素质，是指精神疾病的名称及其概念、精神疾病的症状、诊断方法、治疗方法、药物效益和副作用、治疗过程、预后和精神疾病医疗系统的相关知识。此外，作为诊疗室中患者与精神科医生的桥梁，口译员需要尽量不受自己情绪的影响，用所掌握的知识为二者的沟通作出努力。为此，需要既注意双方的面部表情，又理解患者的苦恼和文化社会背景，并用正确的语言恰当地传达每一次情绪和对话，观察患者和精神科医生对翻译内容是否有相同的理解，坚定地置身于两者的沟通之中^[6]。

精神科医疗口译的“患者拥护”是什么

根据日本护理协会^[9]的说法，“患者拥护”= advocacy 有权利拥护和代言等意思。在护理实践中，护士作为患者的 advocator（权利拥护者、代言人），需要维护患者的权利，帮助患者做出最接近他们价值观和信念的决定，并确保患者作为人的尊严和隐私得到尊重。

从口译员的角度来看，“患者拥护”意味着什么？本节将探讨国际和美国、日本的规定，以及专家的意见。

- 首先，国际医疗口译员协会^[10]（IMIA：International Medical Interpreters Association）为医疗口译员的行为制定了一套道德准则。其中，“口译员有责任维护患者的权利，为了传递信息在合适并必须这样做的情况下，利用他们的专业判断，作为跨文化的中介人士来向医疗服务提供者和患者解释文化和习惯差异。”
- 全美医疗口译委员会^[11]（NCIHC）于2004年7月

发布了“全美医疗口译道德准则”。准则对“患者拥护”的定义如下。当“病人的健康、福祉或尊严受到威胁时，口译员可以充当 advocator（拥护者）。Advocacy（拥护行为）被理解为，有支持形成积极的健康方面的结果的意图，并超越了促进沟通的范畴，为了个人而发生的行为。这种拥护行为，必须要在对情况深思熟虑之后，并且仅在其他非介入类手段无法解决问题的情况下才能使用。”

- 日本的情况，可以参考厚生劳动省的“医疗口译”^[12]教材。该教材中关于权利拥护（Advocacy）提供了如下措辞。“权利拥护（Advocacy）是在患者的生命尊严受到威胁时，使用恰当的知识来判断来保护他们权利的行为。”还进一步指出，“口译员的权利拥护行为，超出了口译员的职责范围，有些国家禁止口译员的这一行为。但本准则中规定，医疗口译在对情况进行恰当分析的基础上，仅在患者的安全和生命受到威胁，处于危险中时，才可以偏离原有的医疗口译的职责，来采取权利拥护的行为。”
- 专家们对口译员的患者拥护的解释则如下所示。饭田^[13]认为，“医疗口译员了解患者和医护人员语言和文化的，以及他们所处的环境，因此他们应致力于向所有人提供合适的医疗服务，并能够进行患者拥护行为。”他/她还指出，“权利拥护不是医疗口译员直接代理或代行，而是协助患者争取和恢复自己的权利。”
- Lourdes Herrera^[14]对“患者拥护”提出了以下观点。“当外国患者因语言障碍而无法为自己说话（无法为自己代言）时，口译者会像“救援者”一样伸出援手”，“需要通过了解生活在日本的外国人的社会和经济状况，并从患者的细微面部表情来读取其文化、家庭和个人情况，提供必要的拥护行为。”“口译员还扮演着向外国人提供信息（信息来源）的角色。患者对口译员有诸多

期待，但口译员必须判断应该何时直接干预，何时寻求他人的帮助。”“口译这份工作，应该是善良和坚持的，并且是令人尊重的援助过程，既给予一定程度上的温暖，又不会过度保护。”

总结上述道德规范和专家意见，虽然部分观点认为口译员所做出的“患者拥护”是“只有在患者处于危险境地，并在没有其他可干预的手段时才能采取的及其罕见的行为。”但作者希望暂且将其定义为“口译员观察患者，当患者处于危险境地时，需要成为患者的代言人以确保患者的权利得到尊重，还需要作为文化的理解者来弥补患者和医护之间的文化差异，以及作为信息提供者，或者作为支持者为患者寻求他人的帮助来协助患者康复”。

结 论

本文探讨了精神科医疗口译的特殊性和“患者拥护”的定义。然而，在实际临床中，从事精神科医疗口译的口译员们究竟如何看待和实践“患者拥护”，以及在实践过程中是否有困难之处。这些将会成为作者未来的研究课题。

鸣 谢

这项研究得到了中日笹川医学奖学金的资助。奖学金帮助我全身心投入到研究活动中。在此我表示衷心的感谢。

引用文献：

- [1] 出入国在留管理厅 在留外国人统计（旧登录外国人统计）统计表
https://www.moj.go.jp/isa/policies/statistics/toukei_ichiran_touroku.html（访问时间：2022年3月1日）
- [2] 厚生劳动省课题 令和元年度残疾人综合福祉推进事业

精神科医疗机构接收外国人患者的现状和问题把握的相关调查 <https://www.mhlw.go.jp/content/12200000/000672477.pdf>（访问时间：2022年3月1日）

- [3] 阿部裕 多文化精神医疗 鹿儿岛：Laguna 出版：2019
- [4] 村松纪子“社区活动中医疗口译员的作用”《医疗口译这份工作》大阪：大阪大学出版社：2013：76
- [5] 长尾 Hiromi “医疗口译的职业伦理规定”《医疗口译入门》东京：松柏社：2007 29-46
- [6] 阿部裕 精神医疗领域中社区口译的必要性 Series 多语言和多文化合作实践研究 16 2013：105-113
- [7] Turner G Onsite Mental Health Interpreting A workshop for Professional Interpreters from MMHA's NT forum
- [8] 押见贵之 精神医疗中的医疗口译 心与文化 2009：8卷：108-113
- [9] 日本护理协会 护理实践信息 临床伦理方法 <https://www.nurse.or.jp/nursing/practice/rinri/text/basic/approach/index.html>（访问时间：2022年3月1日）
- [10] IMIA Code of Ethics <https://www.imiaweb.org/code/default.asp>（访问时间：2022年3月1日）
 IMIA 伦理规定（日语翻译版）<https://www.imiaweb.org/uploads/pages/393.pdf>（访问时间：2022年3月1日）
- [11] 全美医疗口译伦理规定 https://www.migrationpolicy.org/sites/default/files/language_portal/ANationalCodeofEthicsforInterpretersinHealthCareinJapanese_0.pdf（访问时间：2022年3月1日）
- [12] 厚生劳动省 与医疗口译相关的资料 课本《医疗口译》<https://www.mhlw.go.jp/content/10800000/000385181.pdf>（访问时间：2022年3月1日）
- [13] 饭田奈美子“医疗口译员伦理规定解读”《论医疗口译这份工作》大阪：大阪大学出版社：2013：33-47
- [14] Lourdes Herrera“从外国患者的角度看医疗口译的作用”《论医疗口译这份工作》大阪：大阪大学出版社：2013：89-97

◆ 著者联系方法 ◆

周 英

金泽大学人间社会环境研究科 博士后期课程

E-mail：11431984@qq.com

日中笹川医学奨学金制度<学位取得コース>評価書

課程博士：指導教官用



第 44 期

研究者番号：G4408

作成日：2024年3月1日

氏名	劉天驕	LIU TIANJIAO	性別	M	生年月日	1995/03/10
所属機関（役職）	成都市婦女兒童中心醫院醫務部（幹事）					
研究先（指導教官）	京都大学大学院 医学研究科遺伝医学講座分子遺伝学分野（篠原 隆司 教授）					
研究テーマ	α-Klotho を要因とする老化過程における精子幹細胞の微小環境制御 The study on the molecular mechanism of α-Klotho' s regulation of spermatogonial stem cell niche during aging					
専攻種別	<input type="checkbox"/> 論文博士			<input checked="" type="checkbox"/> 課程博士		

研究者評価（指導教官記入欄）

成績状況	良 学業成績係数=	取得単位数
		取得単位数 30 / 取得すべき単位数総数 30
学生本人が行った研究の概要	劉天驕さんは老化が精子形成に及ぼす影響を調べるため、老化モデルである α-Klotho ノックアウトマウスの解析を行いました。このマウスの精巣においてテストステロンの産生の低下と、血液精巣閉鎖を形成する分子の発現の低下していることを見出し、これらが精子形成の破綻に関わっている可能性を示唆する結果を得ました。また、テストステロンを皮下に埋め込み、もしくは皮下注射にて連続投与し、精巣や他の臓器に与える影響を調べました。	
総合評価	【良かった点】 実験手技は着実に増え、日本語は入学時より上達し読み書きに関してはかなり改善されました。	
	【改善すべき点】 日本語の会話の能力はまだ低く、研究室の他のメンバーとのコミュニケーションができていません。 研究に関しては、実験がうまくいかないなど問題が生じた時に自分で解決法を探す態度がまだできていません。	
	【今後の展望】 実験はできるようになりましたが、今後は研究の進め方や、問題が生じた時の対処法など、自立して研究に取り組んでいけるようになるかどうか大きな課題だと思います。	
学位取得見込	奨学金支援終了後3年以内に日本の博士学位を取得できる見込みです。	
評価者（指導教官名） 篠原 隆司		

日中笹川医学奨学金制度<学位取得コース>報告書 研究者用



第44期

研究者番号: G4408

作成日: 2024年3月 12 日

氏名	刘 天骄	LIU TIANJIAO	性別	M	生年月日	1995/03/10
所属機関(役職)	成都市婦女兒童中心医院婦人科(医師)					
研究先(指導教官)	京都大学大学院 医学研究科遺伝医学講座分子遺伝学分野(篠原 隆司 教授)					
研究テーマ	α -Klothoを要因とする老化過程における精子幹細胞の微小環境制御 The study on the molecular mechanism of α -Klotho's regulation of spermatogonial stem cell niche during aging					
専攻種別	論文博士	<input checked="" type="checkbox"/>	課程博士	<input type="checkbox"/>		
1. 研究概要(1) 1) 目的(Goal) Aging is an urgent sociomedical issue which greatly threatens the fertility of population in many societies, especially in the developed countries and regions. It was reported that advanced paternal age brings higher risks of the pre-mature birth, low Apgar scores or admission to a neonatal intensive care department of newborns. The paternal age also improves the incidence rate of multiple congenital defects such as heart malformations as well as oral, palate and lip cleft. In addition, many mental disorders like autism, schizophrenia, bipolar disorder, low intelligence capacity were also more frequently observed with advanced father's age. ¹ The spermatogonial stem cells (SSCs), a rare subpopulation of the spermatogonia, are tasked to self-renew actively to sustain the SSC reservoir and give rise to progenitors poised for eventually differentiating into sperms ² . Spermatogonial stem cell (SSC) transplantation is regarded as a promising technique for treating the infertility of male survivors from cancer therapies before sexual maturation. The SSC transplantation, which reintroduces the SSCs into the seminiferous tubules of recipient's testis, can initiate their spermatogenesis and enable the production of their own biological children. The aging of SSCs is always accompanied by impaired proliferation, epigenetic abnormalities, altered metabolism and even the loss of sperm-forming function ³ , hampering the scientific utilization of SSCs' versatility a lot. The serial transplantation of SSCs into young testes, which enabled the longer than lifetime proliferation of SSCs and also proved their strong proliferation ability ⁴ . This evidence indicated that the SSCs have a unique mode of aging which is likely caused by the deteriorated niche, a protective region for stem cells with surrounding stromal cells. The Klotho gene is a critical gene in regulating phosphate metabolism and senescence. Mice deficient in α -Klotho not only have a phosphate metabolism dysfunction and hyperphosphatasemia due to the impaired urinary phosphate excretion but also show apparent and multiple phenotypes of premature aging, including slower growth, smaller body size, atrophy of multiple organs, vascular calcification, sarcopenia, cardiac hypertrophy and fibrosis, osteopenia, emphysematous lung, hearing impairment, cognitive defects and shortened lifespan. ⁵ Its abnormal expression and functioning was recently found play an essential role in the premature placental senescence and malformation caused by advanced maternal age. ⁶ However, its regulation on the aging of male fertility has not been reported yet. This study aims to investigate the molecular mechanism of Klotho's regulation on the senescence of spermatogonial stem cells and their niche.						
2) 戦略(Approach) (1) investigate the spermatogonial stem cell niche of Klotho testis using immunostaining (2) functional analysis of the blood testicular barrier (BTB) of Klotho testis (3) exogenous supplement of testosterone into Klotho KO male mice and investigate its lifespan, spermatogonial stem cell niche and spermatogenesis						
3) 材料と方法(Materials and methods) (1) Animal: All the experimental protocols including animals were granted by the Institutional Animal Care and Use Committee of Kyoto University. The Klotho-deficient mice were produced by crossing the heterozygous Klotho +/- male and female mice. (2) Testosterone injection: 0.45mg per 0.1ml olive oil were subcutaneously injected into the Klotho KO male mice twice a week since 6 week old. (3) Biotin intrusion experiment: A total volume of 10 ul 7.5mg/ml biotin was injected into each testis when the Klotho-deficient mice turned 10-week-old after anesthesia. Half hour after the injection, the mice were sacrificed, and the testes were removed and processed for immunostaining of Biotin. (4) Macroscopic and histological analysis of testes: Implanted mice were killed at the age of 12 weeks (4 weeks post-implantation). The testes were kept intact in cold PBS and observed under macroscopy. The testes and epididymis were fixed in 10% neutral-buffered formalin and embedded in paraffin blocks. Slides were stained with hematoxylin and eosin and checked for histological analysis						

(5) Immunostaining: Testes were fixed in 4% paraformaldehyde for 2 h at 4° C, and embedded in Tissue-Tek OCT compound (Sakura Finetek, Tokyo, Japan) before cryosectioning. Cryo-sections of 6 μ m thickness were then prepared. The tissue were then treated with 0.1% Triton-X and sodium citrate in phosphate-buffered saline (PBS) for permeabilization. Donkey serum diluted at 10 fold in PBS were applied onto the slide for blocking. The tissues were treated with first antibodies in 4 degree overnight, then incubated with second antibodies in room temperature for 1 hour after washing with PBS. Hoechst were diluted at 1:300 ratio in PBS and then dropped onto the slides and kept for 10 minutes for counter staining.

(6) Serum collection and Enzyme linked immunosorbent assay (ELISA): The blood from the carotid artery of mice will be collected during scarification. The blood would be kept in 4 degree overnight. The serum was collected after centrifugation at 1200rpm for 30min and cryopreserved in -80 degree. The ELISA will be performed for detecting the concentration of testosterone according to producer's protocol.

4) 実験結果 (Results)

We firstly examined the expression of Claudin 3, 5 and 11, as well as the key enzymes of testosterone synthesis (CYP17A1 and HSD3B) in the testes of Klotho KO and WT mice. We noticed that Cldn3 (0.004 ± 0.001 vs. 0.045 ± 0.008 $\mu\text{m}^2/\mu\text{m}$, $p < 0.001$), Cldn11 (0.006 ± 0.017 vs. 0.025 ± 0.006 $\mu\text{m}^2/\mu\text{m}$, $p = 0.01$), and CYP17A1 (0.112 ± 0.112 vs. 58.27 ± 9.82 μm^2 , $p = 0.0005$) are remarkably lower in Klotho KO testes in comparison with the WT, but the expressions of HSD3B and Cldn5 are comparable in both groups. These results imply the impaired BTB and testosterone metabolism in Klotho-deficient testis. Then we performed the Biotin intrusion experiment on the 10 weeks old Klotho KO mice and WT mice's testes ($n = 4$) to confirm whether there is a functional defect of BTB in Klotho KO testes. A total volume of 10 μl 7.5mg/ml biotin was injected into each testis. We observed that the majority of seminiferous tubules in Klotho KO mice's testes are notably more penetrated by biotin, while almost no biotin intrusion could be found in the WT testes ($88.89 \pm 4.54\%$ vs. $6.25 \pm 3.61\%$, $p < 0.0001$). We also detected the mRNA level of Klotho- α in the testes of CTL and W mice (5 Weeks old, $n = 3$) using qPCR. The result shows that α -Klotho's expression in W mice testes is significantly lower than the control group (1.023 ± 0.031 vs. 0.457 ± 0.062 , $p = 0.0012$).

Previous results showed the impaired testosterone metabolism and tight junction between Sertoli cells in Klotho KO testes. As previous studies showed that testosterone could rescue the incomplete tight junction between Sertoli cells and ameliorated the phenotype of aging, we hypothesized that the malfunctioning and lower expression of cldn3 and cldn11 in Klotho KO testes were caused by the lower level of testosterone. We also supplemented the testosterone into Klotho-deficient mice to rescue its fertility. To verify the feasibility of such technique, we treated 4 Klotho KO mice per group with testosterone or pure olive oil respectively. After 6 weeks of injection, we noticed that the external genital organ of the testosterone group became bigger. As we investigate the testosterone and olive oil treated Klotho KO by immunofluorescence, we found that the testosterone-treated Klotho deficient mice not only had a comparable level of Cldn5 as compared with the cholesterol group, but also showed increased level of Cldn3, Cldn11, as well as the GFRA1, Ki67 Positive GFRA1, and PNA, indicating that the testosterone treatment might not only repaired the BTB, but also facilitated its spermatogenesis. In consistent with these findings, the macroscopic and histological investigation of testosterone and cholesterol treated testes and the pathological examination of their epididymis also showed that the testosterone treatment had notably increased the size and weight of Klotho KO testis and facilitated the maturation of sperm in the epididymis compared with the olive oil group.

5) 考察 (Discussion)

We previously reported the intrinsic senescence model of SSC via Jnk-mediated glycolysis activation using long-term cultured SSCs. We noticed that aged SSCs proliferate faster than young SSCs and showed enhanced glycolytic activity, but still kept euploidy and exhibited stable androgenetic imprinting patterns with robust SSC activity, though having shortened telomeres. In consistency with this, the investigation of Klotho-deficient mice model also showed hyperactivation of JNK and enhanced glycolysis. We also reported the significantly smaller size, fewer PNA⁺ tubules, increased proliferation of ZBTB16⁺ cells, and enhanced level of 53BP1 expression in Klotho KO testis.

Although many phenotypes of Klotho-deficient testis were described in our previous work, the detailed molecular mechanism of Klotho's regulation on the spermatogonial stem cell niche and spermatogenesis has not been clearly elucidated. In present study, we observed the impaired testosterone metabolism, functional and structural defects of blood testicular barrier in the Klotho-KO testis, which could be rescued by the exogenous supplement of testosterone. To our surprise, the 4-week implantation of testosterone (from 8 weeks to 12 weeks) not only repaired the BTB of Klotho-deficient testis but also recovered their spermatogenesis. These findings indicated the potential existence of the Klotho-testosterone-BTB pathway. To verify such hypothesis, we plan to perform western blot in our future study. In addition, we would also endeavor to explore the underlying molecular mechanism in detail.

6) 参考文献 (References)

- 1 Janeczko, D., Hołowczuk, M., Orzeł, A., Klatka, B. & Semczuk, A. Paternal age is affected by genetic abnormalities, perinatal complications and mental health of the offspring. *Biomed Rep* 12, 83–88, doi:10.3892/br.2019.1266 (2020).
- 2 Takashima, S. & Shinohara, T. Culture and transplantation of spermatogonial stem cells. *Stem Cell Res* 29, 46–55, doi:10.1016/j.scr.2018.03.006 (2018).
- 3 Schultz, M. B. & Sinclair, D. A. When stem cells grow old: phenotypes and mechanisms of stem cell aging. *Development* 143, doi:10.1242/dev.130633 (2016).
- 4 Ryu, B.-Y., Orwig, K. E., Oatley, J. M., Avarbock, M. R. & Brinster, R. L. Effects of aging and niche microenvironment on spermatogonial stem cell self-renewal. *Stem Cells* 24, 1505–1511 (2006).
- 5 Kuro-O, M. The Klotho proteins in health and disease. *Nat Rev Nephrol* 15, 27–44, doi:10.1038/s41581-018-0078-3 (2019).
- 6 Chen, Z. et al. Advanced maternal age causes premature placental senescence and malformation via dysregulated α -Klotho expression in trophoblasts. *Aging Cell* 20, e13417, doi:10.1111/acel.13417 (2021).

2. 執筆論文 Publication of thesis ※記載した論文を添付してください。Attach all of the papers listed below.

論文名 1 Title	Current perception of transvaginal natural orifice transluminal endoscopic surgery among Chinese female gynecological medical staff					
掲載誌名 Published journal	Asian journal of surgery					
	2022 年 12 月	45 卷(号)	2947 頁 ~	2950 頁	言語 Language	English
第1著者名 First author	Tianjiao Liu	第2著者名 Second author	Dan Feng		第3著者名 Third author	Xin Li
その他著者名 Other authors						
論文名 2 Title	Potential resolution of placenta previa from the 28th-to the 36th-week of pregnancy: A retrospective longitudinal cohort study.					
掲載誌名 Published journal	Placenta					
	2022 年 8 月	126 卷(号)	164 頁 ~	170 頁	言語 Language	English
第1著者名 First author	Xiong Wen	第2著者名 Second author	Xin Li		第3著者名 Third author	Tianjiao Liu
その他著者名 Other authors	Rui Ding, Linbo Cheng, Dan Feng, Duan Duan, Mi Su, Yalan Li, Xiao Yang, Sumei Wei					
論文名 3 Title	Repeated transvaginal natural orifice transluminal endoscopic surgery: An initial Chinese experience					
掲載誌名 Published journal	The Journal of Obstetrics and Gynaecology Research					
	2023 年 8 月	49 卷(号)	2501 頁 ~	2508 頁	言語 Language	English
第1著者名 First author	Dan Feng	第2著者名 Second author	Tianjiao Liu		第3著者名 Third author	Xin Li
その他著者名 Other authors	Jieru Peng, Lu Huang, Li He					
論文名 4 Title	Perioperative outcomes of and predictors for conversion from transvaginal natural orifice transluminal endoscopic tubal surgeries: A retrospective cohort study of 619 patients.					
掲載誌名 Published journal	International Journal of Gynaecology and Obstetrics					
	2023 年 1 月	161 卷(号)	803 頁 ~	811 頁	言語 Language	English
第1著者名 First author	Dan Feng	第2著者名 Second author	Li He		第3著者名 Third author	Xin Li
その他著者名 Other authors	Qiang Zhang, Jieru Peng, Lu Huang, Tianjiao Liu, Yonghong Lin					
論文名 5 Title	Transvaginal natural orifice endoscopic surgery for tubal ectopic pregnancy: A more suitable surgical approach for enhanced recovery after surgery					
掲載誌名 Published journal	Heliyon					
	2024 年 1 月	- 卷(号)	- 頁 ~	- 頁	言語 Language	English
第1著者名 First author	Ying Liu	第2著者名 Second author	Xin Li		第3著者名 Third author	Tianjiao Liu
その他著者名 Other authors	Aijie Xie, Xian Wu, Yujian Jia, Xiaoyan Liao, Wei Cheng, Hui Wang, Fangyuan Zhong, Lijuan Xu, Juan Huang, Siqin					

3. 学会発表 Conference presentation ※筆頭演者として総会・国際学会を含む主な学会で発表したものを記載してくだ

※Describe your presentation as the principal presenter in major academic meetings including general meetings or international me

学会名 Conference				
演題 Topic				
開催日 date	年	月	日	開催地 venue
形式 method	<input type="checkbox"/> 口頭発表 Oral	<input type="checkbox"/> ポスター発表 Poster	言語 Language	<input type="checkbox"/> 日本語 <input checked="" type="checkbox"/> 英語 <input type="checkbox"/> 中国語
共同演者名 Co-presenter				
学会名 Conference				
演題 Topic				
開催日 date	年	月	日	開催地 venue
形式 method	<input type="checkbox"/> 口頭発表 Oral	<input type="checkbox"/> ポスター発表 Poster	言語 Language	<input type="checkbox"/> 日本語 <input type="checkbox"/> 英語 <input type="checkbox"/> 中国語
共同演者名 Co-presenter				
学会名 Conference				
演題 Topic				
開催日 date	年	月	日	開催地 venue
形式 method	<input type="checkbox"/> 口頭発表 Oral	<input type="checkbox"/> ポスター発表 Poster	言語 Language	<input type="checkbox"/> 日本語 <input type="checkbox"/> 英語 <input type="checkbox"/> 中国語
共同演者名 Co-presenter				
学会名 Conference				
演題 Topic				
開催日 date	年	月	日	開催地 venue
形式 method	<input type="checkbox"/> 口頭発表 Oral	<input type="checkbox"/> ポスター発表 Poster	言語 Language	<input type="checkbox"/> 日本語 <input type="checkbox"/> 英語 <input type="checkbox"/> 中国語
共同演者名 Co-presenter				

4. 受賞(研究業績) Award (Research achievement)

名称 Award name	国名 Country		受賞年 Year of	年	月
	国名 Country		受賞年 Year of	年	月

5. 本研究テーマに関わる他の研究助成金受給 Other research grants concerned with your research theme

受給実績 Receipt record	<input checked="" type="checkbox"/> 有 <input type="checkbox"/> 無
助成機関名称 Funding agency	成都市婦女児童中心医院
助成金名称 Grant name	成都市婦女児童中心医院英才計画第3期
受給期間 Supported period	2024 年 1 月 ~ 2025 年 12 月
受給額 Amount received	4,000,000 円
受給実績 Receipt record	<input type="checkbox"/> 有 <input type="checkbox"/> 無
助成機関名称 Funding agency	
助成金名称 Grant name	
受給期間 Supported period	年 月 ~ 年 月
受給額 Amount received	円

6. 他の奨学金受給 Another awarded scholarship

受給実績 Receipt record	<input type="checkbox"/> 有 <input checked="" type="checkbox"/> 無
助成機関名称 Funding agency	
奨学金名称 Scholarship name	
受給期間 Supported period	年 月 ~ 年 月
受給額 Amount received	円

7. 研究活動に関する報道発表 Press release concerned with your research activities

※記載した記事を添付してください。Attach a copy of the article described below

報道発表 Press release	<input type="checkbox"/> 有 <input checked="" type="checkbox"/> 無	発表年月日 Date of release	
発表機関 Released medium			
発表形式 Release method	・新聞 ・雑誌 ・Web site ・記者発表 ・その他()		
発表タイトル Released title			

8. 本研究テーマに関する特許出願予定 Patent application concerned with your research theme

出願予定 Scheduled	<input type="checkbox"/> 有 <input checked="" type="checkbox"/> 無	出願国 Application	
出願内容(概要) Application contents			

9. その他 Others

--

指導責任者(記名) 篠原 隆司



Contents lists available at ScienceDirect

Asian Journal of Surgery

journal homepage: www.e-asianjournalsurgery.com

Letter to Editor

Current perception of transvaginal natural orifice transluminal endoscopic surgery among Chinese female gynecological medical staff



Keywords:

Transvaginal natural orifice transluminal endoscopic surgery
 Female medical staff
 Minimally invasive surgery
 Laparoendoscopy
 Online questionnaire

To the editor,

Natural orifice transluminal endoscopic surgery (NOTES) is a novel minimally invasive surgical (MIS) concept for performing endoscopic procedures via natural orifices.¹ Its feasibility for human clinical application was initially proven by transgastric appendectomy surgery conducted in 2003.² Since then, NOTES has developed rapidly, and surgeons have explored its use through other orifices, such as the intestinal tract and vagina. Notably, transvaginal NOTES (vNOTES) has been shown to outperform many other NOTES approaches due to the availability of greater operative space and easier removal of resected tissues, thus it has become increasingly popular for peritoneal surgeries, especially gynecologic laparoendoscopy, despite some reservations regarding the procedure.³

Theoretically, the acceptance of and preference for vNOTES can vary remarkably among patients and healthcare workers from different cultural, ethnic, and socioeconomic backgrounds, and it can be also expected to change with the development of endoscopic techniques and instruments. In the Western world, several surveys on patients and medical workers have investigated their

perceptions of the vNOTES procedure and yielded paradoxical results.⁴ However, after the introduction of vNOTES in mainland China seven years ago, its familiarity among the public and acceptance among mainland Chinese medical professionals has rarely been reported.⁵ Since healthcare workers' perception and awareness of such novel MIS procedures is probably a prerequisite for its recommendation and popularization, and female medical staff can provide insights from gynecological patients' perspective in hypothetical scenarios, we conducted a citywide online questionnaire survey in Chengdu, China, to investigate Chinese female gynecological health workers' current perceptions of vNOTES and to identify potential factors that contribute to their preference for vNOTES.

In our study, 523 gynecologists and 482 nurses completed the questionnaire. The majority (92.6%) had a positive attitude toward vNOTES. The “prefer vNOTES” group included a much lower proportion of respondents finishing postgraduate education than the “did not prefer vNOTES” group (11.0% vs. 25.7%, $p = 0.003$). They also included significantly more respondents having heard of the vNOTES procedure (83.9% vs. 68.9%, $p = 0.001$) and a strikingly higher proportion of members who had participated in vNOTES training courses (47.1% vs. 11.8%, $p = 0.029$). A significantly higher proportion of participants opted for vNOTES for reasons like safety (73.9% vs. 23.0%, $p < 0.001$), effectiveness (70.8% vs. 25.7%, $p < 0.001$), postsurgical cosmesis (93.7% vs. 73.0%, $p < 0.001$) and less postprocedural pain (71.1% vs. 47.3%, $p < 0.001$) than those in the “did not prefer vNOTES” group (shown in Table 1). Logistic regression revealed that concerns regarding postprocedural cosmesis (odds ratio (OR) = 3.239, $p < 0.001$) and prior awareness of vNOTES (OR = 2.271, $p = 0.004$) were significant predictors of preference for vNOTES, whereas those with higher education levels had a negative coefficient for vNOTES preference (OR = 0.549, $p = 0.003$) (see Fig. 1).

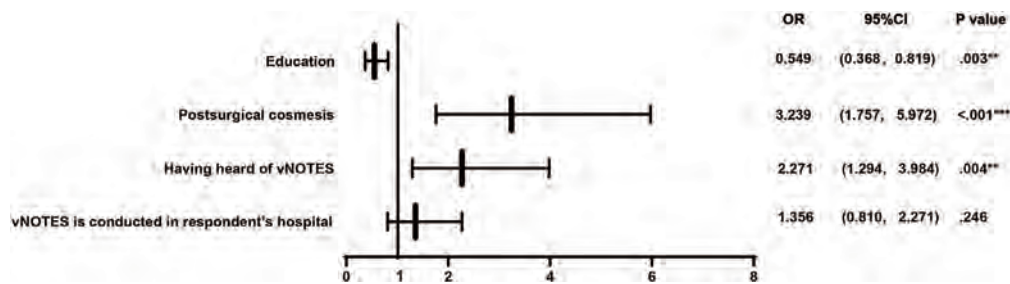


Fig. 1. Logistic regression model for factors that made vNOTES preferable. NOTE: ** $p < .01$, *** $p < .001$. Abbreviations: vNOTES, transvaginal natural orifice transluminal endoscopic surgery.

<https://doi.org/10.1016/j.asjsur.2022.06.117>

1015-9584/© 2022 Asian Surgical Association and Taiwan Robotic Surgery Association. Publishing services by Elsevier B.V. This is an open access article under the CC BY-NC-ND license (<http://creativecommons.org/licenses/by-nc-nd/4.0/>).

Table 1
Subject characteristics and attitudes toward vNOTES in “prefer for vNOTES” group versus “not prefer for vNOTES” group.

Subject characteristics	prefer vNOTES	not prefer vNOTES	X ²	P value
	n = 931(92.6%)	n = 74 (7.4%)		
Age group (years old)			2.871	0.580
20-30	258(27.7%)	22 (29.7%)		
31-40	394(42.3%)	36 (48.6%)		
41-50	204 (21.9%)	13 (17.6%)		
51-60	70 (7.5%)	3 (4.1%)		
≥61	5 (0.5%)	0(0%)		
Occupation			2.462	0.117
Gynecologist	478 (51.3%)	45 (60.8%)		
Nurse	453 (48.7%)	29 (39.2%)		
Educational background			13.762	0.003**
College	203 (21.8%)	14 (18.9%)		
Bachelor	625 (67.1%)	41 (55.4%)		
Master	97 (10.4%)	18 (24.3%)		
Doctoral	6 (0.6%)	1 (1.4%)		
Occupational title			2.271	0.518
Elementary	313 (33.6%)	24 (32.4%)		
Intermediate	354 (38.0%)	27 (36.5%)		
Senior	241 (25.9%)	19 (25.7%)		
Others	23 (2.5%)	4 (5.4%)		
The level of hospital you working for			3.203	0.361
Tertiary A	591 (63.5%)	54 (73.0%)		
Tertiary B	167 (17.9%)	8 (10.8%)		
Secondary A	96 (10.3%)	7 (9.5%)		
Secondary B	77 (8.3%)	5 (6.8%)		
How many years have you practiced medicine?			4.135	0.388
≤3	117 (12.6%)	13 (17.6%)		
3-5	92 (9.9%)	8 (10.8%)		
5-10	200 (21.5%)	16 (21.6%)		
10-20	297 (31.9%)	26 (35.1%)		
≥20	225 (24.2%)	11 (14.9%)		
Have you ever experienced laparoscopic surgery or examination			2.430	0.119
Yes	182 (19.5%)	9(12.2%)		
No	749 (80.5%)	65 (87.8%)		
Have you experienced laparotomy?			2.208	0.137
Yes	397(42.6%)	25 (33.8%)		
No	534 (57.4%)	49 (66.2%)		
Do you have child or children?			1.583	0.208
Yes	804 (93.1%)	60 (81.1%)		
No	127 (13.6%)	14 (18.9%)		
Attitude toward vNOTES				
Do you think postsurgical cosmesis is as important as safety for gynecologic surgery?			21.215	<0.001***
Yes	862 (92.6%)	57 (77.0%)		
No	69 (7.4%)	17 (23.0%)		
Have you ever heard of laparoendoscopic single site surgery?			0.698	0.404
Yes	867 (93.1%)	67 (90.5%)		
No	64 (6.9%)	7 (9.5%)		
(Q10)Have you heard of transvaginal natural orifice transluminal endoscopic surgery (vNOTES)?			10.779	0.001**
Yes	781 (83.9%)	51(68.9%)		
Never	150(16.1%)	23 (31.1%)		
If your answer to Q10 is yes, how do you know about it?	n = 781	n = 51		
Academic conference	488 (62.5%)	25 (49.0%)	3.671	0.055
Training courses	368 (47.1%)	16 (11.8%)	4.776	0.029*
Reading literatures	413 (52.9%)	29 (56.9%)	0.305	0.580
Heard from colleagues	496 (63.5%)	33 (64.7%)	0.057	0.811
Relatives and friends received vNOTES	119 (15.2%)	6 (11.8%)	0.452	0.501
Is vNOTES conducted in your hospital?			4.014	0.045*
Yes	490 (52.6%)	30 (40.5%)		
No	441 (47.4%)	44 (59.5%)		
What is the acceptable complication incidence rate of vNOTES for you to replace the conventional laparoendoscopic gynecologic surgery? (The incidence rate for surgical complications of laparoendoscopy is 0%–3%)			10.220	0.006**
0%–3%	626 (67.2%)	37 (50.0%)		
3%–6%	200 (21.5%)	27 (36.5%)		
6%–9%	105 (11.3%)	10 (13.5%)		
Are you willing to undergo vNOTES (if diagnosed with indication) or recommend it to relatives/friends/families?			84.902	<0.001***
Yes	688 (73.9%)	17 (23.0%)		
No	243 (26.1%)	57 (77.0%)		
If you are a patient or a family member of a patient, for what reason(s) you would prefer to undergo vNOTES (multiple options)?				
Safe	688 (73.9%)	17 (23.0%)	84.902	<0.001***

Table 1 (continued)

Subject characteristics	prefer vNOTES	not prefer vNOTES	X ²	P value
	n = 931(92.6%)	n = 74 (7.4%)		
Effective	659 (70.8%)	19 (25.7%)	63.546	<0.001***
Cosmetic/scarless	874 (93.9%)	54 (73.0%)	42.344	<0.001***
No pain or painless	662 (71.1%)	35 (47.3%)	18.283	<0.001***
Other reasons	6 (0.6%)	9 (12.2%)	61.852	<0.001***
If you are a patient or a family member of a patient, refuse to undergo vNOTES may for (multiple options)?				
Worried about its potential impact on sexual life	210 (22.6%)	27 (36.5%)	7.382	0.007**
Worried about its potential impact on pregnancy and childbirth	193 (20.7%)	29 (39.2%)	13.572	<0.001***
Worried about the failure of the operation	273 (29.3%)	27 (36.5%)	1.680	0.195
Worried about surgical complications	334 (35.9%)	43 (58.1%)	14.455	<0.001***
Other reasons	10 (1.1%)	11 (14.9%)	63.725	<0.001***
Do you think age is a major factor for choosing vNOTES or recommending it to friends and relatives?			3.272	0.070
Yes	330 (35.4%)	34 (45.9%)		
No	601 (64.6%)	40 (54.1%)		
If your answer is yes, what do you think is the most appropriate age for vNOTES	n = 330	n = 34	9.656	0.008**
20-40	227 (68.8%)	16 (47.1%)		
41-55	84 (25.4%)	12 (25.5%)		
>55	19 (5.8%)	6 (17.6%)		
(Q22) Do you think finish childbirth or not is a major factor in the surgical selection of vNOTES or the recommendation of it to your family and friends' choice?			1.002	0.317
Yes	348 (37.4%)	32 (43.2%)		
No	583 (62.6%)	42 (56.8%)		
If your answer to Q22 is yes, do you think you should finish childbirth before undergoing vNOTES?	n = 342	n = 32	0.021	0.885
Yes	265 (77.5%)	24 (75.0%)		
No	83 (22.5%)	8 (25.0%)		
Gynecologists' perspective of vNOTES				
	Prefer vNOTES n = 495	Not prefer vNOTES n = 42	X ²	P value
Would you like to conduct vNOTES in your department?			20.148	<0.001***
Yes	485 (98.0%)	36 (85.7%)		
No	10 (2.0%)	6 (14.3%)		
Do you think the prospect of vNOTES is good?			61.310	<0.001***
Yes	474 (95.8%)	27 (64.3%)		
No	21 (4.2%)	15 (35.7%)		
What do you think make it difficult to popularize vNOTES (multiple options)?				
Difficulty in establishment of surgical platform	294(59.4%)	25(59.5%)	0.002	1.000
Restricted operative visualization	388(78.4%)	38(90.4%)	3.452	0.063
The chopstick effect of single-port laparoscopy makes it difficult to perform vNOTES	376(76.0%)	24(57.1%)	7.213	0.007**
Low acceptance rate among patients	99(20.0%)	12(28.5%)	1.735	0.188
Higher operative cost	201(40.6%)	9(21.4%)	5.979	0.014*
Other-----	10(2.0%)	0(0%)	0.865	0.352
Gynecologists' perspective of vNOTES				
	Prefer vNOTES n = 495	Not prefer vNOTES n = 42	X ²	P value
Would you like to conduct vNOTES in your department?			20.148	<0.001***
Yes	485 (98.0%)	36 (85.7%)		
No	10 (2.0%)	6 (14.3%)		
Do you think the prospect of vNOTES is good?			61.310	<0.001***
Yes	474 (95.8%)	27 (64.3%)		
No	21 (4.2%)	15 (35.7%)		
What do you think make it difficult to popularize vNOTES (multiple options)?				
Difficulty in establishment of surgical platform	294(59.4%)	25(59.5%)	0.002	1.000
Restricted operative visualization	388(78.4%)	38(90.4%)	3.452	0.063
The chopstick effect of single-port laparoscopy makes it difficult to perform vNOTES	376(76.0%)	24(57.1%)	7.213	0.007**
Low acceptance rate among patients	99(20.0%)	12(28.5%)	1.735	0.188
Higher operative cost	201(40.6%)	9(21.4%)	5.979	0.014*
Other-----	10(2.0%)	0(0%)	0.865	0.352

In conclusion, the majority of surveyed female gynecologic healthcare workers had a supportive attitude toward vNOTES. Prior awareness and evaluation of surgical cosmesis had a positive influence on the surgical preference for vNOTES. However, concerns about its impact on sexual life, pregnancy, and childbirth still exist.

Funding

This study was funded by Chengdu High-level Key Clinical Specialty Construction Project, Chengdu Municipal Health Commission Project (No.2021215), Fifth Round of Chengdu Municipal Science and Technology Research Program (No.2021-YF05-00627-SN), and Japan China Sasakawa Medical Fellowship.

Data availability statement

Data of this study can be obtained from the corresponding author upon reasonable request.

Author contributions

Dan Feng conceptualized the study and formulated the questionnaire. Tianjiao Liu, Dan Feng, and Xin Li drafted and revised the manuscript. Tianjiao Liu and Xin Li also participated in statistical analyses. Li He supervised this study and critically reviewed the manuscript.

Declaration of competing interest

The authors declared no conflicts of interest related to this article.

Acknowledgment

We thank all the gynecologists and nurses who participated in our survey.

Appendix A. Supplementary data

Supplementary data to this article can be found online at <https://doi.org/10.1016/j.asjsur.2022.06.117>.

References

1. Rattner D, Kalloo A. ASGE/SAGES working group on natural orifice transluminal

- endoscopic surgery. *Surg Endosc*. 2006;20(2):329–333. October 2005.
2. Rao GV, Reddy DN, Banerjee R. NOTES: human experience. *Gastrointest Endosc Clin N Am*. 2008;18(2).
3. Kho RM. vNOTES: is it the panacea we are all hoping for? *J Minim Invasive Gynecol*. 2021;28(6):1146–1147.
4. Gerntke CI, Kersten JF, Schön G, Mann O, Stark M, Benhidjeb T. Women's perception of transvaginal natural orifice transluminal endoscopic surgery (NOTES): results of a survey of female medical staff and literature review. *Surg Innovat*. 2016;23(2):201–211.
5. Fei YF, Fei L, Salazar M, Renton DB, Hazey JW. Transvaginal surgery: do women want it? *J Laparoendosc Adv Surg Tech*. 2014;24(10):676–683.

Tianjiao Liu¹, Dan Feng¹

The Department of Gynecology of Chengdu Women's and Children's Central Hospital, School of Medicine, University of Electronic Science and Technology of China, Chengdu, People's Republic of China

Xin Li¹

The Department of Obstetrics of Chengdu Women's and Children's Central Hospital, School of Medicine, University of Electronic Science and Technology of China, Chengdu, People's Republic of China

Li He*

The Department of Gynecology of Chengdu Women's and Children's Central Hospital, School of Medicine, University of Electronic Science and Technology of China, Chengdu, People's Republic of China

* Corresponding author. No.1617, Riyue Avenue, Chengdu, Sichuan, 610091, China.

E-mail address: helisichuan@163.com (L. He).

9 March 2022

Available online 2 July 2022

¹ These authors contributed equally to this work.



Contents lists available at ScienceDirect

Asian Journal of Surgery

journal homepage: www.e-asianjournalsurgery.com

Letter to Editor

Current perception of transvaginal natural orifice transluminal endoscopic surgery among Chinese female gynecological medical staff



Keywords:

Transvaginal natural orifice transluminal endoscopic surgery
 Female medical staff
 Minimally invasive surgery
 Laparoendoscopy
 Online questionnaire

To the editor,

Natural orifice transluminal endoscopic surgery (NOTES) is a novel minimally invasive surgical (MIS) concept for performing endoscopic procedures via natural orifices.¹ Its feasibility for human clinical application was initially proven by transgastric appendectomy surgery conducted in 2003.² Since then, NOTES has developed rapidly, and surgeons have explored its use through other orifices, such as the intestinal tract and vagina. Notably, transvaginal NOTES (vNOTES) has been shown to outperform many other NOTES approaches due to the availability of greater operative space and easier removal of resected tissues, thus it has become increasingly popular for peritoneal surgeries, especially gynecologic laparoendoscopy, despite some reservations regarding the procedure.³

Theoretically, the acceptance of and preference for vNOTES can vary remarkably among patients and healthcare workers from different cultural, ethnic, and socioeconomic backgrounds, and it can be also expected to change with the development of endoscopic techniques and instruments. In the Western world, several surveys on patients and medical workers have investigated their

perceptions of the vNOTES procedure and yielded paradoxical results.⁴ However, after the introduction of vNOTES in mainland China seven years ago, its familiarity among the public and acceptance among mainland Chinese medical professionals has rarely been reported.⁵ Since healthcare workers' perception and awareness of such novel MIS procedures is probably a prerequisite for its recommendation and popularization, and female medical staff can provide insights from gynecological patients' perspective in hypothetical scenarios, we conducted a citywide online questionnaire survey in Chengdu, China, to investigate Chinese female gynecological health workers' current perceptions of vNOTES and to identify potential factors that contribute to their preference for vNOTES.

In our study, 523 gynecologists and 482 nurses completed the questionnaire. The majority (92.6%) had a positive attitude toward vNOTES. The “prefer vNOTES” group included a much lower proportion of respondents finishing postgraduate education than the “did not prefer vNOTES” group (11.0% vs. 25.7%, $p = 0.003$). They also included significantly more respondents having heard of the vNOTES procedure (83.9% vs. 68.9%, $p = 0.001$) and a strikingly higher proportion of members who had participated in vNOTES training courses (47.1% vs. 11.8%, $p = 0.029$). A significantly higher proportion of participants opted for vNOTES for reasons like safety (73.9% vs. 23.0%, $p < 0.001$), effectiveness (70.8% vs. 25.7%, $p < 0.001$), postsurgical cosmesis (93.7% vs. 73.0%, $p < 0.001$) and less postprocedural pain (71.1% vs. 47.3%, $p < 0.001$) than those in the “did not prefer vNOTES” group (shown in Table 1). Logistic regression revealed that concerns regarding postprocedural cosmesis (odds ratio (OR) = 3.239, $p < 0.001$) and prior awareness of vNOTES (OR = 2.271, $p = 0.004$) were significant predictors of preference for vNOTES, whereas those with higher education levels had a negative coefficient for vNOTES preference (OR = 0.549, $p = 0.003$) (see Fig. 1).

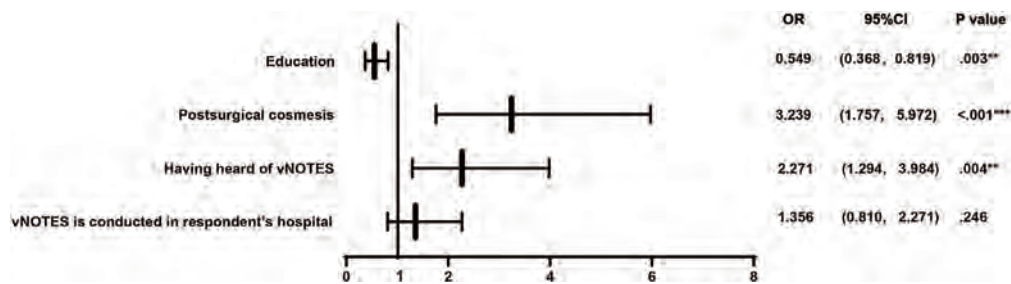


Fig. 1. Logistic regression model for factors that made vNOTES preferable. NOTE: ** $p < .01$, *** $p < .001$. Abbreviations: vNOTES, transvaginal natural orifice transluminal endoscopic surgery.

<https://doi.org/10.1016/j.asjsur.2022.06.117>

1015-9584/© 2022 Asian Surgical Association and Taiwan Robotic Surgery Association. Publishing services by Elsevier B.V. This is an open access article under the CC BY-NC-ND license (<http://creativecommons.org/licenses/by-nc-nd/4.0/>).

Table 1
Subject characteristics and attitudes toward vNOTES in “prefer for vNOTES” group versus “not prefer for vNOTES” group.

Subject characteristics	prefer vNOTES	not prefer vNOTES	X ²	P value
	n = 931(92.6%)	n = 74 (7.4%)		
Age group (years old)			2.871	0.580
20-30	258(27.7%)	22 (29.7%)		
31-40	394(42.3%)	36 (48.6%)		
41-50	204 (21.9%)	13 (17.6%)		
51-60	70 (7.5%)	3 (4.1%)		
≥61	5 (0.5%)	0(0%)		
Occupation			2.462	0.117
Gynecologist	478 (51.3%)	45 (60.8%)		
Nurse	453 (48.7%)	29 (39.2%)		
Educational background			13.762	0.003**
College	203 (21.8%)	14 (18.9%)		
Bachelor	625 (67.1%)	41 (55.4%)		
Master	97 (10.4%)	18 (24.3%)		
Doctoral	6 (0.6%)	1 (1.4%)		
Occupational title			2.271	0.518
Elementary	313 (33.6%)	24 (32.4%)		
Intermediate	354 (38.0%)	27 (36.5%)		
Senior	241 (25.9%)	19 (25.7%)		
Others	23 (2.5%)	4 (5.4%)		
The level of hospital you working for			3.203	0.361
Tertiary A	591 (63.5%)	54 (73.0%)		
Tertiary B	167 (17.9%)	8 (10.8%)		
Secondary A	96 (10.3%)	7 (9.5%)		
Secondary B	77 (8.3%)	5 (6.8%)		
How many years have you practiced medicine?			4.135	0.388
≤3	117 (12.6%)	13 (17.6%)		
3-5	92 (9.9%)	8 (10.8%)		
5-10	200 (21.5%)	16 (21.6%)		
10-20	297 (31.9%)	26 (35.1%)		
≥20	225 (24.2%)	11 (14.9%)		
Have you ever experienced laparoscopic surgery or examination			2.430	0.119
Yes	182 (19.5%)	9(12.2%)		
No	749 (80.5%)	65 (87.8%)		
Have you experienced laparotomy?			2.208	0.137
Yes	397(42.6%)	25 (33.8%)		
No	534 (57.4%)	49 (66.2%)		
Do you have child or children?			1.583	0.208
Yes	804 (93.1%)	60 (81.1%)		
No	127 (13.6%)	14 (18.9%)		
Attitude toward vNOTES				
Do you think postsurgical cosmesis is as important as safety for gynecologic surgery?			21.215	<0.001***
Yes	862 (92.6%)	57 (77.0%)		
No	69 (7.4%)	17 (23.0%)		
Have you ever heard of laparoendoscopic single site surgery?			0.698	0.404
Yes	867 (93.1%)	67 (90.5%)		
No	64 (6.9%)	7 (9.5%)		
(Q10)Have you heard of transvaginal natural orifice transluminal endoscopic surgery (vNOTES)?			10.779	0.001**
Yes	781 (83.9%)	51(68.9%)		
Never	150(16.1%)	23 (31.1%)		
If your answer to Q10 is yes, how do you know about it?	n = 781	n = 51		
Academic conference	488 (62.5%)	25 (49.0%)	3.671	0.055
Training courses	368 (47.1%)	16 (11.8%)	4.776	0.029*
Reading literatures	413 (52.9%)	29 (56.9%)	0.305	0.580
Heard from colleagues	496 (63.5%)	33 (64.7%)	0.057	0.811
Relatives and friends received vNOTES	119 (15.2%)	6 (11.8%)	0.452	0.501
Is vNOTES conducted in your hospital?			4.014	0.045*
Yes	490 (52.6%)	30 (40.5%)		
No	441 (47.4%)	44 (59.5%)		
What is the acceptable complication incidence rate of vNOTES for you to replace the conventional laparoendoscopic gynecologic surgery? (The incidence rate for surgical complications of laparoendoscopy is 0%–3%)			10.220	0.006**
0%–3%	626 (67.2%)	37 (50.0%)		
3%–6%	200 (21.5%)	27 (36.5%)		
6%–9%	105 (11.3%)	10 (13.5%)		
Are you willing to undergo vNOTES (if diagnosed with indication) or recommend it to relatives/friends/families?			84.902	<0.001***
Yes	688 (73.9%)	17 (23.0%)		
No	243 (26.1%)	57 (77.0%)		
If you are a patient or a family member of a patient, for what reason(s) you would prefer to undergo vNOTES (multiple options)?				
Safe	688 (73.9%)	17 (23.0%)	84.902	<0.001***

Table 1 (continued)

Subject characteristics	prefer vNOTES	not prefer vNOTES	X ²	P value
	n = 931(92.6%)	n = 74 (7.4%)		
Effective	659 (70.8%)	19 (25.7%)	63.546	<0.001***
Cosmetic/scarless	874 (93.9%)	54 (73.0%)	42.344	<0.001***
No pain or painless	662 (71.1%)	35 (47.3%)	18.283	<0.001***
Other reasons	6 (0.6%)	9 (12.2%)	61.852	<0.001***
If you are a patient or a family member of a patient, refuse to undergo vNOTES may for (multiple options)?				
Worried about its potential impact on sexual life	210 (22.6%)	27 (36.5%)	7.382	0.007**
Worried about its potential impact on pregnancy and childbirth	193 (20.7%)	29 (39.2%)	13.572	<0.001***
Worried about the failure of the operation	273 (29.3%)	27 (36.5%)	1.680	0.195
Worried about surgical complications	334 (35.9%)	43 (58.1%)	14.455	<0.001***
Other reasons	10 (1.1%)	11 (14.9%)	63.725	<0.001***
Do you think age is a major factor for choosing vNOTES or recommending it to friends and relatives?			3.272	0.070
Yes	330 (35.4%)	34 (45.9%)		
No	601 (64.6%)	40 (54.1%)		
If your answer is yes, what do you think is the most appropriate age for vNOTES	n = 330	n = 34	9.656	0.008**
20-40	227 (68.8%)	16 (47.1%)		
41-55	84 (25.4%)	12 (25.5%)		
>55	19 (5.8%)	6 (17.6%)		
(Q22) Do you think finish childbirth or not is a major factor in the surgical selection of vNOTES or the recommendation of it to your family and friends' choice?			1.002	0.317
Yes	348 (37.4%)	32 (43.2%)		
No	583 (62.6%)	42 (56.8%)		
If your answer to Q22 is yes, do you think you should finish childbirth before undergoing vNOTES?	n = 342	n = 32	0.021	0.885
Yes	265 (77.5%)	24 (75.0%)		
No	83 (22.5%)	8 (25.0%)		
Gynecologists' perspective of vNOTES				
	Prefer vNOTES n = 495	Not prefer vNOTES n = 42	X ²	P value
Would you like to conduct vNOTES in your department?			20.148	<0.001***
Yes	485 (98.0%)	36 (85.7%)		
No	10 (2.0%)	6 (14.3%)		
Do you think the prospect of vNOTES is good?			61.310	<0.001***
Yes	474 (95.8%)	27 (64.3%)		
No	21 (4.2%)	15 (35.7%)		
What do you think make it difficult to popularize vNOTES (multiple options)?				
Difficulty in establishment of surgical platform	294(59.4%)	25(59.5%)	0.002	1.000
Restricted operative visualization	388(78.4%)	38(90.4%)	3.452	0.063
The chopstick effect of single-port laparoscopy makes it difficult to perform vNOTES	376(76.0%)	24(57.1%)	7.213	0.007**
Low acceptance rate among patients	99(20.0%)	12(28.5%)	1.735	0.188
Higher operative cost	201(40.6%)	9(21.4%)	5.979	0.014*
Other-----	10(2.0%)	0(0%)	0.865	0.352
Gynecologists' perspective of vNOTES				
	Prefer vNOTES n = 495	Not prefer vNOTES n = 42	X ²	P value
Would you like to conduct vNOTES in your department?			20.148	<0.001***
Yes	485 (98.0%)	36 (85.7%)		
No	10 (2.0%)	6 (14.3%)		
Do you think the prospect of vNOTES is good?			61.310	<0.001***
Yes	474 (95.8%)	27 (64.3%)		
No	21 (4.2%)	15 (35.7%)		
What do you think make it difficult to popularize vNOTES (multiple options)?				
Difficulty in establishment of surgical platform	294(59.4%)	25(59.5%)	0.002	1.000
Restricted operative visualization	388(78.4%)	38(90.4%)	3.452	0.063
The chopstick effect of single-port laparoscopy makes it difficult to perform vNOTES	376(76.0%)	24(57.1%)	7.213	0.007**
Low acceptance rate among patients	99(20.0%)	12(28.5%)	1.735	0.188
Higher operative cost	201(40.6%)	9(21.4%)	5.979	0.014*
Other-----	10(2.0%)	0(0%)	0.865	0.352

In conclusion, the majority of surveyed female gynecologic healthcare workers had a supportive attitude toward vNOTES. Prior awareness and evaluation of surgical cosmesis had a positive influence on the surgical preference for vNOTES. However, concerns about its impact on sexual life, pregnancy, and childbirth still exist.

Funding

This study was funded by Chengdu High-level Key Clinical Specialty Construction Project, Chengdu Municipal Health Commission Project (No.2021215), Fifth Round of Chengdu Municipal Science and Technology Research Program (No.2021-YF05-00627-SN), and Japan China Sasakawa Medical Fellowship.

Data availability statement

Data of this study can be obtained from the corresponding author upon reasonable request.

Author contributions

Dan Feng conceptualized the study and formulated the questionnaire. Tianjiao Liu, Dan Feng, and Xin Li drafted and revised the manuscript. Tianjiao Liu and Xin Li also participated in statistical analyses. Li He supervised this study and critically reviewed the manuscript.

Declaration of competing interest

The authors declared no conflicts of interest related to this article.

Acknowledgment

We thank all the gynecologists and nurses who participated in our survey.

Appendix A. Supplementary data

Supplementary data to this article can be found online at <https://doi.org/10.1016/j.asjsur.2022.06.117>.

References

1. Rattner D, Kalloo A. ASGE/SAGES working group on natural orifice transluminal

- endoscopic surgery. *Surg Endosc*. 2006;20(2):329–333. October 2005.
2. Rao GV, Reddy DN, Banerjee R. NOTES: human experience. *Gastrointest Endosc Clin N Am*. 2008;18(2).
3. Kho RM. vNOTES: is it the panacea we are all hoping for? *J Minim Invasive Gynecol*. 2021;28(6):1146–1147.
4. Gerntke CI, Kersten JF, Schön G, Mann O, Stark M, Benhidjeb T. Women's perception of transvaginal natural orifice transluminal endoscopic surgery (NOTES): results of a survey of female medical staff and literature review. *Surg Innovat*. 2016;23(2):201–211.
5. Fei YF, Fei L, Salazar M, Renton DB, Hazey JW. Transvaginal surgery: do women want it? *J Laparoendosc Adv Surg Tech*. 2014;24(10):676–683.

Tianjiao Liu¹, Dan Feng¹

The Department of Gynecology of Chengdu Women's and Children's Central Hospital, School of Medicine, University of Electronic Science and Technology of China, Chengdu, People's Republic of China

Xin Li¹

The Department of Obstetrics of Chengdu Women's and Children's Central Hospital, School of Medicine, University of Electronic Science and Technology of China, Chengdu, People's Republic of China

Li He*

The Department of Gynecology of Chengdu Women's and Children's Central Hospital, School of Medicine, University of Electronic Science and Technology of China, Chengdu, People's Republic of China

* Corresponding author. No.1617, Riyue Avenue, Chengdu, Sichuan, 610091, China.

E-mail address: helisichuan@163.com (L. He).

9 March 2022

Available online 2 July 2022

¹ These authors contributed equally to this work.



ORIGINAL ARTICLE

Repeated transvaginal natural orifice transluminal endoscopic surgery: An initial Chinese experience

Dan Feng¹ | Tianjiao Liu¹ | Xin Li¹ | Jieru Peng² | Lu Huang¹ | Li He¹

¹Department of Gynecology, Chengdu Women's and Children's Central Hospital, School of Medicine, University of Electronic Science and Technology of China, Chengdu, China

²Medical Administrative Department, Chengdu Women's and Children's Central Hospital, School of Medicine, University of Electronic Science and Technology of China, Chengdu, China

Correspondence

Li He, Department of Gynecology, Chengdu Women's and Children's Central Hospital, School of Medicine, University of Electronic Science and Technology of China, No. 1617, Riyue Avenue, Chengdu 610091, China.
Email: helisichuan@163.com

Funding information

Chengdu High-level Key Clinical Specialty Construction Project; Chengdu Municipal Health Commission Project, Grant/Award Number: 2021215; Fifth Round of Chengdu Municipal Science and Technology Research Program, Grant/Award Number: 2021-YF05-00627-SN; Japan China Sasakawa Medical Fellowship Program; Chengdu Municipal Medical Research Project in 2023

Abstract

Aims: To investigate the perioperative outcomes and sexual function of patients undergoing repeated transvaginal natural orifice transluminal endoscopic surgery (vNOTES).

Methods: We retrieved the records of patients who underwent vNOTES twice at our institute between April 2019 and December 2022 and analyzed their baseline information and perioperative complications, and compared the pre- and postoperative sexual function of both vNOTES.

Results: Patients' mean age and body mass index were 29.00 ± 3.59 and 30.4 ± 4.00 years and 21.89 ± 3.69 and 22.76 ± 3.88 kg/m², respectively, when receiving the first and second vNOTES. Ectopic pregnancy was the most frequent indication for vNOTES, with 7 cases in the first vNOTES and 11 cases in repeated vNOTES. The interval between the two vNOTESs ranged from 9 days to 38 months. The operation duration (63.33 ± 13.71 vs. 67.33 ± 22.51 min, $p = 0.723$), intraoperative estimated blood loss (32.00 ± 20.42 vs. 30.00 ± 9.26 mL, $p = 0.429$), and duration of postoperative hospital stay (2.20 ± 0.56 vs. 2.40 ± 0.51 days, $p = 0.082$) of both vNOTESs were comparable. No significant differences were found in any of the domains in the comparison of pre-first and post-first vNOTES, pre-second and post-second vNOTES, and pre-first and post-second vNOTES female sexual function index. None of the patients delivered after the second vNOTES.

Conclusion: Repeated vNOTES is safe and feasible. No significant change in the patients' sexual function was found in our cohort after the first and second vNOTES.

KEYWORDS

culdotomy, female sexual function index, incision complications, perioperative complications

INTRODUCTION

Natural orifice transluminal endoscopic surgery (NOTES) uses natural orifices such as the stomach, urethra, rectum, and vagina to access the body cavity and targeted organs. With the development of endoscopic techniques, NOTES has been proven clinically feasible and has achieved better surgical outcomes, especially in averting visible skin scars.¹ However, because of technical difficulties and specific morbidities, most NOTES approaches require highly skilled hands and careful preoperative examination and consultation; thus, they have not gained popularity as expected.²

NOTES performed transvaginally, hereinafter abbreviated as vNOTES, has avoided many demerits of other NOTES. It enables shorter access to the peritoneum and urogenital organs, easier retrieval of large and hard specimens, closure of the incision under direct view, and the use of rigid endoscopes. It also reportedly outperforms other endoscopic techniques because of its better cosmetic outcomes, less pain and intraoperative bleeding, and faster recovery.³ Therefore, vNOTES has been increasingly used to treat benign gynecological diseases.

Although many studies have demonstrated the feasibility and safety of vNOTES for better short-term surgical outcomes compared to other endoscopic techniques,^{4,5} evidence supporting its repeatability is still lacking.^{6,7} Considering that it was not fully elucidated whether the second

Dan Feng, Tianjiao Liu, and Xin Li contributed equally to this study.

vNOTES can be successfully performed without severe adverse surgical outcomes and it is possible that the repeated colpotomy in the second vNOTES might cause undesirable impairment to patients' sexual function and vaginal delivery, research on repeated vNOTES' impact on these issues is desperately needed to fill the knowledge gap.⁶ To this end, this case series retrieved all the 15 repeated vNOTES for benign gynecological indications performed at our institute in recent years and compared the postoperative outcomes and pre- and postoperative sexual function of both vNOTESs, hoping to prove the feasibility and safety of repeated vNOTES.

METHODS

Study design

This is a retrospective study, which investigated a series of patients who underwent vNOTES twice at our institute between April 2019 and December 2022 and analyzed their baseline information (age, education, ethnicity, body mass index [BMI], gravidity and parity history, abdominopelvic surgical history, and comorbidities) and perioperative outcomes (time to establish the surgical entrance, operation duration, intraoperative pelvic adhesion [categorized based on the grading system issued by the American Society for Reproductive Medicine, ASRM], estimated intraoperative blood loss, volume of blood transfusion, pre- and postoperative hemoglobin levels, postoperative pain score [Visual Analog Scale, VAS] of the first to third postoperative days,⁸ and intraoperative complications, including surgical conversion) of both vNOTESs. The VAS consists of a 10 cm-long line with both ends representing the extremes of pain intensity (from painless to extremely painful). The time to establish surgical entrance was defined as the sum of the time taken to expose the cervical part of the vagina and posterior vaginal fornix by clamping, incise the posterior vaginal fornix, and insert the disposable tractor. In addition, when patients were about to undergo vNOTES, their preoperative sexual functions were surveyed using the Female Sexual Function Index (FSFI) scale after obtaining their written consent forms during the preoperative assessment. Postoperative sexual function data were collected 3–6 months after vNOTES. The intervals between the vNOTESs were calculated and recorded. The patients' postoperative childbirth status was also followed up until the end of the study.

Inclusion and exclusion criteria

At our institute, we had similar inclusion and exclusion criteria for the first and second vNOTES, except that the patient requiring the second vNOTES must have a surgical history of a first vNOTES. The inclusion criteria for

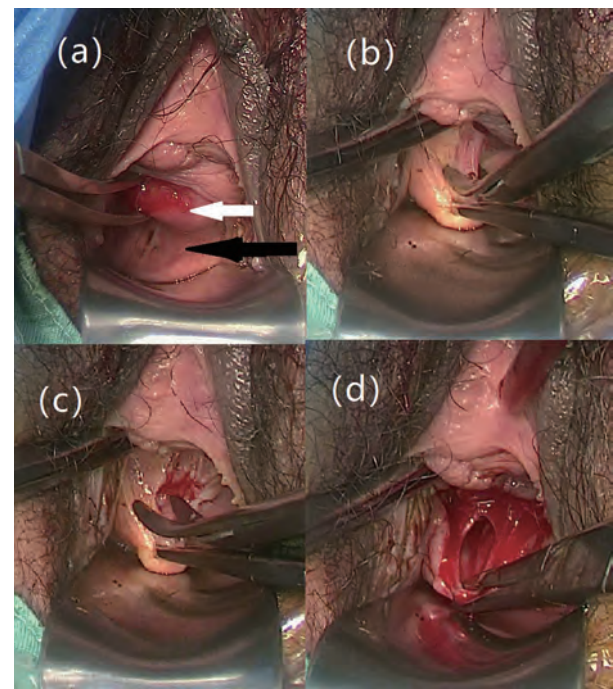


FIGURE 1 Critical steps in establishing the surgical platform of second transvaginal natural orifice transluminal endoscopic surgery (vNOTES). (a) Mucous wrinkles on the posterior vaginal fornix. (b–d) Entering the pelvic cavity through the previous incision.

vNOTES were: (i) laparoscopic surgery was needed for benign gynecological indications; (ii) patients showed willingness to undergo vNOTES. The exclusion criteria for vNOTES were as follows: (i) history of rectal surgery, severe pelvic inflammation, and pelvic radiotherapy; (ii) signs of suspected rectovaginal endometriosis, malignant tumors, or severe pelvic adhesions in preoperative examinations; (iii) not yet experienced sexual intercourse; (iv) not suitable to receive transvaginal surgery due to the risk of infection, including vaginal infections, or massive pelvic hemorrhage potentially necessitating autotransfusion; and, (v) myoma on the lateral wall or posterior and anterior wall of the uterus.

Surgical procedures

The vNOTES approaches in the present study were similar to those described in previous publications, with incisions of both first and second vNOTES made on the posterior vaginal fornix.^{9–12} All surgeries were performed by the same group of highly experienced surgeons. By the end of vNOTES, an anti-cohesive reagent (Gynecare Interceed [Johnson & Johnson, New Jersey, the United States]), was applied if the patient was willing to receive anti-cohesive treatment. The surgical incisions were closed by continuous suturing of both layers of the vaginal wall and peritoneum using a 2–0 absorbable suture. For the second vNOTES, there are two noteworthy

TABLE 1 Patients' baseline information.

Case no.	Age (year) ^a	Age (year) ^b	BMI (kg/m ²) ^a	BMI (kg/m ²) ^b	Gravity ^a	Gravity ^b	Parity ^a	Parity ^b	Vaginal delivery ^a	Vaginal delivery ^b	Cesarean section ^a	Cesarean section ^b
1	25	28	21.6	27.0	0	2	0	0	0	0	0	0
2	26	27	18.5	18.9	1	2	0	0	0	0	0	0
3	35	37	26.7	27.0	1	3	0	0	0	0	0	0
4	26	26	19.3	19.3	2	2	0	0	0	0	0	0
5	30	32	17.1	17.9	3	4	0	0	0	0	0	0
6	30	33	24.0	25.1	7	8	0	0	0	0	0	0
7	25	26	27.0	28.0	2	3	0	0	0	0	0	0
8	26	26	19.1	20.3	0	1	0	0	0	0	0	0
9	26	26	19.8	19.8	1	2	0	0	0	0	0	0
10	31	33	26.0	25.7	4	5	1	1	0	0	1	1
11	36	37	21.2	21.8	3	3	1	1	0	0	1	1
12	30	33	20.3	20.1	3	3	2	2	2	2	0	0
13	27	28	19.5	19.7	0	0	0	0	0	0	0	0
14	29	30	19.2	21.1	1	2	0	0	0	0	0	0
15	33	34	29.0	29.7	5	5	1	1	1	1	0	0
Average	29.00 ± 3.59	30.4 ± 4.00	21.89 ± 3.69	22.76 ± 3.88								

Abbreviation: vNOTES, transvaginal natural orifice transluminal endoscopic surgery.

^aCharacteristics of 1st vNOTES.

^bCharacteristics of 2nd vNOTES.

points (shown in Figure 1): (1) Before performing the culdotomy for establishing the surgical platform of the second vNOTES, special mucous wrinkles on the posterior vaginal fornix, caused by the previous incision and suture, could be easily noticed (Figure 1a); (2) Due to the narrow surgical safe zone of the posterior fornix, we accessed the pelvic cavity via a previous incision located 0.5 cm below the cervicovaginal junction or in the same location as the mucous wrinkles (Figure 1b–d).

FSFI

The FSFI is a validated and widely applied scale with a maximum obtainable score of 95. It comprises 19 questions involving six domains of female sexual experience, including libido, arousal, lubrication, orgasm, satisfaction, and pain.¹³ A score lower than 26.5 indicates impaired sexual function.¹⁴ The score of each domain is determined by the sum of all items in that domain multiplied by the domain factor (desire, 0.6; arousal, 0.3; lubrication, 0.3; orgasm, 0.4; satisfaction, 0.4; pain, 0.4). The overall score is the sum of the six domain scores.

Statistical analysis

SPSS version 25.0 (IBM Corporation, Armonk, NY) and GraphPad Prism (version 9.0.0, GraphPad Software, San Diego, CA) were used for statistical analyses of the present study. Paired Student's *t*-test was performed for each patient's pre- and postoperative FSFI scores of the first and second vNOTESs. Statistical significance was defined as a *p*-value lower than 0.05.

RESULTS

Patients' baseline characteristics

During the study period, there were approximately 3000 patients who underwent their first vNOTES. Among them, 21 patients were initially considered for a second vNOTES, but 6 cases (5 cases of tubal pregnancy and massive pelvic hemorrhage and 1 case of a potentially malignant indication) underwent transumbilical laparoendoscopic single site surgery instead. As a result, there were 15 patients who were willing to undergo a second vNOTES in light of their satisfactory cosmetic outcomes and painless experience in the first vNOTES. Their socio-demographic characteristics are given in Table 1. Their mean age during the first and second vNOTES was 29.00 ± 3.59 and 30.4 ± 4.00 years, respectively. The mean values of their BMI when receiving the first and second vNOTES were 21.89 ± 3.69 and 22.76 ± 3.88 kg/m². Three patients had never experienced pregnancy before their first vNOTES. This number decreased to one

after the second vNOTES. Most patients (11/15) were nulliparous at the time of the first vNOTES. One case had induced labor at the 20th gestational week because of fetal anomalies during the interval between both vNOTES. None of the patients delivered after the second vNOTES. Among the remaining four cases, one patient had experienced vaginal delivery once, one had delivered vaginally twice, and the other two had undergone cesarean section once.

Surgical outcomes of first and second vNOTES

Subsequently, we summarized the clinicopathological characteristics of both the vNOTESs (Table 2). Ectopic pregnancy was the most frequent indication for vNOTES, with 7 cases during the first vNOTES and 11 during the second, followed by ovarian teratoma, with 5 cases during the first vNOTES. The interval between both vNOTES approaches ranged from 9 days to 38 months, with case 4 complicated by persistent ectopic pregnancy after vNOTES salpingostomy, and thus received a vNOTES salpingectomy on the 9th postoperative day. Their postoperative VAS score also remained stable, with only case no. 8 experiencing slightly increased VAS score after the second vNOTES (2 and 1 on the first and second postoperative day of the first vNOTES, respectively vs. 3, 2, and 1 on postoperative Day 1, 2, and 3, respectively). Intriguingly, this patient did not experience any perioperative or postoperative complications during the follow-up, even though the surgical interval was remarkably short. No other perioperative complications were found in either vNOTES among the patients. We also noticed slightly exacerbated intraoperative pelvic adhesion during the first vNOTES in cases 3, 6, and 12, which correspondingly increased the difficulty of repeated vNOTES but did not lead to any surgical conversion. In addition, none of the cases had any postoperative incision complications such as hernia, polypi, or granuloma. The operation duration (63.33 ± 13.71 vs. 67.33 ± 22.51 min, $p = 0.429$), intraoperative estimated blood loss (32.00 ± 20.42 vs. 30.00 ± 9.26 , $p = 0.723$), and postoperative hospital stay (2.20 ± 0.56 vs. 2.40 ± 0.51 , $p = 0.082$) of both vNOTESs were also comparable. However, we noticed a prolonged surgical duration in cases 3, 10, 12, and 15. Moreover, the matched samples *t*-test revealed that the second vNOTES needed a significantly longer time to establish the surgical entrance (3.53 ± 1.36 vs. 4.73 ± 1.58 , $p = 0.023$). Noteworthy, three patients were pregnant at the end of the study period.

Pre- and postoperative sexual function of the first and second vNOTES

The domain and overall scores of the patients' pre- and postoperative FSFI for both vNOTES are listed in Table 3 as mean \pm standard error. We only recorded case 4's pre-first and post-second vNOTES FSFI (due to the



TABLE 2 Clinicopathological features of the first and second vNOTES.

Case no.	Surgical type ^a	Interval between both vNOTES, days	Indication ^a	Indication ^b	Time to reach the abdominal cavity, min		Operation duration, min ^b
					abdominal cavity, min ^a	the abdominal cavity, min ^b	
1	Right ovarian cystectomy	787	Right ovarian teratoma(5 cm)	Left ampullary pregnancy	7	5	70
2	Left ovarian cystectomy	152	Left ovarian teratoma(5.5 cm)	Left ampullary pregnancy	3	4	50
3	Bilateral tubal ligation	283	Infertility; IVF	Infertility; IVF	5	8	60
4	Left Salpingostomy	9	Left ampullary pregnancy	Persistent Ectopic Pregnancy	3	5	60
5	Right salpingostomy	546	Right ampullary pregnancy	Right ampullary pregnancy	2	4	35
6	Left salpingostomy	891	Left ampullary pregnancy	Left ampullary pregnancy	2	6	60
7	Right salpingostomy	692	Right ampullary pregnancy	Left ampullary pregnancy	3	6	80
8	Left ovarian cystectomy	290	Left ovarian teratoma (6.5 cm)	Right ampullary pregnancy	3	4	50
9	Bilateral neosalpingostomy + right ovarian cystectomy	136	Secondary infertility + Right ovarian teratoma (5 cm)	Right ampullary pregnancy	4	6	85
10	Left salpingostomy	940	Left ampullary pregnancy	Right ampullary pregnancy	5	3	60
11	Myomectomy	406	posterior Uterine myoma	Left ampullary pregnancy	3	4	75
12	Right ovarian cystectomy	1156	Right ovarian teratoma (2.0 cm)	Right ovarian mucinous cystadenoma (2.0 cm)	4	3	80
13	Neosalpingostomy + hydrotubation	184	Left hydrosalpinx	Infertility, IVF	3	3	65
14	Right salpingostomy	84	Right tubal pregnancy	Right ampullary pregnancy	2	3	50
15	Left tubal ligation	231	Left hydrosalpinx	Left Hydrosalpinx	4	7	70
Average		452.47 ± 359.00			3.53 ± 1.36	4.73 ± 1.58	63.33 ± 13.71
P-value					0.023 ^c		0.429 ^c

Case no.	Intraoperative estimated blood loss ^a	Intraoperative estimated blood loss ^b	Perioperative complications ^a	Perioperative complications ^b	Postoperative complications ^a	Postoperative complications ^b	VAS score of first 3 postoperative days ^b		Hospital stay ^b
							days ^a	days ^b	
1	30	30	—	—	—	—	1/0	1/1	2
2	30	20	—	—	—	—	1/1	1/1	2
3	20	50	—	—	—	—	2/2/0	2/1/0	3
4	30	20	—	—	Persistent Ectopic Pregnancy	—	1/0	1/1	2
5	20	20	—	—	—	—	2/0	3/1	2
6	20	30	—	—	—	—	2/2/0	2/2/0	3
7	20	30	—	—	—	—	2/1	1/1	2
8	20	30	—	—	—	—	1	2/1	2

(Continues)

TABLE 2 (Continued)

Case no.	Intraoperative estimated blood loss ^a	Intraoperative estimated blood loss ^b	Perioperative complications ^a	Perioperative complications ^b	Postoperative complications ^a	Postoperative complications ^b	VAS score of first 3 postoperative days ^a	VAS score of first 3 postoperative days ^b	Hospital stay ^a	Hospital stay ^b
9	50	50	—	—	—	—	2/1	2/1	2	2
10	20	30	—	—	—	—	1/1	2/1	2	2
11	100	30	—	—	—	—	2/1/0	2/1/1	3	3
12	30	30	—	—	—	—	2/1/0	2/2/0	3	3
13	30	20	—	—	—	—	1/1	2/1	2	2
14	30	30	—	—	—	—	2/2/0	3/1/0	3	3
15	30	30	—	—	—	—	2/0	2/1/0	2	3
Average	32.00 ± 20.42	30.00 ± 9.26	—	—	—	—			2.20 ± 0.56	2.40 ± 0.13
<i>P</i> -value	0.723 ^c								0.082 ^c	

Abbreviations: IVF, in vitro fertilization; VAS, Visual Analogue Scale; vNOTES, transvaginal natural orifice transluminal endoscopic surgery.

^aCharacteristics of 1st vNOTES.

^bCharacteristics of 2nd vNOTES.

^cMatched samples *t*-test.

short surgical interval) and case 15's pre- and post-first vNOTES FSFI (received the surgery 1 month before drafting); all the remaining cases were surveyed all four time points. Three comparisons were conducted between (1) the pre- and postoperative FSFI scores of the first vNOTES, (2) the pre- and postoperative FSFI of the second vNOTES, and (3) the pre-first and post-second vNOTES FSFI. We noticed a slightly lower score in the pain domain of pre- and postoperative FSFI for repeated vNOTES compared to those for the first vNOTES (pre-first vNOTES: 4.96 ± 0.78 ; post-first vNOTES: 4.82 ± 0.79 ; pre-second vNOTES: 4.45 ± 1.39 ; post-second vNOTES: 4.43 ± 1.36). Such difference was also observed in the overall scores (pre-first vNOTES: 24.52 ± 2.44 ; post-first vNOTES: 24.23 ± 2.15 ; pre-second vNOTES: 22.43 ± 6.50 ; post-second vNOTES: 4.43 ± 1.36). However, no significant differences were found in any of the domains or overall scores between the three comparisons.

DISCUSSION

With the unprecedented development of minimally invasive surgical techniques and equipment, the vNOTES approach has gained increasing popularity in general surgery, urology and gynecology. Meanwhile, whether vNOTES can be performed repeatedly has become a huge concern among gynecologists and endoscopists.^{6,7,15,16} Some experts are of the opinion that the re-entry via the culdotomy of previous vNOTES should be avoided,¹⁶ while the clinical evidence supporting such an opinion is still lacking. Traditional laparoendoscopy can easily enter the abdominal cavity through the previous entrance and use new trocar sites on the abdominal walls. However, owing to the limited operative safety zone of the vaginal fornix, the second vNOTES requires a re-incision of the previous incision to establish the surgical access, which may cause potential incisional complications and impact patients' sexual life and childbirth.

To date, reports regarding repeated vNOTES are scarce. The first and only study discussing the feasibility of a second vNOTES complete hysterectomy among patients who underwent the first vNOTES adnexectomy mainly focused on the surgical complications of the second vNOTES and included only 11 patients, most of whom were already in their peri- or postmenopausal period.⁶ Evidence of the safety and impact of repeated non-hysterectomy vNOTES on childbirth and sexual quality of life is still lacking.

vNOTES is an emerging minimally invasive surgical technique, which has not been widely performed worldwide. It has been conducted in our institute for only 4 years.¹⁷ We have performed 3000 cases of vNOTES so far, but because not many patients would suffer from another benign gynecological disease in such a short

TABLE 3 FSFI domain scores before and 3 month after 1st and 2nd vNOTES.

Domain	Pre-1st vNOTES	Post-1st vNOTES	<i>P</i> -value ^a	Pre-2nd vNOTES	Post-2nd vNOTES	<i>P</i> -value ^b	<i>P</i> -value ^c
Desire	3.44 ± 0.66	3.28 ± 0.59	0.164	3.04 ± 0.55	3.13 ± 0.48	0.336	0.365
Arousal	3.04 ± 0.61	3.06 ± 0.62	0.991	3.00 ± 0.70	2.98 ± 0.75	0.752	0.302
Lubrication	4.60 ± 0.71	4.52 ± 0.69	0.573	4.52 ± 0.72	4.67 ± 0.69	0.221	0.221
Orgasm	4.13 ± 0.78	4.16 ± 0.84	0.670	4.14 ± 0.73	4.09 ± 0.63	0.435	0.551
Satisfaction	4.35 ± 0.67	4.40 ± 0.77	0.334	4.51 ± 0.62	4.31 ± 0.59	0.187	0.477
Pain	4.96 ± 0.78	4.82 ± 0.79	0.151	4.45 ± 1.39	4.43 ± 1.36	0.583	0.328
Overall	24.52 ± 2.44	24.23 ± 2.15	0.272	22.43 ± 6.50	22.33 ± 6.49	0.566	0.250

Abbreviations: FSFI, female sexual function index; vNOTES, transvaginal natural orifice transluminal endoscopic surgery.

^aComparison between the pre- and postoperative FSFI scores of the 1st vNOTES.

^bComparison between the pre- and postoperative FSFI scores of the 2nd vNOTES.

^cComparison between the pre-first and post-second vNOTES FSFI.

period after the first vNOTES, we did not have many patients who underwent a second vNOTES. Thus, we only had a few cases of repeated vNOTES, making the study on the repeatability of vNOTES challenging.

There were several intriguing findings regarding the second vNOTES in our study. The postoperative VAS score of both vNOTESs were similar, with only 1 patient having a slightly increased VAS score. We speculate that it might be due to the scarce distribution of nerves in the posterior vaginal fornix, which is also one of the most notable minimal invasive features of the vNOTES technique. There was no significant difference in the operative duration between both vNOTESs in our 15 cases, despite several cases experiencing longer surgical duration in the second vNOTES. We conclude that the prolonged surgical duration experienced by several cases might be caused by more severe pelvic adhesions or lesser surgical experience of the second surgeon. The significantly longer time needed to establish the surgical entrance in the second vNOTES may be caused by a less clear anatomical structure as a result of the first vNOTES.

Since transvaginal access could be accomplished through the posterior or anterior vaginal fornix and even the vaginal residue after the complete hysterectomy, the repeated vNOTES could be categorized into the following situations: (1) vNOTES complete hysterectomy following the first vNOTES via culdotomy in the posterior or anterior vaginal fornix; (2) both vNOTES performed through culdotomy in the posterior vaginal fornix; and (3) both vNOTES established via the anterior vaginal fornix. In clinical practice, the first two situations are the overwhelming majority. Only one publication has explored the feasibility of the first scenario of repeated vNOTES.⁶ In our study, all vNOTESs of the 15 cases, regardless of whether they were performed initially or later, were conducted through posterior fornix culdotomy. Our perioperative findings showed no aggravation of postoperative pelvic adhesion and a comparable incidence rate of surgical complications as the first vNOTES, indicating that repeated vNOTES may be a safe and feasible surgical alternative for patients with a history of posterior fornix entrance vNOTES.

No evidence has been found on the impact of the second vNOTES on patients' sexual well-being so far. Some previously published studies have shown no significant difference in patients' FSFI between vNOTES and conventional laparoscopic opportunistic bilateral salpingectomy.¹⁸ Consistent with this, the 15 cases in our study also had comparable FSFI domain and overall scores, regardless of vNOTES. One potential explanation is that most somatic vaginal innervation is distributed in the distal and anterior parts of the vaginal walls and bypasses the posterior vaginal fornix, thus making the culdotomy, even the repeat culdotomy, least deleterious to sexual function.^{19,20}

Regarding the impact of vNOTES on childbirth, several cases of successful vaginal delivery among patients who underwent the first vNOTES, including ovarian cystectomy, tubal ligation, and myomectomy, have been reported, primarily revealing the relative safety of vNOTES concerning childbirth.^{21,22} However, no evidence of the impact of repeated vNOTES on childbirth has been reported in the literature. Unfortunately, due to the relatively short postoperative follow-up period and small cohort size in our study, after the second vNOTES, none of the patients had delivered vaginally or via cesarean section.

Although several limitations of the current study might hinder the generalizability of our findings, including the small cohort size, various surgical intervals, the potential selection bias, and the fact that the patients have not yet undergone childbirth after the second vNOTES, this case series first reported the sexual functions of patients who underwent vNOTES twice and found no significant change in FSFI and comparable incidence rate of perioperative complications between these two vNOTES. This might be helpful for the minimally invasive surgical approach selection for patients who undergo vNOTES once. Our study provides evidence that the second vNOTES could be successfully conducted without overt impact on patients' postoperative outcomes and sexual function. However, a larger sample size and longer follow-up period are needed to investigate the influence of vNOTES and repeated vNOTES on childbirth.

To sum up, we provide preliminarily evidence that repeated non-hysterectomy vNOTES, which has a comparable incidence rate of perioperative complications

and insignificant impact on patients' sexual function, is safe and feasible.

CONFLICT OF INTEREST STATEMENT

The authors declare no conflict of interest for this article.

DATA AVAILABILITY STATEMENT

The data that support the findings of this study are openly available in Figshare at <http://doi.org/10.6084/m9.figshare.23608890>, Reference number 23.

ETHICS STATEMENT

This study was approved by the ethics committee of our institute (CWCCH-2021122). All information retrieval and questionnaire surveys were conducted with the written consent of each patient. For privacy concerns, their identifiable characteristics were not transcribed from the Hospital Information System.

ORCID

Dan Feng  <https://orcid.org/0000-0002-7324-1548>

Tianjiao Liu  <https://orcid.org/0000-0001-8279-5924>

Xin Li  <https://orcid.org/0000-0002-6734-9034>

Li He  <https://orcid.org/0000-0002-9716-2457>

REFERENCES


- Gauderer MW, Ponsky JL, Izant RJ. Gastrostomy without laparotomy: a percutaneous endoscopic technique. *J Pediatr Surg.* 1980;15(6):872–5.
- Atallah S, Martin-Perez B, Keller D, Burke J, Hunter L. Natural-orifice transluminal endoscopic surgery. *Br J Surg.* 2015;102(2):e73–92. <https://doi.org/10.1002/bjs.9710>
- Brandão P, Almeida A, Ramôa P. vNOTES for adnexal procedures. *J Obstet Gynaecol.* 2021;41(7):1134–8. <https://doi.org/10.1080/01443615.2020.1841124>
- Baekelandt J, de Mulder PA, le Roy I, Mathieu C, Laenen A, Enzlin P, et al. Adnexectomy by vaginal natural orifice transluminal endoscopic surgery versus laparoscopy: results of a first randomised controlled trial (NOTABLE trial). *BJOG.* 2021;128(11):1782–91. <https://doi.org/10.1111/1471-0528.16838>
- Baekelandt JF, de Mulder PA, le Roy I, Mathieu C, Laenen A, Enzlin P, et al. Hysterectomy by transvaginal natural orifice transluminal endoscopic surgery versus laparoscopy as a day-care procedure: a randomised controlled trial. *BJOG.* 2019;126(1):105–13. <https://doi.org/10.1111/1471-0528.15504>
- Nulens K, van Genechten I, Baekelandt J. Repeat vaginal natural orifice transluminal endoscopic surgery: a first feasibility study. *Gynecol Obstet Invest.* 2021;86(1–2):117–22. <https://doi.org/10.1159/000513403>
- Perretta S, Vix M, Dallemagne B, Nassif J, Donatelli G, Marescaux J. Video. Repeated transvaginal notes: is it possible? *Surg Endosc.* 2012;26(2):565. <https://doi.org/10.1007/s00464-011-1923-7>
- Ferreira-Valente MA, Pais-Ribeiro JL, Jensen MP. Validity of four pain intensity rating scales. *Pain.* 2011;152(10):2399–404. <https://doi.org/10.1016/j.pain.2011.07.005>
- Chen X, Liu H, Sun D, Zhang JJ, Fan Q, Shi H, et al. Transvaginal natural orifice transluminal endoscopic surgery for tubal pregnancy and a device innovation from our institution. *J Minim Invasive Gynecol.* 2019;26(1):169–74. <https://doi.org/10.1016/j.jmig.2018.05.013>
- Huang L, Lin Y-H, Yang Y, Gong Z-L, He L. Comparative analysis of vaginal natural orifice transluminal endoscopic surgery versus transumbilical laparoendoscopic single-site surgery in ovarian cystectomy. *J Obstet Gynaecol Res.* 2021;47(2):757–64. <https://doi.org/10.1111/jog.14603>
- Baekelandt J, Vercammen J. IMELDA transvaginal approach to ectopic pregnancy: diagnosis by transvaginal hydrolaparoscopy and treatment by transvaginal natural orifice transluminal endoscopic surgery. *Fertil Steril.* 2017;107(1):e1–2. <https://doi.org/10.1016/j.fertnstert.2016.09.024>
- Lee C-L, Wu K-Y, Su H, Ueng S-H, Yen C-F. Transvaginal natural-orifice transluminal endoscopic surgery (NOTES) in adnexal procedures. *J Minim Invasive Gynecol.* 2012;19(4):509–13. <https://doi.org/10.1016/j.jmig.2012.02.005>
- Rosen R, Brown C, Heiman J, Leiblum S, Meston C, Shabsigh R, et al. The female sexual function index (FSFI): a multidimensional self-report instrument for the assessment of female sexual function. *J Sex Marital Ther.* 2000;26(2):191–208.
- Gerstenberger EP, Rosen RC, Brewer JV, Meston CM, Brotto LA, Wiegel M, et al. Sexual desire and the female sexual function index (FSFI): a sexual desire cutpoint for clinical interpretation of the FSFI in women with and without hypoactive sexual desire disorder. *J Sex Med.* 2010;7(9):3096–103. <https://doi.org/10.1111/j.1743-6109.2010.01871.x>
- Reddy H, Kim SW, Plewniak K. Applications of vaginal natural orifice transluminal endoscopic surgery (vNOTES) in gynecologic surgery. *Curr Opin Obstet Gynecol.* 2022;34(4):220–6. <https://doi.org/10.1097/GCO.0000000000000799>
- Baekelandt J, Noori N, Hofmann L, Mansoor A, Kapurbandara S. Standardised step by step approach to adnexectomy by vaginal natural orifice transluminal endoscopic surgery. *Eur J Obstet Gynecol Reprod Biol.* 2022;274:160–5. <https://doi.org/10.1016/j.ejogrb.2022.05.021>
- Huang L, Feng D, Gu D-X, Lin YH, Gong ZL, Liu DD, et al. Transvaginal natural orifice transluminal endoscopic surgery in gynecological procedure: experience of a women's and children's medical center from China. *J Obstet Gynaecol Res.* 2022;48(11):2926–34. <https://doi.org/10.1111/jog.15402>
- Yassa M, Kaya C, Kalafat E, Tekin AB, Karakas S, Mutlu MA, et al. The comparison of transvaginal natural orifice transluminal endoscopic surgery and conventional laparoscopy in opportunistic bilateral salpingectomy for permanent female sterilization. *J Minim Invasive Gynecol.* 2022;29(2):257–64. <https://doi.org/10.1016/j.jmig.2021.08.009.e1>
- Solomon D, Lentz R, Duffy AJ, Bell RL, Roberts KE. Female sexual function after pure transvaginal appendectomy: a cohort study. *J Gastrointest Surg.* 2012;16(1):183–7. <https://doi.org/10.1007/s11605-011-1706-4>
- Tunuguntla HSGR, Gousse AE. Female sexual dysfunction following vaginal surgery: myth or reality? *Curr Urol Rep.* 2004;5(5):403–11.
- Feng D, He L. Pregnancy and childbirth after transvaginal natural orifice transluminal endoscopic surgery for benign gynecological diseases. *Int J Gynaecol Obstet.* 2021;155:551–2. <https://doi.org/10.1002/ijgo.13820>
- Thomaidis P, Weltermann NJ, Seefeldt CS, Richards DC, Sauerwald A, Heiss MM, et al. Transvaginal hybrid-NOTES procedures-do they have a negative impact on pregnancy and delivery? *Langenbecks Arch Surg.* 2021;406(6):2045–52. <https://doi.org/10.1007/s00423-021-02105-z>
- Dan Feng TL, Xin L, Jieru P, Lu H, Li H. Supplementary file of repeated vNOTES. Figshare (Accessed 30 June 2023). <http://doi.org/10.6084/m9.figshare.23608890>.

How to cite this article: Feng D, Liu T, Li X, Peng J, Huang L, He L. Repeated transvaginal natural orifice transluminal endoscopic surgery: An initial Chinese experience. *J Obstet Gynaecol Res.* 2023;49(10):2501–8. <https://doi.org/10.1111/jog.15757>

CLINICAL ARTICLE

Gynecology

Perioperative outcomes of and predictors for conversion from transvaginal natural orifice transluminal endoscopic tubal surgeries: A retrospective cohort study of 619 patients

Dan Feng¹  | Li He¹  | Xin Li¹  | Qiang Zhang¹ | Jieru Peng² | Lu Huang¹ | Tianjiao Liu¹  | Yonghong Lin¹ 

¹Department of Gynecology, Chengdu Women's and Children's Central Hospital, School of Medicine, University of Electronic Science and Technology of China, Chengdu, People's Republic of China

²Medical Administrative Department, Chengdu Women's and Children's Central Hospital, School of Medicine, University of Electronic Science and Technology of China, Chengdu, People's Republic of China

Correspondence

Yonghong Lin, Department of Gynecology, Chengdu Women's and Children's Central Hospital, School of Medicine, University of Electronic Science and Technology of China, No.1617, Riyue Avenue, Chengdu, Sichuan, 611731, People's Republic of China.

Email: linyhcd2011@163.com

Funding information

Chengdu High-level Key Clinical Specialty Construction Project; Sichuan Provincial Medical Association Project, Grant/Award Number: S19085; the Chengdu Municipal Health Commission Project, Grant/Award Number: 2021215; the Japan-China Sasakawa Medical Fellowship Program

Abstract

Objective: To assess the perioperative outcomes of vNOTES tubal surgeries and to identify predictors of surgical conversion.

Methods: A single-center retrospective cohort study was performed on 619 patients who underwent vNOTES tubal surgeries in our institute from December 2018 to October 2021. Patients were categorized into “converted” or “non-converted” groups based on whether conversion occurred. *t*-test and χ^2 test were performed on demographic and clinicopathologic data to compare their perioperative outcomes. Logistic regression was built to identify predictors for surgical conversions.

Results: The conversion and complication rates of the vNOTES tubal surgeries in the present study were 3.07% and 4.85%, respectively. The “converted group” has a significantly higher percentage of patients with severe pelvic adhesions (9/19 [47.4%]) and pelvic endometriosis (2/19 [10.5%]), which significantly predicates surgical conversion. The “converted group” also had a longer duration of surgery (140.94 ± 88.73 min, $P = 0.002$) and an increased proportion of “converted from vNOTES” patients experienced more than 50 ml of intraoperative blood loss (7/19 [36.9%]). Four patients had intraoperative rectal injuries, and no Clavien–Dindo III–V postoperative complications occurred.

Conclusion: vNOTES tubal surgeries are safe due to low conversion and complication rates. Severe pelvic adhesion and endometriosis are predictors for surgical conversions.

KEYWORDS

intraoperative conversion, risk factors, surgical complication, surgical outcomes, tubal operation, vNOTES

1 | INTRODUCTION

The development and progress of surgical technology over recent decades have led us to adopt many minimally invasive surgical (MIS) options. Natural orifice transluminal endoscopic surgery (NOTES), a

novel MIS concept of accessing the abdominal cavity through natural orifices, has created an innovative, less painful, and scarless surgical alternative to conventional laparoscopy in recent years.¹ Because of the anatomical features of the vagina, transvaginal NOTES (vNOTES) allow easy access to the female internal genital

Dan Feng, Li He, Xin Li and Tianjiao Liu contributed equally to this work.

© 2023 International Federation of Gynecology and Obstetrics.

organs and safe closure of the incision, making them increasingly popular and frequently utilized in the field of gynecology.²

Although vNOTES was proved clinically feasible in 2007,³ it still lacks adequate evidence demonstrating its safety and ineligible risk factors for surgical conversions. However, the rate of complications and intraoperative conversion to other approaches, along with the effectiveness of disease treatment, are the most important immediate judgment criteria for the safety and feasibility of novel procedures like vNOTES. Due to their relatively lower complexity, tubal operations such as ligation, salpingostomy, chromoperturbation, and resection are always the first choice of novice gynecologists learning the vNOTES technique. Additionally, none of the existing publications regarding these vNOTES tubal surgeries presents a sample size larger than 20 patients.⁴ More solid clinical evidence is thus required for better surgical recommendation and consultation of vNOTES.^{5,6} Considering that, understanding why vNOTES tubal surgeries were converted is important and could help gynecologists to make better preoperative decisions. Here we retrospectively reviewed 619 vNOTES tubal surgeries in our institute to investigate the perioperative outcomes, especially surgical conversions, and to identify predictors for conversion.

2 | MATERIALS AND METHODS

2.1 | Study design

This retrospective study analyzed the data on the postoperative outcomes of 619 patients who underwent vNOTES tubal surgeries, mainly for treating ectopic tubal pregnancy, hydrosalpinx, or infertility, in the Department of Gynecology of Chengdu Women's and Children's Central Hospital (CWCCH), Chengdu, People's Republic of China, from December 2018 to October 2021 (Figure 1). In our center, patients who underwent vNOTES tubal surgeries all met following criteria: (1) laparoscopic surgery was required for tubal pathology; (2) patients were willing to receive vNOTES, although the following patients were excluded: (i) those with a history of rectal surgery, severe pelvic inflammatory disease, or pelvic radiotherapy; (ii) patients suspected of rectovaginal endometriosis, malignant tumors, or severe pelvic adhesions; (iii) and those who had not had sexual intercourse.⁷⁻⁹ A 1-month routine follow-up was carried out to investigate patients' short-term postoperative outcomes. Given the relatively narrow operative space, restricted visualization, and technical difficulty associated with vNOTES for delicate suturing in neosalpingostomy and tubal anastomosis for natural conception, these tubal surgeries were rarely conducted transvaginally in our institute. Based on whether vNOTES was converted to other approaches or not, the patients were grouped into "converted from vNOTES" ($n = 19$) and "non-converted vNOTES" ($n = 600$), respectively. Following that, statistical analyses were carried out to compare the postoperative outcomes of the groups and identify the risk factors for surgical conversion.

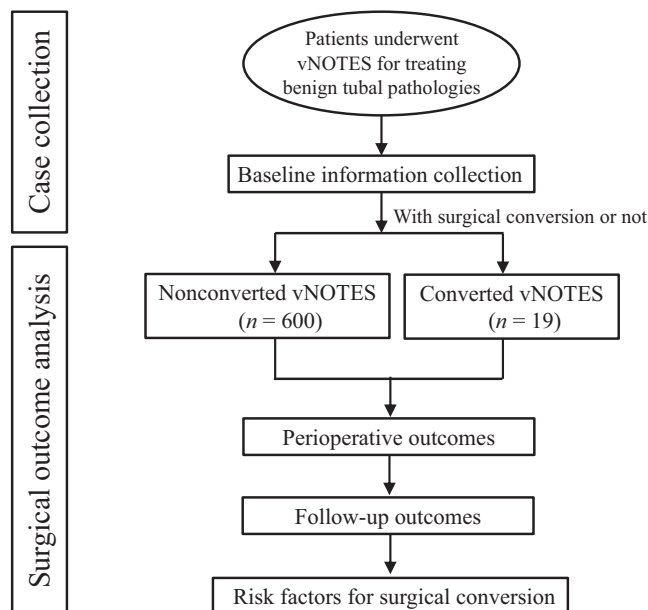


FIGURE 1 Flow diagram of present study.

2.2 | Surgical procedures

The vNOTES tubal surgical technique and instruments used for the present study have been previously described.^{4,9-11} A detailed gynecological physical examination and ultrasonography were performed during the preoperative examination and assessment to rule out severe pelvic adhesion. The surgical procedures involved in the present study included tubal salpingostomy, salpingectomy, tubal ligation, and several instances of chromoperturbation. In the present study, 33 surgeons performed vNOTES tubal procedures and were classified as second-line and third-line surgeons based on their years of experience. There are 21 second-line surgeons in our center, each of whom has at least 10 years of operating experience and has performed more than 500 laparoscopies, including about 30 instances of vNOTES, and 12 third-line surgeons, each of whom has at least 20 years of operating experience and has performed more than 1000 laparoscopies, including more than 60 instances of vNOTES. First-line surgeons (with less than 10 years of operating experience) were regarded as relatively inexperienced and were not permitted to perform the vNOTES surgery as chief operators in our institute; thus they were not included. From the day that vNOTES was performed to the third postoperative day, the Visual Analogue Scale (VAS) was applied to each patient to measure their postoperative pain daily.

2.3 | Baseline information and perioperative characteristics of the patients

We included patients' sociodemographics, such as age, ethnicity, body mass index (BMI, calculated as weight in kilograms divided by the square of height in meters), gravidity, parity, and surgical or gestational histories, as their baseline characteristics. We also

gathered their clinicopathologic characteristics, such as a history of previous abdominal or pelvic surgeries and the presence of uterine pathology, endometriosis or pelvic adhesion, and classified them using consensus criteria, with some modifications due to the relatively narrow field of visualization in the case of vNOTES.^{12,13} The perioperative features of the patients, such as operative duration, postoperative hospital stay, postoperative fever, volume of estimated blood loss, and postoperative pain scores, were also collected. The surgical conversion implied converting a vNOTES procedure to an open abdominal (OA) surgery, transumbilical laparoendoscopic single port (LESS), or conventional multiport laparoscopy (MPL) procedure. The Clavien–Dindo (CD) classification method was applied to categorize the postoperative complications of each surgical patient.¹⁴ We also calculated the uterine volume using the formula for the volume of a prolate ellipsoid, $V = 0.52 \times \text{maximum length} \times \text{anteroposterior diameter} \times \text{transverse diameter}$, for analyzing the uterine size's role in the surgical conversion of vNOTES tubal surgeries.¹⁵

2.4 | Ethics statement

The present study was approved by the Ethics Committee of the CWCCH, and written informed consent was obtained from all patients during their admission. After retrieving the data from the HIS, all personally identifiable information about the patients was deleted.

2.5 | Statistical analyses

All data were analyzed with SPSS version 25 (IBM). The continuous variables were presented as mean \pm standard deviation (SD) and analyzed using a two-sample *t*-test or Mann–Whitney *U*-test as appropriate. The categorical variables were expressed as numbers and percentages and compared using the χ^2 or Fisher exact test unless stated otherwise. A logistic regression was built to determine the predictors for surgical conversion, and the results were presented in the form of odds ratios and 95% confidence intervals (CIs). A *P*-value of less than 0.05 was considered statistically significant.

3 | RESULTS

3.1 | Overall profile of patient cohort

Of the 619 patients included in the present study, only 19 (3.07%) experienced surgical conversion from vNOTES (Table 1), and no patient was lost during the 1-month postoperative follow-up. The entire study cohort included 403 salpingectomies, 49 tubal ligations, including 20 neosalpingostomies, 138 salpingostomies, and 29 tubal chromopertubations, of which six and three of these

procedures were combined with fimbrioplasty and neosalpingostomy, respectively.

3.2 | Demographic and clinicopathologic features of the patients

Both patient groups, “non-converted vNOTES” and “converted from vNOTES,” displayed similar distributions in terms of mean age (31.45 ± 5.53 years vs. 32.42 ± 7.44 years, $P = 0.458$), BMI (21.66 ± 3.15 vs. 20.48 ± 2.46 , $P = 0.107$), and proportion of Han Chinese ethnicity (578/600 [96.3%] vs. 19/19 [100%], $P = 0.395$). Statistically significant differences were also absent in terms of gravidity, parity, cumulative cesarean sections, and previous pelvic or abdominal surgeries between the patients in the groups. The distribution of different procedures between these two groups was also similar, with the majority having undergone salpingectomy (390/600 [65.0%] vs. 13/19 [68.4%], $P = 0.890$). In addition, the proportions of different classes of surgeons conducting the procedures in both groups were also similar, with 256/600 (42.7%) versus 9/19 (47.4%) surgeries performed by second-line surgeons and 344/600 (57.3%) versus 10/19 (52.6%) surgeries performed by third-line gynecologists ($P = 0.683$). Besides, these two groups also had similar uterine volumes (56.47 ± 31.32 vs. 54.14 ± 23.96 , $P = 0.748$) and compositions of concurrent uterine pathologies (myoma 26/600 [4.3%] vs. 1/19 [5.3%]; adenomyoma 7/600 [1.2%] vs. 0, $P = 0.879$).

Notably, the converted group had a significantly lower proportion of patients who underwent vNOTES for treating ectopic pregnancy (370/600 [61.7%] vs. 9/19 [47.4%]) and a bigger proportion for treating tubal hydrosalpinx (191/600 [32.3%] vs. 8/19 [42.1%], $P = 0.036$). A higher percentage of patients in the converted vNOTES group had severe pelvic adhesions (9/19 [47.4%] vs. 0/600 [0.0%], $P < 0.001$) and endometriosis (2/19 [10.5%] vs. 10/600 [1.7%], $P < 0.001$). Additionally, the patients in this group underwent a significantly longer duration of surgery than did the non-converted vNOTES patients (140.94 ± 88.73 min vs. 67.22 ± 27.50 min, $P = 0.002$). The postoperative outcomes of the patients in these two groups also differed significantly. Although the patients between the groups displayed no significant difference in the postoperative pain score for three consecutive days, a significantly larger percentage of patients in the converted vNOTES group stayed hospitalized for longer than a week post-surgery (6/19 [31.6%] vs. 11/600 [1.8%], $P < 0.001$). In addition, a higher proportion of patients in the converted vNOTES group had lost more than an estimated 50 ml of blood intraoperatively (7/19 [36.9%] vs. 17/600 [2.9%], $P < 0.001$).

The perioperative complications in our cohort are listed in Table 2. There were four cases of rectal injury in our cohort, including one full-thickness rectal injury in both groups and two seromuscular injuries in the “converted vNOTES” group. In the non-converted case of full-thickness rectal injury, the surgeon successfully repaired the injured rectum and completed the whole

TABLE 1 Demographics and clinical characteristics of patients who underwent vNOTES tubal surgery without versus with surgical conversions.

Characteristics	Non-converted vNOTES (n = 600 [96.9%])	Converted from vNOTES (n = 19 [3.1%])	P-value
Age (year)	31.45 ± 5.53	32.42 ± 7.44	0.458
BMI ^a	21.66 ± 3.15	20.48 ± 2.46	0.107
Ethnicity			0.395
Han Chinese	578 (96.3%)	19 (100.0%)	
Minority groups	22 (3.7%)	0	
Gravidity			0.609
0	96 (16.0%)	2 (10.5%)	
1	137 (22.8%)	6 (31.6%)	
≥2	367 (61.2%)	11 (57.9%)	
Parity			0.973
0	323 (53.8%)	10 (52.6%)	
1	207 (34.5%)	7 (36.8%)	
≥2	70 (11.7%)	2 (10.5%)	
Cesarean section			0.518
0	480 (80.0%)	17 (89.5%)	
1	96 (16.0%)	2 (10.5%)	
≥2	24 (4.0%)	0	
Vaginal delivery			0.210
0	439 (73.2%)	11 (57.9%)	
1	121 (20.1%)	7 (36.8%)	
≥2	40 (6.7%)	1 (5.3%)	
Previous pelvic or abdominal surgery			0.145
0	354 (59.0%)	15 (78.9%)	
1	177 (29.5%)	4 (21.1%)	
≥2	69 (11.5%)	0	
Chief complaint			0.016
Ectopic pregnancy	371 (62.6%)	9 (47.4%)	
Infertility	28 (4.7%)	1 (5.3%)	
Tubal hydrosalpinx	199 (32.3%)	8 (42.1%)	
Fallopian tube abscess	2 (0.3%)	1 (5.3%)	
Types of tubal surgery			0.890
Salpingostomy	135 (22.5%)	3 (15.8%)	
Salpingectomy	390 (65.0%)	13 (68.4%)	
Tubal ligation	47 (7.8%)	2 (10.5%)	
Chromopertubation	19 (3.2%)	1 (5.3%)	
Chromopertubation combined with fimbrioplasty or neosalpingostomy	9 (1.5%)	0	
Surgeon type			0.683
Second-line	256 (42.7%)	9 (47.4%)	
Third-line	344 (57.3%)	10 (52.6%)	
Uterine volume (cm ³) ^b	56.47 ± 31.32	54.14 ± 23.96	0.748
Concurrent uterine pathology			0.879
None	567 (94.5%)	18 (94.7%)	
Myoma	26 (4.3%)	1 (5.3%)	

TABLE 1 (Continued)

Characteristics	Non-converted vNOTES (n = 600 [96.9%])	Converted from vNOTES (n = 19 [3.1%])	P-value
Adenomyoma	7 (1.2%)	0	
Presence of pelvic adhesions			<0.001
None	155 (25.8%)	4 (21.1%)	
Mild or moderate	445 (74.2%)	6 (31.6%)	
Severe	0	9 (47.4%)	
Presence of pelvic endometriosis			<0.001
Deep endometriosis	0 (0.0%)	2 (10.5%)	
Ovarian endometriosis	6 (1.0%)	0 (0.0%)	
Superficial endometriosis	4 (0.7%)	0 (0.0%)	
None	590 (98.3%)	17 (89.5%)	
Surgical duration (min)	67.22 ± 27.50	140.94 ± 88.73	0.002
Estimated intraoperative blood loss (ml)			<0.001
≤50	583 (97.2%)	12 (63.2%)	
≤100	12 (2.0%)	5 (26.3%)	
≤200	1 (0.2%)	1 (5.3%)	
>200	4 (0.7%)	1 (5.3%)	
Postoperative complications (Clavien–Dindo classification)			0.241
None	576 (96.0%)	17 (89.4)	
I	17 (2.8%)	1 (5.3%)	
II	7 (1.2%)	1 (5.3%)	
III–V	0 (0.0%)	0 (0.0%)	
Postoperative pain score ^c			
Day 0	2.86 ± 0.43	2.95 ± 0.23	0.129
Day 1	2.33 ± 0.69	2.53 ± 0.61	0.225
Day 2	1.49 ± 0.66	1.63 ± 0.68	0.346
Day 3	0.90 ± 0.58	1.16 ± 0.69	0.055
Postoperative hospitalization duration (day)			<0.001
<3	433 (72.2%)	10 (52.6%)	
3–7	156 (26.0%)	3 (15.8%)	
>7	11 (1.8%)	6 (31.6%)	

^aBody mass index (calculated as weight in kilograms divided by the square of height in meters).

^bUterine volume was calculated using the formula for the volume of prolate ellipsoid: $V = 0.52 \times \text{maximum length} \times \text{anteroposterior diameter} \times \text{transverse diameter}$.

^cVisual Analogue Scale (VAS).

procedure in a vNOTES manner. Furthermore, we displayed the more detailed distribution of postoperative complications according to the CD classification (Table 2). The incidence rates of CD I–IV complications in our cohort were 18/619 (2.91%) for CD I, 8/619 (1.29%) for CD II, and zero for CD III and CD IV, respectively. For the CD I complications, there were seven cases of vomiting, four of fever, two of pain (requiring a painkiller), one of wound bleeding, two cases of anemia (requiring iron supplements), and two cases of urinary retention requiring catheterization. As for the CD II complications, all six cases of postoperative pelvic infection occurred in the non-converted vNOTES group, and both groups had one patient with ileus.

3.3 | Risk factors for surgical conversion

For further identification of the risk factors dictating the conversion from vNOTES tubal surgery in our cohort, we performed a logistic regression analysis on the factors relevant to the surgical conversions, including BMI, history of vaginal delivery, history of abdominopelvic surgery, uterine volume, the presence of pelvic adhesion, and endometriosis (Table 3). We found that the presence of severe pelvic adhesion and endometriosis significantly increased the chance of surgical conversion from vNOTES. Patients with severe pelvic adhesion were more than 14 times as likely to be converted to MPL or LESS in comparison with those without pelvic adhesion (adjusted odds ratio [OR] 14.87,

TABLE 2 Perioperative complications of vNOTES tubal surgery.

Complications	Non-converted vNOTES (n = 600)	Converted from vNOTES (n = 19)	All cases (n = 619)
Intraoperative complications	1	3	4 (0.65%)
Full-thickness rectal injury	1 (0.17%)	1 (5.26%)	
Rectal seromuscular injury	0	2 (10.53%)	
Postoperative complications			
CD I	17 (2.83%)	1 (5.26%)	18 (2.91%)
Vomiting	7 (1.17%)	0	7 (1.13%)
Fever (without treatment with antibiotics)	3 (0.50%)	1 (5.26%)	4 (0.65%)
Pain	2 (0.32%)	0	2 (0.32%)
Wound bleeding	1 (0.16%)	0	1 (0.16%)
Anemia requiring iron supply	2 (0.33%)	0	2 (0.32%)
Urinary retention	2 (0.33%)	0	1 (0.16%)
CD II	7 (1.17%)	1 (5.26%)	8 (1.29%)
Postoperative acute pelvic inflammatory disease	6 (1.00%)	0	6 (0.97%)
Incomplete ileus	1 (0.16%)	1 (5.26%)	2 (0.32%)
CD III-V	0	0	0
Total	25 (4.17%)	5 (26.32%)	30 (4.85%)

Abbreviation: CD, Clavien–Dindo classification.

TABLE 3 Logistic regression analysis of risk factors for conversion of vNOTES tubal surgeries.

Variable	P-value	Adjusted OR (95%CI)
BMI ^a	0.421	0.91 (0.75–1.14)
History of vaginal delivery	0.417	1.40 (0.64–3.16)
History of abdominopelvic surgery	0.347	0.60 (0.23–1.76)
Uterine size	0.745	0.99 (0.98–1.01)
Presence of mild or moderate pelvic adhesion	0.582	1.71 (0.19–18.56)
Presence of severe pelvic adhesion	<0.001	14.87 (5.63–40.16)
Presence of endometriosis	<0.001	14.63 (3.93–56.84)

Abbreviations: CI, confidence interval; OR, odds ratio; vNOTES, transvaginal natural orifice transluminal endoscopic surgery.

^aBody mass index (calculated as weight in kilograms divided by the square of height in meters).

95% CI 5.63–40.16, $P < 0.001$). In addition, the presence of endometriosis also significantly increased the chance of surgical conversion from vNOTES (adjusted OR 14.63, 95% CI 3.93–56.84, $P < 0.001$).

3.4 | Clinical characteristics of patients with surgical conversion

We present the major clinicopathologic features of all 19 patients who underwent surgical conversion in Table 4. Generally speaking,

there were two major indications for these conversions, including: (1) failure in entering the abdominal cavity through the posterior vaginal fornix (8 patients); and (2) the procedures could not be completed in a vNOTES manner after the surgical platform had been established (11 patients). For the rectum and posterior uterine wall adhere to each other tightly, thus sealing the posterior fornix. As for the second indication, there were four different situations of surgical conversion, including interstitial tubal pregnancy (2 cases, 18.18%), abnormal location of the fallopian tube (2 cases, 18.18%), an unexpected malignant intraoperative finding (1 case, 9.09%), and serious pelvic adhesions that made it hard to expose the pathological tubes (6 cases, 54.55%). Of note, all three converted rectal injuries were found in patients with the first indication. The planned procedures were one chromopertubation, two tubal ligations, three tubal salpingotomies, and 13 salpingectomies. Two procedures were converted to conventional MPL, and the remaining 17 were converted to the LESS approach. Nine second-line and 10 third-line surgeons performed these surgeries.

4 | DISCUSSION

Lee et al.¹¹ were the first to report on the clinical application of vNOTES in the treatment of ectopic pregnancy. Nowadays, vNOTES is a basic MIS procedure that is frequently performed by novice surgeons learning this MIS technique. Although vNOTES is associated with several desirable postoperative outcomes, including better cosmetic satisfaction, quicker recovery, and less postoperative pain,¹⁶ clinical evidence proving its safety and feasibility is still lacking.⁵ The majority of previous studies on vNOTES have failed to document a

TABLE 4 Key clinicopathological features of patients who underwent surgical conversion in attempted vNOTES tubal surgery.

Patient no.	Type of vNOTES tubal surgery	Age (years)	BMI ^a	Entered the abdominal cavity in a vNOTES manner or not	Presence of pelvic endometriosis	Converted to:	Cause of conversion	Perioperative complication
1	Salpingostomy	29	21.5	Yes	None	LESS	Unpredicted malignance: ovarian dysgerminoma (2 cm)	None
2	Salpingostomy	35	25.0	Yes	None	LESS	Severe pelvic adhesion	None
3	Salpingectomy	28	22.6	Yes	None	LESS	Abnormal location of fallopian tube: the fimbriated extremity as adhered to the anterior wall of uterus	None
4	Salpingectomy	42	22.4	Yes	None	MPL	Severe pelvic adhesion	None
5	Salpingectomy	25	22.0	Yes	None	LESS	Interstitial pregnancy	None
6	Salpingectomy	31	18.9	Yes	None	LESS	Abnormal location of fallopian tube: left fallopian tube was adhered to left round ligament	None
7	Salpingectomy	32	18.4	Yes	None	LESS	Interstitial pregnancy	None
8	Salpingectomy	56	17.6	Yes	None	LESS	Severe pelvic adhesion	None
9	Salpingectomy	28	21.2	Yes	None	LESS	Severe pelvic adhesion	None
10	Tubal ligation	37	21.1	Yes	None	LESS	Severe pelvic adhesion	None
11	Salpingectomy	32	20.8	Yes	None	LESS	Severe pelvic adhesion	None
12	Salpingectomy	31	22.5	No	None	MPL	Severe pelvic adhesion and injury of adjacent organs	Rectal seromuscular injury
13	Tubal ligation	40	25.3	No	None	LESS	Severe pelvic adhesion and injury of adjacent organs	Rectal seromuscular injury
14	Salpingectomy	34	18.8	No	None	LESS	Severe pelvic adhesion	Incomplete ileus
15	Salpingectomy	30	19.5	No	Yes	LESS	Severe pelvic adhesion	None
16	Tubal hydrotubation	25	19.1	No	None	LESS	Severe pelvic adhesion	None
17	Salpingectomy	27	17.7	No	Yes	LESS	The pelvic endometriosis caused adhesion in the Douglas pouch	Full-thickness rectal injury
18	Salpingostomy	26	17.4	No	None	LESS	Severe pelvic adhesion	None
19	Salpingectomy	28	17.3	No	None	LESS	Severe pelvic adhesion	None

Abbreviations: LESS, laparoscopic single port; MPL, multiport laparoscopy; vNOTES, transvaginal natural orifice transluminal endoscopic surgery.

^aBody mass index (calculated as weight in kilograms divided by the square of height in meters).

large enough sample size and detailed perioperative data, and have rarely focused on the aspects of surgical conversion either,^{4,10,17,18} making their conclusions questionable.^{5,6}

The present study first reported the risk factors for the surgical conversion of vNOTES tubal surgeries. Our regression analysis revealed that patients with endometriosis and severe pelvic adhesions had a significantly higher chance of undergoing surgical conversion from vNOTES. Many previous studies also indicated that vNOTES is contraindicated in patients with severe pelvic adhesions, which significantly increase the risk of rectal injury.^{11,18} This is probably because endometriosis and severe pelvic adhesion can result in adhesion formation in the pouch of Douglas, blocking the entry site of vNOTES and causing the surgical conversion.¹⁹ Despite performing detailed preoperative gynecological examinations on patients to avoid such risks, we were still confronted with several cases of "latent" or unpredictable severe pelvic adhesions, making it difficult to enter the abdominal cavity during surgery or resulting in accidentally injury to the rectum of the patient. Some of these patients did not have any prior events of severe pelvic adhesion based on their medical histories and pelvic examinations. However, this does not rule out the use of vNOTES in the treatment of patients with pelvic adhesion. Many studies have reported the detection of Douglas cul-de-sac obliteration and deep endometriosis using medical imaging, especially ultrasonography, which could aid in reducing surgical conversion of vNOTES in our future clinical practice.²⁰⁻²² In the present study itself, patients who were diagnosed with mild or moderate pelvic adhesion were successfully operated on with vNOTES and rarely converted to the OA, MPL, or transumbilical LESS approach.

We also found that factors such as BMI, and history of vaginal delivery or abdominopelvic surgery, including cesarean section, did not increase the risk of surgical conversion. Our findings were almost consistent with a newly published consensus on the safe implementation of vNOTES, which held the view that a previous cesarean section and a high BMI (>30) were not contraindications for vNOTES.⁷ Many other publications have also shown that the vNOTES approach is advantageous for patients with obesity, as surgeons can easily access the pelvic cavity in a transvaginal manner using endoscopic instruments and extract the resected tissue through the vaginal tract.^{11,23,24}

The complication rate in our cohort is comparable to that of a recently published study on vNOTES with a large sample size (4.85% vs. 3.9%), in which all the 1000 surgeries were performed by a high-volume vNOTES expert,²⁵ but the conversion rate of the present study is higher than that study (3.07% vs. 0.4%). We reason that it is because we had a more diverse composition of surgeons, the majority of whom have a much lower caseload and more years' experience of conducting vNOTES than the expert in the other study. The most serious perioperative complication in the present study was rectal injury. There were two full-thickness and two seromuscular rectal injuries. Of these, one full-thickness injury was repaired via vNOTES and the remaining three were converted into MPL or LESS.

In the present study, we attempted to provide solid clinical evidence about the perioperative complications, especially surgical

conversions, of vNOTES tubal surgeries. One of the strengths of the present study is its large sample size. Furthermore, variables such as the primary outcome and incidence of conversion are well documented in the medical records and are not simply subject to interpretation. However, there are a few inherent limitations to the study design. Besides, we only performed a 1-month follow-up, which was relatively short, and did not get long-term postoperative complications data, such as deep dyspareunia and incision granulomas. Another limitation is that the present study only investigated vNOTES complications in treating tubal pathology, which restricted the generalization of our findings to other procedures such as cystectomies, myomectomies, hysterectomies, and oophorectomies. Furthermore, our data were retrospectively collected, which might have introduced information bias and the possibility of data misclassification.

5 | CONCLUSION

vNOTES tubal surgeries are safe due to their low conversion and complication rates. Their surgical conversions are dictated by severe pelvic adhesion and endometriosis.

AUTHOR CONTRIBUTIONS

Dan Feng conceptualized this project. Dan Feng, Li He, and Qiang Zhang completed the data collection. Tianjiao Liu, Dan Feng, and Xin Li drafted the manuscript. Tianjiao Liu, Xin Li, Qiang Zhang, and Jieru Peng participated in the statistical analysis. Li He and Yonghong Lin supervised the project. All the authors contributed substantially to critical revisions of the manuscript.

ACKNOWLEDGMENTS

We gratefully thank the Chengdu High-level Key Clinical Specialty Construction Project, the Chengdu Municipal Health Commission Project (Grant number: 2021215), the Fifth Round of the Chengdu Municipal Science and Technology Research Program (grant number: 2021-YF05-00627-SN), Sichuan Provincial Medical Association Project (grant number: S19085) and the Japan-China Sasakawa Medical Fellowship Program for providing financial support of present study.

CONFLICT OF INTEREST

The authors have no conflicts of interest.

DATA AVAILABILITY STATEMENT

Research data are not shared.

ORCID

Dan Feng  <https://orcid.org/0000-0002-7324-1548>

Li He  <https://orcid.org/0000-0002-9716-2457>

Xin Li  <https://orcid.org/0000-0002-6734-9034>

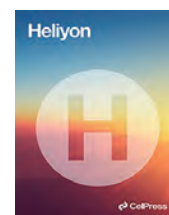
Tianjiao Liu  <https://orcid.org/0000-0001-8279-5924>

Yonghong Lin  <https://orcid.org/0000-0001-7566-8732>

REFERENCES

- Moreira-Pinto J, Lima E, Correia-Pinto J, Rolanda C. Natural orifice transluminal endoscopic surgery: a review. *World J Gastroenterol*. 2011;17(33):3795-3801. doi:10.3748/wjg.v17.i33.3795
- Yoshiki N. Review of transvaginal natural orifice transluminal endoscopic surgery in gynecology. *Gynecol Minim Invasive Ther*. 2017;6(1):1-5. doi:10.1016/j.gmit.2016.11.007
- Zorrón R, Filgueiras M, Maggioni LC, Pombo L, Lopes Carvalho G, Lacerda OA. NOTES. Transvaginal cholecystectomy: report of the first case. *Surg Innov*. 2007;14(4):279-283. doi:10.1177/1553350607311090
- Chen X, Liu H, Sun D, et al. Transvaginal natural orifice transluminal endoscopic surgery for tubal pregnancy and a device innovation from our institution. *J Minim Invasive Gynecol*. 2019;26(1):169-174. doi:10.1016/j.jmig.2018.05.013
- Kho RM. vNOTES: is it the panacea we are all hoping for? *J Minim Invasive Gynecol*. 2021;28(6):1146-1147. doi:10.1016/j.jmig.2021.04.012
- Becerra Garcia FC, Romo-Medrano Mora KE. Our perception of "Women's positive perception of transvaginal NOTES surgery": let the voices be heard, not just counted. *Surg Endosc*. 2010;24(5):1226-1228. doi:10.1007/s00464-009-0750-6
- Kapurubandara S, Lowenstein L, Salvay H, Herijgers A, King J, Baekelandt J. Consensus on safe implementation of vaginal natural orifice transluminal endoscopic surgery (vNOTES). *Eur J Obstet Gynecol Reprod Biol*. 2021;263:216-222. doi:10.1016/j.ejogrb.2021.06.019
- Huang L, He L, Zhang L, et al. Application of the prone position in myomectomy by transvaginal natural orifice transluminal endoscopic surgery. *Wideochir Inne Tech Maloinwazyjne*. 2021;16(1):234-242. doi:10.5114/wiitm.2020.95397
- Huang L, Lin Y-H, Yang Y, Gong Z-L, He L. Comparative analysis of vaginal natural orifice transluminal endoscopic surgery versus transumbilical laparoscopic single-site surgery in ovarian cystectomy. *J Obstet Gynaecol Res*. 2021;47(2):757-764. doi:10.1111/jog.14603
- Baekelandt J, Vercammen J. IMELDA transvaginal approach to ectopic pregnancy: diagnosis by transvaginal hydrolaparoscopy and treatment by transvaginal natural orifice transluminal endoscopic surgery. *Fertil Steril*. 2017;107(1):e1-e2. doi:10.1016/j.fertnstert.2016.09.024
- Lee C-L, Wu K-Y, Su H, Ueng S-H, Yen C-F. Transvaginal natural-orifice transluminal endoscopic surgery (NOTES) in adnexal procedures. *J Minim Invasive Gynecol*. 2012;19(4):509-513. doi:10.1016/j.jmig.2012.02.005
- Johnson NP, Hummelshoj L, Adamson GD, et al. World endometriosis society consensus on the classification of endometriosis. *Hum Reprod*. 2017;32(2):315-324. doi:10.1093/humrep/dew293
- Mettler L, Hucke J, Bojahr B, Tinneberg HR, Leyland N, Avelar R. A safety and efficacy study of a resorbable hydrogel for reduction of post-operative adhesions following myomectomy. *Hum Reprod*. 2008;23(5):1093-1100. doi:10.1093/humrep/den080
- Dindo D, Demartines N, Clavien P-A. Classification of surgical complications: a new proposal with evaluation in a cohort of 6336 patients and results of a survey. *Ann Surg*. 2004;240(2):205-213.
- Goldstein SR, Horii SC, Snyder JR, Raghavendra BN, Subramanyam B. Estimation of nongravid uterine volume based on a nomogram of gravid uterine volume: its value in gynecologic uterine abnormalities. *Obstet Gynecol*. 1988;72(1):86-90.
- Li C-B, Hua K-Q. Transvaginal natural orifice transluminal endoscopic surgery (vNOTES) in gynecologic surgeries: a systematic review. *Asian J Surg*. 2020;43(1):44-51. doi:10.1016/j.asjsur.2019.07.014
- Liu J, Bardawil E, Lin Q, et al. Transvaginal natural orifice transluminal endoscopic surgery tubal reanastomosis: a novel route for tubal surgery. *Fertil Steril*. 2018;110(1):182. doi:10.1016/j.fertnstert.2018.02.139
- Xu B, Liu Y, Ying X, Fan Z. Transvaginal endoscopic surgery for tubal ectopic pregnancy. *JSLs*. 2014;18(1):76-82. doi:10.4293/108680813X13693422519875
- Cranney R, Condous G, Reid S. An update on the diagnosis, surgical management, and fertility outcomes for women with endometrioma. *Acta Obstet Gynecol Scand*. 2017;96(6):633-643. doi:10.1111/aogs.13114
- Reid S, Condous G. Transvaginal sonographic sliding sign: accurate prediction of pouch of Douglas obliteration. *Ultrasound Obstet Gynecol*. 2013;41(6):605-607. doi:10.1002/uog.12469
- Leonardi M, Martins WP, Espada M, Georgousopoulou E, Condous G. Prevalence of negative sliding sign representing pouch of Douglas obliteration during pelvic transvaginal ultrasound for any indication. *Ultrasound Obstet Gynecol*. 2020;56(6):928-933. doi:10.1002/uog.22023
- Arion K, Aksoy T, Allaire C, et al. Prediction of pouch of Douglas obliteration: point-of-care ultrasound versus pelvic examination. *J Minim Invasive Gynecol*. 2019;26(5):928-934. doi:10.1016/j.jmig.2018.09.777
- Lee C-L, Wu K-Y, Su H, Wu P-J, Han C-M, Yen C-F. Hysterectomy by transvaginal natural orifice transluminal endoscopic surgery (NOTES): a series of 137 patients. *J Minim Invasive Gynecol*. 2014;21(5):818-824. doi:10.1016/j.jmig.2014.03.011
- Kaya C, Yıldız Ş, Alay İ, Aslan Ö, Aydinler İE, Yaşar L. The comparison of surgical outcomes following laparoscopic hysterectomy and vNOTES hysterectomy in obese patients. *J Invest Surg*. 2022;35(4):862-867. doi:10.1080/08941939.2021.1927262
- Baekelandt J, Kapurubandara S. Benign Gynaecological procedures by vaginal natural orifice transluminal endoscopic surgery (vNOTES): complication data from a series of 1000 patients. *Eur J Obstet Gynecol Reprod Biol*. 2021;256:221-224. doi:10.1016/j.ejogrb.2020.10.059

How to cite this article: Feng D, He L, Li X, et al. Perioperative outcomes of and predictors for conversion from transvaginal natural orifice transluminal endoscopic tubal surgeries: A retrospective cohort study of 619 patients. *Int J Gynecol Obstet*. 2023;161:803-811. doi:10.1002/ijgo.14653



Research article

Transvaginal natural orifice endoscopic surgery for tubal ectopic pregnancy: A more suitable surgical approach for enhanced recovery after surgery

Ying Liu^{a,1}, Xin Li^{a,*}, Tianjiao Liu^{a,1}, Aijie Xie^a, Xian Wu^a, Yujian Jia^a, Xiaoyan Liao^a, Wei Cheng^a, Hui Wang^a, Fangyuan Zhong^a, Lijuan Xu^a, Juan Huang^a, Siqin Xiu^a, Zhongzhi Li^b, Yalan Li^c, Xue Xiao^{d,**}, Yonghong Lin^{a,***}, Xiaoqin Gan^{a,****}

^a Department of Gynecology and Obstetrics, Chengdu Women's and Children's Central Hospital, School of Medicine, University of Electronic Science and Technology of China, Chengdu, 611731, China

^b Department of Gynecology and Obstetrics, Chongqing University Fuling Hospital, Chongqing, 408099, China

^c Psychiatry Department, Psychosomatic Medical Center, The Fourth People's Hospital of Chengdu, Chengdu, 610036, China

^d Department of Gynecology and Obstetrics, West China Second University Hospital, Sichuan University, Chengdu, 610041, China

ARTICLE INFO

Keywords:

Enhanced recovery after surgery
Salpingectomy
Salpingostomy
Laparoscopic
Transvaginal natural orifice endoscopic surgery
Tubal pregnancy

ABSTRACT

Objective: We aimed to determine the safety of Vaginal natural orifice transluminal endoscopic surgery (vNOTES) in terms of the Enhanced Recovery after Surgery (ERAS) concept for tubal pregnancy surgery and provide a detailed process of vNOTES for tubal pregnancy surgery, including experience and key points for surgeons performing this procedure.

Methods: The Longitudinal Vaginal Natural Orifice Transluminal Endoscopic Surgery Study (LovNOTESS), which was conducted in Chengdu, China. A total of 219 patients who underwent tubal ectopic pregnancy surgery between September 2021 and March 2022. The patients underwent salpingectomy or salpingostomy using transumbilical laparoscopic single-site surgery (LESS) or vNOTES, according to their preferences. This study prospectively collected perioperative and one-year follow-up data on tubal pregnancy outcomes after vNOTES and compared them with those after LESS.

Results: The vNOTES group showed a shorter surgical duration, hospitalization duration, and postoperative exhaust time and a lower analgesic medication usage rate, but it showed a higher surgical conversion rate. The vNOTES approach reduced the postoperative exhaust time by

* Corresponding author. Chengdu Women's and Children's Central Hospital, 1617 Riyue Avenue, Qingyang District, Chengdu, 611731, Sichuan, China.

** Corresponding author. West China Second University Hospital, Sichuan University, No. 20, Block 3, Renmin Road, Chengdu, 610041, China.

*** Corresponding author. Chengdu Women's and Children's Central Hospital, 1617 Riyue Avenue, Qingyang District, Chengdu, 611731, Sichuan, China.

**** Corresponding author. Chengdu Women's and Children's Central Hospital, 1617 Riyue Avenue, Qingyang District, Chengdu, 611731, Sichuan, China.

E-mail addresses: 554989333@qq.com (Y. Liu), xinlicwch@163.com (X. Li), xiaoxuesc@aliyun.com (X. Xiao), linyhcd2011@163.com (Y. Lin), amandine2021@163.com (X. Gan).

¹ These authors contributed equally to this work.

<https://doi.org/10.1016/j.heliyon.2024.e24945>

Received 18 October 2023; Received in revised form 13 January 2024; Accepted 17 January 2024

Available online 20 January 2024

2405-8440/© 2024 Published by Elsevier Ltd. This is an open access article under the CC BY-NC-ND license (<http://creativecommons.org/licenses/by-nc-nd/4.0/>).

approximately 9 h (95% confidence interval [CI]: $-11.93, -5.57$ h, $p < .001$) and the risk of postoperative analgesic drug use by 77% (odds ratio, 0.23; 95% CI: 0.10, 0.61, $p = .023$).

Conclusion: vNOTES can shorten the exhaust time and duration of hospitalization, reduce postoperative pain, and avoid surface surgical scars in tubal pregnancy surgeries, consistent with the ERAS concept. However, more comprehensive preoperative evaluation of patients who choose vNOTES is required to reduce the occurrence of intraoperative conversion.

Trial registration: ChiCTR2100053483.

1. Introduction

Ectopic pregnancy involves implantation of the zygote outside the uterine cavity, and tubal pregnancy is the most common form of ectopic pregnancy [1]. Although the incidence rate of tubal pregnancies is only approximately 0.5%–2.3% [2,3], it is the main cause of early pregnancy death [4,5]. Stable and ruptured tubal pregnancies are primarily treated using surgical procedures, which are divided into salpingostomies and salpingectomies [6,7].

Tubal pregnancy surgeries are routinely performed as daycare surgeries at our department because of the minor surgical damage. While the conventional surgical approach is transumbilical laparoendoscopic single-site surgery (LESS), vaginal natural orifice transluminal endoscopic surgery (vNOTES) has recently emerged as an option [8–11]. The growing relevance of the Enhanced Recovery after Surgery (ERAS) concept requires surgeons to continuously refine their surgical skills to ensure less surgery-related damage and pain, shorter hospital stays, and earlier return to normal life [12–14]. In comparison with LESS, vNOTES shows milder postoperative pain, faster anal exhaust, and complete absence of surface scars, consistent with the concept of ERAS [15–19]. Although the feasibility of vNOTES for tubal pregnancy surgery has been reported, data regarding its safety are limited [8]. Considering its anatomical specificity, this approach may cause damage to adjacent organs such as the bladder or rectum [16,20,21], indicating the need to investigate the safety of vNOTES in tubal pregnancy surgery in terms of the ERAS concept.

Therefore, this study prospectively collected and compared perioperative and one-year follow-up data on tubal pregnancies treated using vNOTES and LESS. Using these data, we aimed to determine the safety of vNOTES in terms of the ERAS concept for tubal pregnancy surgery and provide detailed insights regarding vNOTES for tubal pregnancy surgery, including important considerations for surgeons performing this procedure.

2. Materials and methods

2.1. Study design and participants

This study was based on the Longitudinal Vaginal Natural Orifice Transluminal Endoscopic Surgery Study (LovNOTESS), which was conducted in Chengdu, China (China Clinical Trials Registry ChiCTR2200059282), and was approved by the Institutional Review Board of Chengdu Women and Children's Central Hospital (No. 202130). This subgroup study prospectively collected perioperative and one-year follow-up data of patients with tubal pregnancy who were willing to undergo surgical treatment between September 2021 and March 2022. This study only recruited patients with stable vital signs, and patients suspected of significant abdominal bleeding or hemorrhagic shock underwent emergency surgery. Meanwhile, this study excluded patients with absolute or relative contraindications to vNOTES, such as suspected vaginal infections, severe pelvic adhesions, fallopian tube ovarian abscesses, endometriosis, malignancy, intrauterine pregnancy, potential interstitial ectopic pregnancy (through preoperative ultrasound examination [22]) or sacrouterine nodularity. After informing the patient in detail about the risks associated with the surgery and providing written informed consent, the patient underwent salpingectomy or salpingostomy using LESS or vNOTES according to their preferences. In tubal pregnancies, suspected vaginal infections, severe pelvic adhesions, or lesions located in the interstitial part of the fallopian tubes are contraindications for vNOTES.

2.2. Data collection

The patients' perioperative data were collected from the hospital's electronic medical record system, including data related to the patients' age, duration of amenorrhea, body mass index (BMI), fertility history, previous abdominal surgery, surgical method, surgical approach, maximum diameter of the mass, preoperative and postoperative blood human chorionic gonadotropin (HCG) levels, operation time, pelvic adhesions, surgical conversion, postoperative exhaust time, length of hospital stay, and perioperative complications. The operative time was measured from the time the incision was made to the end of suturing. Postoperative recovery data included the time from the end of the surgery to the first postoperative activity, urination, feeding, and exhaust. For salpingectomy, outpatient follow-up assessments were performed 1 week after surgery and 1 month thereafter; for salpingostomy, patients were required to undergo weekly blood HCG tests until they showed negative results.

2.3. Standard surgical procedures for transumbilical LESS and vNOTES under ERAS

For all patients, the routine procedure for ERAS was as follows: patients fasted for >8 h after consuming fried or fatty foods or

meats, >6 h after consuming light meals or milk, and >2 h after drinking water. Urinary catheters were not routinely placed during surgery. After waking up from anesthesia, the patient was asked to eat light food as soon as possible and get out of bed as soon as possible. For patients who experienced no specific discomfort, discharge was routinely performed on the same day or in the morning after surgery (within 24 h of admission). After discharge, patients were given a 24-h online phone number to contact the doctors in case of adverse events.

All surgeries were performed by the same qualified surgeons in accordance with the same surgical procedures. Patients emptied their bladder before surgery and received an intravenous infusion of 1-g cefazoline 30 min before surgery to prevent infection. The patient was assisted in the lithotomy position and administered general anesthesia. Before performing vNOTES, cervical forceps were used to pull the cervix to ensure good cervical and uterine activity. For vNOTES, the specific operating steps are as follows: 1) The vaginal retractor exposes the cervix, and 2 Allis forceps are used to pull the cervix outward and upward to expose the posterior vaginal fornix; 2. Make a 2 cm transverse incision at the midpoint of the posterior vaginal fornix, cut the whole thickness of the vaginal wall, and then use tissue scissors to separate the tissue to reach the peritoneum; 3) Cut the peritoneum and extend the incision toward 4 and 8 o'clock in the vagina; 4) A disposable double-ring multi-instrument access port (Beijing Aerospace Kadi Technology Development Institute, HK-TH-60.4TY) was inserted into the pelvic cavity through the incision. For the LESS procedure, an incision was made at the navel. The next steps were same in all groups and followed: Pneumoperitoneum was created up to 14 mmHg of CO2 insufflation and a 10-mm 30-degree rigid laparoscope (Karl Storz GmbH & Co. KG, Tuttlingen, Germany) was used for visualization.

2.4. Standard surgical procedures for salpingostomy or salpingectomy

For salpingostomy, an incision was made on the opposite side of the fallopian tube mesentery, at the most prominent point of the pregnancy mass. Bipolar electrocoagulation was performed to create an electrocoagulation band along the long axis of the fallopian tube. The fallopian tube was placed inside a specimen bag to prevent the villi from flowing into the abdominal cavity. Electrocoagulation hooks or scissors were used to cut longitudinally along the long axis of the affected fallopian tube, with a slightly shorter incision length than the pregnancy mass. Non-invasive forceps were used to lift the incision edge of the fallopian tube wall, stretch into a 5-mm flushing suction device along the tube wall into the lumen, use water pressure to separate the villi and blood clots from the tube wall, and drive the villi and blood clots to completely discharge from the incision under water flow. If the villi and blood clots adhered tightly to the tube wall and could not be completely separated by water pressure, non-invasive grasping forceps were used to gently pull the villi tissue and continue to separate the villi from the base of the tube wall under water pressure. The lumen of the fallopian tube was rinsed repeatedly with an NaCl solution to ensure the absence of residual villous tissue. The wound surface of the Fallopian

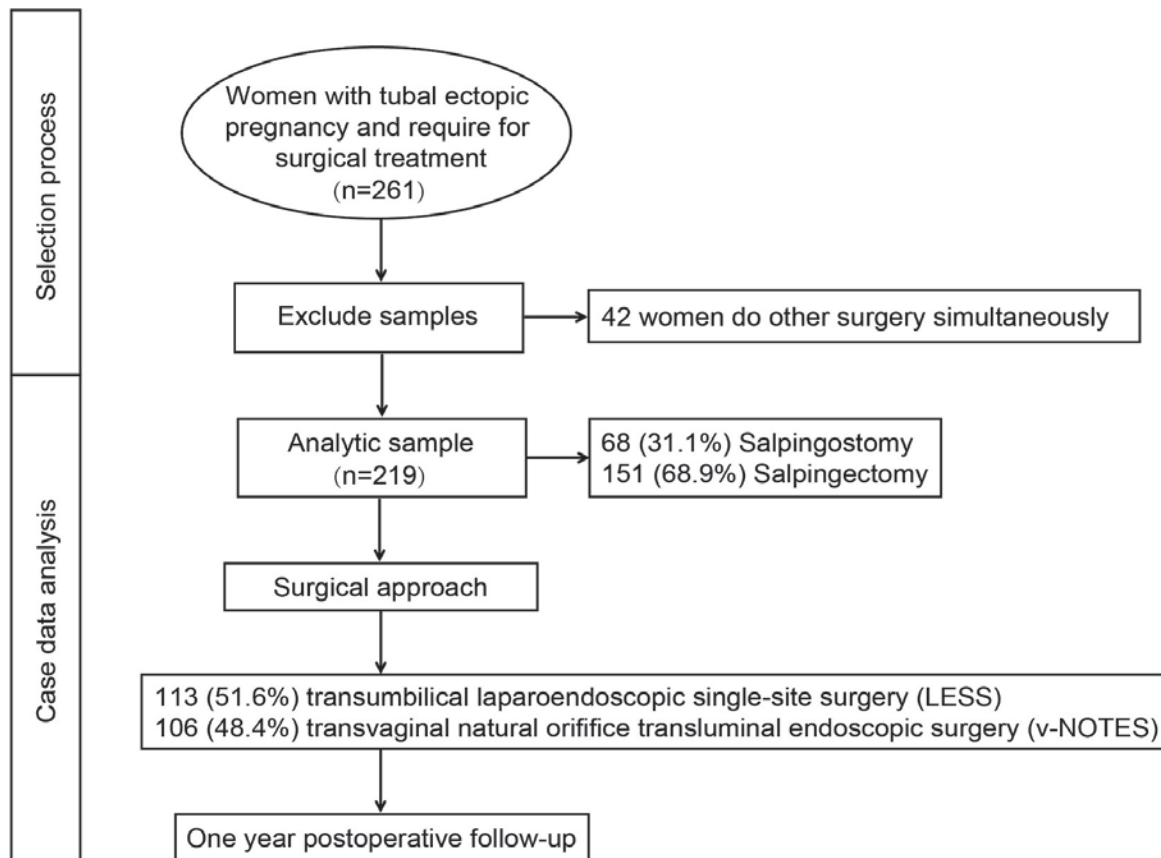


Fig. 1. Selection process for this study.

tube was opened or sutured discontinuously to the mucosal layer.

For salpingectomy, the fimbriated extremity of the fallopian gland was lifted with non-invasive forceps, the mesosalpinx was coagulated with bipolar electrocoagulation, and the mesosalpinx was gradually cut to the isthmus of the oviduct with scissors. After bipolar electrocoagulation of the interstitial part of the fallopian tube, scissors were used to cut the fallopian tube at the electrocoagulation site, and the wound was electrocoagulated to stop the bleeding.

All surgeons and surgical team members follow standardized operating procedures to complete the learning curve [23] and achieve proficiency. If intraoperative injury of large vessels, important organs or bleeding >800 ml, the surgical method will be changed. vNOTES is generally converted to transabdominal single-port laparoscopic surgery, and single-port laparoscopic surgery is converted to multi-ports surgery. Immediately convert to open surgery if there is a life-threatening vascular injury.

The abdominal and vaginal wound were closed with 2-0 absorbed suture and 2-0 barbed absorbable suture respectively. If the patient feels significant pain after surgery, 10 ml of ibuprofen will be given as a single oral analgesic. Use again after 4–6 h if necessary.

2.5. Statistical analysis

SPSS software (version 27.0; IBM Corp., Armonk, NY, USA) were used to perform the all statistical analyses. Fisher's exact or Chi-square tests were used to analyze categorical data, reporting as counts (percentages). The mean \pm standard deviation values of continuous variables were evaluated via Student's t-test and least significant difference Student's t-test. Multivariate linear regression analysis was used to detect the factors influencing intraoperative bleeding, duration of surgery, and postoperative exhaust time. Binary logistic regression was used to analyze the associations between preoperative characteristics and postoperative analgesic medication usage. Covariates were selected according to the different variables in the univariate analysis and factors that were reported to affect the dependent variable in previous studies. All statistical significance was set at $P < .05$ with two-tailed tests.

3. Results

The selection process for the study population is illustrated in Fig. 1. Initially, 261 patients with tubal ectopic pregnancies who were willing to undergo surgical treatment were recruited for the study. After excluding patients who underwent other surgeries simultaneously, the final analysis included 219 patients, of whom 106 (48.4%) underwent vNOTES and 113 (51.6%) underwent LESS. The average age of the patients, duration of amenorrhea, and BMI at recruitment were 31.40 ± 5.45 years, 31.40 ± 5.45 days, and 21.28 ± 3.16 kg/m², respectively. Among these patients, 159 (72.6%) had a history of artificial dilation and curettage abortion, 115 (52.5%) had undergone abdominal surgery, and 30 (13.7%) had a previous ectopic pregnancy. Among the 219 patients, 68 (31.1%) chose salpingostomy and 151 (68.9%) chose salpingectomy (Table 1).

No statistically significant differences were observed in the demographic characteristics of the patients in the LESS and vNOTES groups. Patients in the vNOTES group showed a shorter duration of surgery and hospitalization, a shorter postoperative exhaust time, and a lower analgesic medication use rate, but had a higher surgical conversion rate (Table 2). The reasons for surgical conversion in four cases in the vNOTES group were as follows: the procedure was beyond the scope of the surgical instrument due to adhesion of the fallopian tube to the lateral wall of the pelvic cavity in one case; difficulty stopping bleeding due to the proximity of the mass to the uterine part in one case; and difficulty entering the pelvic cavity due to pelvic adhesions in two cases. All four of these patients were transferred to the LESS group. Perioperative complications in the LESS group included persistent ectopic pregnancy after surgery in one patient, poor incision healing in one patient, and postoperative fever and one patient had; in contrast, perioperative complications in the vNOTES group included persistent ectopic pregnancy after surgery in one patient, postoperative pelvic hemorrhage in one patient, and postoperative fever in two patients had. All patients recovered after undergoing conservative treatment and were discharged without re-surgery.

The volume of intraoperative bleeding can be indirectly used as an indicator of surgical injury, and was further analyzed using

Table 1
Description of the patients demographic characteristics and operation types.

Variables	Total
Patients	219
Age (year)	31.40 ± 5.45
BMI (kg/m ²)	21.28 ± 3.16
Duration of amenorrhea (day)	47.90 ± 10.45
History of abdominal surgery	115 (52.5%)
History of D & C artificial abortion	159 (72.6%)
History of ectopic pregnancy	30 (13.7%)
Surgical approach	
LESS	113 (51.6%)
v-NOTES	106 (48.4%)
Surgical type	
Salpingostomy	68 (31.1%)
Salpingectomy	151 (68.9%)

BMI: body mass index, v-NOTES: vaginal natural orifice transluminal endoscopic surgery, LESS: laparoendoscopic single-site surgery.

Table 2
Description of the patient characteristics by surgical approaches.

Variables	LESS	v-NOTES	P-value
Patients	N = 113	N = 106	
Age (year)	31.60 ± 4.98	31.24 ± 5.86	0.735 ^a
BMI (kg/m ²)	21.38 ± 3.41	21.20 ± 2.97	0.769 ^a
Duration of amenorrhea (day)	46.92 ± 7.95	48.67 ± 12.15	0.374 ^a
History of abdominal surgery	60 (53.1%)	55 (51.9%)	0.756 ^b
Max diameter of mass (cm)	2.94 ± 1.32	2.78 ± 1.19	0.493 ^a
Preoperative HCG (mIU/ml)	2861.12 ± 5765.42	3004.95 ± 5647.45	0.897 ^a
D&C artificial abortion	73 (64.6%)	86 (81.1%)	0.787 ^b
History of ectopic pregnancy	17 (15.0%)	13 (12.2%)	0.293 ^b
Emergency surgery	4 (3.5%)	5 (4.7%)	0.702 ^c
Surgical type			0.215 ^b
Salpingostomy	38 (33.6%)	30 (28.3%)	
Salpingectomy	75 (66.4%)	76 (71.7%)	
Operative information			
Duration of surgery (min)	59.53 ± 21.35	55.94 ± 17.06	0.230 ^a
Bleeding volume (ml)	22.19 ± 31.01	18.02 ± 15.39	0.370 ^a
Pelvic adhesion	35 (31.0%)	32 (30.2%)	0.846 ^b
Surgical conversion	0 (0%)	4 (3.8%)	0.026 ^c
Post-Operative information			
Hemoglobin difference (g/L)	15.65 ± 9.43	13.71 ± 9.23	0.387 ^a
Hospital stay (day)	1.03 ± 0.18	0.60 ± 0.13	0.041 ^a
Exhaust time (hour)	6.05 ± 4.89	4.84 ± 3.90	0.204 ^a
Analgesic medication use	26 (23.9%)	8 (7.6%)	<0.001 ^b
Perioperative complications	3 (2.7%)	4 (3.8%)	0.776 ^c

BMI: body mass index, v-NOTES: vaginal natural orifice transluminal endoscopic surgery, LESS: laparoendoscopic single-site surgery, HCG: human chorionic gonadotropin, D&C: Dilation and Curettage.

^a Average and standard deviation. Student's *t*-Test.

^b Number (percentage). Chi-squared Test.

^c Number (percentage). Fisher Exact Test.

multiple linear regression. The results showed that the amount of intraoperative bleeding was positively correlated with surgical conversion and pelvic adhesions. The bleeding volume increased by approximately 29 mL in cases involving surgical conversion (95% confidence interval [CI]: 17.56, 39.73 mL, $p = .019$) and 19 mL for each 1-grade increase in pelvic adhesion (95% CI: 7.08, 27.39 mL, $p = .043$) (Table 3).

The factors influencing operation time were further analyzed using multiple linear regression, and the results showed that operation duration was correlated with BMI, surgical type, surgical conversion, and pelvic adhesion (Fig. 2A). Salpingostomy, surgical conversion, and each grade of pelvic adhesion increased the operation duration by approximately 10 min (95% CI: 1.24, 18.22 min, $p = .025$), 32 min (95% CI: 16.83, 46.17 min, $p = .037$), and 9 min (95% CI: 5.33, 13.39 min, $p = .012$), respectively (Fig. 2B). Interestingly, the operation duration also increased by approximately 1.4 min when BMI increased by 1 kg/m² (95% CI: 0.24, 2.59 min, $p = .019$).

Early postoperative anal exhaust indicates faster recovery of gastrointestinal function. Multiple linear regression analysis was conducted to investigate the factors influencing postoperative anal exhaust time, and the results showed that exhaust time was correlated with BMI, surgical approach, and pelvic adhesions (Table 4). A 1-kg/m² increase in BMI and an increase one 1 grade in

Table 3
Association between perioperative characteristics and volume of intraoperative bleeding.

Variables	Beta	95% CI	P-value	VIF
R ² = 0.360				
Age (year)	0.09	(-0.87,1.06)	0.849	1.29
BMI (kg/m ²)	-0.25	(-1.86,1.36)	0.760	1.21
Surgical approach (vNOTES)	-5.62	(-15.08,3.84)	0.242	1.04
Surgical type (Salpingostomy)	2.49	(-9.14,14.11)	0.672	1.36
Surgical transfer	28.64	(17.56,39.73)	0.019	1.13
History of abdominal surgery	-2.15	(-7.45,3.15)	0.423	1.15
Duration of amenorrhea	-0.02	(-0.51,0.46)	0.929	1.19
Max diameter of mass	-0.35	(-4.15,3.45)	0.855	1.04
Preoperative HCG	0.01	(0,0.02)	0.146	1.16
Emergency surgery	2.16	(-4.49,8.81)	0.588	1.06
Pelvic adhesion	19.24	(7.08,31.39)	0.043	1.10
Duration of surgery	0.19	(-0.08,0.46)	0.166	1.28
Surgeon	-3.60	(-11.39,4.19)	0.361	1.22

BMI: body mass index, v-NOTES: vaginal natural orifice transluminal endoscopic surgery, HCG: human chorionic gonadotropin.

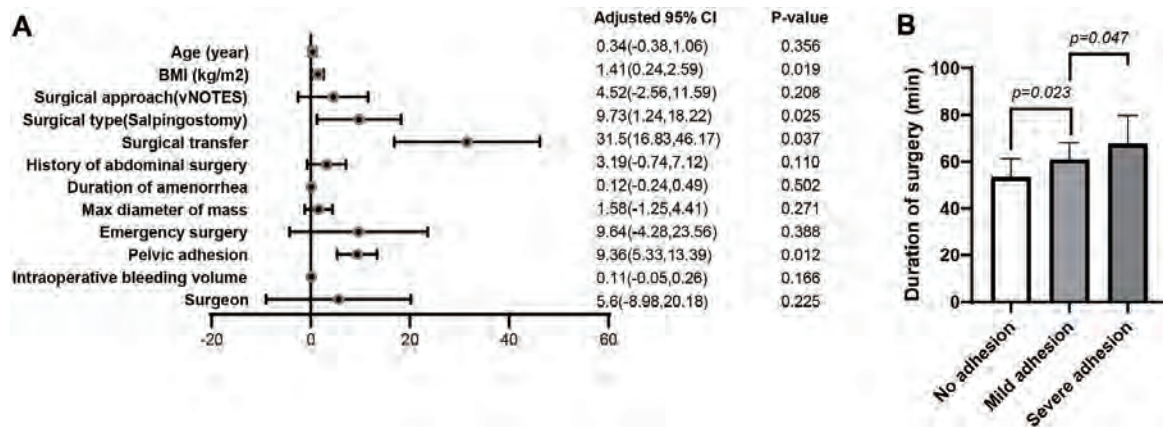


Fig. 2. The influence of surgical characteristics on the operation duration. (A) Multiple linear regression showed that the operation duration was correlated with BMI, surgical type, surgical conversion, and pelvic adhesion. Salpingostomy, surgical conversion, and each grade of pelvic adhesion increased the operation duration by approximately 10 min (95% confidence interval [CI]: 1.24, 18.22 min; $p = .025$), 32 min (95% CI: 16.83, 46.17 min; $p = .037$), and 9 min (95% CI: 5.33, 13.39 min; $p = .012$), respectively. Interestingly, the operation duration increased by approximately 1.4 min when BMI increased by 1 kg/m² (95% CI: 0.24, 2.59 min, $p = .019$). (B) The groups with no adhesions, mild adhesions, and severe adhesions showed significant differences in the duration of surgery.

pelvic adhesion increased the exhaust time by 0.6 h (95% CI: 0.26, 0.85 h, $p = .027$) and 6.7 h (95% CI: 2.90, 10.57 h, $p = .019$), respectively. Notably, the vNOTES approach reduced the postoperative exhaust time by approximately 9 h (95% CI: -11.93, -5.57 h, $p < .001$).

Analgesics are not routinely used after surgery, and patients actively requesting the use of analgesics may be experiencing greater pain and discomfort. The factors influencing postoperative analgesic drug use were analyzed using binary logistic regression, and the results showed that analgesic drug use was correlated with the surgical approach, surgical conversion, and duration of surgery (Table 5). Surgical conversion increased the risk of postoperative analgesic drug use by 102% (odds ratio [OR]: 2.02, 95% CI: 1.34, 3.56, $p = .025$), while vNOTES decreased the risk by 77% (OR:0.23, 95% CI: 0.10, 0.61, $p = .023$). Moreover, the risk of postoperative analgesic drug use increased by 3% when the duration of surgery increased by 1 min (OR:1.03, 95% CI: 1.01, 1.12, $p = .037$).

The patient’s fertility history was followed-up by phone one year after surgery. In the salpingostomy group, more patients chose contraception, mostly because of concerns regarding the recurrence of ectopic pregnancy. In this group, patients planning to conceive had a higher natural conception rate and risk of recurrent tubal pregnancy, and lower rates of infertility or conception through assisted reproductive technologies (Supplementary Table 1).

4. Discussion

Our results showed that vNOTES shortened the exhaust time and hospital stay, reduced postoperative pain, and helped avoid surface surgical scars, consistent with ERAS requirements. In this prospective study, we compared the perioperative characteristics of tubal pregnancy surgery using LESS and vNOTES in terms of the ERAS requirements and collected data on fertility one year after surgery. In addition, the advantages and disadvantages of vNOTES in relation to the ERAS requirements for tubal pregnancy surgery are discussed in detail, providing a theoretical basis for the further development of vNOTES.

The vNOTES and LESS approaches showed no significant differences in intraoperative bleeding, surgical duration, or postoperative

Table 4
Association between postoperative exhaust time and perioperative characteristics.

Variables	Beta	95% CI	P-value	VIF
$R^2 = 0.607$				
Age (year)	-0.01	(-0.33,0.32)	0.963	1.32
BMI (kg/m ²)	0.56	(0.26,0.85)	0.027	1.14
Surgical approach (vNOTES)	-8.75	(-11.93,-5.57)	<0.001	1.07
Surgical type (Salpingostomy)	-2.19	(-5.92,1.55)	0.249	1.28
Surgical transfer	5.68	(-18.31,29.66)	0.201	1.21
History of abdominal surgery	1.31	(-0.64,3.25)	0.187	1.43
Max diameter of mass	0.63	(-0.63,1.88)	0.325	1.04
Emergency surgery	0.42	(-5.55,6.39)	0.889	1.35
Pelvic adhesion	6.73	(2.90,10.57)	0.019	1.16
Intraoperative bleeding volume	-0.03	(-0.09,0.04)	0.415	1.07
Duration of surgery	-0.02	(-0.10,0.07)	0.715	1.22
Surgeon	-0.45	(-1.60,0.71)	0.443	1.12

BMI: body mass index, v-NOTES: vaginal natural orifice transluminal endoscopic surgery.

Table 5

Association between postoperative analgesic medication use and perioperative characteristics.

Variables	Exp(B)	95% CI	P-value
Age (year)	0.94	(0.85,1.02)	0.177
BMI (kg/m ²)	1.01	(0.86,1.18)	0.901
Surgical approach (vNOTES)	0.23	(0.10,0.61)	0.023
Surgical type (Salpingostomy)	1.02	(0.71,1.44)	0.916
Surgical transfer	2.02	(1.34,3.56)	0.025
History of abdominal surgery	0.68	(0.02,1.38)	0.826
Duration of amenorrhea	1.47	(0.89,2.43)	0.128
Max diameter of mass	0.97	(0.92,1.02)	0.255
Emergency surgery	1.29	(0.02,2.31)	0.256
Pelvic adhesion	0.56	(0.03,1.32)	0.545
Postoperative exhaust time	1.02	(0.97,1.06)	0.212
Intraoperative bleeding volume	1.00	(0.98,1.02)	0.791
Duration of surgery	1.03	(1.01,1.12)	0.037
Surgeon	1.45	(0.27,2.02)	0.109

BMI: body mass index, v-NOTES: vaginal natural orifice transluminal endoscopic surgery.

complication rates, indicating that the vNOTES approach is safe and feasible. However, the surgical conversion rate of 3.8% in the vNOTES group was much higher than that in the LESS group (0%). These conversions were primarily attributable to adhesions and the presence of the mass in the uterine part. In such cases, continued surgery under vNOTES may cause damage to neighboring organs; consequently, these patients were converted to LESS. Thus, surgeons should conduct a more comprehensive preoperative evaluation of the patients selected for vNOTES. A history of dysmenorrhea or previous pelvic surgery, difficult uterine activity, and tenderness of sacral ligament nodules may provide important clues for screening of severe pelvic adhesions [24,25]. In addition, vaginal ultrasound can be used for real-time assessment of the sliding of the uterus on the anterior wall of the rectum. If these evaluations indicate severe pelvic adhesions, the vNOTES approach should be avoided. Notably, the lesion was in the uterine part in one case. Due to failure to reach the uterine fundus, the patient underwent transumbilical single-port laparoscopy for hemostasis. This reflects the limitations of vNOTES that for lesions in the uterine fundus, vNOTES is difficult to perform surgery due to limitations in field of view and instrument range. We believe that a combination of these methods can effectively avoid the complications associated with inappropriate patient selection.

In this cohort, the incidence of complications was 3.2%, slightly higher than that associated with LESS in previous studies [21, 26–30]. Among the cases showing complications, two involved persistent ectopic pregnancies, accounting for 2.9% of salpingostomy cases, which was similar to the corresponding percentage reported in previous studies [31,32]. Both patients recovered and were discharged from the hospital after methotrexate administration following surgery, and neither patient required re-surgery. Moreover, the surgical duration in the vNOTES group was shorter than that in the LESS group, although the difference was not statistically significant. This may be due to the smaller chopstick effect caused by the lesion being closer to the platform [33–35]. Our experience suggests that salpingostomy and ovarian cystectomy are more convenient to perform using vNOTES because the lesion site is directly located in front of the approach [36,37].

The timing of postoperative anal exhaust as a part of the discharge evaluation criteria is crucial for evaluating the ERAS mode [38, 39]. In our cohort, the postoperative exhaust time was shorter in the vNOTES group than in the LESS group, which is consistent with previous studies [40]. The vNOTES procedure was performed in the pelvic area, and showed little effect on the upper abdomen. After entering the pelvis, the first step is to push the small intestine into the abdominal cavity, after which the intestine will not be touched again, thereby minimizing intestinal irritation. Additionally, because the vNOTES incision is made in the vaginal vault, this site is insensitive to cutting pain caused by visceral nerve innervation. Lighter postoperative pain encourages patients to get out of the bed early after surgery, which can also promote gastrointestinal recovery and facilitate earlier exhaust [41,42].

The ERAS concept requires less damage to patients, faster postoperative recovery, greater patient comfort, and an earlier return to normal life activities [43–45]. The findings of this study imply that vNOTES is not inferior to or is even more suitable than LESS in terms of the ERAS concept. Moreover, vNOTES offers the advantage of completely eliminating surface scars, making it aesthetically pleasing. However, in patients who choose vNOTES, a more comprehensive preoperative evaluation is required to reduce the occurrence of intraoperative conversion.

The follow-up assessments of the patients' fertility status one year after surgery yielded noteworthy findings. Among the patients who chose salpingostomy because of reproductive reasons, 61.8% chose continuous contraception because of concerns regarding another ectopic pregnancy. However, patients who undergo salpingectomy have fewer options for contraception because they don't have to worry about ectopic pregnancy happening again in the affected fallopian tubes. This situation may also be caused by informed notification from physicians during the perioperative period. As for patients who choose salpingostomy, physicians usually recommend strict contraception for 3–6 months and inform them that the affected fallopian tube will increase the risk of ectopic pregnancy again after surgery. This may increase the psychological pressure on patients, leading them to choose long-term contraception. Although patients undergoing salpingostomy have a slightly higher natural conception rate, they also have a 15.4% chance of recurrent tubal pregnancy. Therefore, further studies are needed to determine which surgical method is the best choice for women with reproductive needs.

The strengths of this study include its prospective design and professional participants. The patients were included on the basis of

strict inclusion and exclusion criteria and a surgical procedure, ensuring a high degree of consistency in demographic characteristics between the two groups. This study compared the perioperative characteristics of the two most advanced surgical methods for tubal pregnancy surgery and preliminarily confirmed the safety and effectiveness of vNOTES for this procedure. In addition, a relatively comprehensive experimental design was implemented by prospectively collecting follow-up data from patients at 1 week, 1 month, and 1 year after surgery.

This pilot study strengthened our understanding of the safety of vNOTES during tubal pregnancy. However, this study had some limitations. First, the sample size of this study was relatively smaller than that of similar studies using Multi-port and LESS. Second, the limitations of the vNOTES technique are the chopstick effect (lack of triangulation resulting from the use of the conventional equipment) and the limited experience of the surgeons. Before performing vNOTES surgery, we suggest that all surgeons and surgical team members should follow standardized operating procedures to complete the learning curve [23]. Third, although this study shows that vNOTES can promote ERAS in patients, it is necessary to grasp the indications of this approach to reduce the occurrence of complications and surgical conversions. Four, since this study is not a randomized clinical trial, we are unable to specify surgical procedures for patients. After fully informing the advantages and disadvantages of the two surgeries, the final decision is based on the patient's wishes. Therefore, in this process, some potential bias factors may be added, which may affect the choice of surgical methods for patients. Five, if there is a conventional surgical group as the control group, it can indeed better demonstrate the advantages of vNOTES. However, due to the fact that our hospital no longer performs routine open surgery and Multi-port laparoscopic surgery except for some large uterine fibroids or malignant tumor surgeries, we do not have enough data as a control. Six, vNOTES has been widely used in gynecology for only 5 years, and the patients in this study were followed-up for only 1 year. Longer follow-up periods with more patients can improve our understanding of the short- and long-term complications of vNOTES and their potential influence on sexual function and fertility. Therefore, large-scale multicenter studies involving more patients, longer time periods, and more types of surgery are needed to further promote the widespread use of vNOTES in the field of gynecology.

5. Conclusions

Our results indicated that vNOTES could shorten the exhaust time and hospital stay, reduce postoperative pain, and avoid surface surgical scars, consistent with the ERAS concept. Thus, vNOTES may be more suitable for ERAS than LESS. However, in patients who choose vNOTES, a more comprehensive preoperative evaluation is required to reduce the occurrence of intraoperative conversion. With the further popularization of minimally invasive and scar free surgery, vNOTES will inevitably achieve longer-term development. Therefore, more and higher quality research is needed to demonstrate its advantages and promote its rapid development.

Capsule

To reflect the safety of vaginal natural orifice transluminal endoscopic surgery (vNOTES) in terms of the Enhanced Recovery after Surgery (ERAS) concept for tubal pregnancy surgery and provide a detailed process of vNOTES for tubal pregnancy surgery, including experience and key points for surgeons performing this procedure.

Funding

Financial support for this study was provided by the Sichuan Provincial Department of Science and Technology (2023YFS0219 and 2023YFS0228), Chengdu Science and Technology Bureau (No: 2021-YF0500530-SN) and the Chengdu Municipal Health Commission (No: 2021074, 2022441, 2023261, 2023413 and 2023475). The funding agencies did not have any role in the design of the study; collection, analysis, and interpretation of data; or in writing the manuscript.

Attestation statement

The subjects in this trial have not concomitantly been involved in other randomized trials. Data regarding any of the subjects in the study has not been previously published unless specified. Data will be made available to the editors of the journal for review or query upon request.

IRB approval

This study was approved by the Institutional Review Board of Chengdu Women and Children's Central Hospital (No. 202130) on June 14, 2021.

Data availability

The datasets generated and analyzed during the current study are not publicly available because of our ongoing prospective study but are available from the corresponding author upon reasonable request.

CRediT authorship contribution statement

Ying Liu: Writing – original draft. **Xin Li:** Writing – original draft. **Tianjiao Liu:** Writing – original draft. **Aijie Xie:** Writing – original draft. **Xian Wu:** Writing – original draft. **Yujian Jia:** Writing – original draft. **Xiaoyan Liao:** Writing – original draft. **Wei Cheng:** Writing – original draft. **Hui Wang:** Writing – original draft. **Fangyuan Zhong:** Writing – original draft. **Lijuan Xu:** Writing – original draft. **Juan Huang:** Writing – original draft. **Siqin Xiu:** Writing – original draft. **Zhongzhi Li:** Writing – original draft. **Yalan Li:** Writing – original draft. **Xue Xiao:** Writing – review & editing, Writing – original draft, Funding acquisition. **Yonghong Lin:** Writing – original draft. **Xiaoqin Gan:** Writing – original draft.

Declaration of competing interest

The authors declare that they have no known competing financial interests or personal relationships that could have appeared to influence the work reported in this paper.

Acknowledgements

The authors would like to thank all participants and researchers who contributed to this cohort study.

Appendix A. Supplementary data

Supplementary data to this article can be found online at <https://doi.org/10.1016/j.heliyon.2024.e24945>.

References

- [1] Y.T. Shen, Y.Y. Yang, P.G. Zhang, L.M. He, R.H. Che, Z. Li, W. Lu, Tubal ectopic pregnancy: a retrospective cohort study on clinical characteristics, treatment options and reproductive outcomes within 5 years, *Arch. Gynecol. Obstet.* 306 (6) (2022) 2055–2062.
- [2] K. Tamai, T. Koyama, K. Togashi, MR features of ectopic pregnancy, *Eur. Radiol.* 17 (12) (2007) 3236–3246.
- [3] G. Oron, T. Tulandi, A pragmatic and evidence-based management of ectopic pregnancy, *J. Minim. Invasive Gynecol.* 20 (4) (2013) 446–454.
- [4] P. Cheng, X.H. Yang, Preservation of the fallopian tube in ectopic tubal pregnancy. An analysis of the outcome of two laparoscopic surgical approaches, *Ann. Ital. Chir.* 93 (2022) 241–247.
- [5] E. Nedopekina, S. Escura, T. Cobo, S.R. Hansson, J.M. Martinez, F. Figueras, M. Lopez, Conservative treatment in non-tubal ectopic pregnancy and predictors of treatment failure, *Eur. J. Obstet. Gynecol. Reprod. Biol.* 257 (2021) 6–10.
- [6] E. Eghbali, M. Azari, A. Jafarizadeh, S. Alihosseini, Spontaneous bilateral tubal ectopic pregnancy preoperatively diagnosed by the ultrasound: a case report, *BMC Pregnancy Childbirth* 23 (1) (2023) 125.
- [7] P. Torok, A. Naem, S. Csehely, V. Chiantera, Z. Sleiman, A.S. Lagana, Reproductive outcomes after expectant and surgical management for tubal pregnancy: a retrospective study, *Minim Invasive Ther. Allied Technol.* (2023) 1–9.
- [8] B. Xu, Y. Liu, X. Ying, Z. Fan, Transvaginal endoscopic surgery for tubal ectopic pregnancy, *J. Soc. Laparoendosc. Surg.* 18 (1) (2014) 76–82.
- [9] Y.W. Kim, B.J. Park, T.E. Kim, D.Y. Ro, Single-port laparoscopic salpingectomy for surgical treatment of tubal pregnancy: comparison with multi-port laparoscopic salpingectomy, *Int. J. Med. Sci.* 10 (8) (2013) 1073–1078.
- [10] G. Ozceltik, D. Simsek, I. Hortu, A.O. Yeniel, I.M. Itil, Transvaginal natural orifice transluminal endoscopic surgery for ectopic pregnancy, *J. Obstet. Gynaecol. Res.* 48 (3) (2022) 843–849.
- [11] G. Ozceltik, A.O. Yeniel, A.O. Atay, I.M. Itil, Transvaginal natural orifice transluminal endoscopic surgery for tubal stump pregnancy, *J. Minim. Invasive Gynecol.* 28 (4) (2021) 750–751.
- [12] J. Ripolles-Melchor, A. Abad-Motos, M. Bruna-Esteban, M. Garcia-Nebreda, I. Otero-Martinez, O.A. Fernandez, M.P. Tormos-Perez, G. Paseiro-Crespo, R. Garcia-Alvarez, M. Am-O, et al., Association between use of enhanced recovery after surgery protocols and postoperative complications after gastric surgery for cancer (POWER 4): a nationwide, prospective multicentre study, *Cir. Esp. (Engl. Ed.)* (2023).
- [13] G. Nelson, C. Fotopoulou, J. Taylor, G. Glaser, J. Bakkum-Gamez, L.A. Meyer, R. Stone, G. Mena, K.M. Elias, A.D. Altman, et al., Enhanced recovery after surgery (ERAS(R)) society guidelines for gynecologic oncology: addressing implementation challenges - 2023 update, *Gynecol. Oncol.* 173 (2023) 58–67.
- [14] J. Gillet, L. Morgado, A. Hamy, C. Casa, S. Mucci, F. Drissi, P. Le Naoures, J.F. Hamel, A. Venara, Does stoma modify compliance with enhanced recovery after surgery programs? Results of a cohort study, *Int. J. Colorectal Dis.* 38 (1) (2023) 100.
- [15] J. Baekelandt, L. Matak, M. Merckx, S. Housmans, J. Deprest, T. Tollens, Posterior rectus fascia prolapse (PREFAP) repair: a new native tissue approach to pelvic organ prolapse via vaginal natural orifice transluminal endoscopic surgery, *Arch. Gynecol. Obstet.* (2023).
- [16] L. Mereu, B. Pecorino, M. Ferrara, M. Siniscalchi, G. Garraffa, M.G. D'Agate, P. Scollo, Cumulative sum analysis of learning curve process for vaginal natural orifice transluminal endoscopic surgery (V-notes) hysterectomy, *J. Minim. Invasive Gynecol.* (2023).
- [17] V.T. Lerner, G. May, C.B. Iglesia, Vaginal natural orifice transluminal endoscopic surgery revolution: the next frontier in gynecologic minimally invasive surgery, *J. Soc. Laparoendosc. Surg.* 27 (1) (2023).
- [18] L. Huang, J. Yu, Y. Li, Z.L. Gong, D. Feng, L. He, Y.H. Lin, Transvaginal natural orifice transluminal endoscopic surgery versus conventional vaginal surgery for sacrospinous ligament fixation of apical compartment prolapse: a retrospective analysis, *BMC Surg.* 23 (1) (2023) 24.
- [19] J. Jung, J.J. Noh, J. Jeon, C.S. Chang, T.J. Kim, Comparison of surgical outcomes of adnexectomy by vaginal natural orifice transluminal endoscopic surgery (vNOTES) versus single-port access (SPA) surgery, *J. Personalized Med.* 12 (12) (2022).
- [20] J. Zhang, Y. Dai, J. Leng, L. Zhu, J. Lang, D. Sun, Hysterectomy and bilateral adnexectomy using transvaginal natural orifice transluminal endoscopic surgery: the role of multichannel abdominal PORT and vaginal support ring, *J. Obstet. Gynaecol. Res.* 47 (7) (2021) 2521–2528.
- [21] M.S. Kim, J.J. Noh, T.J. Kim, Hysterectomy and adnexal procedures by vaginal natural orifice transluminal endoscopic surgery (VNH): initial findings from a Korean surgeon, *Front. Med. (Lausanne)* 7 (2020) 583147.
- [22] M. Elsherbiny, E.T. Lim, K. Ma, Interstitial ectopic pregnancy: laparoscopic cornuostomy, *J. Minim. Invasive Gynecol.* 30 (6) (2023) 439–440.
- [23] L. Huang, L. He, L. Huang, X. Gan, Y. Lin, Z. Xiong, Learning curve analysis of transvaginal natural orifice transluminal endoscopic hysterectomy combined under the standard operating procedure, *Int. J. Gynaecol. Obstet.* 159 (3) (2022) 689–695.
- [24] M. Hui, C. Schwartzburg, A. Bhalwal, Utility of vaginal natural orifice transluminal endoscopic surgery for permanent sterilization after failed attempt at bilateral tubal ligation at the time of previous cesarean section, *J. Minim. Invasive Gynecol.* 29 (10) (2022) 1138–1139.

- [25] X. Guan, E. Bardawil, J. Liu, R. Kho, Transvaginal natural orifice transluminal endoscopic surgery as a rescue for total vaginal hysterectomy, *J. Minim. Invasive Gynecol.* 25 (7) (2018) 1135–1136.
- [26] A. Kale, E. Mağ, G. Basol, E.C. Gundogdu, Y. Aboalhasan, G. Yildiz, B. Kuru, E. Kale, T. Usta, M. Altintas, et al., A new and alternative route: transvaginal natural orifice transluminal endoscopic scarless surgery (vaginal natural orifice transluminal endoscopic surgery) for class 2 and class 3 obese patients suffering from benign and malignant gynecologic pathologies, *Surg. Innovat.* 29 (6) (2022) 730–741.
- [27] I. Tavano, S. Housmans, J. Bosteels, J. Baekelandt, Pregnancy outcome after vaginal natural orifice transluminal endoscopic surgery, a first retrospective observational cohort study, *Gynecol. Obstet. Invest.* 86 (5) (2021) 432–437.
- [28] K. Nulens, R. Kempenaers, J. Baekelandt, Hysterectomy via vaginal Natural Orifice Transluminal Endoscopic Surgery in virgin patients: a first feasibility study, *J. Obstet. Gynaecol.* 42 (1) (2022) 116–121.
- [29] K. Nulens, I. Van Genechten, J. Baekelandt, Repeat vaginal natural orifice transluminal endoscopic surgery: a first feasibility study, *Gynecol. Obstet. Invest.* 86 (1–2) (2021) 117–122.
- [30] L. Huang, Y.H. Lin, Y. Yang, Z.L. Gong, L. He, Comparative analysis of vaginal natural orifice transluminal endoscopic surgery versus transumbilical laparoendoscopic single-site surgery in ovarian cystectomy, *J. Obstet. Gynaecol. Res.* 47 (2) (2021) 757–764.
- [31] E. Wall-Wieler, C.L. Shover, J.M. Hah, S.L. Carmichael, A.J. Butwick, Opioid prescription and persistent opioid use after ectopic pregnancy, *Obstet. Gynecol.* 136 (3) (2020) 548–555.
- [32] S. Akira, Y. Negishi, T. Abe, M. Ichikawa, T. Takeshita, Prophylactic intratubal injection of methotrexate after linear salpingostomy for prevention of persistent ectopic pregnancy, *J. Obstet. Gynaecol. Res.* 34 (5) (2008) 885–889.
- [33] T. Benhidjeb, I. Benhidjeb, M. Stark, S. Kreisel, M. Kruger, J. Pfitzenmaier, J. Schulte am Esch, Women's perception of transgastric and transvaginal natural orifice transluminal endoscopic surgery (NOTES) - impact of medical education, stage of life and cross-cultural aspects, *Int. J. Womens Health* 14 (2022) 1881–1895.
- [34] M.L. Interdonato, P. Scollo, T. Bignardi, F. Massimello, M. Ferrara, G. Donatiello, M. Caretto, P. Mannella, B. Pecorino, M.G. Meroni, et al., Hysterectomy by transvaginal natural orifice transluminal endoscopic surgery: an Italian initial experience, *Front. Med. (Lausanne)* 9 (2022) 1018232.
- [35] A.B. Tekin, M. Yassa, C. Kaya, D. Budak, P.B. Ilter, M.A. Mutlu, C. Usta, O.S. Gunkaya, E. Yavuz, N. Tug, Implementing the transvaginal natural orifice transluminal endoscopic surgery (vNOTES) "first" strategy in benign gynecological surgeries, *Arch. Gynecol. Obstet.* 307 (4) (2023) 1007–1013.
- [36] Y. Jung, A. Rattanaburi, O. Kim, J.H. Park, K.H. Lee, A simple gasless direct suturing technique to achieve ovarian hemostasis during transvaginal natural orifice transluminal endoscopic surgery ovarian cystectomy, *J. Laparoendosc. Adv. Surg. Tech.* 31 (9) (2021) 1046–1050.
- [37] C.B. Li, K.Q. Hua, Transvaginal natural orifice transluminal endoscopic surgery (vNOTES) in gynecologic surgeries: a systematic review, *Asian J. Surg.* 43 (1) (2020) 44–51.
- [38] J. Chen, A.L. Luo, L. Yang, W. Wang, X. Zhou, M. Yang, Nutrition management by a multidisciplinary team for prevention of nutritional deficits and morbidity following esophagectomy, *Braz. J. Med. Biol. Res.* 56 (2023) e12421.
- [39] Z. Wang, Q. Xia, A. Li, Q. Lv, Comparison of the effects of endoscopic submucosal dissection and laparoscopic distal radical surgery on the rehabilitation and quality of life of patients with early gastric cancer, *Am. J. Transl. Res.* 15 (3) (2023) 2183–2190.
- [40] Q. Hou, X. Li, L. Huang, Y. Xiong, D. Feng, Q. Zhang, X. Zeng, Y. Yang, T. Liu, Y. Li, et al., Transvaginal natural orifice endoscopic surgery for myomectomy: can it be a conventional surgery? *Front. Surg.* 9 (2022) 1013918.
- [41] X. Lv, C. Li, M. Tang, D. Yuan, Y. Zhong, Y. Xie, Study of the effect of pain on postoperative rehabilitation of patients with uterine malignant tumor, *Front. Surg.* 9 (2022) 1052800.
- [42] N. Zhang, J. Miao, Q. Zheng, The effect of nursing intervention on patients with inguinal hernia and its influence on self-management ability, *Contrast Media Mol. Imaging* 2022 (2022) 4965709.
- [43] Z. Lin, C. Yang, Y. Wang, M. Yan, H. Zheng, Comparison of prolonged postoperative ileus between laparoscopic right and left colectomy under enhanced recovery after surgery: a propensity score matching analysis, *World J. Surg. Oncol.* 20 (1) (2022) 68.
- [44] N. Kugelman, O. Lavie, N. Cohen, M. Schmidt, A. Reuveni, L. Ostrovsky, H. Dabah, Y. Segev, Enhanced recovery after surgery is feasible and beneficial and should be the standard in major gynecological surgeries, *Isr. Med. Assoc. J.* 23 (11) (2021) 725–730.
- [45] O.I. Tkachenko, S.H. Chetverikov, O.V. Bondar, V.Y. Maksymovskiy, M. Chetverikov, V.V. Chetverikova-Ovchynnyk, Implementation of the enhanced recovery after surgery protocol for patients with peritoneal carcinomatosis undergoing cytoreductive surgery and hyperthermic intraperitoneal chemoperfusion, *Contemp. Oncol.* 25 (2) (2021) 133–139.